

MARTIN MARIETTA ENERGY SYSTEMS LIBRARIES



3 4456 0251537 5

CENTRAL RESEARCH LIBRARY
DOCUMENT COLLECTION

ORNL-4422
UC-10 - Chemical Separations Processes
for Plutonium and Uranium

ty. 2

CHEMICAL TECHNOLOGY DIVISION
ANNUAL PROGRESS REPORT
FOR PERIOD ENDING MAY 31, 1969

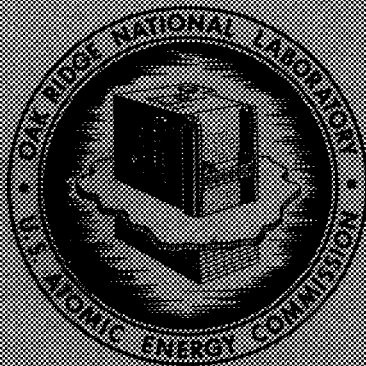
OAK RIDGE NATIONAL LABORATORY
CENTRAL RESEARCH LIBRARY
DOCUMENT COLLECTION

LIBRARY LOAN COPY

DO NOT TRANSFER TO ANOTHER PERSON

If you wish someone else to see this
document, send in name with document
and the library will arrange a loan.

ORNL-4422
13 6377



OAK RIDGE NATIONAL LABORATORY
operated by
UNION CARBIDE CORPORATION
for the
U.S. ATOMIC ENERGY COMMISSION

Printed in the United States of America. Available from Clearinghouse for Federal
Scientific and Technical Information, National Bureau of Standards,
U.S. Department of Commerce, Springfield, Virginia 22151
Price: Printed Copy \$3.00; Microfiche \$0.65

LEGAL NOTICE

This report was prepared as an account of Government sponsored work. Neither the United States, nor the Commission, nor any person acting on behalf of the Commission:

- A. Makes any warranty or representation, expressed or implied, with respect to the accuracy, completeness, or usefulness of the information contained in this report, or that the use of any information, apparatus, method, or process disclosed in this report may not infringe privately owned rights; or
- B. Assumes any liabilities with respect to the use of, or for damages resulting from the use of any information, apparatus, method, or process disclosed in this report.

As used in the above, "person acting on behalf of the Commission" includes any employee or contractor of the Commission, or employee of such contractor, to the extent that such employee or contractor of the Commission, or employee of such contractor prepares, disseminates, or provides access to, any information pursuant to his employment or contract with the Commission, or his employment with such contractor.

Contract No. W-7405-eng-26

CHEMICAL TECHNOLOGY DIVISION

ANNUAL PROGRESS REPORT

for Period Ending May 31, 1969

D. E. Ferguson - Division Director
K. B. Brown - Assistant Division Director
R. G. Wymer - Chemical Development
 Section A Chief
R. E. Blanco - Chemical Development
 Section B Chief
M. E. Whatley - Unit Operations Section Chief
H. E. Goeller - Process Design Section Chief
R. E. Brooksbank - Pilot Plant Section Chief

OCTOBER 1969

OAK RIDGE NATIONAL LABORATORY
Oak Ridge, Tennessee
operated by
UNION CARBIDE CORPORATION
for the
U.S. ATOMIC ENERGY COMMISSION

MARTIN MARIETTA ENERGY SYSTEMS LIBRARIES



3 4456 0251537 5

Reports previously issued in this series are as follows:

ORNL-2392	Period Ending August 31, 1957
ORNL-2576	Period Ending August 31, 1958
ORNL-2788	Period Ending August 31, 1959
ORNL-2993	Period Ending August 31, 1960
ORNL-3153	Period Ending May 31, 1961
ORNL-3314	Period Ending May 31, 1962
ORNL-3452	Period Ending May 31, 1963
ORNL-3627	Period Ending May 31, 1964
ORNL-3830	Period Ending May 31, 1965
ORNL-3945	Period Ending May 31, 1966
ORNL-4145	Period Ending May 31, 1967
ORNL-4272	Period Ending May 31, 1968

Contents

SUMMARY.....	vii
1. MOLTEN-SALT REACTOR PROCESSING.....	1
1.1 Molten-Salt Breeder Reactor Processing Flowsheet Analysis.....	1
1.2 Measurement of Distribution Coefficients in Molten-Salt–Metal Systems.....	15
1.3 Solubilities of Thorium and Protactinium in Bismuth.....	23
1.4 Metal-Transfer Process for Rare Earth–Thorium Separation.....	25
1.5 Development of a Molten Salt–Bismuth Electrolytic Cell.....	27
1.6 Reductive Extraction Engineering Studies.....	31
1.7 Simulated Molten-Salt–Liquid-Bismuth Contactor Studies.....	33
1.8 Corrosion Control by Use of a Frozen Layer of Salt.....	36
1.9 MSRE Fuel Salt Processing.....	39
1.10 Preparation of ^{233}U Fuel for the MSRE.....	42
1.11 Distillation of MSRE Fuel Carrier Salt.....	44
2. DEVELOPMENT OF AQUEOUS PROCESSES FOR FAST REACTOR FUELS.....	48
2.1 Shipping and Receiving.....	49
2.2 Head-End Processing.....	56
2.3 Removal of Volatile Fission Products.....	67
2.4 Dissolution and Feed Preparation.....	69
2.5 Solvent Extraction with TBP.....	74
2.6 Extraction of Plutonium with Amines.....	82
2.7 Removal of Iodine from Off-Gas.....	83
2.8 Radiation and Shielding Studies.....	88
2.9 Criticality Studies.....	100
3. DEVELOPMENT OF METHODS FOR PROCESSING HTGR FUELS.....	107
3.1 Head-End Burn-Leach Methods for Processing HTGR Fuel.....	107
3.2 Mechanical Head-End Methods for Processing HTGR Fuel.....	111
3.3 Application of the Burn-Grind-Leach Process to Irradiated Fuel.....	114
4. WASTE TREATMENT AND DISPOSAL.....	120
4.1 Engineering, Economic, and Safety Evaluations.....	121
4.2 High-Level Radioactive Waste.....	136

4.3	Intermediate-Level Radioactive Waste.....	144
4.4	Separation of Radioactive Xenon and Krypton from Other Gases by Using Permselective Membranes	150
5.	TRANSURANIUM-ELEMENT PROCESSING.....	154
5.1	TRU Operations.....	154
5.2	Isolation and Purification of TRU Products.....	164
5.3	Development of Chemical Processes.....	166
5.4	Special Projects	173
5.5	Transplutonium Element Research.....	175
6.	DEVELOPMENT OF THE THORIUM FUEL CYCLE	183
6.1	Preparation of ThO_2 - $^{233}\text{UO}_2$ Fuel for HTLTR.....	183
6.2	Demonstration of the Engineering-Scale Production of ThO_2 - UO_2 Microspheres	187
6.3	Microsphere Forming, Drying, and Firing Studies	190
6.4	^{233}U Storage and Distribution.....	199
7.	SOL-GEL PROCESSES FOR THE URANIUM FUEL CYCLE.....	203
7.1	Preparation of UO_2 Sols by Solvent Extraction	203
7.2	UO_2 - PuO_2 and PuO_2 Sol-Gel Process Development	211
7.3	Preparation of UO_2 - PuO_2 and PuO_2 Materials.....	214
7.4	Microsphere Forming, Drying, and Firing Studies	216
7.5	Development of High-Performance Fuel Materials.....	223
7.6	Plutonium Storage Facility	228
8.	SOL-GEL PROCESSES FOR ISOTOPIC HEAT SOURCES.....	230
8.1	Laboratory Studies of $^{238}\text{PuO}_2$ Sol-Gel Process.....	230
8.2	Developmental Studies in a Glove-Box System.....	234
8.3	Assistance to Mound Laboratory.....	235
8.4	Curium Sol-Gel Studies.....	237
9.	SPECIAL SOL-GEL PROCESSES.....	239
9.1	Sol Preparation	239
9.2	Scaleup of the Precipitation-Washing-Peptization Sol Process.....	241
9.3	Incorporation of Carbon into Metal Oxide Sols.....	244
9.4	Preparation of Porous Oxides	244
9.5	Microsphere Forming.....	247
10.	SEPARATIONS CHEMISTRY RESEARCH.....	252
10.1	Extraction of Metal Sulfates and Nitrates by Amines	252
10.2	New Separations Agents.....	252
10.3	Beryllium Purification by Solvent Extraction.....	255
10.4	Recovery of Uranium from Commercial Phosphoric Acid.....	256
10.5	Rapid High-Resolution Chromatography.....	259

10.6	Actinide and Lanthanide Intragroup Separations by Displacement Elution from Ion Exchange Resins	261
10.7	Separations by Precipitation	263
10.8	Equilibria and Mechanisms of Extraction	265
10.9	Relative Potentials of the Bk(IV)/Bk(III) and Ce(IV)/Ce(III) Couples.....	266
10.10	Kinetics of Metal Ion Extractions by Organophosphorus Acids.....	267
10.11	Aggregation and Activity Coefficients in Solvent Phases	268
11.	CHEMICAL APPLICATIONS OF NUCLEAR EXPLOSIONS.....	272
11.1	Copper Ores.....	272
11.2	Recovery of Oil from Shale	273
12.	BIOCHEMICAL SEPARATIONS	276
	MACROMOLECULAR SEPARATIONS.....	276
12.1	Development of Reversed-Phase Chromatography Systems for Separating Transfer Ribonucleic Acids.....	276
12.2	Engineering Scaleup of Biological Macromolecular Separations Techniques.....	276
12.3	Separation of Transfer Ribonucleic Acids from <i>B. subtilis</i> A-12.....	281
12.4	Separation of Aminoacyl-RNA Synthetases.....	281
12.5	Separation of Ribosomal Ribonucleic Acids.....	282
	BODY FLUIDS ANALYSIS.....	284
12.6	Prototype Analyzers.....	284
12.7	Separation Systems.....	287
12.8	System Components.....	290
12.9	Identification of Body Fluid Constituents.....	292
12.10	Analytical Results	293
12.11	Data Acquisition and Analysis.....	297
12.12	Literature Survey.....	299
13.	IRRADIATION EFFECTS ON HETEROGENEOUS SYSTEMS	300
13.1	Effects on Aqueous Sols	300
14.	SPECTROPHOTOMETRIC STUDIES OF SOLUTIONS OF LANTHANIDES AND ACTINIDES.....	304
14.1	Spectra of Aqueous $\text{Pr}(\text{NO}_3)_3$ and $\text{Nd}(\text{NO}_3)_3$ to 356°C	304
14.2	Temperature Effects on Aqueous Am^{3+} Complexes.....	304
14.3	Emission Spectra of the Transuranium Elements.....	305
14.4	Densities of Aqueous KCl and UO_2SO_4 to 374°C	305
15.	REACTOR EVALUATION STUDIES	306
15.1	Optimization Studies of the Reprocessing Industry in an Expanding Nuclear Economy.....	306
15.2	The Oak Ridge Systems Analysis Code.....	309

16. PREPARATION AND PROPERTIES OF ACTINIDE OXIDES.....	312
16.1 Electrophoretic Studies of Urania and Thoria-Urania Sols.....	312
16.2 Investigation of Lanthanide Sols	314
16.3 Mathematical Models of Colloidal Systems.....	315
17. CHEMISTRY OF CARBIDES, NITRIDES, AND CARBONITRIDES.....	316
18. SAFETY STUDIES OF FUEL TRANSPORT.....	322
18.1 Research.....	322
18.2 Contacts with Private Industry.....	324
18.3 CTD Cask Evaluation Program.....	324
19. NUCLEAR-POWERED AGRO-INDUSTRIAL COMPLEXES: SPECIAL STUDIES.....	325
20. SITING OF FUEL REPROCESSING PLANTS AND WASTE MANAGEMENT FACILITIES.....	326
21. CHEMICAL ENGINEERING RESEARCH.....	329
21.1 Development of the Stacked-Clone Contactor.....	329
22. ASSISTANCE PROGRAMS.....	333
22.1 Eurochemic Assistance Program.....	333
22.2 Evaluation of Radiation Resistance of Selected Protective Coatings (Paints).....	333
PUBLICATIONS, SPEECHES, AND SEMINARS.....	338

Summary

1. MOLTEN-SALT REACTOR PROCESSING

1.1 Molten-Salt Breeder Reactor Processing Flowsheet Analysis

The proposed flowsheet for processing a 1000-Mw (electrical) single-fluid MSBR is given. It is based on reductive extraction and processing of the reactor salt to isolate protactinium on a 3-day cycle and to remove rare earths on a 30-day cycle.

A rare earth removal system based on reductive extraction is described, and calculations for steady-state performance are given. Graphs that indicate the importance of the number of stages, the separation factors, the bismuth flow rate, and the fraction of ThF_4 that is reduced in the electrolytic cell are included.

A computer code has been developed to perform steady-state material balance calculations that describe the nuclear, chemical, and physical processes occurring in the fuel stream of an MSBR. The code allows investigation of the effects of chemical processing on the nuclear performance of an MSBR, as well as the determination of fission product inventories and heat generation rates. The buildup of transuranium isotopes, the production of activation products by neutron capture in the carrier salt, and chain-branching in the decay of fission products are considered.

1.2 Measurement of Distribution Coefficients in Molten-Salt-Metal Systems

The equilibrium distributions of uranium, zirconium, plutonium, protactinium, rare earths, thorium, and other elements between several $\text{LiF-BeF}_2\text{-ThF}_4$ salts and liquid bismuth solutions were determined at 525 to 700°C in support of the development of a reductive extraction process for single-fluid MSBR fuels. Uranium was found to be practically inseparable from zirconium; however, it should be possible to separate uranium from protactinium (U-Pa separation factor of at least 15) and from plutonium (U-Pu separation factor of about 10). Plutonium-protactinium separation factors of about 10

can be achieved when the reductant concentration in the bismuth phase is very low. Protactinium-thorium separation factors were greater than 2000 in the systems tested. However, rare-earth-thorium separation factors were only in the range of 1 to 3.5, indicating that this separation will be difficult. Californium and americium behaved much like plutonium, while curium was slightly more difficult to extract (Pu-Cm separation factor of about 10). Variation of the salt composition produced only slight changes in the respective separation factors. In general, the separation factors decreased with increasing temperature.

1.3 Solubilities of Thorium and Protactinium in Bismuth

The solubility of thorium in bismuth was measured over the temperature range of 450 to 817°C. The data can be expressed as: $\log S$ (wt ppm Th) = $7.717 - 3850/T$. By using the reductive extraction technique, the solubility of protactinium in bismuth was found to be about 1200 ppm at 500°C, and was estimated to be 4500 ppm at 600°C. Nickel was found to react with thorium in bismuth solution to produce an insoluble phase in which the Ni/Th atom ratio was about 1. The mutual solubilities of thorium and nickel in bismuth at 600°C can be expressed as a mole fraction solubility product: $K_{sp} = X_{\text{Ni}}X_{\text{Th}} = 6.2 \times 10^{-7}$.

1.4 Metal-Transfer Process for Rare Earth-Thorium Separation

The transfer of rare earths from an $\text{LiF-BeF}_2\text{-ThF}_4$ donor salt through a thorium-bismuth solution to an acceptor salt is being tested as an alternative to reductive extraction for effecting the rare earth-thorium separation. In our initial experiments, about 35% of the lanthanum present in $\text{LiF-BeF}_2\text{-ThF}_4$ (72-16-12 mole %) was transferred to an equimolar amount of LiCl-LiF (80-20 mole %) at 600°C; however, the thorium decontamination factor was only about 10. Other acceptor salts tested gave poorer results.

1.5 Development of a Molten Salt-Bismuth Electrolytic Cell

Electrolytic cells will be required for the operation of reductive extraction systems in an MSBR fuel processing plant. The cells will be used to oxidize materials in Bi stream effluents from extraction contactors, as well as to reduce Li and Th for introduction into Bi streams that are fed to the contactors.

Experiments have been carried out in quartz cells (4 in. OD) using Bi pools as the electrodes and 66-34 mole % LiF-BeF₂ as the electrolyte. Current densities up to 4.5 amp/cm² were observed. The current was linearly dependent on applied voltage, suggesting that there is essentially no limiting current in the range covered by the experiments.

Because corrosive conditions will exist in the vicinity of anodic surfaces, we plan to protect such surfaces with a layer of frozen salt. A small, all-metal, static cell has been installed for use in studying this method of operation.

A system is being built to allow the testing of a variety of electrolytic cell designs under steady-state conditions. Provisions have been made for circulating up to 0.5 gpm Bi and 0.25 gpm salt through the cell containment vessel, sampling the inlet and outlet streams from the cell, and visually observing operation of the cell.

Heat transfer and mass transfer are important considerations in the design and operation of electrolytic cells. Attempts are being made to predict values for heat and mass transfer in electrolytic cells in order to provide a basis for evaluating cell designs and for interpreting data from experiments with cells.

1.6 Reductive Extraction Engineering Studies

Equipment for semicontinuous engineering experiments on reductive extraction has been installed in Bldg. 3592. Mass transfer between molten salt (72-16-12 mole % LiF-BeF₂-ThF₄) and molten bismuth will be studied at 600°C under various countercurrent flow conditions in several packed or baffled columns. Attempts will be made to correlate mass transfer performance with hydrodynamic conditions (flooding, holdup, specific interfacial area, etc.) that may be inferred from measurements of pressure drop through the column by analogy with results from a mercury-water system.

1.7 Simulated Molten-Salt-Liquid Bismuth Contactor Studies

A mercury-water system is being used to allow the selection of the types of contactors to be tested with

actual process fluids. With this system, quantitative data are being obtained for flooding rates, pressure drop, dispersed-phase holdup, and backmixing in the continuous phase; in addition, qualitative information on flow patterns and drop size is being accumulated. Equations defining the relationships of the hydrodynamic conditions in a dispersed-flow column have been developed; the values of constants in these relationships are being evaluated for several packing materials.

1.8 Corrosion Control by Use of a Frozen Layer of Salt

Equipment is being developed for use in the continuous removal of UF₄ from a salt stream by countercurrent contact of the salt with F₂ in a salt-phase-continuous system. This equipment will be protected from corrosion by freezing a layer of salt on the vessel wall; the heat necessary for maintaining molten salt adjacent to frozen salt will be provided by the decay of fission products in the salt stream. A series of experiments was recently concluded in which salt and an inert gas were contacted countercurrently in a 5-in.-diam, 8-ft-high column having an internal heat source.

These experiments demonstrated that a frozen salt layer can be formed and maintained at fluid flow and heat-transfer conditions approximating those expected for processing fuel from a 1000-Mw (electrical) MSBR.

1.9 MSRE Fuel Salt Processing

After test runs with the KOH-KI scrubber for fluorine disposal had been completed, about 224 kg of uranium was recovered from the MSRE flush and fuel salt. Known uranium losses were less than 0.1%. Gross beta and gamma decontamination factors were 1.2×10^9 and 8.6×10^8 respectively. Corrosion of the vessel averaged about 0.1 mil/hr. After fluorination, the corrosion product fluorides were reduced and then filtered to provide a carrier salt having a lower concentration of metallic contaminants than the original carrier salt.

1.10 Preparation of ²³³U Fuel for the MSRE

A total of 63 kg of ⁷LiF-²³³UF₄ salt (73-27 mole %) containing 39 kg of uranium (91.4% ²³³U, 222 ppm of ²³²U) was prepared for refueling the Molten-Salt Reactor Experiment. The uranium oxide was converted to LiF-UF₄ in nickel-lined equipment located in cell G of the Thorium-Uranium Recycle Facility. The product salt was packaged in containers of various capacities and shipped in shielded casks to the MSRE site.

1.11 Distillation of MSRE Fuel Carrier Salt

The nonradioactive phase of the MSRE distillation experiment was completed, and equipment installation preparatory to distillation of a 48-liter batch of irradiated fuel carrier salt is now under way at the MSRE. The nonradioactive phase involved distillation of six 48-liter batches of MSRE fuel carrier salt (four of which contained 0.1 to 0.3 mole % NdF_3). Distillation rates were measured and condensate samples were taken in order to assess the importance of concentration polarization and entrainment. The temperature of the still pot was varied from 950 to 1025°C, and the condenser pressure was varied from 0.05 to 2 mm Hg.

The distillation rate was found to be limited by the frictional pressure loss through the passage between the vaporization and condensation surfaces, and a correlation relating distillation rate to still pot pressure and condenser outlet pressure was developed. Distillation rates up to 1.5 ft³ of salt per day per square foot of vaporization surface were observed; this rate is adequate to permit distillation to be used as a process step.

Only minor difficulties were encountered in the operation of the equipment. Neither concentration polarization or entrainment was evident. A postoperational inspection of the equipment showed that it was in satisfactory condition for radioactive operations.

2. DEVELOPMENT OF AQUEOUS PROCESSES FOR FAST REACTOR FUELS

2.1 Shipping and Receiving

Economic considerations will require the transport of spent nuclear fuel from individual reactor stations to a central reprocessing facility. Investigations and studies during this report period have indicated that relatively short-cooled LMFBR spent fuel can be safely and economically shipped, provided certain changes in cask construction and operation (from those currently employed for LWR fuel) are effected. The first of these changes is the use of a highly effective, low-vapor-pressure heat transfer medium (sodium in lieu of air or water) within the cask fuel cavity. The second is the use of a high-strength, tough, high-temperature-resistant material for the biological shield (steel in lieu of lead). The third is the use of sealing systems that will be less susceptible to mechanical and thermal damage, plus the use of highly effective energy-absorbing devices to limit impact loads to levels that are considerably below the point at which significant cask deformation would occur.

Preliminary tests have been made to support the contention that heat can be adequately transported within a sodium-filled shipping container. Other early tests with reduced-scale steel shipping casks and with energy absorbers have also been encouraging.

2.2 Head-End Processing

Material balance flowsheets were prepared for the reprocessing of Atomic International (AI) reference oxide fuel assemblies at the rate of 5 metric tons per day. The flowsheets relate the quantities of uranium, plutonium, fission products, and stainless steel which will be encountered at different stations in a reprocessing plant.

The steady-state temperatures of the centermost fuel rod contained in shrouded hexagonal assemblies of LMFBR fuel suspended in a quiescent inert gas atmosphere were determined for radioactive decay heat release rates from 0 to 25 w per foot of a single fuel rod and for rod surface emissivities of 0.3 to 1.0. Because these results showed the need for auxiliary cooling, calculations were also made to determine the requirements necessary to maintain a typical assembly at any preselected temperature.

A dismantling operation is being investigated and developed as the first head-end processing step in the preparation of spent LMFBR fuel for Purex processing. A study was made of the Fast Flux Test Facility, demonstration, and follow-on reactor assemblies. Several cropping and slitting methods, as well as a method for dissection or disassembly to single fuel rods, were included. An abrasive disk saw and a slitting saw were selected for the cropping of end hardware and for shroud removal respectively. The study showed that the head-end processing of fast breeder fuel could be simplified considerably if the fuel rods could be pushed or withdrawn from the sheath.

The shearing of an assembly, multirod arrays, and single rods was analyzed. Three methods were found to be attractive; the advantages and disadvantages of each are summarized.

Two methods, induction melting and compaction, were studied for reducing approximately 1.75 metric tons of stainless steel waste (~88% void fraction) per day. Induction melting was favorably recommended by the commercial industry.

2.3 Removal of Volatile Fission Products

Studies of a head-end treatment for removing iodine, krypton, xenon, and tritium from irradiated oxide fuels

were continued. Only about 10% of the ^{85}Kr was removed from low-burnup (1800 Mwd/ton) 20% PuO_2 -80% UO_2 by heating fuel rod segments in oxygen at 450 to 750°C. However, more than 95% of the tritium was removed. With high-burnup (100,000 Mwd/ton) 20% PuO_2 -80% UO_2 , about 98% of the ^{85}Kr was released by oxidizing for 3 hr at 450°C and then 7.5 hr at 750°C. Increasing the oxidation temperature to 850°C decreased the amount of ^{85}Kr released to about 80%. At this temperature, about 32% of the gamma-emitting radionuclides in the fuel sample also volatilized, and the stainless steel cladding disintegrated. In tests with short-cooled UO_2 , more than 90% of the ^{131}I and more than 69% of the ^{133}Xe and ^{85}Kr were volatilized during an oxidation treatment at 750°C.

A rotary kiln has been selected as possibly the most promising type of equipment for performing the heating-oxidation treatment. A small (5 kg/hr) rotary unit has been purchased for engineering experiments.

2.4 Dissolution and Feed Preparation

In dissolution tests with a variety of stainless-steel-clad, irradiated PuO_2 - UO_2 fuel specimens, recoveries of at least 99.8% of the plutonium from most specimens were obtained by leaching with boiling 8 *M* HNO_3 . The relatively high plutonium losses obtained for several specimens are attributed to apparent nonhomogeneity of a small fraction of the fuel. This refractory fraction can be dissolved by adding HF to the dissolver solution. In one experiment, decreasing the length of the sheared fuel sections from 1.75 in. to 0.75 in. increased the amount of plutonium dissolved in boiling 4 *M* HNO_3 in 6 hr from about 85% to 99.7%. The amount of stainless steel cladding dissolved in boiling 4 to 8 *M* HNO_3 was usually less than 5%; addition of HF to the leach solution greatly increased the attack on the cladding.

2.5 Solvent Extraction with TBP

In a tracer-level batch countercurrent demonstration of the first-cycle Purex flowsheet using 15% TBP-*n*-dodecane (NDD), recoveries of plutonium and uranium were higher than 99.9%, and decontamination factors from fission products across the extraction-scrub system were as follows: 700 from ^{95}Zr , 260 from ^{95}Nb , >180 from ^{103}Ru , >400 from ^{144}Ce , >2800 from ^{137}Cs , >3000 from $^{140}\text{Ba-La}$, and 1.2 from ^{131}I . Essentially complete recovery of plutonium from the solvent and reasonably efficient separations from uranium were obtained by partitioning with dilute nitric

acid while reducing only part of the plutonium with Fe(II) or U(IV).

Iodine, in the form of a mercury-iodine complex, was extracted efficiently ($D_a^0 = 20$ -50) from 0.02 to 2 *M* HNO_3 with TBP-NDD. The complex contains about one mole of Hg^{2+} per mole of iodine. The extraction coefficient decreased to low values (<1) at high acid concentrations and at high mercury/iodine mole ratios.

Batch cyclic tests using actual fuel solutions and a ^{60}Co radiation source continued to indicate that problems arising from solvent radiation damage will not seriously affect the Purex process efficiency when short-cooled LMFBR fuels are processed in pulsed columns.

In laboratory studies, rate constants were determined for the decomposition of TBP in nitric acid solutions at 50 and 75°C. The presence of zirconium apparently greatly increased the decomposition rate. The distribution of dibutylphosphoric acid (the principal TBP decomposition product) between TBP-NDD and solutions of sodium carbonate or nitric acid was determined.

2.6 Extraction of Plutonium with Amines

The use of secondary amine extraction as an alternative to ion exchange for the final purification of plutonium continued to show promise. In a batch countercurrent test demonstrating the recovery of plutonium from a simulated second-TBP-cycle product solution with 0.3 *M* di(tridecyl)amine in diethylbenzene, more than 99.9% of the plutonium was recovered in four extraction and four scrub stages. Stripping the extract with 0.15 *M* HNO_3 yielded a product solution containing 50 g of plutonium per liter.

2.7 Removal of Iodine from Off-Gas

Iodine decontamination factors of 10^3 or higher were obtained in scrubbing air streams containing iodine in the forms of elemental iodine, methyl iodide, or higher alkyl iodides with mercuric nitrate-nitric acid solutions. The rate of reaction of methyl iodide with the mercury scrub solution increased as the temperature and the mercuric ion and nitric acid concentrations were increased. The mercury-iodine complex was extracted from the scrub solution with several organic extractants, but stripping of the iodine (and mercury) from the solvents was difficult.

The combination of a catalytic oxidation treatment to destroy organic solvent contaminants, followed by sorption of iodine on iodized charcoal, appears to be a

promising method for removing iodine from process off-gases. A number of different organic compounds including methyl iodide, alcohols, and solvent extraction diluents were completely decomposed by passing air streams containing the organic material through a 2-in. bed of Hopcalite ($\text{MnO}_2\text{-CuO}$) catalyst at 350 to 500°C.

2.8 Radiation and Shielding Studies

Analytical studies were made as part of a continuing program to develop information on the radiation properties and shielding requirements of spent LMFBR fuels. The most significant accomplishments during the year involved the compilation of basic nuclear data for approximately 700 nuclides of importance, the development of a computer code (ORIGEN) for calculation of the transient concentrations of nuclides, and the analysis of radiation control and shielding requirements of certain operations in the recycle of LMFBR fuels.

2.9 Criticality Studies

A series of survey criticality calculations were made to aid in the conceptual design of LMFBR fuel reprocessing equipment. The results indicate that there is considerable incentive to develop fixed and soluble neutron absorbers for use in such equipment.

3. DEVELOPMENT OF METHODS FOR PROCESSING HTGR FUELS

3.1 Head-End Burn-Leach Methods for Processing HTGR Fuel

Several small-scale engineering studies of fluidized-bed burning were made in a 2-in.-diam fluidized-bed burner, using both simulated (graphite plus SiC-coated microspheres) and crushed prototype Ft. St. Vrain fuel. No operating problems were encountered, and the burner ash was free flowing. Breakage of particle coatings of the simulated fuel ranged from 1 to 10%. A leaching test of the ash from burned, crushed prototype fuel indicated that the coatings on 0.5% of the UO_2 and 5.5% of the ThO_2 particles were broken during the burning step.

An initial fixed-bed burning test was made to determine if dilution of the reagent gas with CO_2 could be used to help control the high burning temperatures (>1000°C) expected. It was found that the temperatures of the graphite blocks could easily be controlled

by adjusting the CO_2 flow. Approximately 60 to 80% of the admitted CO_2 was converted to CO.

Preliminary tests were carried out to determine if the alumina heat-transfer media present in the fluidized-bed burner ash could be separated from the fertile and fissile particles in a gas particle classifier, using a geometry similar to a fluidized-bed burner. By using a programmed gas flow rate, about 99.5% of the alumina could be separated from the heavy fertile-fissile particles. However, separation of fertile from fissile particles in the equipment sized for alumina separation does not appear to be feasible.

3.2 Mechanical Head-End Methods for Processing HTGR Fuel

Several graphite fuel sections, similar to Ft. St. Vrain HTGR fuel, were fabricated for use in small-scale engineering tests of proposed comminution and particle separation steps. These fuel sections contained fertile particles (ThO_2 kernels) with either two layers of isotropic carbon (i.e., BISO coating) or two layers of isotropic carbon plus a SiC layer placed in the middle of the outer carbon layer (i.e., TRISO coating), and fissile particles (UO_2 kernels) with TRISO coatings. Suitably sized feed for the fluidized-bed burner was produced using either a jaw crusher with a $\frac{5}{8}$ -in. setting between the jaws or a hammer mill set to produce $\frac{3}{4}$ -in. product. The size range of the product obtained from either a roll crusher with the rolls set $\frac{5}{8}$ in. apart or a hammer mill set to produce $\frac{3}{4}$ -in. product was unsatisfactory. Leaching tests of material that had been crushed in the hammer mill set to produce a $\frac{3}{4}$ -in. product indicate that the coatings on 2.2% of the UO_2 particles and 1.1% of the ThO_2 particles did not survive the crushing step.

3.3 Application of the Burn-Grind-Leach Process to Irradiated Fuel

Reprocessing studies of HTGR-type fuels were initiated using irradiated Dragon fuel compacts provided by the British O.E.C.D. Dragon project. Dragon fuel contains only a single size of fuel particles but otherwise is similar in many respects to the Ft. St. Vrain fuel. The major head-end steps (crushing, sawing, burning, sieving, grinding, and leaching) have been scouted. Standardized experimental procedures and techniques have been developed. Experiments were designed to test the feasibility of present concepts for recycling HTGR fuels. In the Ft. St. Vrain fuel, the fissile ($\sim 200\text{-}\mu\text{-diam}$) and fertile ($\sim 400\text{-}\mu\text{-diam}$) particles

are coated with a silicon carbide barrier layer to prevent the migration of fission products. For the planned fuel cycle, this barrier layer must be capable of surviving irradiation and head-end reprocessing steps through burning so that the fertile and fissile particles can be separated by a sizing technique to minimize recycle of ^{237}U .

In hot-cell tests with irradiated and unirradiated compacts, particle breakage has been shown to be strongly dependent on irradiation and the primary fuel crushing parameters. Breakages of about 7.6 and 3% were experienced for irradiated and unirradiated fuel, respectively, when crushers with a final jaw opening of $\frac{1}{8}$ in. were used. A breakage of 0.35% was obtained for an unirradiated compact when a jaw opening of $\frac{5}{8}$ in. was used. Hacksawing through the compact resulted in the breakage of essentially all the particles that were touched by the blade. These studies will be extended to two-particle Ft. St. Vrain type fuels as they become available.

Gas release studies have shown that ^{85}Kr is released after the silicon carbide coatings are ruptured. Heating in an inert gas stream greatly accelerates the release rate. About 40% of the tritium found in these experiments was outside the fuel particle and was released in the fluidized-bed burning step. About 58% of the tritium was released in the second burning step, after the fuel particles had been ruptured.

Processing Dragon fuel using the crush-burn-grind-leach flowsheet gave process losses to the solid residues (shards and alumina) of as much as 0.2% uranium, 0.6% thorium, and about 10% of the gamma-emitting fission products.

The crush-burn-grind-leach flowsheet appears to be promising as indicated by these tests with hot pressed compacts of the Dragon fuel. Similar tests must be performed on the prismatic fuel of the Ft. St. Vrain type.

4. WASTE TREATMENT AND DISPOSAL

4.1 Engineering, Economic, and Safety Evaluations

We have begun a systematic review of the wastes that are expected to accumulate from the aqueous reprocessing of fuels from light-water, fast breeder, and gas-cooled reactors, to determine the most economical approaches to their management within the technology that is being developed. The initial part of this survey is devoted to the preparation of fuel reprocessing flowsheets and characterization of the principal liquid and solid wastes. Also, we have estimated the characteristics

of various combinations, or blends, of the individual waste streams that represent alternative methods of waste management. Based on the estimated physical properties of the solidified wastes and considerations of heat dissipation, all wastes considered to date could be solidified and encapsulated in 6-in.-diam containers after interim liquid storage times ranging from 30 days to about two years. This is believed to be an acceptable interval from the standpoints of safety and economics. Subsequent analyses will estimate the economic incentives or penalties for management of the wastes as (1) separate streams, (2) in the various combinations indicated, and (3) as a function of liquid storage time.

4.2 High-Level Radioactive Waste

The major objectives of the chemical development work are to characterize the principal wastes that are expected from the reprocessing of power-reactor fuels and to produce and characterize solids that could be formed from these wastes for permanent storage. High-level wastes from a representative type of fast breeder reactor (LMFBR), high-temperature gas-cooled reactor (HTGR), light-water-cooled reactor (LWR), and molten-salt breeder reactor (MSBR) are being studied. These data are needed to evaluate the feasibility, economics, and safety of various waste management programs.

The physical and chemical properties of solutions and solidified wastes from the aqueous reprocessing of fuels from LMFBR's, HTGR's, and LWR's were characterized. In addition, a method was developed for preparing dispersions, rather than solutions, of the solidified wastes in a glassy matrix by using the pot calcination process. The latter has been successfully demonstrated previously. A dispersion should have a good balance of properties, such as low leach rates (because of the glassy continuous phase), and high thermal conductivities (because of the crystalline dispersed phase). Simulated aqueous high-level wastes from reprocessing LMFBR and LWR fuels were dispersed in borosilicate glass and lead silicate glass, respectively, at 900°C in a semicontinuous manner using a 2-in.-diam, 12-in.-high type 304 stainless steel pot in a 5-kw furnace. Simulated solid waste powder from processing HTGR fuel was dispersed in a lead silicate glass at 800°C using the same equipment; the measured thermal conductivity of this dispersion was $1.73 \text{ Btu hr}^{-1} \text{ ft}^{-1} \text{ }^\circ\text{F}^{-1}$ at 600°C, a fourfold increase over that of the waste powder.

An initial study of the radiolysis of 67-33 mole % $\text{LiF}\text{-BeF}_2$ in a ^{60}Co source at 50°C indicated a possible

fluorine production rate corresponding to a $G(F_2)$ value of 0.005 or an equivalent production of HF by hydrolysis of the salt with traces of moisture.

Detailed calculations were made of the maximum temperature rise in cylinders containing solidified high-level wastes. These calculations show that, if future high-level wastes from processing fuels from advanced reactors are to be solidified after out-of-reactor times as short as one year or less with a requirement that the centerpoint temperature not exceed 900°C , they must be either diluted with inert solids or stored as materials having significantly higher thermal conductivities than those of calcines.

Methods proposed for the disposal of gaseous wastes include the conversion of ^{131}I and ^{129}I (half-lives, 8.05 days and 1.6×10^7 years) to stable solid compounds for storage, and storage of krypton as a gas after it has been separated from the inert xenon. ^{133}Xe and ^{131}Xe (half-lives, 5.27 and 12 days) can be released to the atmosphere after a few months, whereas ^{85}Kr (half-life, 10.76 years) must be retained for the long term. The solid waste products would be sealed in a stainless steel primary containment vessel (pot) for additional safety during temporary storage and shipment to a government disposal area. Both primary and secondary containment, as opposed to simple pressurized tank storage, seem desirable for the more mobile gases. Several alternative primary containment methods, in which stainless steel pots serve as secondary containment vessels, were considered. These methods include entrapment in molecular sieves or clathrates and dispersion as a foam or as microampules in glass, plastic, or metal media. The advantages and disadvantages of these methods are presented, but the lack of definitive experimental, engineering, and economic information precludes precise comparisons.

4.3 Intermediate-Level Radioactive Waste

New waste management concepts indicate that only wastes containing a negligible amount of long-lived alpha-emitting nuclides will be considered as intermediate- or low-level wastes and processed for burial above the water table. A process has been developed for the incorporation of such wastes in asphalt or polyethylene prior to burial. Inorganic or organic solutions or slurries are mixed with emulsified road asphalt, molten asphalt, or molten polyethylene, and the water or volatile organic material is evaporated and the temperature of the product is raised to about 160°C . The product, containing salts or organic residue, flows into a disposable drum. Incorporation in asphalt re-

quires that the materials be neutral or alkaline, while incorporation in polyethylene is possible with all classes of materials except oxidizing acids. Polyethylene is equal to, or better than, asphalt on most bases.

An assessment was made of the safety aspects of producing and storing asphalt or polyethylene products containing oxidizing salts. The burning characteristics of asphalt or polyethylene containing 40 to 75 wt % sodium nitrate or sodium nitrite were determined with small samples in air. The nitrate-asphalt, nitrite-asphalt, and nitrate-polyethylene samples ignited at 330, 275, and 440°C respectively. The asphalt samples burned vigorously, while the polyethylene samples burned slowly. Studies of phase separation as a function of time and temperature showed that the salts begin to separate from the asphalt at temperatures above 60°C . Therefore, products with power densities as high as $40 \text{ Btu hr}^{-1} \text{ ft}^{-3}$, which is about eight times the power density of a typical intermediate-level waste concentrate, could be stored in 55-gal drums before phase separation would become a problem. The explosive hazards of the nitrate-asphalt system were studied by detonating blasting jelly in 1- to 2-kg samples of the mixture confined in 4-in. sched 80 steel pipes. Only a sample containing 10 wt % asphalt and 90 wt % NaNO_3 , with about 50% voids, could be detonated. Irradiation of samples in a ^{60}Co source showed that asphalt-nitrate products could reach 50% void volumes at an absorbed dose of about 10^9 rads; however, polyethylene-nitrate samples showed no signs of voids at this dose. It was concluded that asphalt and polyethylene are good media for incorporating intermediate-level radioactive wastes that do not contain oxidizing materials. Incorporation in asphalt is not recommended for wastes containing oxidants. Polyethylene may be acceptable for this purpose; however, further studies would be required to fully assess the safety of the system.

The engineering development of the asphalt process was concluded with the successful demonstration of the incorporation of a 20 wt % sodium metaborate solution containing 10% excess caustic in asphalt. This solution was used to simulate the waste that is formed during discharge of the primary loop of power reactors. Thus, to date, the wiped-film evaporator has been used to incorporate simulated neutralized second-cycle Purex waste, sodium aluminate decladding waste, ORNL evaporation bottoms, and the sodium metaborate waste without difficulty. Waste-to-emulsified asphalt feed ratios of 2.0 to 3.3 were investigated for waste feed rates of 6.5 to 10.8 gph; products containing 39 to 58 wt % solids were obtained. The evaporator was operated

at a temperature of 200°C with a rotor speed of 295 rpm. Product temperatures in excess of 130°C were required in order to achieve smooth operation and to obtain products characterized by low residual water contents and satisfactory leach rates. The decontamination factor for sodium between feed and condensate was about 2000 under optimum operating conditions. Salt accumulation, in two runs with low throughput, increased wiper blade wear from less than 0.1 to 2–3 mils/hr. Generally, solids buildup can be controlled by increasing the throughput or by decreasing the evaporator wall operating temperature. The equipment is being modified in preparation for the demonstration of incorporation of wastes in polyethylene.

4.4 Separation of Radioactive Xenon and Krypton from Other Gases by Using Permselective Membranes

A new technique for supporting silicone rubber membrane resulted in increased permeability without decreasing the separation factor for the gases. This development decreases the estimated cost of a membrane cascade by about 37%. Irradiation studies indicated that the membrane has satisfactory resistance (i.e., not more than a 10% change in permeability) to radiation damage at levels up to 1×10^8 rads. A radiation dose of 1.22×10^7 rads is predicted for removing the noble gases from a reactor containment vessel 30 days after a nuclear incident. Replacement of membranes after irradiation to 10^8 rads would increase the operating costs of a membrane cascade for removing the noble gases from the off-gas of a reactor fuel processing plant by a maximum of \$4000 per year.

5. TRANSURANIUM-ELEMENT PROCESSING

The USAEC Heavy Element Production Program is centered in two main facilities at ORNL – the High Flux Isotope Reactor (HFIR) and the Transuranium Processing Plant (TRU). During this report period, which corresponds to the third year of operation of these facilities, 16 mg of californium was recovered. This quantity is more than twice that recovered in the previous two years combined. A milestone of this year's production was the recovery, in two campaigns, of fermium fractions that contained a total of about 2×10^8 atoms. Eighty-two shipments were made to customers throughout the country. A major achievement of the year, following an intensive study of the problem, was the demonstration of a system for the removal of iodine from the plant ventilation streams. This system will permit the processing of targets after only one week of cooling.

The phases of the program that are under the direction of the Chemical Technology Division, including the operation of TRU, isolation and purification of products, development of chemical processes, and some chemical studies of the actinide elements, are reported here. Target fabrication work, which is directed by the Metals and Ceramics Division, is described in detail in reports issued by that Division.

5.1 TRU Operations

The Transuranium Processing Plant (TRU) is primarily a production facility in which: (1) targets that have been irradiated in the HFIR are processed to isolate and purify the transuranium elements, and (2) americium and curium are fabricated into recycle targets for additional irradiation in the HFIR.

This was the third year of operation for TRU. During the first two years, processing and recovery steps, through the partitioning of the transplutonium elements, and target fabrication were demonstrated in several major campaigns.

This year, two major target campaigns were carried out, and another campaign completed the processing of the raffinate solution that resulted from earlier SRP plutonium recovery processing. In the first target campaign, 14 plutonium-bearing targets, which comprised the first group of targets that had been irradiated entirely in the HFIR, were processed. In the second target campaign, six curium recycle targets that were fabricated in TRU last year were processed. A total of approximately 16 mg of ^{252}Cf was processed in these two campaigns; this is more than twice the total amount processed during the first two years. Einsteinium products (including einsteinium produced by reirradiation of some of the californium) totaled 97 μg this year; only 16 μg was produced last year. Each of the target-processing campaigns produced about 10^8 atoms of ^{257}Fm , the first usable amounts of fermium that have been recovered at TRU. Eighty-two shipments of transuranium elements were made to experimenters at ten laboratories throughout the country.

Minor improvements were made in some of the processing steps this year, but the overall processing sequence remained unchanged. On the other hand, several important improvements and additions to the equipment were made. For example, tantalum equipment was installed for the LiCl-based anion exchange process. In addition, the equipment used for Tramex solvent extraction was replaced; it was becoming difficult to operate because of wear, corrosion, and damage. The new equipment is operated with the

organic phase continuous instead of the aqueous phase continuous.

We had no difficulty in partitioning actinides, using the new tantalum equipment for the LiCl-based anion exchange process. All product fractions were taken based on continuous in-line alpha monitoring of the column effluent line and on neutron and gamma scans of the tantalum column. Such indications as the green color from nickel during its elution and the red glow from the curium band on the column were clearly not needed.

The Hepex solvent extraction process for partitioning actinides was tested in-cell, using the new Tramex equipment, and was found to be satisfactory for use in TRU. During this testing, 275 μg of californium was separated from 100 g of curium and 90 g of americium.

The Hepex process performs basically the same function as the LiCl-based anion exchange process. It is well suited to large batches, whereas ion exchange is better for handling our usual 10- to 30-g batches. In the Hepex process, the transcurium actinides are extracted into di(2-ethylhexyl)phosphoric acid, and the americium-curium-bearing aqueous raffinate is collected as one product. The transcurium elements, which constitute the second product, are stripped from the solvent, using 5 M HCl.

Equipment was installed in-cell and is being placed in operation for making americium-curium oxide microspheres, by the sol-gel method, for use in fabricating recycle targets for the HFIR. The major remaining difficulties are: (1) high losses during the washing of americium-curium hydroxide during sol formation, and (2) clustering in the sphere-forming column. We routinely produce sols that are stable for as long as 24 hr and are now searching for run conditions, and combinations of drying solvent and additives, that will result in the formation of gel microspheres that are satisfactory for fabrication of recycle targets.

The target fabrication equipment has continued to operate satisfactorily. Three second-cycle curium targets, 9 plutonium targets, and 14 rabbits, which contained ^{249}Bk , ^{252}Cf , or ^{253}Es , were fabricated.

The optimum irradiation period for producing ^{253}Es from ^{252}Cf was found to be less than one reactor cycle. Therefore, we have started to irradiate californium in the HFIR hydraulic rabbit facility. Two HFIR rabbits, containing a total of 2.3 mg of ^{252}Cf , were irradiated intermittently in the hydraulic tube for a total of 10 days each (four irradiation periods separated by 10- to 18-day intervals for decay). Initially, we recovered 12 μg of einsteinium that was rich in the heavier isotopes, ^{254}Es and ^{255}Es , from the irradiated ^{252}Cf ; then,

after a suitable period to allow the ^{253}Cf to decay, we recovered 6 μg of ^{253}Es in a second cycle of processing.

A major accomplishment during this report period was the development of an off-gas treatment system for limiting the release of radioiodine from TRU during the processing of short-cooled targets. The processing of short-cooled targets is necessary in some instances, for example, to recover the maximum possible amount of ^{253}Es , which has a half-life of 20 days. The main feature of the treatment system is a bed of oxidation catalyst that converts organic vapors to CO_2 and H_2O and thereby protects a bed of KI-impregnated charcoal from being poisoned against iodine retention. Earlier attempts to trap radioiodine, using charcoal beds, were unsuccessful because organic vapors quickly poisoned the charcoal. We confined most of the iodine-bearing off-gas to a 3-cfm stream, and installed the iodine removal system in this small stream. The treatment system was composed of a caustic scrubber to remove acid vapors, a heater, a bed of oxidation catalyst (operated at 350°C), a cooler, and the charcoal bed. The 3-cfm off-gas stream was decontaminated from ^{131}I by a factor (DF) as high as 10^4 .

No target failures have occurred this year, although a number of targets have been irradiated for longer periods of time, and to higher burnups, than the ones that failed two years ago.

We are developing a nondestructive method for assaying the ^{252}Cf content of neutron sources and shipping containers. Weighed discs of aluminum are activated by fast-neutron emissions from ^{252}Cf and then assayed by gamma-ray spectrometry for the activation product ^{24}Na . The precision of the method is excellent for sources containing a few hundred micrograms of ^{252}Cf .

5.2 Isolation and Purification of TRU Products

Product finishing operations and the final purification and isolation of transplutonium elements are accomplished in equipment that is installed in cell 5 in TRU and in supporting shielded-cave facilities. Special separations and the final processing of main-line products will continue to be performed in the cell 5-shielded-cave complex because the equipment and handling procedures available there are optimum for present program needs.

Plant processing provides two product fractions by LiCl-based anion exchange: an americium-curium fraction and a transcurium fraction. We have continued to process these fractions in cell 5 by procedures that have been described in previous progress reports. Portions of the americium-curium product were processed to sepa-

rate the contained elements by selectively precipitating americium as an Am(V)-potassium double carbonate. Berkelium was separated from residual actinides by oxidation to Bk^{4+} with $NaBrO_3$ and subsequent extraction from 8 M HNO_3 into di(2-ethylhexyl)phosphoric acid. Fermium, einsteinium, and californium were isolated from each other and from other residual actinides by selective elution from cation exchange resin with ammonium α -hydroxyisobutyrate. Purified products from these separations included 40 g of ^{244}Cm , 10 g of ^{243}Am , 1.6 mg of ^{249}Bk , 17 mg of ^{252}Cf , 88 μg of ^{253}Es , and approximately 3×10^8 atoms of ^{257}Fm .

Various special separations were also made; these include: isolation of 24 μg of second-growth ^{253}Es (daughter of ^{253}Cf) and 260 μg of ^{248}Cm , both of which had grown into the purified californium products during storage, and separation of 50 μg of ^{249}Cf that had grown into ^{249}Bk . In other processing, approximately 3 g of curium containing 9% ^{246}Cm was purified from residual americium and converted to the oxide for calutron separation of ^{246}Cm ; approximately 4 g of curium with a high concentration of ^{245}Cm was similarly processed for calutron separation of ^{245}Cm ; and 275 μg of californium rich in the 249, 250, and 251 isotopes was isolated and purified from the plant Hepex test.

5.3 Development of Chemical Processes

Laboratory support was provided to investigate chemical problems that arose during high-activity-level processing in TRU. We continued the development of processes to prepare oxides for HFIR targets and special irradiations, and ^{252}Cf source fabrication methods were developed. Also, we continued to investigate methods for separating californium, einsteinium, and fermium, recovering plutonium, partitioning actinides, and isolating berkelium.

Development of the sol-gel method for preparing americium-curium oxide microspheres was continued. Simplified equipment concepts for sol preparation were demonstrated. The precipitated metal hydroxide was washed in an inverted-cone fluidized-bed washer and produced 31 g of mixed oxides.

A technique for incorporating milligram quantities of ^{252}Cf into HFIR target pellets was also developed and demonstrated. This process consists in adding californium nitrate solution to a rare earth sol, which can then be formed into microspheres and incorporated into pellets. Additional techniques were developed for preparing alpha-contained sources of ^{252}Cf . These

entail: (1) encapsulation of the ^{252}Cf in a small quartz sphere (approximately 3 mm), which can then be welded into a small metal container, (2) adsorption on a small metal ion exchange column, followed by pyrolysis of the resin and processing of the column into a standard pellet configuration, and (3) electrodeposition of transplutonium elements on platinum or stainless steel plates. Deposition of 400 μg of metal per square centimeter of plate area has been demonstrated.

The laboratory development of high-pressure ion exchange technology was continued. Studies of the LiCl-based anion exchange system were directed toward (1) a single one-step process for small quantities of irradiated curium, and (2) a cation exchange system that utilizes the complexing behavior of various aminopolyacetic acids and actinides. The use of the latter system for separating actinides and lanthanides and for partitioning actinides reduces corrosion problems, but is chemically complex. However, the variety of ligands available for study makes accomplishment of the desired separations promising.

Laboratory development of the Pubex, Hepex, and modified Berkex processes was continued. These processes are now sufficiently established and reliable to meet present program needs.

Continued laboratory development of an extraction process for actinide partitioning (Hepex) led to its successful demonstration on a plant scale. It was found that single-stage separation factors between californium and curium could be increased from approximately 15 to greater than 30 by appropriate pretreatment of the organic extractant.

Laboratory studies of the Berkex process, in which berkelium is oxidized to Bk^{4+} with $NaBrO_3$ and extracted from 8 M HNO_3 into HDEHP, indicate that the unstable bromate compound can be replaced by a chromate compound, and that satisfactory berkelium isolation can be accomplished with much lower concentrations of HNO_3 and bromate than previously considered necessary.

5.4 Special Projects

A number of special projects were undertaken in cooperation with other groups, both at ORNL and elsewhere. These cooperative efforts included the fabrication of irradiation capsules containing ^{253}Es for the production of short-lived ^{254m}Es , and the encapsulation of several ^{252}Cf neutron sources. We also prepared several lots of curium for calutron separation and assisted with an experiment designed to produce and identify ^{258}Fm .

5.5 Transplutonium Element Research

A systematic study of actinide element chemistry and of comparative lanthanide element chemistry is being made to increase our basic understanding of actinide systems. This program includes the investigation of problems involving solution chemistry, with particular emphasis on the formation of complexes and on the preparation of solid actinide compounds that will be characterized by x-ray diffraction, electron microscopy, thermogravimetry, and differential thermal analysis.

The investigation of lanthanide sulfate complexes by amine extraction was extended to americium. As expected, the americium complexes and their formation constants proved to be very similar to those found for europium. The species and their thermodynamic (zero ionic strength) constants for formation from the uncomplexed species Am^{3+} were: AmSO_4^+ , $K_{01} = 6.24 \times 10^3$; $\text{Am}(\text{SO}_4)_2^-$, $K_{02} = 4.43 \times 10^5$; and $\text{Am}(\text{SO}_4)_3^{3-}$, $K_{03} = 2.27 \times 10^5$. The existence of a dinuclear complex $\text{Am}_2(\text{SO}_4)_3$ was suggested, as was $\text{EuAm}(\text{SO}_4)_3$ when both europium and americium were present. No evidence for a higher sulfate complex, $\text{Am}(\text{SO}_4)_4^{5-}$, was found. Ancillary computer programs were improved, particularly to allow calculation of the fractional distribution of all species at each sulfate ion concentration. Experimental difficulties that caused scatter of data were largely resolved, and improved methods of sampling and of counting, using an extractive liquid scintillator, were developed.

Laboratory studies were made to improve and simplify methods for preparing anhydrous chlorides of the lanthanides as stand-ins for trivalent actinides. The best results have been obtained with $\text{NH}_4\text{Cl} + \text{HCl}$ in conjunction with a programmed temperature rise from 200 to 500°C. However, phosgene gas in a fluidized bed at 500°C offers some operational advantages and shows enough promise to warrant further study. Thus far, no method that has been tested has provided effective chlorination of Yb_2O_3 , which represents the heaviest lanthanides.

Based on electron microscopic, x-ray diffraction, and thermogravimetric measurements, the study of trends and differences in the crystallization behavior of lanthanide hydroxide preparations was extended to the entire series. This study showed that the lanthanides can be divided into two groups, based on crystallizing times and the microstructures obtained for the hydroxides. The diffraction patterns obtained for the first group indicate that the structures are hexagonal; however, the second group gave diffraction patterns which are much more complex. In parallel studies of

the actinide elements, hydroxide preparations of curium, berkelium, and californium were examined. Crystalline forms of these materials were observed; however, it has not been possible, as yet, to unambiguously characterize the crystal structure from the diffraction patterns obtained.

Thermal analysis, in conjunction with x-ray analysis, was used in the study of plutonium carbide systems; emphasis was centered on carbides that had been prepared by dispersing carbon in plutonia sol (see Sect. 7.5). Construction of a microthermogravimetric balance was completed and checked out with lanthanide compounds.

Several research projects were conducted in collaboration with the Transuranium Research Laboratory (TRL). The berkelium fluoride and metal systems were characterized by x-ray diffraction. Low- and high-temperature forms of BkF_3 were found to be orthorhombic and trigonal respectively. Berkelium metal was characterized as a double hexagonal close-packed structure. The formal potential for Bk(III)-Bk(IV) oxidation in 1.1 *N* H_2SO_4 was determined to be 1.37 v, and a method of determining the II-III oxidation potentials of the transplutonium elements was developed by determining the electron transfer spectra of reducible lanthanides and then using this calibration curve to estimate the potentials for actinides.

6. DEVELOPMENT OF THE THORIUM FUEL CYCLE

6.1 Preparation of ThO_2 - $^{233}\text{UO}_2$ Fuel for HTLTR

Thirty-two kilograms of ThO_2 - $^{233}\text{UO}_2$ microspheres containing thorium and uranium in a 3:1 mole ratio were prepared for use in the High Temperature Lattice Test Reactor at the Pacific Northwest Laboratory; the ^{233}U contained 6 ppm of ^{232}U . Microspheres were formed from sols that had been prepared by employing solvent extraction of nitrate ion from a mixed thorium nitrate-uranium nitrate solution. Both the sol preparation and the microsphere forming operation were carried out in equipment designed for alpha containment. Operation of the equipment involved in the sol preparation was trouble free. Initially, problems encountered in the semiremote operation of sphere forming equipment resulted in low yields of product. However, as operating experience was gained, these problems were circumvented; in the final runs, 95% yields were obtained. Microspheres were coated with pyrolytically deposited carbon by the ORNL Metals and Ceramics Division prior to shipment.

6.2 Demonstration of the Engineering-Scale Production of $\text{ThO}_2\text{-UO}_2$ Microspheres

The procedures and equipment proposed for preparing $\text{ThO}_2\text{-UO}_2$ microspheres in TURF were demonstrated for a reference HTGR recycle fuel composition. Both process and equipment operation were satisfactory throughout ten days of continuous operation of the amine solvent extraction system to prepare sol containing 120 kg of $\text{ThO}_2\text{-UO}_3$. The overall material balances were 100.2 and 100.4% of the (Th + U) for the sol preparation and concentration steps respectively. In general, operation of the sphere-forming column was satisfactory; however, the gel dryers required modifications to prevent temperature excursions and cracking of the microspheres.

6.3 Microsphere Forming, Drying, and Firing Studies

Experience gained in operating microsphere forming columns to prepare kilogram quantities of oxide microspheres from hydrosols has permitted us to make a number of generalizations about column size and dimension ratios needed to accomplish various tasks related to the formation of microspheres. Similar microsphere forming columns of the same general type can be characterized by a single dimension, the minimum column inside diameter. Average bed loading of 10 to 20 vol % seems reasonable. Typically, about half the bed volume is in a cylindrical section at the top of the column. Small microspheres can be prepared, without fluidization, by gelation during free fall through the length of the column. Reasonable column lengths are possible when the droplets are not too large; for example, 360- μ -diam sol droplets can be gelled in a column 8 ft long using 2-ethyl-1-hexanol (2EH). Even shorter column lengths are possible if smaller droplets are formed.

In a study of the chemistry of microsphere formation, a factorial experiment designed to delineate the effects of three variables was carried out. The variables studied were water content, nitric acid concentration, and Ethomeen S/15 concentration in the 2EH. In addition to eight variations in alcohol composition, five different ThO_2UO_3 sols were used. Results showed that the nature and the history of the sols were as important as the composition of the alcohol in determining the quality of the microsphere product. In general, it was found that the Ethomeen S/15 concentration was the most important of the three variables studied. The experiment, as designed, permitted the evaluation of

"cross effects," or effects produced by the interaction of two or more variables. Two cross effects were found: those between nitric acid and Ethomeen S/15 and those between water and Ethomeen S/15. Microspheres of acceptable quality were obtained with 2EH with low Ethomeen contents. The sensitivity of the microsphere formation process to small changes in composition of the 2EH suggested the desirability of an alcohol sidestream recycle system, which would effectively purify the alcohol after a limited time in the column. Scrubbing with Na_2CO_3 solution has been found to be effective for removing nitric acid from the alcohol and thus preventing its reaction with the surfactant in the distillation system that is used to remove water from the alcohol. Such a system would be supplemented by a surfactant, water, and acid infusion system in the alcohol recycle circuit. An alternative approach to recycle is total distillation of the 2EH to completely purify it. This would be followed by reintroduction of nitric acid, surfactant, and water by infusion, as indicated above.

6.4 ^{233}U Storage and Distribution

ORNL serves as a national distribution center for ^{233}U . The ^{233}U facility, which contains a small batch leacher, a batch dissolver, and a single-cycle solvent extraction system, is capable of purifying ^{233}U at the rate of 25 kg per week. The ^{233}U received during 1968 amounted to 50 kg (not including the 34 kg of ^{233}U received for the TRUST facility), or 41% of that received in 1967. The weight of ^{233}U shipped during 1968 was 52 kg, or 87% of that shipped in 1967.

The TRUST (Thorium Reactor Uranium Storage Tank) facility was built to store a metric ton of highly enriched uranium (76.5% ^{235}U , 9.7% ^{233}U) in the form of a uranyl nitrate solution. The material is the uranium product from the Indian Point Reactor fuel; it was purified by solvent extraction at the Nuclear Fuel Services plant in West Valley, New York. The solution will be stored indefinitely since the ^{232}U content (120 ppm) prohibits its direct refabrication into fuel elements, and the low ^{233}U content makes it of little interest for reactors demonstrating the thorium fuel cycle.

The TRUST transfer operations were completed in 22 days. The overall average radiation exposure was 21 mrem/man-day. The maximum exposure for a single day was 160 mrem.

7. SOL-GEL PROCESSES FOR THE URANIUM FUEL CYCLE

7.1 Preparation of UO_2 Sols by Solvent Extraction

A new process [the CUSP (Concentrated Urania Sol Preparation) process] for the preparation of concentrated ($\geq 1 M$) urania sols directly by solvent extraction has been developed in the laboratory and tested in engineering-scale equipment. Suitability of the resulting sols for use in the preparation of microspheres has been demonstrated. In the process, nitrate ion is extracted continuously at a controlled rate from a U(IV) nitrate-formate solution by an organic solution of Amberlite LA-2 (a high-molecular-weight secondary amine). By following a prescribed conductivity-temperature-time schedule, we can prepare concentrated urania sols that are characterized by a high degree of crystallinity, stability, and a high U(IV) content.

The solvent extraction process previously used for the preparation of urania sols consisted of a multistage extraction of nitrate, with a digestion step between the first and second stages. It was limited to the preparation of dilute ($< 0.3 M$) urania sols, which, on concentration to $1 M$, showed variations in gelling and microsphere forming properties. Laboratory studies to determine the reasons for the variation in sol properties showed that the sols prepared according to this flowsheet contained a large and variable fraction of amorphous solids. Basic to the development of the new process was the discovery that simple heating of an acid-deficient U(IV) polymer solution to the crystallization temperature usually does not promote a high degree of crystallization per se; the extraction of nitrate at the crystallization temperature is also required. Once crystallization has been initiated, however, it appears to proceed rapidly, releasing nitric acid. Nitrate extraction is accelerated at this point to minimize the oxidation of U(IV) to U(VI) species. By extracting the nitrate at a controlled rate, monitoring the extraction by measuring the conductivity of the aqueous phase, and controlling the temperature of extraction as indicated by conductivity readings, we found that concentrated, stable, highly crystalline sols could be reproducibly prepared.

7.2 UO_2 - PuO_2 and PuO_2 Sol-Gel Process Development

Urania sols prepared by the CUSP process (see Sect. 7.1) have been mixed with high-nitrate plutonia sols prepared by solvent extraction to yield mixed sols that form good-quality microspheres if mixing and forming are carried out within 24 hr. It has not yet been found

feasible to prepare a plutonia sol suitable for direct use in sol-gel processes by solvent extraction; however, a high-nitrate sol, which has a NO_3^-/Pu mole ratio that is usually considered to be unacceptably high, is readily prepared by a simple extraction with amine or *n*-hexanol. This high-nitrate sol, although unsuitable for sol-gel sphere forming techniques per se, becomes acceptable when properly mixed with a UO_2 sol. This approach circumvents problems stemming from the redox reaction of Pu(IV) with U(IV) and avoids the necessity of handling solids, which is required in other mixed sol preparation procedures. At present, this work is being done on a laboratory scale; considerable developmental effort is needed before successful engineering scaleup will be possible.

7.3 Preparation of UO_2 - PuO_2 and PuO_2 Materials

We still must rely on the precipitation-peptization process for preparing the UO_2 sols and the baking-peptization process for preparing the PuO_2 sols that are used in forming $^{235}\text{UO}_2$ - PuO_2 microspheres and shards for irradiation capsule tests. During the past year we have substantially improved the reliability of our sphere forming operations with these mixed sol systems by removing formic acid from the urania sol prior to mixing and by using a new solvent-surfactant system for sphere forming. A deleterious aging effect has been observed when the mixed sols are permitted to stand for 24 hr or longer before being used to form microspheres.

7.4 Microsphere Forming, Drying, and Firing Studies

The chemical conditions required for satisfactory forming, drying, and firing of gel spheres depend, in part, on the characteristics of the sol. Satisfactory long-term operation of sphere forming columns requires additions of surfactants to the alcohols used in the forming column. Our criteria to demonstrate satisfactory operation are 1 hr for satisfactory initial conditions, 50 hr for an adequate surfactant addition schedule, and 200 hr as a practical test of excessive accumulations of other constituents in the alcohol. Initial surfactant concentrations and addition schedules were determined for seven sols.

7.5 Development of High-Performance Fuel Materials

The carbides, nitrides, and carbonitrides of uranium and plutonium are potential fuel materials in future fast

reactors because of their high-performance characteristics, namely, small molar volumes, high thermal conductivities, and high melting points. All of these materials can be prepared by a sol-gel method, starting with oxide sols to which carbon black has been added. For carbide preparation, the carbothermic reduction of the oxide is carried out in an argon or a helium atmosphere, whereas the preparation of nitrides and carbonitrides must be carried out under nitrogen. The preferred method of supplying the carbon is to introduce it as carbon black directly into the oxide sol, thereby forming a codispersed sol of high stability. Our present laboratory development effort has the objectives of demonstrating the capability of this method for preparing dense pellets and microspheres of these materials, and of studying the physical chemistry of the reactions in order to determine the best conditions to carry out these carbothermic syntheses.

We have previously shown that this method can be used to prepare ThC_2 , $(\text{Th,U})\text{C}_2$, and U(C,N) , starting with oxide sols prepared by standard ORNL methods. The work has now been extended to include UC and PuC; also, some preliminary work on $(\text{U,Pu})\text{C}$ has been done. We have prepared dense microspheres of UC, at both hyper- and hypostoichiometric compositions, with low residual oxygen contents. Work still in progress on PuC shows that the carbide conversion can be carried out but that further efforts will be necessary in order to obtain essentially single-phase product with a low oxygen content. The feasibility of working with mixed UO_2 - PuO_2 -C sols and gels has been demonstrated; however, problems similar to those encountered with PuC still remain to be solved.

By studying the reactions of dense UO_2 microspheres with graphite (to form UC_2) and of dense UC_2 microspheres with N_2 [to give U(C,N)], we have gained a better understanding of these reactions than would be possible from the direct study of the fast reactions occurring on a microcrystalline scale in an oxide-C gel. We have determined kinetic parameters and rate-controlling mechanisms for these two reactions.

7.6 Plutonium Storage Facility

A facility for safely storing and handling plutonium has been built in Building 3019 to meet the needs for developmental work involving the sol-gel flowsheet for fast reactor fuels. This facility is located in the basement adjacent to the Metals and Ceramics Division alpha laboratory. It has a capacity of 100 kg of plutonium in solid (fluoride) or liquid (nitrate) form. The liquid handling portion of the facility is a doubly

contained 150-gal tank filled with borosilicate glass Raschig rings.

Construction was completed during the year. The checking of instrumentation and the calibration of vessels are in progress.

8. SOL-GEL PROCESSES FOR ISOTOPIC HEAT SOURCES

Plutonium-238 is potentially an important isotopic power source. Its possible uses include applications in the space program and in devices for cardiac patients. The preparation and the use of ^{238}Pu have been studied at several locations.

Because significant progress had been made in the application of sol-gel technology to the production of $^{239}\text{PuO}_2$ microspheres, the developmental effort was extended to include ^{238}Pu . Much of the work with ^{239}Pu was found to be applicable to ^{238}Pu .

Sol-gel developmental work with curium, which has already proved useful for isotopic power sources, was also carried out.

8.1 Laboratory Studies of $^{238}\text{PuO}_2$ Sol-Gel Process

Microspheres of $^{238}\text{PuO}_2$ had been successfully prepared on a laboratory scale (10 g of ^{238}Pu), but difficulties were encountered in scaleup experiments. Investigation showed that the primary cause of the difficulties was degradation of the plutonium polymer by HNO_3 . Minor process changes were made to overcome this problem. These changes resulted in the successful preparation of $^{238}\text{PuO}_2$ sols and microspheres in batches containing as much as 50 g of ^{238}Pu .

8.2 Developmental Studies in a Glove-Box System

Flowsheet developmental studies were carried out in a glove-box facility, which has a capacity of 150 g of plutonium per day. In this work, ^{239}Pu was used as a stand-in for ^{238}Pu . During these studies, a total of 2.5 kg of dense $^{239}\text{PuO}_2$ microspheres was prepared for use in the development of fuel forms for isotopic power sources.

Flowsheet development included a demonstration of the peptization of hydrous plutonia precipitate at a reduced NO_3^-/Pu mole ratio and at an increased slurry concentration. In addition, the operation of a drying column with a minimum of turbulence was demonstrated, and an improved firing technique was developed.

8.3 Assistance to Mound Laboratory

The installation at Mound Laboratory of equipment to produce 150-g batches of $^{238}\text{PuO}_2$ microspheres was completed, and a program of extensive checking-out and modification was carried out. Developmental work associated with the formation of sols and microspheres was continued during the fabrication and installation of the system; as a result, several equipment improvements were made. Further work with the ORNL system is awaiting the outcome of large-scale (>50 g of plutonium per batch) work being conducted by Mound Laboratory personnel, using ^{238}Pu in similar equipment in shielded glove boxes.

8.4 Curium Sol-Gel Studies

The rare-earth sol-gel process had previously been adapted for use in preparing mixed americium-curium oxide. An additional 31 g of oxide was prepared during this report period; simplified equipment concepts for sol preparation were demonstrated, and a permanent sol-gel equipment rack was designed and installed in the Transuranium Processing Plant.

9. SPECIAL SOL-GEL PROCESSES

The versatility of the sol-gel process and the ease with which it can be adapted to prepare a variety of ceramic bodies of different shapes and sizes has led to numerous requests for specially prepared materials. Application of sol-gel methods to the preparation of materials to be used for purposes other than nuclear fuel or isotopic heat sources is reported here.

9.1 Sol Preparation

The precipitation-washing-peptization procedure previously developed for preparing rare earth sols has been used to prepare hydroxide and/or hydrous oxide sols of various metals, including Y, Fe, Zr, Hf, Al, Ti, Am, Cm, Bk, and Cf, as well as the rare earths. In each case, the original precipitate that forms when a metal salt solution is added to ammonium hydroxide consists of small amorphous particles from 20 to 50 Å in diameter. Digestion at elevated temperature converts these precipitates to crystalline forms that can be peptized; however, the conversion times vary widely for the different metal hydroxides. For those hydroxides requiring digestion times of days or months, it is convenient to form fluid sols by vigorous agitation of the gelatinous solids.

Mixed $\text{ZrO}_2\text{-Y}_2\text{O}_3$ and $\text{PuO}_2\text{-ThO}_2$ materials were prepared by blending sols in the desired ratio and converting the resulting sols to the oxides.

9.2 Scaleup of the Precipitation-Washing-Peptization Sol Process

Equipment was built and used to prepare 100- to 200-g batches of sol by the precipitation-washing-peptization process that was originally developed for preparing rare earth sols. Titania sol was prepared in this equipment to demonstrate large-scale operations.

9.3 Incorporation of Carbon into Metal Oxide Sols

Positively charged oxide sols (such as UO_2 , ThO_2 , and $\text{ThO}_2\text{-UO}_3$) that are composed of small crystallites were found to act as protective colloids toward carbon black, forming very stable and fluid codispersed sols at carbon/metal mole ratios as high as 15. On the other hand, positively charged sols containing large crystallites (e.g., europium hydroxide or autoclaved ZrO_2) and negatively charged sols (such as SiO_2) do not exhibit this protective action; instead, they become viscous at relatively low carbon concentrations. Carbon has been satisfactorily dispersed into specially prepared ZrO_2 , TiO_2 , HfO_2 , and CeO_2 sols.

9.4 Preparation of Porous Oxides

Porous ZrO_2 microspheres in the 2- to 20- μ -diam range were prepared by burning carbon out of $\text{ZrO}_2\text{-C}$ gel spheres or by controlling the sintering conditions (low temperature and minimum time) to limit the densification of zirconia gel spheres. Burning carbon out of the $\text{ZrO}_2\text{-C}$ gel spheres produced porosities of 61 and 70%, whereas controlled sintering of ZrO_2 gel spheres at 400°C produced porosities of approximately 25%.

Porous U_3O_8 shards for testing as potential HFIR fuel were formed by controlled oxidation and sintering of UO_2 gel. Porosity was a function of firing conditions. Shards of UO_2 containing about 23% porosity were produced by converting UO_2 sol to gel shards via air drying at 110 to 150°C, then firing in air at a temperature that was increased (at 200°C/hr) to 1000°C. Materials that volatilize during oxidation-densification (e.g., carbon or sulfate) can be added to urania sol to produce porosity in the final oxide.

9.5 Microsphere Forming

Recent developmental work has been directed at improving methods for preparing microspheres that are

less than 100 μ in diameter. Both the two-fluid nozzle operated at high organic-fluid flow rates and electrostatic dispersion from hypodermic needles show promise. In the case of the two-fluid nozzle, the most important variable (and the one primarily used to control the sol droplet size) is the turbulence of the organic fluid in the nozzle. A dimensionless relationship between operating variables and sol-drop size has been derived from experimental data. About 60 wt % of the spheres formed in the two-fluid nozzle at turbulent flows are between 0.7 d_{50} and 1.4 d_{50} (where d_{50} is the mean diameter).

Preliminary results obtained by electrostatic dispersion from a hypodermic needle indicate good control of size range. Conditions preset to produce 50- to 100- μ -diam microspheres gave an 80 wt % yield in the desired range.

10. SEPARATIONS CHEMISTRY RESEARCH

New separations methods and reagents are being developed, principally for uses in radiochemical processing but also for other purposes extending from extractive metallurgy to biochemical separations. Reagents developed in the former ORNL raw-materials program and subsequent studies continue to show extended utility. The program in separations chemistry can be divided into three parallel and interdependent types of research activity: (1) descriptive chemical studies (Sects. 10.1, 10.2, and 10.5–10.7) of the reactions of substances to be separated and of separations reagents, of the controlling variables in particular separations, and of new potential reagents and methods; (2) development (Sects. 10.3–10.6) of selected separations and methods into specific complete processes, both where no workable process exists and where existing processes can be improved, carried where warranted to the point that large-scale performance can be predicted; and (3) fundamental chemical studies (Sects. 10.6–10.11) of the species, equilibria, and reaction mechanisms involved in separations systems, both to increase knowledge and to help define potential applications.

10.1 Extraction of Metal Sulfates and Nitrates by Amines

As part of the program that is concerned with surveying the extraction characteristics of many metals from various systems, data were obtained for extractions of 16 metals from Li_2SO_4 –0.2 *N* H_2SO_4 (ranging from 0.3 to 5 *N* sulfate) and LiNO_3 –0.2 *N* HNO_3 (0.5 to 10 *N* nitrate) solutions with representative primary,

secondary, tertiary, and quaternary amines. Extraction coefficients higher than 1 were obtained only for V(V), Zr(IV), Nb(V), Mo(VI), Pd(II), and U(VI) in the sulfate system and for Zr(IV), Mo(VI), Pd(II), Eu(III), Hg(II), and U(VI) in the nitrate system.

10.2 New Separations Agents

We are continuing to investigate, for potential utility in solvent extraction or other separations methods, compounds that are (1) newly available commercially, (2) submitted by manufacturers for testing, or (3) specially procured for testing of class or structure.

We obtained a sample of methyltrioctylphosphonium dimethylphosphate, which is readily convertible to methyltrioctylphosphonium chloride or carbonate. It has usefully low solubility in the corresponding aqueous solutions, 1 *M* HCl or 1 *M* Na_2CO_3 . It appears similar to the analogous commercial quaternary ammonium compound, Adogen 464. Two other quaternary phosphonium compounds examined showed excessive aqueous solubility.

Three unsymmetrical dialkylsulfoxides were synthesized for comparison with the symmetrical dialkylsulfoxides previously studied. One alkyl group of each is methyl, and the other is a large branched alkyl group containing 9 to 15 carbons. Each of the three compounds dissolved readily in xylene and did not distribute excessively to aqueous solutions. Each extracted iron(III) from chloride solutions (as did another methyl-alkyl-sulfoxide, but not any symmetrical dialkylsulfoxide tested), confirming that there is a fundamental difference between the two classes of sulfoxides.

10.3 Beryllium Purification by Solvent Extraction

Additional evaluation tests of the solvent extraction process (quaternary ammonium carbonate extractant) for preparing very pure beryllium hydroxide showed that the purity of the product is greatly improved by adding EDTA to the scrub, strip, and product wash solutions. A product containing only 140 parts of sulfur and 60 parts of total metal impurities per million parts of BeO was prepared. A study of methods for decreasing the boron contamination (20 to 30 parts per million parts of BeO) of the products was begun.

10.4 Recovery of Uranium from Commercial Phosphoric Acid

A promising solvent extraction process for recovering uranium from commercial wet-process phosphoric acid

was developed and demonstrated successfully in small-scale batch tests. In this process, the uranium is extracted with the synergistic reagent combination of di(2-ethylhexyl)phosphoric acid plus trioctylphosphine oxide in a kerosene diluent. After the extract is scrubbed with water to remove phosphoric acid, the uranium is stripped with ammonium hydroxide--ammonium carbonate solution and precipitated from this solution by heating. Economic feasibility of the process will depend on maintaining losses of the expensive extraction reagents at a tolerable level. Total chemical reagent costs for the process are estimated to be in the range of \$0.89 to \$2.78 per pound of U_3O_8 ; variations within this range would depend mainly on the amount of solvent loss that is assumed.

10.5 Rapid High-Resolution Chromatography

In the continuing study of the high-resolution chromatography obtainable with very finely divided sorbents, the factors contributing to peak-broadening are being examined. With small columns and tubing, the chief factor appears to be gradient-broadening, which is thought to result from laminar flow through the effluent tube. Similar washing-out patterns were obtained with a moderately long effluent tube preceded by a packed column, an empty column, or no column. The material of the tube (i.e., Teflon, polyethylene, or stainless steel) had no significant effect. Injected air bubbles were markedly effective in maintaining a sharp concentration gradient, but interfered with dropwise sample collection.

10.6 Actinide and Lanthanide Intragroup Separations by Displacement Elution from Ion Exchange Resins

In scoping tests, several aminopolyacetic acids, singly and in pairs, were used as chelating agents to elute neodymium and praseodymium from Dowex 50 cation exchange resin. Good separations of these elements were obtained with hydroxyethylethylenediaminetetraacetic acid (HEDTA) and diethylenetriaminepentaacetic acid (DTPA). Ethylenediaminetetraacetic acid (EDTA) and (with heated column) 1,2-diaminocyclohexanetetraacetic acid (DCTA) gave excellent separations but required a barrier metal ion to prevent precipitation of the free acids on the H^+ -form resin. Nitrilotriacetic acid (NTA) gave fair separation and did not precipitate in a heated column; however, it did precipitate from the cooled eluate. Unsatisfactory results were obtained with iminodiacetic acid (IDA).

When the chelating agents were combined in pairs, separation was considerably improved in some instances

(i.e., HEDTA + IDA, + NTA, or + HIMDA, hydroxyethyliminodiacetic acid), but not in others (HEDTA + DTPA, + EDTA, or + DCTA).

Hot-cell tests of transplutonium actinide separations were made with HEDTA, NTA, IDA, and 2-hydroxypropane-1,3-diaminetetraacetic acid (HPDTA), and various combinations of these. The experimental feed solution contained ^{241}Am , ^{244}Cm , ^{252}Cf , and ^{253}Es in 0.25 *M* HNO_3 . HPDTA (10 g/liter at pH 8.0) gave good separation of the actinides into four fractions: (1) Es, 30% of Cf, < 0.1% of Cm; (2) 70% of Cf, 0.2% of Cm; (3) 80% of Cm, trace Am; (4) Am, 19% of Cm. Under the conditions used in these tests, little or no separation was obtained with HEDTA alone or with HEDTA + IDA or HEDTA + NTA; however, the poor resolution was probably due, in part, to insufficient quantities of the actinides on the resin for efficient performance of displacement (in contrast to chromatographic) elution.

10.7 Separations by Precipitation

A study of the oxidation of berkelium in the presence of cerium and excess iodate confirmed the expected homogeneous coprecipitation. Precipitation of the trace berkelium is even more complete than that of the carrier cerium, and gives good separation from most other metals.

A study of the kinetics of the foregoing coprecipitation showed that, when the precipitation is not too rapid, the concentrations of berkelium and cerium decrease according to the Doerner-Hoskins model,

$$\log [\Sigma Bk]_i / [\Sigma Bk]_f = k\lambda \log [\Sigma Ce]_i / [\Sigma Ce]_f.$$

The coefficient $k\lambda$ is approximately 3, so that dissolved berkelium is depleted more rapidly than is cerium. However, since $k \approx 10$ from other measurements (Sect. 10.9), $\lambda \approx 0.3$, which indicates that cerium would be the more rapidly depleted solute if the precipitation were not controlled by the redox reaction.

10.8 Equilibria and Mechanisms of Extraction

We have begun a detailed investigation of the extraction of iron(III) from hydrochloric acid solutions by *p*-xylene solutions of the unsymmetrical methyl-4,8-dimethylnonylsulfoxide. This compound is one of a series of unsymmetrical methylalkylsulfoxides, all of which, in contrast to a series of symmetrical dialkylsulfoxides, extract iron chloride. With a variable sulfoxide concentration and a constant hydrochloric acid concentration (8 *M*), the log-log slope of the extraction

coefficient E vs [sulfoxide] was 2.4, suggesting the formation of a mixture of $\text{FeCl}_x\text{H}_{x-3} \cdot 2\text{R}_2\text{SO}$ and $\text{FeCl}_x\text{H}_{x-3} \cdot 3\text{R}_2\text{SO}$. The possible analogy of this extraction to the extraction of iron by ether suggests that these compounds may actually be $\text{HFeCl}_4 \cdot 2\text{R}_2\text{SO}$ and $\text{HFeCl}_4 \cdot 3\text{R}_2\text{SO}$; however, at present, we are unable to estimate the chloride ratio in the extracted complex since we have not, as yet, varied the chloride concentration independently of the acid concentration.

10.9 Relative Potentials of the Bk(IV)/Bk(III) and Ce(IV)/Ce(III) Couples

The difference between the formal potentials of the Bk(IV)/Bk(III) and Ce(IV)/Ce(III) couples at 25°C in nitric acid solutions was measured by using a selective extraction system to permit the separation of Bk^{4+} and Ce^{4+} (low concentrations) from Bk^{3+} and Ce^{3+} (higher concentrations) for analysis.

$$E_{\text{Ce}} - E_{\text{Bk}} = 0.059 \log \left(\frac{[\text{Bk(IV)}]/[\text{Bk(III)}]}{[\text{Ce(IV)}]/[\text{Ce(III)}]} \right) \approx 0.06 \text{ v .}$$

No absolute value is assigned to E_{Bk} because of discrepancies in the published values for E_{Ce} .

10.10 Kinetics of Metal Ion Extractions by Organophosphorus Acids

An improved technique for measuring extraction kinetics, with continuous closed-loop flow sampling and automatic counting, permitted both improved precision and longer uninterrupted runs. With the improved precision, the extraction of iron(III) by HDEHP is best fitted by

$$\frac{\text{rate}}{[\text{Fe}]} = r = \frac{(r_{1m} + r_{1d})(r_{2s} + r_{2d} + r_{2df})}{r_{1m} + r_{1d} + r_{2s} + r_{2d} + r_{2df}},$$

where

$$r_{1m} = 5.5 \times 10^{-4} [\Sigma\text{HA}]^{0.5}/[\text{H}^+],$$

$$r_{1d} = 1.8 \times 10^{-3} [\Sigma\text{HA}]/[\text{H}^+],$$

$$r_{2s} = 1.5 \times 10^{-7} [\text{H}^+]/[\text{Fe}],$$

$$r_{2d} = 9.0 \times 10^{-6} [\Sigma\text{HA}]^{1.5}/[\text{H}^+]^2,$$

$$r_{2df} = 1.2 \times 10^{-5} [\Sigma\text{HA}]^2/[\text{H}^+]^2.$$

In the much more complicated kinetics of the extraction of beryllium by HDEHP, the rate changes

with time in each run. The extraction is moderately slow at the start (commensurate with iron extraction rates), decreases in 1 to 3 hr to a lower rate, and then rises gradually over a 10- to 15-hr period to a higher rate, where it finally becomes proportional to the aqueous beryllium concentration (i.e., where it is first order with respect to beryllium).

10.11 Aggregation and Activity Coefficients in Solvent Phases

Previously reported difficulties with leaks in a commercial diaphragm sensitive manometer appear to have been eliminated in a newer design of the sensing head. Use of two of the new heads (pressure ranges, 3 mm and 100 mm Hg) in our differential vapor pressure system has given the most accurate vapor pressure depression data that we have obtained to date. With this improvement, osmotic coefficients were redetermined for benzene solutions of three reference standard solutes, triphenylmethane, azobenzene, and benzil. The results were well fitted by a new empirical three-parameter equation.

Methyl-4,8-dimethylnonylsulfoxide was determined to be monomeric in water-saturated benzene solution by use of a matched-thermistor dynamic osmometer. However, constant readings could not be obtained when hydrochloric acid was also present; thus the latter solutions will require isopiestic measurement.

Quantitative measurements of the extraction of water by organic solutions of tri-*n*-octylamine and six of its salts were completed.

11. CHEMICAL APPLICATIONS OF NUCLEAR EXPLOSIONS

11.1 Copper Ores

In the leaching of a new chimney-rock sample, about 50% of the ^{90}Sr and 30 to 35% of the ^{106}Ru were dissolved in the pH range 1 to 2. The amounts of dissolved ^{125}Sb and ^{137}Cs decreased from about 12% at pH 1 to 2 to 4% at pH 2. Of these isotopes, only ^{106}Ru contaminated the copper that was recovered from the leach liquor by cementation. The ^{106}Ru contamination of cement copper products decreased as the copper concentration of the liquor increased.

11.2 Recovery of Oil from Shale

The tritium contamination of oil that was retorted from shale after 25 days of exposure to tritiated water vapor was found to be directly dependent on tempera-

ture in the range of 45 to 97°C. Tritium contamination of the shale increased as the shale particle size increased. Tritium was removed from contaminated shale by heating the shale in a stream of moist air, but the efficiency of this treatment decreased as the size of the shale chunks increased. Tritium was also effectively removed from contaminated shale by immersing the shale in hot water. Attempts to scrub tritium from contaminated shale oil, however, were not successful.

12. BIOCHEMICAL SEPARATIONS

MACROMOLECULAR SEPARATIONS

12.1 Development of Reversed-Phase Chromatography Systems for Separating Transfer Ribonucleic Acids

A new reversed-phase system that is based on a phosphonium analog (trioctylmethylphosphonium dimethylphosphate) of existing quaternary ammonium chloride reversed-phase chromatography systems was investigated for use in separating *E. coli* B tRNAs. Good resolution of tRNAs was obtained. An interesting feature of the chromatograms was the wide separation of the two alanine tRNAs.

12.2 Engineering Scaleup of Biological Macromolecular Separations Techniques

Approximately 860 mg of purified formylmethionine 1 tRNA and 700 mg of valine tRNA were recovered from mixed *E. coli* B crude tRNA. These purified samples have been distributed by the sponsoring agency, the National Institute of General Medical Sciences. Another production campaign was initiated, and crude tRNA was prepared from 77 kg of *E. coli* K-12 MO7 by an improved flowsheet that yielded four times as much tRNA per kilogram of cells as in the previous campaign. About 920 mg of purified phenylalanine 2 tRNA has been prepared by RPC-4 reversed-phase chromatography. Study of the DEAE-cellulose chromatography system has given a better understanding of this system.

12.3 Separation of Transfer Ribonucleic Acids from *B. subtilis* A-12

A large batch of transfer RNAs has been prepared from *B. subtilis* A-12, and methods for the isolation of the purified tRNAs are being investigated. Good resolution of individual tRNAs has been obtained on RPC-4 columns.

12.4 Separation of Aminoacyl-RNA Synthetases

A general flowsheet that is suitable for scaleup to any batch size has been devised for the recovery of aminoacyl-RNA synthetases. The activity of the methionyl-RNA synthetase has been increased 50-fold through purification on DEAE-cellulose and hydroxylapatite columns. The leucyl-RNA synthetase, on the other hand, has proved to be extremely labile and, to date, its activity has been increased only eightfold.

12.5 Separation of Ribosomal Ribonucleic Acids

Gram quantities of ribosomal ribonucleic acid (rRNA) have been prepared from *E. coli* cells. Methods that have been studied for separating component rRNAs include gel permeation chromatography and reversed-phase chromatography. Partial separation of rRNAs was achieved on beaded agarose columns; however, a more complete separation was obtained by reversed-phase chromatography using the RPC-2 system. A NaCl gradient solution was used to elute the rRNAs. Lower-molecular-weight RNAs appeared to be eluted first. Chromatographic fractions were analyzed by gel electrophoresis using polyacrylamide-agarose gels.

BODY FLUIDS ANALYSES

12.6 Prototype Analyzers

Three prototype analyzers for detecting and quantifying uv-absorbing constituents and one prototype analyzer for detecting and quantifying carbohydrates have been built and sent to other laboratories for evaluation. An advanced uv-analyzer prototype of much smaller size has also been built and is being tested.

12.7 Separation Systems

Improvements have been made in the ion exchange separation media used in both types of analyzers, and a commercial source of such ion exchange resin is now available. A technique for dynamically loading ion exchange resin columns has been perfected, and the effects of pH on chromatographic separation have been determined. We are developing a computer program that can predict the elution position and the peak shape of a known compound if the dependence of its distribution coefficient on buffer concentration and temperature is known. Fundamental studies on gradient elution chromatography are continuing.

12.8 System Components

A small, dual-beam, dual-wavelength uv photometer has been developed for use with the advanced uv analyzers. A small, six-port sample injection valve that is capable of operation up to 5000 psi has also been developed and tested extensively.

12.9 Identification of Body Fluid Constituents

The chromatographic positions of 143 uv-absorbing compounds and 48 carbohydrates have been established. Twenty-one uv peaks and three carbohydrate peaks from urine chromatograms have been definitely identified by spectral and chemical methods; an additional 18 uv peaks and 13 carbohydrate peaks have been identified tentatively by their chromatographic properties. The effect of chemical structure on elution position has been established, and the use of gel chromatography and enzymatic hydrolysis of urine prior to analysis has been shown to be useful in identification.

12.10 Analytical Results

The results of analyzing urine and blood sera from eight normal subjects during two different sampling periods indicate that normal persons have very similar excretion patterns. A number of pathologic urine samples have been examined, and the presence of some of the metabolites of the drug, phenacetin, have been established.

12.11 Data Acquisition and Analysis

A small digital computer has been purchased for use as an on-line computer for real-time data acquisition and evaluation from two or more chromatographs. A computer program for evaluating chromatographic information as it is acquired has been developed and tested.

12.12 Literature Survey

An annotated bibliography on urine constituents and analyses was completed for the period 1964–1966. Over 3000 literature citations were found, with reference to over 1000 molecular constituents with molecular weights less than 1000.

13. IRRADIATION EFFECTS ON HETEROGENEOUS SYSTEMS

The effects of ^{60}Co gamma irradiation on various inorganic aquasols were studied. Aged hydroxide sols of

the lanthanides were essentially unaffected. Irradiation of a freshly prepared $\text{Eu}(\text{OH})_3$ sol produced some transient effects, primarily in electrical conductivity; however, the stability of the sol was not detectably affected. Streaming currents of sols of bentonite and alumina were decreased by irradiation; blue-colored, but not red-colored, gold sols showed similar behavior.

14. SPECTROPHOTOMETRIC STUDIES OF SOLUTIONS OF LANTHANIDES AND ACTINIDES

Spectrophotometric techniques for studying aqueous solutions, especially of the lanthanides, actinides, and transition elements, are being developed and exploited. Studies of non- or low-alpha-active solutions at temperatures less than 100°C are accomplished by regular techniques, while a special spectrophotometer system that is capable of operating at temperatures up to 380°C and pressures up to 10,000 psi has been built to provide containment for alpha-active materials. The latter system has been used in a standard laboratory for studying temperature effects (25 to 380°C) on aqueous $\text{Pr}(\text{NO}_3)_3$, $\text{Nd}(\text{NO}_3)_3$, and UO_2SO_4 , and will be further used to study other lanthanides and low-alpha-active materials before it is moved into a laboratory designed for studying materials that are highly alpha active. In conjunction with the spectrophotometric studies, the densities of aqueous solutions of lanthanides and actinides are being measured over the temperature range 25 to 400°C .

15. REACTOR EVALUATION STUDIES

This program, which is a joint effort with other ORNL Divisions, especially the Reactor Division and the Metals and Ceramics Division, has the primary purpose of assisting the USAEC in evaluating the technical feasibility and economics of various nuclear power concepts being developed, or being considered for development, under the U.S. civilian power program. Work in this Division during the past year was devoted primarily to the development of linear programming models for use in the planning of optimal nuclear power systems in the United States. Other work in the Division included principal responsibility for preparation of the report of the Fuel Recycle Task Force, assistance in preparation of the report of the Systems Analyses Task Force, evaluation of fuel cycle costs for metallic uranium-fueled pressurized-water reactors, estimation of costs for on-site vs off-site fuel cycle facilities and shipping associated with liquid-

metal-cooled fast breeder reactors, and initiation of studies to develop a dynamic programming model for the optimization of nuclear power systems.

16. PREPARATION AND PROPERTIES OF ACTINIDE OXIDES

Studies on sols of urania, thoria-urania, and various lanthanide hydroxides were continued. It was found that oxidation of nitrate-stabilized UO_2 sols leads to two colloidal charge-carrying species, as was previously observed for chloride-stabilized systems. In the case of the nitrate-stabilized sol, the more highly oxidized particles have a lower zeta potential, whereas the reverse situation is found in the chloride-stabilized system. In both systems, CO_2 will reversibly displace the stabilizing ion.

Several lanthanide hydroxide sols were used in studies of the effects of aging on the streaming current. All of the sols examined thus far have shown differences in behavior for a day or two after preparation, but appear to reach steady state after 7 to 10 days. Theoretical studies of colloidal systems were continued.

17. CHEMISTRY OF CARBIDES, NITRIDES, AND CARBONITRIDES

Fundamental studies of the reactions of the uranium and thorium carbides, nitrides, and carbonitrides with aqueous solutions were continued. Uranium mononitride dissolved readily in 0.5 to 15.8 M HNO_3 , yielding a yellow solution containing uranyl, ammonium, and nitrite ions, and an off-gas composed of N_2 , NO , N_2O , and NO_2 (with 8 to 16 M HNO_3). The quantities of the various nitrogen-containing products were functions of acid concentration, reaction temperature, and time of reaction. Ammonium ion was an intermediate in the oxidation of the nitride nitrogen to free nitrogen.

The uranium carbonitride used ($\text{UC}_{0.6}\text{N}_{0.4}$) in these studies was inert at 80°C in water and in 6 M NaOH . The carbonitride reacted with 6 M HCl at 25°C and with 6 M H_2SO_4 at 80°C , producing primarily CH_4 , NH_4^+ , H_2 , and U^{4+} , and, in the case of 6 M H_2SO_4 , $\text{U}(\text{SO}_4)_2 \cdot 4\text{H}_2\text{O}$. In the reactions of the carbonitride with 0.5 to 15.8 M HNO_3 , nitrous acid, NO , and N_2 were the major products. Twenty to 70% of the carbon was found as CO_2 , while the remainder formed nitric acid-soluble organic compound(s). The NH_4^+ and the organic species, as yet unidentified, were intermediate reaction products that slowly oxidized to N_2 and CO_2 respectively.

18. SAFETY STUDIES OF FUEL TRANSPORT

This program was organized in early 1966 to identify and resolve problems involving the transport of irradiated fuel elements from a reactor to a reprocessing site and to develop an *Irradiated Fuel Shipping Cask Guide* (originally designated as an *Irradiated Fuel Shipping Cask Criteria*) for the Division of Reactor Development and Technology.

The *Guide* was completed during this reporting period and is available as ORNL-TM-2410. It establishes suitable engineering standards for the design, fabrication, and inspection of irradiated fuel shipping casks by providing information on structural integrity, shielding, heat transfer, criticality, and materials of construction. A considerable amount of emphasis is placed on quality control during the fabrication of a cask.

The *Guide* is presently being revised to incorporate newly developed data, as well as comments that have been received from recipients of the report.

19. NUCLEAR-POWERED AGRO-INDUSTRIAL COMPLEXES: SPECIAL STUDIES

Several members of the Chemical Technology Division continued their participation in the agro-industrial studies which were begun during the summer of 1967. Work this year has included: (1) a continuation of the general study of industrial processes and their application at a number of possible coastal desert energy center sites throughout the world, (2) a more detailed study of nuclear-powered complexes in the Middle East, and (3) a study of aquaculture (controlled cultivation of seafood) as a component of agro-industrial complexes.

19.1 General Studies

The continuation of work on the technical and economic evaluation of nuclear-powered industrial and agro-industrial complexes has entailed refinement of old data, procurement of new information (where possible), and the completion of a series of reports on the nuclear energy center work.

The cost of nuclear power was evaluated for fast breeder and thermal breeder reactors as a function of size and interest rate. The sensitivity of the final cost of power to various assumptions such as load factor and capital costs was tested. An increase of 25% in the assumed capital cost of a nuclear power plant was found to add 0.4 mill/kwhr to the cost of power.

The cost of water was represented as a range, in which the upper bound was defined as the water cost

associated with a single-purpose plant using bypass steam and the lower bound was determined from the incremental cost of adding water production to a power-only plant. For a 10% cost of money and a water output of 500 million gallons per day, the cost ranges were: Advanced Breeder Reactor-Vertical Tube Evaporator (ABR-VTE), 17.5 to 28.5 ¢/1000 gal; Light Water Reactor-Multistage Flash Evaporator (LWR-MSF), 25.5 to 36 ¢/1000 gal. The comparative benefits of using single-purpose (water-only) and dual-purpose (water and power) nuclear energy sources were evaluated for agricultural production. Results showed that benefits were about 30% higher for the dual-purpose plant.

The effect of a delay in the startup of a large agro-industrial complex was studied by a cash flow analysis, using the following assumptions: (1) full production during the first year; (2) 50% production the first year and full production during the second year; and (3) 25% production the first year, 50% production the second year, and full production during the third year. The corresponding internal rates of return, 14.8, 13.9, and 12.8%, indicate that the project returns would be very sensitive to any delay in startup.

The manufacturing costs of hydrogen and oxygen were estimated for water electrolysis plants using two types of advanced electrolytic cells: porous electrode cells and high-temperature vapor-phase cells. Electrolytic plants producing 40 million std ft³ of hydrogen and 860 tons of oxygen per day were compared with fossil fuel plants which utilize steam reforming and partial oxidation processes at the same hydrogen production rates. Electricity required for the electrolytic process, using a porous electrode cell, would have to cost from 0.8 to 2.3 mills/kwhr in order for this process to compete economically (i.e., "break even") with the various fossil fuel processes. If an oxygen credit of \$4/ton was assumed, this break-even power cost range would increase to 1.5 to 3 mills/kwhr.

The computer codes for determining the manufacturing costs of the products studied last year (ammonia, phosphorus, aluminum, salt, caustic-chlorine, and secondary products) were combined and revised; subroutines for seawater products (potassium chloride, potassium sulfate, magnesium chloride, and magnesium metal) and the production of acetylene and ethylene by the plasma arc process were added to the code. A study that compared the cost of producing iron and steel via the blast furnace route with the cost of production in electric pig iron and electric and basic oxygen steel furnaces was completed.

19.2 Middle East Studies

Studies of the application of the nuclear-powered agro-industrial complex concept to five countries in the Middle East (Egypt, Israel, Lebanon, Jordan, and Syria) were begun under AEC sponsorship in reply to the Strauss-Eisenhower proposal and the Baker Resolution, which was passed by the U.S. Senate in 1968. These studies were continuations of the general studies described above, but also included implementation studies, marketing analysis subcontract studies (industry: Union Carbide, Corporate Marketing Research, New York, and agriculture: A. D. Little, Inc.), an architectural-engineering study (Bechtel Corp.), and a financial study (to be assigned). Technical proposals for complexes at sites in Egypt and Israel were prepared and reviewed with the governments of these nations during November 1968 and April 1969 respectively. Joint study efforts, including exchanges of personnel, were arranged with both nations. A study of an internationalized complex for the Sinai (El Arish) area was also made.

The study involving an Egyptian proposal is presently farther advanced than the other studies. According to this proposal, a series of energy centers would be constructed along Egypt's western Mediterranean coast to provide water for the irrigation of about three million acres of coastal desert by the turn of the century. The first center, which might be located at El Hammam (40 miles west of Alexandria) would include four 2500-Mw (thermal) reactors, each of which would produce 250 million gallons of water per day and 500 Mw (electrical), built at two-year intervals; each unit would provide irrigation water for 60,000 acres of farmland. Most of the generated power would be absorbed by the Egyptian power grid. Industry at the site would include a one-million-ton-per-year salt works (using evaporator effluent as feed), a 1000-ton/day caustic-chlorine plant for seawater treatment and secondary industry, and a mixed fertilizer plant for the newly created farms. Power would also be used to produce electric-furnace phosphorus at the phosphate rock deposits on the Red Sea or the Upper Nile.

19.3 Studies on Aquaculture

We investigated the benefits that might be derived from including aquaculture — the intensive cultivation of finfish and shellfish under controlled conditions — in an agro-industrial complex. The major synergistic ad-

vantage lies in the utilization of large volumes of flowing water (saline and fresh) that enter into and exit from the nuclear desalination unit. Conceptually, a flowing stream would improve the water environment in such a manner that the growth potential of all fish (both seawater and fresh water species) would be benefited. It would provide a constant oxygen supply and flush away wastes, leaving a clean environment. Coupled with temperature optimization, the control of water conditions could increase fish yields and upgrade product quality significantly.

Aquaculture could supply economic and nutritive benefits to the overall agro-industrial project. High-value foods (e.g., shrimp) could be cultivated for export and provide for fast capital regeneration. Finfish, cultured intensively, could aid in relieving serious protein diet deficiencies that prevail among the populations of many developing countries.

Conceivably, aquaculture could best be practiced in the stream of seawater that cools the evaporator and is pumped back to sea as waste. The current VTE-MSF evaporator design specifies a 40°F rise in temperature and one billion gallons per day (BGD) of outfall for every BGD of fresh water produced. To illustrate the benefits of utilizing this stream for the culture of shrimp, a hypothetical operation at an energy center at El Hammam (Arab's Gulf), Egypt, was considered. Seawater at a mean temperature of 69°F would have to be blended with outfall water at 109°F in the ratio of 1.5:1 in order to obtain water with a mean temperature of 85°F, the temperature at which shrimp growth is maximized. Culture in a controlled-temperature environment yields two crops of shrimp annually that are of equal or better quality and market value than the one crop that can be produced in a similar volume of variable-temperature seawater. The anticipated annual gross income from shrimp would be \$10 million, assuming two crops annually, a yield of 1000 lb of shrimp per acre per crop, a total acreage of 5000, and a price of \$1/lb for the shrimp produced (20 to 30 shrimp per pound, heads off). Land improvement costs could range as high as \$8000/acre and still yield a 20% return on investment.

Studies of the cultivation of oysters was also begun.

20. SITING OF FUEL REPROCESSING PLANTS AND WASTE MANAGEMENT FACILITIES

The Chemical Technology Division participated in a study of long-range considerations involved in the siting of commercial fuel reprocessing plants and waste management facilities. The objectives of the study

were: (1) to identify factors that will influence growth patterns of the commercial fuel reprocessing and waste management industry, and (2) to explore the need, and recommend bases for, a national siting policy that would present minimum impediment to the growth of economic nuclear power while fully satisfying the requirements of public health and safety.

The principal conclusions of the study are concerned with: (1) the need for standards or regulations, (2) factors that influence the sizes of sites, (3) the safety and economics of large fuel reprocessing plants, (4) alternative schemes for the management of high-level wastes, (5) the effects of shipping radioactive materials, and (6) the question of whether reprocessing and waste facilities should be located on private lands.

21. CHEMICAL ENGINEERING RESEARCH

A stacked-clone contactor containing nine clones per stage and having reduced physical size and stage holdup was constructed, and initial evaluation tests were made.

A new type of contactor, a pulsed stacked-clone contactor, is being developed; a first model has been built and tested. A model small enough to fit in a glove box is now being designed.

Conceptual designs of scaled-up contactors indicate that machines with 300 clones per stage, and possibly more, can be designed and built.

22. ASSISTANCE PROGRAMS

22.1 Eurochemic Assistance Program

The Laboratory has continued to coordinate, for the USAEC Division of International Affairs, the exchange of technical information between Eurochemic and the USAEC production sites and national laboratories. The residence of a U.S. Technical Advisor to Eurochemic at Mol, Belgium, was terminated in January 1969. Eurochemic has performed successful processing campaigns on both low-enriched and highly enriched feeds.

22.2 Evaluation of Radiation Resistance of Selected Protective Coatings (Paints)

Tests to evaluate commercial protective coatings have been continued, using systems that were supplied principally by manufacturers with a recent or renewed interest in marketing their products in the nuclear field. Eighty coatings (seven generic types) supplied by nine manufacturers are being tested by exposure to a ^{60}Co gamma source with an intensity of 6×10^5 r/hr and a

temperature range of 40 to 50°C. The epoxies and phenolics that were continuously exposed until failure occurred were found to exhibit the greatest resistance at an average of 3.7×10^9 rads in air and 1×10^9 rads in deionized water.

A United States of America Standards Institute paint standard, "Protective Coatings (Paints) for Light Water Nuclear Reactor Containment Facilities," has been written and is now being reviewed. It is scheduled for completion by June 1969.

1. Molten-Salt Reactor Processing

The Oak Ridge National Laboratory is actively engaged in the development of a molten-salt breeder reactor which would produce low-cost power while producing its own fuel, ^{233}U , from ^{232}Th in amounts larger than it consumes. It would use a molten fluoride salt, $\text{LiF-BeF}_2\text{-ThF}_4$ (72-16-12 mole %), as a fluid fuel and graphite as a moderator. This reactor, which is described in detail in other reports, will succeed as a breeder only if the ^{233}Pa (27.4-day half-life) can be isolated at a rate significantly higher than its decay rate, and if the rare earth fission products are removed on a cycle of between 30 and 100 days. The development of an on-site, compact, low-inventory, high-performance, economical processing plant to effect these removals is the responsibility of the Chemical Technology Division. A proposed process that employs liquid-liquid extraction of the reactor salt with a bismuth phase containing reductants appears to offer a means to this end; therefore, it has been the major subject of our studies.

Data obtained previously provided good qualitative assurance that Pa, Th, and U could be separated by reductive extraction; however, we had very little information on the behavior of rare earths under reductive extraction conditions with a single-fluid reactor salt. During this report period, our understanding of the chemistry of reductive extraction has significantly improved, and reliable distribution coefficients for our system have been determined, not only for protactinium, uranium, and thorium but also for most of the actinides. The refinement of these data has increased our confidence in the chemical feasibility of the protactinium isolation part of the process. Revised calculational analyses, which have been made for the steady-state operation with ^{233}U and for initial operation with ^{239}Pu , show adequate Pa, Th, and U and/or Pu separation and indicate sufficient stability of the process against operational upset.

Distribution coefficients for most of the rare earths encountered in our system have been deter-

mined with sufficient accuracy to allow flowsheet analysis. Because the separation of the rare earths from thorium will require high flow rates of bismuth, the contactor development is complicated and a large electrolytic unit to prepare the necessary reductant will be required. Our calculations show that these penalties are probably acceptable if more attractive process alternatives are not found.

Our engineering development program is progressing to an experimental phase. We are now ready to contact molten fluoride salt with molten bismuth in a small packed tower and to observe mass transfer in this system under simulated process conditions. We have been encouraged in our development of electrolytic cells for the process by successful results with salt and bismuth in simple static experiments.

Our development work on the distillation of fluoride salts, originally directed toward the recovery of LiF and BeF_2 from the fuel salt of a two-fluid MSBR, will reach a climax when we distill about 1 ft³ of ^{235}U fuel salt from the initial MSRE loading.

1.1 MOLTEN-SALT BREEDER REACTOR PROCESSING FLOWSHEET ANALYSIS

Proposed Reductive Extraction Flowsheet

The process flowsheet envisioned for a single-fluid MSBR is based on reductive extraction and assumes that the reactor salt will be processed through the Pa isolation and the rare earth removal systems on a 3-day and a 30-day cycle respectively. The present version of the flowsheet, scaled for a 1000-Mw (electrical) MSBR, is shown in Fig. 1.1. The Pa isolation system and the rare earth removal system will be described in more detail in later sections.

The Pa isolation system exploits the fact that Pa is intermediate in nobility between U and Th. A

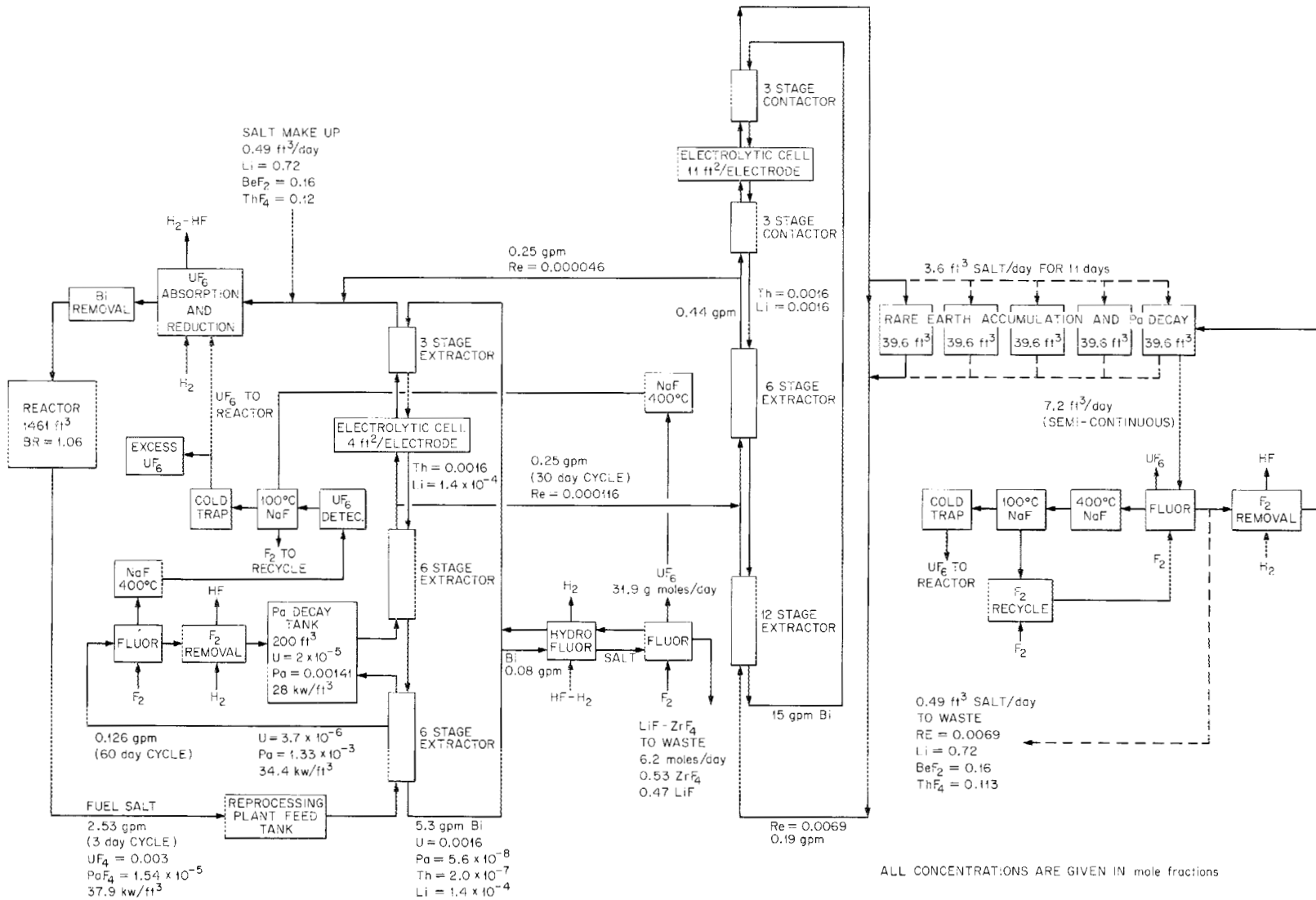


Fig. 1.1. Proposed Reductive Extraction Processing Flowsheet for a 1000-Mw(electrical) Single-Fluid MSBR. All concentrations are in mole fractions.

molten salt stream is withdrawn from the reactor on a three-day cycle (2.5 gpm) and is fed countercurrently to a 5.3-gpm liquid bismuth stream in a seven-stage contactor. If the reductant (Th plus Li) concentration in the Bi stream entering the contactor is adequate, the U in the salt will transfer to the downflowing Bi stream in the lower part of the contactor. The Pa, however, will concentrate midway up the cascade, where most of the Pa in the reactor system can be held by diverting the salt through a suitably large volume (200 ft³). Under steady-state conditions, the ²³³Pa decays to ²³³U at the same rate that it enters the tank from the reactor. (Calculated concentration profiles in the extraction column are discussed in a later section.) The concentrations of both Pa and U in the salt leaving the column are negligible; however, the concentration of rare earths at this point is about the same as that in the reactor. Approximately 10% (0.25 gpm) of the salt stream leaving the Pa isolation column will be processed for removal of rare earths. The remaining salt passes through an electrolytic oxidizer-reducer, where Li and Th are reduced at a flowing Bi cathode and become part of the metal stream fed to the column. At the anode of the cell, Bi is oxidized to BiF₃, which will be soluble in the molten salt. The salt stream containing BiF₃ is countercurrently contacted with the Bi stream leaving the extraction column in order to oxidize U, Pa, and other materials, which, after oxidation, transfer to the salt stream and return to the reactor.

The concentration of U or Pa must be known at some reference point in the column if the reductant concentration in the Bi stream fed to the column is to be controlled. The U concentration is determined by fluorinating approximately 5% of the salt entering the Pa decay tank and analyzing the resulting gas stream for UF₆. Means for collecting the UF₆ from this operation, as well as from other fluorination operations, and for returning this material to the fuel salt are provided. The UF₆ is simultaneously absorbed into the molten salt and reduced to UF₄ by a hydrogen sparge. Bismuth will be removed from the salt in a separate step before the salt is returned to the reactor.

Approximately 1.5% (0.08 gpm) of the Bi stream leaving the extraction column will be hydrofluorinated in the presence of a salt stream for removal of the seminoble metals (Ga, Ge, Cd, In, Sn, and Sb), corrosion products (Fe, Ni, and Cr), and fission product Zr. The salt will be recycled between

the hydrofluorinator and a fluorinator (where U is removed). The principal components that accumulate in the salt are LiF and ZrF₄; the expected steady-state composition is 47-55 mole % LiF-ZrF₄, which has a liquidus temperature of 520°C.

Salt that is free of U and Pa but contains rare earths is fed to the center of a 24-stage extraction column at the rate of about 0.25 gpm, which is sufficient to process the volume of salt in the reactor in 30 days. The salt flows countercurrent to a 15-gpm Bi stream containing Th and Li. Typically, 60% of the rare earths are extracted from the salt stream in the upper part of the column (resulting in a removal time of 50 days), and the rare earth concentration is increased to approximately 0.69 mole % in the lower part of the column. A portion of the salt leaving the column returns to the reactor, while the remainder is fed to the electrolytic cell complex; the net effect is the addition of Th and Li to the Bi stream and the transfer of the extracted rare earths from the Bi phase to the returning salt. Both the anode and the cathode are flowing streams of Bi. A Bi-Li stream generated at the cathode of the cell is fed to the three-stage contactor, which effectively removes the ThF₄ from the incoming salt. This salt stream, which picks up BiF₃ as it passes the anode, then flows countercurrent to the Bi stream entering the complex from the rare earth removal column in order to oxidize the rare earths, Th, and Li from the Bi.

Salt containing 0.69 mole % rare earths is withdrawn from the system at the rate of 0.49 ft³/day. The active metal fission products (Sr, Cs, Ba, and Rb), which are also present in the salt at a concentration equal to that in the reactor, are removed on a 3000-day cycle. Withdrawal is accomplished by using a set of 40-ft³-capacity tanks sequentially. This arrangement limits the rate at which rare earths could inadvertently return to the reactor. This salt will be fluorinated to recover uranium when necessary.

Isolation of Protactinium

System performance for the proposed flowsheet for isolating protactinium from a single-fluid MSBR (Fig. 1.2) has been recalculated using current data on reduction potentials and thorium solubility. Calculations were made for an MSBR fueled with uranium, as well as for initial operation of an MSBR fueled with plutonium. According to the flowsheet,

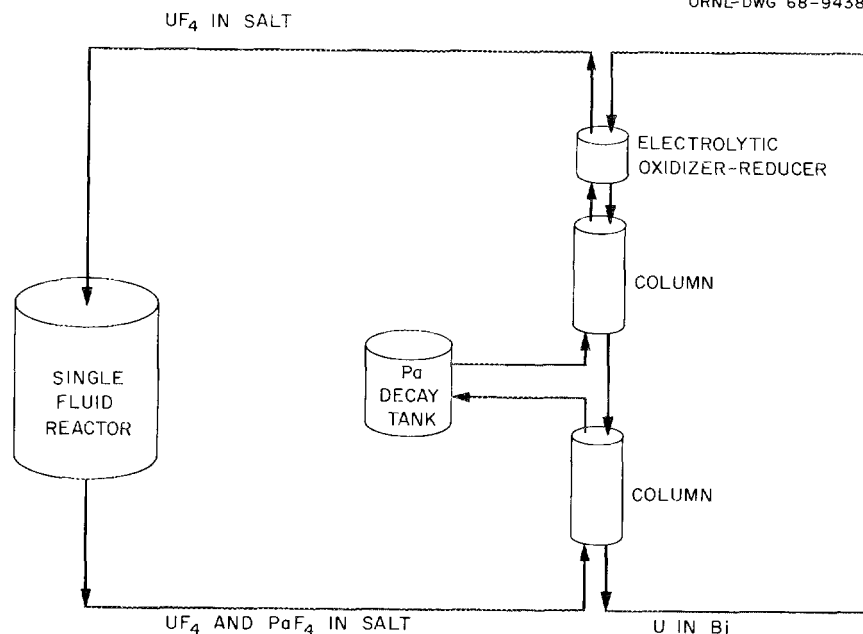


Fig. 1.2. Scheme for Isolating Protactinium in a Single-Fluid MSBR.

fuel salt from the reactor enters the bottom of the extraction column and flows countercurrently to a stream of bismuth containing reduced metals. Ideally, the metal stream entering the top of the column contains sufficient Th and Li to extract only the U and Pu entering the system. The system exploits the fact that Pa is less noble than U and Pu but more noble than Th. Both U and Pu are preferentially extracted in the lower part of the column, while Pa refluxes in the center. High protactinium concentrations are produced in the salt and metal streams. Most of the protactinium in the system can be isolated by diverting the salt stream through a tank of sufficient size (about 200 ft³).

Calculations have been made for both steady-state and transient system performance. The following values were assumed for the calculations: fuel salt composition, 71.7-16-12-0.3 mole % LiF-BeF₂-ThF₄-UF₄; reactor volume, 1461 ft³; processing rate, 2.5 gpm (three-day cycle); operating temperature, 600°C; reactor power, 1000 Mw (electrical); and Pa decay tank volume, 200 ft³. The Th and Li concentrations in the Bi stream being fed to the column were 0.0016 and 1.4×10^{-4} mole fraction respectively. In the calculations for an MSBR fueled with plutonium, the salt composition was assumed to be 71.8-16-12-0.2 mole % LiF-BeF₂-ThF₄-PuF₃; other values were the same as those given above.

Steady-State Performance for Case of MSBR

Fueled with Uranium. -- Calculated concentration profiles in the extraction column are shown in Fig. 1.3. The U concentration in the salt increases from the inlet value of 0.003 mole fraction to approximately 0.004 mole fraction in the first stage because of the reduction of U(IV) to U(III). It then decreases steadily to negligible values at the salt outlet. The concentration of Pa in the salt increases from the inlet value of 1.39×10^{-5} mole fraction to a maximum of 0.0021 mole fraction, then decreases to negligible values near the salt outlet. The concentration of Th in the Bi stream decreases from about 0.00132 mole fraction in the upper part of the column to 7.9×10^{-8} mole fraction near the Bi outlet. The concentration of Li in the Bi decreases from about 0.00124 mole fraction in the upper part of the column to about 0.00011 mole fraction at the bottom of the column.

The concentrations of U and Pa in the salt entering the decay tank are 1.25×10^{-5} and 1.325×10^{-3} mole fraction respectively. The concentrations of U and Pa in the decay tank are 2.63×10^{-5} and 1.312×10^{-3} mole fraction respectively. Under ideal steady-state operating conditions, approximately 93% of the Pa present in the reactor system would be held in the decay tank. However, it is likely that the actual amount of Pa isolated from the reactor will be somewhat below this value be-

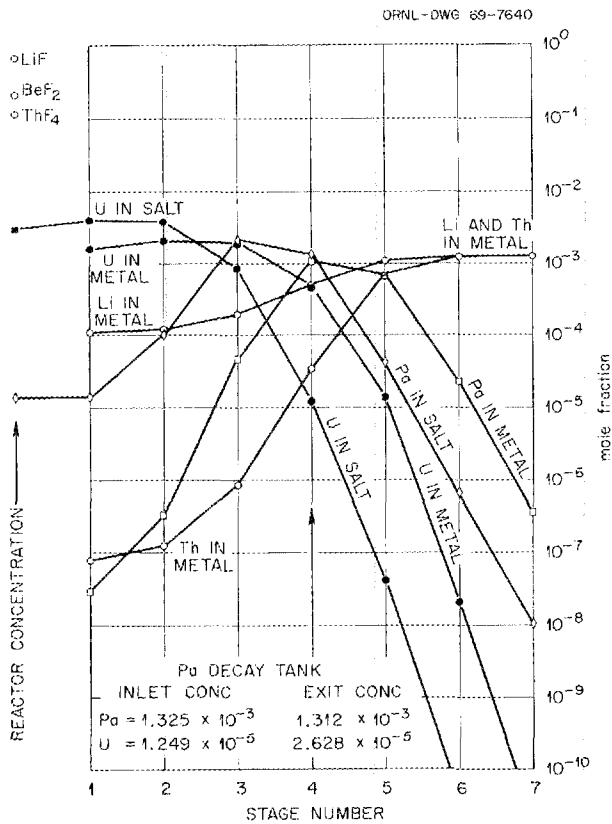


Fig. 1.3. Calculated Concentration Profiles in Reductive Extraction Column.

cause of an inability to maintain optimum operating conditions.

The variation of the calculated steady-state protactinium concentration in the reactor and in the decay tank with bismuth flow rate is shown in Fig. 1.4. The minimum protactinium concentration in the reactor is obtained when the bismuth flow rate is just sufficient to extract the uranium entering the system. At slightly higher bismuth flow rates, protactinium will also be extracted since it is the next component in order of decreasing nobility. At bismuth flow rates slightly lower than the optimum rate (about 5.3 gpm), some of the uranium will not be extracted; instead, it will displace protactinium from the decay tank, forcing the latter to flow out the top of the column if the flow rate is not corrected. In either case, some protactinium would be allowed to return to the reactor, and the effectiveness of the system would be diminished.

The flowsheet has several very desirable characteristics, including: (1) a negligible holdup of fissile ²³³U in the isolation system, (2) an almost immediate return of newly produced ²³³U to the reactor system, and (3) a closed system that precludes loss of protactinium, ²³³U, or other components of the fuel salt. Since the performance of the system is sensitive to variations in operating conditions, attention has been given to methods for controlling the system and for making the perform-

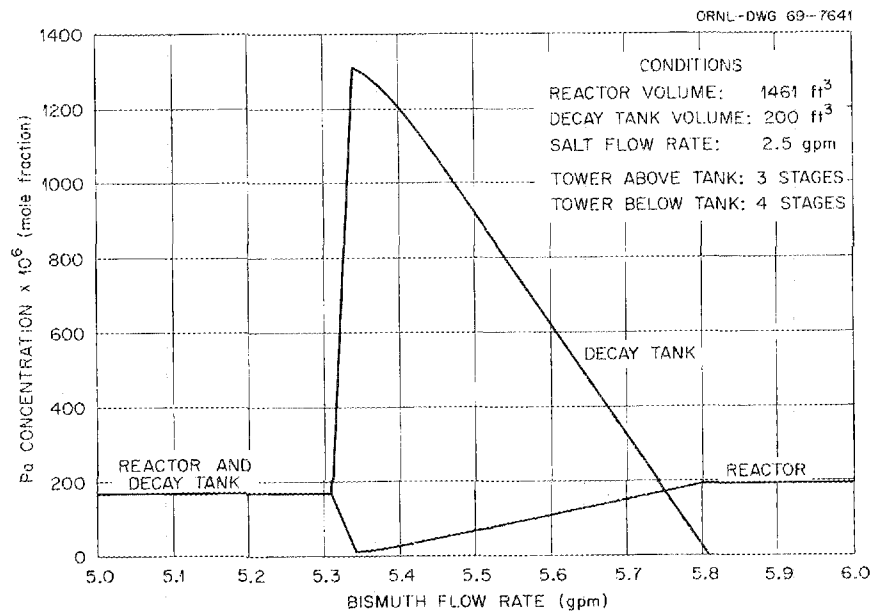


Fig. 1.4. Variation of Calculated Steady-State Protactinium Concentration in the Reactor and in the Decay Tank with Bismuth Flow Rate.

ance less dependent on operating conditions. Removal of uranium from the center of the column makes the system less sensitive to minor changes in operating conditions (see Fig. 1.5). For example, removal of 2% of the uranium in the salt entering the decay tank results in complete stabilization of the system with respect to bismuth flow variations (below the optimum flow rate) as large as 1.03% of the optimum. The uranium concentration in the salt, which is very sensitive to small changes in operating conditions near optimum con-

ditions, increases by a factor of 5000 for a decrease in bismuth flow rate of only 0.037%.

Transient Performance for Case of MSBR Fueled with Uranium. — Calculations were also made to show the transient behavior of the protactinium isolation system. Since the uranium concentration in the salt entering the decay tank had been shown to be very sensitive to operating conditions when these conditions were near optimum, measurement of this concentration was chosen as the means of controlling the system (see Fig. 1.6). It was as-

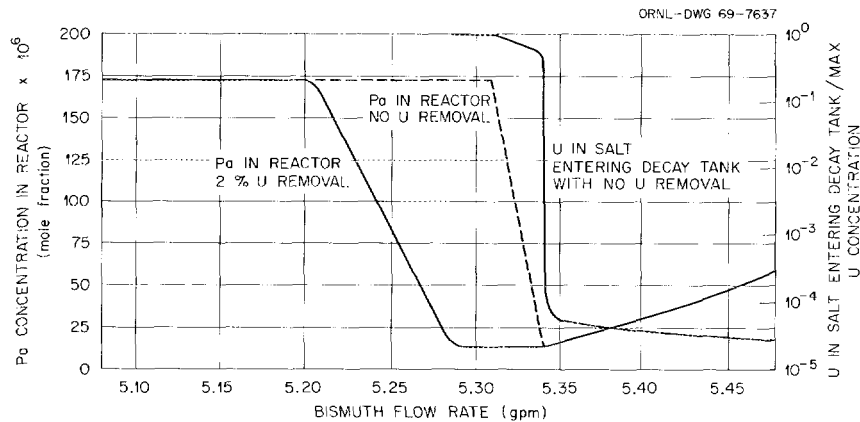


Fig. 1.5. Effect of Uranium Removal and Bismuth Flow Rate on Protactinium Concentration in Reactor and Uranium Concentration in Salt Entering Decay Tank.

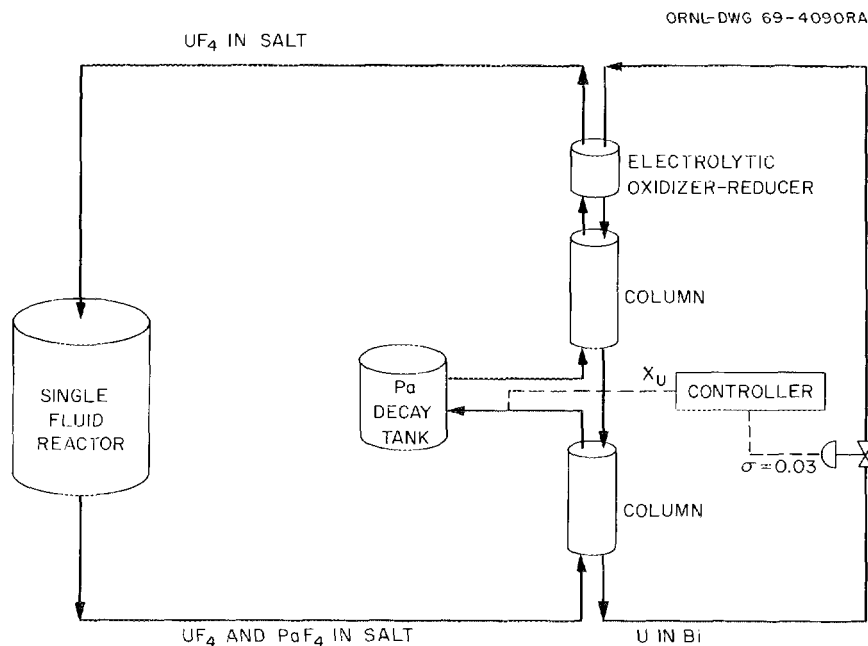


Fig. 1.6. Schematic Diagram Showing Method for Controlling Metal Flow Rate by Measurement of Uranium Concentration in Salt Entering Protactinium Decay Tank.

sumed that the uranium concentration in the salt entering the decay tank could be measured by fluorinating approximately 5% of the stream. The measured uranium concentration would then be used by a controller having proportional, integral, and derivative actions to control the bismuth flow rate through the columns. A random error distributed normally about the controller output and having a specified standard deviation (usually 5%) was considered to be imposed on the control system. The system was assumed to operate for a specified time interval (0.06 day) at each bismuth flow rate selected by the control system. During this period, the extraction columns were assumed to operate at steady state; however, the reactor and decay tank were treated as perfectly mixed vessels having inlet concentrations equal to the column effluent concentrations.

The calculated system response is shown in Fig. 1.7 for an initial protactinium concentration of 10^{-4} mole fraction in the reactor. (The reactor volume

used for the transient calculations was 1000 ft^3 , which was an earlier estimate than the current 1461 ft^3 .) This concentration is seen to decrease to approximately 4×10^{-5} mole fraction, which is acceptably low. This value would be expected to be even lower for a larger reactor volume. It is believed that control of the protactinium isolation system in the manner suggested is practical.

Steady-State Performance for Case of MSBR Fueled with Plutonium. — An MSBR may be fueled initially with plutonium, which would remain in the reactor system during the time required for the ^{233}Pa and ^{233}U inventories to build up. Since the separation factor between Pu and Pa is only about one-half that between U and Pa, we would expect the isolation of Pa from a Pu-fueled system to be more difficult than from a U-fueled system. A typical calculated concentration profile in the extraction column for a Pu-fueled system is shown in Fig. 1.8. It was assumed that the Pa inventory in the system was the steady-state value but that a neg-

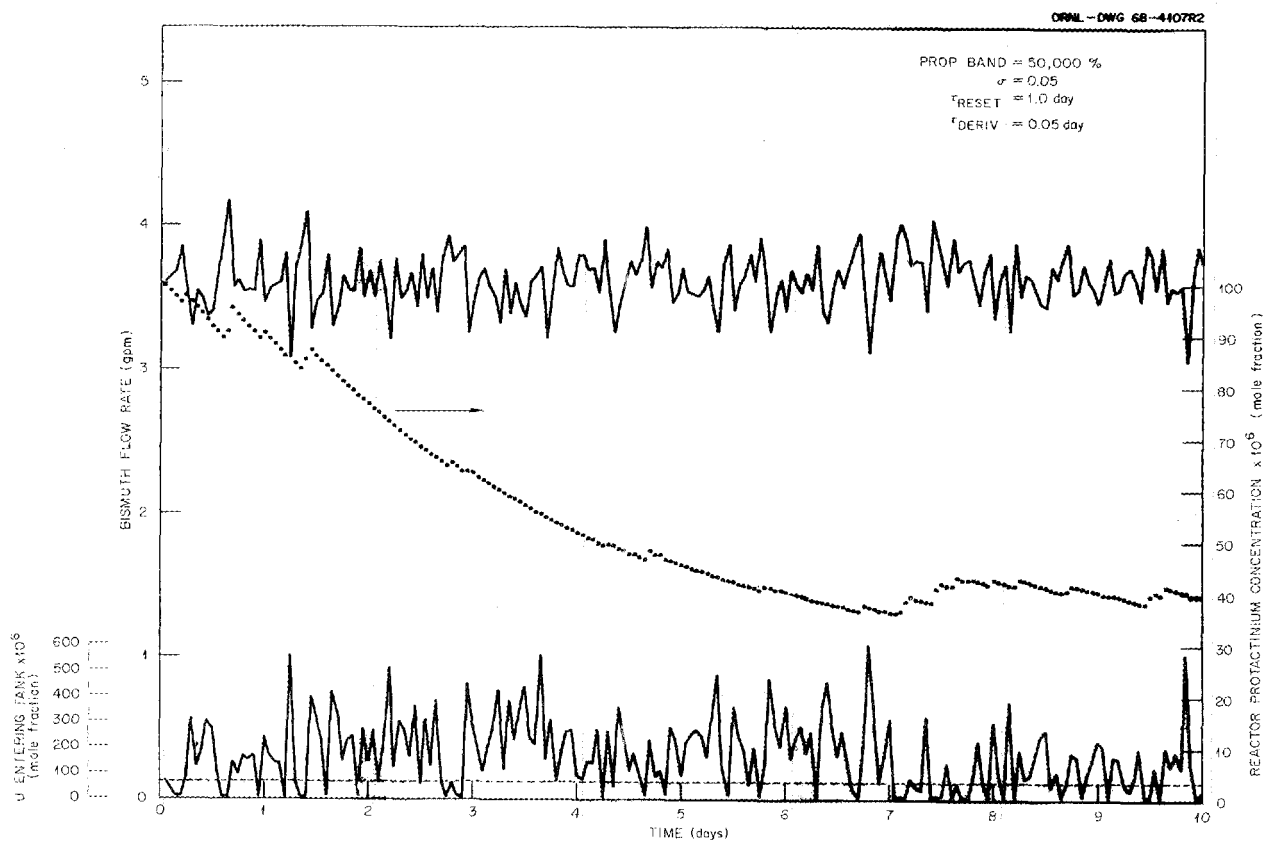


Fig. 1.7. Control of Protactinium Isolation Process Through Measurement of Uranium Concentration in Salt Entering Decay Tank. Random error in bismuth flow rate is shown.

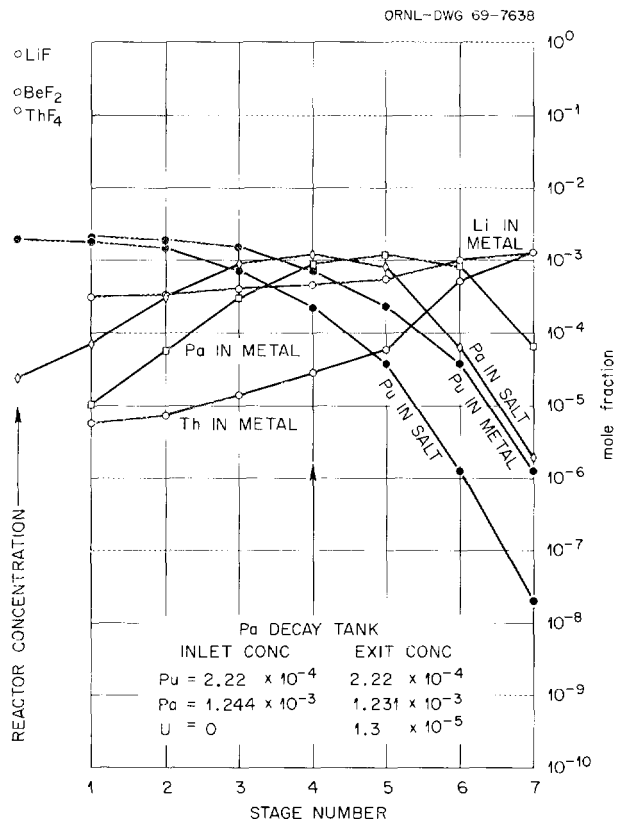


Fig. 1.8. Calculated Concentration Profiles in Reductive Extraction Column for Plutonium-Fueled System.

ligible quantity of uranium was present; although this condition will not actually exist, results from such a case should indicate the relative ease or difficulty to be encountered in isolating Pa from a system fueled with Pu. The Pu concentration in the salt decreases steadily from the inlet value of 0.002 mole fraction to negligible values at the salt outlet. The concentration of Pa in the salt increases from the inlet value of 2.5×10^{-5} mole fraction to a maximum of 1.244×10^{-3} mole fraction, then decreases to negligible values. The concentration of Th in the Bi stream drops from 1.26×10^{-3} mole fraction in the upper part of the column to 5.6×10^{-6} mole fraction at the Bi outlet. The concentration of Li in the Bi decreases from about 1.23×10^{-3} mole fraction in the upper part of the column to about 3.2×10^{-4} mole fraction at the column exit.

The concentrations of Pu and Pa in the salt entering the decay tank are 2.22×10^{-4} and 1.244×10^{-3} mole fraction respectively. The concentration of Pa in the decay tank is 1.231×10^{-3} mole fraction. Under ideal steady-state operating conditions, approximately 87% of the Pa present in the reactor system would be held in the decay tank.

The variation of Pa concentration in the reactor and in the decay tank with bismuth flow rate is shown in Fig. 1.9. The results indicate that isolation of Pa in a reactor fueled with Pu would be feasible.

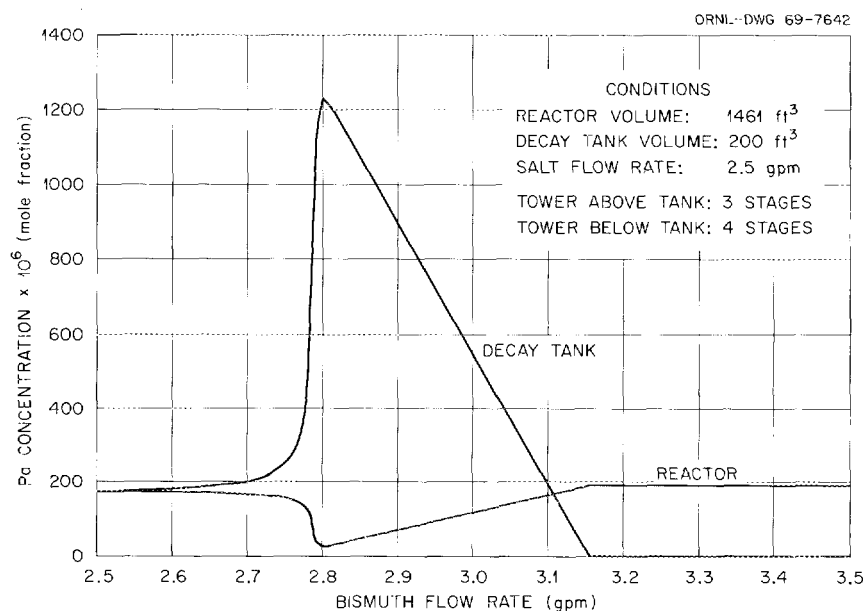


Fig. 1.9. Isolation of Protactinium from an MSBR Fueled with Plutonium.

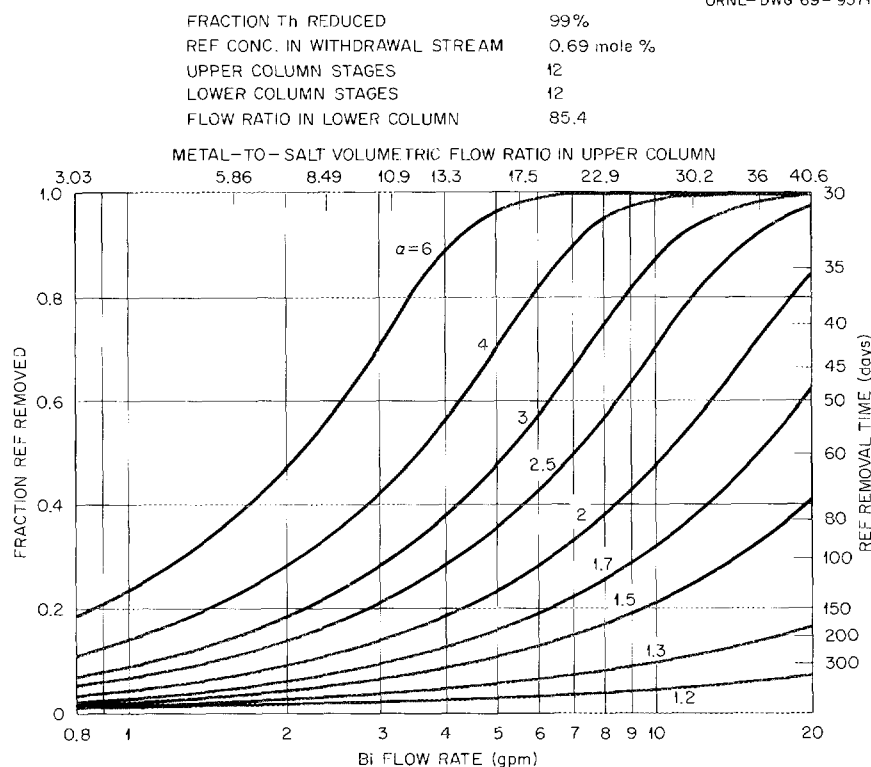


Fig. 1.11. Effects of Bismuth Flow Rate and Rare Earth-Thorium Separation Factor on Fraction of Rare Earths Removed with a 24-Stage Column.

flow ratio in the upper column is about 34 for this Bi flow rate.

System performance for the same operating conditions given above, except that a 12-stage extraction column was used, is shown in Fig. 1.12. In this case, a Bi flow rate of approximately 23 gpm would be required to obtain a rare earth removal efficiency of about 69% for a separation factor of 2.

The effect of the fraction of ThF_4 reduced in the electrolytic cell on rare earth removal is shown in Fig. 1.13 for a separation factor of 2. Operating conditions included a 24-stage column and a rare earth concentration of 0.0069 mole fraction in the withdrawal stream. It should be noted that the importance of this parameter is equal to, if not greater than, that of the other parameters considered. The removal efficiency is significantly decreased when the fraction of ThF_4 reduced is decreased from 99 to 90%; the system becomes ineffective if less than 50% of the ThF_4 is reduced. The concentration of rare earths in the withdrawal stream has essentially no effect on removal efficiency in the range of interest.

The separation factors for several of the rare earths have been determined for a bismuth stream, saturated with thorium, in contact with 72-16-12 mole % $\text{LiF-BeF}_2\text{-ThF}_4$.¹ The separation factors under reference conditions of column operation (see Table 1.1) are expected to be 1.3 for Eu, 1.7 for Pm, 1.8 for La, 2.0 for Sm, 3.0 for Nd, and 3.5 for Ce. The removal times, which range from about 225 days for Eu to approximately 30 days for Nd and Ce, are considered adequate.

Material Balance Calculations for the Reactor System

A computer code has been developed to perform steady-state material balance calculations that describe in detail the nuclear, chemical, and physical processes taking place in the fuel stream of an MSBR. Such calculations are necessary to deter-

¹MSR Program Semiann. Progr. Rept. Feb. 28, 1969, ORNL-4396 (in press).

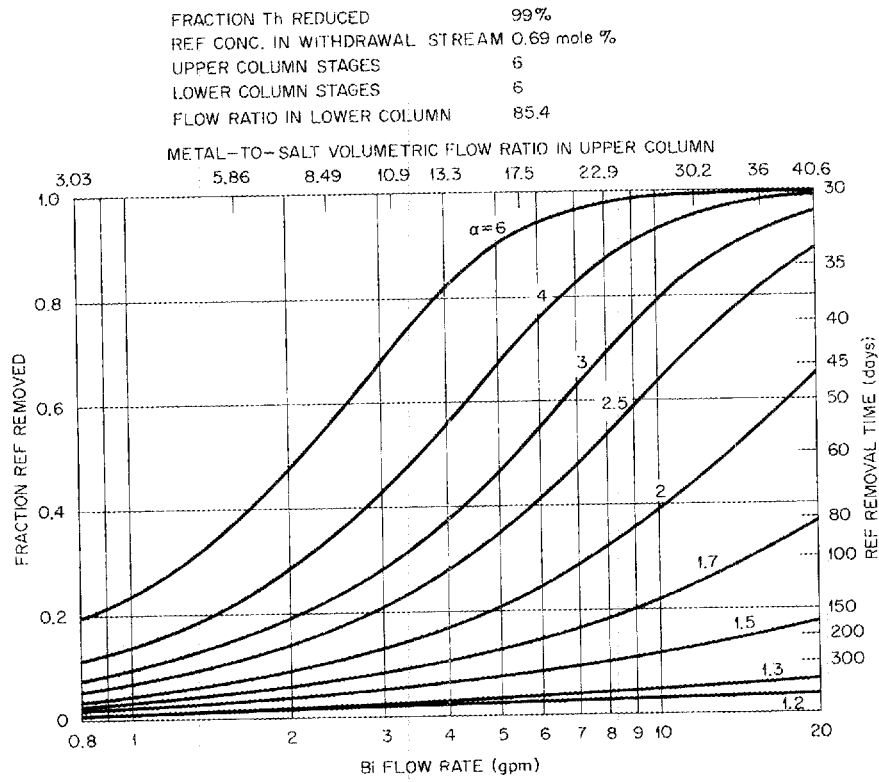


Fig. 1.12. Effects of Bismuth Flow Rate and Rare Earth-Thorium Separation Factor on Fraction of Rare Earths Removed with a 12-Stage Column.

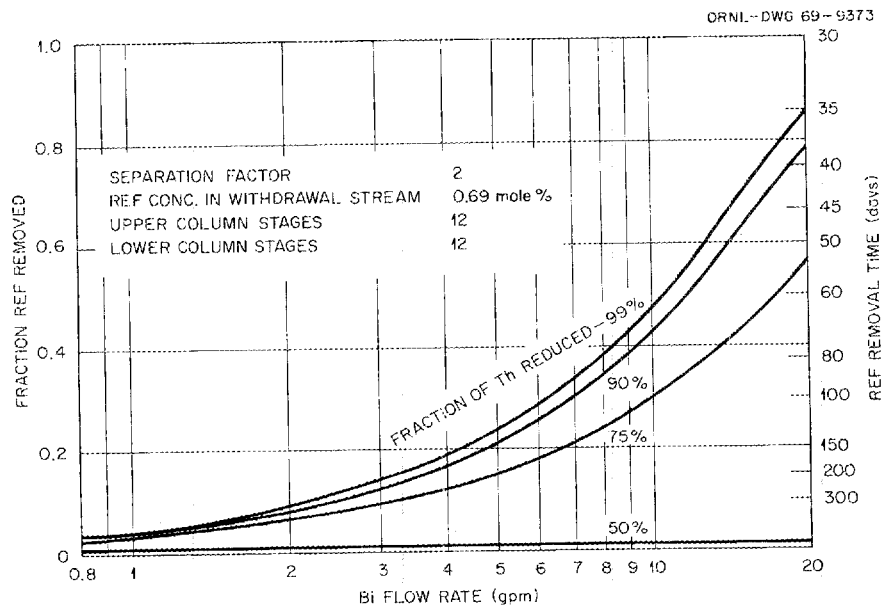


Fig. 1.13. Effects of Fraction of Thorium Reduced and Bismuth Flow Rate on Rare Earth Removal.

Table 1.1. Removal Times for Various Rare Earths at Reference Conditions^a

Rare Earth	Separation Factor	Removal Time (days)
Pm	1.7	63.8
Nd	3.0	30.6
Sm	2.0	43.5
La	1.8	47.7
Eu	1.3	222.0
Ce	3.5	30.3

^aReference conditions include a total of 24 stages and a Bi flow rate of 15 gpm.

mine fission product inventories and heat generation rates, to specify flow rates of streams in the chemical processing plant, and to investigate the effects of changes in chemical processing on the nuclear performance of the MSBR. The code also takes into account the buildup of transuranium isotopes, the production of activation products by neutron capture in the carrier salt, and chain-branching in the fission product decay schemes not included in earlier investigations.²

MSBR Nuclear Data Compilation. — In order to perform these calculations, a library of nuclear data for MSBR applications has been compiled. This library contains half-lives and radioactive decay schemes, three-group neutron capture cross sections, and beta and gross gamma disintegration energies for 687 nuclides. Of these, 178 are isotopes of elements that comprise the carrier salt, graphite, and structural materials and their activation products, 461 are fission products and their daughters, and 48 are isotopes of the actinide elements and their daughters. The radioactive decay schemes include beta and positron emission to isomeric states and ground states of daughter nuclides, alpha emission, and isomeric transition. These decay schemes are based primarily on the compilation of Lederer *et al.*³ The three-group cross-section library consists of a thermal cross

section, a resonance integral, and a fast cross section that was obtained by averaging a cross section over an MSR spectrum given by Prince for $E > 1$ Mev.^{4,5} Where possible, the thermal cross sections and resonance integrals have been corrected for non- $1/v$ behavior by using the data of Prince.^{4,5} In addition to the total neutron absorption cross section, the library contains, for each group, the fraction of neutron captures that lead to fission and (n,γ) , (n,α) , (n,p) , and $(n,2n)$ reactions. These data are based primarily on the compilations of Stehn *et al.*⁶ and Drake.⁷ The fission product library also includes direct fission yields from five fissionable species, ^{233}U , ^{235}U , ^{238}U , ^{232}Th , and ^{239}Pu , based on the data of Katcoff.⁸ The beta-plus-gamma disintegration energies were calculated by using the computer code SPECTRA written by E. D. Arnold, ORNL. This code computes the average energy of a beta particle by integrating the Fermi beta-ray spectrum, taking into account changes in spin and parity.⁹ A new computer code, which reads the data in this nuclear library from cards and prepares an array of transition coefficients to be used in material balance calculations (see below), has been written.

MSBR Material Balance Calculations. — For many purposes it is adequate to consider the recirculating fuel salt in a proposed MSBR to be a well-mixed fluid at steady-state conditions. Under these conditions, the average concentration of a nuclide, i , in the salt is given by the equation

$$0 = FN_{i0} + V \sum_j e_{ij} \lambda_j N_j + \phi V_c \sum_k f_{ik} \sigma_k N_k + \phi V_c \sum_m y_{im} \sigma_{im} N_m - (\lambda_i V + \sigma_i \phi V_c + F + P_i) N_i, \quad (1)$$

where

N_i = concentration of species i , atoms/cc,

N_{i0} = feed concentration of species i , atoms/cc,

⁴B. E. Prince, *MSR Program Semiann. Progr. Rept. Feb. 28, 1967*, ORNL-4119, pp. 79–83.

⁵B. E. Prince, *MSR Program Semiann. Progr. Rept. Aug. 31, 1967*, ORNL-4191, pp. 50–58.

⁶J. R. Stehn *et al.*, BNL-325, 2d ed., Suppl. 2, Vols. I–III (1964).

⁷M. K. Drake, *Nucleonics* **24**, 108 (1966).

⁸S. Katcoff, *Nucleonics* **18**, 163 (1960).

⁹E. D. Arnold, *Handbook of Shielding Requirements*, ORNL-3376 (1964), p. 21 ff.

²J. S. Watson, L. E. McNeese, and W. L. Carter, *MSR Program Semiann. Progr. Rept. Aug. 31, 1967*, ORNL-4191, pp. 245–47.

³C. M. Lederer, J. M. Hollander, and I. Perlman, *Table of Isotopes*, 6th ed., Wiley, New York, 1967.

- F = volumetric flow rate of fuel salt, cc/sec,
 V = fuel salt volume, cc,
 V_c = reactor core volume, cc,
 ϕ = volume- and energy-averaged neutron flux, $\text{bam}^{-1} \text{sec}^{-1}$,
 λ_i = radioactive disintegration constant of species i , sec^{-1} ,
 σ_i = spectrum-averaged neutron cross section, barns,
 σ_{fi} = fission cross section of species i , barns,
 e_{ij} = fraction of disintegrations by species j which lead to formation of species i ,
 f_{ik} = fraction of neutron captures by species k which lead to formation of species i ,
 y_{im} = fission yield of species i from fission of species m ,
 P_i = effective chemical processing rate for species i , cc/sec.

This equation, which is a generalization of that given in ref. (2), is a statement of the fact that, under steady-state conditions, the rate of input of species i into the system by direct feed, radioactive decay of precursors, neutron capture, and fission must equal the rate of loss of species i by radioactive decay, neutron capture, flow out of the system, and chemical processing. Consideration was also given to the following: (1) the loss of Xe and Kr isotopes by diffusion into the graphite moderator, followed by neutron capture or radioactive decay, (2) the production of Xe and Kr isotopes by diffusion into the graphite moderator, followed by neutron capture or radioactive decay, and (3) the production of Xe and Kr isotopes in the fuel salt by migration of gaseous neutron capture products out of the graphite, using a model developed by Kedl and Houtzeel.¹⁰ Provisions are also made in the code for migration of noble gases and noble metals to recirculating bubbles in the fuel salt.¹¹ The bubbles are treated as a separate well-mixed region of fixed residence time in which radioactive decay may take place. Daughter products that are neither

noble gases nor noble metals are assumed to return to the fuel salt.

The volume-averaged thermal flux and the ratio of the resonance flux per unit lethargy to the thermal flux, both of which are required in order to compute the spectrum-averaged cross sections for use in Eq. (1), are obtained from the output of the ROD reactor design code for a given reactor configuration and fuel processing scheme.¹² The ROD code is a multiregion, six-group neutron diffusion code which is used for the primary design and evaluation calculations for the MSBR. Equation (1) is a coupled system of N linear algebraic equations in N unknowns of the form

$$0 = \sum_{k=1}^N a_{ik} X_k + b_i, \quad i = 1, 2, \dots, N. \quad (2)$$

A code has been developed to solve this system of equations which employs the Gauss-Seidel iteration technique, a well-known numerical method that can be shown to converge, provided the coefficients a_{ik} fulfill certain restrictions.¹³

The code requires, as input, the fuel salt volume, the core volume, the graphite volume, the removal times of the elements by chemical processing, and the solubility and mass transfer coefficients for migration of the noble gases to the graphite. In addition, the nuclear library and the three-group weighting factors for the reactor spectrum (described above) are required. The output consists of the composition of the fuel stream (in g-moles/cc and mole fraction of each isotope), the level of neutron poisoning, and the beta and gamma specific power for each nuclide in w/cc. The code also computes the flow rates (in g/day), the compositions, and the power of the various streams of fission products leaving the primary fuel salt loop.

The material balance code is used with a version of the ROD reactor design code to permit calculations to be made for a given reactor configuration over a range of processing conditions. ROD is used to determine the absorption rates in thorium and uranium for an assumed "lumped" fission product poisoning; and the converged absorption rates for the actinide elements from ROD are then

¹⁰R. J. Kedl and A. Houtzeel, *Development of a Model for Computing ^{135}Xe Migration in the MSRE*, ORNL-4069 (1967).

¹¹F. N. Peebles, *Removal of ^{135}Xe from Circulating Fuel Salt of the MSBR by Mass Transfer to He Bubbles*, ORNL-TM-2245 (1968).

¹²O. L. Smith, W. R. Cobb, and H. T. Kerr, *MSR Program Semiann. Progr. Rept. Aug. 31, 1968*, ORNL-4344, p. 68.

¹³L. Lapidus, *Digital Computation for Chemical Engineers*, McGraw-Hill, New York, 1967.

used by the material balance code in computing inventories and poisoning for the individual fission product nuclides and in calculating a new lumped fission product poisoning for use by ROD. This process is repeated until the lumped fission product poisoning calculated by the two codes is satisfactorily close; at this point, all concentrations, absorption rates, etc., are known for the assumed operating conditions.

MSBR Processing Plant Design Calculations. —

Calculations were made for a 2250-Mw (thermal) single-fluid reactor containing 1460 ft³ of fuel salt of approximate composition 71.7-16-12-0.3 mole % LiF-Bef₂-ThF₄-UF₄. The gases Xe, Kr, and tritium have low solubilities in the fuel salt and can be removed by sparging the salt with helium.^{11,14} The noble metals (As, Se, Nb, Mo, Tc, Ru, Rh, Pd, Ag, and Te) do not form fluorides in the salt but appear in the gas space of the fuel pump bowl. They plate out on the graphite and vessel walls as free metals.¹⁵ A 50-sec residence time in the fuel salt was assumed for the noble gases and noble metals as they migrated to the helium bubbles. It was assumed that these materials circulate in the

gas space, which was treated as a well-mixed volume that was stripped on a 110-sec cycle. The plating out of the noble metals on surfaces was not treated as a separate removal mechanism; that is, all noble metals that were removed from the fuel salt were assumed to be present in the stream resulting from stripping the gas space on a 110-sec cycle. A 200-day removal time was assumed for Zr and the seminoble metals (Ga, Ge, Cd, In, Sn, and Sb).

The rare earth fission products, with the exception of Eu, would be removed on a 50-day cycle; a 225-day cycle would be used for Eu. The active metals (Rb, Cs, Sr, and Ba) will be removed by salt discard on a 3000-day cycle. The halogens (I and Br) will be removed from the salt during fluorination on a 50-day cycle.

Table 1.2 gives the processing cycle times, flow rates, and heat generation rates of the principal groups of fission products being withdrawn from the primary salt loop of the MSBR. It is seen that these streams contain about 1.5% of the reactor power and that 90% of this power is generated in the noble gas and noble metal streams. Table 1.3 gives the chemical compositions of these streams of fission products. The most important fission product poisons are listed in Table 1.4. Studies that will give additional information on the effect of chemical processing rates on the nuclear performance of the MSBR are now in progress.

¹⁴R. J. Kedl, *MSR Program Semiann. Progr. Rept. Aug. 31, 1968, ORNL-4344*, pp. 72-75.

¹⁵S. S. Kirslis and F. F. Blankenship, *MSR Program Semiann. Progr. Rept. Aug. 31, 1968, ORNL-4344*, pp. 115-42.

Table 1.2. Processing Cycle Times, Flow Rates, and Heat Generation Rates of Fission Product Streams in a 2250-Mw (thermal) MSBR

Chemical Group	Processing Cycle Time ^a	Flow Rates		Heat Generation Rate (Mw)
		(g/day)	(moles/day)	
Noble gases	50 sec ^b	496.3	4.337	11.37
Noble metals	50 sec ^b	685.4	6.173	16.03
Halogens	50 days	1.9	0.016	0.02
Rare earths	50 days	718.6	5.245	1.29
Zr and seminoble metals	200 days	299.5	3.193	0.43
Active metals	3000 days	79.9	0.740	0.94
Total		2281.6	19.70	30.08

^aThe removal time for each element except europium is assumed to be equal to the processing time for its chemical group. Europium is removed from the fuel salt on a 225-day cycle.

^bIn addition to a 50-sec residence time in the salt, the noble gases and noble metals are assumed to circulate in helium bubbles with a residence time of 110 sec.

Table 1.3. Chemical Composition of MSBR Processing Streams

Noble Gases		Noble Metals		Halogens	
Element	Mole Fraction	Element	Mole Fraction	Element	Mole Fraction
Xe	0.556	Te	0.391	I	0.764
Kr	0.443	Nb	0.317	Br	0.236
T	0.001	Mo	0.174		
		Others	0.118		
Rare Earths		Zr and Semimoble Metals		Active Metals	
Element	Mole Fraction	Element	Mole Fraction	Element	Mole Fraction
Ce	0.382	Zr	0.986	Sr	0.603
Nd	0.250	Sn	0.008	Cs	0.242
Y	0.111	Sb	0.005	Ba	0.141
La	0.103	Others	0.001	Rb	0.014
Pr	0.094				
Others	0.060				

Table 1.4. Fission Product Poisons in a 2250-Mw (thermal) Single-Fluid MSBR

Nuclide	Poisoning $\times 10^2$ (absorptions per fissionable absorption)	Concentration $\times 10^6$ (mole fraction)
^{149}Sm	0.631	0.15
$^{135}\text{Xe}^a$	0.500	9.0×10^{-5}
^{143}Nd	0.160	9.1
^{147}Pm	0.150	3.0
^{151}Sm	0.146	0.43
^{153}Eu	0.044	1.2
^{90}Sr	0.044	608
^{155}Eu	0.039	0.050
^{152}Sm	0.037	0.81
^{145}Nd	0.035	8.0
^{143}Pr	0.025	3.8
^{148}Pm	0.025	0.038
^{93}Zr	0.024	64
^{154}Eu	0.022	0.26
^{137}Ba	0.013	46
^{150}Sm	0.013	1.6
^{148m}Pm	0.012	6.6×10^{-3}
^{141}Ce	0.011	7.2
^{149}Pm	0.010	0.11
^{139}La	0.006	12

^aA ^{135}Xe poison fraction of 0.005 is a fixed design value.

1.2 MEASUREMENT OF DISTRIBUTION COEFFICIENTS IN MOLTEN-SALT-METAL SYSTEMS

During the past year, chemical development of the reductive extraction method¹⁶⁻¹⁹ for the processing of single-fluid MSBR fuels has been continued. Laboratory work has consisted mainly of the measurement of the equilibrium distribution of uranium, zirconium, protactinium, plutonium, rare earths, and other elements between LiF-BeF_2 - ThF_4 solutions and liquid bismuth solutions. The distribution coefficients

$$D_M = \frac{\text{mole fraction of component } M \text{ in the metal phase}}{\text{mole fraction of component } M \text{ in the salt phase}}$$

at a given temperature can be expressed as

$$\log D_M = n \log C_{L_1} + \log I,$$

¹⁶L. E. McNeese and M. E. Whatley, *MSR Program Semiann. Progr. Rept. Feb. 29, 1968*, ORNL-4254, p. 248.

¹⁷L. M. Ferris, *MSR Program Semiann. Progr. Rept. Aug. 31, 1968*, ORNL-4344, p. 292.

¹⁸Chem. Technol. Div. Ann. Progr. Rept. May 31, 1968, ORNL-4272, p. 14.

¹⁹MSR Program Semiann. Progr. Rept. Feb. 28, 1969, ORNL-4396 (in press).

where C_{Li} is the lithium concentration in the metal phase (at. %), I is a constant, and n is the valence of the species in the salt phase. This expression comes directly from the thermodynamic treatment²⁰ of the equilibria involved in the two-phase systems.

Under the experimental conditions used, the bismuth phase could be saturated with thorium without changing the composition of the salt significantly. When the metal phase is saturated with thorium, the distribution coefficients for the various components are the highest attainable in the system. This condition provides a convenient reference point for the correlation of data. Following the convention used previously,¹⁷ distribution coefficients obtained when the metal phase is saturated with thorium are designated as D^{max} , and the separation factors ($\alpha = D_A/D_B$) are denoted by α^* .

Extraction of U, Zr, Pa, Pu, and Th from Single-Fluid MSBR Fuels

The equilibrium distribution of uranium, protactinium, zirconium, and plutonium between several typical LiF-BeF₂-ThF₄ single-fluid MSBR fuel salts and liquid bismuth solutions has been measured. The behavior of these elements is of primary interest in the protactinium isolation portion of the reference reductive extraction flowsheet.¹⁸ Previous studies^{17,18} utilizing LiF-BeF₂-ThF₄ (69.2-19.4-11.4 mole %) as the salt phase established that the extractability of protactinium was between that of uranium and thorium, and that the respective separation factors were high enough to allow isolation of the protactinium. Extraction of zirconium (a major fission product) from LiF-BeF₂-ThF₄ salts had received little, if any, attention. Preliminary work²¹ with LiF-BeF₂ (66-34 mole %) indicated that zirconium would behave like a rare earth fission product. Data obtained in the present study using LiF-BeF₂-ThF₄ (72-16-12 mole %) show that this is not the case. The possibility of using plutonium as a fuel in an MSBR (particularly during startup) has often been considered;²² consequently,

its behavior in a reductive extraction process required study.

All experiments involving zirconium and some of those with uranium were conducted in mild-steel apparatus using the procedure described previously.^{17,18} The other experiments were conducted in a system in which the components that contacted the salt and bismuth (i.e., crucible, sparge tube, and thermowell) were all fabricated of molybdenum. Use of molybdenum allowed simultaneous HF-H₂ treatment of the salt and bismuth, making it possible to conduct several experiments in sequence in the same apparatus using only one initial charge of protactinium. In a typical experiment, 100 to 150 g of salt and about 200 g of bismuth were loaded into the molybdenum crucible. A few milligrams of ²³³Pa contained in hydrofluoric acid solution was evaporated onto about 1 g of LiF; then the LiF containing the ²³³Pa, along with any uranium or plutonium desired, was added to the system. In several experiments in which uranium was present, the ²³³U isotope was used to facilitate accurate analysis. The salt and bismuth were sparged first with 50% HF--50% H₂ for about 24 hr to remove oxide impurities, and then for 3 to 4 hr with pure hydrogen to reduce noble-metal fluorides (Ni, Bi, Mo, etc.). The two phases were then sparged with purified argon to remove all residual hydrogen. Extraction of the various components (U, Pa, Pu, etc.) from the salt into the bismuth was effected by the incremental addition of crystal-bar thorium to the system. The first piece of thorium usually contained about 1 mc of ²³³Pa (via irradiation), which allowed immediate gamma counting of the samples. Thus a rapid indication of the progress of the experiment could be obtained. Filtered samples of each phase were taken at least 4 hr after each addition of thorium. Analyses of these samples provided the data necessary for the calculation of the distribution coefficients. In each experiment, the system was equilibrated under an argon atmosphere. The argon was purified by passage through two traps filled with uranium turnings; the first was held at about 625°C, while the second was maintained at 200 to 300°C.

In most of the previous studies,^{17,18,21,23} the valence of the uranium species in the salt phase during extraction was assumed to be 4. Thermo-

²⁰J. H. Shaffer *et al.*, *Reactor Chem. Div. Ann. Progr. Rept. Dec. 31, 1966*, ORNL-4076, p. 34.

²¹D. M. Moulton *et al.*, *Reactor Chem. Div. Ann. Progr. Rept. Dec. 31, 1967*, ORNL-4229, p. 41.

²²R. E. Thoma, *Chemical Feasibility of Fueling Molten Salt Reactors with PuF₃*, ORNL-TM-2256 (June 20, 1968).

²³D. M. Moulton, W. R. Grimes, and J. H. Shaffer, *MSR Program Semiann. Progr. Rept. Feb. 28, 1968*, ORNL-4254, p. 153.

dynamic considerations,^{24,25} using data for LiF-BeF₂ (66-34 mole %) at 600°C, indicate that significant concentrations of a tetravalent uranium species should exist in the salt phase only when the lithium concentration in the metal phase is less than about 2 wt ppm (0.006 at. %). At higher lithium concentrations, the uranium species in the salt phase should be primarily trivalent. The results of our recent experiments, using refined analytical methods, show that this was generally the case for uranium in LiF-BeF₂-ThF₄ solutions at 600°C. Our results can be illustrated by the plot of $\log D_U$ vs $\log D_{Li}$ (Fig. 1.14) that was prepared by using data obtained in two separate experiments at 600°C with LiF-BeF₂-ThF₄ (72-16-12 mole %). The line has a slope of 3, with the lowest lithium distribution coefficient corresponding to a lithium concentration in the metal phase of about 0.004 at. %. Similar data were obtained in experiments with other salt compositions; in general, the uranium appeared to be primarily trivalent whenever the uranium distribution coefficient was greater than about 0.05. The only exception occurred in an experiment with LiF-ThF₄ (73-27 mole %) at 650°C in which the transition from U(IV) to U(III) in the salt phase apparently was detected. A plot of $\log D_U$ vs $\log C_{Li}$ gave a line of slope 3 when the lithium concentration in the metal phase was greater than about 0.04 at. % (Fig. 1.15), whereas the data obtained at lower lithium concentrations were represented better by a line of slope 4. The ²³³U concentrations in the bismuth phase in the region where U(IV) appeared to predominate in the salt phase were sufficiently high to permit accurate alpha pulse-height analysis. The lowest concentration encountered was 1.72×10^6 alpha counts $\text{min}^{-1} \text{g}^{-1}$, which is equivalent to 172 ppm.

Uranium and zirconium data from two experiments at 600°C using LiF-BeF₂-ThF₄ (72-16-12 mole %) are shown in Fig. 1.16. The slope of this plot of $\log D_{Zr}$ vs $\log D_U$ is 1.33, as would be expected if the uranium existed as a trivalent species in the salt. More importantly, these data show that uranium and zirconium will behave almost identically in the proposed reductive extraction process. Un-

doubtedly, special provision will have to be made to remove zirconium from the system at one point in the process.

The results of previous studies¹⁷ indicated that protactinium would exist as a tetravalent species in the salt phase in a reductive extraction system. Additional experimentation has verified this conclusion. This is illustrated by the plots of $\log D_{Pa}$ vs $\log D_U$ and $\log D_{Th}$ shown in Fig. 1.17. These data were obtained with LiF-BeF₂-ThF₄ (72-16-12 mole %) at 600°C. The slope of the Pa-Th line is 1, as expected from two tetravalent species; the slope of the Pa-U plot is 1.33, which is consistent with the presence of tetravalent protactinium and trivalent uranium in the salt phase. Protactinium was found to be tetravalent in the ex-

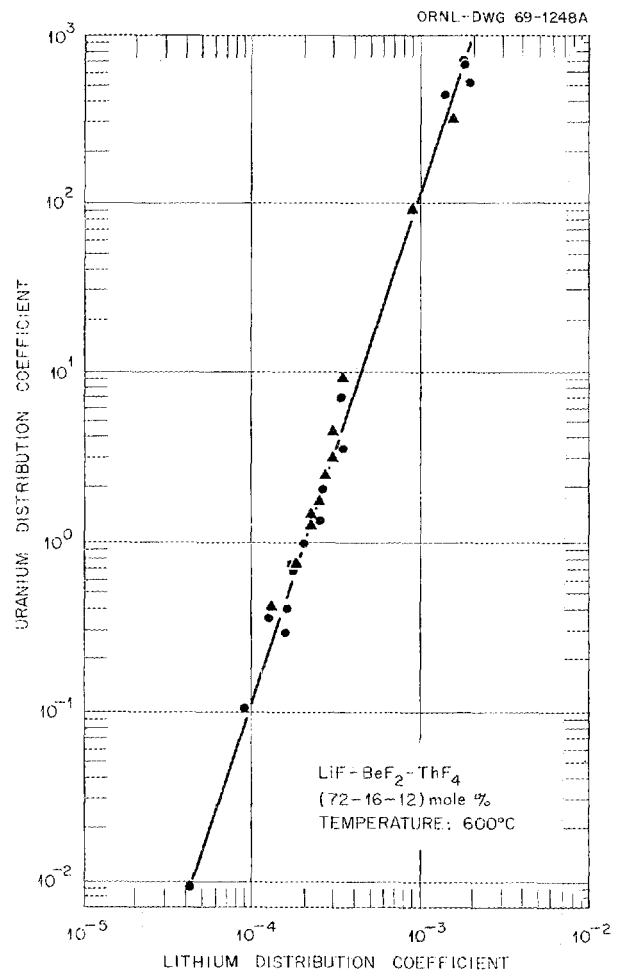


Fig. 1.14. Equilibrium Distribution of Uranium Between LiF-BeF₂-ThF₄ (72-16-12 mole %) and Bismuth Solutions at 600°C.

²⁴L. M. Ferris, *Some Aspects of the Thermodynamics of the Extraction of Uranium, Thorium, and Rare Earths from Molten LiF-BeF₂ into Liquid Li-Bi Solutions*, ORNL-TM-2486 (March 1969).

²⁵C. F. Baes, Jr., "The Chemistry and Thermodynamics of Molten Salt Reactor Fluoride Solutions," in *Thermodynamics*, Vol. II, p. 409, IAEA, Vienna, 1966.

periment with LiF-ThF_4 (73-27 mole %), as shown in Fig. 1.15.

Plutonium was expected to exist as a trivalent species in the salt phase in these systems. This

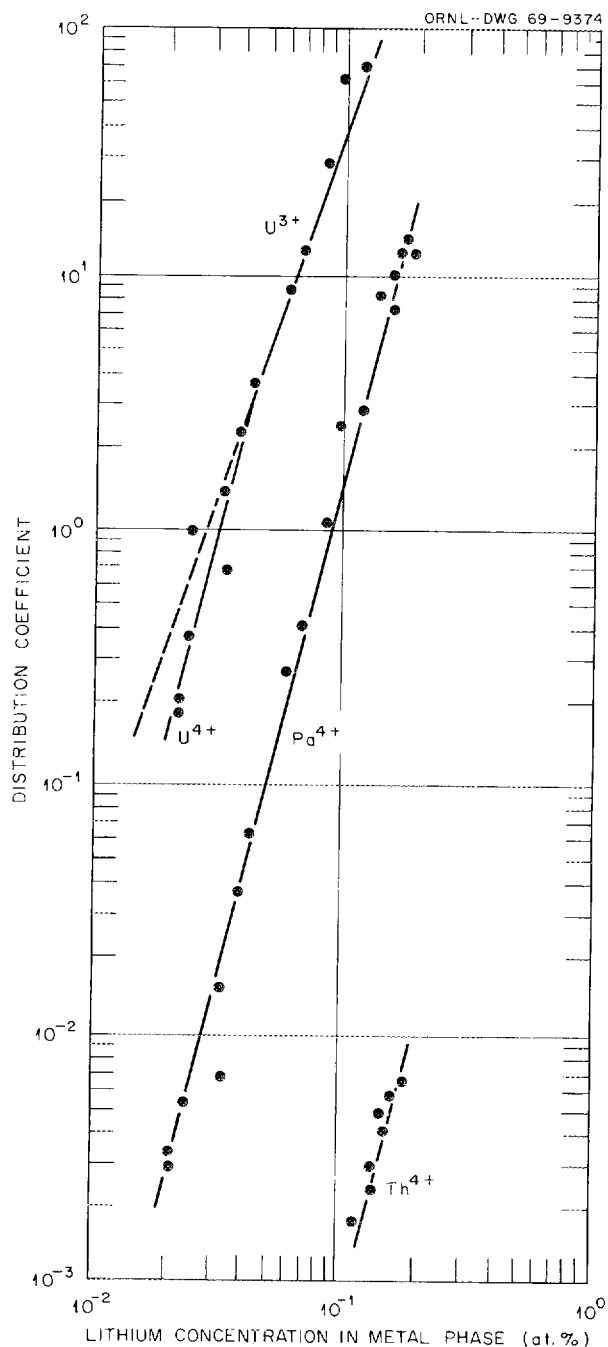


Fig. 1.15. Distribution Coefficients Obtained with LiF-ThF_4 (73-27 mole %) and Bismuth Solutions at 650°C .

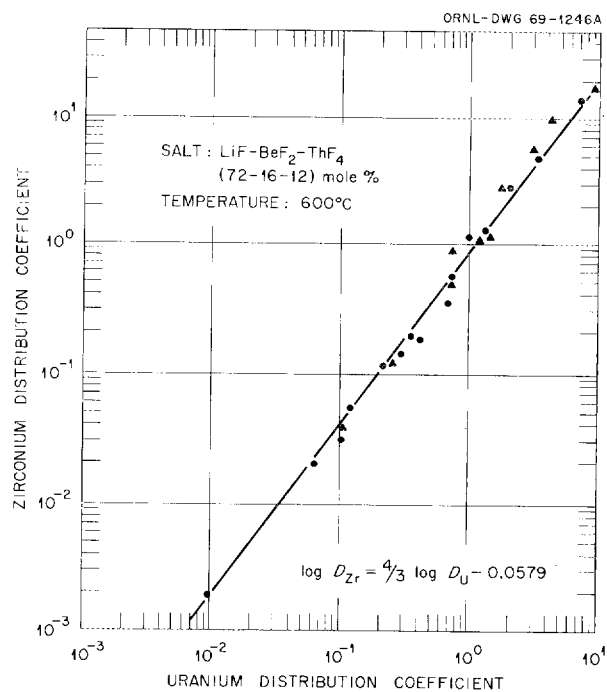


Fig. 1.16. Equilibrium Distribution of Uranium and Zirconium Between $\text{LiF-BeF}_2\text{-ThF}_4$ (72-16-12 mole %) and Bismuth Solutions at 600°C .

expectation was confirmed in the two experiments in which plutonium was used.

Most of the distribution coefficient data obtained so far for uranium, protactinium, zirconium, plutonium, and thorium are compiled in Table 1.5 as equations of the form: $\log D = n \log C_{\text{Li}} + \log I$. These equations were obtained by visually fitting what appeared to be the most representative lines of integral slope through the experimental data. Close inspection of these equations reveals that the distribution coefficients at a given lithium concentration vary in a regular manner as the composition of the salt is changed. The difference in Pa-Th behavior is most noticeable; for example, with the salts containing about 12 mole % ThF_4 , the Pa-Th separation factor increased from about 2100 to 4400 as the "free fluoride" equivalence¹⁷ of the salt increased from -4 to +13 (see Fig. 1.18). Free fluoride equivalence (FF) is defined by:

$$\text{FF} = \text{LiF (mole \%)} - 2\text{BeF}_2 \text{ (mole \%)} \\ - 3\text{ThF}_4 \text{ (mole \%)} .$$

The fact that the Pa-Th separation factors obtained with LiF-BeF_2 (66-34 mole %) and LiF-ThF_4 (73-

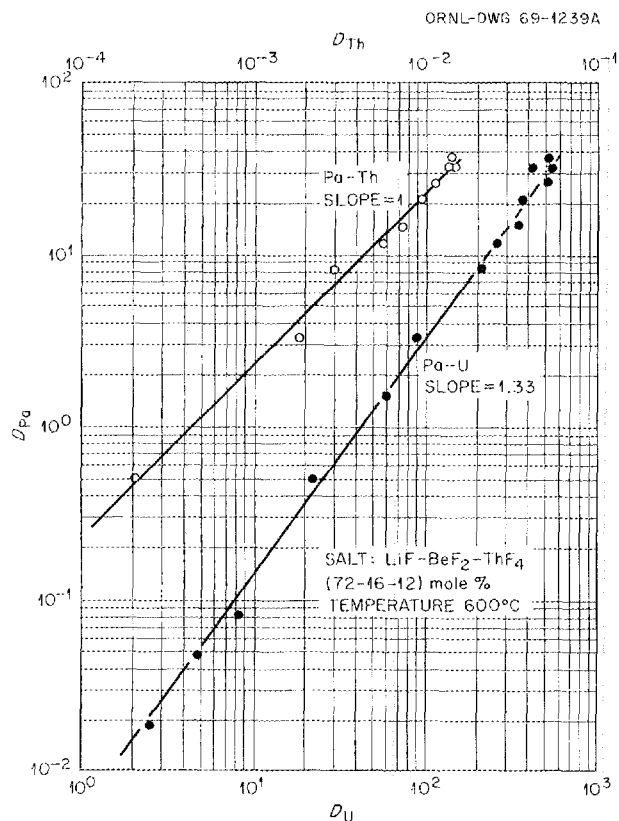


Fig. 1.17. Distribution of Protactinium, Uranium, and Thorium Between LiF-BeF₂-ThF₄ (72-16-12 mole %) and Bismuth Solutions at 600°C.

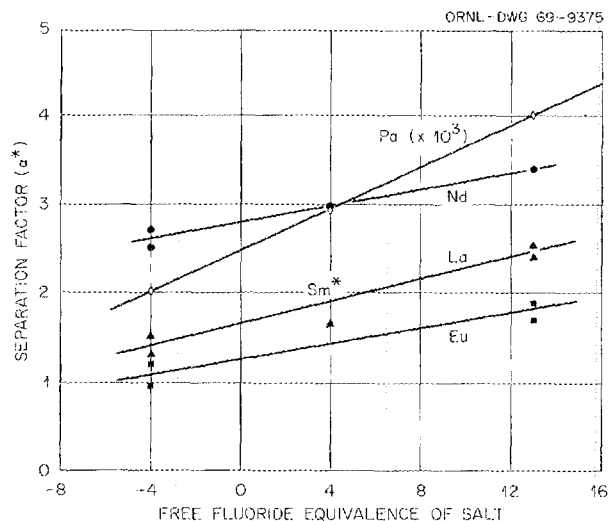


Fig. 1.18. Effect of Free Fluoride Equivalence of LiF-BeF₂-ThF₄ Salts on Rare Earth-Thorium and Protactinium-Thorium Separation Factors at 600°C. Concentration of ThF₄ in the salts is about 12 mole %.

27 mole %) do not correlate with those obtained with salts containing about 12 mole % ThF₄ emphasizes that the free fluoride concept is far from ideal. The U-Pu separation factor was about 10 in the two systems in which plutonium was present. Both the U-Pa and Pu-Pa separation factors are variable since the species do not have the same valence. When the bismuth phase was saturated with thorium ($D_{Th}^{max} = 0.0145$ for salts in which the ThF₄ concentration is 12 mole %), the U-Pa separation factor was about 15 to 20 regardless of the salt composition. These data show that, for MSBR fuel salts containing about 12 mole % ThF₄, separation of uranium from protactinium should be relatively easy, especially if the reductant concentration in the metal phase is kept low. The Pu-Pa separation will be more difficult; however, separation factors greater than 10 can probably be achieved by maintaining a very low reductant concentration in the metal phase.

In several experiments, distribution coefficients for the various components were determined as a function of temperature under conditions where the metal phase was saturated with thorium. The effect of temperature on the metal-thorium separation factors obtained with LiF-BeF₂-ThF₄ (72-16-12 mole %) is shown in Fig. 1.19. It is obvious that these separation factors increase regularly with decreasing temperature.

Extraction of Thorium and Rare Earths from Single-Fluid MSBR Fuels

Distribution coefficients for thorium and several rare earths have been measured using a variety of LiF-BeF₂-ThF₄ solutions in which the ThF₄ concentration was about 12 mole %. The experimental procedure¹⁷ was very similar to that described in the previous section. The data obtained at 600 and 700°C are given in Table 1.6. The rare earth-thorium separation factors generally were in the range of 1 to 3.5 over the range of conditions investigated. As illustrated in Fig. 1.18, the data obtained at 600°C correlate well with the calculated free fluoride equivalence of the salt. Increasing the temperature from 600 to 700°C usually produced a small decrease in the separation factor (Table 1.6). The effect of temperature on La-Th and Sm-Th separation factors was studied more extensively in two separate experiments with LiF-BeF₂-ThF₄ (72-16-12 mole %). The bismuth phase was saturated with thorium in each case. About four pairs

Table 1.5. Equilibrium Distribution of Uranium, Protactinium, Plutonium, Thorium, and Zirconium Between LiF-BeF₂-ThF₄ Salts and Bismuth Solutions

Salt Composition (mole %)			Free Fluoride Equivalence	Temperature (°C)	Equilibrium Expression	Pa-Th Separation Factor (D_{Pa}/D_{Th})
LiF	BeF ₂	ThF ₄				
69.2	19.4	11.4	-4	600	$\log D_{Th} = 4 \log C_{Li} + 2.077$ $\log D_{Pa} = 4 \log C_{Li} + 5.398$ $\log D_U = 3 \log C_{Li} + 5.817$ $\log D_{Pu} = 3 \log C_{Li} + 4.796$	2100
66	34	0	0	600	$\log D_{Th} = 4 \log C_{Li} + 2.453$ $\log D_{Pa} = 4 \log C_{Li} + 6.026$ $\log D_U = 3 \log C_{Li} + 5.971$	3700
72	16	12	4	600	$\log D_{Th} = 4 \log C_{Li} + 1.653$ $\log D_{Pa} = 4 \log C_{Li} + 5.144$ $\log D_U = 3 \log C_{Li} + 5.484$ $\log D_{Pu} = 3 \log C_{Li} + 4.518$ $\log D_{Zr} = 4 \log C_{Li} + 7.254$	3000
75	13	12	13	600	$\log D_{Th} = 4 \log C_{Li} + 1.152$ $\log D_{Pa} = 4 \log C_{Li} + 4.798$ $\log D_U = 3 \log C_{Li} + 5.231$	4400
73	0	27	-8	650	$\log D_{Th} = 4 \log C_{Li} + 0.849$ $\log D_{Pa} = 4 \log C_{Li} + 4.222$ $\log D_U = 3 \log C_{Li} + 4.655 (D_U > 1)$	2360

of samples were taken at each of several temperatures between 525 and 750°C. Average values for the respective distribution coefficients and α^* are given in Table 1.7. The value for α^*_{Sm-Th} was about 2, regardless of the temperature, whereas α^*_{La-Th} decreased from about 2 to 1.5 as the temperature was increased from 525 to 750°C. These results are consistent with the earlier observation¹⁷ that temperature had no significant effect on α^* . The results obtained in this study are in good agreement with those obtained by other workers.²⁶

It is interesting to note that the average values of D_{Th}^{max} obtained at 600 and 700°C (Table 1.6) correspond to thorium concentrations in the bismuth of about 1850 and 5600 wt ppm respectively. These values are in excellent agreement with those obtained by direct measurement of the solubility of thorium in bismuth¹⁷ (see also Sect. 1.3).

Although the rare earth-thorium separation factors increased slightly with increasing free fluoride equivalence of the salt, no significant enhancement of the separation factors over those obtained with the reference carrier salt, LiF-BeF₂-ThF₄ (72-16-12 mole %), appears to be possible by changing the salt composition.

²⁶D. M. Moulton, W. R. Grimes, and J. H. Shaffer, MSR Program Semiann. Progr. Rept. Aug. 31, 1968, ORNL-4344, p. 174.

Table 1.6. Distribution of Thorium, Rare Earths, and Lithium Between LiF-BeF₂-ThF₄ Salts and Thorium-Saturated Bismuth Solutions at 600 and 700°C

Salt Composition (mole %)			Rare Earth	Free Fluoride Equivalence	Temperature (°C)	D^{\max}			
LiF	BeF ₂	ThF ₄				Li	Th	Rare Earth	α^*
						$\times 10^{-3}$	$\times 10^{-2}$	$\times 10^{-2}$	
69.2	19.4	11.4	Eu ²⁺	-4	600	1.45	1.35	1.3	0.96
			Eu ²⁺			1.59	1.30	1.5	1.2
			La ³⁺			1.61	1.51	2.0	1.3
			La ³⁺			1.49	1.44	2.1	1.5
			Nd ³⁺		1.65	1.53	4.2	2.7	
			Nd ³⁺		1.62	1.49	3.8	2.5	
			La ³⁺		700	4.60	4.0	6.0	1.5
			Nd ³⁺			4.23	4.94	13.9	2.8
72	16	12	La ³⁺	+4	600	1.88	1.45	2.3	1.6
			Sm ^a			1.88	1.54	3.2	2.1
			Nd ³⁺			2.16	1.40	4.2	3.0
			Pm ^b				2.5	1.7 ^c	
			Sm ^a		700	5.02	4.55	9.7	2.1
			Nd ³⁺			5.29	4.41	8.6	1.9
75	13	12	Eu ²⁺	+13	600	2.28	1.49	2.8	1.9
			Eu ²⁺			2.33	1.50	2.6	1.7
			La ³⁺			2.43	1.40	3.5	2.5
			La ³⁺			2.40	1.36	3.3	2.4
			Nd ³⁺		2.40	1.50	5.6	3.7	
			Eu ²⁺		700	6.19	3.92	6.7	1.7
			La ³⁺			6.48	4.35	7.6	1.8
			Nd ³⁺			6.95	4.11	14.0	3.4

^aThe average valence of Sm in this experiment was 2.7, indicating that both Sm²⁺ and Sm³⁺ were present in the salt.

^bThe valence of the Pm species in the salt phase was not determined in this experiment.

^cThe thorium analyses for this experiment are not yet available; this value for α^* was calculated using $D_{\text{Th}}^{\max} = 0.014$.

Table 1.7. Effect of Temperature on Rare Earth-Thorium Separation Factors

Salt: $\text{LiF}\cdot\text{BeF}_2\cdot\text{ThF}_4$ (72-16-12 mole %).

Bismuth was saturated with thorium in each case.

Temperature (°C)	Rare Earth	Th Concentration in Bi (ppm)	D_{RE}	D_{Th}	$\alpha_{\text{RE-Th}}^*$
525	La	843	0.0125	0.00633	1.97
	Sm	785	0.0115	0.00589	1.95
560	La	1,290	0.0206	0.00968	2.13
	Sm	1,210	0.0189	0.00908	2.08
600	La	2,082	0.0251	0.0156	1.60
	Sm	2,080	0.033	0.0156	2.11
650	La	3,830	0.0448	0.0287	1.56
	Sm	3,788	0.0562	0.0284	1.98
700	Sm	6,022	0.0962	0.0452	2.13
750	La	10,230	0.113	0.0768	1.47
	Sm	8,772	0.113	0.0658	1.72

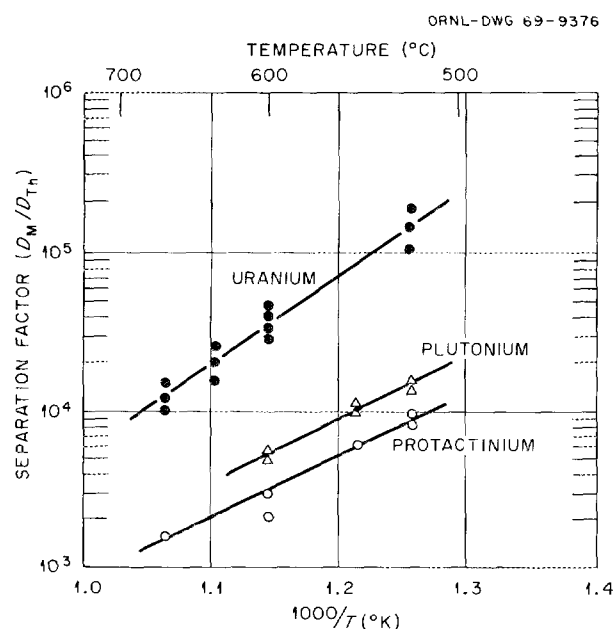


Fig. 1.19. Variation of Metal-Thorium Separation Factors with Temperature. Data obtained with $\text{LiF}\cdot\text{BeF}_2\cdot\text{ThF}_4$ (72-16-12 mole %). Bismuth phase was saturated with thorium at each temperature.

Extraction of Transuranium Elements from $\text{LiF}\cdot\text{BeF}_2\cdot\text{ThF}_4$ (72-16-12 mole %) at 600°C

The behavior of the transuranium elements must be considered in a reductive extraction process for an MSBR that is initially fueled with plutonium. In this connection, experiment PE11 was conducted, using $\text{LiF}\cdot\text{BeF}_2\cdot\text{ThF}_4$ (72-16-12 mole %) as the salt phase, to determine the behavior of Pu, Am, Cm, and Cf. In this experiment, 100 g of the salt was contacted with 200 g of Bi at 600°C. In addition to its listed composition, this salt initially contained the following: (in ppm) ^{231}Pa , 100; ^{239}Pu , 4500; and (in counts $\text{min}^{-1}\text{g}^{-1}$) ^{241}Am , 2×10^7 ; ^{243}Am , 2.5×10^6 ; ^{244}Cm , 6×10^6 ; and ^{252}Cf , 1.5×10^5 . The Pa and transuranium elements were transferred to the Bi phase by the incremental addition of crystal-bar Th to the system. The results of this experiment are shown graphically in Fig. 1.20. The Pu, Cf, and Am are seen to be nearly inseparable, with Cm being the only transuranium element that is well separated from the others. The separation factor for Am and Cm is about 7. The separation factor for Cm and Nd (data from a prior experiment) is about 200. From

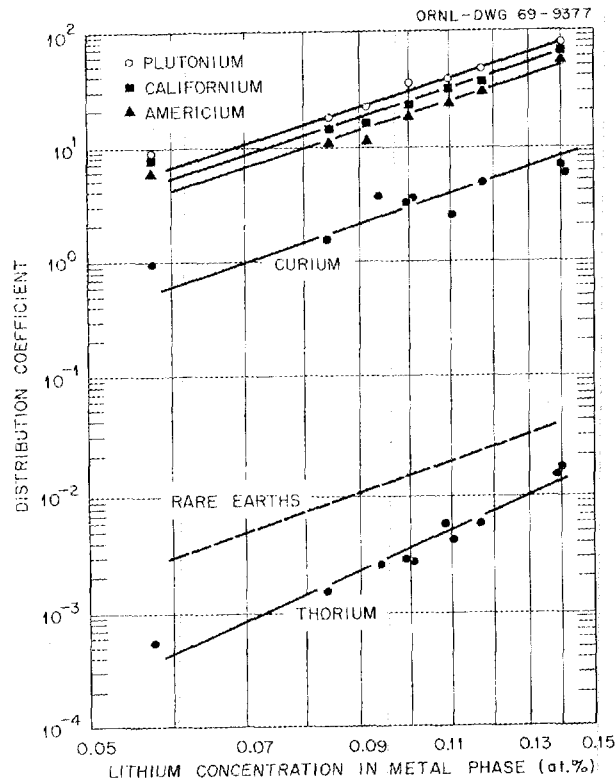


Fig. 1.20. Distribution of the Actinide Elements Between $\text{LiF-BeF}_2\text{-ThF}_4$ (72-16-12 mole %) and Bismuth Solutions at 600°C .

this information, we would expect the Cm to behave much like Pa and to accumulate in the Pa isolation vessel. If the fuel is processed on a fairly short cycle, this isolation of the Cm would prevent the buildup of higher transuranium elements. The Am would follow the Pu. All of the transuranium elements studied are easily separated from the rare earths; thus, reductive extraction may be a useful technique for this separation.

1.3 SOLUBILITIES OF THORIUM AND PROTACTINIUM IN BISMUTH

Knowledge of the solubilities of thorium, protactinium, and other metals in bismuth is essential to the development of the reference reductive extraction process¹⁸ for a number of reasons. The solubility of thorium in bismuth is equivalent to the

maximum reductant concentration attainable in the bismuth at a given temperature. Calculations²⁷ have shown that, in order to achieve the desired operating conditions, the solubility of protactinium in bismuth should be as high as that of thorium. Furthermore, insoluble intermetallic compounds can be formed under some conditions. Throughout our studies of the reductive extraction process, we have been constantly alert to solute interactions in the bismuth phase that could decrease the solubility of thorium and/or result in the formation of an insoluble intermetallic phase. The data obtained in this program show that the solubility of thorium at 600°C (about 2000 ppm) is not affected by the presence of uranium and zirconium at concentrations of 2000 ppm, either singly or in combination. Similar results were obtained with uranium, plutonium, and thorium; solutions containing about 2000 ppm of thorium and at least 2000 ppm of uranium and plutonium have been produced. Lithium and lanthanum, in concentrations up to about 1000 ppm, had no detectable effect on the thorium solubility. Nickel was the only element encountered in this work that had a marked effect; consequently, its interaction with thorium in bismuth solution was studied more extensively.

Solubility of Thorium in Bismuth

Measurements of the solubility of thorium in bismuth were made over the temperature range of 450 to 817°C . In one experiment, the system was contained in a mild-steel crucible; all samples were taken with stainless steel, vacuum-type filters. In another experiment, the system was contained in a molybdenum crucible, and the samples were taken with either molybdenum or molybdenum-coated stainless steel filters. Purified argon was used as the cover gas in each experiment. The data obtained are plotted in Fig. 1.21; the line shown is:

$$\log S (\text{wt ppm Th}) = 7.717 - 3850/T.$$

Within the limits of experimental error, the values obtained using the molybdenum crucible and samplers were the same as those obtained using the mild-steel crucible. These data are in good agreement with those reported by Greenwood,²⁸ but are

²⁷Chem. Technol. Div. Ann. Progr. Rept. May 31, 1968, ORNL-4272, p. 20.

²⁸G. W. Greenwood, *The Solubilities of Uranium and Thorium in Liquid Bismuth*, AERE-M/R-2234 (June 1957).

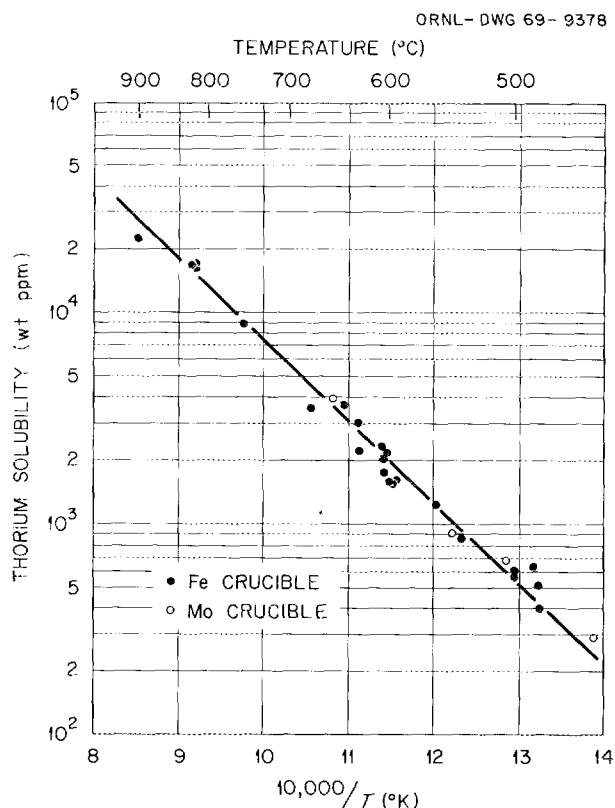


Fig. 1.21. Solubility of Thorium in Bismuth.

lower than those given by Hayes and Gordon²⁹ and by Bryner and Brodsky.³⁰

Solubility of Protactinium in Bismuth

In the reductive extraction process being evaluated, it is desirable that the solubility of protactinium in bismuth be at least as high as that of thorium. An estimate of the solubility of protactinium in bismuth was obtained in the following experiment: About 100 mg of ²³¹Pa was dissolved in 100 g of LiF-BeF₂ (66-34 mole %) by hydrofluorination in the presence of 50 g of bismuth. After stripping residual HF and H₂ from the salt with pure argon, crystal-bar thorium was added to the system at 600°C until about 95% of the protac-

tinium had transferred to the bismuth phase. The protactinium concentration in the bismuth, by analysis, was 2078 ppm. The thorium concentration, by analysis, was about 300 ppm; however, this value was probably incorrect, based on the distribution coefficient data obtained in a later experiment. The actual thorium concentration was probably about 60 ppm. The temperature of the system was reduced to 550°C without changing the protactinium concentration in the metal phase detectably. However, at 500°C, the protactinium concentration in the bismuth decreased to about 1200 ppm, with a corresponding decrease in the protactinium material balance. The protactinium concentration of 2078 ppm and a material balance of nearly 100% were re-established when the system was reheated to 550°C. Using distribution coefficient data obtained in other experiments at various temperatures, the metal phase at 500°C was estimated to contain no more than 10 ppm each of lithium and thorium; the solid phase probably contained less than 20% thorium. Thus, the value of 1200 ppm obtained at 500°C appears to be very close to the true solubility of protactinium in bismuth at this temperature. Over the temperature range of 500 to 700°C, the heats of solution of uranium, thorium, and plutonium bismuthides are nearly the same³¹ (Fig. 1.22). Assuming that protactinium behaves similarly, the solubility of protactinium in bismuth at 600°C is estimated to be about 4500 ppm.

Toward the end of the experiment outlined above, sufficient UF₄ was added to the system to effect oxidation of some of the protactinium from the metal phase. Under the equilibrium conditions established, the metal phase contained about 668 ppm of Pa and 1090 ppm of U, with corresponding uranium and protactinium material balances of nearly 100%. Thus, the mutual solubility of uranium and protactinium in bismuth appears to be high.

Mutual Solubility of Thorium and Nickel in Bismuth

The effect of nickel on the solubility of thorium in bismuth at 600°C has been investigated in two recent experiments. The system was contained under an argon atmosphere in a mild-steel crucible in experiment 5639, and in a molybdenum crucible

²⁹E. E. Hayes and P. Gordon, *The Solubility of Uranium in Liquid Metals and Alloys*, TID-2501-De1. (1957), p. 115.

³⁰J. S. Bryner and M. B. Brodsky, *Proc. Intern. Conf. Peaceful Uses At. Energy*, 2nd, Geneva, 1958, 7, 209 (1958).

³¹J. A. Lane, H. G. MacPherson, and F. Maslan (eds.), *Fluid Fuel Reactors*, Addison-Wesley Publishing Co., Inc., Reading, Mass., 1958, p. 724.

ORNL-DWG 68-11057A

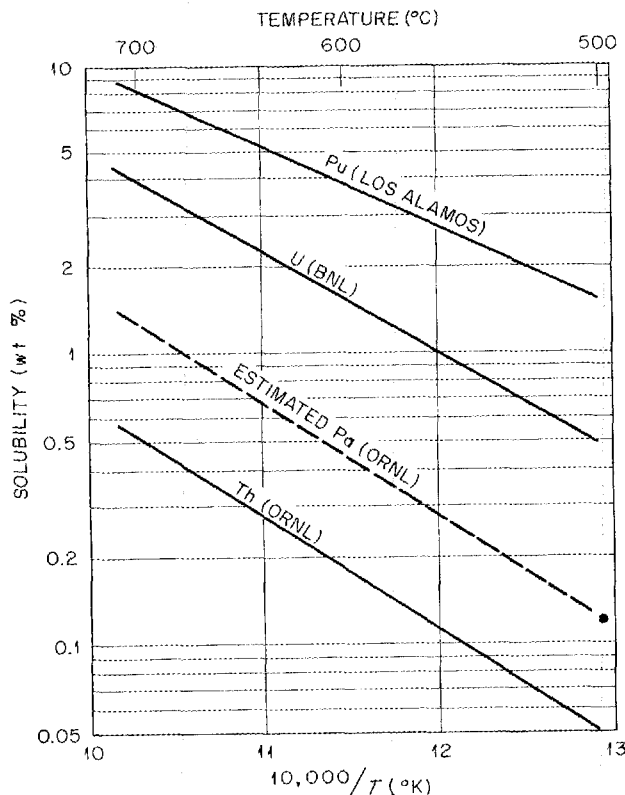


Fig. 1.22. Solubilities of Actinide Metals in Liquid Bismuth.

in experiment LA-1. Initially, sufficient crystal-bar thorium was added to just saturate the bismuth at 600°C; lanthanum, at a concentration of about 1000 ppm, was also present in experiment LA-1. Then, small portions of nickel were added to the systems. After each addition, a period of at least 4 hr was allowed for the attainment of equilibrium before a filtered sample of the liquid phase was taken for analysis. The results are shown in Fig. 1.23. The values denoted by solid circles in experiment 5639 were obtained by back-titration with crystal-bar thorium. The data from these experiments can be expressed as a mole fraction solubility product,

$$K_{sp} = X_{Th} X_{Ni} = 6.2 \times 10^{-7},$$

over the range of concentrations investigated. This is the type of behavior that would be expected if the Th/Ni atom ratio in the solid phase were 1, as apparently was the case here. Material balance calculations (taking into account the amounts of material added or removed from the system) gave

ORNL-DWG 69-9379

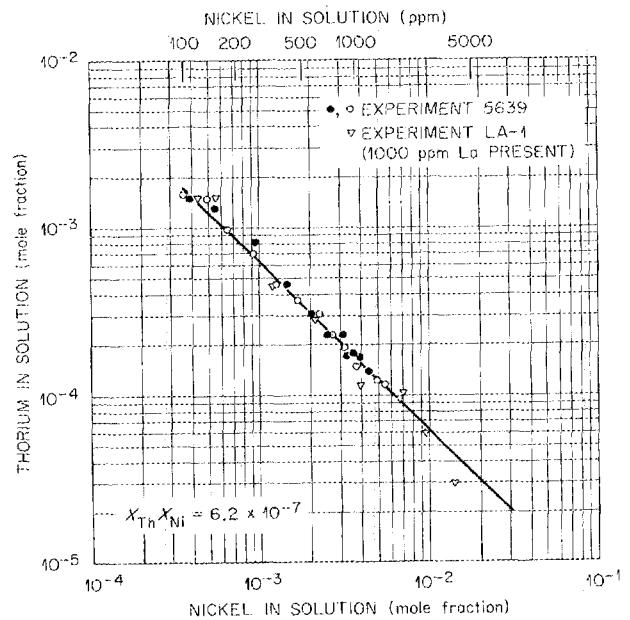


Fig. 1.23. Mutual Solubility of Thorium and Nickel in Bismuth at 600°C.

Th/Ni atom ratios in the solid phase of 0.89 to 0.99 throughout each experiment. Preliminary analyses of the solid phase³² indicate that it is probably a ternary bismuthide, ThNiBi₂, but it could be a thorium-nickel compound. The data indicate that a bismuth solution saturated with thorium at 600°C could accommodate up to about 100 ppm of Ni before a thorium- and nickel-containing solid would precipitate. Additional evidence to this effect was obtained in experiment 5639. After back-titration with thorium, a large excess of crystal-bar thorium was added to the system to ensure that the bismuth was saturated with thorium; then, about six samples of the liquid phase were removed for analysis. The average thorium and nickel concentrations in the liquid were about 2000 and 100 ppm respectively. It was also noted that the lanthanum concentration in the liquid phase remained constant even when the nickel concentration was 5000 ppm.

1.4 METAL-TRANSFER PROCESS FOR RARE EARTH-THORIUM SEPARATION

Because the rare earth-thorium separation factors attainable by reductive extraction are some-

³²L. M. Ferris and F. J. Smith, ORNL Chemical Technology Division, unpublished data.

what lower than desired, alternative methods for effecting this separation are being sought. One possibility is the selective transfer of the rare earths from the $\text{LiF-BeF}_2\text{-ThF}_4$ donor salt through a liquid metal phase to an acceptor salt. All oxidation-reduction equilibria between the respective salts and the metal phase must be satisfied. Differences in the chemical activities of the various species in the two salts provide the driving force for the transfer of a given component, starting with nonequilibrium conditions. At equilibrium, the desired conditions are those where (1) a large fraction of the rare earth is present in the acceptor salt, and (2) the thorium decontamination factor

Experimentally, this technique was tested using an $\text{LiF-BeF}_2\text{-ThF}_4$ donor salt, which initially contained the rare earth, that was separated from the acceptor salt by a thorium-saturated bismuth phase. In each experiment, the number of moles of donor salt was equal to the number of moles of acceptor salt. The equilibrium distribution of thorium, lithium, and the rare earth among the three phases was then determined at about 600°C . (Beryllium and the anionic species do not transfer in these systems.) In each system tested, equilibrium was reached in less than 48 hr without agitation of any of the phases. The results of the experiments are given in Table 1.8. It is seen that none of the ac-

$$DF_{\text{Th}} = \frac{(\text{mole fraction Th in donor}) (\text{mole fraction RE in acceptor})}{(\text{mole fraction Th in acceptor}) (\text{mole fraction RE in donor})}$$

is high (hopefully greater than 100).

Table 1.8. Rare Earth-Thorium Separations in Metal-Transfer Experiments
(At equilibrium, with equal moles of donor and acceptor salts. Bismuth phase saturated with thorium.)

Donor Salt	Acceptor Salt	Temperature ($^\circ\text{C}$)	Rare Earth	Amount of Rare Earth Transferred (%)	Thorium Decontamination Factor
$\text{LiF-BeF}_2\text{-ThF}_4$ (75-13-12 mole %)	LiF-BeF_2 (66-34 mole %)	600	Eu(II)	39	21
$\text{LiF-BeF}_2\text{-ThF}_4$ (75-13-12 mole %)	LiF-BeF_2 (66-34 mole %)	600	La(III)	6.4	3.5
$\text{LiF-BeF}_2\text{-ThF}_4$ (72-16-12 mole %)	LiF-BeF_2 (57-43 mole %)	600	La(III)	5 ^a	3 ^a
$\text{LiF-BeF}_2\text{-ThF}_4$ (72-16-12 mole %)	LiCl	640	La(III)	4.1	b
$\text{LiF-BeF}_2\text{-ThF}_4$ (72-16-12 mole %)	LiCl-LiF (90-10 mole %)	640	La(III)	20	23
$\text{LiF-BeF}_2\text{-ThF}_4$ (72-16-12 mole %)	LiCl-LiF (80-20 mole %)	640	La(III)	35	12
$\text{LiF-BeF}_2\text{-ThF}_4$ (72-16-12 mole %)	LiCl-LiF (80-20 m mole %)	600	La(III)	34	10
$\text{LiF-BeF}_2\text{-ThF}_4$ (72-16-12 mole %)	LiBr	600	La(III)	1.4	
$\text{LiF-BeF}_2\text{-ThF}_4$ (72-16-12 mole %)	LiBr-LiF (90-10 mole %)	600	La(III)	9	20

^aCalculated from distribution coefficient data from separate experiments with the respective salts.

^bContamination of the LiCl with a trace of the $\text{LiF-BeF}_2\text{-ThF}_4$ salt precluded determination of this value. The thorium DF should be greater than 300 based on the distribution coefficient data obtained in other experiments.³³

ceptor salts used fulfilled both of the desired criteria. Significant transfer of lanthanum was achieved using LiCl-LiF solutions as the acceptor; however, the thorium decontamination factor was only in the range of 10 to 20. Studies³³ with pure LiCl indicate that high thorium decontamination factors could be achieved but that only a small fraction of a trivalent rare earth such as lanthanum or neodymium would be transferred. The search for an acceptor salt that provides the desired results is continuing.

1.5 DEVELOPMENT OF A MOLTEN SALT-BISMUTH ELECTROLYTIC CELL

Experiments with Static Cells

An electrolytic oxidizer-reducer is an essential part of the proposed flowsheets³⁴ for the removal of protactinium and of rare earths from a single-fluid MSBR. Reactions at the cell anode are related to the oxidation of metals from Bi streams exiting from extraction columns, while reactions at the cathode are related to the preparation of Bi streams, containing Th and Li metal, that are fed to the extraction columns. The anode and cathode current densities are important because they determine the size of the electrolytic cells. The concentrations of materials to be oxidized from the Bi are so low that they will present a rate limitation if they are selectively oxidized. The diffusion-limited current density for oxidation of uranium from bismuth at a uranium concentration of 0.0016 mole fraction was estimated to be 0.15 amp/cm² (based on uranium diffusivity in bismuth of 2.5×10^{-5} cm²/sec,³⁵ a diffusion layer thickness of 5×10^{-3} cm, and a bismuth volume of 21.3 cc/g-atom). This corresponds to an anode area of 21.7 ft² for the Pa isolation system. The area can be considerably decreased by oxidizing the major component present in the anode, bismuth. Although this oxidation produces BiF₃, a corrosive material, the presence of such material is more desirable than using very large anode areas.

³³F. J. Smith, ORNL Chemical Technology Division, unpublished data.

³⁴L. E. McNeese and M. E. Whatley, *MSR Program Semiann. Progr. Rept. Feb. 28, 1968*, ORNL-4254, p. 248.

³⁵J. C. Hesson, H. E. Hootman, and L. Burris, Jr., *Electrochem. Technol.* 3, 240 (1965).

The BiF₃, which dissolves in the molten fluoride electrolyte, can be used to oxidize the materials from the incoming bismuth stream by counter-current contact.

Although a flow-type electrolytic cell will be used in the processing system, a considerable amount of information can be gained from tests with static cells during the period in which facilities for testing flow cells are being built. Therefore, two series of experiments were carried out in static cells made of quartz. A static quartz cell was also used in a scouting test for simulating the generation of heat by using ac rather than dc power. In addition, a static cell made entirely of metal was installed. Results of experiments with these cells are given below.

Quartz Cell Experiments Using DC Power. --

The quartz cell shown in Fig. 1.24 consists of a flat-bottomed quartz tube (4 in. OD) with metal flanges. The bottom of the cell contains a quartz divider, which gives two equal compartments about 3 in. deep. The compartments were filled with bismuth to within about $\frac{1}{2}$ in. of the top of the divider to produce electrodes with an exposed area of about 30 cm² each. A 6-in. layer of molten salt (66-34 mole % LiF-BeF₂) covered the electrodes and served as the electrolyte. Two molybdenum tubes contained within quartz sleeves were introduced from the top of the vessel through the molten salt and terminated near the bottom of the electrode compartments; they served as the electrode leads as well as gas sparge lines. Means for obtaining filtered samples of salt or bismuth were provided.

Prior to each series of experiments, the bismuth was sparged with hydrogen at 700°C for about 16 hr. About 1.8 kg of molten salt that had been previously purified by hydrofluorination, hydrogen reduction, and filtration was then introduced into the cell. Viewing slits were provided in the furnace to allow observation of the salt-Bi interface in the vicinity of the quartz divider. Prior to the transfer of molten salt to the cell, the bismuth surfaces were shiny, although a small amount of surface film on the bismuth was noted. After its transfer to the cell, the salt was colorless and quite transparent. A flow of argon cover gas was maintained through the gas space above the salt, and a slight positive pressure was maintained in order to prevent air leakage. A 0- to 12-v dc power supply that had a maximum output of 250 amp was used. Both the cell current and

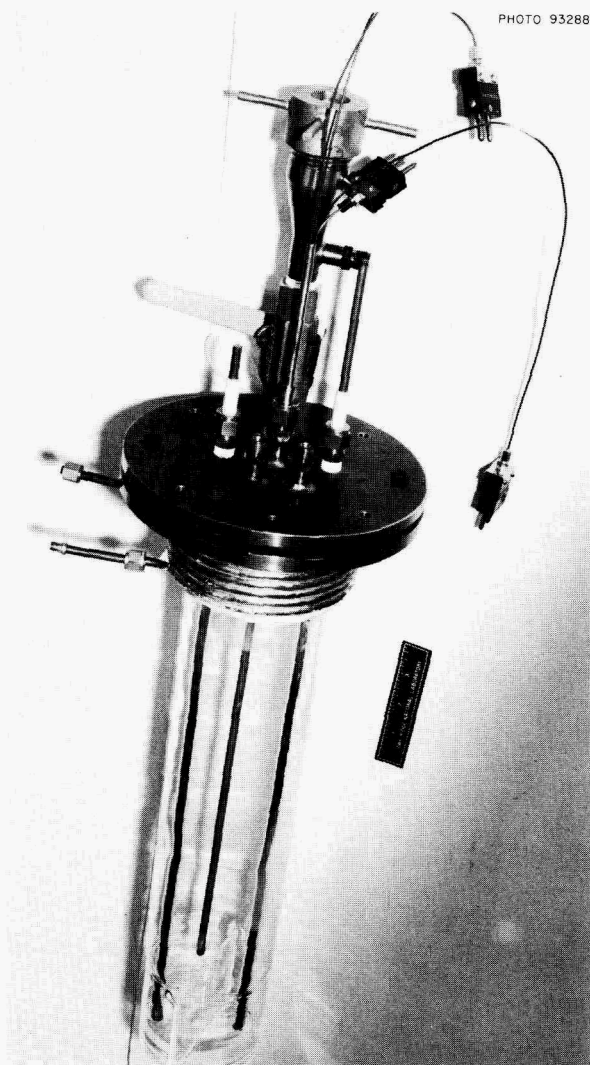


Fig. 1.24. Static Electrolytic Cell Made of Quartz.

the potential difference between the electrodes were recorded continuously.

During each series of experiments, the voltage applied across the electrodes was increased, in increments of about 0.6 v, from an initial value of 2.6 v, and operation of the cell was observed. Neither the salt nor the bismuth electrodes were sparged with gas during the first series of experiments; however, the cathode was sparged with argon during most of the second series.

The initial potential difference between the bismuth electrodes was less than 0.05 v (i.e., below recorder sensitivity). The cell potential increased rapidly to 2 v after passage of 60 coulombs in 10 sec, to 2.1 v after 625 coulombs

in 125 sec, and to 2.25 v after 9300 coulombs in 61 min. The cell potential remained at about 2.2 v thereafter. The potential was decreased by mixing the cathode via argon sparging; however, sparging the anode produced no change in cell potential. The plot of current density vs voltage from the experiments (Fig. 1.25) suggests that there is essentially no limiting current in the range covered by the experiments. The slight decrease in cell resistance shown in one of the curves resulted from an increase in cell temperature and is consistent with published values³⁶ for the specific conductivity of the molten LiF-BeF₂ mixture used. The highest average current density obtained was 4.5 amp/cm² (4180 amp/ft²). Higher current densities would be expected as the applied potential is increased.

During each series of runs, the formation of very finely divided dark material was noted at the anode. This material was observed to spread slowly throughout the salt during the first 10 min

³⁶S. Cantor (ed.), *Physical Properties of Molten-Salt Reactor Fuel, Coolant, and Flush Salts*, ORNL-TM-2316 (August 1968), p. 14.

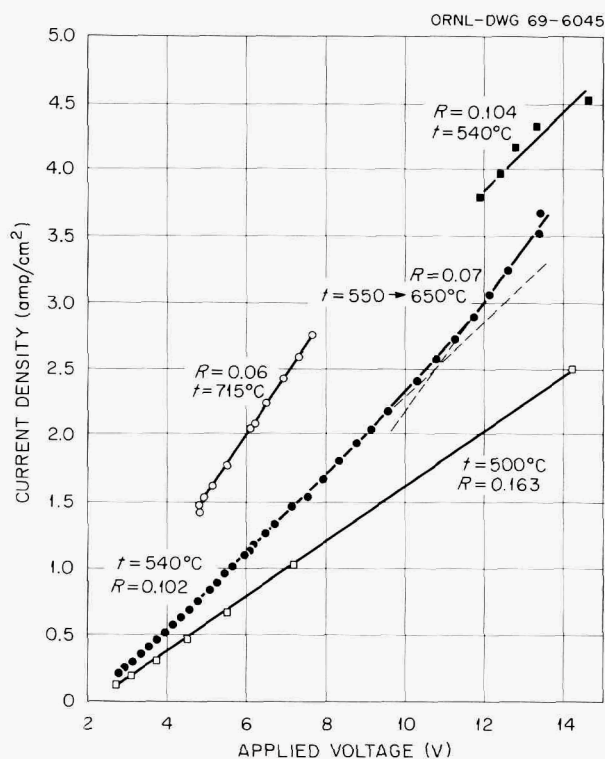


Fig. 1.25. Variation of Current Density with Applied Potential for Quartz Cell Experiments.

of operation of the first cell. Circulation of the salt during this period was slight and resulted from thermal convection. The salt was opaque during the remainder of the operation; however, it became transparent after the cell had stood overnight, and only a small amount of dark material was noted at the salt-bismuth interface. During operation of the second cell, the salt immediately above the anode became light brown after 10 sec (60 coulombs). At this point, the cathode was sparged with argon; the salt remained transparent during the sparging. Then the anode was stirred by an argon sparge, resulting in the dispersion of the material that had collected above the anode throughout the salt (which then appeared light brown). The formation of black material at the anode continued for an additional 125 sec (625 additional coulombs). After standing overnight, the salt became transparent again, with only a small amount of black material present. No further formation of black material was noted during several additional hours of cell operation. During this time, the salt was circulated by means of an argon sparge in the cathode chamber.

Gas was evolved from the anode during cell operation, even at a current density as low as 0.15 amp/cm^2 . Mass spectrometric analysis of off-gas samples showed the gas to be SiF_4 . The SiF_4 concentration in the samples increased as the cell current density was increased. The gas was produced on the anode side of the quartz divider that separated the bismuth anode and the cathode, and was produced only during or immediately after the passage of current. These observations strongly suggest that the evolution of gas was the result of reaction of BiF_3 (produced at the anode) with the quartz divider.

There was no evidence of fluorine evolution during cell operation. Only after the cell had shorted internally (arcing was noted between the electrodes) did the KI-starch solution (through which the cell off-gas passed) become lightly tinted. The bismuth concentration in the salt (probably BiF_3) increased with the number of coulombs passed through the cell, although the concentration was only 10 to 50% of that which would result if only BiF_3 had been produced and all of it had remained in the salt.

Quartz Cell Experiment Using AC Power. — The purpose of this experiment was to determine the feasibility of using ac power for simulating heat generation in cells designed for use with dc power.

The procedures for cell preparation were the same as those for the dc runs except that a low-voltage ac power supply was used. The calculated cell resistance was 0.16 ohm at 500°C for the ac run, as compared with 0.15 ohm at 515°C for the subsequent dc run in the same cell. Visible changes at the salt-metal interface were not significantly different from those observed during dc runs. The quartz cell was attacked by the fluoride salt, but to a lesser degree (especially at the electrode divider) than in the dc runs. A residual voltage of 0.2 v was measured after the ac run; this indicates that a slight amount of rectification took place.

The cell was operated for 2-hr periods at current densities of 2.6 and 3.2 amp/cm^2 ; the resulting steady-state cell temperatures were 660 and 750°C respectively. One of the electrodes was sparged with argon during these periods to promote the circulation of salt. The cell was also operated for a short time at a current density of 5 amp/cm^2 . Less black, suspended material was produced than in comparable dc runs. This material disappeared when the cell temperature was maintained at 660°C or higher, but reappeared when the cell temperature was decreased to about 500°C . This may reflect changes in the solubility of the material in the salt.

Based on the results of this experiment, we conclude that ac power can be used to simulate heat generation in cells designed for use with dc power.

Experiment with All-Metal Static Cell. — Although the initial experimental work on the development of electrolytic cells utilized quartz as a convenient container material, this material will not be suitable for long-term usage. The most corrosive condition in a cell will exist in the vicinity of anodic surfaces where oxidation occurs. Although cathodic surfaces must resist attack by liquid bismuth, the corrosion problem in this area is not considered severe. We plan to protect all anodic surfaces other than liquid bismuth surfaces by a frozen salt layer. A small, all-metal static cell has been installed for study of this method of operation.

The main body of the cell is a 6-in.-diam, 18-in.-long sched 40 mild-steel pipe with a flat, $\frac{1}{4}$ -in.-thick bottom. The cell body is the cathode container. The upper part of the cell is flanged; the upper flange is electrically insulated from the cell body. The anode of the cell (shown in Fig.

1.26 before assembly) is a double-walled, fluid-cooled cup having an inside diameter of 1.75 in. (gross electrode area, 15.5 cm²) and an outside diameter of 2.75 in. The cup is suspended from the top flange by two $\frac{1}{4}$ -in. tubes that serve as the coolant (N₂ and water) inlet and outlet, as well as the electrical connection to the anode. Provision was made for raising and lowering the anode cup. Viewing ports are available on the top flange, and provision is made for sampling the salt or bismuth without introducing air into the system.

The cell has been charged with 16.3 kg of bismuth that was previously treated with H₂ at 700°C for 16 hr and molten salt (4.5 kg of 66-34 mole % LiF-BeF₂) that had been purified by hydrofluorination, hydrogen reduction, and filtration. Initially, the system will be tested to determine whether a frozen salt layer can be formed on the outer surfaces of the anode cup. Electrolysis experiments will follow.

Design of a Continuous Electrolytic Cell Testing System

A system is being built to continuously circulate molten salt and bismuth through an electrolytic cell at 500°C (Fig. 1.27). The electrolytic cell containment vessel, which has provisions for

cooling, sampling, and visually observing the cell, will permit a variety of cell designs to be tested. Design criteria for the cells are being developed, based on tests of static cells that are under way. Tentatively, the cell will have anode and cathode areas of about 0.1 ft² each and will be supplied with approximately 1500 amp at 10 to 20 v. Bismuth and salt flow rates up to 0.5 and 0.25 gpm, respectively, are provided. The system external to the cell consists of a mixer-settler tank (to equilibrate the salt and bismuth streams from the cell) and gas lift pumps and gravity-head-type orifice flowmeters (for return of the streams to the cell). Low-carbon steel will be used for most of the system that will be in contact with salt or bismuth. The agitator shaft and impeller, along with several of the transfer lines and the internal piping in the electrolytic cell containment vessel, will be made of molybdenum. Outlet nozzles on the mixer-settler vessel have been coated with vapor-deposited tungsten. Provisions have been made for inserting corrosion test coupons in the system.

Gas lifts were selected as the simplest method for pumping salt and bismuth. Since gas lift performance data could not be found for high-density liquids such as bismuth, tests of the air lift pumping of mercury were made at approximately 25°C. For a total lift height of 34 in., a lift tube diameter of 0.3 in., and a fractional submergence of

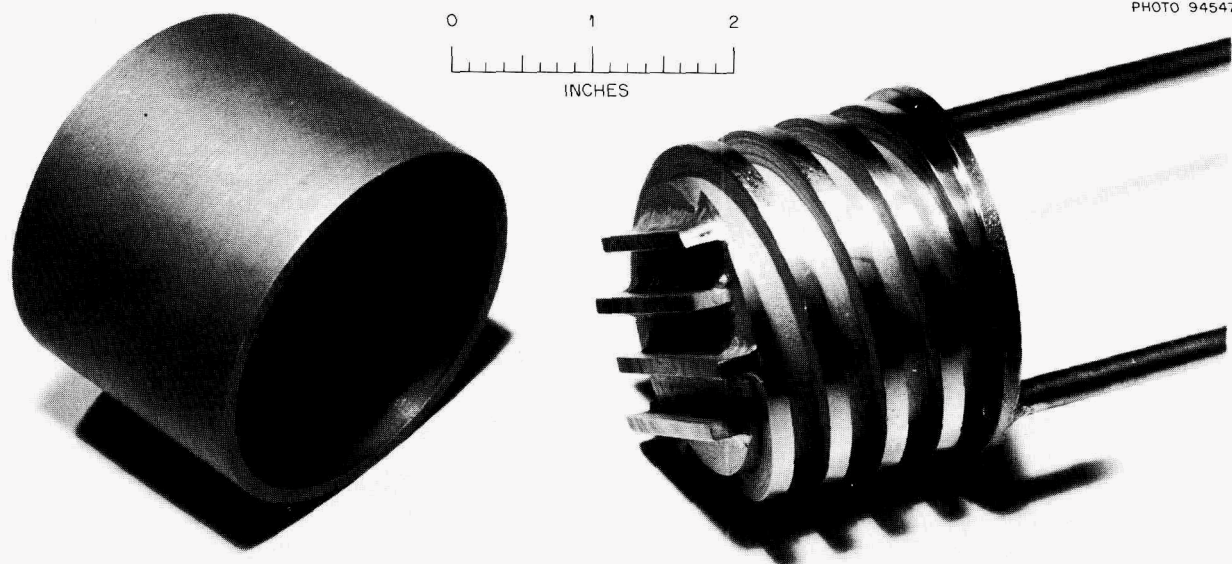


Fig. 1.26. Photograph of Anode Cup Before Assembly.

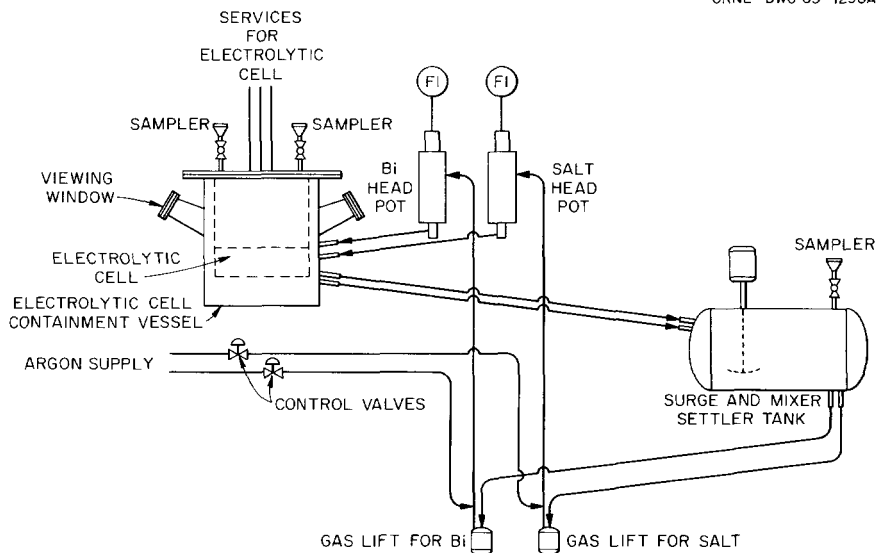


Fig. 1.27. Continuous Electrolytic Cell Testing System.

0.54, the maximum mercury pumping rate was 0.26 gpm at an air flow rate of 4.0 std liters/min. It is estimated that an argon flow rate of 1.5 std liters/min will be required for pumping bismuth at 500°C. Two lift tubes will be operated in parallel on the bismuth stream; only one will be used on the salt stream. The flow rates will be regulated by varying the gas flow to the lift. A head pot with a baffled annulus that eliminated entrainment and damped surges in the gas lift liquid discharge was designed and tested.

Heat and Mass Transfer Analysis of Electrolytic Cells

Heat transfer and mass transfer are important considerations in the design and operation of electrolytic cells. Studies that are in progress for characterizing heat and mass transfer in electrolytic cells will provide a basis for the evaluation of various cell designs and for interpreting data obtained from experiments with the cells.

An analytical study of mass transfer in electrolytic cells has been undertaken to aid in understanding or predicting current efficiencies, current densities, and conditions that will reduce beryllium at the cathode or that will saturate the cathode metal interface with thorium. This study will complement and help to elucidate the parallel

experimental program. Since the system is complicated and few of the transport parameters are known, considerable simplification is necessary, as well as justified. The geometry of the cell is reduced to a simple one-dimensional system, and the hydrodynamics are simplified to perfectly mixed phases separated by stagnant films on both sides of the salt-metal interfaces. Transport through the metal film is by Fickian diffusion; within the salt films, however, electric potential as well as concentration gradients are treated. We are considering simplifications that can be made to the model, and we are gathering information regarding ionic species that may be present in electrolytic cells. Approximate values of parameters are also being sought.

The resistivity of the molten salt electrolyte is relatively high (about 0.5 ohm-cm). Therefore, significant quantities of heat will be produced by I^2R losses in the electrolyte. The distribution of power density and temperature is being calculated for geometries of interest.

1.6 REDUCTIVE EXTRACTION ENGINEERING STUDIES

Equipment for semicontinuous engineering experiments on reductive extraction has been installed in Bldg. 3592. Mass transfer between molten salt (72-16-12 mole % $\text{LiF}-\text{BeF}_2-\text{ThF}_4$) and

molten bismuth will be observed at 600°C under various countercurrent flow conditions in any of several packed or baffled columns. Attempts will be made to correlate mass transfer performance with hydrodynamic conditions (flooding, holdup, specific interfacial area, etc.), which may be inferred from measurements of pressure drop through the column by analogy with results from a mercury-water system.

Equipment for these experiments is shown schematically in Fig. 1.28. Except where noted, mild steel is the material of construction. The column, C-7, is 0.82 in. ID \times 2 ft long (packed length); it will be packed with $\frac{1}{4}$ -in. right circular cylinders of molybdenum for the first experiments. To the right of the column is the salt head tank, T-6, which will be used for monitoring the pressure of the salt fed to the column. The pressure of the argon cover gas above T-6 and C-7 will be equal; hence the salt feed pressure will be a good measure of the pressure drop through the column. A pressure drop of 3 to 6 ft of salt is expected at maximum flow rates.

The bismuth feed and catch tank, T-1 and -2, and the salt feed and catch tank, T-3 and -4, are of similar design; that is, they are concentric cylinders of about 15-liter working capacity. The stainless steel salt-and-metal treatment vessel, T-5, contains a graphite crucible (working ca-

capacity, \sim 40 liters) in which salt and metal may be hydrofluorinated.

Flowing stream samplers, FS-9 and FS-10, are mounted on the effluent lines from the column. These will allow up to seven samples to be taken from each stream during the course of a run. In addition, each tank is equipped with a sampler through which up to four samples may be taken.

Salt and bismuth will be transferred through $\frac{3}{8}$ - and $\frac{1}{2}$ -in. lines, respectively, containing freeze valves (shown as dips in the lines) to route the flow. Salt and metal streams from T-5 will pass through fritted molybdenum filters to remove particulate material.

In addition to the components shown in Fig. 1.28, there are supply systems for HF, purified H_2 , and purified argon, as well as a vacuum system and an off-gas system designed to handle these materials.

With this equipment, about 15 liters each of salt and bismuth may be transferred by argon pressurization (\leq 25 psig) at flow rates ranging from 0.05 to 0.5 liter/min. The first experiments will consist of hydrodynamic studies in which salt and bismuth will flow countercurrently at volumetric flow ratios ranging from 10:1 to 1:10. During these experiments, the salt-phase pressure drop will be observed. It is believed that bismuth holdup, limiting flow, flooding, and some measure

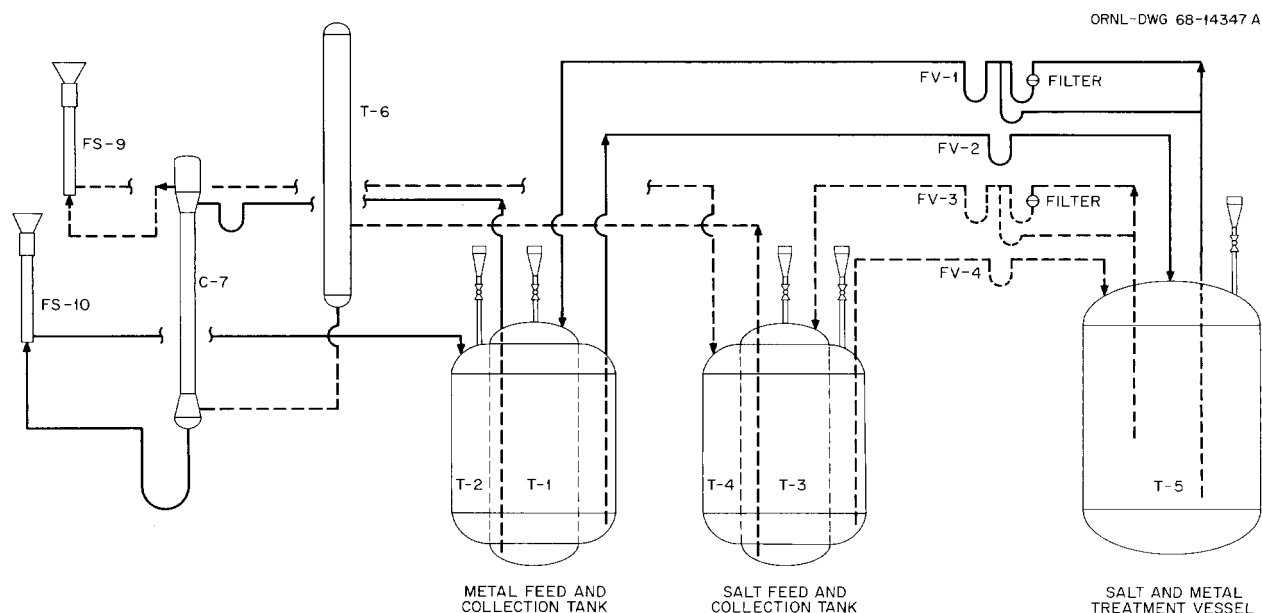


Fig. 1.28. Simplified Salt and Metal Flowsheet.

of specific interfacial area may be inferred from the pressure drop by analogy to similar experiments with a water-mercury system.

After the operators have gained some experience with the system and are confident of its performance, uranium tetrafluoride will be added to the salt phase for mass-transfer experiments. Metallic thorium will be added to the bismuth as a reductant.

It is expected that the height equivalent of a theoretical stage for mass transfer in this system will be 1 to 2 ft. With this estimate and equilibrium data from laboratory experiments, stage-by-stage calculations have been performed for one-, two-, and three-stage columns with various concentrations of uranium in the salt, and of thorium in the bismuth, at metal-to-salt flow ratios ranging from 10:1 to 1:10. From these calculations it appears that the optimal conditions for observing the number of stages obtained will be at volumetric metal-to-salt flow ratios from 5:1 to 1:1, with a uranium fluoride concentration in the salt phase between 500 and 1000 ppm and a thorium concentration in the bismuth between 500 and 1000 ppm. Because of the high distribution coefficient for uranium, the difference in effluent uranium concentration for one, two, and three stages will be small. For this reason, it is not felt that a more sophisticated mass-transfer model is warranted. Consequently, the effects of specific interfacial area, axial backmixing, etc. will not be investigated individually; mass-transfer performance will be evaluated only as a number of theoretical stages achieved with a 2-ft column height. The number of stages will, however, vary with operating conditions.

1.7 SIMULATED MOLTEN-SALT-LIQUID-BISMUTH CONTACTOR STUDIES

The proposed method for removing protactinium and fission products from a single-fluid molten-salt breeder reactor (or from the blanket salt of two-fluid reactors) involves reductive extraction by liquid bismuth containing lithium and thorium reductants. Equipment is needed to efficiently contact streams of salt and bismuth. The properties of these fluids are very different from those of aqueous and organic fluids conventionally used in liquid-liquid extraction equipment.

Since the correlations used to design liquid-liquid extraction systems are based upon condi-

tions far removed from those of interest, experimental data from systems similar to the molten-salt-bismuth system are needed. Because experiments with bismuth and molten salt are difficult, a mercury-water system is being used to allow selection of contactor types for testing with actual process fluids. This simulated system will provide quantitative data on flooding rates, pressure drop, holdup, and backmixing, as well as qualitative information on flow patterns and drop size.

One similar study has been reported; Johnson and co-workers³⁷ at Argonne National Laboratory studied a column that was packed with $\frac{3}{16}$ -in. Berl saddles, using water and Wood's metal. Their observed flooding rates were not adequately predicted by conventional correlations.

The experiments to date have been carried out in a 1-in.-ID, 2-ft-long glass column. Mercury is circulated through the column by a diaphragm pump containing tantalum check valves. Distilled water is circulated through the column by a small centrifugal pump. Ball valves, which are located at each end of the 1-in. column, allow flow to and from the column to be stopped instantaneously for holdup measurements. Each end of the column contains a section of 2-in. pipe; these sections (packed with the material of interest) allow lower velocities (to permit coalescence of droplets) and provide space for the inlet and outlet lines. Thus far we have tested Teflon Raschig rings ($\frac{3}{16}$ and $\frac{1}{4}$ in. OD) and solid right circular cylindrical packing of two sizes: $\frac{1}{4}$ in. and $\frac{1}{8}$ in. The column diameter should be about twice the present size in order to avoid wall effects with $\frac{1}{4}$ -in. packing; however, we are currently restricted to the smaller diameter because of the limited capacity of the mercury pump.

There are apparently two different flow conditions under which the column can operate. These are illustrated in Figs. 1.29 and 1.30. Figure 1.29 shows a photograph of the column packed with $\frac{3}{16}$ -in. Raschig rings through which the metal travels downward in channels. This type of behavior is typical of that observed for all flow rates tested with this packing and with the small $\frac{1}{8}$ -in. solid cylinders. Figure 1.30 is a photograph of the column with $\frac{1}{4}$ -in. Raschig rings. The small increase in packing diameter causes a dramatic change in the behavior of the dispersed metal

³⁷T. R. Johnson *et al.*, ANL-7325, pp. 30-32.

phase. The metal moves down the column in the form of small droplets that seldom coalesce and that remain intact for considerable distances down the column. This flow behavior is typical of that encountered with $\frac{1}{4}$ -in. Raschig rings or $\frac{1}{4}$ -in. solid packing. However, as the flow rates approach flooding conditions, some "channel" flow begins to occur. The dispersed or droplet flow is more desirable since it provides a significantly greater interfacial area than channel flow. Thus it may be advantageous to operate the salt-metal columns with $\frac{1}{4}$ -in. or larger packing.

Flooding occurred at approximately the same conditions with $\frac{3}{16}$ -in. Raschig rings and with $\frac{1}{4}$ -in. solid cylinders, that is, at equal (volumetric)

flow rates of the two phases when the superficial velocities reached approximately 90 ft/hr or 650 gal ft⁻² hr⁻¹. We investigated flooding rates for a range of flow ratios and found that the flooding curves could be approximated by straight lines with near-unity negative slopes when the square roots of the two phase velocities were plotted against each other. The $\frac{1}{4}$ -in. Raschig rings gave considerably higher flooding rates. At equal flow rates, flooding did not occur until the superficial velocity of each phase reached approximately 190 ft/hr.

Pressure drop and dispersed phase holdup data for a 2-ft length of the 1-in.-diam column packed with $\frac{1}{4}$ -in. Raschig rings are shown in Figs. 1.31

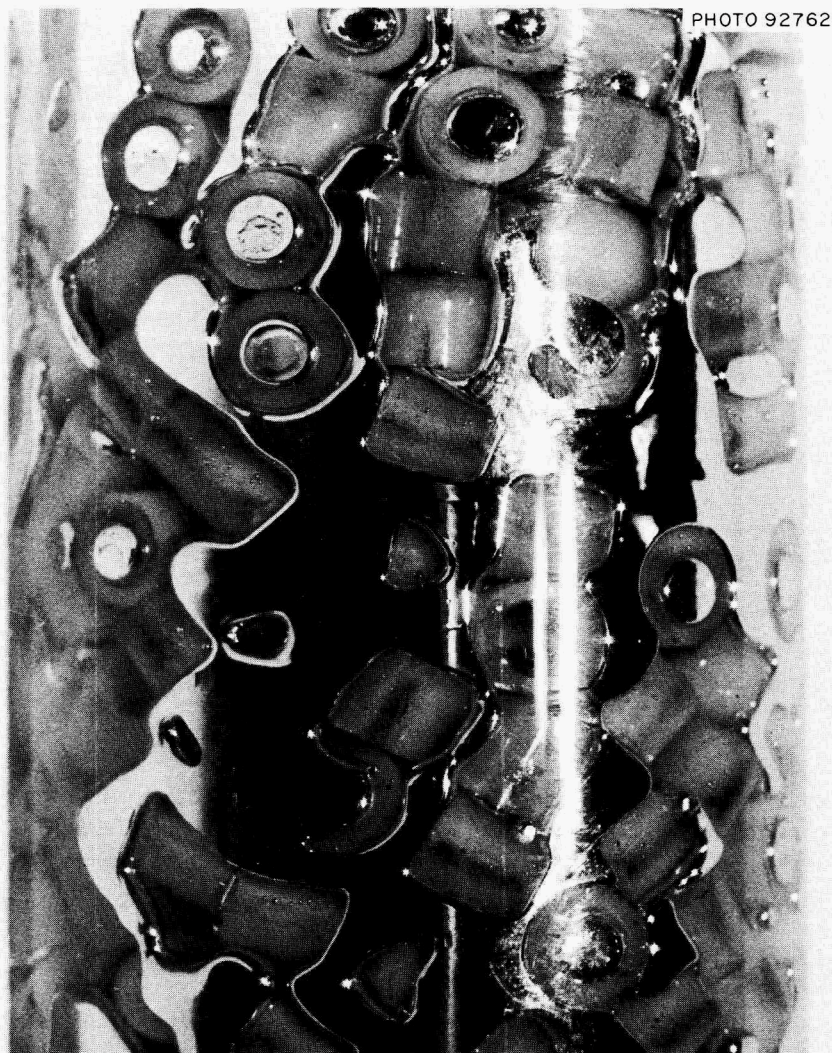


PHOTO 92762

Fig. 1.29. Mercury-Water Column Operated with $\frac{3}{16}$ -in. Polyethylene Raschig Rings.

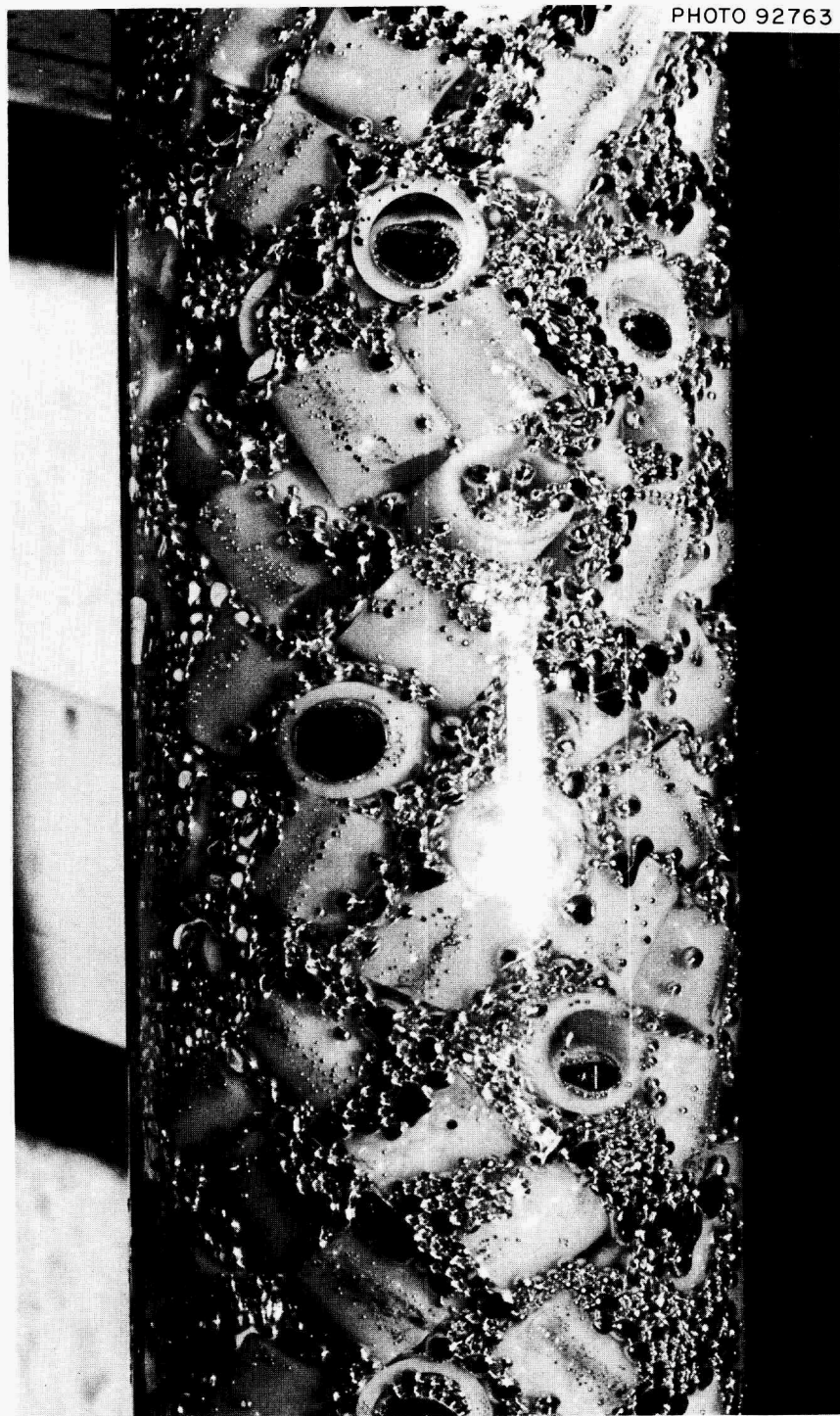


Fig. 1.30. Mercury-Water Column Operated with $\frac{1}{4}$ -in. Polyethylene Raschig Rings.

and 1.32. These results are similar to all the data obtained with other packing materials. Pressure drop and holdup for larger packing sizes (where the mercury is well dispersed) may be related by the semiempirical equations:

$$\frac{\Delta P}{L} = k_1 V_s X + k_2 \left(\frac{C}{1-X} \right) X,$$

and

$$V_s = \frac{g}{g_c} \frac{\Delta \rho}{k_1} - \frac{\Delta P}{L} - k_3 D,$$

where

ΔP = pressure drop due to flow (e.g., total pressure drop across the column less the static head),

L = length of column,

V_s = superficial slip velocity,

X = holdup,

C, D = continuous- and dispersed-phase superficial velocities,

$\Delta \rho$ = density difference,

$k_1, k_2,$ and k_3 = constants.

Thus, the hydrodynamic conditions (holdup, pressure drop, and, by implication, flooding rates) in a column with dispersed flow can be related using only three constants ($k_1, k_2,$ and k_3). Unfortunately, only two of the four packing materials tested gave dispersed flow, and evaluation of the relationship between the hydrodynamic variables will require data from additional packing materials. We are now considering larger packing materials for the processing system; therefore, a 2-in.-ID column and a larger mercury pump have been installed to permit $\frac{3}{8}$ - and $\frac{1}{2}$ -in. packing materials to be tested.

Studies of axial mixing in packed columns are also under way. With the high flow ratios required for some process flowsheets, axial mixing of the continuous phase (salt) appears to be very important in determining the column height equivalent of a theoretical stage. We plan to study both ordinary packed columns and columns that have been modified to reduce axial mixing.

1.8 CORROSION CONTROL BY USE OF A FROZEN LAYER OF SALT

Equipment is being developed for the continuous removal of UF_4 from a salt stream by counter-current contact of the salt with F_2 in a salt-phase-

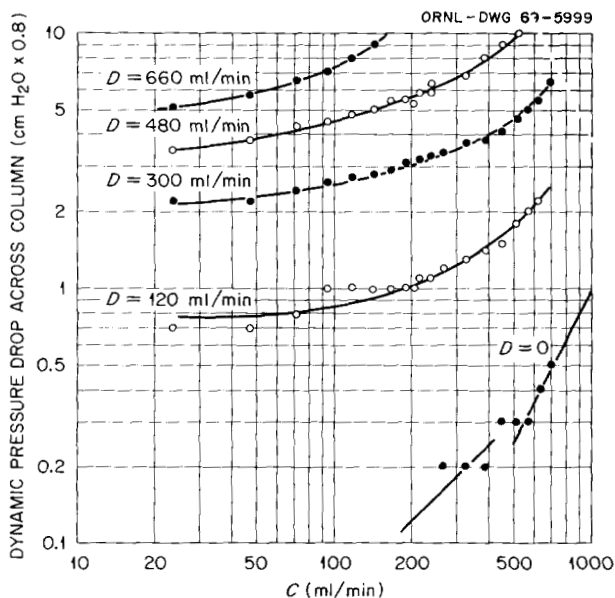


Fig. 1.31. Pressure Drop Across the 1-in.-diam, 2-ft-long Mercury-Water Column Packed with $\frac{1}{4}$ -in. Raschig Rings.

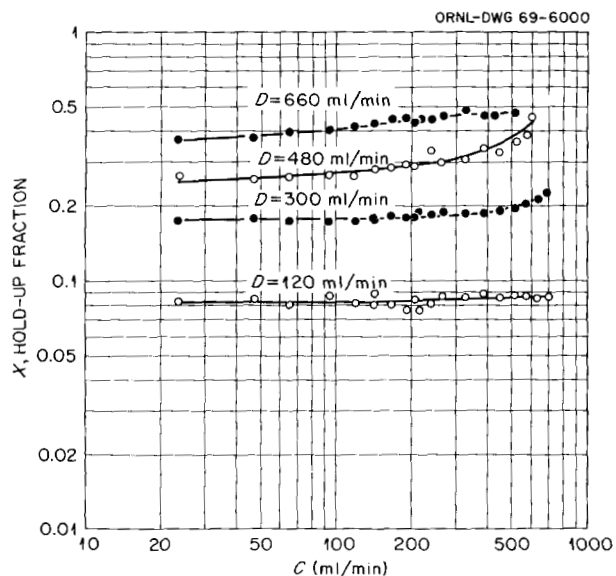


Fig. 1.32. Dispersed-Phase Holdup in the 1-in.-diam, 2-ft-long Mercury-Water Column Packed with $\frac{1}{4}$ -in. Raschig Rings.

continuous system. The equipment will be protected from corrosion by freezing a layer of salt on the vessel wall; the heat necessary for maintaining molten salt adjacent to frozen salt will be provided by the decay of fission products in the salt stream. In a series of recently concluded experiments (total of 24) using countercurrent flow of salt and an inert gas, we demonstrated that a frozen salt layer can be formed and maintained at conditions of fluid flow and heat transfer approximating those expected for processing fuel from a 1000-Mw (electrical) MSBR.

The experimental equipment described previously³⁸ consisted of a 5-in.-diam, 8-ft-high column fabricated from sched 40 nickel pipe. An internal heat source consisting of three Calrod heaters contained in a $\frac{3}{4}$ -in.-diam sched 40 pipe was used to simulate a volume heat source in the molten salt. The salt mixture was 66-34 mole % LiF-ZrF_4 , which has a liquidus temperature of 595°C and a phase diagram similar to the LiF-BeF_2 system. Since the principal objective of the work was to demonstrate that a uniform layer of frozen salt could be established and maintained at expected heat generation rates, we chose to substitute argon for fluorine, thereby simplifying the experimental procedures.

For the final set of experiments, the insulation was stripped from the test section, and the air cooling coils were removed to permit heat loss by radiation and natural convection. The primary purpose was to obtain a more nearly uniform surface temperature (and hence a uniform frozen salt thickness) throughout the test section.

As a means of confirming the thickness of the frozen salt, as indicated by the internal thermocouples, the molten salt in a few selected experiments was quickly drained from the column after a period of steady-state operation so that radiographs could be made. Over the 3.5-in. elevation range covered by the array of internal thermocouples, the thickness varied by as much as 20%; however, the thickness in the plane of the nominal $\frac{1}{2}$ -in.-deep thermocouple was in good agreement with that calculated from temperature measurements. This calculation is illustrated in Fig. 1.33 for a typical experiment and assumes simple radial flow of heat to the outer surface of a thick-

walled cylinder. The metal wall constituted a negligible resistance to heat flow because of its much higher coefficient of thermal conductivity. The most consistent interpretation of the experimental data was obtained by using only two thermocouples to locate the interface: the internal thermocouple located 0.66 in. from the metal wall and the adjacent wall thermocouple. The entire array of internal thermocouples was not usable because: (1) the embedded thermocouple nearest the interface caused a local perturbation, (2) the tip of the thermocouple nearest the wall appeared to change position during the course of the experiment, and (3) surface temperatures varied axially over the length of the thermocouple array.

Following the final experiment, the test section was sawed into portions to permit visual examination of the frozen salt layer and direct measurement of internal thermocouple locations (Fig. 1.34). The salt thickness was very uniform over the central portion of this test section, and the concentricity of the frozen layer throughout approximately a 30-in. length of the section indicated

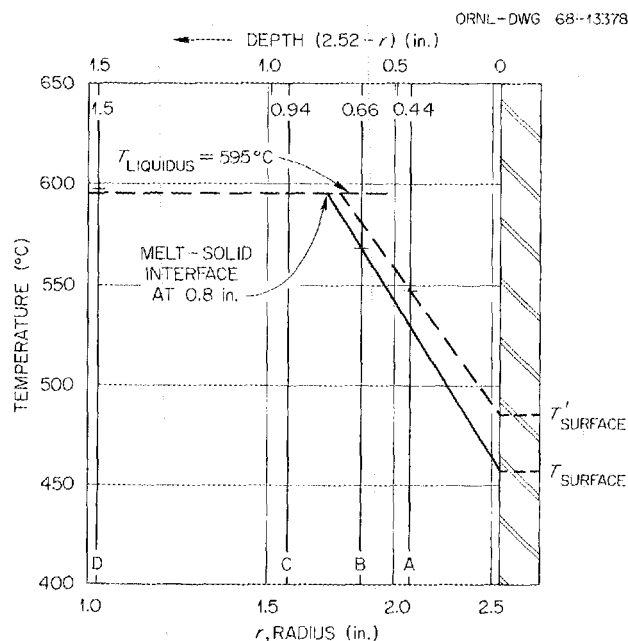


Fig. 1.33. Salt Temperature vs Radius in 5.04-in.-ID Column. Thickness of frozen salt = 0.80 in. by the preferred method of extrapolating from a surface temperature through temperature of adjacent thermocouple to liquidus temperature. Positions of internal thermocouples are direct measurements from postoperation examination.

³⁸Chem. Technol. Div. Ann. Progr. Rept. May 31, 1968, ORNL-4272, p. 2.

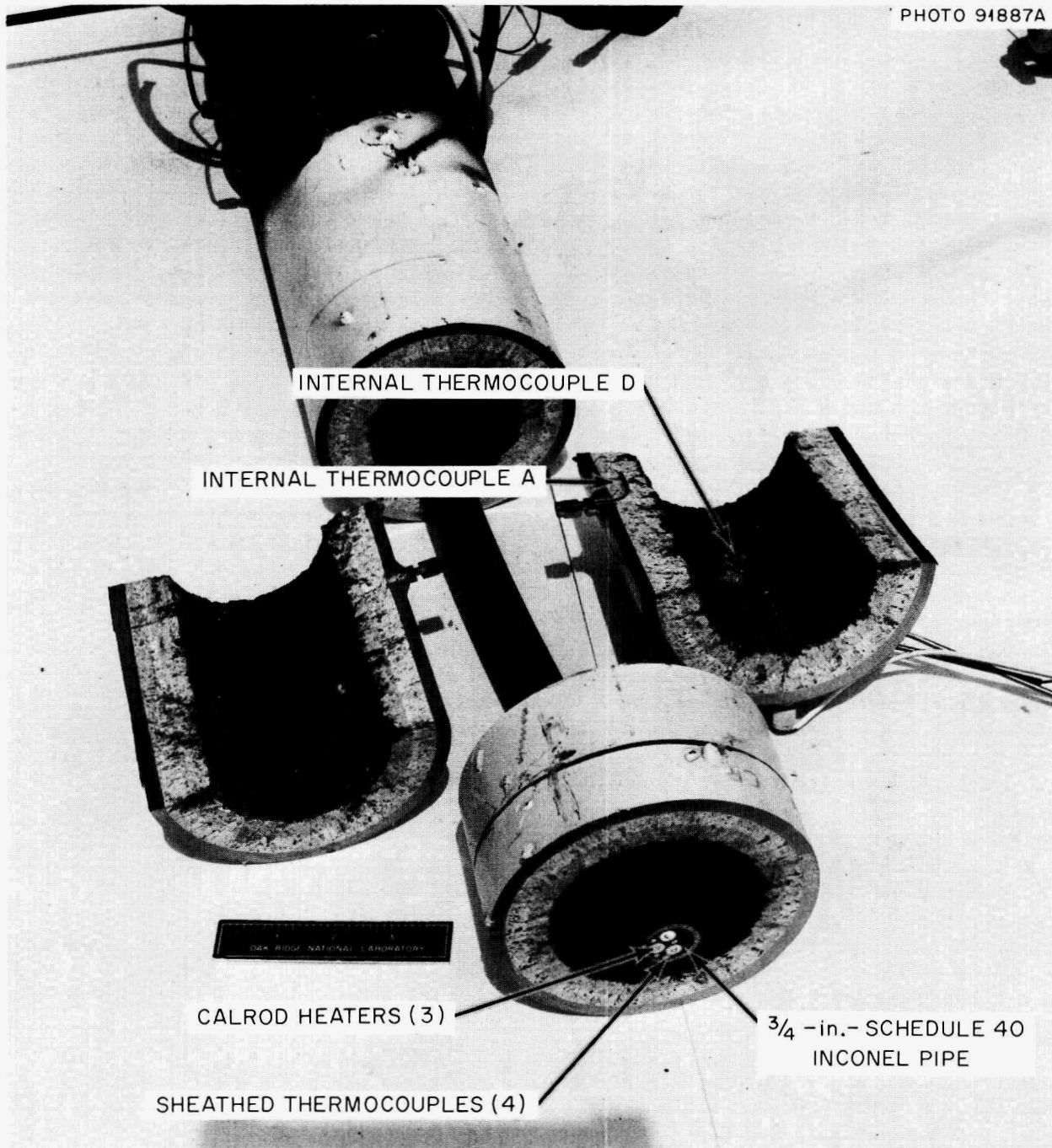


Fig. 1.34. View of the Central Portion of the Test Section. Upper end of the test section is in the foreground.

that the off-axis feed point for the argon caused no undesirable effects on the uniformity of the thickness of the frozen layer.

The inferred thickness of frozen salt for the series of 24 experiments ranged from about 0.10 to 1.10 in. The equivalent volume heat generation rate ranged from 34,000 to 190,000 Btu hr⁻¹ ft⁻³. Because the cooling coils did not provide adequately uniform surface temperatures at the lower heat fluxes, the column tended to freeze completely across at heat generation rates below 50,000 Btu hr⁻¹ ft⁻³.

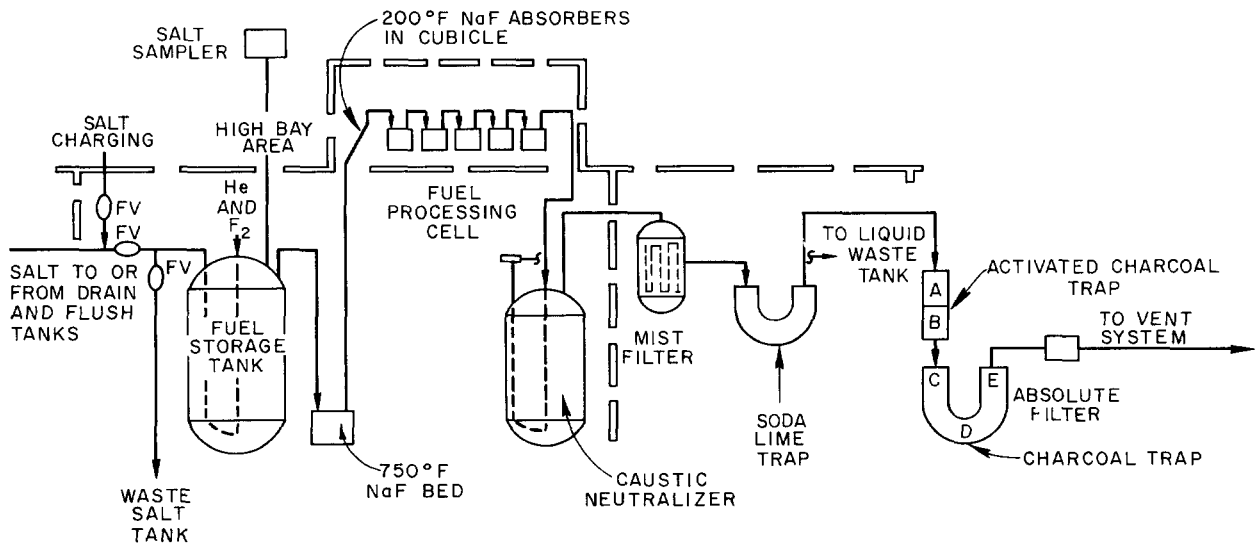
1.9 MSRE FUEL SALT PROCESSING

After operating for slightly more than one equivalent full-power year with a 33% ²³⁵UF₄ fuel, the MSRE was shut down on March 26, 1968, for removal of the uranium from the carrier salt in preparation for the ²³³U phase of the reactor program. After four months of testing and modifications, during which the fluorine disposal system was changed from a system based on the gas-phase reaction with SO₂ to the aqueous KI-KOH scrubber, processing of the flush salt began.

Process and Equipment

The flowsheet used is shown in Fig. 1.35. The steps represented by this flowsheet are as follows:

The 70-ft³ batch of molten salt is transferred, under pressure, from the reactor drain tank to the fuel storage tank. The salt is then cooled to within 50°F of the liquidus temperature (850–875°F) before sparging with fluorine is initiated. After the UF₄ is converted to UF₅, volatilization of UF₆ begins. The gas stream is passed through a NaF bed held at 750°F for removal of some of the volatile fluorides of metals such as Nb, Ru, and Sb. The decontaminated UF₆ then passes through a series of NaF absorbers, held at 200°F, where the UF₆ and some corrosion product MoF₆ are absorbed. The UF₆ volatilization and absorption are followed by mass flowmeters at the inlet and the outlet of the series of absorbers and by the heat of absorption in each absorber. Fluorination is stopped before any uranium reaches the final absorber in order to prevent any loss of uranium to the aqueous scrubber. The scrubber is charged with 1300 liters of 2 M KOH–0.33 M KI; 0.2 M K₂B₄O₇ is added as a nuclear poison. The scrubber solution is replaced before 50% of the KOH has been consumed; the fluorine being fed to the scrubber is diluted to less than 50% with helium. The mist filter removes hydrated oxides of molybdenum from the scrubber exit gas stream, and the soda-lime trap prevents traces of fluorine from reaching the charcoal traps. Any radioactive iodine not removed by the scrubber will be removed by the charcoal traps.



ORNL-DWG 68-8994A

Fig. 1.35. MSRE Fuel Processing System.

When fluorination is complete, the temperature is increased to 1200°F to reduce the corrosion product fluorides. The NiF_2 is reduced by hydrogen sparging, while the FeF_2 and CrF_2 are reduced by the addition of zirconium metal. The reduced metals are removed by filtration through an Inconel fibrous metal filter³⁹ before the carrier salt is returned to the reactor drain tank.

All the equipment, except the absorbers, is located in shielded cells in the reactor building; the absorbers are in a sealed cubicle in the operating area. A shielded salt sampler for taking dip samples after fluorination and reduction is also located in the operating area.

Processing of the Flush Salt

The flush salt contained about $6\frac{1}{2}$ kg of uranium that had accumulated during seven flushes of the reactor system. Since only about one-half of this uranium had decayed less than a year, the flush salt served as a final low-level test of the system. Using an average fluorine utilization of about 15%, the uranium in the salt was reduced to 7 ppm in less than 7 hr. After 10 hr of hydrogen sparging for NiF_2 reduction, followed by 25 additional hr of hydrogen sparging with 1 kg of zirconium, analysis of the filtered salt showed 76 ppm of chromium, while the nickel concentration had been reduced from 516 to 26 ppm.

Processing of the Fuel Salt

The fuel salt uranium was recovered in six runs. The absorber weight increases are shown in Table 1.9. These absorbers were loaded with high-surface-area NaF (HSA, $1\text{ m}^2/\text{g}$) except as noted. The low-surface-area (LSA) NaF has the advantage of higher loading capacity, as seen in Fig. 1.36; however, it has a slower reaction rate, thereby requiring operation at temperatures above 200°F. Higher loading with LSA NaF was obtained at lower temperatures where the lower reaction rate permitted deeper penetration into the NaF pellets. Table 1.10 shows the fluorine flow rates and utilizations obtained. Utilizations were

calculated from the mass flowmeter readings, which provided a continuous indication of the UF_6 content of the gas stream.

After correction for uranium daughter activity, gross beta and gamma decontamination factors (DF's) of 1.2×10^9 and 8.6×10^8 , respectively, were calculated. The gamma DF would have been higher if some metallic ^{95}Nb had not been blown into the line and flowmeter filter upstream of the absorber at the end of the salt transfer from the drain tank. This was the only radioactive material found in a measurable amount on the absorbers. Of the 400 mc of ^{129}I calculated to still remain in the salt, 74% was found in the scrubber solution from the first two runs. None was detected in the charcoal traps. The 560 g of plutonium in the salt remained there during the fluorination.

Corrosion of the Hastelloy N processing tank was somewhat less extensive than expected from previous pilot-plant fluorinations. The corrosion rate, calculated from the increase in the Ni, Fe, and Cr contents of the salt, averaged approximately 0.1 mil/hr. About 10 kg of reduced metals was produced. Nickel analyses of the filtered salt showed that the reduction and the filtration of nickel were complete. Because of unreliable iron analyses, chromium analysis was used to determine the end of reduction. It was expected that iron would be reduced before the chromium. From subsequent reactor operations, however, it appears that the concentrations of residual FeF_2 and residual CrF_2 were equal (35 ppm) since

Table 1.9. Calculation of Uranium Recovery from Absorber Weight Increases

Absorber	Run No.					
	1	2	3	4	5	6
1	12.50 ^a	11.95 ^a	10.64	11.46	13.49 ^a	10.45
2	9.78	12.84 ^a	13.11 ^a	11.53	14.43 ^a	12.45
3	3.49	8.35	11.89	11.22	12.39	0.55
4	0.06	0.61	5.72	9.82	8.93	0.00
5	0.00	0.09	0.09	0.15	0.00	0.00
Total	25.83	33.84	41.45	44.18	49.24	23.45
Total 217.99 kg U						

³⁹R. B. Lindauer and C. K. McGlothlan, *Design, Construction and Testing of a Large Molten Salt Filter*, ORNL-TM-2478 (March 1969).

^aLow-surface-area NaF ($0.063\text{ m}^2/\text{g}$).

ORNL-DWG 68-11623

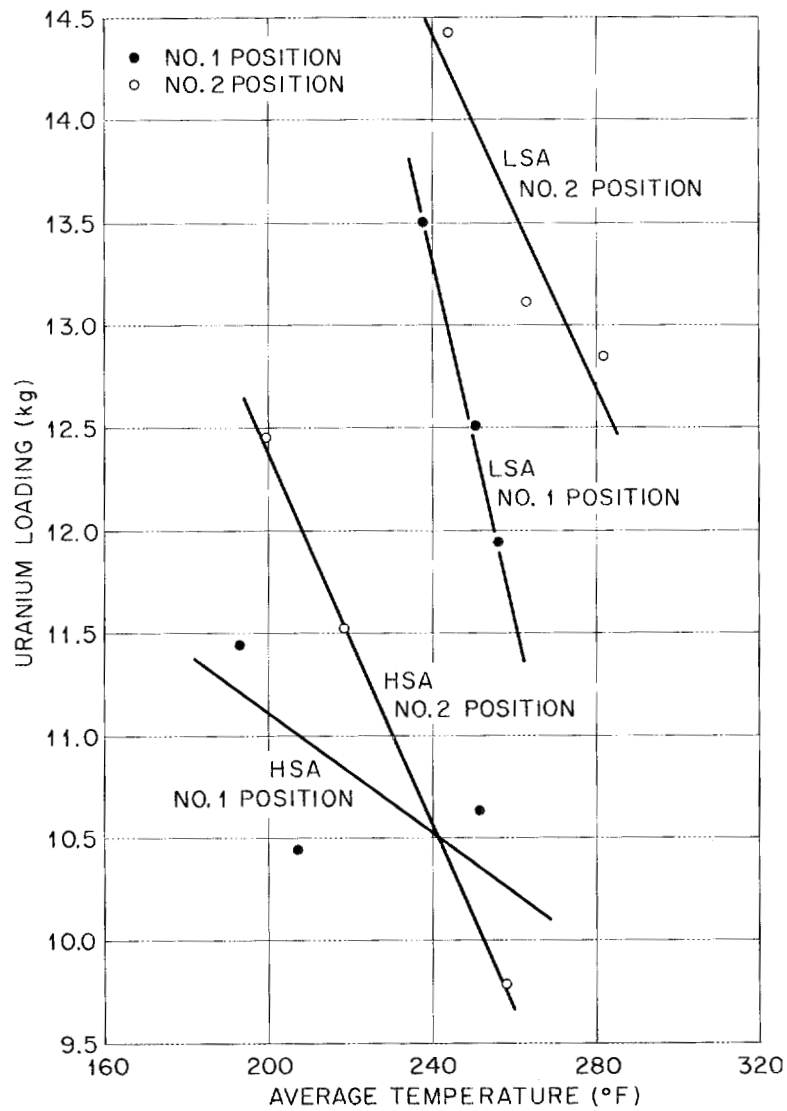


Fig. 1.36. Comparison of LSA and HSA NaF Loading.

Table 1.10. Fuel Salt Fluorination Data

Run	Fluorine Sparge			Volatilized U (kg)	Percent F ₂ Utilization	
	Time (hr)	Flow Rate (liters/min)	Volume (liters)		Average	Maximum ^a
Before	7.33	33.9	14,870		70	
UF ₆ breakthrough						
1	2.42	26.9	3,760	25.83	32	34
2	5.68	17.1	5,830	33.84	27	41
3	6.67	16.3	6,540	41.45	30	35
4	7.03	16.2	6,850	44.18	31	38
5	8.70	12.1	6,300	49.24	37	46
6	8.57	16.8	8,650	23.45	13	30
Total			52,800	217.99		

^aFrom mass flowmeter readings.

there was a rapid increase in chromium concentration from 34 to 67 ppm at the start of reactor operations.

1.10 PREPARATION OF ^{233}U FUEL FOR THE MSRE

The MSRE has been refueled with an enriching salt concentrate, $^7\text{LiF}\cdot^{233}\text{UF}_4$ (73-27 mole %). Sixty-three kilograms of this concentrate was prepared in cell G of the Thorium-Uranium Recycle Facility. Its preparation in a shielded cell was required because of the high ^{232}U content (222 ppm) of the ^{233}U .

Uranium oxide was reduced to UO_2 by treatment with hydrogen, the UO_2 was converted to UF_4 by hydrofluorination, LiF was added, and the eutectic was formed by fusing the components. The eutectic mixture, $\text{LiF}\cdot\text{UF}_4$ (73-27 mole %), was purified by treatment with hydrogen, which reduced the corrosion products to metal and subsequently allowed for their removal by filtration. The quality of the product was well within the requirements established for the MSRE.

The fuel concentrate, containing 39 kg of uranium (91.4% ^{233}U), was packaged in nine variable-capacity (0.5 to 7 kg of uranium) shipping containers for addition to the reactor fuel drain tank and in 45 enrichment capsules, each containing 96 g of uranium, for addition to the bowl of the fuel recirculating pump. A total of 35.6 kg of fuel (32.48 kg of ^{233}U) was shipped in shielded carriers to the MSRE to accommodate the reactor enrichment schedule, and 3.4 kg of the fuel was stored.

Process and Equipment

A summary of processing procedures and a description of equipment used to prepare the MSRE fuel concentrate were described in the preceding annual report.⁴⁰ A complete description of the MSRE fuel preparation and its delivery to the reactor is given in the project report.⁴¹

⁴⁰Chem. Technol. Div. Ann. Progr. Rept. May 31, 1968, ORNL-4272, pp. 28-33.

⁴¹J. M. Chandler and S. E. Bolt, *Preparation of Enriching Salt $^7\text{LiF}\cdot^{233}\text{UF}_4$ for Refueling the Molten Salt Reactor*, ORNL-4371 (March 1969).

The chemical flowsheet shown in Fig. 1.37 was used to produce the $^7\text{LiF}\cdot\text{UF}_4$ salt from the uranium oxide and lithium fluoride starting materials. A 13.2-kg batch of uranium, as oxide, was treated batchwise in a nickel-lined cylindrical stainless steel (304 L) vessel $7\frac{5}{16}$ in. in diameter. The expanded bed of $^{233}\text{UO}_3$ was heated for 2 hr at 550°C in a helium atmosphere to remove, by pyrolysis, any traces of ammonium compounds or other volatiles remaining from previous chemical processing. The bed was then cooled to 400°C before hydrogen treatment was started. This temperature was sufficiently low to accommodate the temperature rise resulting from the exothermic reaction of hydrogen with UO_3 . The concentration of hydrogen (in helium) was initially adjusted to 5 vol % and gradually increased to 50 vol % during the first 4 hr of treatment. The temperatures within the bed were monitored by an internal probe with 12 thermocouples that were placed at 2-in. intervals along the vertical axis of the bed. The temperatures rose in response to an increase in hydrogen concentration and then became constant after the initial excursion. The procedure of incrementally increasing the hydrogen concentration was repeated until the hydrogen:helium volume ratio was 1:1; the gaseous flow rate during this time was 2 liters/min.

The location of the reaction zone and the zone movement inside the 24-in.-high bed were clearly defined by the temperature profile. As the reaction progressed, the reaction zone rose, in the form of a band, up through the bed.

After the temperature excursion resulting from the initial increase in hydrogen flow had subsided (approximately 12 hr), the temperature of the furnace was increased, at the rate of $30^\circ\text{C}/\text{hr}$, until the bed temperature was $525 \pm 25^\circ\text{C}$. The reduction operation was continued at this temperature with 50 vol % hydrogen-50 vol % helium until 50 to 100% excess over the stoichiometric amount of hydrogen had been passed through the bed.

Hydrogen utilization within the bed was 100% until the reaction zone approached the top of the powder bed; then a slight decrease was observed. Hydrogen usage was determined by a material balance of the gas flowing into the reaction vessel, as measured by rotameters, and the gas outflow, as measured by the in-cell wet test meter.

The conversion of UO_2 to UF_4 by hydrofluorination, using HF gas diluted with hydrogen, began at

OVERALL REACTION	
$UO_3 + H_2 + 4HF \rightarrow UF_4 + 3H_2O$	
$UF_4 + LiF \rightarrow UF_4 \cdot LiF$	
27% - 73% EUTECTIC COMPOSITION	
CHARGE UO_3 :	~13.2 kg U AS UO_3
HEAT TREAT UO_3 :	3 TO 5 hr DIGESTION AT 550°C; COOL TO 400°C.
HYDROGEN REDUCTION: $UO_3 \rightarrow UO_2$	START 5% H_2 AT 400°C AND INCREASE TO 50% H_2 ; TEMPERATURE RISES TO 490°C; TREAT AT 500-550°C AT 100% USAGE OF H_2 ; COOL TO 400°C.
HYDROFLUORINATION: $UO_2 \rightarrow UF_4$	START 5% HF IN H_2 AT 400°C; INCREASE TO 40% HF IN H_2 ; TEMPERATURE INCREASES TO 450°C; WHEN HF USE DECREASES BELOW 80%, INCREASE THE TEMPERATURE TO 630°C STEPWISE UNTIL HF USE BECOMES 0; COOL TO 150°C.
EUTECTIC FORMATION: $UF_4 + LiF \rightarrow UF_4 \cdot LiF$	ADD EXACT QUANTITY OF LiF ; MELT UNDER 30% H_2 ; DIGEST AT 850°C FOR 3 TO 5 hr; COOL TO 700°C.
EUTECTIC PURIFICATION: $MO + HF \rightarrow MF + H_2O$ $MF + H_2 \rightarrow M^0 + HF$	PURGE MELT 24 TO 30 hr AT 700°C WITH 20% HF IN H_2 ; TREAT WITH H_2 FOR 75 TO 150 hr.
PRODUCT PURITY:	UNFILTERED SAMPLE ANALYZED FOR OXIDE CONTENT. FILTERED SAMPLE ANALYZED FOR METALLIC IMPURITIES.

Fig. 1.37. Chemical Flowsheet for the Low-Temperature Process for Preparing the MSRE Fuel Concentrate.

400°C and was completed at 625°C. Five to seven days were required for the conversion.

At the beginning of the hydrofluorination step, the composition of the gas was 95 vol % hydrogen—5 vol % HF; the flow rate of the mixture was 2 liters/min. Over a period of 3 to 4 hr, the HF concentration was incrementally increased to 40 vol % as the exothermic reaction caused the temperature to rise from 400 to 450°C. After the HF concentration of the hydrofluorinating mixture had reached 40 vol %, the reaction zone traveled, in the form of a band, up through the bed (in a manner similar to that observed during the hydrogen reduction) as the UO_2 was converted to UF_4 .

A total of 13.5 kg of uranium, as UO_2 , was converted to UF_4 in each of three runs; only minor differences in the runs were noted.

The eutectic mixture UF_4 -LiF (27-73 mole %) was formed by adding the stoichiometric quantity of lithium fluoride powder to the uranium tetrafluoride powder and fusing the mixture. The temperature of the reaction vessel containing the stratified UF_4 and LiF powders was increased to 855°C in order to liquefy the lithium fluoride (mp,

835°C). The resulting melt was digested at this temperature for 3 hr while it was sparged with hydrogen (at a flow rate of 0.2 liter/min) to reduce any extraneous compounds that might have been introduced during the LiF addition. Then the 9-in.-deep pool of eutectic salt (mp, 490°C) was treated with 20 vol % HF—80 vol % hydrogen (flow rate, 2.4 liters/min) for 24 hr at a temperature of 700°C to remove the last trace of oxide from the salt prior to the hydrogen purification procedure.

The eutectic salt was purified by bubbling pure hydrogen gas (3 to 10 ppm of H_2O) at a flow rate of 2 std liters/min through the melt held at 700°C. The product was very pure and met all MSRE specifications. Table 6 in ref. 41 gives the chemical analysis of the fuel shipments to the MSRE; Table 7 in this reference gives the isotopic analysis of the uranium.

Eight transfer operations were necessary to convey the three 13.5-kg batches of eutectic salt mixtures from the reaction vessel to the intermediate transfer vessel and then to the various shipping container assemblies. The transfers were made by applying helium gas pressure over

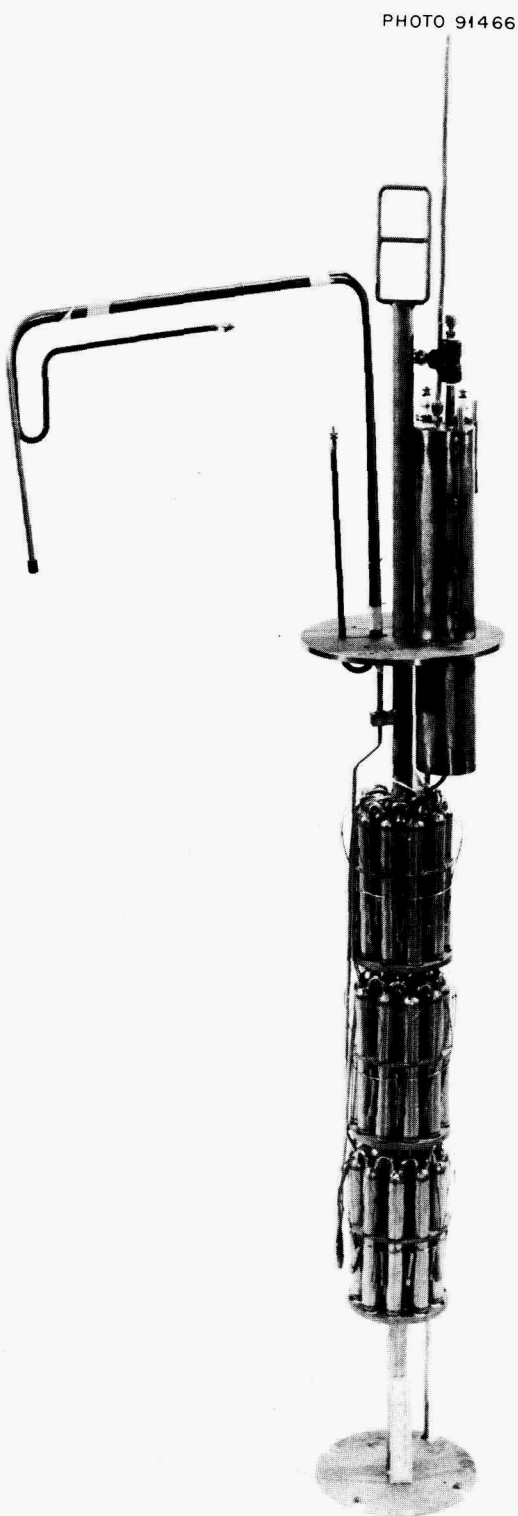


Fig. 1.38. Filling Array Consisting of 45 Capsules.

a pool of molten salt at 600°C . The salt was forced out of the dip line, through a heated transfer line ($\frac{3}{8}$ -in.-OD \times 0.065-in.-wall type 200 nickel tubing) and salt filter, to the receiving vessel.

Five salt transfers were required to fill the three product container assemblies. The first array (Fig. 1.38) consisted of 45 enrichment capsules, each of which was $\frac{3}{4}$ in. in diameter and 6 in. long and designed to contain 96 g of uranium. The capsules were connected in series and arranged in three 15-capsule decks. The second array, which was of similar design, consisted of four $2\frac{1}{2}$ -in.-diam by 34-in.-long cans connected in series for filling operations. Each was designed to contain 7 kg of uranium when loaded at 600°C . The third array contained a group of six $2\frac{1}{2}$ -in.-diam by variable-length cans that were designed to contain 0.5 to 3 kg of uranium (2 cans, 0.5 kg each; one can, 1 kg; one can, 2 kg; and one can, 3 kg). One can was used to store excess material that was blown back from the other five cans after they had been filled to overflow. The assorted sizes were needed to facilitate starting the reactor.

Preparatory to transfer, the shipping container assemblies were stripped of thermocouples, overflow pots, heaters, and supporting hardware. The containers were separated from each other by cutting the interconnecting tubing. The 45 enriching capsules were clipped and trimmed, and their lifting bails were tested with a 15-lb pull. Each was drilled for draining and venting and then identified and weighed. They were packaged in groups of six in carousel shipping containers. The $2\frac{1}{2}$ -in.-diam product cans were removed from the filling arrays, and a lifting bail was installed on one end of each can. A stopper was inserted in the bottom end of the can to minimize the loss of salt during handling and shipment. The shipping containers were weighed before shipment to the MSRE.

1.11 DISTILLATION OF MSRE FUEL CARRIER SALT

The nonradioactive phase of the MSRE distillation experiment was completed on June 18, 1968, and installation of equipment for distillation of a 48-liter batch of fluorinated fuel salt from the reactor has been started at the MSRE. The nonradioactive phase of the experiment involved distilling six 48-liter batches of MSRE fuel carrier

salt (four of which contained 0.1 to 0.3 mole % NdF_3). During these runs, vaporization rates were measured, and samples of the condensate were taken to assess the effect of concentration polarization and entrainment on operation of the equipment.

Essentially the same procedure was used in each run. The still is shown prior to installation in Fig. 1.39. Molten salt was charged to the feed tank at 600°C from a heated storage vessel. After the storage vessel was disconnected, the still pot was heated to 900 to 950°C , and the system pressure was reduced to 5 mm Hg. The feed tank was

pressurized to about 0.5 atm to force salt into the still pot, and the condenser pressure was decreased to 0.05 to 0.1 mm Hg to initiate vaporization at an appreciable rate. At this time, the liquid level in the still pot was switched to automatic control, and salt was fed to the still pot in this mode at a rate slightly greater than the vaporization rate. The argon feed valve to the feed tank remained open (forcing more salt into the still pot) until the liquid level in the still pot rose to a given point; the valve was then closed until the salt level dropped to another set point. After about one still pot volume had been processed, the

PHOTO 89051

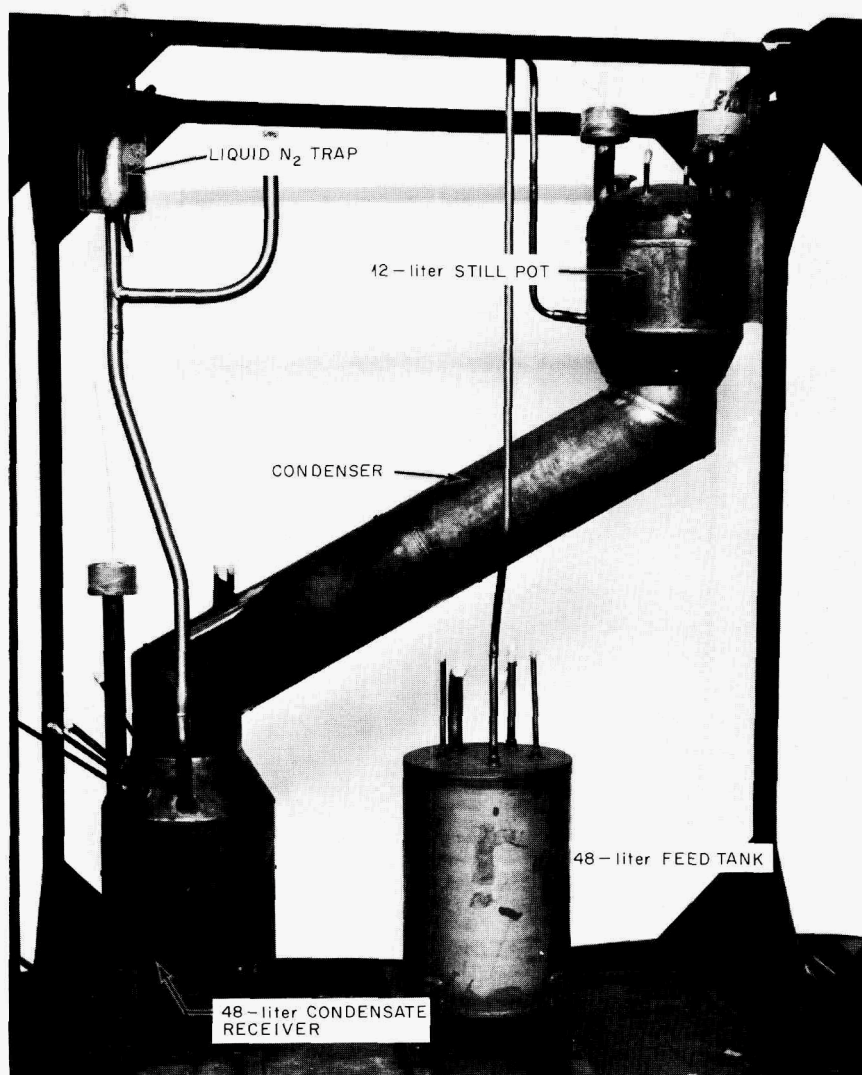


Fig. 1.39. MSRE Distillation Experiment Prior to Installation.

temperature of the still was raised to the desired operating point (approximately 1000°C). When the desired quantity of salt had been distilled, distillation was stopped by increasing the condenser pressure to 5 mm Hg. Then, 8 to 10 liters of the initial salt mixture was used to flush the high-melting salt from the still pot and to produce a salt mixture in the still having a liquidus temperature of less than 700°C.

During each run, distillation rates were determined by measuring the rate of rise of the condensate level in the receiver. The steady-state rate measurements for each run, and the operating conditions under which they were determined, are shown in Table 1.11.

The distillation rate is fixed by the conditions that the frictional pressure loss through the passage between the vaporization and condensation surfaces equals the difference between the vapor pressure of the salt in the still pot and the pressure at the lower end of the condenser. Thus, the distillation rate can be increased by either increasing the still pot temperature, which increases the salt vapor pressure, or decreasing the condenser pressure. A correlation of the distillation rate with the salt vapor pressure (P_1) and the condenser pressure (P_2) is shown in Fig. 1.40. The salt vapor pressure was assumed to be that of salt of the composition 90-7.5-2.5 mole % LiF-BeF₂-ZrF₄.⁴² A mixture of this composition produces vapor having a composition of approximately 65-30-5 mole % LiF-BeF₂-ZrF₄ and hence should approximate the composition of material in the still pot at steady state.

The correlation in Fig. 1.40 was suggested by a steady-state mechanical energy balance for isothermal flow of an ideal gas through a conduit of constant cross section. This balance shows that the flow rate is a function of the difference in the squares of the upstream and downstream pressures. Although the conditions were not isothermal and the flow cross section was not uniform, Fig. 1.40 shows a fair correlation of all the distillation rate data. The calculated range of the salt vapor pressure (P_1) was from 0.70 to 1.28 mm Hg, and the measured range of the condenser pressure (P_2) was 0.055 to 0.5 mm Hg.

Table 1.11. Distillation Rates During Nonradioactive Distillation Experiment

Run No.	Still Temperature (°C)	Condenser Pressure (mm Hg)	Distillation Rate (ft ³ ft ⁻² day ⁻¹)
MSS-C-1	990	0.5	1.15
MSS-C-1	990	0.3	1.20
MSS-C-1	990	0.055	1.25
MSS-C-2	1005	0.07	1.50
MSS-C-3	1004	0.075	1.56
MSS-C-4	1020	0.065 ^a	1.63
MSS-C-5	950	0.08	0.66
MSS-C-5	1000	0.08	1.21
MSS-C-5	1025	0.08	1.95
MSS-C-6	1000	0.08	1.40

^aCondenser pressure may have been higher; a ZrF₄ plug occurred in the vacuum line in this run.

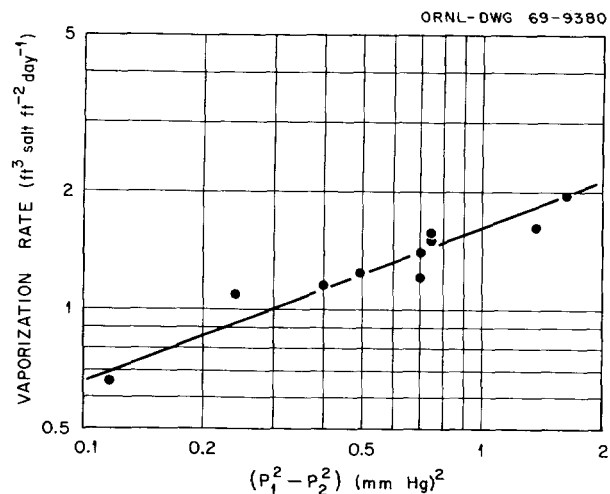


Fig. 1.40. Dependence of Vaporization Rate on Estimated Still Pot Pressure (P_1) and Pressure at End of Condenser (P_2).

For operation under conditions where the vapor pressure of the still pot material is 1 mm Hg or greater, distillation rates of 1.5 ft³ of salt day⁻¹ ft⁻² or greater can be obtained. Rates of this order are adequate to permit distillation to be used as a process step.

Concentration polarization in the still pot, or entrainment of liquid droplets from the still pot,

⁴²R. B. Briggs, *MSR Program Semiann. Progr. Rept.* Aug. 31, 1965, ORNL-3872, p. 126.

could seriously limit the separation of slightly volatile materials from the more-volatile LiF and BeF₂. The extent of polarization or entrainment was determined by analyzing condensate samples taken during the course of a run for NdF₃. The ratio of NdF₃ concentration in the condensate to the average NdF₃ concentration in the still, denoted by *R*, should be constant and should approximate the relative volatility of NdF₃ with respect to LiF.

In the first run in which NdF₃ was included in the feed salt, *R* varied (randomly) between 1.4×10^{-4} and 3.5×10^{-4} for about 2.5 still pot volumes of collected condensate. This value is comparable to the measured relative volatility⁴³ of NdF₃, which is 1.4×10^{-4} . In later runs (MSS-C-5 and MSS-C-6), the values of *R* were as high as 5.5×10^{-2} ; however, it is believed that the high values were the result of contamination by flush salt (on the condenser walls and in the sample reservoir) from previous runs. Neither concentration polarization nor entrainment was evident in the run from which data are considered most reliable.

Two difficulties were encountered: (1) condensed ZrF₄ and unidentified molybdenum compounds in the vacuum line completely restricted flow on two occasions, and (2) a deposition of nickel and iron in the salt feed line to the still almost stopped the flow after the first two runs and caused a noticeable restriction in the replacement feed line after the fourth run.

The major metallic constituents of the deposition in the vacuum line were zirconium and molybdenum. The first restriction was removed by cutting into the vacuum line; the second was removed during the last run by heating the vacuum line to about 950 to 1050°C, thereby redistributing the material. Examination of the vacuum line

during postoperational inspection showed that the free cross section of the pipe at the point of exit from the receiver was equivalent to about 50% of the original cross section. The material obstructing the vacuum line analyzed 39.4% zirconium and 11.6% molybdenum; F⁻ and O²⁻ were the major anions.

The cause for the metal deposition in the salt feed line is not completely understood. Two possible sources of the deposited material are: suspended metals and/or dissolved fluorides introduced with the feed salt, and corrosion products. The possibility that system corrosion may have been a factor is suggested by the composition of the deposits, ~0.9 wt % Co and 0.7 to 2 wt % Mo (both of these metals are constituents of Hastelloy N), and of the plug in the vacuum line (high molybdenum content). The extent of corrosion necessary to produce the materials found would be very small and could not have been detected by the wall thickness measurements. Another possible source of corrosion products is the corrosion coupons in the still pot (although no coupon was severely corroded). A hypothesis for the reduction and deposition of dissolved fluorides is based on the observation that higher-valence fluorides are, in general, more volatile than lower-valence fluorides of the same element. This condition causes the still pot salt to be reducing in nature with respect to the feed salt and could cause reduction and deposition of relatively noble metals at the entrance to the still pot.

Postoperational inspection showed the still to be in satisfactory condition for radioactive operation. Wall thickness measurements over the still pot and at both ends of the condenser showed an average decrease in wall thickness of only 1.6 mils. Length and diameter measurements showed changes of only 0.026 in. between points about 50 in. apart. Visual inspection of the inside of the still pot revealed that the metal was in good condition. The walls were shiny, and there was no evidence of pitting or cracking. Radiography also showed no evidence of physical change.

⁴³J. R. Hightower, Jr., and L. E. McNeese, *Measurement of the Relative Volatilities of Fluorides of Ce, La, Pr, Nd, Sm, Eu, Ba, Sr, Y, and Zr in mixtures of LiF and BeF₂*, ORNL-TM-2058 (January 1968).

2. Development of Aqueous Processes for Fast Reactor Fuels

Beginning in the 1980's, reprocessing of large quantities of fissile material from LMFBR reactors will be required. The problems that will be encountered during the reprocessing of this material will be different from those that have been encountered with light-water reactor (LWR) fuels for the following reasons: (1) The major fissile material in LMFBR reactors is plutonium rather than ^{235}U . (2) The fissile content of the LMFBR fuel is higher, by a factor of about 7 in the core section and by a factor of about 3 when all the material to be processed is considered, than that of the LWR fuel. (3) The average fission product content will be somewhat higher (the localized fission product content may be three times higher) than that encountered in LWR fuel. (4) The specific power of the LMFBR is higher, by a factor of about 5, than that of the LWR. (5) Processing of the LMFBR fuel after short decay periods will be advantageous, owing to the high fissile content (and high inventory costs) of the core material.

The Purex solvent extraction process, which is employed by nearly every major fuel processing facility in existence today, will be applicable in the processing of LMFBR fuels. The process versatility, the ease of adaptation of the process to continuous high-capacity throughput, and the vast operating experience that has been attained in the major processing facilities make this aqueous solvent extraction process an obvious and reliable choice. It appears feasible, with plant modifications, to process fuel from early LMFBR reactors, where preprocessing decay is acceptable, in existing fuel reprocessing facilities.

Aqueous reprocessing is most economically accomplished in large central facilities to which fuel is shipped from various reactor sites. The problem of fuel shipment, which is difficult even with LWR fuels, is aggravated in the case of LMFBR fuels

by the high specific power of the fuel and the need to ship after only short decay times. We have been working toward development of equipment and techniques for shipment that will ensure safety and containment under accident conditions, as well as the adequate dissipation of fission product decay heat by natural (unaided) means.

The preparation of LMFBR fuel for solvent extraction is more difficult than that of LWR fuel because of increased heat generation, vastly increased amounts of radioiodine (if the fuel is processed after short decay periods), and the presence of substantial quantities of relatively difficult-to-dissolve plutonium and fission products. We are making studies of the dissolution rates for irradiated fuel and of equipment that will be suitable for the accomplishment of certain of the mechanical operations (e.g., shearing). Improved containment of each equipment item and reduction of the quantity of contaminated off-gas are among the primary goals.

Disposal of the tritium that is produced during the fissioning of uranium and plutonium is not currently a problem because of the relatively small amount being produced. However, when the nuclear capacity expands by several orders of magnitude and the size and number of processing facilities increase, there will be a definite need to minimize the discharge of tritium to the environment. A process that, hopefully, will isolate the tritium prior to its dilution with dissolver solution is under development. (If the tritium becomes mixed with the dissolver solution, its isolation and recovery will be impractical.) This process involves an oxidative heat treatment, which will also liberate other volatile fission products such as iodine, xenon, and krypton.

The treatment of off-gas is a major consideration in the processing of fuels that have been

cooled less than 120 days. Removal efficiencies for radioiodine of 10^8 will be required for large-scale plants which process fuel that has been cooled for about 30 days. While no processing facility in existence today has the capacity (or the need) for this degree of removal, our tests of the catalytic oxidation of organic iodides in the off-gas from the TRU facility have produced encouraging results; we now believe that such a plant is not beyond reasonable attainment. In the processing of short-decayed fuels, substantial quantities of radioactive xenon will also be present in the off-gas streams; it, along with ^{85}Kr , can be removed by various known means and by other rare gas removal methods that are being developed.

The solvent extraction processing of LMFBR fuels must take into consideration (1) higher plutonium contents and (2) increased fission product activity in the feed. The second problem will cause difficulty in both plutonium valence control (necessary for good plutonium recovery) and solvent stability. The first will affect process and/or equipment design (to avoid criticality), as well as the choice of reductant to be used in the partitioning step. Neither of these problems appears to be serious in view of currently available information and of existing means for operating within the limitations.

Our work has been directed, in a considerable measure, toward clear definitions of the problems and a delineation of the most profitable areas of investigation. In the future we expect to develop the equipment and the process flowsheet conditions that are required to demonstrate safe and economic shipment and the processing of short-cooled LMFBR fuel. While this is a challenging problem, we are confident that the solution lies in the extension of current practice and/or technology.

2.1 SHIPPING AND RECEIVING

The reprocessing of spent fuels from LMFBR facilities is economically similar to other manufacturing operations in which a large capital investment is required for satisfactory accomplishment of the task. Small-capacity plants cannot be competitive with large-capacity plants; hence, spent fuel from several reactors located over a considerable area must be transported to a central reprocessing facility.

The shipment of fuels from LMFBR's will be more difficult than shipment of fuel from light-water reactors (LWR's) because of the higher specific power at which LMFBR's operate and because of the economic need to reprocess LMFBR fuel after short decay times. The LMFBR fuels are generally expected to be encased within a wrapper that will impede dissipation of heat from the fuel subassembly; in addition, the fueled portion of the LMFBR subassembly comprises only a small percentage (less than 25% in some instances) of the total subassembly length, whereas nearly all of the length of an LWR subassembly is fueled.

Cask Concept

A shipping cask that employs a single vessel to contain the fuel subassemblies and the heat transfer media (primary coolant) in which the fuel subassemblies are immersed can make more efficient use of the shielded space than is possible with a number of small containers. For this reason, we revised the previously proposed shipping cask concept, in which six individually sealed shipping containers were housed within a large steel shield, to one in which a single vessel with two or more relatively small openings in one end is used to contain many (18 to 36) subassemblies. This revision will permit more effective use of the shielding, and will not present any greater hazard during shipment than multiple containers within a single shield.

Our criteria for operating temperatures have been revised to some extent. That is, we are now assuming that the temperature of the fuel subassembly will never reach, either in normal operation or in an emergency in which no outside cooling can be supplied, a temperature greater than 1275°F . This should improve the probability of retention of fission products within the cladding of each fuel rod and reduce the probability of gross contamination of the primary coolant, even under accident conditions. Previously we had allowed an even higher temperature (1500°F) for the container wall, which was to be made of high-temperature-resistant steel, and had taken the position that failure of fuel rod cladding due to high temperature during the emergency condition would be acceptable. Although such a concept is acceptable under the existing Federal regulations, the current self-imposed restriction is more conservative.

Engineering Evaluation

An engineering evaluation of LMFBR fuel shipment was made during the past year. The objectives were as follows: (1) to determine if safe and economical fuel shipment can be achieved, (2) to suggest fertile areas for development and investigation, and (3) to enumerate the various problem areas and to evaluate possible solutions to these problems. It was concluded that, while increased provisions for safety must always be accompanied by additional expense, shipment of even short-cooled fuel can be accomplished safely at an acceptable cost. Extra safety features can be included, and costs can be reduced, if steel is used as the material of construction. (It is suitable for use at elevated temperatures, has high strength, and is very tough.) It will be necessary that adequate seals for openings in the containment vessel be developed and demonstrated and that the resistance of the containment structure, in general, be proved under conditions set forth in the applicable regulations. The coolant or heat transfer medium should be a fluid because of the need to transport heat over relatively long distances. The preferred liquid coolant, as determined in this evaluation, was sodium, which

does not introduce any new material to LMFBR fuel subassemblies or materially increase the difficulty of removing the sodium originally contained in these subassemblies; further, we do not believe that the presence of a highly reactive metal within the shipping container will significantly increase the hazard of shipment. Increases in decay time in order to minimize shipping problems will be difficult to justify economically, since it can be shown that one week's inventory charge is comparable to the freight cost for shipping 20 times the fuel weight for a distance of 2000 miles. Therefore, if safety can be ensured, economic considerations will dictate that fuel be shipped as soon as it can reasonably be processed. The effect of certain parameters was investigated (see Table 2.1). It should be noted that the temperatures and weight ratios indicated are only approximate. The calculations were based on Atomics International (AI) reference oxide fuel.

Heat Transfer Studies

Temperature profiles were calculated for casks filled with AI reference oxide fuel subassemblies,

Table 2.1. Effects of Selected Parameters^a on Fuel Shipping Cask Characteristics

Parameter	Basis for Comparison	Condition	Temperature (°F)		Shielding to Fuel Ratio (W_s/W_f)
			Outside Skin	Fuel Rod	
Decay time	36 subassembly	20-day-cooled	710	1155	40
		90-day-cooled	510	805	27
Excess hardware	18 subassembly, 20-day-cooled	Full length (17 ft 8 in.)	555	895	56
		Cropped (7 ft 8 in.)	780	1270	49
Shipment quantity	20-day-cooled	6 subassemblies	400	610	106
		18 subassemblies	555	895	56
		36 subassemblies	710	1155	40
Shielding design	18 subassembly, 20-day-cooled	Uniform shielding	520	872	83
		Graded shielding	555	895	56
Shielding material	18 subassembly, 20-day-cooled	Steel	555	895	56
		Uranium	670	995	34

^aUnless otherwise noted, all shielding is steel, graded in thickness, and all fuel subassemblies are shipped full length.

surrounded by metallic sodium. The assumption was made that no convection would occur. Figure 2.1 shows the temperature profile to be expected within a shipping cask containing 18 subassemblies that have been allowed to decay 21 days. It can be seen that the maximum temperature (1460°F) to be achieved within the cask under the assumed conditions is unacceptable as the desired maximum temperature of 1275°F is exceeded.

Available literature does not provide adequate information to permit estimation of the degree of heat transport that will be accomplished by thermal convection in systems in which the flow pattern is not controlled; however, it does provide values of heat transfer coefficients that can be expected at a surface located within a large body of fluid. Crude estimates of the potential for heat transport via thermal convection indicated that excellent distribution of heat within a fluid-filled shipping cask is possible, particularly if the

fluid is relatively nonviscous and possesses a high heat capacity per unit volume. In order to obtain at least qualitative data concerning the feasibility of heat transport by thermal convection, a device (Fig. 2.2) was constructed to simulate certain features of a shipping cask. The length-to-diameter ratio of this device is much greater than that for a shipping cask containing a number of fuel subassemblies; therefore, the relative temperature gradient from the point of heat generation to the end of the cask would be expected to be greater than that found in a shipping cask. Temperatures observed within this water-filled test device along the vertical center line and at various sections along the length of the cask are shown in Fig. 2.3. The amount of heat, per unit cross section, moving axially in this device was roughly equivalent to twice the axial heat rate in a shipping cask loaded with 21-day-cooled AI reference oxide fuel subassemblies. In actuality, the resistance to flow

ORNL-DWG 69-3555A

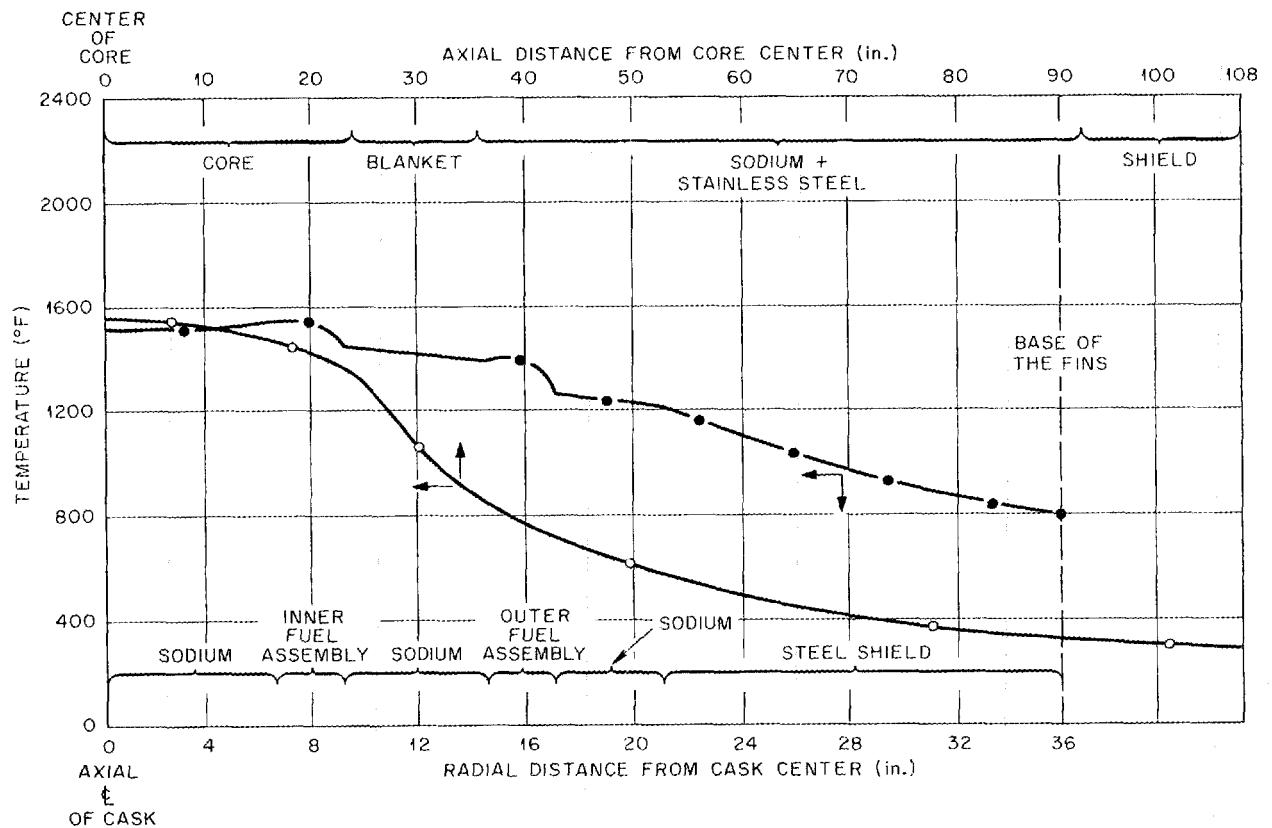


Fig. 2.1. Calculated Temperatures Within a Shipping Cask Containing 18 Atomic International Reference Oxide Reactor Subassemblies at 21 Days Decay. Thermal convection of sodium was assumed to be negligible.

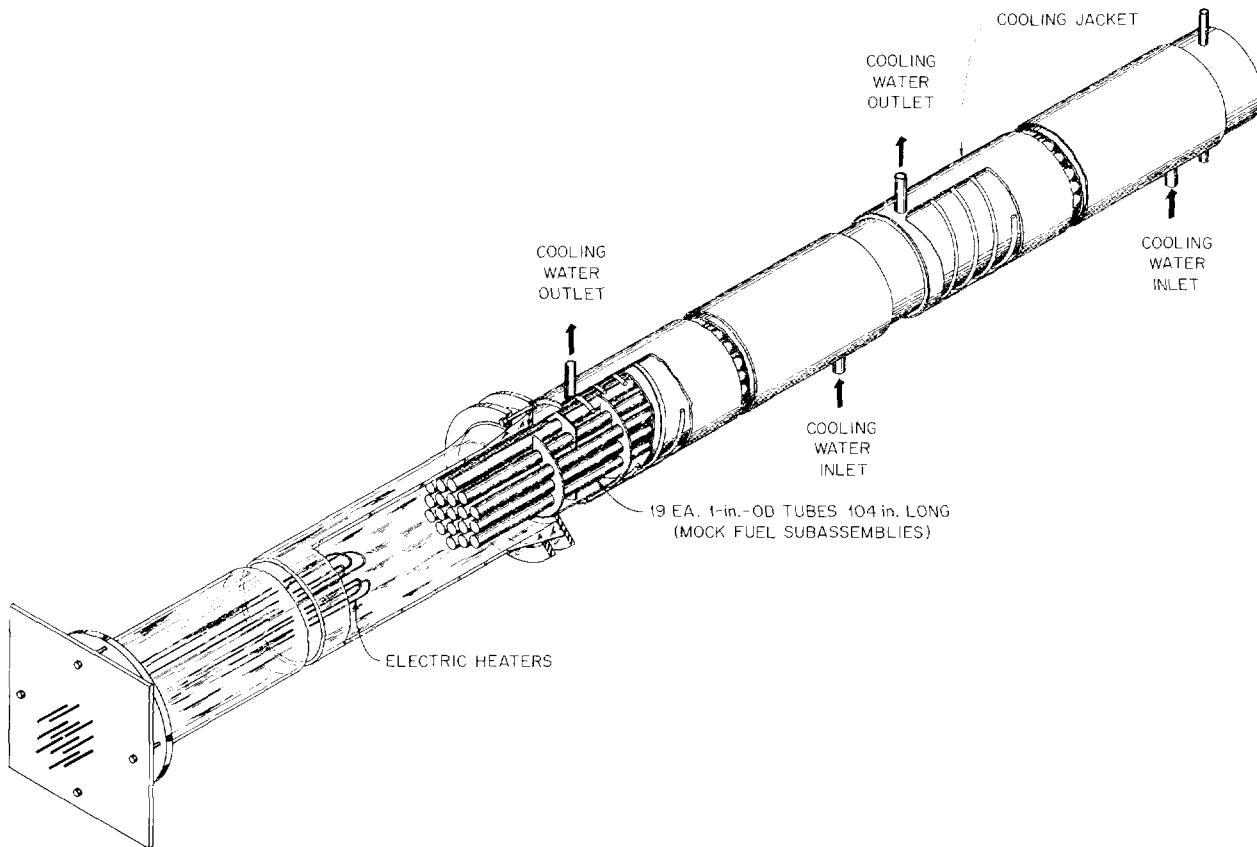


Fig. 2.2. Device for Studying Heat Transport by Thermal Convection.

within this test device is greater than would be encountered in a full-scale shipping cask because the passageways for flow are narrower than those in a cask. As a heat transport medium in a thermal convection system, sodium is not expected to be as effective as water; however, we believe that it will be quite satisfactory. The test device described above will be operated with mercury as a stand-in for sodium. Although the results obtained with mercury will not be exactly the same as those for sodium, mercury should more closely approximate the operation of the sodium-filled system than does the water-filled system. Further, the use of mercury may permit us to understand the heat transport mechanism more fully.

Two other systems under construction will provide information concerning heat dissipation from fuel subassemblies located within the cask. The first of these is an electrically heated mockup

of an AI reference oxide fuel subassembly that is housed within a 10-in.-diam pipe. This unit is completely installed and is now ready for testing. The tests will include determinations of thermal conductivity within the fuel bundle when it is filled with liquid sodium. We will also collect some qualitative information about the convective heat transfer within the 10-in. pipe and within the fuel bundle, both in the horizontal position and at an angle of 15° from horizontal. We will also operate this test unit under vacuum to determine its radiation emissivity, with an inert gas (probably argon) and with a helium gas primary coolant both at atmospheric and at approximately 10-atm pressure. After the cask has been in sodium service, we will recheck the emissivity coefficient. The second of the devices (see Fig. 2.4) is intended to demonstrate the feasibility of distribution of

heat within a large shipping cask by means of thermal convection. This unit constitutes one-half of the total length of a shipping cask that could contain 36 subassemblies of the same dimensions as are found in the AI reference oxide fuel subassembly. The unit is to be built only half-length since the motion of fluid should be the same in both ends of the cask; also, introduction of power to the middle of a vessel would be very difficult. This unit is to be operated with sodium as the primary coolant. At the conclusion of this test, we should have irrefutable evidence of the temperature profile that can be expected within a shipping cask containing a large number of short-decayed fuel subassemblies. No questions concerning scaleup should exist because results with this unit should apply to a full-scale cask even though the length of the unit is only half that expected for a cask. This equipment has been designed, and fabrication was started early in May. Completion of construction and testing is expected by the end of 1969.

Cask Integrity

Federal regulations require that a cask be capable of surviving a series of hazards without releasing a significant quantity of fission products to the environment and without a significant loss of shielding. The stipulated series of hazards include a 30-ft free fall of the cask onto an unyielding object, a 40-in. free fall onto a 6-in.-diam steel piston, exposure to a 1475°F fire for a period of 30 min, and immersion in water. When maximum temperatures to be attained by fuel in a shipping cask during the preceding series of hazards are calculated, the general practice has been to assume loss of coolant. Water, which is customarily used in the United States as a primary coolant, has the disadvantage of having a high vapor pressure at elevated temperatures; thus, it is assumed that this material will be lost in the course of a fire. The retention of coolant within the cask fuel cavity is vital to the maintenance of safety and the improvement of the economics

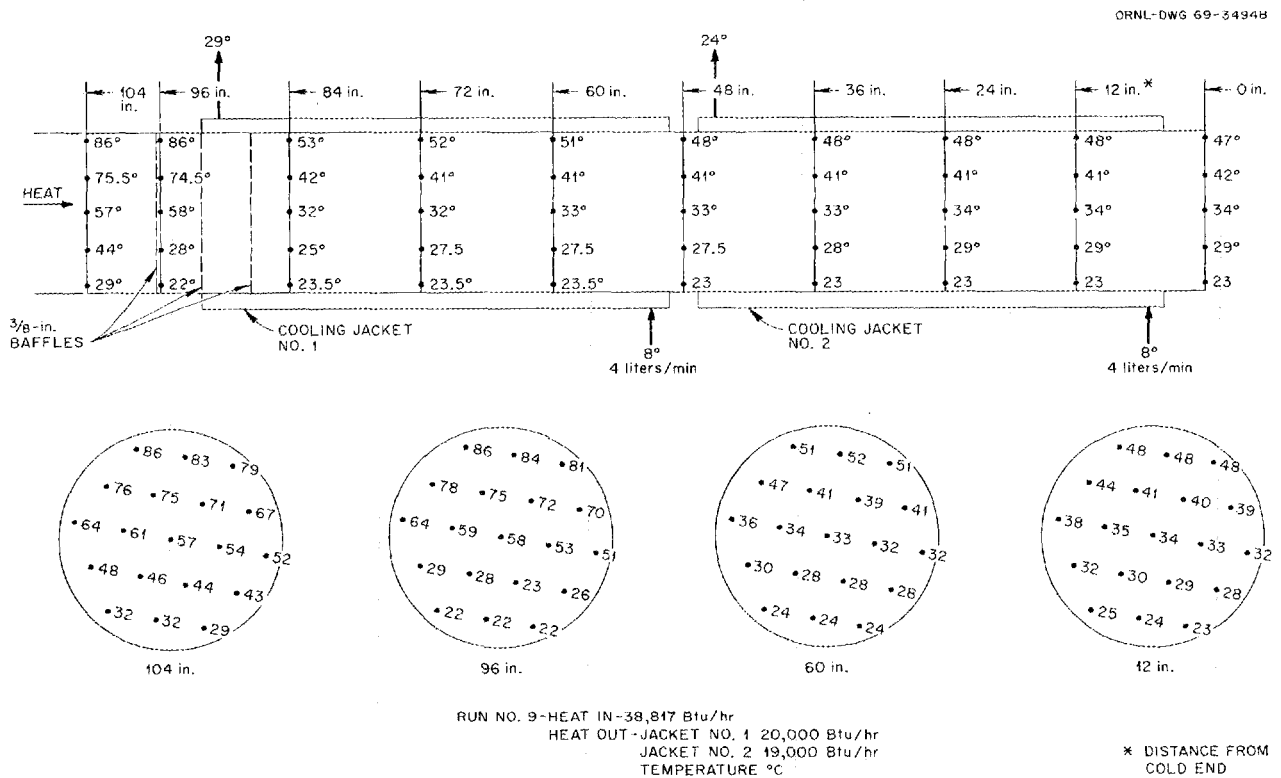


Fig. 2.3. Convective Heat Transport Test Data for Conditions Under Which Both Jackets Are Operational.

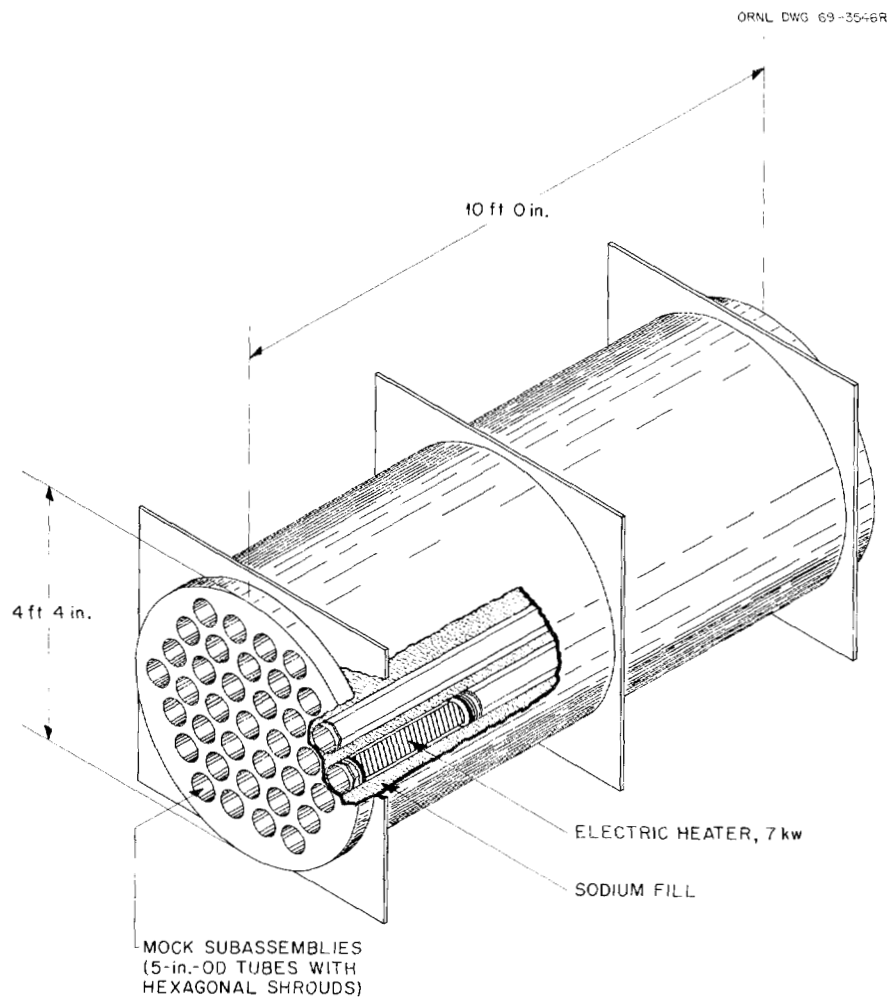


Fig. 2.4. Full-Scale, Half-Length Mockup of a Large Shipping Cask Fuel Cavity for Transporting LMFBR Spent Fuel.

of shipping high-specific-power, relatively-short-decayed LMFBR fuels. During this report period, our work has been aimed exclusively at developing better sealing methods and more rugged containers to withstand the various environments to which they might be subjected. Although no tests with regard to the fire hazard have been carried out, we believe that the use of steel for both the container and the shield will be better than using a container of lead-filled steel and a primary coolant of sodium. An all-steel cask will be resistant to fire and will show a slower response to outside thermal influences than will a lead-filled cask.

Our studies and developmental work to improve cask integrity have involved: (1) reducing the stresses applied to the cask as a result of im-

pact with other objects; (2) increasing the probability of survival of cask closure seals via changing their location, method of mounting, etc.; (3) surveying the various kinds of seals that are available and the probability of their successful application in a shipping cask; and (4) constructing cask models to determine whether or not there is a predictable relationship between the damage that is suffered by a small-scale unit and the damage that will be sustained by a large-scale unit when both units are subjected to the same hazard.

The impact stresses to which a cask is subjected when it contacts an unyielding object can be reduced by locating sacrificial fins around the perimeter of the cask. Fins are also useful for promoting heat dissipation.

One alternative means for reducing impact loads involves the use of wheels mounted around the cask and tied to it by uniform cross-section spokes. The wheel rims are connected to each other by means of compression members in such a manner that the cask is nested within a cage which is capable of absorbing all the kinetic energy of the cask and can, therefore, bring it to a halt at a controlled rate of deceleration prior to its contact with another object. A test of a one-eighth scale model was partially successful. This unit (Fig. 2.5) reduced the velocity of the cask by about 25% (thus absorbing about 50% of the kinetic energy of the cask) before the spokes broke. It can be seen that damage to the cask was superficial in spite of the absence of fins and of the fact that only 50% of the energy had been removed from the cask prior to its contact with the unyielding object. The cask was filled with water and equipped with a Conoseal joint mounted on the end of a 1-in. pipe that was attached to the cask cavity by means of standard pipe threads. The Conoseal joint was determined to be undamaged by the impact to which it was exposed; no leakage was observed. The calculated g loading was on the order of 1000. Posttest examination of this cask model,

plus results from other tests of "properly constructed" tensile specimens, have provided assurance that the objective of absorbing all kinetic energy in a sacrificial crash frame can be achieved.

Our studies of seals and the probability of survival of a seal after an impact and fire lead us to believe that the seal should not constitute a part of the vessel shielding and should be made of a metal having mechanical properties at least as good as those of the material of construction of the cask. Further, we are convinced that the sealing surface should be removed as far as practical from the point of impact in order to minimize the probability of deformation of the sealing surface. We have designed, and are planning to construct and test, a sealing system which is mounted in a manner that will permit the cask head to be significantly deformed without deformation of the sealing surface.

A number of seals appear to be acceptable for use in a liquid-metal-filled cask for fast-breeder-reactor fuel subassemblies; these include metal Vee rings (such as are made by Haskel and Parker-Hannifin), the Conoseal (which is manufactured by the Marman Division of the Aeroquip Corporation), and the Grayloc seal (product of the Gray

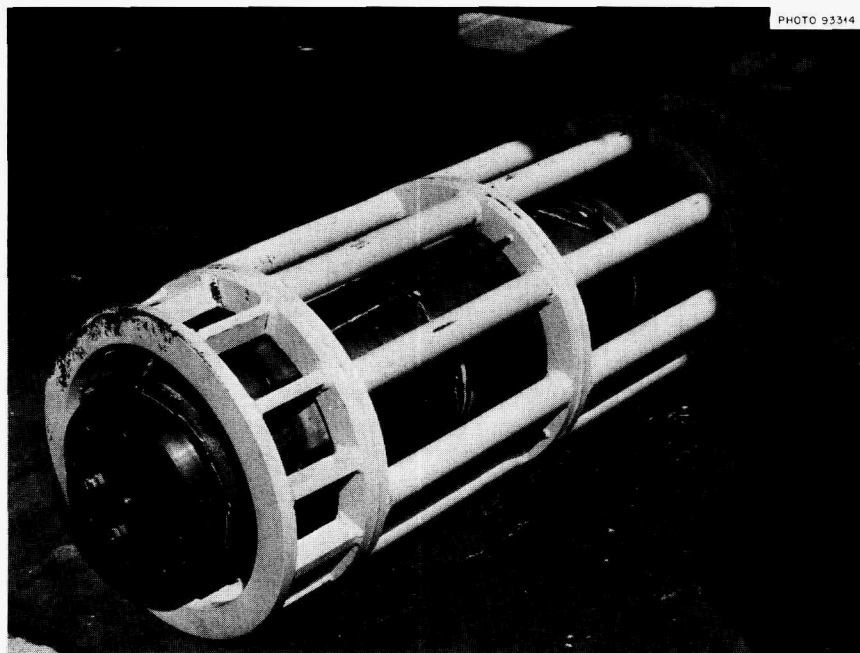


Fig. 2.5. One-Eighth Scale Model of Cask-Frame Assembly After Impact from 30-ft Free Fall.

Tool Company). We plan to carry out tests that will provide a basis for comparing and evaluating the merits of these and other sealing systems.

Many tests have been made with steel-encased, lead-shielded fuel shipping casks to establish that the deformations and failures suffered by small casks on impact are comparable to those sustained by large casks under similar conditions. We have designed a number of small specimens that will be tested to determine the relationship of such deformations in steel casks. If this relationship can be established, then the testing of various steel cask designs can be carried out at small scale and at relatively low cost to prove the capability of various designs to withstand the hazards specified in the Federal regulations.

2.2 HEAD-END PROCESSING

The head-end processing of LMFBR fuel involves those operations which are necessary to properly prepare LMFBR fuel for the recovery of the fissile and fertile materials by the Purex process. The principal operations are: dismantling (cropping, deshrouding, dissection), shearing (single rods, multirod arrays, and canned or uncanned assemblies), and disposal of inert waste metal components. The principal objective of the first two operations is to produce severed fuel of a size that will allow dissolution of the core material without significant dissolution of the stainless steel cladding.

During the past year (1) a conceptual design of a 5-metric ton/day central head-end reprocessing facility for short-decayed (30-60 day) fuels was made; (2) material balance flowsheets were prepared for AI reference oxide fuel; (3) we began an analysis of decay heat dissipation problems in the head-end steps by making steady-state calculations of the temperature of the center fuel rod in LMFBR arrays and of the auxiliary cooling requirements to maintain a preselected temperature; (4) the dismantling (cropping) and shearing operations were analyzed; (5) the conversion of waste metal to a more convenient form for handling and disposal was studied; and (6) scoping studies of a melt-decladding backup process for the present mechanical head-end steps were begun.

Head-End Processing Facility Concept

We have completed an initial conceptual design of a central head-end processing facility for preparing spent LMFBR fuel for Purex processing (see Fig. 2.6). This concept will ensure that all principal problem areas are revealed and systematically included in the research and development program. The conceptual facility includes the following processing steps: decanning and dismantling, singularization, removal of volatile fission products (voloxidation), shearing, leaching, leached hull monitoring, and treatment of inert waste metal to facilitate handling and disposal. This section is concerned only with the mechanical head-end steps. Voloxidation and leaching are discussed in Sects. 2.3 and 2.4 respectively.

In the facility shown in Fig. 2.6, canned or uncanned fuel assemblies shipped in sodium, inert gas, or inert liquid coolant are received and, depending upon the circumstances, are stored in water, sodium, inert gas, or inert liquid coolants. The assemblies (canned or uncanned) are withdrawn from storage as needed and sent to the dismantling operation where the ends of the can (in the case of canned assemblies) and the end hardware of the fuel are removed by a cropping operation.

The cropped fuel assemblies can be decanned, deshrouded, dissected (reduced to single fuel rods or to groups of rods), and sent to the appropriate shear feeder. Options permit the shearing of fuel as single rods, multirod arrays, or as the cropped, uncanned or cropped, canned fuel assembly. Single-rod and multirod shears may be preferred to shears designed for use with fuel bundles because (1) they are small and maintenance is inexpensive, (2) the control of heat dissipation is simple, and (3) the sheared product is more readily handled in subsequent processing steps. The product may be comprised of pieces of fuel rods, wire spacers, grids, shroud sections, and severed reflector rods. The simplest product may consist only of severed fuel rods and spacer wires.

The sheared fuel passes through a diverter or valving unit, which routes the empty, unfueled gas plenum sections and the core and blanket portions to separate transfer chutes. Sheared

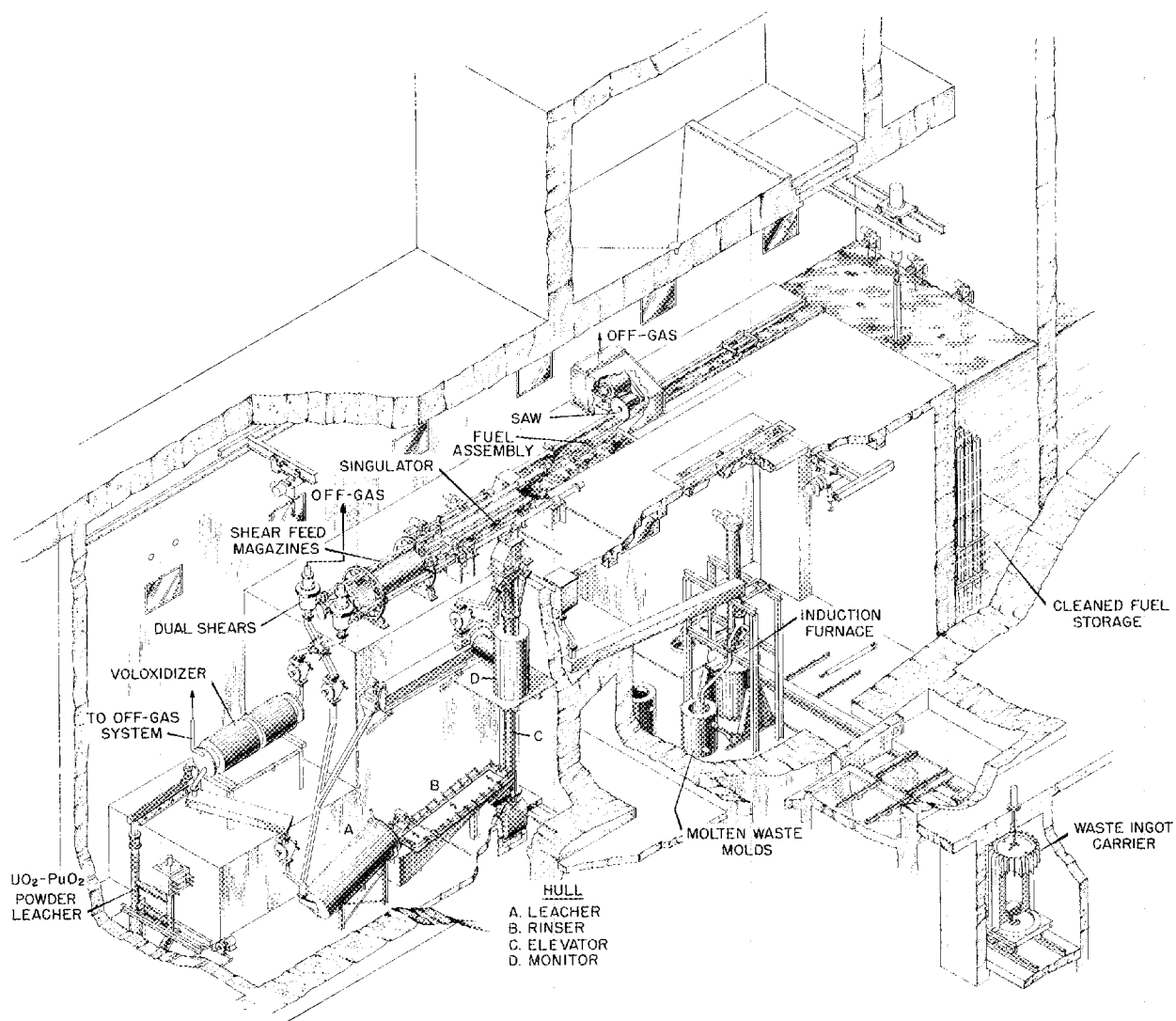


Fig. 2.6. Conceptual Head-End Processing Facility for LMFBR Fuel. The mechanical head-end processing portion of the conceptual central processing facility prepares the spent fuel for recovery, using aqueous Purex methods. Here, the inert end hardware is removed by a saw, the assembly is dismantled into individual rods by a singulator, and arrays of up to 100 rods are sheared and fed to a voloxidizer. This unit converts UO_2 - PuO_2 to U_3O_8 - PuO_2 , releasing fission product gases. The leached cladding and inert hardware are melted and disposed of as metallic ingots.

pieces containing core and blanket materials are sent to a volatile fission gas removal step (see Sect. 2.3), while the fragments of plenum go to a hull leacher. In the fission gas release step, sheared fuel can be first treated (heated, oxidized, etc.) to remove volatile fission gases and sodium and then be sent directly to a dissolver.

Leached hulls, wire spacers, grids, shrouds, etc., are rinsed, monitored, and recycled to a hull leacher (if residual fissile and fertile materials are detected) or to a step that converts them to a form more suitable for handling and waste disposal. All of the processing steps listed require extensive development and evaluation. The study of broken fuel in the canned or uncanned state merits considerable emphasis since there is no reference technology available. The disassembly of LMFBR fuel appears to be much more difficult than that of LWR fuel, primarily because of the close-fitting shroud of the former. In general, handling is also more complex because of decay heat emission and the long lengths (~18 ft) involved. For example, if fuel rods or multirod arrays are processed, their frail spaghetti-like structure will require the development of appropriate nondestructive handling techniques.

In general, the conceptual design study showed that the basic mechanical operations that are useful in processing LWR fuels could also be applied to LMFBR fuel. However, owing to the special properties of LMFBR fuel, such as high heat emission, sodium contamination, and the presence of large volumes of radioactive off-gas, and criticality and other related problems, an extensive research and developmental program will be necessary to produce the reliable head-end processing steps required. To reliably obtain a processing rate of 5 metric tons/day or greater, dual mechanical head-end processing lines would probably be required.

LMFBR Flowsheet Calculations

Material balance flowsheets were prepared for the reprocessing of AI reference oxide fuel assemblies at the rate of 5 metric tons (uranium, plutonium, and fission products) per day. The flowsheets are for the following four types of reprocessing operations:

1. Core and axial blanket assemblies (see Fig. 2.7).
2. Radial blanket inner ring and outer ring type I assemblies.
3. Radial blanket outer ring type II assemblies.
4. Homogenized fuel assemblies based on the scheduled removal rate from the reactor (see Fig. 2.8).

The primary purpose of the material balance flowsheets is to relate the quantities of materials (uranium, plutonium, fission products, and stainless steel) that will be encountered at different stations in a reprocessing plant. Consequently, the concentrations given in the aqueous reprocessing steps are somewhat arbitrary and should not necessarily be interpreted as the optimum conditions.

In each flowsheet, the mechanical head-end process is linked to the aqueous reprocessing by two different paths, concepts A and B. In concept A, the stainless steel hulls and wires remain with the oxide fuel through the dissolver; in concept B, the stainless steel is mechanically separated from the oxide fuel between the heating and dissolution steps. The specific treatment of the resulting products depends on whether boric acid (H_3BO_3) is added as a soluble poison. When the soluble poison is present, the (U + Pu) concentration of the product from the dissolver is fixed at 1 M, and the feed to the first TBP cycle is adjusted to 70 g of (U + Pu) per liter. In the absence of the soluble poison, the plutonium concentration of the product from the dissolver is set at a maximum of 7 g per liter, and the feed to the first TBP cycle is maintained at maximum concentrations of either 7 g of plutonium per liter or 70 g of (U + Pu) per liter (if the plutonium concentration is less than 7 g per liter).

Decay Heat Dissipation

A computer code, HEX, was developed to determine the steady-state temperatures of shrouded hexagonal arrays of LMFBR fuel rods generating heat by radioactive decay. Heat transfer between fuel rods within an assembly was assumed to be by radiation only, while heat dissipation from the shroud encapsulating the array was assumed to be both by radiation and natural convection to the surroundings. The cladding temperature of the center rod was calculated as a function of heat

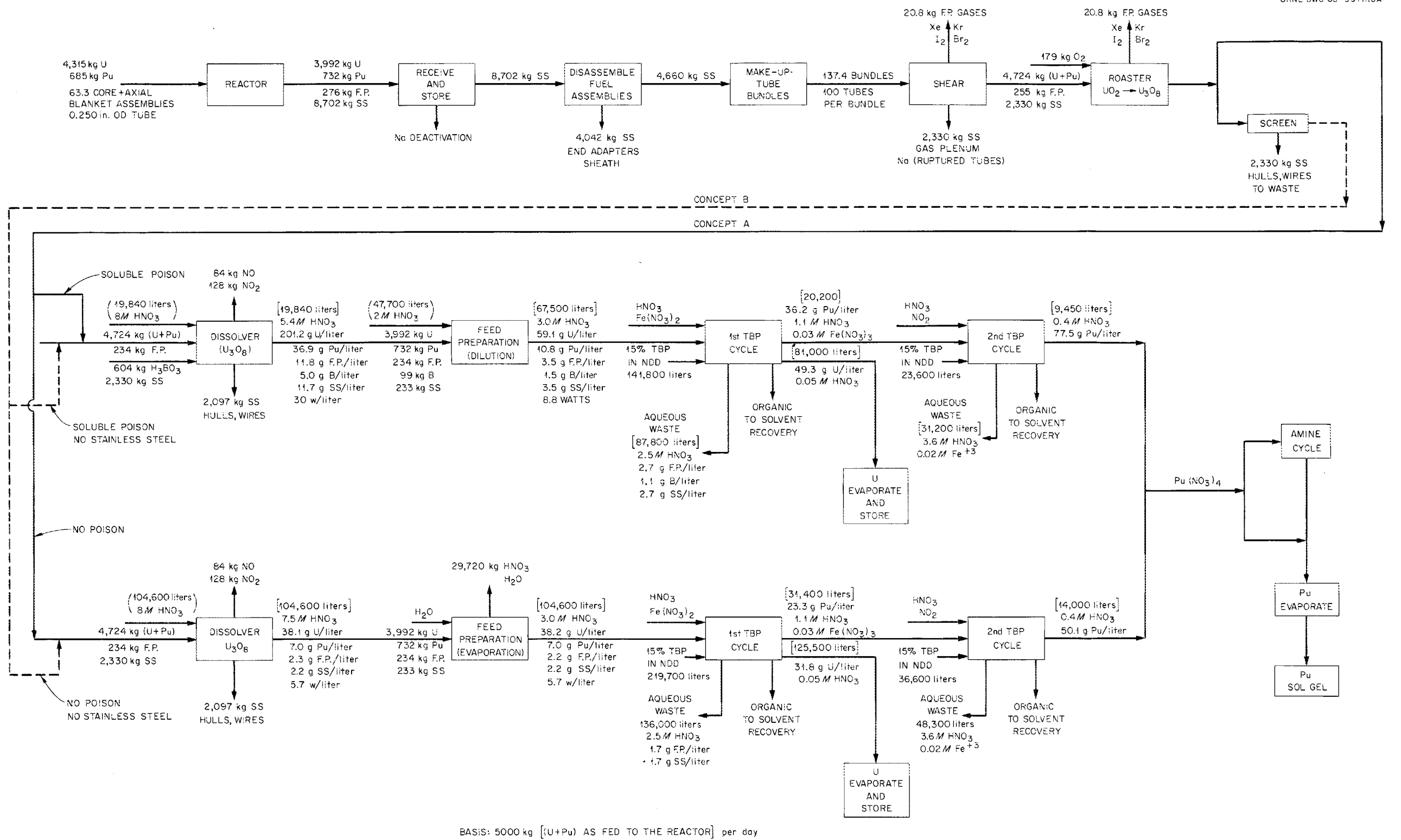


Fig. 2.7. Reprocessing Plant Material Balance for LMFBR Core and Axial Blanket Assemblies.

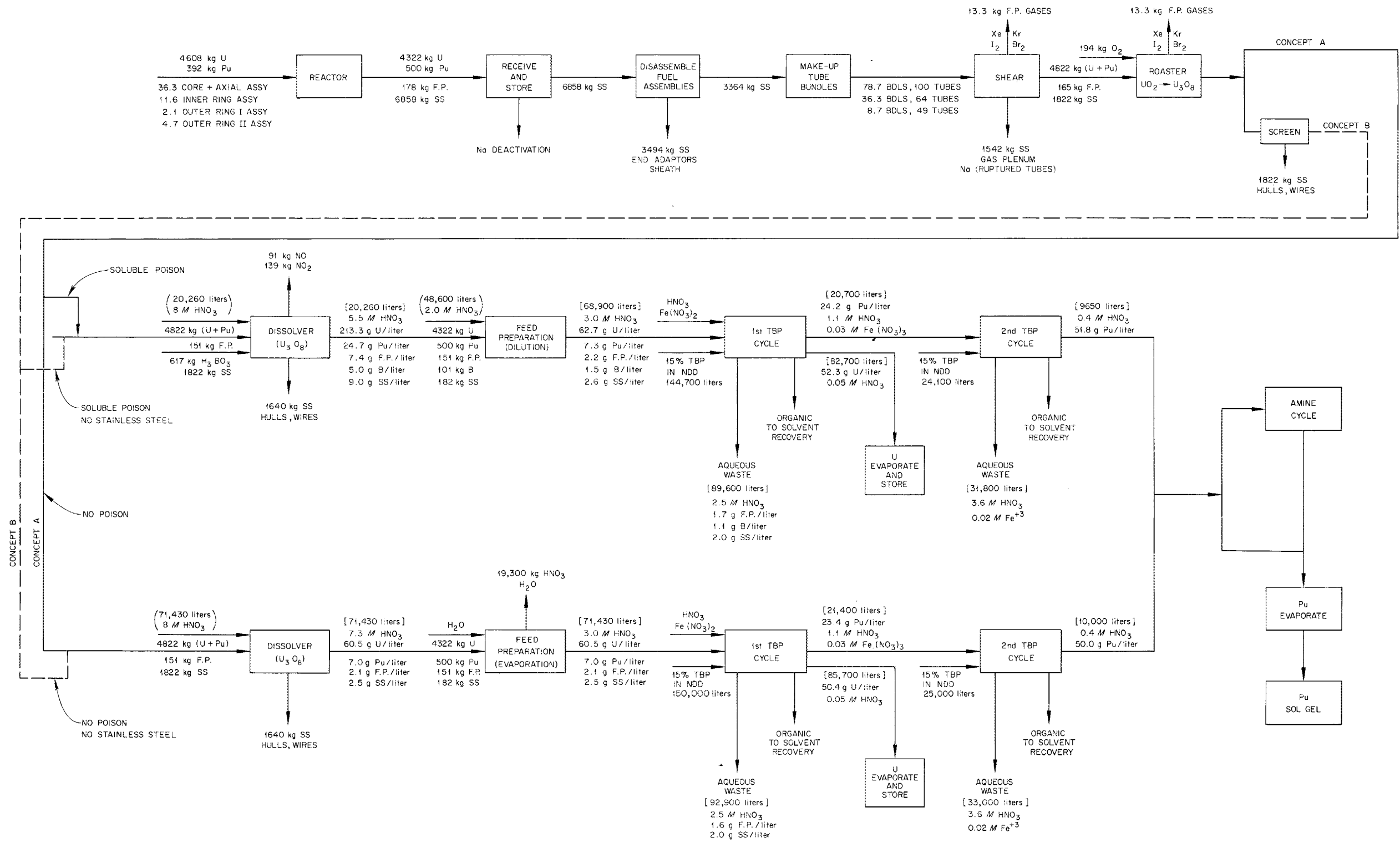


Fig. 2.8. Reprocessing Plant Material Balance for Homogenized LMFBR Fuel Assemblies.

generation rate for the Fast Flux Test Facility (FFTF), Atomics International (AI), Babcock and Wilcox (B&W), General Electric (GE), and Combustion Engineering (CE) fuel assemblies suspended vertically in an argon atmosphere at 120°F for emissivities of 0.3, 0.5, and 1.0. Curves for an emissivity of 1.0 are shown in Fig. 2.9. These curves, when compared with curves for other emissivities, show the pronounced dependence of temperature upon emissivity and the need for the experimental determination of this parameter. As an indication of the decay times corresponding to the linear powers, the linear powers of 10-, 30-, and 150-day-cooled AI fuel are 19.3, 11.2, and 4.3 w per foot of rod. From the curve for AI fuel (Fig. 2.9) and with 1275°F as the maximum allowable cladding temperature, it can be seen that for an emissivity of 1.0 the steady-state temperature exceeds 1275°F for any fuel assembly with a power greater than 5.5 w/ft (corresponding to fuel cooled 100 days). Thus, there is obviously a need for auxiliary cooling of shorter-decayed fuel.

Figure 2.10 shows the center rod temperature of a 217-rod array for the more general case of any

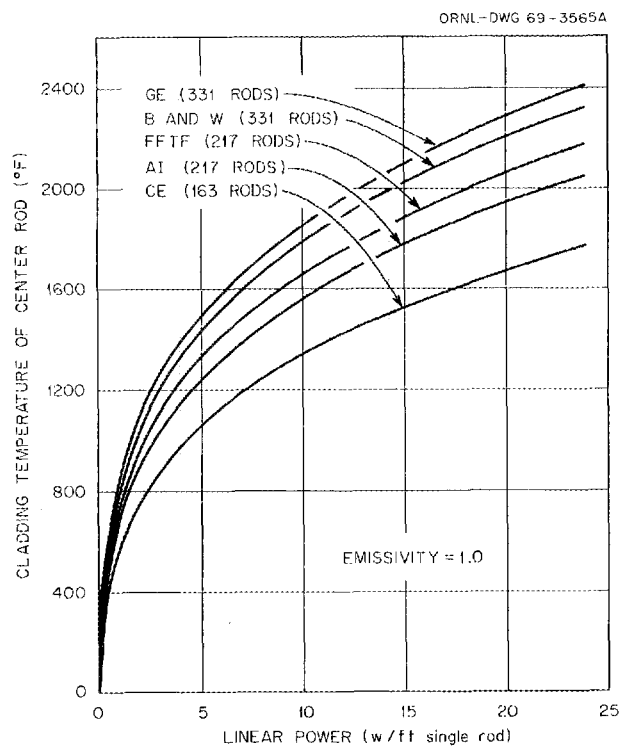


Fig. 2.9. Steady-State Center Rod Temperatures of LMFBR Fuel Assemblies.

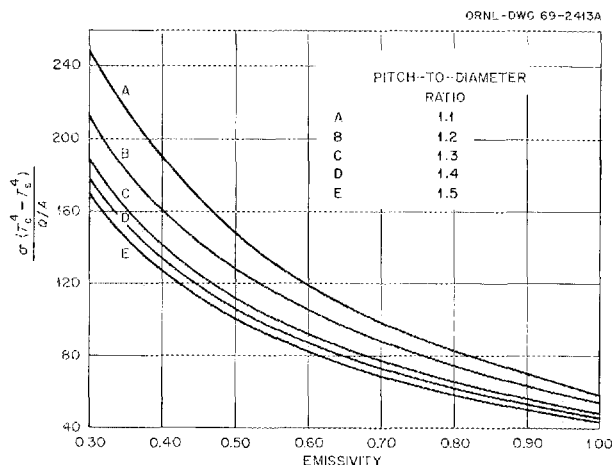


Fig. 2.10. Dimensionless Center Rod Temperature for a 217-Rod LMFBR Shrouded Hexagonal Array of Fuel.

value of rod surface heat flux, Q/A , for emissivities over the range 0.3 to 1.0 and pitch-to-diameter ratios of 1.1 to 1.5. The HEX computer code can also be used to generate similar plots for any size hexagonal array. Since the ordinate in Fig. 2.10 is dimensionless, any set of consistent units can be used. The temperatures are absolute, and the quantity σ is the Stefan-Boltzmann constant.

The sheath temperature, T_s , may be found from a heat balance equating the heat generated within the fuel rod array to the heat dissipated by the shroud to the surroundings.

A computer program has been written to calculate the hottest temperature in a fuel assembly as a function of the flow rate of gas through the bundle. All of the heat generated within the fuel element is assumed to be dissipated by convection to the gas flowing through the assembly, whereas the heat dissipated from the exterior of the assembly by radiation and natural convection is neglected. This is a reasonable approximation as long as the calculations are done for fairly high gas flow rates. Variation of temperature along the length of the element is taken into account. The cooling gas requirement for an AI reference fuel assembly to maintain a preselected temperature is shown in Fig. 2.11 for shrouded hexagonal arrays that have decayed 10, 21, 30, and 60 days.

Dismantling of Multirod Assemblies

A dismantling operation is being investigated and developed as the first head-end step in the

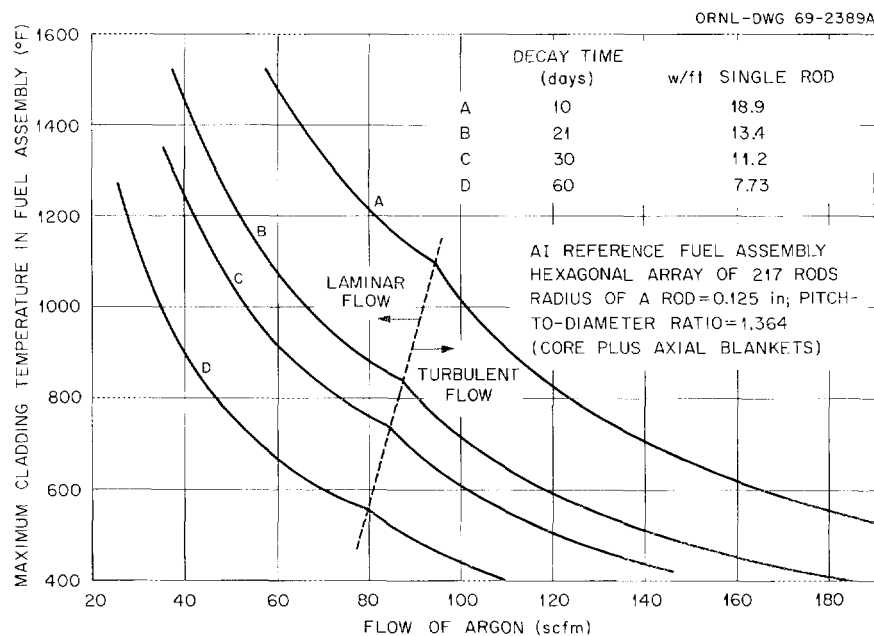


Fig. 2.11. Cooling Gas Requirement for a Typical Shrouded LMFBR Fuel Assembly.

preparation of spent LMFBR fuel for Purex processing.

The dismantling of multirod fuel assemblies usually involves one or all of the following operations: (1) decanning, (2) removal of the massive end hardware, (3) displacement of fuel rods from a shroud or sheath, (4) removal of fuel rods from a system of grids, and (5) cutting of metallic strips binding subbundles or subassemblies. The dismantling of assemblies, 5 to 8 in. in diameter and up to 18 feet long, and the removal of the end hardware (cropping), along with the shrouds (slitting), are desirable in order to prevent the massive waste metal from being included in subsequent processing steps. It may also be desirable to further disassemble or dissect a dismantled assembly to obtain single fuel rods, or small arrays of rods, to aid in the dissipation of heat in the shearing, volatile fission gas release, and dissolution steps.

A study was made of the FFTF, demonstration, and follow-on reactor fuels to determine if they could be dismantled in a manner similar to that used for LWR reactor assemblies. Included were several cropping and slitting methods and a method for dissection or disassembly, as follows:

1. *Abrasive Cutting.* Both wet and dry cutting are applicable to LMFBR assemblies; wet cutting is about 20% slower. Dry cutting rates

are normally 2.5 to 3 in.³/min, using a ¼-in.-thick blade, and the blade wear is 1:2 (i.e., 1 part blade per 2 parts metal). A holding clamp on either side of the cut is required to hold the assembly rigid and to minimize wheel breakage. Wet and dry wheel speeds are about 8,000 and 15,000 standard fpm respectively. At an optimistic cutting rate of 2.5 in.³/min for irradiated steel, a cutting time of about 1.1 min would be required to crop a typical fuel rod radially through the sheath and lower end fittings; about 2 min would be required to slit the 144-in.-long shroud.

2. *Friction Cutting.* A circular steel blade operated at about 22,000 standard fpm contacts the work surface, generating temperatures above 600°C at the point at which work is being done; this reduces the tensile strength of the material and makes the cutting easy. With this type of cutting, the LMFBR assembly sheath would deform before enough pressure could be developed to generate the heat required for effective cutting; however, the method could probably be developed for removing the massive end pieces.
3. *Electrolytic Grinding (ELG).* This method involves the use of a conductive grinding wheel and an electrolyte (salt-water) that flows between the wheel and the assembly, thus com-

pleting an electric circuit which removes the stock metal as a metallic hydroxide. About 90 to 95% of the material is removed by electrochemical action, while only 5 to 10% is removed by abrasive action; therefore, wheel wear is slight. Approximately 0.1 in.³ of metal is removed per 1000 amp per minute. A maximum current density of about 3000 amp/in.² can be attained. It would require 23.5 min to slit the sheath of a typical LMFBR fuel. Thus, the slow cutting rates of the ELG do not make it attractive for cropping and slitting operations.

4. *Roll Cutting.* A special tube cutting device, which uses pipe-cutter wheels and performs in a manner similar to that of conventional pipe cutters, could be adapted for severing LMFBR sheaths. However, the proposed high-burnup rates of the LMFBR fuel may negate the use of roll cutters because of the extreme hardness of irradiated metal. Also, longitudinal cuts on the sheath with a nibbler-roll cutter combination would be difficult on hardened metal since the LMFBR shrouds do not appear to have a rigid cross section and would tend to deform rather than be cut.
5. Other methods considered include: (1) lixiviation,¹ (2) torch cutting, and (3) the drilling out of spotwelds, if applicable. None of these methods appears as attractive as abrasive cutting, slitting, or some other similar techniques.

To summarize, abrasive disk cutting, which is currently being used to crop LWR fuels at Nuclear Fuel Services, Inc., is the most attractive method for cropping LMFBR fuel. This method appears to be superior because it permits cutting into an open shaped configuration containing springs, solid steel rods, ceramic disks, unfilled tubing, nickel reflector rods, etc. with minimal holding pressures.

A slitting saw was selected in preference to abrasive cutting for shroud removal. Cutting in the close proximity of fuel rods with an abrasive disk is not very practical because of blade wear

during a given cut. In addition, a slitting saw operates at a much slower speed (~100 rpm) as compared with several hundred rpm for an abrasive saw, thus making the collection and containment of waste metal much easier. The following is a set of selected cutting conditions based on Martensitic stainless steel of a Rockwell C hardness of 43 (to simulate irradiated stainless steel):

Blade – 6 in. in diameter; stagger tooth with chip removal clearance; 30 to 36 teeth; 133 rpm; high-speed steel or Carboloy
 Feed – 48 in./min; saw rotation in the upmilling position. (Upmilling is defined as rotation such that the object on which work is being done tends to be lifted from the holddown device.)

Shearing Analysis

The shearing requirements for LMFBR fuels appear to be basically similar to those for LWR fuel. However, LMFBR fuel presents several additional problems; for example, intact or broken fuel must be sheared in the presence of sodium, and broken or intact fuel and the can surrounding it must be sheared simultaneously. Presently, there is no existing technology for the shearing of canned fuel or assemblies (or subassemblies) in the presence of sodium or other coolants. The shearing of Yankee Atomic and Dresden LWR fuels has been successfully demonstrated by Nuclear Fuel Services, Inc.; however, the shearing of these LWR fuels is simpler than the shearing of high-burnup, short-cooled LMFBR fuels because of special problems associated with the latter: (1) the generation of large quantities of decay heat, (2) the release of fission gases, (3) the production and containment of very fine core and cladding particulates, and (4) the presence of liquid metal coolants. At the present time, it appears desirable to develop a capability for shearing canned LMFBR assemblies, uncanned assemblies, subassemblies or groupings of fuel rods, and single fuel rods. A summary of bundle, multirod, and single-rod shearing data is presented in Table 2.2.

Conversion of Cladding and Inert Metal for Solids Waste Handling

In the reprocessing of LMFBR fuel, approximately 1.75 metric tons of waste stainless steel must be

¹J. Van Impe, J. P. Rombaux, and R. Gilbert, "Simultaneous Cutting and Lixiviation Head-End Process Step for Spent Nuclear Fuel Processing Plants by Electrolytic Way," presented at the International Conference of the Constructive Uses of Atomic Energy (Joint ANS-AIF Sponsorship), November 10-14, 1968, Washington, D.C.

Table 2.2. A Survey of Three Types of Shearing Operations for LMFBR Fuel

Full-Size Assembly Shear	Multirod Shear	Single-Rod Shear
Advantages		
<ol style="list-style-type: none"> 1. Eliminates or reduces the magnitude and complexity of (1) assembly handling equipment, (2) disassembly machinery, (3) rod singulator, and (4) multirod handling machine. 2. Technology has been largely proved in industry with spent LWR fuel. 3. Reduces the frequency but not necessarily the magnitude of maintenance or downtime. 4. Reduces in-process fuel inventory. 5. Less cell space required than for complete systems of other concepts. 6. Reduces fuel and waste handling. 7. One shear would probably meet proposed production requirement. 8. Problem of contamination spread from ruptured rods is less. 	<ol style="list-style-type: none"> 1. Eliminates most decay heat removal problems. 2. Less inert material in subsequent process equipment than for the assembly shear. 3. Physically smaller than an assembly shear. 4. Less fission gas released per cut than with an assembly shear. 5. Less specific static and dynamic localized floor and building loads than the assembly shear. 6. Remote maintenance and replacement easier than for the large assembly shear. 7. Cost of the shear is less than that of an assembly shear. 	<ol style="list-style-type: none"> 1. Easily handled remotely because of small physical size. 2. Decay heat removal is not a problem. 3. Less fission gas release per cut and easier subsequent control. 4. A minimum of inert material is sent to subsequent process steps. 5. Batch (criticality) problems are minimized. 6. Shorter sheared lengths possible. 7. Standby units of parallel lines economically feasible. 8. Shear cost is less than for the other concepts.
Disadvantages		
<ol style="list-style-type: none"> 1. More difficult to maintain and replace due to its physical size. 2. Increase in quantity and physical size of inert material in subsequent process equipment. 3. Decay heat dissipation problems. 4. More fission gas released per cut than with other concepts. 5. May encounter difficulty in shearing short lengths. 6. Potential for increasing criticality problems. 7. Increases specific static and dynamic localized floor load. 8. More force or energy is required per cut. 9. Shear cost is the highest. 	<ol style="list-style-type: none"> 1. Disassembly or dissection to sub-assemblies required. 2. May require rod singulator and bundling machine. 3. More difficult to maintain and replace than a single-rod shear. 4. Specific static and dynamic localized floor loads increased as compared with a single-rod shear. 5. It may be more difficult to shear short lengths than with the single-rod shear. 6. Specific cost of shear is higher than a single-rod shear. 7. More force or energy is required per cut than a single-rod shear. 8. No established technology. 	<ol style="list-style-type: none"> 1. Complete disassembly to individual fuel rods required. 2. Singulator machine is necessary. 3. Potential problems with feeder due to the short cycle time. 4. Probable shorter blade life. 5. No established technology.

handled and discarded for each metric ton of fuel (U + Pu + fission products) processed. This stainless steel waste is comprised of stainless steel end fittings, shrouds, reflector rods, wire spacers, grids, and cladding. A significant reduction in the void fraction (~88%) of the waste would be advantageous in its handling, shipping, and ultimate disposal. The calculated amounts of stainless steel components produced per metric ton of typical LMFBR fuel (U + Pu) are presented in Table 2.3.

Two methods for converting and reducing the bulk volume of the waste have been evaluated: (1) induction melting, and (2) compaction. A manufacturer of induction furnaces was consulted on the proposed application of melting down stainless steel wastes. His recommendation was favorable. In this concept, the furnace would be initially provided with a heel of molten metal before it is charged with the various waste metal components. This technique is necessary in order to initiate the melting of metallic shapes with large void fractions. The molten metal waste is finally cast into ingots, thereby reduc-

ing the waste to a minimal volume. The principal disadvantage of using induction heating is that the ceramic furnace liners must be replaced from time to time. Presently, liners can only be replaced manually. Thus, techniques for remote replacement would have to be developed.

Scoping studies of the compaction of the cladding and wire spacers were made, and some trial compactions (see Fig. 2.12) were carried out through the courtesy of the Milwaukee Foundry Equipment Division of SPO, Incorporated. The upper three briquettes shown in the figure gave the most favorable results. Compression tests made at 21,380 psi on 4.37-in.-diam columns of stainless steel hull and wire (0.250-in.-OD, 10-mil-wall tubes; and 0.093-in.-OD wire) resulted in a volume reduction of 83%. The density of the stainless steel prior to compression was 12% of theoretical; after compression, it was 70% of theoretical. The induction melting and compaction methods are sufficiently promising to warrant continued investigation, development, and evaluation.

Table 2.3. Calculated Quantities of Stainless Steel Waste Generated During the Reprocessing of LMFBR Fuel

Basis of Calculation: Atomics International reference oxide fuel core plus axial blanket assembly

Core (U + Pu) = 49.9 kg

Axial Blanket (U + Pu) = 29.1 kg

89.6 kg UO₂-PuO₂ per assembly

1-metric ton (U + Pu)/day plant = 12.68 assemblies processed per day

	Weight of SS per Assembly (kg)	Volume of Sheared Cladding per Assembly (liters)	Bulk Density (g/cc)	Volume per Assembly After Crushing (liters)	Crushed Bulk Density (g/cc)	Weight of SS per kg of (U + Pu)(kg)
Core and axial blanket:						
cladding + wire + end plug	36.77	26.84	1.37 ^a	6.57	5.6 ^a	0.465
Gas plenum:						
cladding + wire + end plug	36.77	26.84	1.37 ^a	6.57	5.6 ^a	0.465
Bottom end adaptor	14.51	9.82 ^b	1.48	2.59	5.6	0.184
Upper end adaptor	6.69	3.70 ^b	1.81	1.19	5.6	0.085
Shroud	42.62	57.63 ^b	0.74	7.61	5.6	0.539
Total	137.36	124.83		24.53		1.738

^aExperimental data.

^bMinimum calculated volume per assembly.

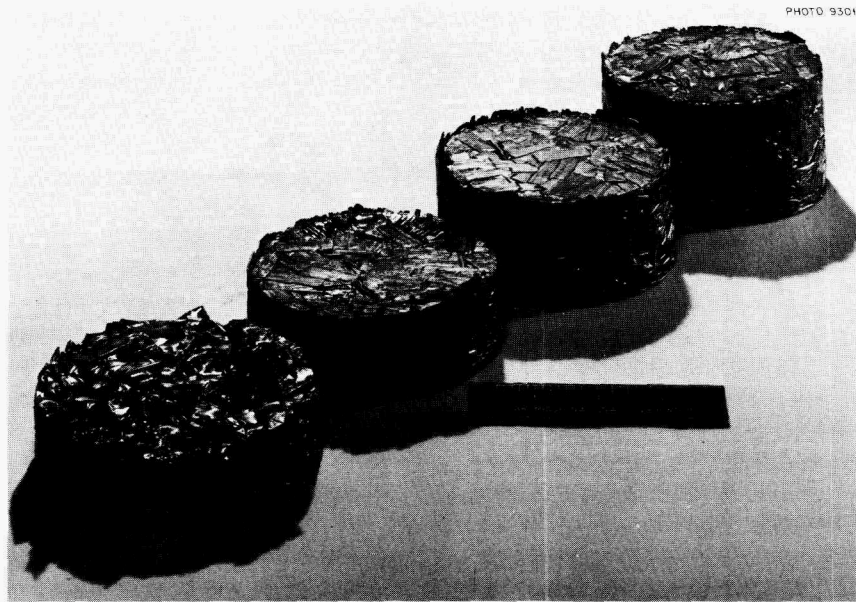


Fig. 2.12. Compaction of 1-in. Cut Lengths of 0.250-in.-OD \times 0.010-in.-Wall Stainless Steel Cladding and 0.093-in.-OD Spacer Wire. Briquetting press force on 4.5-in. cylinder at 21,380 psi increased the bulk density of the stainless steel from 12 to 70% of theoretical.

Alternative Processing Methods

Alternative methods are being considered as backup measures for the shear-leach process because of the number, nature, and magnitude of the problems associated with some of the mechanical processing operations in the handling of short-decayed, high-specific-activity, sodium-contaminated fast-breeder-reactor fuel. Chemical decladding with sulfuric acid is not practical because of safety considerations (i.e., reactions with sodium metal occur) and because of losses of fissile material to the decladding solution as well as to large volumes of waste that are inherent in the process. There are, however, metallurgical means that could be used to remove the cladding essentially quantitatively, with relatively little loss of fissile material. Argonne National Laboratory is proposing to use molten zinc at a temperature of about 800°C to dissolve the steel cladding, whereas the Belgians have proposed the use of a copper-antimony alloy to accomplish the same task. The British and the Russians have done some work on the decladding of uranium by melting the stainless steel. This latter process

appears to be the most attractive of the three alternatives because of the compact nature of the waste produced and because of the availability of materials of construction for the containment of molten stainless steel.

Tests made thus far have been of a scouting nature. In these tests, in which a number of specimens were melted at 1500 to 1700°C, it was observed that the surface tension of molten stainless steel is sufficiently high to float uranium pellets (density of 10.5 g/cc) on the surface. The high surface tension creates problems relative to the separation of the stainless steel from the uranium pellets. In tests in which 0.270-in.-diam uranium pellets and stainless steel cladding were supported in a 0.625-in.-diam alumina tube, at an angle of about 5° from the horizontal, only about 50% of the cladding material was fully separated from the uranium pellets (see Fig. 2.13). In another test in which uranium pellets clad in stainless steel were supported vertically on zirconia rubble, the stainless steel was separated essentially completely from the uranium pellets. Future tests will be designed to study different methods for separating the molten steel from the oxide pellets.

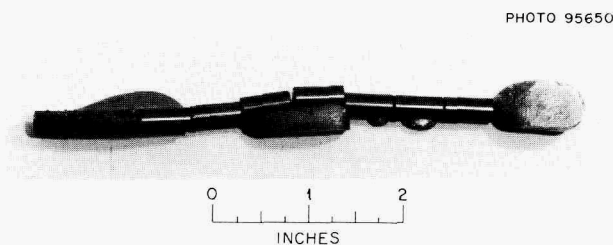


Fig. 2.13. Results of a Melt-Declad Experiment Designed to Separate Urania Pellets from the Stainless Steel Cladding.

2.3 REMOVAL OF VOLATILE FISSION PRODUCTS

As the nuclear power industry grows and the number and size of the fuel reprocessing plants increase, the release of radioactive noble gases, tritium, and iodine to the environment will become a much more important consideration than at present. In the future, the removal of essentially all radionuclides from the plant off-gas may be required. The removal of iodine from process off-gases, which requires careful control even in present reprocessing plants, will become much more difficult when short-cooled LMFBR fuels are processed.

We previously described exploratory tests of a new head-end processing step (termed voloxidation) designed to release volatile fission product gases from the fuel prior to aqueous processing.² The objective of this step is to transfer the iodine, krypton, xenon, and tritium from the fuel into a relatively small volume of gas from which they can be efficiently removed in concentrated form for storage or permanent disposal. Extrapolating from information in the literature and from our preliminary experiments, we are hopeful that this objective can be met by heating the oxide fuel to some reasonable temperature in oxygen or an inert gas stream.

Most of the information concerning the volatilization of fission products deals with UO_2 rather than with $(\text{U}, \text{Pu})\text{O}_2$ and was developed principally from studies relating to reactor safety (fuel melt-down) or LWR fuel processing by oxidation-reduction, fluidized-bed fluoride volatility, or other methods.³⁻⁵ The release of fission product gases from irradiated fuels is controlled by a diffusion process. The rate of release appears to be enhanced by: (1) decreasing the diffusion

path length by oxidation of the fuel to a powder form, and by (2) increasing the diffusion rate by heating to temperatures up to the melting point. The high melting point of oxide fuels ($> 2500^\circ\text{C}$) makes the melting of irradiated fuels a less attractive alternative than the oxidative-powdering approach. Some of the literature indicates that the presence of PuO_2 in mixed oxides suppresses the oxidation of UO_2 to U_3O_8 , but other references indicate that it may be possible to accomplish the powdering by the use of temperatures of 600°C or higher.³

We are studying the effects of many variables (temperature, sweep-gas composition and volume, plutonium concentration and burnup of the fuel, etc.) on the efficiency of the release of the fission product gases. The pieces of sheared fuel rods or fuel segments or particles are heated in quartz or nickel reactors in a stream of oxygen or an inert gas. The off-gases are passed through a series of aqueous scrubbers, molecular sieves, and charcoal traps to capture the fission products. The oxidized fuel is then dissolved in acid, and the off-gases are passed through a similar train of absorbers to obtain a material balance.

Tests with Low-Burnup Fuels

In a series of tests with 1-in. sections of stainless-steel-clad low-burnup (1800 Mwd/ton) 20% PuO_2 -80% UO_2 , heating the fuel in oxygen at temperatures in the range of 450 to 750°C for 4 to 11 hr usually dislodged only about 10% of the fuel from the cladding and removed only about 10% of the krypton. Removing the fuel from the cladding and crushing it to a powder prior to the heating-oxidation treatment did not increase the amount of krypton removed. In all of these tests, however, more than 95% of the tritium was removed from the fuel. The behavior of iodine could not be followed since all of the ^{131}I had decayed.

²Chem. Technol. Div. Ann. Progr. Rept. May 31, 1968, ORNL-4272, p. 41.

³J. H. Goode, ORNL, personal communication, January 1969.

⁴G. W. Parker et al., *Out-of-Pile Studies of Fission-Product Release for Overheated Reactor Fuels at ORNL, 1955-1965*, ORNL-3981 (July 1967).

⁵G. Brand and E. Murbach, *Pyrochemical Reprocessing of UO_2 by AIROX - Summary Report*, NAA-SR-11389 (August 1965).

Cyclic Oxidation-Reduction Treatment. — A cyclic treatment similar to that used in the Atomic International Airox Process⁵ was tried. A charge of 0.5- to 1.0-in.-long sections of a fuel rod was heated alternately in argon-4% hydrogen and in oxygen. Four cycles of treatment at 650 to 750°C over a period of 21 hr removed only about 10% of the krypton from the fuel. The fuel was not dislodged from the cladding, and we do not know if a significant fraction of the UO_2 was oxidized during the oxidation treatments.

Tests with High-Burnup Fuels

Short sections of NUMEC 316L stainless-steel-clad, mechanically blended 20% PuO_2 -80% UO_2 , irradiated to 100,000 Mwd/ton and decayed about 16 months, were heated in a slow (50 cc/min) flow of oxygen for 3 hr at 450°C and then 7.5 hr at 750°C. (NUMEC reported that 43% of the noble gases had previously been released from this fuel upon puncturing of the fuel rod.) The oxidation treatments volatilized a total of about 98% of the remaining ^{85}Kr , even though none of the fuel was dislodged from the cladding:

Oxidation Treatment	^{85}Kr Removed (% of total)
3 hr at 450°C	58.6
4 hr at 750°C	34.6
3.5 hr at 750°C	4.6
Total	97.8

Significant fractions of fission product Ru, Cs, Sb, and Nb also were volatilized. Most of this material, as well as about 2% each of the uranium and plutonium, were found on the walls of the quartz "burner" and in the burner head, which contained a glass wool filter (Table 2.4). About 3% of the ^{106}Ru and 8% of the ^{137}Cs penetrated to a trap containing type 5A molecular sieve, which was attached to the gas exit on the head of the burner. The ^{85}Kr was adsorbed at -78°C on activated charcoal traps located downstream of the molecular sieve.

We oxidized the segmented remnants of another NUMEC fuel rod (316L stainless-steel-clad, coprecipitated 20% PuO_2 -80% UO_2 , irradiated to 100,000 Mwd/ton) at 850°C. In this experiment, we volatilized millicurie quantities of a submicron cesium "smoke," which passed through a NaOH scrubber and a 2-in.-diam disposable "absolute" filter and was carried to the charcoal traps used to retain ^{85}Kr . Cesium contamination of the traps prevented an absolute determination of the quantity of ^{85}Kr released by the oxidation procedure. However, based on the amount of ^{85}Kr expected in the initial fuel and the amount found in the oxidized fuel, only about 80% of the ^{85}Kr was released by the 5-hr oxidation treatment. About 32% of the gamma-emitting radionuclides in the fuel sample also were volatilized in this experiment.

In a third experiment, sections of NUMEC stainless-steel-clad mechanically blended 20% PuO_2 -80% UO_2 (irradiated to 100,000 Mwd/ton)

Table 2.4. Distribution^a of Uranium, Plutonium, and Fission Products After Oxidation at 750°C

Procedure: Fuel rod segments heated in oxygen for 3 hr at 450°C and then 7.5 hr at 750°C.

	Oxidized Fuel + Cladding	Burner Walls	Burner Head	Molecular Sieve	Activated Charcoal
Uranium	97.9	1.3	0.9	Trace	
Plutonium	96.6	1.9	1.5	Trace	
^{85}Kr	2.2	Not detected			97.8
^{95}Nb	90.6	9.4			
^{106}Ru	56.7	6.3	34.2	2.7	
^{125}Sb	73.1	19.7	~6.7		
^{137}Cs	71.0	18.8	2.4	7.9	
^{144}Ce	96.5	2.5	0.8		

^aPercent of total found.

were oxidized for 6 hr at 800°C. Again, the fuel pellets did not disintegrate; one pellet split in half lengthwise but was intact otherwise. Based on the expected ^{85}Kr concentration in the initial fuel and the ^{85}Kr concentration in the oxidized fuel, about 87% of the krypton was removed by the voloxidation treatment.

Oxidation of Cladding

In the tests at 800 and at 850°C, the stainless steel cladding disintegrated into powder and flakes; this did not occur at 750°C. Weight-gain measurements indicated that 85 to 95% of the stainless steel was converted to oxides. The oxygen attack on the cladding is apparently affected by the irradiation as well as the temperature of oxidation. Unirradiated type 316 and 304L stainless tubing segments, when heated in air for 5 hr at 850°C, turned black on the surface but showed essentially no weight gain.

Tests with Short-Cooled Fuels

The behavior of iodine could not be followed in the above experiments because the ^{131}I had completely decayed during the long cooling period (two years) of the fuel. We are irradiating fuel rods containing sol-gel 15% PuO_2 -85% UO_2 in the ETR and will run fission product release experiments with these specimens after less than 50 days of cooling. We will use a single-rod shear to cut the fuel rods; then we will oxidize the segments in a stainless steel burner.

In preparation for these tests, we performed a 2^3 factorial experiment that was designed to show the separate effects of temperature, oxygen concentration, and gas flow rate on the volatilization of ^{85}Kr , ^{131}I , and ^{133}Xe during the high-temperature oxidation of UO_2 to U_3O_8 . We oxidized 1-g batches of short-decayed (<30 days) UO_2 under the following conditions:

Temperature	450 and 750°C
Oxygen concentration	25 and 75%
Gas flow rate	0.2 and 1.0 cfh

Statistical analysis indicated that the temperature was the principal factor governing the release of all of these fission products, although the higher gas flow rate (1 cfh) may have had a slightly bene-

ficial effect on the removal of ^{131}I from the oxide. At the higher temperature, more than 90% of the ^{131}I and more than 69% of the ^{85}Kr and ^{133}Xe were volatilized.

Processing Unit Concepts

Two engineering equipment concepts, a rotary kiln and a heated fixed bed, are being considered for the removal of fission product gases from sheared lengths of LMFBR fuel. At present, the former is preferred. A preliminary rotary kiln concept is shown in Fig. 2.14. The tumbling action in such a unit would tend to remove the oxidized surface and expose fresh fuel surfaces to the oxygen. If the fuel can be oxidized successfully to produce a powder, then the mechanical separation of the powdered fuel from the stainless steel hulls and spacer wires may be possible. This would greatly ease solids transport problems in the dissolver system.

An electrically heated rotary kiln consisting of a cylindrical retort 6.5 in. in diameter by 7 ft long has been purchased for engineering experiments. The retort is mounted on trunnion rolls and can be rotated with a chain drive at speeds in the range of 1 to 13 rpm. Material to be processed is fed into the retort by means of a sealed vibratory feeder at a maximum rate of about 5 kg/hr. The kiln is equipped with a cylindrical sleeve containing lifting flights to cascade material through the gas stream; the seals permit internal gas pressures up to 2 in. H_2O (gage).

2.4 DISSOLUTION AND FEED PREPARATION

Data on the leaching of irradiated fast reactor fuels are very limited. Information is needed concerning the dissolution rate and the metal recoveries to be expected as a function of the preparation history, the burnup, and the postirradiation temperature history of the fuel. We are procuring irradiated oxide fuels from as many sources as possible for testing. In addition to metal recovery data, information concerning the composition and physical characteristics of the leach residues is being obtained. Particular attention is also being given, both in laboratory and hot-cell studies, to the behavior of iodine in the dissolver-condenser system and to the use of fumeless dissolving

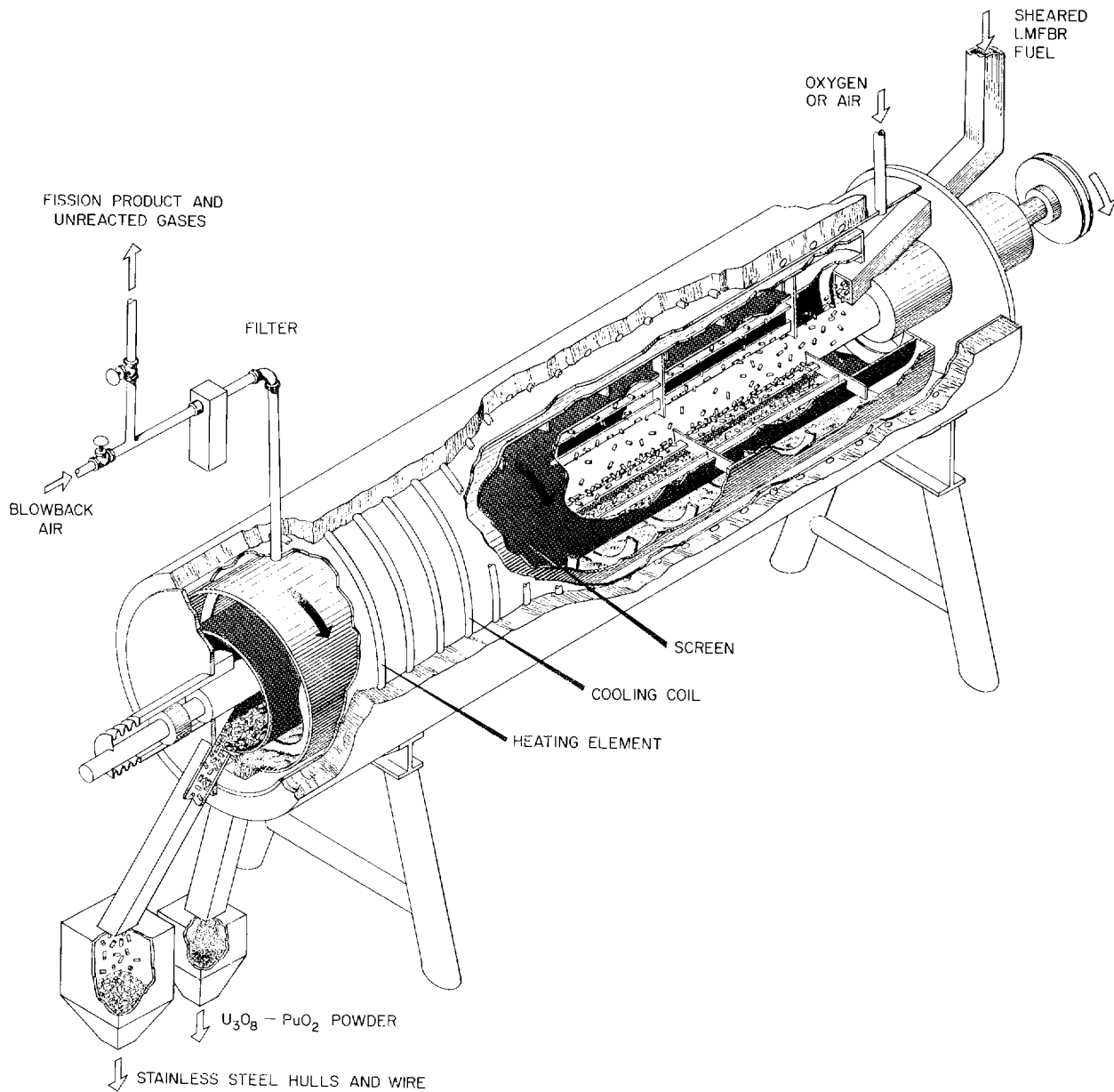


Fig. 2.14. Preliminary Concept of a Rotary Kiln for Removal of Volatile Fission Products from Sheared LMFBF Fuel.

techniques for minimizing the volume and the fume content of the off-gas to allow easier separation and containment of the iodine and possibly the ^{85}Kr and ^{133}Xe .

The dissolution of $\text{PuO}_2\text{-UO}_2$ fuels in nitric acid is affected by: (1) the percentage of PuO_2 in the fuel, (2) the type of mixture and degree of homogeneity of the fabricated fuel, and (3) the irradiation level. Pure PuO_2 dissolves in nitric acid only in the presence of fluoride ion. However, the use of fluoride is undesirable because it leads to corrosion problems during processing. Solid solutions of $\text{PuO}_2\text{-UO}_2$ (up to 35% Pu) dissolve readily in nitric acid. High irradiation levels and high temperatures in the fuel rods tend to produce a more homogeneous (i.e., more soluble) product from fuels not initially in solid solution; however, the outer radius of the fuel does not always reach sufficiently high temperatures in the reactor to ensure conversion to a solid solution. Consequently, for maximum leachability, care should be taken in fabricating mechanically blended fuels to ensure the formation of a solid solution by control of particle size, blending, and sintering time and temperature.

More than 25 dissolution experiments were made this year with samples of mechanically blended, sol-gel, and coprecipitated 5 to 28% $\text{PuO}_2\text{-UO}_2$ (irradiated from 1800 to 100,000 Mwd/ton) to determine the effects of the leaching time, temperature, and leachant composition. The results of these experiments are being correlated with fabrication and irradiation data for the samples and with dissolution data from 21 earlier tests made with coprecipitated 20% $\text{PuO}_2\text{-80% UO}_2$ that had been irradiated from 9000 to 99,000 Mwd/ton.

Results of the leaching experiments with stainless-steel-clad fuel pieces are summarized in Table 2.5. Many of the experimental conditions used were part of scouting experiments for defining flowsheet parameters (e.g., dissolution time cycles, etc.). In many cases, conditions were not optimal and the amounts of undissolved plutonium in the residues were relatively high. Also, the small amounts of the fuel samples available in most cases precluded systematic study of the effects of leaching variables on recoveries obtainable from any one sample. Interpretation of the data in Table 2.5 and other data from the experiments, therefore, is difficult, because of the large number of variables. However, these data (and other data

not shown for the experiments) indicate the following:

1. Recoveries of 99.8% or higher of the plutonium can usually be obtained by leaching for up to 12 hr with boiling 8 M HNO_3 . Most of the fuel dissolves rapidly; however, a small fraction of the plutonium dissolves quite slowly and, in some cases, is essentially insoluble in 8 M HNO_3 . Uranium recoveries are almost always higher than plutonium recoveries. In instances when high plutonium losses occur, apparently some of the plutonium in the fuel is wholly or partially segregated from the uranium and hence is in refractory form. The refractory residues can be dissolved by adding 0.05 M HF to the leach solution.
2. Not enough data are available to determine in what manner and to what extent the leachability of the fuel is affected by the fuel fabrication history or the oxidation treatment for removing volatile fission products.

Rate of Dissolution

Three 2-hr leaches with boiling 8 M HNO_3 dissolved 99.6% of the plutonium and more than 99.9% of the uranium from stainless-steel-clad coprecipitated 20% $\text{PuO}_2\text{-80% UO}_2$ that had been irradiated to about 2000 Mwd/ton (Table 2.6). The almost identical uranium and plutonium leaching rates ($\sim 94.5\%$ in the first 2 hr) indicate that more than 99% of the irradiated fuel was homogeneous.

Dissolution data for three samples of high-burnup (100,000 Mwd/ton) 20% $\text{PuO}_2\text{-80% UO}_2$ with boiling 8 M HNO_3 are shown in Table 2.7. All of the samples had undergone an oxidation treatment to remove volatile fission products prior to leaching. Plutonium recoveries of 99.2 to 99.9% were obtained from two of the samples in 9.5 to 12 hr of leaching. However, with the third sample, 8.9% of the plutonium was still undissolved after four 2-hr leaches. Since more than 99% of the uranium was dissolved from this sample in 4 hr, it appears that the fuel was nonhomogeneous. The oxides for runs 23 and 37 are reputed to be from the same batch and irradiated in the same capsule. If this is true, it is difficult to understand how the plutonium dissolution characteristics of the two samples could be so different. Conceivably, the plutonium analysis of the residue in run 23 could be incorrect; however, rechecking of the analysis

was not possible because of the small amount of material available.

Figure 2.15 shows the effect of the length of the sheared fuel on the overall dissolution rate in boiling 4 M HNO₃ of stainless-steel-clad sol-gel (U,Pu)O₂, irradiated to 20,000 Mwd/ton. The use of 4 M HNO₃ rather than the usual 8 M HNO₃ in the first two leaches magnified the geometry (exposed surface) effects. The use of 7 or 8 M HNO₃ that was 0.04 or 0.05 M in HF, respectively, for the third leach increased the leaching rate and

provided plutonium recoveries of more than 99.8% in 8.5 to 10 hr of total leaching time.

Attack on Cladding

The stainless steel cladding of irradiated LMFBR fuel specimens dissolves in nitric acid more readily than the cladding of LWR fuels. Dissolution is relatively rapid at the start of leaching but decreases to a slow rate during the latter part of the leach, indicating that the surface

Table 2.5. Results Obtained by Leaching Irradiated PuO₂-UO₂ Fuels in Boiling Nitric Acid

Run No.	% PuO ₂	Approximate Burnup (Mwd/ton × 10 ⁻³)	Fuel Type ^a	Weights		Oxidation Temp. (°C)	Leaching		Residue wt (mg)	Undissolved	
				Fuel + Cladding (g)	Fuel (g)		HNO ₃ (M)	Total Time (hr)		U (%)	Pu (%)
1	5	10	b	9.4	6.7	c	8	3.5	9	0.06	0.11
2	5	10	b	9.1	6.0	c	8	7.5	49	0.13	1.0
3	5	20	b	9.2	6.5	c	8 ^d	7.5	13	0.01	0.04
4	5	20	b	9.4	5.9	c	8	3.0	141	0.06	10.2
5	20	20	?	4.0	1.7	450	4	3.0	21	0.18	0.47
6	20	20	CP	4.8	1.2	c	4	12.0	84	1.04	1.7
7	20	22	MB	5.7	1.1	c	8	6.0	47	1.3	1.3
8	20	50	CP	7.0	1.8	750	4 + 8	7.0	134	0.09	1.51
9	20	55	MB	8.3	1.4	750	4 ^d + 8 ^d	5.3	163	0.06	0.41
10	20	53	MB	5.2	0.6	c	4	10.5	<10	<0.01	<0.01
11	20	20	SG	5.8	4.7	c	4 + 8 ^d	9.0	239 ^e	<0.01	0.01
12	20	20	SG	3.7	2.4	c	4 + 8 ^d	9.0	435 ^e	<0.01	0.02
13	20	20	SG	12.6	10.2	c	4 + 7 ^d	8.0	498 ^e	0.04	0.13
17	20	2	CP	20.7	19.4	c	8	8.0	244	<0.01	<0.01
18	20	2	CP	20.6	17.4	c	8	7.0	108	0.01	0.06
19	20	2	CP	22.5	17.8	c	8	8.0	220	0.02	0.13
22	20	2	CP	22.7	19.6	c	8	6.0	188	0.04	0.41
26	20	2	CP	35.5 ^f	28.5	c	8	6.0	30	0.05	0.07
23	20	100	MB	8.0	2.1	750	8	8.0	1170	0.48	8.9
36	20	100	CP	10.4	1.9	850	8	9.5	3555 ^g	0.33	0.82
37	20	100	MB	10.1	6.2	800	8	12.0		0.15	0.08
15	28	70	CP	18.9	15.3	c	4	8.5	560	0.07	0.14
16	28	73	CP	4.0	2.6	c	13	6.0	63	<0.01	<0.01

^aCP = coprecipitated; MB = mechanically blended; SG = sol-gel.

^bMixture of mechanically blended and coprecipitated oxides.

^cNot oxidized.

^dContained 0.05 M HF.

^eContained undissolved ThO₂ from melted insulator pellet.

^fSulfex deacid.

^gMostly powdered, oxidized stainless steel. Bulk pieces of cladding are not included in the residue weights listed in this column.

layer is probably activated during irradiation. The circulating sodium coolant in the reactor is expected to leach chromium from the surface of the stainless steel during irradiation and to reduce its passivity to the leaching solutions. In addition, the loss of chromium, possibly coupled with irradiation effects, reduces the resistance of the cladding to oxidation. While unirradiated stainless steel tubing is dulled slightly by exposure to air at 850°C (weight gain, ~0.1%), samples of stainless steel cladding from fuel irradiated to 100,000 Mwd/ton under LMFBR conditions flaked and powdered in air at 800°C and gained 36% in weight.

The amount of cladding dissolved (based on iron analyses of the leach solutions) with boiling 4 to 8 M HNO₃ has varied from less than 1% to about

Table 2.6. Leaching of Coprecipitated 20% PuO₂-80% UO₂ with Boiling 8 M HNO₃ (Run 22) (~2000 Mwd/ton burnup)

Leach No.	Leach Time (hr)	Amount Dissolved (% of total)	
		Uranium	Plutonium
1	2	94.5	94.3
2	2	4.4	4.5
3	2	1.0	0.8
Residue		0.04	0.41

Table 2.7. Leaching of NUMEC 20% PuO₂-80% UO₂ with Boiling 8 M HNO₃ (~100,000 Mwd/ton burnup)

Leach No.	Amount Dissolved (% of total)								
	Run 23 ^a			Run 36 ^a			Run 37 ^a		
	Time (hr)	U	Pu	Time (hr)	U	Pu	Time (hr)	U	Pu
1	2	98.5	84.5	5.5	99.1	98.0	4	99.4	98.8
2	2	0.6	3.9	2	0.5	0.9	4	0.4	1.0
3	2	0.3	1.7	2	0.1	0.3	4	0.1	0.1
4	2	0.1	1.0						
Residue		0.5	8.9	0.33	0.82		0.15	0.08	

^aDescription of samples is in Table 2.5.

10% but is usually less than 5%. Addition of HF to the leach solution greatly accelerates the attack on the cladding; about 25% of the cladding was dissolved in one test.

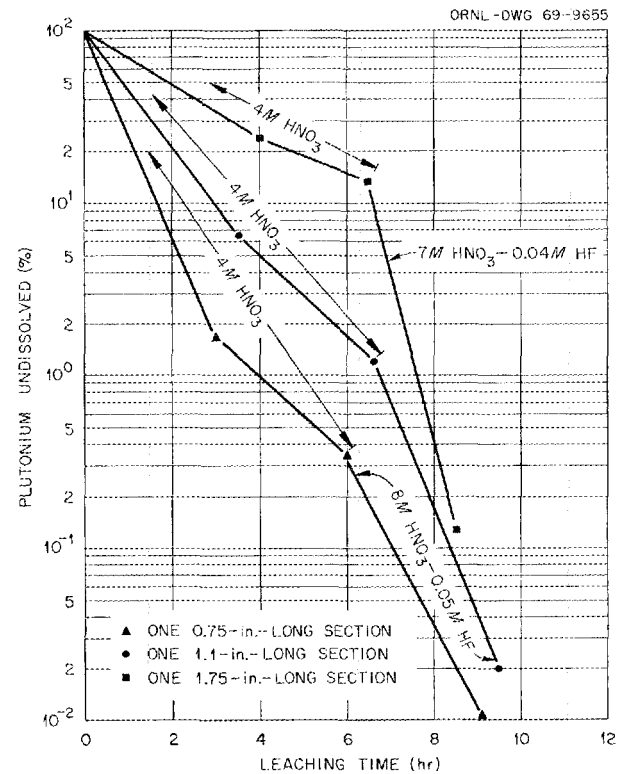


Fig. 2.15. Effect of Sheared Fuel Length on the Dissolution of Stainless-Steel-Clad Irradiated 20% PuO₂-80% UO₂ in Boiling Nitric Acid.

Leach Residues

In addition to undissolved plutonium and uranium, the leach residues contained stainless steel metals (probably as small particles of stainless steel), from 20 to 88% of the total ^{106}Ru , and undetermined amounts of Mo, Pd, Rh, Zr, Mn, Al, and Si.

Iodine Behavior During Dissolution and Feed Adjustment

We plan to remove essentially all of the iodine from the nitric acid solution of LMFBR fuels by volatilizing it as I_2 prior to solvent extraction. Minimizing the amount of iodine that is allowed to contact the organic extractants should simplify off-gas treatment problems and avoid possible difficulties caused by the presence of iodine in the solvent extraction system. The partial pressure of iodine over nitric acid solutions is being determined as a guide for studies of the iodine removal process.

Several effects that are important in studying the behavior of iodine in nitric acid solutions are summarized in the following list. Although these effects have been observed in various experimental tests, little quantitative information has been obtained on the equilibria involved or on the reaction kinetics.

1. Iodide is easily oxidized to volatile free iodine (I_2) in nitric acid solutions. The literature indicates that nitrous acid, an impurity normally present to some degree in nitric acid, is more effective kinetically in the oxidation process than nitric acid.
2. Nitric acid at high concentrations is capable of oxidizing free iodine to iodate (or possibly periodate). These species are not volatile. The effect is strongly dependent on acid concentration, and is best observed at concentrations greater than 8 M.
3. Nitrous acid is capable of reducing iodate to the free iodine state in nitric acid solution. This is a favorable factor that limits the formation of iodate during dissolution of the fuel since the nitrous acid that is generated by reaction of HNO_3 with UO_2 acts as a holding reductant. The tendency toward iodate formation is greater if the solution is digested after the reaction with UO_2 is complete, particularly if the dissolver-condenser system is of a design that tends to trap volatilized iodine (i.e.,

the dissolver is connected to a reflux condenser).

4. The volatilization of iodine from nitric acid solution depends on the form of the iodine present (i.e., free iodine volatilizes readily), the iodine partial pressure, and the amount of gas sparging that is used for transpiration of the iodine. The partial pressure of free iodine in nitric acid increases with temperature and is relatively high above the solid iodine sublimation temperature of 82°C . However, there are no reliable data on the partial pressure and activity coefficients of iodine in nitric acid fuel dissolver solutions or on the species that may be present.
5. The oxidizing or reducing power induced by radiation of the iodine-bearing solution may be an important factor affecting the iodine valence. Initial tests indicate that radiation can both induce the formation of iodate and promote its reduction to free iodine.

2.5 SOLVENT EXTRACTION WITH TBP

Initial emphasis in the solvent extraction studies has been on establishing flowsheet conditions for the interim processing of LMFBR fuels in an existing plant.⁶ The first-cycle solvent extraction flowsheet⁶ is based on the use of 15% TBP and feeds of subcritical concentrations (≤ 5.0 g of fissile plutonium per liter) in existing geometrically unrestricted equipment. The overall process calls for the coextraction and partitioning of plutonium from uranium in the first cycle, followed by a TBP cycle and an ion exchange (or amine extraction) cycle for further purification of the plutonium. Several alternative flowsheets are also being studied. In addition, where pertinent, the studies are being expanded to include those of a more general nature in order to define the most suitable flowsheets for use in plants designed specifically for processing LMFBR fuels.

Extensive studies are being made to obtain a better understanding of the factors affecting solvent degradation and to evaluate our tentative conclusion that problems arising from solvent radiation damage sustained during the processing

⁶E. L. Nicholson, *Preliminary Investigation of Processing of Fast-Reactor Fuel in an Existing Plant*, ORNL-TM-1784 (May 8, 1967).

of short-cooled LMFBR fuels will not seriously impair the efficiency of the Purex process.

Flowsheet Development

In a tracer-level batch countercurrent test, fission product decontamination factors (DF's) were determined for the extraction-scrub system of the first-cycle Purex flowsheet. Recoveries of both plutonium and uranium were higher than 99.9%, and fission product DF's were as follows: 700 from ^{95}Zr , 260 from ^{95}Nb , >180 from ^{103}Ru , >400 from ^{144}Ce , >2800 from ^{137}Cs , >3000 from $^{140}\text{Ba-La}$, and 1.2 from ^{131}I .

The solvent used in this test was 15% TBP in *n*-dodecane (NDD), and the scrub was 2 M HNO_3 . Eight extraction and three scrub stages were used; the feed/solvent/scrub ratios were 1.0/1.8/0.3. The feed was 3 M in HNO_3 and contained 7.2 g of Pu(IV) and 66 g of uranium per liter; some solution obtained from the leaching of a mixture of long-decayed $\text{PuO}_2\text{-UO}_2$ and short-decayed UO_2 was added to provide fission products.

Partitioning of Plutonium from Uranium. — The use of ferrous nitrate⁷ (stabilized with hydrazine) as an alternative to ferrous sulfamate for reducing plutonium in the partitioning step continued to show promise. Elimination of ferrous sulfamate avoids the formation of large amounts of sulfate, which represents a waste problem and also interferes severely with plutonium extraction in the second TBP cycle.

Very efficient partitioning of plutonium from uranium was obtained earlier⁸ in a batch countercurrent test using 0.2 M HNO_3 –0.2 M $\text{Fe}(\text{NO}_3)_2$ –0.013 M N_2H_4 solution. The amount of Fe(II) supplied was equivalent to twice the stoichiometric amount required for reducing the plutonium. We have shown in recent tests that, if the acid concentration in the strip solution is kept low, the partitioning of plutonium and uranium can be accomplished with reduction of only part of the plutonium. In a batch countercurrent test using only about 25% of the stoichiometric amount of Fe(II) needed for reduction of all of the plutonium, more than 99.9% of the plutonium was stripped

Table 2.8. Batch Countercurrent Partitioning of Plutonium and Uranium, with Reduction of Only Part of the Plutonium

Organic feed: 15% TBP–NDD containing 2.94 g of Pu and 31.4 g of U per liter

Strip solution: 0.15 M HNO_3 –0.02 M $\text{Fe}(\text{NO}_3)_2$ –0.01 M N_2H_4

Flow ratios, feed/strip/scrub: 6/1/1

Stage	Concentration in Organic Phase (g/liter)		Concentration in Aqueous Phase (g/liter)	
	Pu	U	Pu	U
Strip-4	0.0012	24.2	0.55	47.0
-3	0.079	31.2	6.6	62.6
-2	1.05	33.1	18.9	63.0
-1	2.23	32.5	19.2	52.5
Organic feed	2.94	31.4		
Scrub-1	2.52	32.4	20.5	44.0
-2	3.00	26.0	20.0	28.9
-3	3.44	17.0	17.7	14.4

(Table 2.8). The strip solution was 0.15 M HNO_3 –0.02 M $\text{Fe}(\text{NO}_3)_2$ –0.01 M hydrazine. The uranium concentration of the plutonium product solution was about 14 g/liter (8% of the total uranium). This, of course, could have been decreased to a much lower level by the addition of more scrub stages. A highly effective separation of the uranium from the plutonium product should not be necessary since further removal of uranium will be obtained in the final purification (ion exchange or amine extraction) cycle. Under these conditions, most of the plutonium is stripped as Pu(IV); the reductant improves the separation efficiency in the plutonium-dilute end of the system. The presence of the reductant is particularly important if the solvent contains a significant concentration of dibutylphosphoric acid (TBP degradation product) since this compound retains plutonium.

Efficient partitioning was also demonstrated using U(IV) reductant (see Fig. 2.16). Partitioning with U(IV) has been studied extensively^{9,10} in the

⁷D. E. Horner, *The Use of Ferrous Nitrate as a Plutonium Reductant for Partitioning Plutonium from Uranium in the Purex Process*, ORNL-4383 (April 1969).

⁸Chem. Technol. Div. Ann. Progr. Rept. May 31, 1968, ORNL-4272, pp. 49–50.

⁹C. S. Schlea et al., *Uranium(IV) Nitrate as a Reducing Agent for Plutonium(IV) in the Purex Process*, DP-808 (1963).

¹⁰H. A. C. McKay, R. J. W. Streeton, and A. G. Wain, *Mixer-Settler Runs to Study Uranium(IV) as a Reductant in Uranium-Plutonium Separation*, AERE-R-4381 (1963).

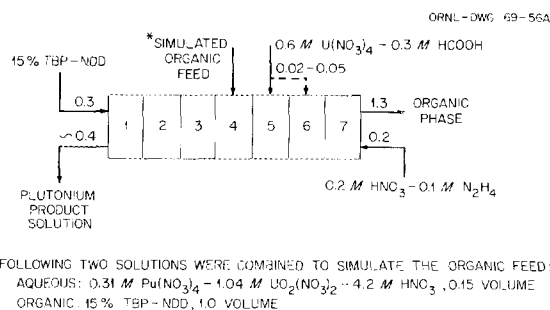


Fig. 2.16. Partitioning with Dilute Acid-Uranous Nitrate.

United States and Europe; it is presently used in Europe on a production basis. Our tests were conducted in a glove box furnished with an inert (argon) atmosphere. A series of batch counter-current tests were made with uranous nitrate solutions (stabilized with formic acid) that had been obtained from a facility that prepares uranous nitrate solutions for sol-gel studies. Preliminary tests showed that formic acid was not an adequate stabilizer in the solvent extraction system; therefore, hydrazine was added to the nitric acid solution fed to the last stage. The system had four stripping and three scrub stages. Varying the amount of added uranous ion from 130 to 50% of the stoichiometric amount required to reduce all of the plutonium did not significantly affect the results. In each experiment, more than 99.9% of the plutonium, along with about 3% of the uranium, was stripped from the organic phase. The amount of uranium contamination could be decreased by using more scrub stages. Usually the uranous nitrate was added to stage 5; however, when 50% of the stoichiometric amount of U(IV) was used, it was necessary to add it to stage 6 to obtain essentially complete plutonium removal.

Second-Cycle Studies. — The plutonium product stream from the first-cycle partitioning step contains Pu(III), which must be oxidized to Pu(IV) prior to extraction in the second TBP cycle. We are evaluating the use of NO gas as an alternative to NaNO_2 , which is usually used as the oxidant but has the disadvantage of contributing sodium to the waste. In a recent test, complete oxidation of the plutonium was obtained with considerably less than the stoichiometric amount of NO. In this test, finely dispersed bubbles of NO gas were passed at the rate of 2 cc/min through 100 ml of simulated first-cycle product solution at room

temperature. The solution was 2.2 M in HNO_3 and 0.03 M in hydrazine and contained 1.8 g of uranium, 21 g of Pu(IV), and 4.2 g of Pu(III) per liter. Within 1 hr, more than 99.9% of the plutonium was in the form of Pu(IV). The oxidation was considerably more efficient than in earlier tests at 0.5 M HNO_3 concentration.

These results suggest that nitrous acid is formed, presumably by the reaction



and are in accord with the known autocatalytic oxidation of Pu(III) with HNO_2 . Other investigators have shown that the rate of this oxidation reaction is proportional to the first power of the HNO_2 and Pu(III) concentrations and to the second power of the HNO_3 concentration.¹¹

More than 99.8% of the plutonium was extracted with 15% TBP-NDD in a batch countercurrent demonstration of the second-cycle flowsheet with a feed that was 4 M in HNO_3 and contained 18 g of Pu(IV) per liter. The system had five extraction and three scrub stages, and the aqueous/organic phase ratio was 1/0.9. The plutonium was readily stripped with dilute nitric acid containing a small amount of Fe(II) to ensure complete stripping of the plutonium. Addition of a plutonium reductant is particularly important if the solvent happens to contain significant concentrations of TBP degradation products. We expect that the second-cycle product solution will have a plutonium concentration of about 50 g/liter.

Alternative Flowsheets

Co-stripping of the plutonium and uranium with dilute acid is being examined as an alternative to partitioning in the first TBP cycle. In the alternative method, the separation of plutonium from uranium is accomplished by first coextracting the two metals with TBP and then partitioning in the second cycle (this is a common arrangement of the Purex flowsheet); selective removal of plutonium from the first-cycle product solution by an anion exchange resin process or by amine extraction (see Sect. 2.6) may be used instead of partitioning if

¹¹E. K. Duker, "Kinetics and Mechanisms for the Oxidation of Trivalent Plutonium by Nitrous Acid," *J. Am. Chem. Soc.* **82**, 9 (1960).

desired. In a batch countercurrent demonstration of the co-stripping step, more than 99.9% of the plutonium and about 99.7% of the uranium were stripped in seven stages with 0.01 M HNO₃ at an organic/aqueous phase ratio of 1.5/1.

Extraction of Iodine in the Presence of Mercuric Ion

Mercuric ion is known to form strong complexes with iodine in aqueous solutions.¹² The addition of mercuric salts to process solutions has been used to control the release of radioiodine from processing plants.^{13,14} During the development of the Thorex Process,¹⁵ it was noted that the mercury-iodine complex was extracted from acid-deficient nitrate solutions by TBP. In studies of the extraction of the complex into TBP-NDD from acid solutions, we have found that the extraction is reversible and is dependent upon the acid, mercury, and TBP concentrations. Also, we have found that the mercury-iodine complex is strong enough (at least outside of a radiation field) to greatly hinder the reaction of iodine with the solvent phase. For example, when elemental iodine was extracted and the organic phase was aged one week, only 20% of the iodine could be stripped with 0.1 M Na₂S₂O₃ solution. On the other hand, 93% of the iodine was stripped from solvent containing mercury-iodine complex after aging one week. In another comparison test, more than 99% of the mercury-iodine complex that had been aged for 42 days in 15% TBP-NDD was stripped in one contact with 5.6 M HNO₃ containing 0.1 M Hg²⁺, but only 20% of the iodine was

stripped with this solution when the aged organic phase contained only elemental iodine.

Coefficients for the distribution of the mercury-iodine complex between 15% TBP-NDD and nitric acid-mercuric nitrate solutions are given in Table 2.9. In these tests, the mercury-iodine complex was extracted into the solvent and the solvent phase was then contacted with nitric acid solutions, some of which contained mercuric salts. The distribution coefficient, D_a^0 , decreased from about 50 with 0.02 M HNO₃ in the aqueous phase to 0.42 at 8 M HNO₃. Adding 0.05 M Hg²⁺ to the aqueous phase (3.6 M HNO₃) decreased the distribution coefficient by a factor of 6.

Based on tests with ²⁰³Hg and ¹³¹I tracers, the extracted complex, which is colorless, contains one mole of mercury per mole of iodine. Extraction coefficients for the complex are approximately proportional to the second power of the TBP concentration. Additional data for the extraction of the mercury-iodine complex with TBP and other extractants are given in Sect. 2.7.

Table 2.9. Distribution of Mercury-Complexed Iodine Between 15% TBP-NDD and Nitric Acid

Organic phase: 15% TBP-NDD containing mercury-iodine complex (initial mercury and iodine concentrations each about 5×10^{-4} M)

Aqueous phase: HNO₃ or HNO₃-Hg(NO₃)₂ solutions

Contact: 10 min at phase ratio of 1/1

Approximate Final Aqueous HNO ₃ Concentration (M)	Iodine Distribution Coefficient (D_a^0)				
	Mercury Concentration in Aqueous Phase (M)				
	0	0.01	0.05	0.1	0.2
0.02	50				
0.2	35				
2	20				
3.6	2.3	0.75	0.37	0.31	0.25
5.6	0.88				0.043
8	0.42				0.0085

¹²C. H. Holm, *Retention of Iodine in Process Solutions by Mercuric Salts*, HW-21103 (1951).

¹³G. K. Cederberg and D. K. Macqueen, *Containment of Iodine-131 Released by the RaLa Process*, IDO-14566 (1961).

¹⁴S. R. Smith, "Suppression of Radioiodine Release from a Radiochemical Separations Plant," *Nucl. Appl.* 5, 20-23 (1968).

¹⁵R. H. Rainey, A. B. Meservey, and R. G. Mansfield, *Laboratory Development of the Thorex Process*, Progress Report Dec. 1, 1955 to Jan. 1, 1958, ORNL-2591.

Solvent Stability

Studies of the effect of radiation on the Purex process were continued. In experiments with a ^{60}Co radiation source, the presence of zirconium and ruthenium in the system during irradiation had no apparent effect on the results. In hot-cell cyclic tests with fuel solutions prepared from irradiated $\text{PuO}_2\text{-UO}_2$, no effects of irradiation were found when the solvent radiation dose was about $0.3 \text{ whr liter}^{-1} \text{ cycle}^{-1}$.

Tests with ^{60}Co Source. — In cyclic tests previously reported,¹⁶ 15% TBP–NDD solvent was irradiated by a ^{60}Co source while being mixed with $3 \text{ M HNO}_3\text{-}0.4 \text{ M UO}_2(\text{NO}_3)_2$, and samples of the irradiated solvent were then subjected to characterization tests. No effects of irradiation on zirconium and ruthenium extractions were detected when the solvent radiation dose was $0.3 \text{ whr liter}^{-1} \text{ cycle}^{-1}$. Since studies by others have indicated that TBP degradation is more rapid when zirconium is present, another series of tests was run at this radiation dose level with zirconium and ruthenium (as well as ^{106}Ru and $^{95}\text{Zr-Nb}$ tracers) present during the irradiation. The zirconium and ruthenium concentrations in the nitric acid–uranyl nitrate solution were 0.9 and 0.3 g/liter respectively. The tests consisted of three cycles of extraction–irradiation, stripping, and solvent cleanup ($0.3 \text{ M Na}_2\text{CO}_3$ wash).

The ^{106}Ru extraction coefficient in each cycle for both irradiated and nonirradiated (control) solvent was about 0.004. The $^{95}\text{Zr-Nb}$ coefficient was 0.005 for nonirradiated solvent and ranged from 0.003 to 0.004 for the irradiated solvent. About 50% of the extracted ^{106}Ru and 10 to 20% of the extracted $^{95}\text{Zr-Nb}$ were retained by the organic phase after the uranium was stripped with 0.01 M HNO_3 . However, the residual activity was removed from the solvent by the carbonate wash.

Hot-Cell Cyclic Tests. — Two cyclic test runs of five cycles each were made to demonstrate that LMFBR fuels can be handled effectively by the Purex process. The available quantities of irradiated fuels were much too limited to allow operation of even a small continuous system for any significant time. Consequently, batch cross-current contacting methods were used in demonstrating the process. Also, since the fuels had been cooled for

two to three years, short-cooled UO_2 was added prior to dissolution to provide short-lived fission products. In one of the tests, the radiation power density of the fuel solution was increased by a factor of about 10 by “spiking” the solution with ^{90}Sr (in order to increase the solvent radiation dose during extraction). Results of the two runs using a 15% TBP flowsheet were satisfactory; phase separation was good and fission product DF’s were approximately as expected. A solvent radiation dose of about $0.3 \text{ whr liter}^{-1} \text{ cycle}^{-1}$, which we estimate is possibly several times higher than should occur when 30-day-cooled mixed core and blanket fuel is processed in pulsed columns by the 15% TBP flowsheet, had no observable effect on the solvent performance.

To prepare aqueous feed for these tests, long-cooled prototype LMFBR fuel specimens, irradiated from 10,000 to 64,000 Mwd/ton, were dissolved along with some irradiated UO_2 that had decayed for less than two weeks. The feed solution was then concentrated 2.4-fold by evaporation to adjust the metal and acid concentrations to the desired level. Sodium nitrite was added prior to the evaporation to hold the plutonium in the quadrivalent state. The concentrate was cooled and diluted with 0.5 M HNO_3 until a final HNO_3 concentration of 3 M was obtained. More than 99% of the plutonium in the adjusted feed was in the form of Pu(IV).

The average burnup of the dissolved fuel was about 39,000 Mwd/ton, which is slightly higher than the expected burnup of mixed core and blanket material from the A1 reference reactor. The ionic concentrations of the fission products in the feed solution should have been approximately equivalent to those that will be encountered in the processing of short-cooled LMFBR fuel, although the activity level of the solution was much lower because the fuel dissolved in the solution had been cooled for a long period of time. Part of this feed solution was spiked with a small volume of “cold” $\text{Sr}(\text{NO}_3)_2$ solution and used in the first cyclic test. The balance of the solution was spiked with $^{90}\text{Sr}(\text{NO}_3)_2$ solution (to bring its beta power density to about 2 w/liter) and then used as feed for the second cyclic test.

To ensure that all of the plutonium was quadrivalent, sodium nitrite was added to the feed solution; then the feed solution was heated to 50°C for 0.5 hr. Analyses of a sample of the feed (2.03 beta w/liter) for the second run showed that the plu-

¹⁶Chem. Technol. Div. Ann. Progr. Rept. May 31, 1968, ORNL-4272, p. 51.

tonium valence [$>97\%$ Pu(IV)] did not change over a period of 3.5 weeks.

A complete process cycle involved: (1) contacting the solvent for 30 min with the feed, (2) scrubbing the extract with four successive volumes of scrub solution (2 M HNO₃, 20 g of uranium and 6 g of plutonium per liter), (3) co-stripping the plutonium and uranium with 0.1 M HNO₃, and (4) washing the solvent with dilute sodium carbonate solution. The aqueous phase from (1) was contacted six additional times with fresh solvent to complete the extraction of plutonium. The estimates of the solvent radiation doses obtained are considered to be conservative since only the dose received during the 30-min extraction contact was considered. The smaller doses received during phase separation and during the subsequent operations of the process cycle were ignored. In addition, absorption of only beta energy was considered since the solution volumes were small and a large fraction of the gamma energy would have escaped from the extractor. Absorption of alpha energy was also neglected since it would have been small as compared with the beta dose. With these assumptions, the estimated solvent doses were 0.04 whr liter⁻¹ cycle⁻¹ in the first run and 0.33 whr liter⁻¹ cycle⁻¹ in the second.

The principal conclusions that can be derived from the data obtained in these runs are listed below:

1. Plutonium (and uranium) recoveries from the feed were consistently more than 99.9%, showing that there was no unextractable plutonium [i.e., plutonium polymer or Pu(III)] in the feed.
2. Fission product DF's (feed to strip product) were erratic, varying over a wide range throughout the five cycles of each run. Presumably, much of the variation was due to difficulties in analysis. For almost all fission products, average DF's for the five cycles were higher for run 2 (the higher radiation level) than for run 1. In run 2 the average DF's were: 9×10^4 from ¹⁰⁶Ru, 1×10^4 from ⁹⁵Zr, 5×10^4 from ¹⁴⁴Ce, 5×10^4 from ¹³⁷Cs, and 3×10^2 from ¹³¹I. There was no decrease in DF's with cycling. Rather, the lowest DF's for most radionuclides were obtained in the first cycle.
3. In each cycle, 10 to 15% of the ¹³¹I in the feed was extracted in the first contact; a total of 50 to 80% was extracted in the seven extraction

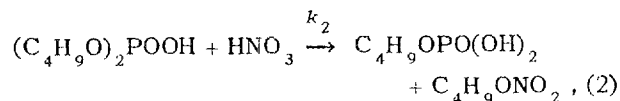
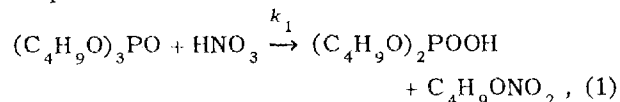
contacts. There was a gradual accumulation of ¹³¹I in the washed solvent with cycling, indicating some formation of alkyl iodides, which were not removed significantly by the carbonate wash treatment. Decontamination factors from iodine were in the range of 200 to 600.

4. No precipitates or slow-breaking emulsions formed in either run.
5. In summary, these tests confirm results of the ⁶⁰Co tests and indicate that, in the processing of short-cooled LMFBR mixed core and blanket fuel in pulsed columns, no serious problems should arise from radiation degradation of the solvent. However, this preliminary conclusion needs confirmation in tests of longer duration with short-cooled fuels.

Rate of Decomposition of TBP and Precipitation of Its Decomposition Products. — As part of the study of the stability of TBP in nuclear fuel processing, we are measuring the rate of decomposition of TBP dissolved in aqueous nitric acid solution as a function of acidity, temperature, radiation, and selected fission products. Most of the experiments have been performed in the presence of only a very small quantity of undissolved TBP since our first objective is to distinguish the rate of TBP decomposition in the aqueous phase from the rate in the organic phase.

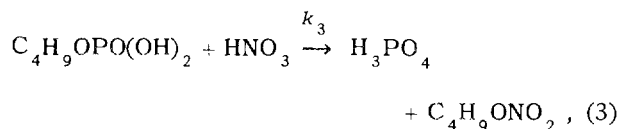
The experiments involved heating 300 to 400 ml of a nitric acid solution at 50 or 75°C, providing constant agitation, and maintaining a quantity (usually about 1 ml) of undissolved TBP in the system to keep the aqueous phase saturated with it. Periodically, 10- to 50-ml samples of the solution were removed and the products were analyzed.¹⁷

We have completed eight experiments at 50 and 75°C, including one at 50°C in the presence of ⁶⁰Co gamma radiation at a power density of 0.033 w/liter. By assuming the successive dealkylation steps



¹⁷A. H. Kibbey and W. Davis, Jr., *Methylation and Gas Chromatographic Analysis of the Decomposition Products of Tributyl Phosphate*, ORNL-TM-2289 (Aug. 1, 1968).

and



we derived equations relating the concentrations of HDBP, H_2MBP , and H_3PO_4 to k_1 , k_2 , k_3 , and S_o (the solubility of TBP in the aqueous phase). By nonlinear least-squares analysis we obtained the rate constants shown in Table 2.10. The product $k_1 S_o$ can be obtained with reasonable accuracy in all experiments since this term can be calculated from HDBP-concentration data alone.

The solubilities of TBP in aqueous nitric acid solutions have not, to our knowledge, been reported at temperatures above 50°C nor at HNO_3 concentrations greater than 3 M. However, we used the data of Higgins, Baldwin, and Soldano¹⁸ to estimate the necessary values (see Table 2.10). Dividing $k_1 S_o$ by S_o gives the values of k_1 (Table 2.10).

The significance of these rate constants may be evaluated, to a first approximation, in terms of the solubility of zirconium dibutyl phosphate in aqueous 1 to 5 M HNO_3 solutions. As previously reported,¹⁹ this solubility is on the order of 0.01 millimole/liter. In recent duplicate sets of experiments at 50 and 75°C in 3 and 5 M HNO_3 , and at initial concentrations of 0.25 and 0.5 g of zirconium per liter, the extent of zirconium precipitation was sevenfold greater than would be expected from the rate constants in Table 2.10, which refer to zirconium-free solutions. Thus, for example, if we multiply by 7 the term $k_1 S_o = 1.5 \times 10^{-3}$ millimole liter⁻¹ hr⁻¹ (Table 2.10, 50°C , 3 M HNO_3 , ^{60}Co gamma irradiation), we obtain about 0.01 millimole liter⁻¹ hr⁻¹. Comparison of this number with the solubility of zirconium dibutyl phosphate indicates that precipitation of this compound could occur if a solvent extraction process misoperation caused aqueous and organic phases to be separated in the primary extraction section for about 1 hr. This is only a first approximation of the significance of TBP decomposition, but it implies that a not-un-

reasonable misoperation could lead to precipitation of zirconium butylphosphates if the operating temperature were as high as 50°C .

Solvent Treatment. — The principal material formed during the decomposition of TBP is dibutylphosphoric acid (HDBP). Since HDBP forms strong complexes with uranium and plutonium as well as with some of the fission products, the presence of even small amounts in the solvent during the extraction-stripping cycle can lead to losses of uranium and plutonium as well as reduced decontamination of the final product. To prevent buildup, the HDBP is removed from the solvent after the strip cycle by an alkaline wash. To obtain a better understanding of the efficiency that can be expected in the solvent wash, the distribution of sodium dibutylphosphate (Na-DBP) labeled with ^{32}P was measured between TBP-NDD and sodium carbonate solutions. In addition, coefficients for the distribution of HDBP between TBP-NDD and 0 to 3.0 M HNO_3 were determined as a guide to the amount of HDBP that may be scrubbed from the organic phase by the various aqueous solutions that it encounters prior to the solvent wash.

The coefficients (D_o^a) for the distribution of Na-DBP between TBP-NDD and aqueous sodium carbonate solutions decreased with increasing TBP concentration. Coefficients of 1×10^4 , 8×10^3 , 5×10^3 , and 1×10^3 , respectively, were obtained on contacting 10, 15, 20, and 30 vol % TBP-NDD containing 10^{-3} M HDBP with 0.3 M Na_2CO_3 at a phase ratio of 1/1. Tests with larger amounts of HDBP in the system showed that the distribution coefficient did not change as long as there was excess sodium carbonate present. For example, the coefficient for the distribution of Na-DBP between 15% TBP-NDD and 0.05 M Na_2CO_3 –0.55 M Na-DBP solution was 7.6×10^3 . Adding NaNO_3 to an aqueous phase concentration of 2 M did not affect the coefficient.

Distribution coefficients (D_o^a) of about 0.34, 0.19, 0.15, 0.11, and 0.09 were measured for HDBP between 15 vol % TBP-NDD and 0.1, 0.5, 1.0, 2.0, and 3.0 M HNO_3 respectively. The coefficients were also measured with nitric acid solutions containing ruthenium or zirconium in concentrations similar to those expected in actual process operations. The presence of 3×10^{-3} M ruthenium did not change the distribution of the HDBP. However, the presence of 1×10^{-2} M zirconium caused precipitation (due to precipitation of zirconium dibutylphosphate, see above) in each case except for the

¹⁸C. E. Higgins, W. H. Baldwin, and B. A. Soldano, *Effects of Electrolytes and Temperature on the Solubility of Tributyl Phosphate in Water*, *J. Phys. Chem.* **63**, 113 (1959).

¹⁹W. Davis, Jr., and H. H. Carmichael, *Solubility of Zirconium Dibutyl Phosphate in Solvent Extraction Solutions*, ORNL-2857 (January 1960).

Table 2.10. Rate Constants for Aqueous-Phase Decomposition of TBP, HDBP, and H₂MBP

Temp. (°C)	HNO ₃ Conc. (M)	No. of Points	$k_1 S_o \times 10^3$ (millimoles/liter·hr)	S_o (millimoles/liter) ^a	$k_1 \times 10^3$ (hr ⁻¹)	$k_2 \times 10^3$ (hr ⁻¹)	V_{TBP}/V_{aq}	Remarks
50	1	4	0.34	1.23	0.28		<10 ⁻²	
50	3	4	0.86	1.61	0.53		<10 ⁻²	
50	5	4	0.99	2.11	0.47		<10 ⁻²	
50	3	3	0.20	1.61	0.12	2.6	1.5 to 8	15% TBP in NDD as a second phase.
50	3	11	1.5	1.61	0.93	4.3	<10 ⁻²	Irradiated in ⁶⁰ Co source at the rate of 0.033 w/liter.
75	1	4	4.8	1.24	3.9		<10 ⁻²	
75	3	4	10.3	2.32	4.4	1.7	<10 ⁻²	
75	5	17	7.1	4.35	1.6	7.1	<10 ⁻²	

^aCalculated from parameters of ref. 18.

Table 2.11. Effect of Zirconium on HDBP Distribution Between 15% TBP-NDD and Nitric Acid

HDBP Conc. (M)	HDBP Distribution Coefficient (D_o^a)					
	1 M HNO ₃		2 M HNO ₃		3 M HNO ₃	
	No Zr	0.01 M Zr	No Zr	0.01 M Zr	No Zr	0.01 M Zr
10 ⁻⁵	0.15	0.29	0.11	0.034	0.088	0.012
10 ⁻⁴	0.15	0.23	0.11	0.029	0.092	0.022
10 ⁻³	0.16	<i>a</i>	0.11	0.0081	0.095	0.0028

^aPrecipitation occurred.

2 M and 3 M HNO₃ aqueous phases when 10⁻³ M HDBP was present in the organic phase. With HDBP concentrations of 10⁻⁴ and 10⁻⁵ M, precipitation occurred only in the contacts with 0.5 and 0.1 M HNO₃ solutions. The distribution coefficients in the tests that did not show precipitation varied from almost twice to only about 3% of the value obtained when no zirconium was present, depending on the initial concentration of HDBP and the acid concentration of the aqueous phase (Table 2.11).

The coefficients for the distribution of HDBP between 15 vol % TBP-NDD and water were 200, 63, and 47 when the HDBP concentrations in the solvent were 10⁻⁵, 10⁻⁴, and 10⁻³ M HDBP respectively. The presence of a small amount of uranium in the solvent that was 10⁻⁵ M in HDBP decreased the coefficient to a value of about 1.

2.6 EXTRACTION OF PLUTONIUM WITH AMINES

Studies of the use of extraction by secondary amines^{20,21} as an alternative to ion exchange for the final purification of plutonium continued to show promise. The secondary amines, unlike the tertiary amines, can be easily stripped with dilute nitric acid.

Diluent Compatibility

One limitation sometimes encountered in amine extraction systems is the tendency for the amine

²⁰Chem. Technol. Div. Ann. Progr. Rept. May 31, 1967, ORNL-4145, p. 55.

²¹Chem. Technol. Div. Ann. Progr. Rept. May 31, 1968, ORNL-4272, p. 54.

nitrate salt or the amine salt-metal salt complex to separate as a third liquid phase. Preliminary compatibility tests with four secondary amines showed, as expected from previous experience, that there is much less tendency for a third phase to form in aromatic diluents such as diethylbenzene (DEB) than in aliphatic diluents such as *n*-dodecane. A third phase did not form when 0.5 M solutions (in DEB) of di(tridecyl)amine, Amberlite LA-1, *N*-benzylheptadecylamine, or Amine S-24 were contacted with 7 M HNO₃ or 1 M HNO₃-1 M Th(NO₃)₄ solution in the temperature range of 25 to 60°C. Thorium was used as a stand-in for plutonium; eventually, of course, the results obtained with thorium will need confirmation with plutonium solutions. In earlier tests, 0.3 M di(tridecyl)amine in DEB was loaded to 27 g of plutonium per liter without the formation of a third phase.

When *n*-dodecane was used as the diluent, it was necessary to add a long-chain alcohol, such as tridecanol (TDA), to the solvent phase to avoid third phase formation. All four of the amines mentioned above required the addition of TDA when they were contacted with the 1 M HNO₃-1 M Th(NO₃)₄ solution; the amounts required were 2 to 5% for Amine S-24 and di(tridecyl)amine and 10 to 20% for the other two amines.

Plutonium Stripping

The elution of plutonium from ion exchange resins is very slow. Also, the French have reported that the stripping of plutonium with sulfuric acid from tertiary amines is slow. However, the stripping of plutonium from secondary amines with nitric acid is rapid. In batch stripping with 0.5 M HNO₃ of 0.3 M di(tridecyl)amine in DEB loaded

with 18 g of plutonium per liter, stripping at 23°C was complete within 1 min, both at organic/aqueous phase ratios of 1/1 and 5/1. The aqueous-phase plutonium concentrations in these tests were 17 and 65 g/liter, respectively, corresponding to stripping coefficients of about 14 and 11.

Data for the stripping of plutonium with 0.15 M and 0.5 M HNO₃ from 0.3 M di(tridecyl)amine in DEB containing about 13 g of plutonium per liter are shown in Fig. 2.17. These data indicate that more than 99.5% of the plutonium could be recovered from the solvent with 0.15 M HNO₃ in three ideal stripping stages to give a product solution containing 60 g of plutonium per liter. Similar results could be obtained with 0.5 M HNO₃ in five ideal stages.

Batch Countercurrent Runs

In a batch countercurrent test demonstrating the recovery of plutonium from a simulated second-TBP-cycle product solution (adjusted to 5 M HNO₃ concentration) with 0.3 M di(tridecyl)amine in DEB, more than 99.9% of the plutonium was recovered in four extraction and four scrub stages (Table 2.12). The scrubbed extract from this run was stripped with 0.15 M HNO₃ in a four-stage batch countercurrent system. Stripping was more than 99.8% complete; the product solution was 0.6 M in nitric acid and contained 50 g of plutonium per liter. Phase separation was rapid (<1 min) in the extraction system but relatively slow (2 to 3 min) in the stripping system.

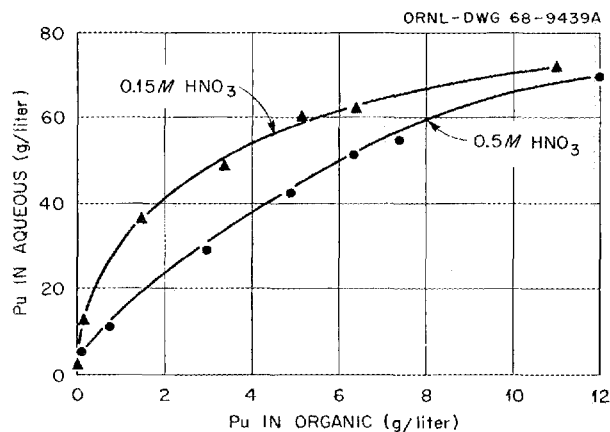


Fig. 2.17. Stripping Plutonium from 0.3 M Di(tridecyl)amine in Diethylbenzene with Dilute Nitric Acid.

Table 2.12. Results Obtained in the Batch Countercurrent Extraction of Plutonium with Di(tridecyl)amine

Feed: 5 M HNO₃, 32.9 g Pu/liter
 Organic: 0.3 M di(tridecyl)amine in DEB
 Scrub: 4.5 M HNO₃
 Stages: 4 extraction, 4 scrub
 Relative flows: feed/organic/scrub = 1.0/2.5/0.25

Stage No.	Pu Concentration (g/liter)		Plutonium Extraction Coefficient (E_a^o)
	Organic	Aqueous	
Scrub-4	12.1	10.0	1.2
-3	12.8	12.6	1.0
-2	13.3	16.4	0.8
-1	13.4	22.6	0.6
Aqueous feed		32.9	
Extraction-1	13.2	14.7	0.9
-2	6.7	1.6	4.2
-3	0.93	0.18	5.2
-4	0.14	0.018	7.8

Separation from Uranium. -- In an alternative flowsheet being investigated, the uranium and plutonium are co-stripped from TBP with dilute acid in the first cycle (see Sect. 2.5) and the plutonium is then recovered from this solution (after adjustment of the HNO₃ concentration to 5–6 M) and separated from the uranium by amine extraction. In a batch countercurrent demonstration of this separation with 0.3 M di(tridecyl)amine in DEB, more than 99% of the plutonium was recovered from a simulated first-cycle product solution in seven extraction and four scrub stages. The decontamination factor for uranium was about 200.

2.7 REMOVAL OF IODINE FROM OFF-GAS

Retention of iodine will be the major problem in treating the off-gas from the processing of short-cooled LMFBR fuels since plant retention factors of 10⁷ to 10⁸ will be required, assuming that the fuel is processed after only 30 to 60 days of cooling. It is evident that the method, or combination of methods, used for removing iodine from the off-gas must be of high integrity and capable of re-

moving not only elemental iodine but also organic iodides, particulate iodine, and possibly other iodine species. It is also evident that more than one, possibly several, iodine removal systems will be needed in the processing complex in order to obtain the high decontamination factors required. We are evaluating all known promising iodine removal methods and will develop additional chemical and engineering data where necessary. Presently, our efforts are concentrated on developing two treatment methods that have shown considerable promise: (1) scrubbing the gas with mercuric nitrate--nitric acid solutions that are known to be effective for removing elemental iodine and recently have been shown to be effective also for organic iodides (see below), and (2) passing the gas through a catalytic oxidation unit to destroy organic vapors and to convert organic iodides to elemental iodine, followed by sorption of the iodine on iodized charcoal.

Scrubbing Iodine from Gas Streams with Mercuric Solutions

Mercuric ion forms strong complexes with iodine in aqueous nitric acid solutions and is sometimes added to the aqueous phase to minimize iodine evolution during fuel dissolution or solution storage.²² In addition, $\text{Hg}(\text{NO}_3)_2$ - HNO_3 solutions have been used successfully to scrub iodine from plant off-gas streams.^{23,24} As far as we know, however, no one has investigated their use specifically for removing alkyl iodides from gas streams. Methyl iodide (and other alkyl iodides) is much more difficult to remove than elemental iodine and often limits the decontamination factor obtained across liquid or solid absorption systems. For example, sodium hydroxide solutions, which absorb elemental iodine, are ineffective for absorbing methyl iodide. In addition to their known ability for absorbing elemental iodine, we have found that $\text{Hg}(\text{NO}_3)_2$ - HNO_3 solutions are very effective for scrubbing both methyl iodide and higher alkyl iodides from gas streams. The $\text{Hg}(\text{NO}_3)_2$ - HNO_3 scrub system, therefore, potentially represents a

high-efficiency system for removing iodine in its more important forms from plant off-gases.

A series of 14 runs was made to determine the effect of changes in temperature and in the mercury and nitric acid concentrations on the efficiency of scrubbing methyl iodide from air. In these tests, air containing $\text{CH}_3^{131}\text{I}$ -traced methyl iodide was bubbled through three scrubbers in series, the first containing 100 ml (about 7-in. height of liquid) and the other two containing 50 ml of scrub solution each. The air leaving the scrubbers was passed through a cold trap at -84°C and then through two iodized charcoal (type 727 from Barnebey-Cheney) traps, each about 1 in. in depth.

Decontamination factors of 10^3 or higher were obtained across the three scrubbers in all tests (Table 2.13). The absorption efficiency increased as the temperature and the concentrations of mercury and nitric acid were increased. Decreasing the methyl iodide concentration in the feed air streams by factors of 15 to 30 (and at the same time increasing the total volume of air passed by a factor of 4) decreased the decontamination factor by factors of 5 to 20.

The observed improvement in efficiency of methyl iodide removal with an increase in nitric acid concentration is opposite to the effect found by British workers for removal of elemental iodine. It appears that the iodine removal efficiency, when the iodine in the feed air stream is in the form of methyl iodide, depends on: (1) the rate of decomposition of methyl iodide, which increases as the acid concentration and temperature are increased; and (2) the efficiency of the retention of iodine by the solution, which is dependent on the stability of the mercury-iodine complex. Sparging tests indicated that the stability of the complex decreases as the acid concentration is increased:

	Concentration (M)			Iodine Released to Sparge Gas (%)
	HNO_3	Hg	I	
	0.1	0.005	0.001	0.003
	5	0.005	0.001	0.19
	5	0.01	0.001	0.003

As expected, the retention of iodine was improved by increasing the mercury/iodine mole ratio in the solution. In these tests, 57 liters of air was sparged, over a 19-hr period, through 50 ml of the

²²S. R. Smith, *Nucl. Appl.* 5, 20 (1968).

²³R. W. Stromatt, *Removal of Radio-Iodine from Purex Off-Gas with Nitric Acid and with Nitric Acid-Mercuric Nitrate Solutions*, HW-55735 (1958).

²⁴G. K. Cederberg and D. K. MacQueen, *Containment of Iodine-131 Released by the RaLa Process*, ID-14566 (1961).

Table 2.13. Removal of Methyl Iodide from Air by Scrubbing with $\text{Hg}(\text{NO}_3)_2\text{-HNO}_3$ Solutions

Conditions: 100 ml/min of air containing methyl iodide passed through three scrubbers in series at room temperature; air was dispersed into the scrub solution through a coarse glass frit; air leaving scrubbers was passed consecutively through a -84°C cold trap and two treated charcoal traps.

Approximate CH_3I Conc. in the Air (mg/liter)	Total Air Passed (liters)	Scrub Solution		Iodine Distribution (% of total found)						Iodine Decontamination Factor Across Scrub System ^a
		Hg (M)	HNO_3 (M)	Scrubbers			Cold Trap	Charcoal Traps		
				1 (100 ml)	2 (50 ml)	3 (50 ml)		1	2	
14	9	0.1	1	99.7	0.24	<0.002	<0.002	<0.002	<i>b</i>	$>2 \times 10^4$
		0.05	1	97.5	2.3	0.16	0.003	0.007	<0.002	1×10^4
		0.03	1	94.8	4.7	0.46	0.006	0.013	<0.002	5×10^3
		0.1	0.1	98.5	1.4	0.10	<0.002	<0.002	<0.002	$>2 \times 10^4$
		0.1	2	99.1	0.87	0.043	<0.002	<0.002	<0.002	$>2 \times 10^4$
		0.1	5	99.9	0.054	0.018	0.003	<0.002	<i>b</i>	2×10^4
		0.03	5	99.1	0.87	0.048	0.005	<0.002	<0.002	1×10^4
		0.2	8	99.9	0.039	0.037	<i>b</i>	<0.002	<0.002	$\sim 10^4$
1.1	36	0.1	0.1	72.5	21.9	5.7	0.01	0.006	<0.003	5×10^3
0.8				99.7 ^c	0.2 ^c	0.08 ^c	0.03	<0.003	<0.003	3×10^3
0.5		0.1	1	98.8	1.2	<0.02	0.05	0.007	<0.003	1×10^3
0.8				98.8	1.1	0.08	<0.03	<0.003	<0.003	$>2 \times 10^3$
0.8		0.1	5	99.4	0.4	0.2	<0.03	<0.003	<0.003	$>2 \times 10^3$

^aRatio of the total amount of iodine found in the scrubbers to the total found in the cold trap and charcoal traps.

^bNot analyzed.

^cScrubber operated at 50°C .

solution containing iodine at room temperature. Iodine released from the solution was caught in charcoal traps.

Mercury solutions were also highly effective for scrubbing higher alkyl iodides from air streams. In tests with two scrubbers in series, DF's of more than 10^3 were obtained for scrubbing iodine, present as *n*-butyliodide and *n*-octyliodide, from the air. The scrub solution used in these particular tests was 0.2 *M* in Hg^{2+} and 8 *M* in HNO_3 ; the efficiency at lower acid concentrations has not yet been determined. Also, some runs were made with *n*-dodecyliodide, but experimental problems were encountered owing to the low volatility of this compound. Although material balances were poor, the *n*-dodecyliodide apparently was removed from the air fairly efficiently ($\text{DF} > 100$).

Absorption in Packed Columns. — The scrubbing of iodine from air streams was also studied using three 2-in.-diam columns in series, each packed with 24 in. of 0.25-in. Berl saddles. A decontamination factor for methyl iodide of about 1800 was obtained. In this test, a total of 3700 liters of air containing an average of about 0.9 mg of CH_3I per liter was passed through the columns at the rate of 2 liters/min. Each column contained 750 ml of 0.05 *M* $\text{Hg}(\text{NO}_3)_2$ –0.2 *M* HNO_3 and was operated at room temperature with the aqueous phase continuous. To simulate the countercurrent flow of solution and gas, 150- to 250-ml volumes of solution were advanced through the columns at 3-hr intervals. Under these conditions, the spent scrub solution contained about 0.01 *M* iodine, equivalent to a mercury/iodine mole ratio of about 5/1. Of the iodine in the scrub system, about 90% was in the first, 9% in the second, and 0.7% in the third column.

In a run with elemental iodine (~ 0.34 mg per liter in the air stream), the decontamination factor was 1950. The distribution of iodine in the columns was considerably different in this run than in the run with CH_3I , showing, as expected, that the reaction of I_2 is more rapid than CH_3I with the scrub solution. About 97.7, 2.1, and 0.16% of the iodine was in the first, second, and third columns respectively.

Mercury-Iodine Complexes. — In operating the scrub system, a mercury/iodine mole ratio of at least 4 must be maintained to avoid precipitation of HgI_2 . Titrations of mercuric nitrate–nitric acid solutions with potassium iodide solutions are being made in attempts to identify the complex species

present in solution. Addition of KI to the colorless solution containing mercuric ion produces a localized yellow puddle that rapidly changes to a red-orange precipitate and then disappears. With 0.1 *M* Hg^{2+} solutions, the formation of a permanent precipitate occurs at a mercury/iodine mole ratio of about 3.9 in 0.1 *M* HNO_3 and at about 3.1 in 5 *M* HNO_3 . Precipitation is apparently complete at a mole ratio of 0.5. At a ratio of 0.25, the precipitate is completely redissolved. The point at which the precipitate disappears does not vary with changes in the nitric acid concentration.

Extraction of the Mercury-Iodine Complex. — If mercury solutions are used for scrubbing radioiodine from the processing plant off-gas, presumably the spent scrub solution can be stored and then recycled after most of the ^{131}I has decayed. However, ^{129}I , which has a long half-life and a low discharge limit, would accumulate in the solution. To obtain more efficient recycle of the scrub solution, some convenient method for removing iodine from the solution is needed. Solvent extraction of the iodine showed some promise in preliminary tests.

As described in Sect. 2.5, the mercury-iodine complex is extracted with TBP; however, the extraction coefficients are low when excess mercury is present. As expected, the complex was extracted more strongly by diamylamylphosphonate (DAAP) and by trioctylphosphine oxide (TOPO) than by TBP. Coefficients for the extraction of the complex (as measured by iodine extraction) from 1 *M* HNO_3 –0.1 *M* Hg^{2+} –0.01 *M* KI solution with 0.3 *M* solutions of TBP, DAAP, or TOPO in *n*-dodecane were 1.4, 3.1, and 29.3 respectively. A 0.1 *M* Adogen 364 (tertiary amine) solution gave an extraction coefficient of 3.8. The mercury/iodine mole ratio in the solvent phase was 1 with all solvents except TOPO, in which case it was 2. Coefficients for the extraction of mercury from 1 *M* HNO_3 (no I^- present) were 0.09 with Adogen 364 and about 0.01 with the TBP, DAAP, and TOPO solutions. These data indicate that iodine could be extracted from the scrub solution with a loss of only 1 to 2 moles of mercury per mole of iodine.

The stripping of iodine (and mercury) from the solvents with alkaline solutions was more difficult than had been expected. For example, contacting the TOPO and DAAP solvents with 1 *M* NaOH for 10 min at room temperature stripped only 3% and 43% of the iodine respectively. With the DAAP solvent, 78% was stripped with 1 *M* NaOH in 10

min at 60°C. Of a variety of stripping agents tested, $\text{Na}_2\text{S}_2\text{O}_3$ solutions gave the best results. A 0.1 M $\text{Na}_2\text{S}_2\text{O}_3$ solution stripped 99.6% of the iodine from the DAAP solvent in 10 min at room temperature. Although the results for stripping of mercury were somewhat erratic, they tended to be similar to those for iodine. Small amounts of precipitate formed, but most of the stripped mercury was found dissolved in the aqueous phase.

Other Scrub Solutions

A large number of solutions of inorganic and organic reagents and combinations of reagents were tested for effectiveness in removing methyl iodide from air streams. Although some of the solutions were effective, none of them appeared as attractive as mercury solutions for process use. The best results were obtained with a 1 M ethanolamine solution in dimethylsulfoxide, which gave an iodine decontamination factor of more than 2500 across a two-stage scrub system. A 1 M NaOH solution in 100% ethanol gave a decontamination factor of 57 at room temperature and 1430 at 50°C. Decontamination factors in the range of 60 to 70 across the two-stage system were obtained with a 0.1 M solution of a quaternary ammonium compound (Adogen 464 in the carbonate form) in 97% diethylbenzene-3% tridecanol and with a 1 M solution of ethanolamine in 100% ethanol.

Catalytic Oxidation of Organic Vapors

Iodized charcoal is highly effective for sorbing iodine both in the form of methyl iodide and as elemental iodine; however, experience at the Transuranium Processing Plant (TRU) at ORNL has shown that organic vapors in the process off-gas are also sorbed on the charcoal and adversely affect iodine sorption. We are studying²⁵ the destruction of organic impurities in process air streams by catalytic oxidation. The objective is to convert the organic materials to carbon dioxide and water prior to passing the gas stream through a charcoal bed. This should avoid loading of the charcoal bed with organic solvents that decrease the iodine removal efficiency. Efficient decompo-

sition of organic vapors was obtained with Hopcalite ($\text{MnO}_2\text{-CuO}$) catalyst in preliminary tests. Eventually we also plan to test other catalysts. The combination of a Hopcalite treatment followed by sorption of iodine on iodized charcoal was used successfully to prevent iodine release in a recent processing campaign at TRU (see Sect. 5.1).

Several different organic materials including methyl iodide were decomposed very efficiently by passing an air stream (velocity, 80 fpm) containing one of the organic materials through a 2-in. bed of Hopcalite at about 350°C:

Organic	Extent of Decomposition (%)
Diethylbenzene	99.99+
Amsco 125-82	99.99+
Denatured alcohol	99.9+
2-ethyl-1-hexanol	99.8+
Methyl iodide	99.9+

Upstream and downstream concentrations of the organic compound were monitored by gas chromatography with either flame ionization or electron capture detection. Although it was not proved that conversion of the organics to CO_2 and H_2O , rather than to intermediate organic compounds, was quantitative, no organic compounds except the usual trace of methane (air normally contains 2 ppm of CH_4 , which is not decomposed by the Hopcalite treatment) were detected in the effluent gas. In tests with *n*-dodecane, some unidentified low-boiling hydrocarbons were found in the effluent gas when the oxidation temperature was 350°C, but conversion to CO_2 and H_2O appeared to be almost quantitative at 500°C.

Heating the Hopcalite catalyst for 1 hr at 400, 500, 600, or 700°C decreased the catalyst surface area from an initial value of 132 m^2/g to 123, 68, 17, and 11 m^2/g respectively. Heating for 6 and 60 hr decreased the surface area to 104 and 15 m^2/g , respectively, at 400°C, and to 94 and 12 m^2/g at 600°C. It has not been shown that the oxidation efficiency of the Hopcalite was decreased by the heat treatments but, since there is frequently a significant relationship between catalytic activity and surface area, the thermal stability of the Hopcalite is of concern and is being given further study.

²⁵R. E. Adams, R. D. Ackley, and Zell Combs of the ORNL Reactor Chemistry Division are participating in these studies.

2.8 RADIATION AND SHIELDING STUDIES

This activity is part of a continuing program of analytical studies with the objective of developing information on the radiation properties and shielding requirements associated with the recycle of LMFBR fuels. The work involves compilation and correlation of basic nuclear data including decay schemes, nuclear cross sections, radiation sources and energy spectra, and thermal power; development of computer programs for calculating transient concentrations of radionuclides in LMFBR fuel; calculation of dose attenuation kerma for shield materials of interest; and applications of these data to LMFBR fuel cycle processes.

The most significant accomplishments during the past year involved the compilation of basic nuclear data for approximately 700 nuclides of importance in spent LMFBR fuels; the development of a computer code, ORIGEN, for calculating transient concentrations of nuclides; and the analysis of radiation control and shielding requirements of certain operations in the recycle of LMFBR fuels. These will be described in the following sections.

Compilation of Nuclear Data

An extensive compilation of nuclear data was prepared for use in computer programs that calculate transient concentrations of nuclides in LMFBR fuels. The compilation includes data for 47 actinides, 461 fission products, and 178 nuclides that may be formed by the activation of materials of construction or inert fuel materials. The data include nuclear decay schemes (negatron, positron, and alpha decay, isomeric transition, and spontaneous fission), one-group cross sections for important types of neutron-induced reactions ($n-\gamma$, n -fission, $n-2n$, $n-3n$, $n-\alpha$, and $n-p$), the radiant energy evolved by nuclear decay, and yields of fission products from the fast fission of ^{235}U , ^{238}U , and ^{239}Pu .

The one-group neutron cross sections in the compilation were generated by numerical integration of multigroup and/or differential cross section data over the LMFBR core spectrum shown in Fig. 2.18. Theoretical models were used to estimate the energy-dependent cross sections for which experimental data are not available. The assumed spectrum is a smoothed version of that computed by Kusters and Metzneroth²⁶ for a typical LMFBR

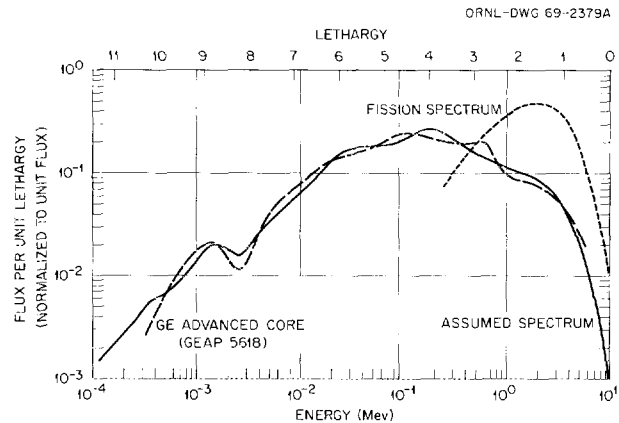


Fig. 2.18. Comparison of the Assumed LMFBR Core Flux Spectrum with the Fission Spectrum and the Spectrum Computed for the General Electric Follow-On Advanced Design.

core composition. It agrees well with the core-averaged spectra computed by General Electric personnel for alternative 1000-Mw (electrical) LMFBR follow-on designs.²⁷ The assumed spectrum is generally somewhat softer in LMFBR axial blankets, but it has been found to be adequate for estimation purposes since the derived cross sections provide a reasonable estimate of plutonium production in LMFBR blankets. Although core spectra could be appreciably softer in LMFBR's that use a beryllium moderator to achieve a negative sodium void coefficient, a hard spectrum with appropriate engineered safety features is currently favored because of economic considerations.

The prediction of heat generation properties of individual fission products has often been unsatisfactory because of uncertainties in the average energies of negatron and positron reactions. Average beta energies for the current compilation were calculated with the computer program SPECTRA,²⁸ based on data and/or estimates of the maximum negatron or positron energy and the degree of forbiddenness of the transition.

²⁶H. Kusters and M. Metzneroth, *The Influence of Some Important Group Constants on Integral Fast Reactor Quantities*, ANL-7120 (Oct. 1965), p. 431.

²⁷*Comparison of Two Sodium-Cooled 1000 Mwe Fast Reactor Concepts -- Task I Report of 1000 Mwe LMFBR Follow-On Work*, GEAP-5618 (June 1968), p. 109.

²⁸E. D. Arnold, *Handbook of Shielding Requirements and Radiation Characteristics of Isotopic Power Sources for Terrestrial, Marine, and Space Applications*, ORNL-3576 (April 1964).

The complete compilation of nuclear data for LMFBR's (as well as similar compilations for LWR's, HTGR's, and MSBR's) are available for distribution upon request.

The ORIGEN Code

A computer code, ORIGEN, was developed to predict the concentrations of individual isotopes in the spent fuel elements when their initial compositions and the burnup characteristics of the reactor are known. This code solves a simultaneous set of first-order ordinary differential equations of the form:

$$\frac{dN_i}{dt} = \sum_j e_{ij} \lambda_j N_j + \bar{\phi} \sum_k f_{ik} \sigma_k N_k + \bar{\phi} \sum_m y_{im} \sigma_{tm} N_m - (\lambda_i + \bar{\phi} \sigma_i) N_i, \quad i = 1, 2, \dots, n, \quad (1)$$

given $N_i(0)$, and where

N_i = concentration of species i , g-atom/metric ton,

$\bar{\phi}$ = volume-, energy-, and time-averaged neutron flux, barn⁻¹ sec⁻¹,

λ_i = radioactive disintegration constant of species i , sec⁻¹,

σ_i = spectrum-averaged neutron cross section of species i , barns,

σ_{fi} = spectrum-averaged fission cross section of species i , barns,

e_{ij} = fraction of disintegrations by species j , which lead to formation of species i ,

f_{ik} = fraction of neutron captures by species k which lead to formation of species i ,

y_{im} = fission yield of species i from fission of species m ,

t = time, sec.

This equation is a statement of the fact that the rate of change of the concentration of each individual nuclide is equal to its rate of production from radioactive decay, neutron absorption, and fission, minus its own rate of loss by radioactive decay and neutron absorption. Equation (1) is applied for a series of time steps in which the average flux is taken to be constant. The flux in

each time interval may be read in as input to the code, or can be computed by the code from the average specific power in the time interval. For these conditions, Eq. (1) is a linear first-order ordinary differential equation with constant coefficients of the form

$$\dot{\mathbf{x}} = \mathbf{A} \mathbf{x}, \quad (2)$$

where \mathbf{x} is an n dimensional vector containing the isotopic composition, \mathbf{A} is an $n \times n$ transition matrix, and the initial conditions, $\mathbf{x}(0)$, are given. The formal solution to Eq. (2) can be shown to be:

$$\mathbf{x}(t) = \exp(\mathbf{A}t) \mathbf{x}(0), \quad (3)$$

and the problem is reduced to generating the matrix function $\mathbf{C} = \exp(\mathbf{A}t)$ for each time step from the transition matrix. The computer code generates this function by expanding in a power series for $\exp(\mathbf{A}t)$:

$$\mathbf{C} = e^{\mathbf{A}t} = \mathbf{I} + \mathbf{A}t + \frac{(\mathbf{A}t)^2}{2!} + \dots + \frac{(\mathbf{A}t)^n}{n!}. \quad (4)$$

The solution of Eq. (2) is obtained for each nuclide as

$$x_i = \sum_{j=1}^n \left(\sum_m C_{ij}^m \right) x_j, \quad i = 1, 2, \dots, m. \quad (5)$$

Here C_{ij}^m is the m th term in the power series expansion of the element C_{ij} in the \mathbf{C} matrix. Each term in the expansion is generated from the preceding row by a recursion relation

$$C_{ij}^m = \frac{t}{m} \sum_{k=1}^n C_{ik}^{m-1} A_{kj}, \quad (6a)$$

$$C_{ij}^0 = \delta_{ij}, \quad (6b)$$

making it necessary to store only one row of the \mathbf{C} matrix. In order to accelerate the computational algorithm and to avoid loss of precision in the summation of the series (6), asymptotic solutions of the nuclide chain equations are used to obtain concentrations of individual isotopes for which the time t exceeds ten half-lives.

ORIGEN requires as input a library of nuclear data containing half-lives, decay schemes, cross

Mwd/metric ton. The concentrations, activities, and specific powers of approximately 700 isotopes comprising the cladding, fission products, and fuel were computed at reactor discharge and for a series of ten decay times after discharge. Typical results are presented in summary form in Tables 2.14 to 2.17.

Radiation Source Data

Spent Fuel. – Typical photon release rate and spectrum data for LMFBR fuel as a function of

postirradiation time are presented in Fig. 2.19. These data were calculated with the PHOEBE³⁰ program, assuming irradiation to a burnup of 100,000 Mwd/metric ton at an average specific power of 125 Mw/metric ton. At short decay times, shielding requirements are determined primarily by the 1.55-Mev gamma group that originates predominantly from the decay of ¹⁴⁰Ba-¹⁴⁰La. At longer

³⁰E. D. Arnold, *PHOEBE – A Code for Calculating Beta and Gamma Activity and Spectra for ²³⁵U Fission Products*, ORNL-3931 (July 1966).

Table 2.15. Radioactivity of Actinides in Spent LMFBR Core Fuel as a Function of Decay Time

Burnup = 80,000 Mwd/metric ton

Specific power = 148.15 Mw/metric ton

Nuclide activities are given in curies per metric ton (U + Pu) charged to core

	Charged to Reactor	Discharged from Reactor	After Cooling Times of:				
			30 days	90 days	150 days	3 years	30 years
²²⁸ Th + daughters	0	0.00519	0.0060	0.00816	0.0107	0.0744	0.202
²³² U	0	0.00595	0.00668	0.00812	0.00949	0.0249	0.0337
²³⁴ U	0	0.135	0.142	0.156	0.171	0.397	2.52
²³⁷ U	0	302,000	13,900	29.2	0.0617		
²³⁸ U	0.260	0.239	0.239	0.239	0.239	0.239	0.239
²³⁷ Np	0	0.124	0.127	0.127	0.127	0.134	0.391
²³⁹ Np	0	81,500,000	11,900	137	137	137	136
²³⁶ Pu	0	0.946	0.931	0.894	0.859	0.458	0.000643
²³⁸ Pu	43,800	30,700	30,800	31,000	31,100	31,000	25,200
²³⁹ Pu	7,940	7,120	7,150	7,150	7,150	7,150	7,140
²⁴⁰ Pu	11,400	11,600	11,600	11,600	11,600	11,500	11,500
²⁴¹ Pu	2,970,000	1,660,000	1,650,000	1,640,000	1,620,000	1,420,000	325,000
²⁴² Pu	34.2	35.2	35.2	35.2	35.2	35.2	35.2
²⁴¹ Am	0	4,120	4,320	4,730	5,140	11,100	40,500
^{242^m} Am	0	239	239	239	239	236	209
²⁴² Am	0	393,000	239	239	239	236	209
²⁴³ Am	0	137	137	137	137	137	136
²⁴² Cm	0	204,000	181,000	140,000	109,000	2,130	171
²⁴³ Cm	0	107	107	106	106	100	55.7
²⁴⁴ Cm	0	3,430	3,420	3,400	3,380	3,060	1,090
Total	3,030,000	167,000,000	1,920,000	1,840,000	1,790,000	1,480,000	422,000

Table 2.16. Fission Product Activity of Spent LMFBR Core Fuel as a Function of Decay Time

Burnup = 80,000 Mwd/metric ton

Specific power = 148.15 Mw/metric ton

Nuclide activities are given in curies per metric ton (U + Pu) charged to core

	On Discharge from Reactor	After Cooling Times of:				
		30 days	90 days	150 days	3 years	30 years
^3H	2,340	2,330	2,310	2,290	1,980	432
^{85}Kr	24,900	24,800	24,500	24,300	20,600	3,610
^{86}Rb	8,150	2,670	288	31		
^{89}Sr	2,240,000	1,500,000	674,000	303,000	1.01	
$^{90}\text{Sr} + ^{90}\text{Y}$	209,000	206,000	204,000	204,000	191,000	98,200
^{91}Y	3,080,000	2,170,000	1,070,000	527,000	7.56	
^{95}Zr	7,050,000	5,120,000	2,700,000	1,420,000	59.2	
^{95m}Nb	141,000	109,000	57,300	30,200	1.26	
^{95}Nb	6,970,000	6,510,000	4,460,000	2,660,000	126	
$^{99}\text{Mo} + ^{99m}\text{Tc}$	13,950,000	8,510	0.00289			
$^{103}\text{Ru} + ^{103m}\text{Rh}$	14,480,000	8,570,000	3,000,000	1,049,000	0.0675	
$^{106}\text{Ru} + ^{106}\text{Rh}$	6,820,000	6,460,000	5,760,000	5,140,000	862,000	0.00698
^{110m}Ag	4,650	4,280	3,630	3,080	231	
^{110}Ag	323,000	557	472	401	300	
^{111}Ag	505,000	31,600	123	0.482		
^{113m}Cd	341	340	337	334	294	77.3
^{115m}Cd	954	558	224	85.0		
^{119m}Sn	49.9	46.0	38.9	32.9	2.39	
^{121m}Sn	142	142	142	142	138	108
^{123m}Sn	2,070	1,750	1,250	900	4.74	
^{125}Sn	153,000	16,700	200	2.40		
^{125}Sb	50,500	50,700	48,800	46,700	24,000	23.4
^{125m}Te	17,100	17,900	18,700	18,600	9,960	9.7
^{126}Sb	10,200	1,940	73.8	6.85	4.36	4.36
^{127}Sb	846,000	4,040	0.0888			
$^{127m}\text{Te} + ^{127}\text{Te}$	1,023,000	315,000	213,000	145,600	354	
^{129m}Te	818,000	446,000	131,000	38,600		
^{129}Te	1,960,000	286,000	84,100	24,800		
^{129}I	0.129	0.131	0.132	0.133	0.133	0.133
^{131}I	4,320,000	336,000	1,920	10.9		
^{131m}Xe	45,100	15,100	581	17.9		
$^{132}\text{Te} + ^{132}\text{I}$	12,140,000	20,500	0.0583			
^{133}Xe	7,920,000	181,000	67.5	0.0252		
^{134}Cs	78,600	76,500	72,400	68,400	28,500	3.16
^{136}Cs	365,000	73,800	3,010	123		
$^{137}\text{Cs} + ^{137m}\text{Ba}$	515,000	514,000	512,000	510,000	480,000	257,000
$^{140}\text{Ba} + ^{140}\text{La}$	12,960,000	2,690,000	104,500	4,060		
^{141}Ce	6,760,000	3,580,000	991,000	275,000		
^{143}Pr	6,380,000	1,850,000	89,000	4,270		
$^{144}\text{Ce} + ^{144}\text{Pr}$	6,820,000	6,180,000	5,340,000	4,620,000	458,000	
^{147}Nd	2,830,000	434,000	10,300	242		
^{147}Pm	812,000	822,000	792,000	758,000	382,000	302
^{148m}Pm	177,000	108,000	40,000	14,900		

Table 2.16 (continued)

	On Discharge from Reactor	After Cooling Times of:				
		30 days	90 days	150 days	3 years	30 years
^{151}Sm	10,900	10,900	10,900	10,800	10,600	8,620
^{154}Eu	2,530	2,520	2,500	2,490	2,220	690
^{155}Eu	209,000	202,000	190,000	178,000	66,200	2.14
^{156}Eu	304,000	77,600	4,850	303		
^{160}Tb	34,100	25,600	14,400	8,070	0.906	
^{161}Tb	47,400	2,330	5.61	0.0135		
$^{162}\text{Gd} + ^{162m}\text{Tb}$	24,200	22,800	20,400	18,140	3,020	
Total curies/metric ton	621,000,000	48,800,000	26,800,000	18,200,000	2,540,000	370,000
Beta power, w/metric ton	4,140,000	100,000	62,100	48,700	6,980	586
Gamma power, w/metric ton	2,210,000	95,600	43,900	25,700	1,840	494

Table 2.17. Cladding Activity of Spent LMFBR Core Fuel as a Function of Decay Time

Burnup = 80,000 Mwd/metric ton

Specific power = 148.15 Mw/metric ton

Nuclide activities are given in curies per metric ton (U + Pu) charged to core

	On Discharge from Reactor	After Cooling Times of:				
		30 days	90 days	150 days	3 years	30 years
^{14}C	0.0584	0.0584	0.0584	0.0584	0.0583	0.0581
^{32}P	2,310	539	29.4	1.61		
^{33}P	13.5	5.86	1.11	0.210		
^{51}Cr	61,700	29,200	6,550	1,470		
^{54}Mn	150,000	140,000	122,000	107,000	12,200	
^{55}Fe	76,000	74,300	71,200	68,100	34,100	25.5
^{59}Fe	10,300	6,520	2,590	1,030		
^{58}Co	410,000	307,000	171,000	95,500	10.00	
^{60}Co	1,350	1,330	1,310	1,280	908	25.9
^{59}Ni	2.13	2.13	2.13	2.13	2.13	2.13
^{63}Ni	67.8	67.7	67.6	67.6	66.3	54.1
Total	1,270,000	559,000	375,000	274,000	47,400	108

decay times, shielding requirements are determined primarily by the 2.38-Mev group, to which a primary contributor is ^{144}Ce - ^{144}Pr .

The estimated neutron source strength of spent LMFBR fuel is compared with that from light water reactor (LWR) fuel in Table 2.18. The isotopic content of those nuclides which constitute impor-

tant neutron sources were calculated with the ORIGEN code. Most of the neutrons originate from spontaneous fission in the isotopes ^{242}Cm and ^{244}Cm . These results indicate that the neutron source in spent LMFBR core fuel will be greater than from enriched uranium LWR fuel but less than from plutonium recycle LWR fuel.

Table 2.18. Estimated Neutron Source Strength of Spent Power Reactor Fuels

Isotope	LWR ^a			LWR-Pu Recycle ^a			LMFBR ^b		
	Isotope Content ^c (g/ton)	Neutron Source		Isotope Content ^c (g/ton)	Neutron Source		Isotope Content ^c (g/ton)	Neutron Source	
		α -n	SF ^d		α -n	SF ^d		α -n	SF ^d
		(sec ⁻¹ ton ⁻¹ × 10 ⁻⁶)			(sec ⁻¹ ton ⁻¹ × 10 ⁻⁶)			(sec ⁻¹ ton ⁻¹ × 10 ⁻⁶)	
²³⁸ Pu	160	5.0	0.4	45	1.4	0.1	1,800	55.6	4.8
²³⁹ Pu	5400	0.4	0.0	1500	0.1	0.0	120,000	8.6	0.0
²⁴⁰ Pu	2200	0.6	2.0	1000	0.3	0.9	52,000	14.	49.
²⁴¹ Am	62	0.4	0.0	60	0.4	0.0	1,400	8.2	0.0
²⁴² Cm	4.4	52.9	87.7	35	418.	693.	48	574.	952.
²⁴⁴ Cm	30	7.3	326.	510	124.	5560.	42	10.2	459.
Total		66.	416		544.	6250		670.	1460.
Overall total		480			6800			2130	

^aFuel had been irradiated to a burnup of 33,000 Mwd/metric ton and allowed to cool for 150 days.

^bFuel had been irradiated to a burnup of 100,000 Mwd/metric ton and allowed to cool for 60 days.

^c"Ton" in this table refers to metric ton of fuel as charged to the reactor.

^dSF = spontaneous fission.

Plutonium Product. — Based on experimental data from LWR's and estimated cross sections in LMFBR's, the neutrons from spontaneous fission and α -n reactions constitute the most important source of penetrating radiation in the plutonium product (and recycle plutonium feed); by comparison, the primary gamma rays of high yield have relatively low energy and are easily shielded. The transient activities of the products of the decay of plutonium having the isotopic composition of LWR products are shown in Table 2.19. These plutonium composition data were calculated with the ORIGEN program, assuming a fuel burnup of 33,000 Mwd/metric ton at a specific power of 30 Mw/metric ton in the Diablo Canyon reactor. The predominant source of radiation dose from lightly shielded plutonium of this composition is the 0.06-Mev gamma ray that occurs in nearly 100% of the disintegrations of ^{241}Am . This gamma radiation is effectively removed by a shield of $\frac{1}{8}$ to $\frac{1}{4}$ in. of lead. The hard gamma radiation (predominantly the 2.62- and 0.58-Mev gamma rays that occur in 100%

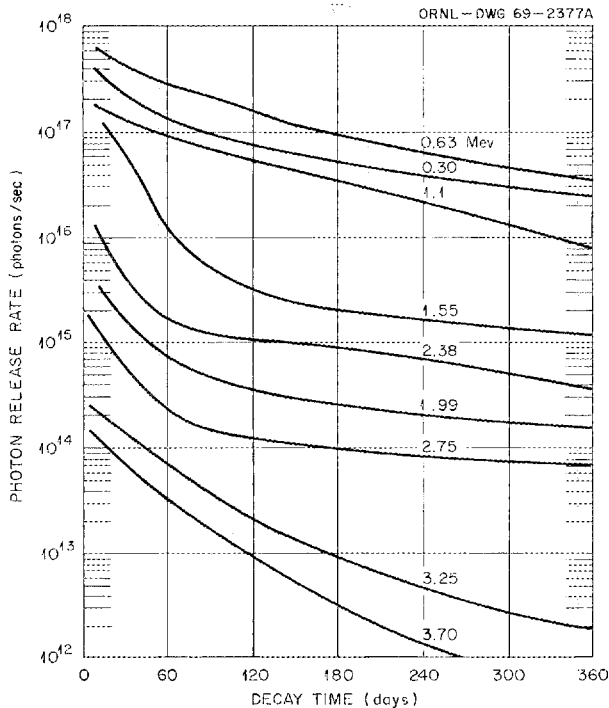


Fig. 2.19. Effect of Postirradiation Decay Time on the Photon Release Rate of Fission Products Resulting from the Irradiation of 1 Metric Ton of LMFBR Fuel to 100,000 Mwd/metric ton at an Average Specific Power of 125 Mw/metric ton.

of the disintegrations of ^{208}Tl) resulting from the daughters of ^{236}Pu decay begins to give dose rates comparable to those from the neutron sources after plutonium post-purification times of greater than one year. Since plutonium is generally stored as a nitrate solution, a relatively simple ion exchange treatment for removing most of the ^{236}Pu daughter activity may be employed, if necessary, before shipment or fabrication of fuel.

Estimates of the isotopic composition and neutron source strength of fuel core charges for LMFBR's and LWR's are shown in Table 2.20. These data reflect current estimates that the plutonium recycled from LMFBR's will contain less ^{236}Pu and ^{238}Pu than plutonium recycled from LWR's. The neutron source strengths per unit of each plutonium isotope are based on relatively abundant experimental information.³¹⁻³³ The primary sources of neutrons are those from ^{238}Pu α -n reactions with oxygen and spontaneous fission of ^{240}Pu . The energy spectra of these neutron sources^{34,35} and shield attenuation kerma for various materials^{36,37} are also available.

Shield Requirements for LMFBR Spent Fuel Shipping Casks. — Calculations were made using the SDC code³⁸ to determine gamma shielding requirements for a 36-element spent fuel shipping cask for LMFBR core plus axial blanket fuel (Table 2.21). The calculations were made as a function of position above the midplane of the active portion of the element. Since the cask is used to ship entire assemblies, including the non-fueled portions that constitute approximately two-

³¹E. D. Arnold, "Neutron Sources," Chapter 2.1.2 in *IAEA Engineering Compendium on Radiation Shielding*, Springer-Verlag, 1968.

³²G. M. Matlack and C. F. Metz, *Radiation Characteristics of Plutonium-238*, LA-3696 (October 1967).

³³D. H. Stoddard and E. L. Albenesius, *Radiation Properties of ^{238}Pu Produced for Isotopic Power Sources*, DP-984 (July 1965).

³⁴T. R. Herold, "Neutron Spectrum of $^{238}\text{PuO}_2$," *Nucl. Appl.* 4(1), 19-22 (1968).

³⁵M. E. Anderson, *Neutron Energy Spectra of ^{239}Pu , ^{238}Pu , $^{238}\text{Pu-F}$, and $^{238}\text{Pu-}^{18}\text{O}$ (α ,n) Sources*, MLM-1422 (October 1967).

³⁶R. A. Robinson et al., *Brayton Cycle Radioisotope Heat Source Design Study - Phase I (Conceptual Design) Report*, ORNL-TM-1691 (August 1967), pp. 87-93.

³⁷W. E. Unger, *^{238}Pu Neutron Shielding Computation Comparisons*, ORNL-TM-1632 (Aug. 30, 1966).

³⁸E. D. Arnold and B. F. Maskewitz, *SDC, A Shielding-Design Calculation Code for Fuel Handling Facilities*, ORNL-3041.

Table 2.19. Isotopic Activity of Plutonium Product from a Light Water Reactor as a Function of Cooling Time

Radioactivity expressed as curies per metric ton of fuel charged to reactor.

Nuclide	Cooling Time (days)					
	0	3	30	300	3,000	30,000
^{208}Tl	0.0	1.45×10^{-8}	1.39×10^{-4}	1.91×10^{-2}	5.05×10^{-1}	3.58×10^{-1}
^{212}Pb	0.0	4.03×10^{-8}	3.86×10^{-4}	5.30×10^{-2}	1.40	9.94×10^{-1}
^{212}Bi	0.0	4.03×10^{-8}	3.86×10^{-4}	5.30×10^{-2}	1.40	9.94×10^{-1}
^{212}Po	0.0	2.58×10^{-8}	2.47×10^{-4}	3.39×10^{-2}	8.97×10^{-1}	6.36×10^{-1}
^{216}Po	0.0	1.04×10^{-6}	4.39×10^{-4}	5.30×10^{-2}	1.40	9.94×10^{-1}
^{220}Rn	0.0	1.04×10^{-6}	4.39×10^{-4}	5.30×10^{-2}	1.40	9.94×10^{-1}
^{224}Ra	0.0	1.04×10^{-6}	4.39×10^{-4}	5.30×10^{-2}	1.40	9.94×10^{-1}
^{228}Th	0.0	6.26×10^{-6}	6.16×10^{-4}	5.30×10^{-2}	1.40	9.94×10^{-1}
^{232}U	0.0	4.20×10^{-3}	4.16×10^{-2}	3.80×10^{-1}	1.73	9.94×10^{-1}
^{234}U	0.0	4.67×10^{-3}	4.67×10^{-2}	4.66×10^{-1}	4.52	3.45×10^1
^{236}U	0.0	1.24×10^{-5}	1.24×10^{-4}	1.24×10^{-3}	1.24×10^{-2}	1.24×10^{-1}
^{237}Np	0.0	2.25×10^{-7}	2.24×10^{-5}	2.21×10^{-3}	1.94×10^{-1}	7.55
^{236}Pu	5.32×10^1	5.31×10^1	5.21×10^1	4.35×10^1	7.21	1.12×10^{-7}
^{238}Pu	2.03×10^5	2.03×10^5	2.02×10^5	2.01×10^5	1.90×10^4	1.07×10^5
^{239}Pu	3.63×10^4	3.63×10^4	3.63×10^4	3.63×10^4	3.63×10^4	3.62×10^4
^{240}Pu	5.22×10^4	5.22×10^4	5.22×10^4	5.22×10^4	5.22×10^4	5.18×10^4
^{241}Pu	1.36×10^7	1.36×10^7	1.35×10^7	1.30×10^7	8.77×10^6	1.70×10^5
^{242}Pu	1.56×10^2	1.56×10^2	1.56×10^2	1.56×10^2	1.56×10^2	1.56×10^2
^{241}Am	0.0	1.69×10^2	1.68×10^3	1.65×10^4	1.36×10^5	3.46×10^5
Total	1.39×10^7	1.39×10^7	1.38×10^7	1.33×10^7	9.18×10^6	7.11×10^5

thirds of the total length, less shielding is required for the upper and lower portions and the cask is tapered to eliminate excessive shield weight.

The estimated neutron dose rate at 8 ft from the surface of LMFBR spent fuel shipping casks is compared with that from LWR fuel shipping casks in Table 2.22. These estimates indicate that supplementary hydrogenous shields on the outside of the cask may be required for both types of fuel.

Shield Requirements for LMFBR Spent Fuel Reprocessing Cells. — Figure 2.20 presents the results of SDC calculations which permit estimation of the required thicknesses of normal concrete cell

walls for LMFBR fuel processing plants. The higher burnup and the specific power of LMFBR fuel necessitate the use of $\frac{1}{2}$ to 1 ft of additional shielding as compared with a comparable mass of LWR fuel at the same post-irradiation decay time.

Plutonium Product Handling and Fabrication

A reliable method for estimating dose rates in gloved enclosure lines for the preparation of recycle UO_2 - PuO_2 fuels involves a comparison with the relatively abundant experience in preparing

Table 2.20. Estimates of the Isotopic Content and Neutron Source Strength of PuO₂ Recycle Fuels

	Isotope						Total
	²³⁸ U	²³⁶ Pu	²³⁸ Pu	²³⁹ Pu	²⁴⁰ Pu	²⁴¹ Pu	
LMFBR Core^a							
Isotope content, g/kg (U + Pu)	761.6	1.4 × 10 ⁻⁶	1.7	163.4	50.8	13.9	8.5
wt % in Pu		0.6 × 10 ⁻⁶	0.72	68.57	21.30	5.83	3.58
Neutron source, neutrons sec ⁻¹ kg (U + Pu) ⁻¹							135,000
From SF			4,500		48,000		14,000
From α-n			42,000	11,000	12,000	3,500	33
LMFBR Core^b							
Isotope content, g/kg (U + Pu)	781.3	23 × 10 ⁻⁶	2.6	129.5	51.8	26.0	8.76
wt % in Pu		11 × 10 ⁻⁶	1.2	59.2	23.7	11.9	4.0
Neutron source, neutrons sec ⁻¹ kg (U + Pu) ⁻¹							164,000
From SF			6,900		49,000		15,000
From α-n			65,000	8,700	13,000	6,600 ^c	34
LWR Pu Recycle Core^b							
Isotope content, g/kg (U + Pu)	956.4	4.6 × 10 ⁻⁶	0.52	25.8	10.3	5.2	1.7
wt % in Pu		11 × 10 ⁻⁶	1.2	59.2	23.7	11.9	4.0
Neutron source, neutrons sec ⁻¹ kg (U + Pu) ⁻¹							33,000
From SF			1,400		9,800		2,900
From α-n			13,000	1,700	2,500	1,300 ^c	6.6

^aMixed plutonium from LMFBR core-blanket recycle.

^bPlutonium from LWR recycle.

^cFrom ²⁴¹Am, assuming one year of post-separation decay.

$^{233}\text{UO}_2\text{-ThO}_2$ fuels.³⁹ This comparison is valid since both the hard gamma radiation from the ^{232}U daughters and the neutrons from plutonium are insensitive to self-shielding effects in the source. The ^{208}Tl is the dominant source of hard-gamma

radiation in the daughters of ^{232}U . The 2.62- and 0.58-Mev gamma radiation that occurs in 100% of the disintegrations of ^{208}Tl generally contributes at least 50% of the total dose rate from lightly shielded sources and nearly all of the dose from heavily shielded sources. For unshielded sources, 32 disintegrations of ^{208}Tl would yield the same penetrating dose as 1 disintegration generating a neutron by $\alpha\text{-n}$ reaction with oxygen (see Table 2.23). This dose ratio remains approximately con-

³⁹R. E. Brooksbank, J. P. Nichols, and A. L. Lotts, "The Impact of Kilorod Operational Experience on the Design of Fabrication Plants for $^{233}\text{U-Th}$ Fuels," AEC Symposium Series 12 (Feb. 1968), pp. 321-40.

Table 2.21. Cask Shield Thicknesses for 36 Atomics International Reference
Oxide Core -- Axial Blanket Elements

Cask has inside diameter of 53 in. Gamma shield requirement is based on a dose rate of 10 mrad/hr at 8 ft from the surface of the cask.

Height Above Midplane (cm)	Thickness of Iron Required (cm)			Thickness of Uranium Required (cm)		
	Decay Time (days)			Decay Time (days)		
	20	60	150	20	60	150
0	52.5	47.9	44.2	17.6	16.1	14.8
10	52.3	47.9	44.2	17.6	16.1	14.8
20	52.3	47.9	44.2	17.6	16.1	14.8
30	52.3	47.9	44.2	17.6	16.1	14.8
40	52.3	47.9	44.2	17.6	16.1	14.8
51	52.2	47.9	44.2	17.6	16.1	14.8
61	52.1	47.8	44.1	17.6	16.1	14.8
66	52.0	47.6	43.9	17.6	16.1	14.8
71	51.8	47.4	43.8	17.6	16.0	14.8
76	51.5	47.2	43.5	17.6	16.0	14.7
81	51.1	46.8	43.2	17.4	15.9	14.6
86	50.7	46.3	42.7	17.2	15.6	14.4
91	50.0	45.7	42.0	16.9	15.3	14.0
96	49.2	44.8	41.2	16.4	14.8	13.5
101.5	48.2	43.8	40.1	15.6	14.1	12.8
106.5	47.0	42.6	38.9	14.8	13.2	11.9
111.5	45.7	41.2	37.4	13.7	12.2	11.0
121.5	42.3	37.7	33.8	11.4	10.0	8.8
131.5	37.9	33.2	29.2	9.1	7.8	6.8
141.5	32.8	28.0	24.0	8.5	7.2	6.2
151.5	27.1	22.5	19.0			
168.5 and above	24.9	21.6	19.0			

Table 2.22. Estimated Neutron Dose Rates at a Distance of 8 ft from the Surfaces of LWR and LMFBR Shipping Casks

The combined neutron and gamma dose rate should be less than 10 mrem/hr for exclusive-use shipments.

Fuel	Inside Diameter (ft)	Active Length (ft)	No. of Elements	Shield	Types of Supplementary Shield		Neutron Dose Rate at 8 ft (mrem/hr)
					Inside	Outside	
LWR	4	12	4 PWR or 10 BWR	{ 8 in. Pb + 2.5 in. Fe	Air or Al	None	18
					Water	None	0.6
					Air or Al	2 in. water ^a	5.0
LWR-Pu recycle	4	12	4 PWR or 10 BWR	{ 8 in. Pb + 2.5 in. Fe	Air or Al	None	250
					Water	None	8.0
					Air or Al	6 in. water + 2 in. Fe ^b	5.0
LMFBR core	1.8	4	36	20 in. Fe	Sodium	None	20
					Sodium	2 in. water ^a	5.0

^aAn equivalent shield may be made with 2 in. of Benelex 70 or 6 in. of normal concrete.

^bAn equivalent shield may be made with 16 in. of normal concrete.

stant since the two sources are shielded by an equal amount of concrete.

Table 2.24 presents an analysis of recycle UO_2 - PuO_2 production that could conceivably be performed in existing glove-box lines; the radiation dose to the operators would be equal to that experienced in preparing $^{233}\text{UO}_2$ - ThO_2 fuels. The portion of the Babcock and Wilcox line described in the first column of Table 2.24 was used to prepare calcined 3% UO_2 -97% ThO_2 containing 1 ppm of ^{233}U from UNH and denitrated ThO_2 , using the sol-gel process in an unshielded glove-box line. The production rate was 3.9 kg per shift. Conceptually, the same dose rate to operators, 130 mrem per man per week, would apply if the line were used to produce UO_2 - PuO_2 for LMFBR cores (from LWR recycle plutonium) at the rate of 7.6 kg of fuel per 8 hr.

The second column shows results obtained at Savannah River in the processing of 40 kg of ^{233}U containing 244 ppm of ^{232}U at the rate of 0.8 kg per shift through their unshielded "B" line. The UNH was precipitated, filtered, calcined to UO_3 - U_3O_8 , and packaged in aluminum cans. Equivalent operator dose rates would be predicted from similar processing steps to prepare coprecipitated UO_2 - PuO_2 at the rate of about 10 kg per shift.

The third column shows results obtained in the ORNL Kilorod program for preparing 3% UO_2 -97% ThO_2 containing 1 ppm of ^{232}U by the sol-gel process at the rate of 6.3 kg per shift. Since this line is shielded with the equivalent of 2 in. of lead

Table 2.23. Effect of Shield Thickness on the Dose Rate from a Unit Point Source of ^{208}Tl Gamma Radiation^a and a Unit Point Source of Neutrons^b from α -n Reactions with Oxygen

Shield	$4\pi r^2 D(r)$, [(mrem/hr)/(dis or n/sec)] · cm ²	
	²⁰⁸ Tl Gamma Radiation	α -n Neutrons
1/8 in. Pb	0.0045	0.142
2 in. Pb	0.00055	~0.1
1 ft concrete	0.00066	0.065
2 ft concrete	0.000064	0.0041
3 ft concrete	0.0000056	0.00017

^a1 dis/sec.

^b1 neutron/sec.

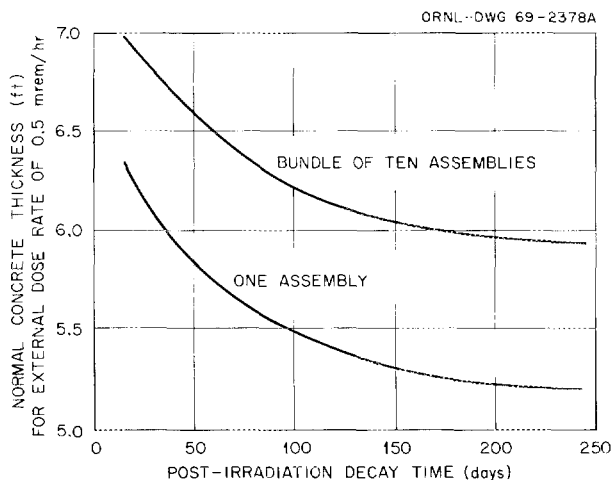


Fig. 2.20. Normal Concrete Shield Requirements (0.5 mrem/hr External Dose Rate) of Cell Walls for LMFBR Fuel Reprocessing Plants as a Function of Decay Time. Assemblies have active length of 4 ft, are located 3 ft from the inner concrete wall, and contain 50 kg of fuel irradiated to a burnup of 100,000 Mwd/metric ton at an average specific power of 125 Mw/metric ton.

to provide dose attenuation by a factor of 10, the average dose to operators was 19 mrem per man per week. Equivalent dose rates would be predicted for processing $\text{UO}_2\text{-PuO}_2$ at the rate of 11 kg per shift if the line were shielded with 15 in. of normal concrete to provide the same factor of 10 for dose attenuation.

The last two columns show conceptual lines for the sol-gel production of either $\text{UO}_2\text{-ThO}_2$ (containing 1 ppm of ^{232}U at 24 days postseparation or 10 ppm of ^{232}U at 5 days postseparation) or $\text{UO}_2\text{-PuO}_2$ such that the operator dose rate will not exceed 40 mrem per man per week. The production rate of either fuel in the unshielded line is 3.5 kg per shift, while that in the shielded line (1 ft of concrete for $\text{UO}_2\text{-PuO}_2$) is 14 kg per shift.

Table 2.25 presents current best estimates of the maximum capacities of lines for preparing two kinds of $\text{UO}_2\text{-PuO}_2$ fuels as a function of shielding thickness. In lightly shielded glove-box lines, it is estimated that LMFBR (LWR Pu recycle) and LWR (LWR Pu recycle) fuels can be prepared at maximum rates of 10 and 50 kg/day (3 shifts/day) respectively. The rates increase by about a factor of 4 if the operation is made semiremote with the installation of 1-ft-thick concrete shielding (al-

though it is probably unreasonable to fabricate LWR fuel at the rate of 200 kg/day by this technique).

2.9 CRITICALITY STUDIES

The objective of these studies is to develop evaluated criticality data for application to the aqueous processing of LMFBR fuels. The work, which is being performed with the assistance of the staff of the Y-12 Critical Experiments Facility, involves compilation of basic data and liaison with other critical experiment groups, calculation of critical parameters, the performance of selected critical experiments to validate calculations for systems containing fixed and soluble neutron absorbers, and application of the critical data to specific items of process equipment.

A series of survey criticality calculations were performed this year to aid in the conceptual design of LMFBR fuel reprocessing equipment.^{40,41} These calculations were made with the one-dimensional neutron transport code, ANISN,⁴² using the S_4 approximation and 16-group Hansen-Roach⁴³ cross sections supplemented with locally generated cross-section sets for ^{241}Pu and ^{242}Pu . The computational procedure was checked by calculating results of critical experiments for systems containing ^{239}Pu at various moderating ratios; the calculated neutron multiplication factors were consistently high by 0 to 5% with respect to those determined experimentally. The computational procedure cannot yet be validated for systems containing high concentrations of ^{240}Pu , ^{241}Pu , ^{238}U , and other neutron absorbers because of the paucity of experimental data for such systems. The following sections will summarize the criticality considerations in the aqueous processing of LMFBR fuels and present results of some of the calculations.

Spent Fuel Shipping. — The minimum critical mass of plutonium in a compact array of typical

⁴⁰D. W. Magnuson, *Criticality Calculations for Light Water Reactor and Liquid Metal Fast Breeder Reactor Fuels*, Y-DR-9 (March 1969).

⁴¹D. W. Magnuson, *Criticality Calculations for the Design of Large Pulsed Extraction Columns*, Y-DR-12 (March 1969).

⁴²W. W. Engle, Jr., *A User's Manual for ANISN*, K-1693 (Mar. 30, 1967).

⁴³G. E. Hansen and W. H. Roach, *Six and Sixteen Group Cross Sections for Fast and Intermediate Critical Assemblies*, LAMS-2543 (December 1961).

Table 2.24. Estimation of Dose Rates in Gloved Enclosure Lines for Sol-Gel Preparation of $\text{UO}_2\text{-PuO}_2$ for LMFBR Core Fuel (with LWR Recycle Plutonium) by Analogy with $^{233}\text{UO}_2\text{-ThO}_2$ Experience

	Babcock and Wilcox	Savannah River	ORNL Kilorod	Conceptual Lines	
				Unshielded	Shielded
General Line Characteristics					
Operator dose rate, mrem per man per 40 hr	130	200	19.5	40	40
Number of operators per shift	1.33	3	2	3	3
Shield attenuation factor	1.0	1.0	0.1	1.0	0.25
Unit dose factor, ^a rem/curie ^{208}Tl processed	36	100	55	55	55
$\text{UO}_2\text{-ThO}_2$ Preparation					
Fuel processing rate, kg $\text{UO}_2\text{-ThO}_2$ per shift	3.9	0.8	6.3	3.5	14
Batch size, kg $\text{UO}_2\text{-ThO}_2$	12	0.4	10	5.5	22
^{208}Tl activity, curies/kg $\text{UO}_2\text{-ThO}_2$	0.00024	0.0015	0.00022	0.000124	0.000124
^{232}U content, mg/kg $\text{UO}_2\text{-ThO}_2$	1.1	220	0.99	$\binom{1}{24}$ or $\binom{10}{5}$	$\binom{1}{24}$ or $\binom{10}{5}$
Effective postseparation time, days	40	3.75	40		
Shield, in. of lead	0	0	2.2	0	1.3
Equivalent $\text{UO}_2\text{-PuO}_2$ Preparation					
Fuel processing rate, kg $\text{UO}_2\text{-PuO}_2$ per shift	7.6	9.7	11.3	3.5	14
Batch size, kg $\text{UO}_2\text{-PuO}_2$	23	4.8	18	5.5	22
Neutron source, curies/kg $\text{UO}_2\text{-PuO}_2$	0.0000076	0.000047	0.0000069	0.0000039	0.0000039
Shield, in. of concrete			15		12
in. Pb	$\frac{1}{4}$	$\frac{1}{4}$		$\frac{1}{4}$	

^aThis factor has been normalized to include effects of material holdup, cleaning and maintenance operations, and shielding.

LMFBR core fuel assemblies flooded with sodium and reflected by steel or lead is not known accurately at present but may be estimated to be in the range of 700 kg.⁴⁴ Even larger masses would result if the elements were spaced slightly farther apart than in the reactor or if they were interspersed with radial blanket elements. These esti-

mates imply that, from a criticality point of view, virtually entire LMFBR cores could be shipped at one time in a single cask if features are provided to ensure that the sodium is not displaced by a more efficient moderator such as water.

It is anticipated that reactor critical experiments will provide sufficient information to determine the necessary criticality parameters of LMFBR casks that are filled with sodium or gas. Special critical experiments, perhaps using boron-stainless steel plates between assemblies or mockups of assemblies, will become necessary if subcriticality

⁴⁴D. Okrent, *Summary of Intercomparison Calculations Performed in Conjunction with Conference on Safety, Fuels and Core Design in Large Fast Power Reactors*, ANL-7120 (October 1965), pp. 3-23.

Table 2.25. Estimated Maximum Capacities of Lines for Preparing $\text{UO}_2\text{-PuO}_2$ as a Function of Reactor Type and Shield Thickness

Operator dose rate = 40 mrem/week.

Type of Operation	LMFBR Core (LWR Recycle Pu)		LWR-Pu Core (LWR Recycle Pu)	
	Concrete Shield Thickness (in.)	Capacity [kg ($\text{UO}_2\text{-PuO}_2$)/day]	Concrete Shield Thickness (in.)	Capacity [kg ($\text{UO}_2\text{-PuO}_2$)/day]
Gloved enclosures ^a	0 ^b	10	0 ^b	50
Semiremote ^a	12	40	12	(200)
Remote ^c	15	100	9	100
	21	500	15	500
	23	1000	17	1000

^aAssumes process equipment installed 1 ft from inner wall of enclosure and dose results by analogy with $^{233}\text{U-ThO}_2$ experience.

^bAssumes $\frac{1}{8}$ in. of lead for shielding soft gamma radiation.

^cAssumes that process vessels (which contain no more than 20% of daily throughput) are installed 2 ft from the inner surface of the shield and that the dose rate at the operating surface is 1.0 mrem/hr.

must be ensured when water is assumed as the moderator.

Spent Fuel Storage, Handling, and Chopping. —

The calculated results presented in Fig. 2.21 illustrate that the minimum critical masses of plutonium in dry chopped fuel or arrays of elements are in the hundreds of kilograms and increase as the inverse 1.0-to-2.0 power of the apparent density of the fuel. In this and subsequent figures the notations "charge" and "discharge" PuO_2 and $(\text{Pu} + \text{U})\text{O}_2$ refer to plutonium oxide and a mixture of oxides having Pu/(U + Pu) weight ratios of 0.247 and 0.243 respectively. The isotopic composition of the plutonium "charge" is 66% ^{239}Pu , 27% ^{240}Pu , 5% ^{241}Pu , and 2% ^{242}Pu , whereas that of the "discharged" plutonium is 62% ^{239}Pu , 31% ^{240}Pu , 5% ^{241}Pu , and 2% ^{242}Pu . No significant criticality limitations are expected in dry or liquid-metal-cooled storage, handling, and chopping of LMFBR elements. It may become necessary to limit the number of elements in steaming equipment for removal of sodium.

Fuel Element Dissolvers. — The calculations summarized in Figs. 2.22 to 2.25 were performed to aid in the selection of conceptual designs for LMFBR fuel element dissolvers. Critical masses, volumes, and dimensions were calculated over virtually the entire range of possible hydrogen moderation to generate estimates of minimum crit-

ical parameters for all possible suspensions of undissolved fuel solids in solutions of partially dissolved fuel. A summary of these estimated critical parameters is presented in Table 2.26. It has been assumed that the settling of fuel particles in dissolvents will result in solid volume fractions no greater than 0.6.

The first five rows of Table 2.26 illustrate that suspensions of pure PuO_2 in water or dilute dissolvent can result in a minimum critical fissile mass of 1 kg or less, minimum critical volumes of

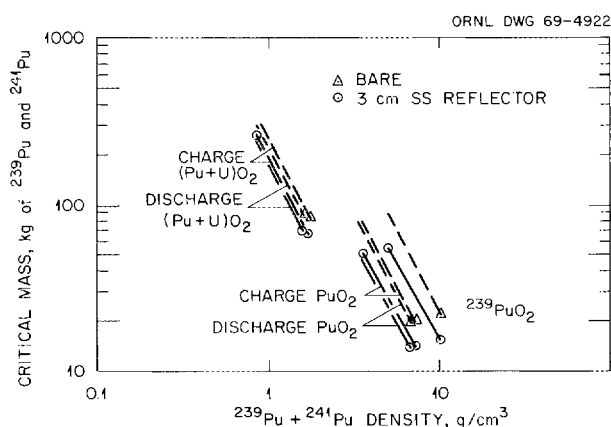


Fig. 2.21. Critical Masses for Spheres of $^{239}\text{PuO}_2$, LMFBR Charge PuO_2 , and LMFBR Discharge $(\text{Pu} + \text{U})\text{O}_2$ at Various Densities.

only several liters, cylinder diameters of less than 5 in., and slab thicknesses less than 3 in. Such limitations on these parameters are potentially required under conditions in which the UO_2 might be

leached preferentially from the UO_2 - PuO_2 (e.g., in the dissolution of unirradiated, mechanically blended pellets) or if plutonium polymer formation is possible. Line 6 of the table shows, however, that the effect of making the dissolvent 0.4 M in cadmium is to materially increase these parameters.

The remaining seven rows of Table 2.26 show the appreciably larger values of the minimum critical parameters that will result with the use of

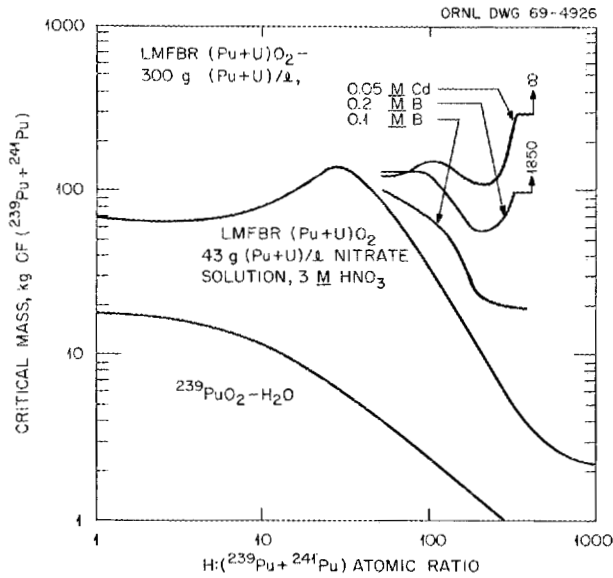


Fig. 2.22. Critical Masses of Spheres for Various Plutonium Fuels Reflected by 3-cm-thick Stainless Steel.

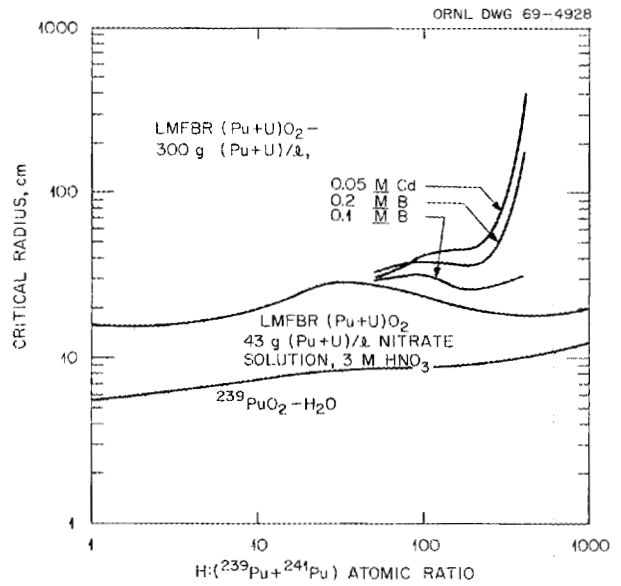


Fig. 2.24. Critical Radii for Infinite Cylinders of Various Plutonium Fuels Reflected by 3-cm-thick Stainless Steel.

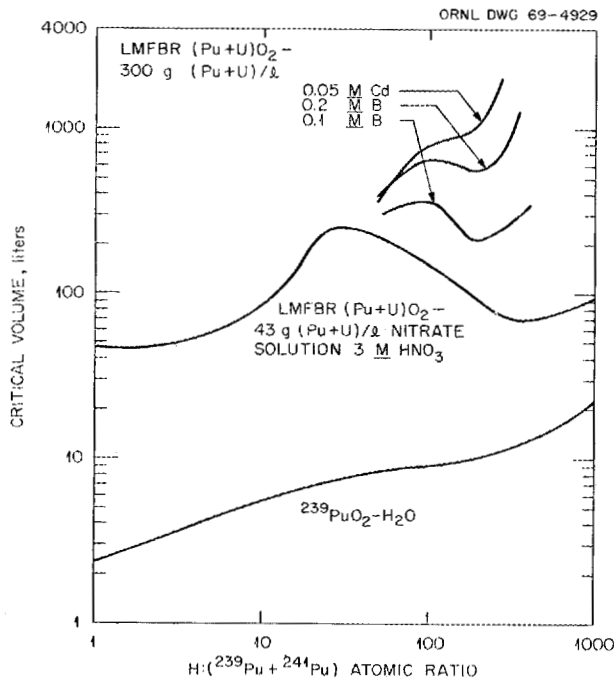


Fig. 2.23. Critical Volumes for Spheres of Various Plutonium Fuels Reflected by 3-cm-thick Stainless Steel.

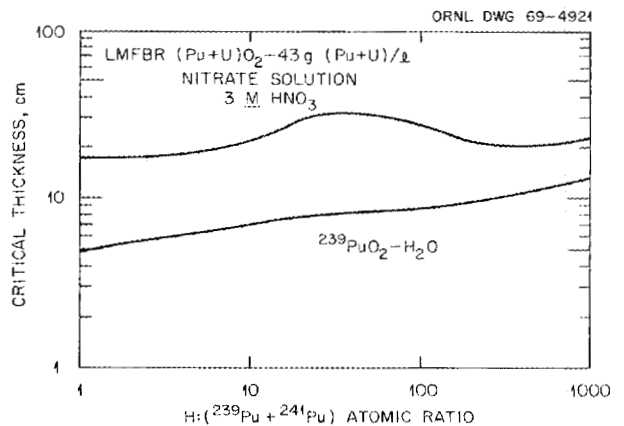


Fig. 2.25. Critical Thicknesses of Infinite Slabs for Various Plutonium Fuels Reflected by 3-cm-thick Stainless Steel.

Table 2.26. Calculated Critical Parameters for 60 vol % Fuel Oxide Solids in Various Solutions for Various Reflector Conditions

Fuel Solid	Solution ^a	H/(²³⁹ Pu + ²⁴¹ Pu) for 60% Solids	Reflector		Critical Sphere ^b		Infinite Cylinder Diameter (in.)	Infinite Slab Thickness (in.)
			Material	Thickness (cm)	Mass (kg of ²³⁹ Pu + ²⁴¹ Pu)	Volume (liters)		
²³⁹ PuO ₂	Water	1.75	Bare		27.2 (0.86)	4.6	6.1	3.3
²³⁹ PuO ₂	Water	1.75	SS	3	17.5 (0.62)	2.9	4.6	2.2
²³⁹ PuO ₂	Water	1.75	Water	15	11.2 (0.48)	1.8	3.5	0.9
LWR-PuO ₂	Water	2.41	SS	3	17.0 (1.0)	3.8		
LMFBR-PuO ₂	43 g (Pu + U)/liter	2.39	SS	3	18.5 (~1)	4.6	5.5	2.6
LMFBR-PuO ₂	300 g (Pu + U)/liter, 0.4 M Cd	2.05	SS	3	20.0	5.0		2.7
LMFBR-(Pu + U)O ₂	43 g (Pu + U)/liter	10.2	SS	3	84. (2.3)	86. (65.)	15.7	8.6
LMFBR-(Pu + U)O ₂	300 g (Pu + U)/liter, 0.2 M Cd	8.74	SS	3	90.	92.	15.9	9.0
LMFBR-(Pu + U)O ₂	300 g (Pu + U)/liter, 0.4 M Cd	8.55	SS	3	96.	98.	16.1	9.2
LMFBR-(Pu + U)O ₂	300 g (Pu + U)/liter, 1.0 M Cd	7.89	SS	3	110.	112.	17.3	9.8
LMFBR-(Pu + U)O ₂	300 g (Pu + U)/liter, 0.2 M Cd	8.74	Soln.	15 ^c	72.	74.		
LMFBR-(Pu + U)O ₂	300 g (Pu + U)/liter, 0.4 M Cd	8.55	Soln.	15 ^c	86.	88.		
LMFBR-(Pu + U)O ₂	300 g (Pu + U)/liter, 1.0 M Cd	7.89	Soln.	15 ^c	106.	108.		

^aAll solutions (except water) were 3 M in HNO₃.

^bValues in parentheses are minimum values at higher H:Pu ratios; other values are minimal at 60 vol %.

^cAn infinite reflector of solution was simulated by returning all leakage neutrons at 15 cm. Pu in reflector not included in the mass value.

cadmium as a soluble poison if it can be assumed that the $\text{UO}_2\text{-PuO}_2$ fuel particles will not materially change in composition during dissolution. The effect of the presence of the $^{238}\text{UO}_2$ is to increase the critical parameters in the low moderation range in which the cadmium absorption is not effective. The presence of stainless steel hulls mixed with the oxide fuel would enhance this effect, but the hulls were omitted in this analysis for conservatism. The effect of the cadmium in solution is to ensure that no more restrictive limits will apply in the intermediate range of moderation. In principle, boron in solution would serve this purpose to a lesser extent. Natural boron, near its solubility limit of about 0.2 M, has neutron absorption properties comparable to those of cadmium at about 0.05 M. The dispersions of $\text{UO}_2\text{-PuO}_2$ in dissolvents containing cadmium have fissile masses greater than 70 kg; minimum critical cylinder diameters and slab thicknesses are in the range of 15 and 9 in. respectively.

Present data indicate that the selective leaching of UO_2 from irradiated $\text{UO}_2\text{-PuO}_2$ is probably negligible; however, this must be substantiated. A variety of critical experiments should be performed to validate the methods for computing critical parameters of dispersions of mixed $\text{UO}_2\text{-PuO}_2$ solids in solutions containing cadmium and boron. In addition, critical experiments should be performed to validate specific equipment designs as the development of LMFBR dissolution hardware approaches plant scale.

Pulsed Extraction Columns. — The Nuclear Fuels Services fuel reprocessing plant employs a 10-in.-diam extraction column to process (U + Pu) fuel, using the Purex process, at the rate of about one ton/day. The expanded top section of the column contains 1% boron–stainless steel to make the column critically safe at the anticipated maximum plutonium concentration. The rationale for the use of a 10-in.-diam column generally assumes that administrative control will be exercised to prevent the effect of reflux from concentrating the plutonium in the column to greater than about 35 g/liter. A more conservative assumption, that is, that reflux is not detected before the solvent becomes saturated with plutonium (at about 120 g of plutonium per liter), would require that column diameters be limited to about 8 in.

Boron–stainless steel is not generally considered suitable for use as a material of construction for pulse plates (which are subject to vibration

and difficult to inspect periodically) because plates made of this material have poor resistance to corrosion and require mechanical (rather than welded) fasteners due to their brittleness. Development work for reactor control plates has revealed that alloys of stainless steel could probably contain sufficient quantities of rare earths, such as gadolinium, to provide safety from the standpoint of criticality without suffering any appreciable change in their mechanical and chemical properties.

The calculations presented in Fig. 2.26 were performed to estimate the critical diameters of pulsed columns that would use pulse plates made of gadolinium–stainless steel. A plate thickness of $\frac{1}{8}$ in. was assumed for most of these calculations in an attempt to estimate the effect of the normally $\frac{3}{16}$ -in.-thick plates which have holes in 23% of the cross-sectional area. From these data it is estimated that the effect of incorporating pulse plates containing about 0.3 wt % gadolinium at a 1.5-in. plate spacing would be to allow essentially unlimited column diameters for the customary assumption of a maximum plutonium concentration of about 35 g/liter [$\text{H}/(^{239}\text{Pu} + ^{241}\text{Pu}) = 1000$] or a diameter of about 9.5 in. for the more conservative assumption of a maximum plutonium concentration of about 120 g/liter [$\text{H}/(^{239}\text{Pu} + ^{241}\text{Pu}) = 220$]. At a 1-in. plate spacing and with pulse

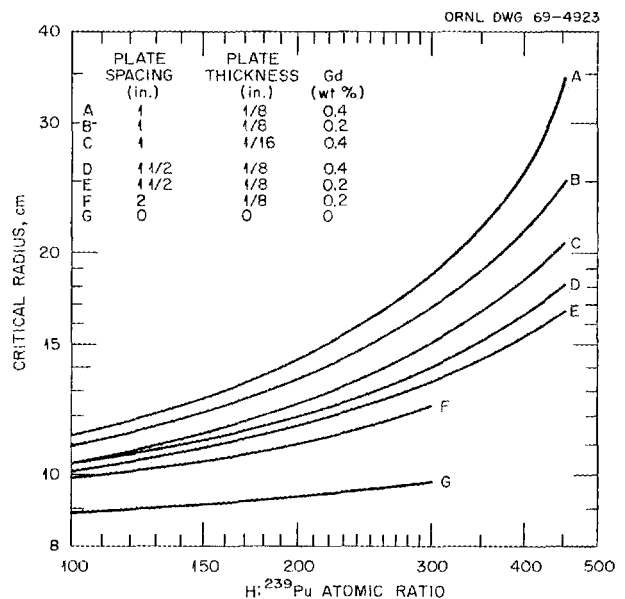


Fig. 2.26. Critical Radii for Pulsed Extraction Columns That Have Gadolinium–Stainless Steel Plates and Are Reflected by 3-cm-thick Stainless Steel.

plates containing 0.4 wt % gadolinium, the critical column diameters would be about 16 and 11.8 in. for plutonium concentrations of 80 and 120 g/liter respectively.

Such large column sizes can contribute to the economy of plants for processing power reactor fuels (LWR as well as LMFBR) at rates of 5 tons/day or greater. Confirmation of the estimates presented above would require selected critical experiments to validate the poisoning effect of gadolinium and to determine the geometrical effects of the holes in the pulse plates, experiments to validate the corrosion resistance of the gadolinium--stainless steel, and studies to generate designs that will ensure appropriate plate spacing and integrity during the intended service life.

Stacked-Clone Contactors. -- Future aqueous reprocessing plants may use stacked-clone contactors, which have the advantage of short contact times and small shielded cell requirements. Such contactors will have relatively unrestrictive criticality requirements because of the low fissile inventory in the contactor and the relative simplicity

of poisoning the metal blocks to minimize interaction between contactors.

Plutonium Storage. -- The use of large tanks packed with borosilicate glass Raschig rings is currently the preferred technique for interim storage of purified plutonium solutions in processing plants. Evidence indicates that solutions of the normal storage concentration, approximately 200 g of plutonium per liter, will remain subcritical and that the product will not become contaminated by leaching of boron from the rings. However, we have not yet determined that borosilicate glass Raschig rings will have a suitably long service life in solutions of high exposure plutonium with associated high alpha and beta radiation levels.

Plutonium Product Shipping. The shipment of plutonium solution in 10-liter polypropylene bottles in "bird cages" is currently considered safe but is relatively expensive. Larger containers incorporating either high surface-to-volume geometry or fixed neutron absorbers could improve the economics by decreasing handling and bulk shipping charges.

3. Development of Methods for Processing HTGR Fuels

The development of methods for reprocessing graphite-based HTGR fuels was continued. Hot-cell experiments were performed, and an engineering evaluation of alternative head-end methods for preparing fuels for solvent extraction was made. Additional development of the Thorex solvent extraction process was deferred, pending definition of the head-end steps. Development is proceeding as outlined in the tentative flowsheet published previously¹ and includes dissection, crushing, burning, separation of the fertile, fissile, and alumina bed particles from each other, crushing of the fertile particles, and burning and leaching of the crushed particles. An arbitrary limit for the cross-over of ^{235}U and ^{233}U has been established as a reprocessing and fuel cycle objective; that is, the loss of ^{233}U to the ^{235}U reject stream should not exceed 5%, or the transfer of ^{235}U to the ^{233}U recycle stream should not exceed 10%, or some combination of these, such that the total economic penalty incurred does not exceed 0.015 mill/kwhr.

3.1 HEAD-END BURN-LEACH METHODS FOR PROCESSING HTGR FUEL

The burn-leach portion of a proposed flowsheet for reprocessing Ft. St. Vrain HTGR fuel, and subsequently recovering the fertile and fissile materials, is being developed and evaluated in small-scale engineering studies. The Ft. St. Vrain reactor is being built for Public Service of Colorado by Gulf General Atomic. The present investigation includes: (1) fluidized-bed burning tests of both simulated and crushed prototype fuel, (2) initial scoping tests of an engineering-scale, fixed-bed unit for burning fuel blocks, and (3) preliminary tests of a gas classification technique for sepa-

rating the alumina fluidized-bed media from the fissile and fertile fuel particles.

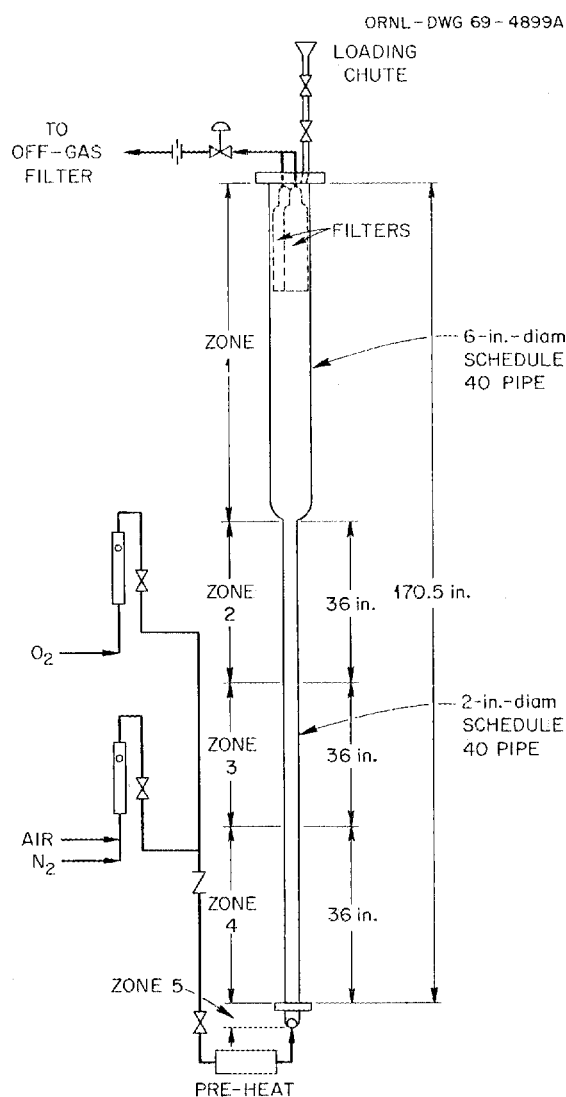


Fig. 3.1. Schematic Drawing of 2-in.-diam Fluidized-Bed Burner.

¹Chem. Technol. Div. Ann. Progr. Rept. May 31, 1968, ORNL-4272, p. 57.

Fluidized-Bed Burning

A 2-in.-diam fluidized-bed reactor that had been previously used for fluoride-volatility experiments was modified for use as a fluidized-bed burner (Fig. 3.1). A series of tests were made using SiC-coated ThO₂ particles and crushed graphite to simulate crushed HTGR fuel (Table 3.1). No temperature excursions or plugging phenomena were observed during these runs. Wall temperatures were easily controlled, and the burner ash was free-flowing. Examination of the burner ash showed no agglomeration of the particles, although some agglomeration of the Al₂O₃ fluidized-bed media was noticed in the residue from a high-temperature (950 ± 25°C) test. In two tests with pure oxygen, the percentage of particles with broken SiC coatings (determined by sieve analyses and microscopic examination of the residue) was erratic, ranging from about 10% in a test at 750°C to 1–2% in a test at 950°C. The high percentage of broken particles in the 750°C test is not understood since no operating excursions were observed and ThO₂ particles from the same batch were used for all experiments.

In one test (run HTGR-BT-13), we used fuel obtained by crushing a fueled prototype graphite sample in a hammer mill (–³/₄-in. grate spacing). Pure oxygen was used at a superficial velocity of

1.25 fps, and wall temperatures were maintained at 800 ± 50°C. Oxygen utilization was greater than 95% during the major burning phase, and no plugging phenomena or wall "hot spots" were observed. The burner ash was free-flowing and passed a 20-mesh screen (Table 3.2). Most of the ThO₂ par-

Table 3.2. Sieve Analyses of Burner Ash from Run HTGR-BT-13

Size Fraction (mesh)	Weight Percent	Remarks
+20	0	None
–20 +35	12.25	Mostly ThO ₂ particles
–35 +50	2.25	Mostly UO ₂ particles; a few bare ThO ₂ particles
–50 +60	0.12	Mostly shards of SiC coating
–60 +80	47.19	Al ₂ O ₃ ^a
–80 +100	16.35	Al ₂ O ₃ ^a
–100 +120	11.4	Al ₂ O ₃ ^a
–120	7.49	Al ₂ O ₃ ^a

^aNo intact ThO₂ or UO₂ kernels were observed in these fractions.

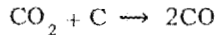
Table 3.1. Data for Fluidized-Bed Burning Tests with Simulated Fuel

	Test No.		
	BT 3	BT 5	BT 7
Reactor charge			
SiC-coated ThO ₂ particles, g	300	220	220
Crushed graphite, g	2400	1600	1600
–90-mesh Norton RR Al ₂ O ₃ , g	2000	2000	2000
Operating conditions			
Reagent gas	Oxygen	Air	Oxygen
Reagent gas flow rate, fps	1.25 at 750°C	1.25 at 750°C	1.25 at 800°C
Operating wall temp., °C	750 ± 25	750 ± 25	950 ± 25
Oxygen utilization, %	95	95	95
Burner residue			
Ash, g	2282	2166	2204
Description	Free-flowing	Free-flowing	Free-flowing
Particle breakage, %	~10	3 to 4	1 to 2

ticles were in the 20- to 35-mesh fraction, while the UO_2 particles appeared in the 35- to 50-mesh fraction (see Table 3.2). Leaching tests indicate that the coatings on 2.7 and 6.6% of the UO_2 and the ThO_2 particles, respectively, were broken. Correcting these values by subtracting breakage values obtained during the crushing step yields values of 0.5 and 5.5% for the UO_2 and ThO_2 particles, respectively, that were broken during the burning and subsequent size fractionation steps.

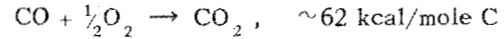
Fixed-Bed Burning

An initial fixed-bed burning test was made, using the equipment shown in Fig. 3.2, to determine whether dilution of the reagent gas with CO_2 could be used to control the high burning temperatures ($>1000^\circ\text{C}$) expected. In addition, the net reaction



was expected to absorb about 29 kcal of heat per mole of carbon and help to cool the burner. The

heat from the reaction



would be released in the external burner, where it could be dissipated more easily. The product CO_2 could be recycled, if desired. Such a system, if feasible, would overcome the difficulties previously experienced in controlling temperatures in fixed-bed burners. Two unfueled Ft. St. Vrain hexagonal graphite blocks (14.17 in. across the flats, 13 in. high) were stacked, one on top of the other, on the grate in the furnace and heated to 700°C before the air flow (65 cfm) was started. Ignition occurred when the temperature of the graphite blocks was approximately 725°C . When the temperature of the blocks reached about 1100°C , the primary burner off-gas analyzed 9% CO_2 and 21% CO , indicating that approximately one-half of the CO_2 formed had subsequently been converted to CO . At this point, CO_2 was admitted to the system, and the temperature stabilized at about 1150°C with a CO_2 liquid flow rate of 1 lb/min; however, it decreased to

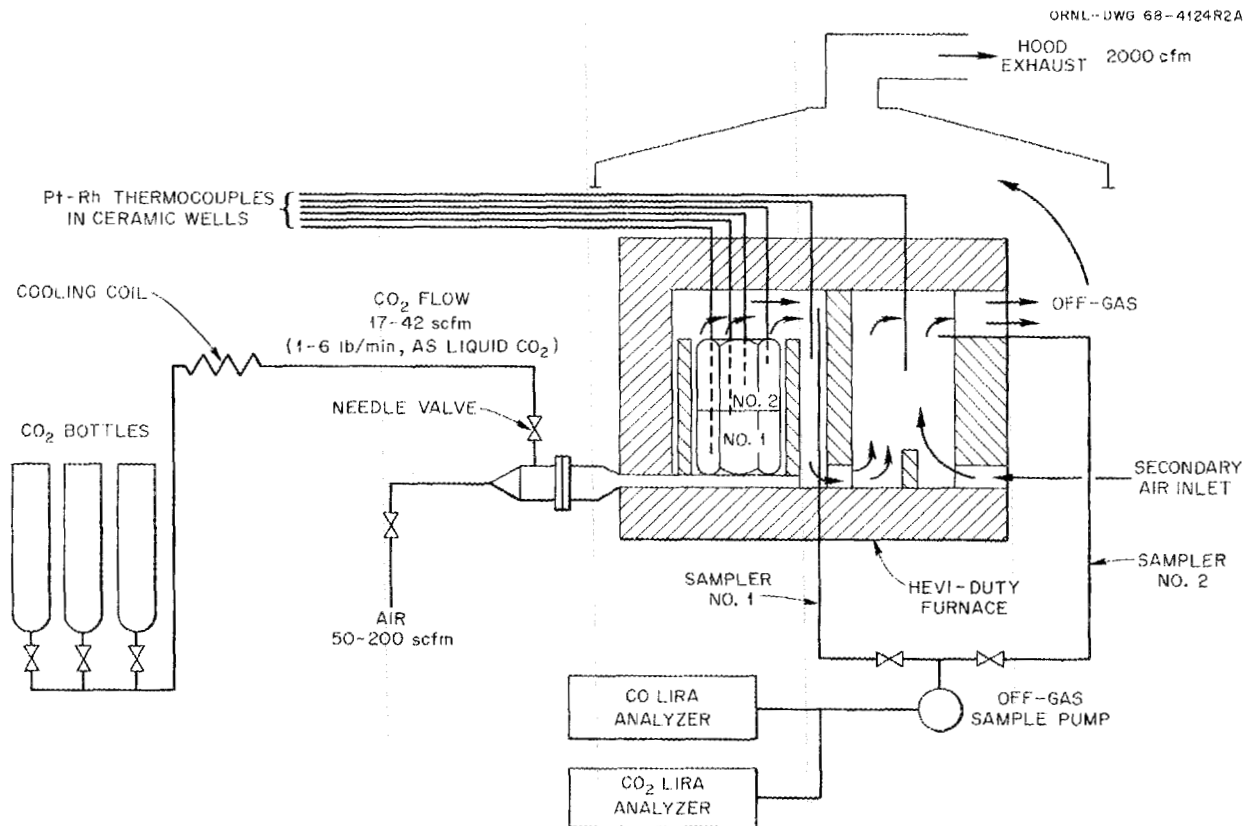


Fig. 3.2. Flow Diagram for Fixed-Bed Graphite Burning Test.

around 1000°C when the CO₂ flow rate was increased to 3 lb/min. During this time, the air flow was constant at 65 cfm. Block temperatures were easily controlled by adjusting the CO₂ flow rate. Overall, approximately 60 to 80% of the admitted CO₂ was converted to CO.

Examination of the partially burned graphite blocks (see Fig. 3.3*b*) indicated that burning had been uniform. (An unburned block is shown in Fig. 3.3*a* for comparison.) Small-scale tests will be made to determine the behavior of the SiC-coated fuel particles when they are burned under similar conditions.

Classification of Fluidized-Bed Burner Ash

The fluidized-bed ash will be classified to produce three fractions: fertile fuel particles, fissile fuel particles, and alumina (the fluidized-bed media). Tests were performed to ascertain the

feasibility of making these separations in a simple gas particle classifier using a geometry similar to a fluidized-bed reactor (Fig. 3.4). The alumina used in these tests was -90-mesh Norton RR grade, and the fuel particles were SiC-coated ThO₂ microspheres (483 ± 86 μ in diameter; density, 3.44 g/cm³) of approximately the same size as the fissile particles. A programmed gas flow was used because violent spouting of the bed occurred with the superficial gas velocities needed to elutriate the alumina. The results of a typical test are shown in Fig. 3.5. The gas flow was started slowly and increased to an initial flow rate of 8.6 cfm (air) when the bed expanded and fluidization occurred. Then it was increased at 15-min intervals until it reached 14.1 cfm, where it was held for 45 min. About 99.5% of the charged alumina was collected in the cyclone. No ThO₂ beads were found in the elutriated alumina. Thus, it is probable that gas particle-classification equipment can be designed for separating alumina from the fertile

ORNL-DWG 69-4975

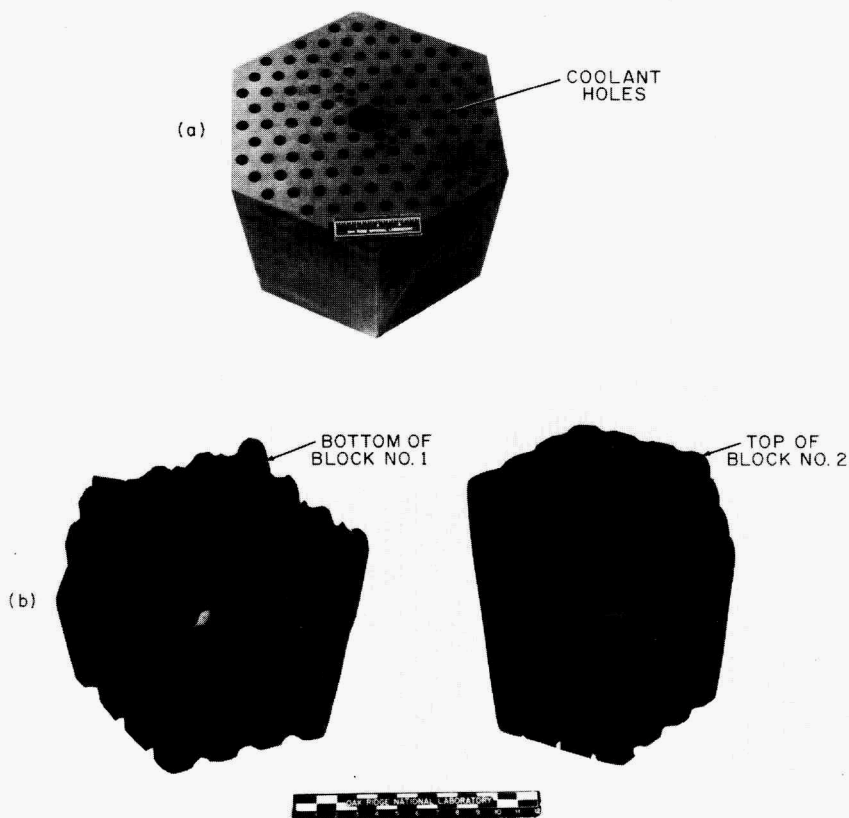


Fig. 3.3. Unfueled Ft. St. Vrain Graphite Blocks. (a) Unburned; (b) partially burned. Block No. 2 in (b) was arranged on top of Block No. 1 during burning.

and fissile particles, provided that the alumina particles do not agglomerate during the fluidized-bed burning step. Separation of fertile particles from fissile particles in the equipment sized for

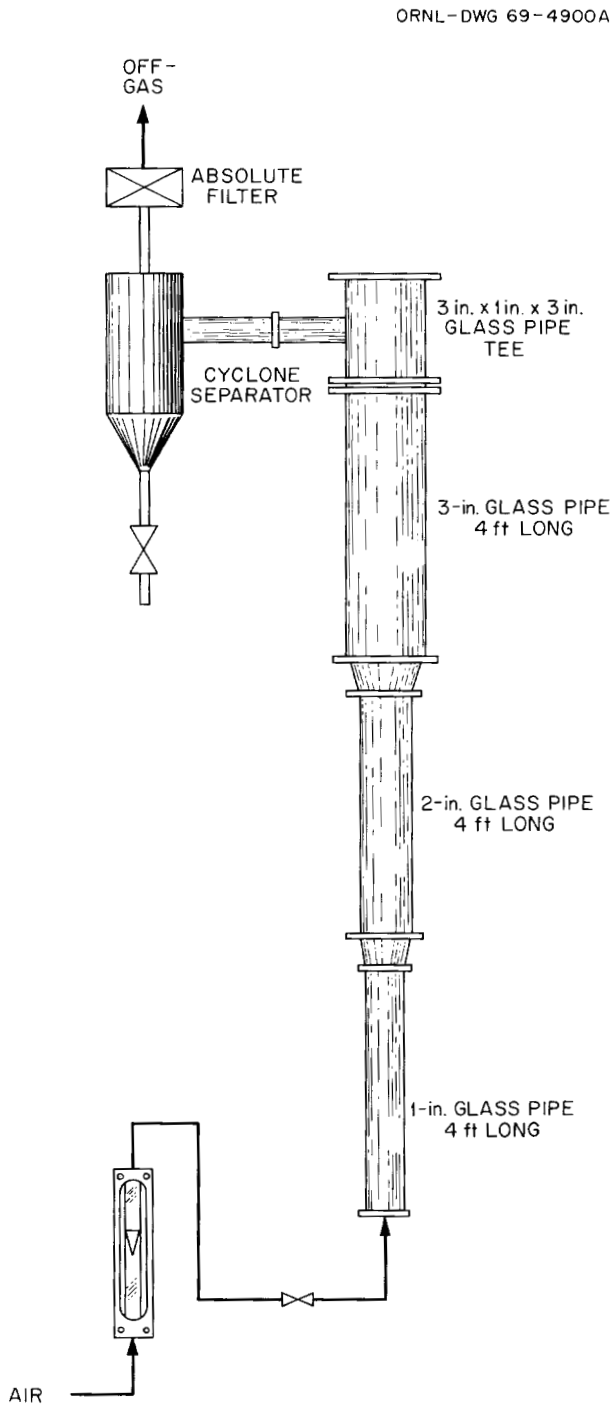


Fig. 3.4. Fluidized-Bed Particle Classifier.

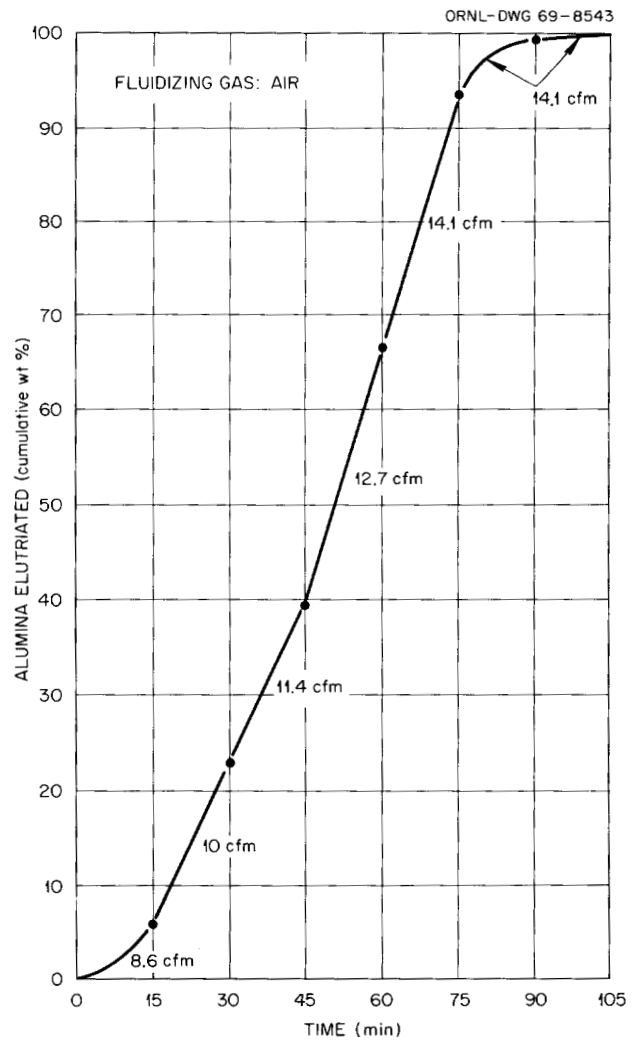


Fig. 3.5. Elutriation of Alumina in a Fluidized-Bed Particle Classifier.

efficient alumina separation does not appear to be feasible because of the high gas velocities required.

3.2 MECHANICAL HEAD-END METHODS FOR PROCESSING HTGR FUEL

Small-scale engineering studies are being made to develop and evaluate the mechanical head-end portion of the proposed reprocessing flowsheet for recovering fertile and fissile material from Ft. St. Vrain HTGR graphite fuel blocks. A number of graphite fuel sections containing fuel sticks comprised of fertile particles (ThO_2 kernels) with

either BISO² or TRISO³ coatings and fissile particles (UO₂ kernels) with TRISO coatings were fabricated for evaluating proposed comminution and particle separation steps. Investigations of both the product size distribution and the extent of fuel-particle-coating breakage during comminution of the graphite fuel sections in a hammer mill, jaw crusher, and roll crusher were begun.

Fabrication of Prototype Graphite Fuel Sections

Nineteen graphite fuel sections were fabricated for use in small-scale engineering evaluation studies using two types of fuel sticks (0.43 in. in diameter and 10 in. long) that had been made in a

²BISO refers to two layers of pyrolytic carbon: a porous buffer layer, followed by a thicker, nonporous protective layer.

³TRISO refers to three layers: the two layers of isotropic pyrolytic carbon, as defined in ref. 2, plus a layer of SiC placed in the middle of the outer carbon layer.

cooperative program with the Metals and Ceramics Division. Type I fuel sticks that contained 400- μ -diam ThO₂ kernels with BISO coatings and 100- μ -diam UO₂ kernels with TRISO coatings were prepared. In the type II fuel sticks, both the ThO₂ and UO₂ particles had TRISO coatings. Pie-shaped fuel samples (one-sixth of a hexagonal Ft. St. Vrain fuel block) were prepared by placing a fuel stick in each of the available fuel holes (36 sticks per pie-shaped section). The holes were then sealed with graphite plugs and epoxy resin, and the fuel sticks were heat treated at 1000°C for approximately 3 hr in an inert gas atmosphere to carbonize the binder. Eleven type I and four type II pie-shaped test sections (see Fig. 3.6), as well as four smaller type II sections, were fabricated.

Crushing

Graphite fuel samples containing fuel particles from a type II fuel stick were crushed in several

PHOTO 92975



Fig. 3.6. Pie-Shaped HTGR Graphite Fuel Sections (Prototype Ft. St. Vrain Fuel).

Table 3.3. Typical Size Distribution of Crushed Graphite Fuel Sections

Size Fraction	Jaw Crusher ^a Product (wt %)	Roll Crusher ^b Product (wt %)	Hammer Mill Product		
			2 $\frac{1}{4}$ -in. Grate Spacing		3 $\frac{3}{4}$ -in. Grate Spacing ^c
			(wt %)		
+ $\frac{3}{4}$ in.	8.8 ^d	31.9	26.8	2.2 ^d	3.2 ^d
- $\frac{3}{4}$ + $\frac{1}{2}$ in.	31.5 ^d	30.9	19.0	9.0 ^d	12.2 ^d
- $\frac{1}{2}$ + 4 mesh	20.2 ^d	25.9	17.0	33.0 ^d	30.8 ^d
-4 + 12 mesh	10.1	3.6	9.3	14.5	14.6
-12 + 20 mesh	9.1	3.0	8.7	11.1	11.7
-20 + 35 mesh	14.6	4.0	14.2	19.8	18.0
-35 + 50 mesh	1.6	0.2	1.4	3.6	2.6
-50 + 80 mesh	1.3	0.3	1.1	2.5	2.5
-80 mesh	3.3 ^e	0.3 ^e	2.0 ^e	4.8 ^e	4.4 ^e

^aUsing $\frac{5}{8}$ -in. spacing between jaws.

^bUsing $\frac{5}{8}$ -in. spacing between rolls.

^cTwo runs were made at this spacing.

^dNo fuel particles were found in these fractions.

^eContained only a few pieces of broken UO₂ + ThO₂ kernels.

types of comminution devices to evaluate their capability for producing a fluidized-bed-burner feed of suitable size without excessive breakage of particle coatings. These scoping tests were made with a hammer mill,⁴ a jaw crusher,⁵ and a roll mill with 8-in.-diam rolls.⁶ The resulting crushed material was sieved, the particle size distribution was determined (Table 3.3), and leaching tests were made to ascertain the extent of particle coating breakage.

The largest chunks of graphite in the + $\frac{3}{4}$ -in. size fractions were found (1) in the hammer mill test with the 2 $\frac{1}{4}$ -in. grate spacing (i.e., a 2 × 2 × 5 in. piece), and (2) in the roll mill test with a $\frac{5}{8}$ -in. spacing between rollers (i.e., a $\frac{1}{2}$ × 2 × 6 in. piece). Although pieces of this size would burn satisfactorily in a static bed burner, they would cause heat-transfer and gas channeling problems in a fluidized-bed burner. The sized fractions from

each crushing test were examined to determine their contents of fuel particles. Particles were found in each fraction from the roll crushing test and the hammer mill test with the 2 $\frac{1}{4}$ -in. grate spacing. Only a very few particles, which usually adhered to the side of a fuel hole, were found in the +4-mesh or larger-size fractions from the jaw crusher tests and the hammer mill tests using a $\frac{3}{4}$ -in. grate spacing. If the graphite in these fractions were discarded or burned in a large secondary burner, the fuel particle loss would be less than 0.05% and the primary burner load would be reduced by about 45%. In all tests, the amount of fines (-80-mesh) material produced was not excessive and would probably cause no problem in the fluidized-bed burner.

Particle coating breakage was determined by leaching the jaw crusher, roll crusher, and hammer mill products with Thorex dissolvent (13 M HNO₃ - 0.04 M F⁻ - 0.10 M Al³⁺). The results for one fuel sample, which had been crushed in the hammer mill to produce - $\frac{3}{4}$ -in. material, indicate that the coatings on 2.2% of the UO₂ particles and 1.1% of the ThO₂ particles did not survive the crushing step.

⁴Type A, Jeffrey Swing Hammer.

⁵Model No. 1, Denver Fire Clay Co.

⁶Laboratory Unit, Sturtevant Mill Co.

3.3 APPLICATION OF THE BURN-GRIND-LEACH PROCESS TO IRRADIATED FUEL

With the cooperation of the British O.E.C.D. Dragon project, seven unirradiated and ten irradiated Dragon fuel compacts have been received at ORNL. These fuel compacts are being used for feasibility studies of head-end processing steps (e.g., crushing, burning, sieving, grinding, and leaching) and to accumulate basic engineering data on the release of fission gases and the losses of fissile and fertile materials. These studies will lay the groundwork for head-end reprocessing of American HTGR fuels, as exemplified by the fuel proposed for the Ft. St. Vrain reactor being built for Public Service of Colorado.

One of the most important concepts of the fuel cycle for the Ft. St. Vrain reactor fuel is the use of separate fertile and fissile fuel particles of different sizes, each coated with a barrier layer of silicon carbide. This SiC coating must survive all head-end steps so that at least 90% of the burned-up fissile (^{235}U) particles can be separated from the fertile (thorium- ^{233}U) particles by a sizing operation after irradiation. Another important objective is the essentially complete recovery of the ^{232}Th and the ^{233}U . The Ft. St. Vrain fuel particles are described in Table 3.4. Although the Dragon fuel contains only a single size of fuel particle, it can be used to perform many pertinent tests.

The flowsheet proposed for use in reprocessing Ft. St. Vrain reactor fuel (Fig. 3.7) was used in the hot-cell tests with Dragon fuel compacts. In these tests, the compacts were usually crushed in a laboratory model jaw crusher, using a standardized crushing procedure (Fig. 3.8). Scouting work involving comparisons of different size reduction techniques was also started since appreciable particle breakage occurred when the standard technique was used with irradiated compacts. Representative samples of crushed fuel were prepared by a coarse powder splitting technique (Fig. 3.9). These samples were used in pairs to determine significant values for particle breakage, recoveries, losses, and residue compositions. The experiments have been designed to compare the results obtained for irradiated compacts with those obtained for unirradiated compacts under similar conditions.

Size Reduction Studies

The normal size reduction procedure consists of passing the fuel through a laboratory model jaw crusher⁷ twice, using a jaw clearance of about $\frac{1}{8}$ in. on the second pass. This was designed to provide good feed for a miniature fluidized-bed burner. Hollow cylinders (similar to Dragon compacts) machined from graphite were used to standardize the

⁷Model 20830, Denver Fire Clay Co.

Table 3.4. Description of Reference Ft. St. Vrain and Standard Dragon Fuels

	Ft. St. Vrain		Dragon
	Fissile	Fertile	Mixed
Composition	(Th/U) C_2	ThC_2	(Th/U) $\text{C}_{2.4}$
Th/U ratio	4.25		10
Kernel diameter, μ	200	400	457
Buffer (pyrolytic carbon) coating, μ	50	50	25
SiC coating, μ	20	20	17
Total diameter of SiC-coated particle, μ	340 ± 74	540 ± 124	541
Isotropic pyrolytic carbon coating, μ	50	60	57
Total diameter of coated particle, μ	440 ± 94	660 ± 144	655
Nominal screen size of SiC-coated particle, mesh	-40 +60	-25 +40	-25 +40

procedure. The crusher products were sieved, and the size distributions were determined (Fig. 3.10). A relatively large number of coated fuel particles, which had been freed from the graphite matrix, accumulated in the +42-mesh fractions in both the irradiated and the unirradiated compacts.

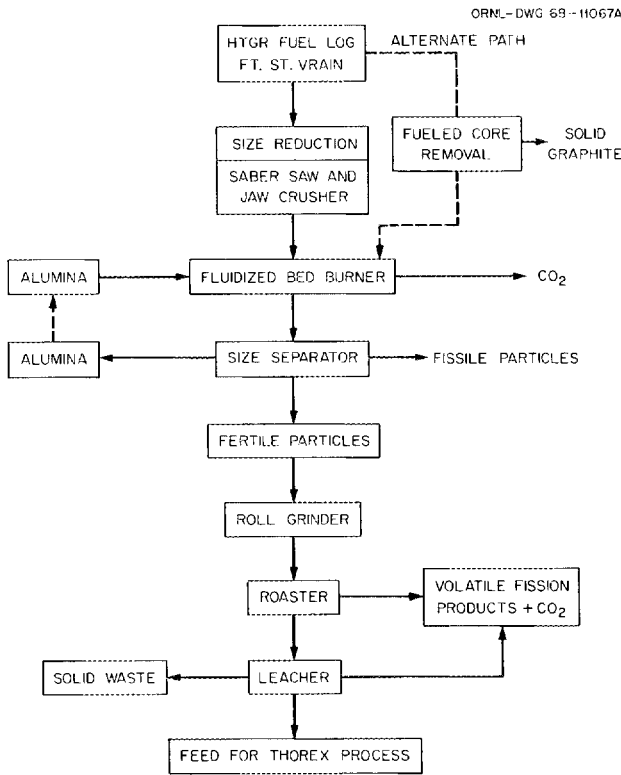


Fig. 3.7. Proposed Head-End Reprocessing Flowsheet for HTGR Fuels.

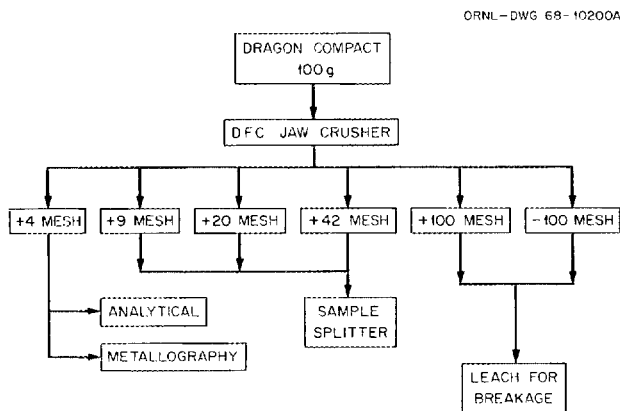


Fig. 3.8. Procedure Used to Crush and Sieve Dragon Fuel.

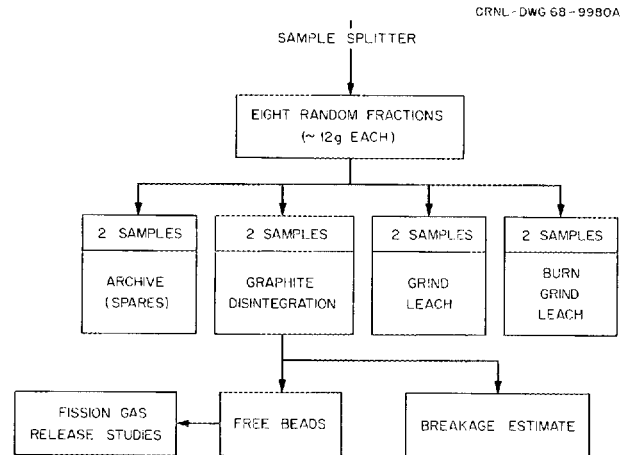


Fig. 3.9. Block Diagram of Technique Used for Sampling Crushed Fuel in Head-End Studies of Dragon Fuel.

A series of tests was designed to compare size reduction techniques, namely, hacksawing, standard crushing at $\frac{1}{8}$ -in. jaw opening, and crushing with the jaws wide open, for use with unirradiated and irradiated Dragon fuel compacts. The results of several of the tests are reported in Table 3.5, although the series is not complete. All four compacts used in these tests contained the same type of fuel (see Table 3.4).

In two separate tests using our standard crushing procedure to disintegrate unirradiated compacts, about 8 or 9% of the compact was reduced to fines less than +42 mesh; however, the total breakage of particles was less than half this value. In a single test using an irradiated compact, 10.6% of the compact was reduced to fines and 7.6% of the fuel particles were broken.

In a single test using the crusher with a $\frac{5}{8}$ -in. jaw opening, the unirradiated compact splintered into four nearly equal segments (similar to the hacksawed pieces described below). Only 0.42% of the compact was reduced to fines and 0.35% of the total particles were broken. Clearly, the jaw opening of the crusher is a major factor in particle breakage.

Since hacksawing has been proposed as a means for providing crusher feed from fuel logs, the effect of sawing through fueled portions was studied. The amount of generated fines is proportional to the amount of sawing employed; consequently, its absolute value is not significant in these tests. However, the fraction of particles broken by the saw

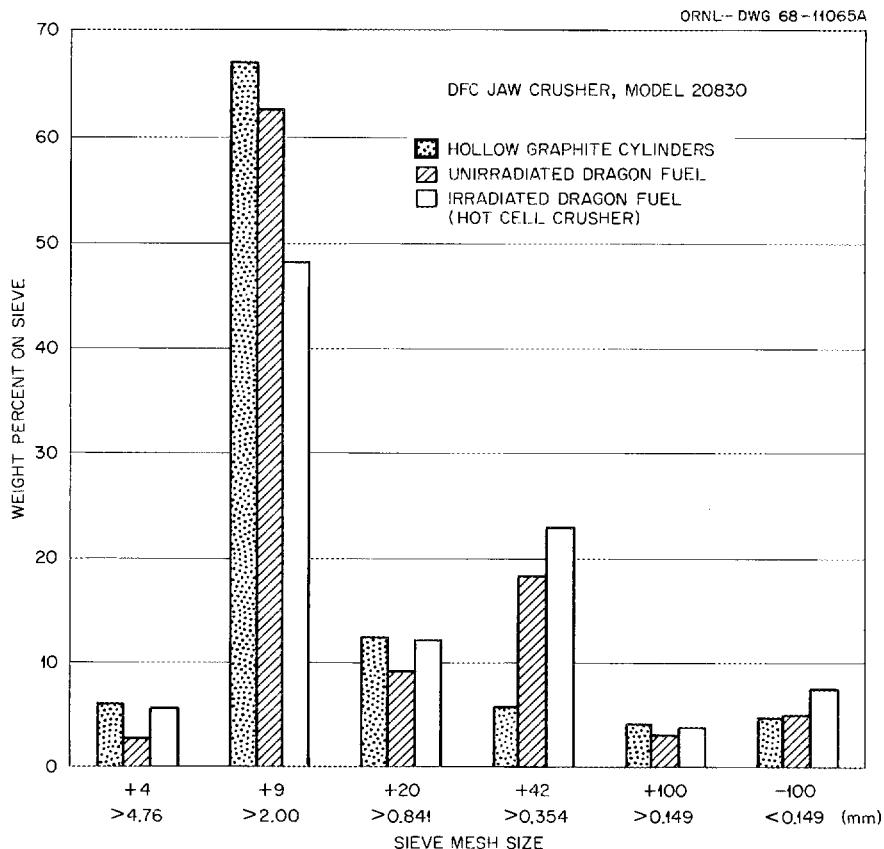


Fig. 3.10. Size Distribution of Crusher Products Obtained from Hollow Graphite Cylinders, and from Irradiated and Unirradiated Dragon Fuel.

cuts is significant. As shown in Table 3.5, the percentage of broken particles exceeds the proportion of the compact that is reduced to fines by about 20%.

One may conclude that the total percentage of particles broken during crushing increases as the crusher product size is reduced. At present, it appears that particle breakage during crushing will not be excessive for feed that is prepared for full-size burners. Hacksawing through fueled channels will fracture essentially all particles in the path of the blade; however, limited cutting through fueled channels could be advantageous to the overall process costs.

Release of Fission Products from HTGR (Dragon) Fuel During Head-End Processing

Two tests were made to study the release of fission gases during the crush-burn-grind-burn-leach

head-end treatment of irradiated HTGR fuel [pyrolytic carbon-SiC-pyrolytic carbon-coated (U/Th) $C_{2.4}$ bonded in a graphite matrix] from the O.E.C.D. Dragon reactor. The first sample was leached with white fuming nitric acid to disintegrate the graphite prior to the burning test. The recovered particles and the second sample of crushed fuel were burned separately in a fluidized bed in an air-oxygen mixture at 750°C. In each case, the SiC-coated fuel particles were recovered by sieving and ground to -60 mesh in a Waring Blendor. The sieved, ground product was burned in oxygen at 750°C and leached with Thorex reagent (13 M HNO₃-0.1 M Al-0.05 M F⁻). Off-gas releases in each step were monitored by trapping tritium on molecular sieves at room temperature and ⁸⁵Kr on charcoal that had been cooled to the temperature of dry ice. The results are given in Table 3.6.

Only an insignificant amount of rare gases (⁸⁵Kr) was released before the silicon carbide coatings

Table 3.5. Comparison of Two Size Reduction Techniques, Crushing and Hacksawing, as Related to Dragon Fuel Particle Breakage

All samples were leached with 13 M HNO₃-0.1 M Al-0.05 M HF without further grinding

Description of Test	Fraction of Sample Reduced to Fines ^a (%)	Fraction of Loose Broken Particles (%)	Fraction of Other Broken Particles (%)	Total Fraction of Broken Particles (%)
A. Unirradiated Dragon Compacts				
Compact 8232				
Standard crushing procedure (~ $\frac{1}{8}$ -in. jaw)	7.5	2.0 ^b	0.8 ^b	2.8 ^b
Compact 8233				
Standard crushing procedure (~ $\frac{1}{8}$ -in. jaw)	8.9 ^b	~2.5	~1.3	3.8 ^b
Hacksaw (~ $\frac{1}{16}$ -in. blade)	5.8 ^c	5.6	1.4	7.0
Wide open crusher ^d (~ $\frac{5}{8}$ -in. jaw)	0.42	0.03	0.32	0.35
B. Irradiated Dragon Compacts				
Compact 8368				
Standard crushing procedure (~ $\frac{1}{8}$ -in. jaw)	10.6	3.9 ^b	3.7 ^b	7.6 ^b
Compact 8375				
Hacksaw (~ $\frac{1}{16}$ -in. blade)	7.3 ^e	6.7	2.1	8.8

^aTypically -42-mesh material.

^bAverage of two determinations.

^cIncludes 0.7% +42-mesh material (intact particles).

^dFour large segments were obtained (similar to hacksaw sections).

^eIncludes 0.2% +42-mesh material (intact particles).

Table 3.6. Fractions of ⁸⁵Kr and Tritium Released from HTGR Fuel (Dragon) During Head-End Processing Steps

	Fraction Released (%) to Off-Gas During				Fraction Left in Solution (%)	Total Found ^a (mc/g)
	Fluidized-Bed Burning	Grinding	Static-Bed Burning	Leaching		
Test 1						
⁸⁵ Kr	0.55	98.85 ^b	0.42	0.18		1.17
³ H ^c	7.3 ^d	^e	46.6	44.2	1.8	0.026
Test 2						
⁸⁵ Kr	0.02	38.38	61.41 ^b	0.18		0.97
³ H	39.6	0.9	57.5	1.5	0.6	0.044

^aUncorrected for minor handling losses.

^bPreheating in helium included.

^cData are believed to be incomplete (see ref. d below).

^dSolutions from the graphite disintegration step prior to burning were not analyzed for tritium content.

^eThe same molecular sieve was used for both grinding and burning.

were broken. Results of test 2 (Table 3.6) indicate that about 38% of the ^{85}Kr is released in the unheated grinding step (i.e., when the silicon carbide coatings are broken), while about 61% is released when the broken particles are heated and burned. Results of test 1 indicate that almost all of the rare gases are released from the irradiated carbide fuel during grinding, if the broken particles are preheated in a stream of helium.

Tritium was released in a different manner. The particles used in test 1 had been recovered from a graphite matrix disintegration step using white fuming nitric acid. We believe that some tritium, originally present outside the silicon carbide-coated particles, was removed to the first leach liquor (and, therefore, lost to our experiment). Thus the tritium data for test 1 are incomplete. In addition, in test 1, the amount of ^3H released to the off-gas (i.e., $\sim 44\%$) during leaching does not agree with values previously obtained for ^3H during dissolution. (Usually, tritium is retained by the leach liquor and is not released to the dissolver off-gas.) We believe that a heel of tritium was left on the trap from the burning step and was recovered after the leaching step when the trap was reused.

In test 2, we used a clean series of tritium traps and crushed fuel that had not been exposed to dissolvent. About 40% of the tritium was released in the first burning step, indicating that some of the tritium may have passed through the SiC coatings. (It is also possible that this tritium came from a nonfission source, for example, neutron reactions in the external coatings or matrix.) Very little tritium was released when the coatings were ruptured. Most of the remainder of the tritium was released when the broken particles were heated up and burned.

Crush-Burn-Grind-Leach Studies

Two samples of crushed fuel from compact 8232 (unirradiated) and compact 8368 (irradiated) were burned in a fluidized bed of alumina at 750°C . Run conditions are given in Table 3.7. After the burning step, the alumina was separated from the silicon carbide-coated beads by sieving through a 42-mesh screen.

The beads were shattered in a Waring Blendor and leached twice with Thorex reagent to yield a +42-

mesh liquid product and a residue. The alumina fraction was leached twice with Thorex reagent to yield an alumina bed liquid product and a residue (Table 3.8). The heavy metal content of each of the alumina fractions was about the same as that found previously in the crushed fuel burner feed (Table 3.5). Therefore, we conclude that the fluidized-bed burning step did not contribute significantly to the total particle breakage.

Heavy metal losses to the total residues (the main process loss) were about 0.2 and 0.6% for uranium and thorium, respectively, for the irradiated compact. About 10% of the total fission products were retained, principally by the shards (Table 3.9). It should be noted that these results are for a single cycle of the alumina with fuel containing only a small percentage of broken particles. Retention by the alumina may increase under other, less-favorable conditions.

In conclusion, the results of the Dragon fuel tests indicate that the proposed flowsheet for HTGR fuels is promising. Similar tests with irradiated Ft. St. Vrain fuel will be necessary in order to extend these results to the actual fuels. Particle separation and uranium and thorium crossover studies must also be included.

Table 3.7. Operating Ranges for Fluidized-Bed Burning Studies

Conditions: Conical fluidized bed, 0.62 in. to $1\frac{3}{8}$ in. ID by 6 in. long
Cylindrical settling section, $1\frac{3}{8}$ in. ID by 3 in. long; stainless steel

Fuel charge (-4 mesh)	~ 12 g
Al_2O_3 (-80 +100 mesh)	~ 15 g
O_2 flow, ml/min	225 to 450
N_2 flow, ml/min	0 to 1680
Temperature inside fluidized bed, $^\circ\text{C}$	700 to 800
Fluidizing velocity, fps	0.3^a to 3.2
Burning rate, g/min (max)	0.12 to 0.24
Oxygen utilization	15 to 50%

^aNo N_2 flow; bed was probably not fluidized.

Table 3.8. Results of Crush-Burn-Grind-Leach Studies Using Dragon Fuel

Sample	Heavy Metal	Percentage of Heavy Metals Found in				Total Loss of Heavy Metals to Residue
		+42-Mesh Product	+42-Mesh Residue	Alumina Bed Product	Alumina Bed Residue	
8232 (Unirradiated)						
R4	U	99.5	0.01	0.41	0.06	0.07
	Th	99.3	0.08	0.55	0.07	0.15
R8	U	99.3	0.02	0.64	0.006	0.03
	Th	99.2	0.04	0.74	0.02	0.06
8368 (Irradiated)						
R5	U	96.7	0.17	3.08	0.03	0.20
	Th	96.2	0.44	3.22	0.15	0.59
R6	U	96.9	0.14	2.92	^a	>0.14
	Th	95.2	0.51	4.34	^a	>0.51

^aNo heavy metals found in this sample.

Table 3.9. Retention of Fission Products by Solid Residues from the Burn-Grind-Leach Flowsheet

Component	Retention by	
	Shards (av. %)	Alumina (av. %)
Total gamma emitters	10.0	0.35
⁹⁵ Zr	~25.0	0.26
¹⁰⁶ Ru	2.0	0.58
¹³⁴ Cs	10.8	0.18
¹³⁷ Cs	9.9	0.16
¹⁴⁴ Ce	8.8	0.16

4. Waste Treatment and Disposal

The objectives of the waste treatment and development program are to develop a comprehensive waste management system for nuclear wastes, including final disposal of the radioactive residues, and to estimate the cost of this operation. A comprehensive waste management flowsheet, which outlined the development program, was presented previously.¹ The program has been revised to include the newer concepts that are gaining acceptance in the atomic energy community (Fig. 4.1). These concepts include: (1) the eventual transfer

of all radioactive wastes from private atomic installations to a government-owned area for final disposal; (2) the solidification of all wastes within five years of their generation as a preparation for shipment to, and disposal at, a government-owned area; (3) the recognition of only two types of aqueous radioactive wastes: high-level and low-level (intermediate-level wastes are considered to be transitory and would be combined with high- or low-level wastes, depending on the contents of long-lived alpha-, beta-, or gamma-emitting nuclides); and (4) the burial of low-level waste residues below the water table as opposed to surface burial, which is permitted at present in government-owned disposal areas.

¹Chem. Technol. Div. Ann. Progr. Rept. May 31, 1965, ORNL-3830, p. 96.

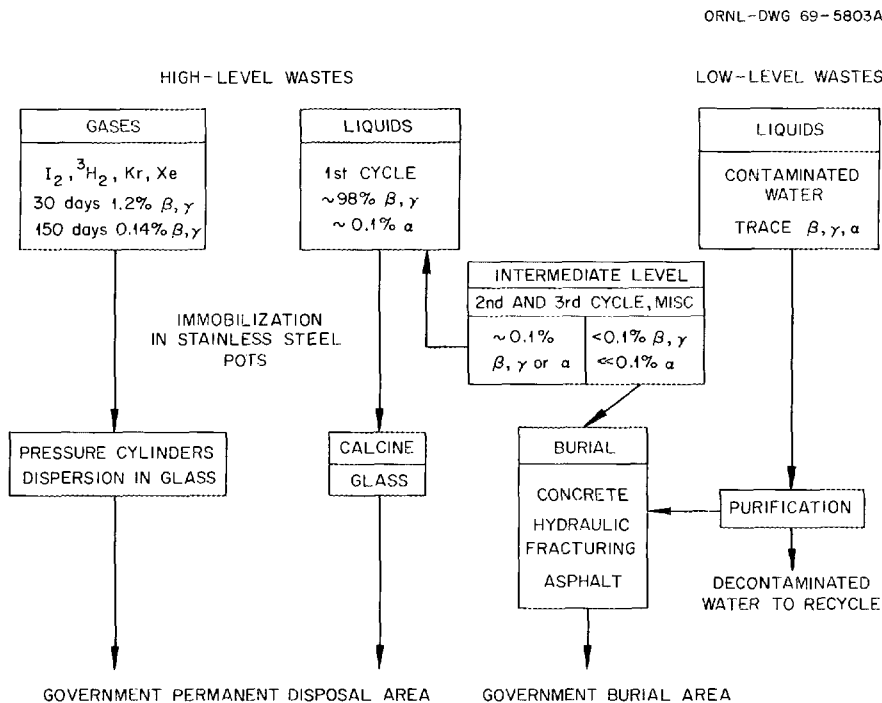


Fig. 4.1. Waste Management Development Program. Distribution of radionuclides is representative of a fuel reprocessing plant.

4.1 ENGINEERING, ECONOMIC, AND SAFETY EVALUATIONS

A systematic review of the wastes that are expected to accumulate from the reprocessing of power-reactor fuels by aqueous methods has been undertaken in order to determine the most economical approaches to their management within the technology that is now available or is presently being developed. A principal assumption of this study is that all wastes arising directly from the reprocessing contain long-lived, biologically hazardous isotopes (e.g., plutonium isotopes, ^{90}Sr , ^{129}I) which must be retained and isolated from man's environment virtually forever. In terms of today's technology, this implies the eventual solidification of these wastes and encapsulation of the residues in high-integrity containers for shipment to a government-owned and -administered repository.

In the initial part of the survey that is reported here, generalized flowsheets are developed for reprocessing spent fuels from a representative type of light-water reactor (LWR), fast breeder reactor (LMFBR), and high-temperature gas-cooled reactor (HTGR). The principal liquid and cladding wastes are characterized in each case. Finally, the characteristics of the solids that could be formed from liquid wastes with little or no extension of current technology are estimated for use in economic and safety analyses that are to be made of available alternatives.

Reactor Design and Operating Characteristics

Three 1000-Mw (electrical) reactors whose design and performance characteristics have been previously defined were chosen as representative types for this study (Table 4.1). The LWR is a pressurized-water type, fueled with Zircaloy-clad UO_2 (3.3% ^{235}U). The reactor operates at an average power level of 34.8 Mw/metric ton and achieves a fuel exposure of 33,000 Mwd/metric ton.

The LMFBR is fueled with stainless-steel-clad UO_2 -15.6% PuO_2 in the core and stainless-steel-clad, slightly enriched UO_2 in the axial and radial blankets. Fuel exposures of 80,000 Mwd/metric ton at a specific power of 175 Mw/metric ton, 2500 Mwd/metric ton at 5.5 Mw/metric ton, and 8100 Mwd/metric ton at 10 Mw/metric ton are achieved in the core, the axial blanket, and the radial blanket

respectively. The projected refueling cycle is once every 153 days when one-third of the core and axial blanket and about three-sixteenths of the radial blanket are discharged. In this study, we assume that the core and blankets will be mixed proportionately ("homogenized") prior to processing, yielding a fuel mixture having an average burnup of 33,000 Mwd/metric ton at a specific power of 58 Mw/metric ton.

The HTGR fuel consists of coated microspheres held in vertical holes in graphite blocks by means of a carbonized resin binder. Three types of particles are used: ThC_2 fertile particles, $^{235}\text{UC}_2$ fuel particles, and ThO_2 - $^{233}\text{UO}_2$ recycle particles. All of these particles are triplex-coated, with a buffer coating and an outer coating of pyrolytic carbon and an intermediate coating of SiC. A full core loading consists of 3560 hexagonally shaped graphite fuel blocks, each about 31 in. long and 14 in. across the flats. An average fuel exposure of 84,000 Mwd/metric ton at a power level of 52 Mw/metric ton is achieved.

Process Flowsheets and Waste Compositions

Wherever possible, reprocessing flowsheets that avoided the addition of chemicals which might be particularly troublesome in subsequent waste management operations were developed. Specifically, to prevent the accumulation of sodium and sulfate ions in the waste streams, nitrogen oxide, U(IV)-hydrazine, and $\text{Fe}(\text{NO}_3)_2$ -hydrazine are used in lieu of NaNO_2 and ferrous sulfamate for plutonium valence adjustments. Product losses are taken as 0.1% (based on NFS experience) and 0.03% (based on ORNL hot-cell experience)² of the Pu in the LWR and LMFBR fuel claddings respectively; 0.1% of the Pu and U in the aqueous raffinate; and 0.01% of the Pu and U in the solvent during stripping (which ultimately appears in the solvent regenerate solution). The spent solvent is regenerated with 0.1 volume of 0.3 M Na_2CO_3 solution per volume of solvent in the case of TBP, and 0.1 volume of 1.0 M Na_2CO_3 solution per volume of solvent in the case of the amine.

LWR Fuels. — In the processing of LWR fuels (Fig. 4.2), a chop-leach head-end method is used, followed by a standard Purex solvent extraction procedure for separating the uranium and plutonium

²J. H. Goode, ORNL, personal communication, January 8, 1969.

Table 4.1. Summary of Reactor Design and Performance Characteristics

	LWR ^a	LMFBR ^b	HTGR ^c
Fuel form	Oxide pellets	Oxide pellets	Oxide, carbide microspheres
Power, Mw (thermal)	3083	2500	2457
Thermal efficiency, %	35.4	40	40.7
Core			
Avg. sp. power, Mw/metric ton	34.8	175	52
Burnup, Mwd/metric ton	33,000	80,000	84,000
Charge, metric tons	88.6 (U)	12.6 (U + Pu)	36 (Th + U)
Enrichment, %	3.3 (²³⁵ U)	15.6 (²³⁹ Pu)	~7 (²³³ U + ²³⁵ U)
Refueling interval, full-power days	~365	153 ^d	~365
Refueling fraction	$\frac{1}{3}$	$\frac{1}{3}$ ^d	$\frac{1}{4}$
Fuel element	Square	hex ^d	} hex graphite block, 31 in. } long by 14 in. across flats
Rods/element	204	217 ^d	
Elements/reactor	193	252 ^d	3560
Rod length, with plenum, in.	148	144 ^d	31
Clad material	Zircaloy-4 (Inconel spacers)	304 SS ^d	SiC, C
Clad outside diam, in.	0.422	0.25 ^d	0.026, 0.017
Clad wall thickness, in.	0.0243	0.015 ^d	0.005, 0.007
Axial blanket			
Avg. sp. power, Mw/metric ton		5.5	
Burnup, Mwd/metric ton		2500	
Charge, metric tons		7.32 (U)	
Enrichment, %		0.3 (²³⁵ U)	
Radial blanket			
Avg. sp. power, Mw/metric ton		10	
Burnup, Mwd/metric ton		8100	
Charge, metric tons		26.7 (U)	
Enrichment, %		1.96 (²³⁵ U)	
Refueling interval, full-power days		153	
Refueling fraction		$\sim \frac{3}{16}$	
Fuel element		hex	
Rods/element		169, 91	
Elements/reactor		39, 87	
Rod length, with plenum, in.		84, 72	
Clad material		304 SS	
Clad outside diam, in.		0.35, 0.51	
Clad wall thickness, in.		0.015	

^aJackson & Moreland and S. M. Stoller Associates, *Current Status and Future Technical and Economic Potential of Light Water Reactors*, WASH-1082 (March 1968).

^bK. Buttrey *et al.*, *Liquid Metal Fast Breeder Reactor Task Force Fuel Cycle Study*, NAA-SR-MEMO-12604 (January 1968).

^cJ. J. Shefcik and R. E. Norman, Gulf General Atomic, Inc., communication to R. S. Lowrie, ORNL, November 1968.

^dAlso applicable to the axial blanket which is an integral unit with the core assembly.

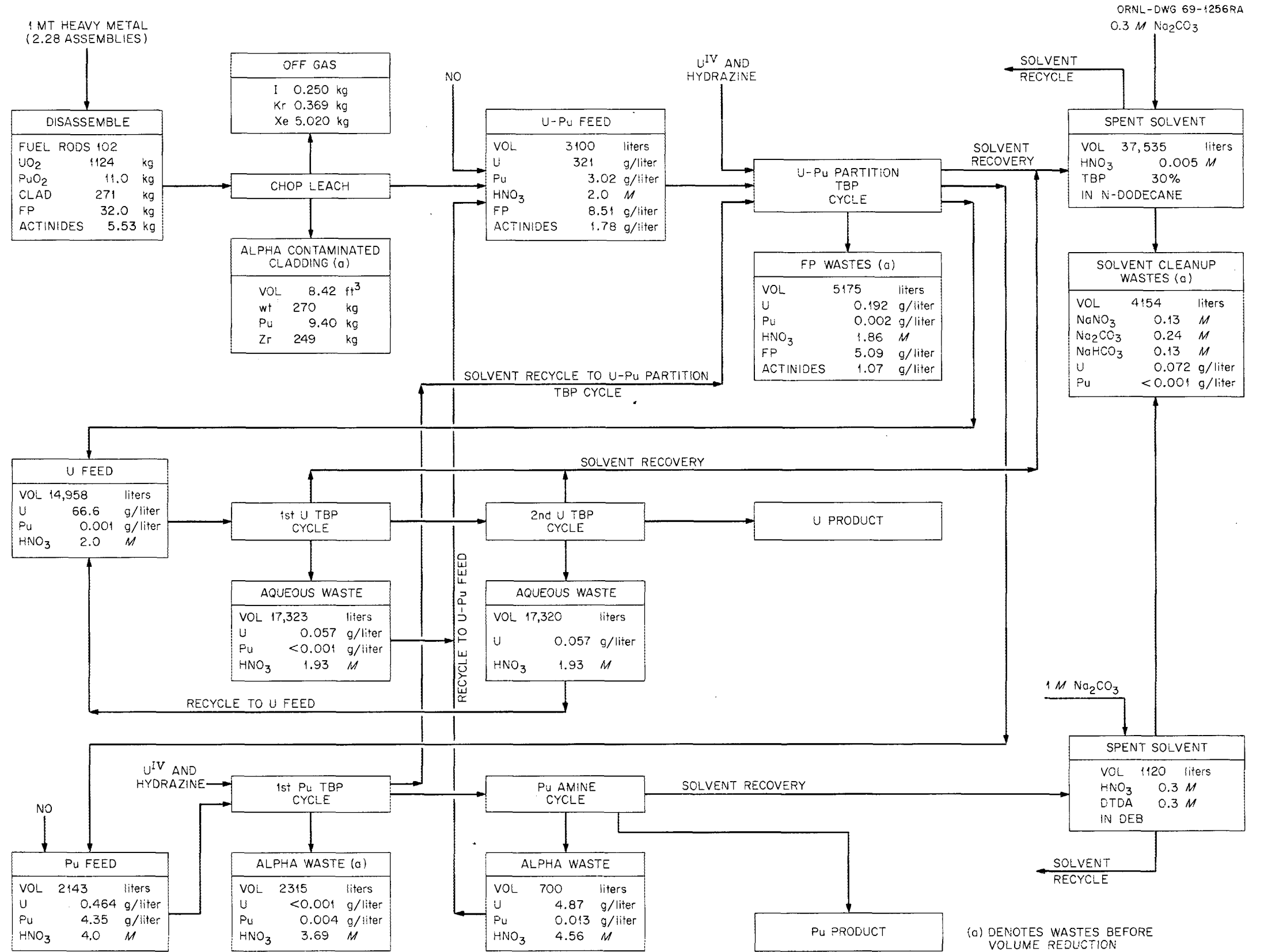


Fig. 4.2. Wastes Generated in Reprocessing of LWR Fuel. Fuel exposure, 33,000 Mwd/metric ton at a specific power of 30 Mw/metric ton.

and subsequently purifying the uranium, followed by an amine extraction for the final purification of plutonium.

Compositions, after concentration, of the four liquid wastes from LWR fuel reprocessing are given in Table 4.2. The iron, nickel, and chromium in the concentrated fission product and alpha-active wastes are present as corrosion products. The caustic scrubber waste volumes and concentrations are based on the loss of 1% of the HNO_3 that was charged to the dissolver.

LMFBR Fuels. — The flowsheet for processing LMFBR mixed core and blanket fuel is based on developmental work still in progress (see Sect. 2); hence, a number of alternatives are considered (Fig. 4.3). Following a mechanical disassembly of the fuel element and separation of hardware that has only induced activity associated with it, the fuel tubes are sheared and heated to about 700°C in an oxygen atmosphere for removal of volatile

fission products. The oxide fuel is then leached from the stainless steel cladding with HNO_3 . Laboratory tests have shown that probably about 1%, but occasionally as much as 10%, of the cladding will dissolve during leaching (Sect. 2.2). Accordingly, concentrations of stainless steel in the solvent extraction feed corresponding to these two percentages are considered. Primary and alternative dissolution and solvent extraction flowsheets are given. Both utilize a TBP partitioning cycle, and TBP and amine purification cycles for plutonium, but in neither case is the uranium purified to an extent necessary for fuel recycle. The primary flowsheet relies on concentration and geometry for criticality control and on ferrous ion for reduction of the plutonium in the TBP cycles. The alternative flowsheet, assuming about 300 g of uranium and plutonium in the feed, uses boron as a soluble poison for criticality control and U(IV) plus hydrazine for reduction of the plutonium. The com-

Table 4.2. Compositions of LWR Aqueous Processing Wastes

Component	Concentrations ^a (g/liter)			
	(1) Fission Product Waste	(2) Alpha-Active Waste	(3) Solvent Cleanup Waste	(4) Caustic Scrubber Waste ^b
U^{6+}	0.80	0.018	0.26	
Pu^{6+}	0.008	0.16	0.001	
H^+	0.95	1.01		
Na^+			66.2	345
Fe^{3+}	0.6	0.2		
Ni^{2+}	0.08	0.02		
Cr^{3+}	0.08	0.02		
Fission products ^c	21.1	Trace	Trace	Trace
Actinides	4.43	Trace	Trace	Trace
CO_3^{2-}			56.7	
HCO_3^-			30.1	
NO_3^-	98.0	62.9	30.6	930
PO_4^{3-}	0.1		Trace	

^aConcentrations are based on volumes, in gal/metric ton, of 330 for (1), 15 for (2), 280 for (3), and 3 for (4).

^bBased on 1% HNO_3 loss from process.

^cBased on a fuel exposure of 33,000 Mwd/metric ton.

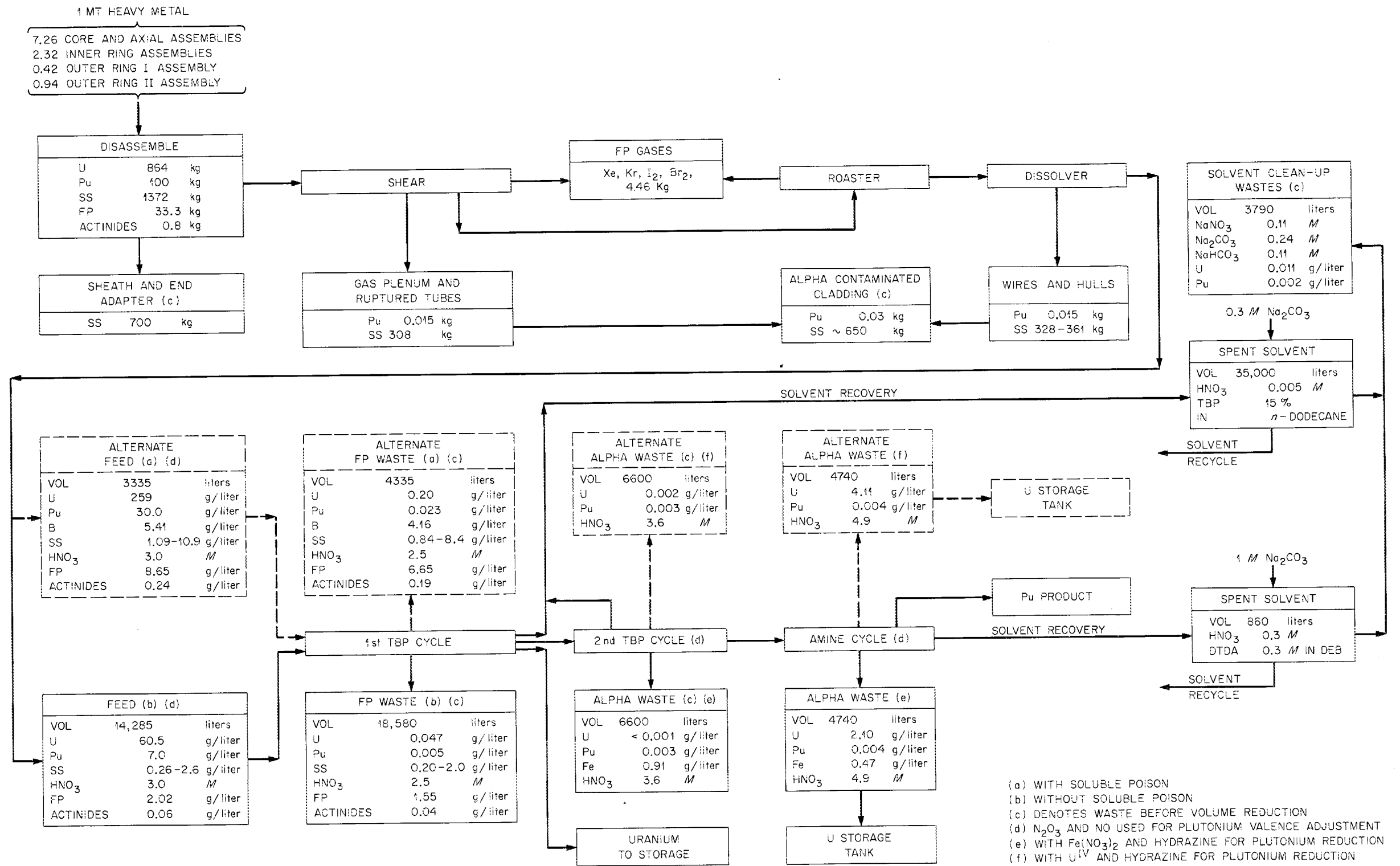


Fig. 4.3. Wastes Generated in Reprocessing of Homogenized LMFBR Fuel Assemblies. Fuel exposure, 33,000 Mwd/metric ton at a specific power of 58 Mw/metric ton.

Table 4.3. Compositions of LMFBR Aqueous Processing Wastes
(Mixed Core and Blankets)

Component	Concentrations ^a (g/liter)							
	Fission Product Wastes				Alpha-Active Wastes		(7) Solvent Cleanup Wastes	(8) Caustic Scrubber Wastes ^b
	Without Boron		With Boron		(5) With Fe(NO ₃) ₂ Reductant	(6) With U ⁴⁺ Reductant		
	(1) 1% Cladding Dissolved	(2) 10% Cladding Dissolved	(3) 1% Cladding Dissolved	(4) 10% Cladding Dissolved				
Fe ³⁺	2.10	21.0	2.10	21.0	105			
Cr ³⁺	0.55	5.54	0.55	5.54				
Ni ²⁺	0.26	2.6	0.26	2.62				
U ⁶⁺	0.69	0.69	0.69	0.69		0.23	0.04	
Pu ⁶⁺	0.08	0.08	0.08	0.08	0.35	0.35	0.005	
H ⁺	1.01	1.01	1.01	1.01	1.01	1.01		
Na ⁺							58.2	345
H ₃ BO ₃			82.5	82.5				
CO ₃ ²⁻							51.4	
NO ₃ ⁻	109	195	109	195	413	62.3	25.3	930
HCO ₃ ⁻							24.9	
Fission products ^c	23.1	23.1	23.1	23.1	Trace	Trace	Trace	Trace
Actinides ^c	0.64	0.64	0.64	0.64	Trace	Trace	Trace	Trace

^aConcentrations are based on volumes, in gal/metric ton, of 330 for fission product wastes [(1), (2), (3), (4)], 15 for alpha-active wastes [(5), (6)], 280 for (7), and 3 for (8).

^bBased on 1% HNO₃ loss from process.

^cBased on an average exposure of 33,000 Mwd/metric ton.

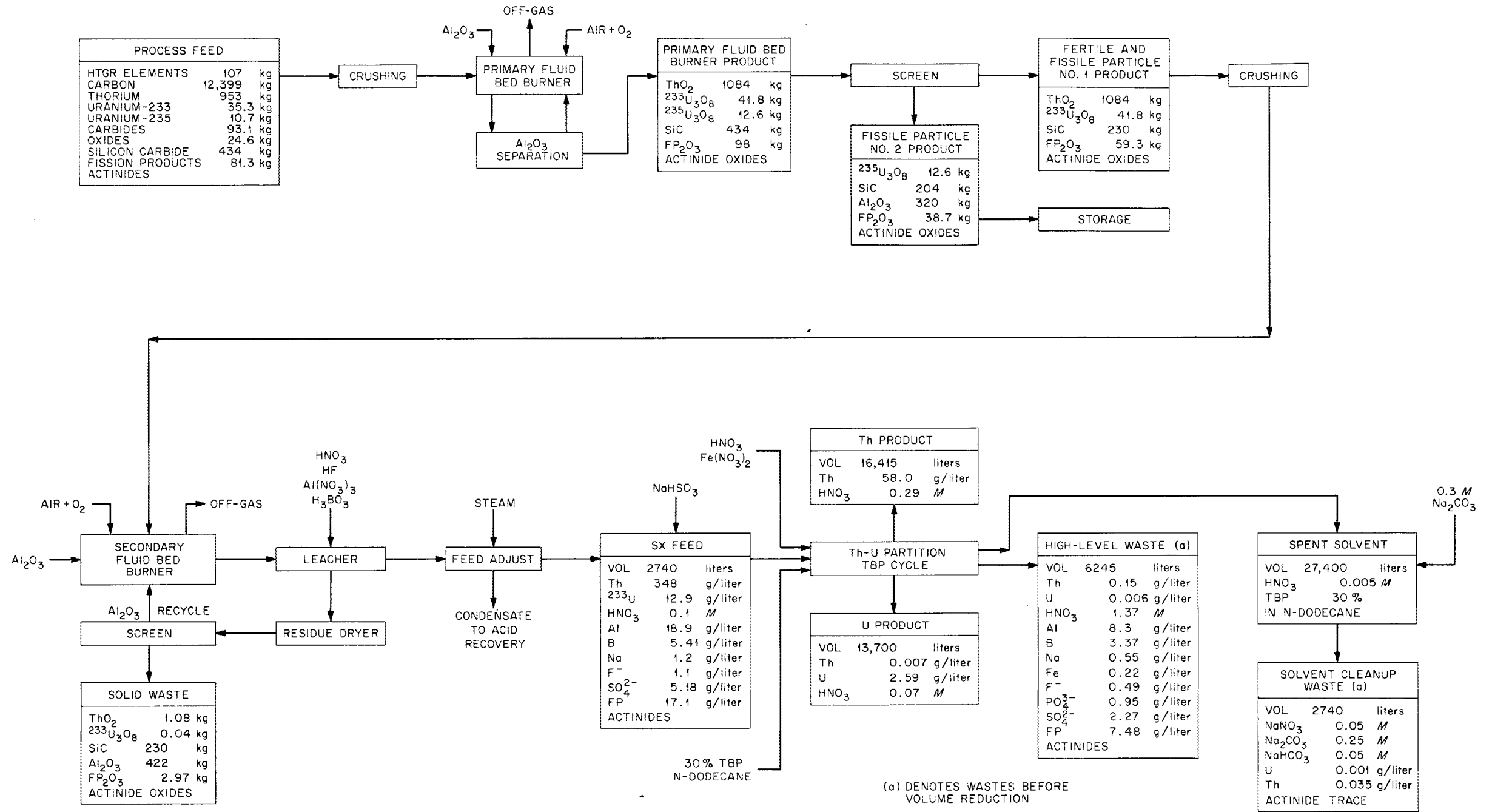


Fig. 4.4. Wastes Generated in Reprocessing of HTGR Fuel. Fuel exposure of 84,000 Mwd/metric ton at a specific power of 52 Mw/metric ton.

Table 4.4. Compositions of HTGR Processing Wastes

Component	Concentrations ^a (g/liter)		
	(1) Fission Product Waste	(2) Solvent Cleanup Waste	(3) Caustic Scrubber Waste ^b
U ⁶⁺	0.020	0.006	Trace
Th ⁴⁺	0.523	0.167	Trace
H ⁺	1.01		
Al ³⁺	28.5		
Na ⁺	1.81	66.9	327
Fe ³⁺	0.76		
Fission products	25.7	Trace	Trace
Actinides	c	Trace	Trace
NO ₃ ⁻	286	15.0	882
F ⁻	1.66		
SO ₄ ²⁻	7.81		
PO ₄ ³⁻	3.27	Trace	
CO ₃ ²⁻		145.4	
HCO ₃ ⁻		14.8	
H ₃ BO ₃	46.6		

^aConcentrations based on volumes, in gal/metric ton, of 480 for (1), 150 for (2), and 10 for (3).

^bBased on 1% HNO₃ loss from process.

^cActinide concentration not estimated to date.

positions of the concentrated wastes, taking into consideration the flowsheet alternatives shown in Fig. 4.3, are given in Table 4.3.

HTGR Fuels. — The flowsheet for processing HTGR fuels (Fig. 4.4) is based on methods being developed at ORNL³⁻⁵ and Gulf General Atomic.⁶ The fuel block is crushed prior to burning the graphite in a fluidized bed of Al₂O₃, and the residual fertile and fissile particles are separated

from the Al₂O₃ by screening. The ²³⁵U fuel particles are also separated from the fertile and recycle particles by screening, and are not processed further. A roll grinder is used to crush the silicon carbide coating of the fertile and recycle particles, the residual carbon is burned off in a secondary fluidized bed of Al₂O₃, and the residue is leached with a mixture of nitric, hydrofluoric, and boric acids. Finally, the thorium and uranium are separated from fission products and from each other by the Thorex solvent-extraction process.

Compositions of the three principal liquid wastes from this process are given in Table 4.4. The fission product waste and the ²³⁵U fuel particles contain about 57 and 40%, respectively, of the fission products present in the spent fuel. The final 3% is found in the solid waste from the secondary fluidized-bed burner and leacher (Fig. 4.4).

³R. S. Lowrie, ORNL, personal communication, January 3, 1969.

⁴Chem. Technol. Div. Ann. Progr. Rept. May 31, 1968, ORNL-4272, pp. 56-67.

⁵V. C. A. Vaughen, J. R. Flanary, J. H. Goode, and H. O. G. Witte, *Hot-Cell Evaluation of the Burn-Leach Method for Processing Irradiated Graphite-Base HTGR Fuels*, ORNL-4120 (in press).

⁶J. J. Shefcik, *Central Reprocessing Plant for HTGR Fuels*, GAMD-8382 (Oct. 16, 1967).

Characteristics of Solid Wastes. – Estimated characteristics of the residues obtained from evaporation and heating aqueous wastes to 900°C are given in Tables 4.5–4.7. In addition to the solids obtained from solidifying the individual waste streams derived from the flowsheets, solidification of several combinations of these streams is considered. For convenience, the solid waste components are generally expressed as oxides; however, in a few instances some elements are expressed as tetraborates, sulfates, and fluorides. To estimate certain characteristics of the final solids, it was sometimes necessary to add components to prevent volatilization, at temperatures up to 900°C, of certain species present in the wastes. Most importantly, sodium and boron were retained by the addition of either NaOH or B₂O₃ in the proper proportion to form thermally stable sodium tetraborate. The sodium tetraborate melts at about 740°C, resulting in either a dispersion of the waste oxides in a continuous phase (50 to 70 vol %) of sodium tetraborate, or, as in the case of the solvent cleanup and caustic scrubber wastes, in an essentially single-phase melt of sodium tetraborate. Densities were calculated from the known theoretical densities of the pure components, assuming that specific volumes are additive on a weight-fraction basis. Effective thermal conductivities, k_e , were calculated using a quasi-theoretical equation of the form,

$$k_e = Ak_c / (1 - V_d^{1/3}),$$

where A is a constant obtained empirically, k_c is the conductivity of the continuous phase, and V_d is the volume-fraction of the dispersed phase. For the calcines in this study, A is taken to be 1.0; for the melts or dispersions, A is taken to be 0.85. For the calcines, k_c is assumed to be that of air at 500°C, or 0.034 Btu hr⁻¹ ft⁻¹ °F⁻¹; for the dispersions, it is assumed to be that of glassy sodium tetraborate at 500°C, or 0.55 Btu hr⁻¹ ft⁻¹ °F⁻¹.

The weights and volumes of cladding wastes from LWR and LMFBR fuels, given in Tables 4.5 and 4.6, were calculated from fuel element specifications, assuming that cladding and associated hardware is compacted, on the average, to 70% of theoretical density. The calculated neutron-induced and plutonium activities associated with these materials as a function of decay time are given in Table 4.8, assuming plutonium losses to the clad-

ding of 0.1% and 0.03% for LWR and LMFBR fuels respectively. In the Zircaloy-4 cladding from LWR fuel, the ⁹⁵Zr-Nb activity predominates for about the first half-year following discharge from the reactor; however, rather substantial contributions from ⁶⁰Co, ⁵⁵Fe, and ⁶³Ni prevail thereafter. The latter nuclides are derived from the Inconel (~22 kg) that is used for spacers in the fuel elements. The type 304 stainless steel cladding from LMFBR fuel has more radioactivity, but fewer curies of plutonium, associated with it for the first ten years after discharge than does the Zircaloy-4. In estimations of the induced activity in LMFBR cladding, only the part of the cladding that is in actual contact with the oxide fuel was considered; the activity induced in the remaining cladding and hardware should not contribute more than an additional few percent.

Minimum Ages for Encapsulation

Although wastes can be stored safely in the form of liquids for limited periods of time in properly designed systems, the risks associated with liquid storage are greater than those associated with storage as solids in less elaborate, but comparably contained, systems. There is, therefore, an incentive from the standpoints of safety and economics during storage to solidify wastes at the earliest practical time following their generation. Estimates of the minimum ages for encapsulation of the solidified wastes characterized in Tables 4.5–4.7 in long, cylindrical containers (6, 12, and 24 in. in diameter) are given in Table 4.9. Only those wastes, or combinations of wastes, that have significant power densities associated with them are considered. (The case numbers in Table 4.9 correspond to those given to the respective wastes in the previous tables.) The minimum ages were calculated, using 900°C as the maximum allowable center-line temperature of the wastes, for a container standing in air. The isotopic power levels, assuming that each reactor operates with an 85% load factor, are given in Fig. 4.5. The temperature drop between the center line and the wall of the container was calculated from

$$T_c - T_w = \frac{QR^2}{4k_e},$$

Table 4.5. Characteristics of LWR Solidified Aqueous Processing Wastes

Characteristic	(1) Fission Product Waste	(2) Alpha-Active Waste	(3) Solvent Cleanup Waste	(4) Caustic Scrubber Waste	(5) Cladding	Combinations		
						(6)	(7)	(8)
						1 + 2 + 3	1 + 2 + 4	1 + 2 + 3 + 4
Composition, kg/metric ton								
U ₃ O ₈	1.17	0.001	0.317			1.49	1.17	1.49
PuO ₂	0.011	0.011	0.001		0.01 ^a	0.023	0.022	0.023
Na ₂ B ₄ O ₇			307	17.1		307	17.1	324
Fe ₂ O ₃	1.07	0.016				1.09	1.09	1.09
Cr ₂ O ₃	0.15	0.002				0.15	0.15	0.15
NiO	0.13	0.001				0.13	0.13	0.13
P ₂ O ₅	0.09		Trace			0.09	0.09	0.09
FP oxides	31.5	Trace	Trace			31.5	31.5	31.5
Actinide oxides	6.28	Trace	Trace			6.28	6.28	6.28
Zircaloy-4, Inconel					270			
Weight, kg/metric ton	40.4	0.031	307	17.1	270	348	57.5	365
Volume, ft ³ /metric ton	0.74 ^b	0.001 ^b	4.58 ^c	0.26 ^c	2.12 ^d	4.80 ^c	0.48 ^c	5.06 ^c
k _e , Btu hr ⁻¹ ft ⁻¹ °F ⁻¹ at 500°C	0.26	0.26	0.55	0.55	3.6 ^e	0.74	2.05	0.72
Density, g/ml	1.92 ^b	2.07 ^b	2.37 ^c	2.37 ^c	4.5 ^d	2.56 ^c	4.21 ^c	2.55 ^c

^aAssumes 0.1% Pu loss to cladding.

^bProduct assumed to be 70% voids.

^cProduct assumed to be void-free.

^dCladding compressed to 70% of theoretical density.

^eConductivity at 100°C.

Table 4.6. Characteristics of LMFBR Solidified Aqueous Processing Wastes

Characteristic	Fission Product Wastes				Alpha-Active Wastes		(7) Solvent Cleanup Wastes	(8) Caustic Scrubber Wastes	Cladding		Combinations			
	Without Boron		With Boron		(5) With Fe(NO ₃) ₃ /2 Reductant	(6) With U ⁴⁺ Reductant			(9) Alpha-Contaminated	(10) Induced Activity Only	(11) 1 + 5 + 7 + 8	(12) 2 + 5 + 7 + 8	(13) 3 + 5 + 7 + 8	(14) 4 + 5 + 7 + 8
	(1) 1% Cladding Dissolved	(2) 10% Cladding Dissolved	(3) 1% Cladding Dissolved	(4) 10% Cladding Dissolved										
Composition, kg/metric ton														
Fe ₂ O ₃	3.75	37.5	3.75	37.5	8.52						12.27	46.02	12.27	46.02
Cr ₂ O ₃	1.01	10.1	1.01	10.1							1.01	10.1	1.01	10.1
NiO	0.42	4.17	0.42	4.17							0.42	4.17	0.42	4.17
PuO ₂	0.11	0.11	0.11	0.11	0.02	0.02	0.01		0.03 ^a		0.14	0.14	0.14	0.14
U ₃ O ₈	1.02	1.02	1.02	1.02		0.02	0.05				1.07	1.07	1.07	1.07
Na ₂ B ₄ O ₇			86.5	86.5			270	17.1			287	287	287	287
FP oxides	34.2	34.2	34.2	34.2	Trace	Trace	Trace	Trace			34.2	34.2	34.2	34.2
Actinide oxides	0.91	0.91	0.91	0.91	Trace	Trace	Trace	Trace			0.91	0.91	0.91	0.91
Stainless steel									650	700				
Weight, kg/metric ton	41.4	88.0	128	175	8.54	0.04	270	17.1	650	700	337	384	337	384
Volume, ft ³ /metric ton	0.81 ^b	1.84 ^b	1.53 ^c	1.84 ^c	0.19 ^b	0.0003 ^b	4.03 ^c	0.255 ^c	4.17 ^d	4.50 ^d	4.58 ^c	4.89 ^c	4.58 ^c	4.89 ^c
k _e , Btu hr ⁻¹ ft ⁻¹ °F at 500°C	0.26	0.26	1.02	1.41	0.26	0.26	0.55	0.55	9.0 ^e	9.0 ^e	0.78	0.94	0.78	0.94
Density, g/ml	1.81 ^b	1.69 ^b	2.95 ^c	3.35 ^c	1.56 ^b	2.90 ^b	2.37 ^c	2.37 ^c	5.50 ^d	5.50 ^d	2.60 ^c	2.77 ^c	2.60 ^c	2.77 ^c

^aAssumes 0.03% Pu loss to cladding.

^bProduct assumed to be 70% voids.

^cProduct assumed to be void-free.

^dCladding compressed to 70% of theoretical density.

^eConductivity at 100°C.

Table 4.7. Characteristics of HTGR Solidified Processing Wastes

Characteristic	(1) Fission Product Waste	(2) Solvent Cleanup Waste	(3) Caustic Scrubber Waste	(4) Fluidized-Bed Burner Waste	Combinations	
					(5) 1 + 2 + 3	(6) 1 + 2 + 3 + 4
Composition, kg/metric ton						
U ₃ O ₈	0.042	0.004		0.042	0.046	0.088
ThO ₂	1.08	0.108		1.08	1.19	2.27
Al ₂ O ₃	86.9			422	86.9	509
Al ₂ (SO ₄) ₃	16.9				16.9	16.9
AlPO ₄	7.62				7.62	7.62
Fe ₂ O ₃	1.97				1.97	1.97
Na ₂ B ₄ O ₇ ^a	100	166	54.1		235 ^b	524 ^c
AlF ₃	4.44				4.44	4.44
FP oxides	56.4			2.97	56.4	59.4
Actinide oxides	<i>d</i>	Trace	Trace	<i>d</i>	Trace	Trace
SiC				230		230
Weight, kg/metric ton	276	166	54.1	656	410	1355
Volume, ft ³ /metric ton	2.99 ^e	2.48 ^e	0.81 ^e	21.1 ^b	5.00 ^e	15.6 ^e
k _e , Btu hr ⁻¹ ft ⁻¹ °F ⁻¹ at 500°C	2.27	0.55	0.55	0.26	1.41	2.27
Density, g/ml	3.26 ^e	2.37 ^e	2.37 ^e	1.10 ^f	2.90 ^e	3.06 ^e

^a12.5 kg of sodium per metric ton added to balance boron; an additional 31.2 kg of Na₂B₄O₇ per metric ton added to give 50% dispersion.

^b35.7 kg of boron per metric ton added to balance sodium.

^c35.7 kg of boron per metric ton added to balance sodium; an additional 289 kg of Na₂B₄O₇ per metric ton added to give 50% dispersion.

^dActinides not estimated to date.

^eAssumed to be void-free.

^fAssumed to be 70% voids.

Table 4.8. Activation of the Cladding from One Metric Ton of Heavy Metal Charged to the Reactor

Element or Nuclide	LWR ^a (Zircaloy-4)					LMFBR Mixed Core and Blankets ^b (Type 304 Stainless Steel)				
	Kilograms Charged	Curies Remaining After				Kilograms Charged	Curies Remaining After			
		150 Days Decay	1 Year Decay	3 Years Decay	10 Years Decay		30 Days Decay	1 Year Decay	3 Years Decay	10 Years Decay
C	0.02					0.18				
Nd	0					1.74				
Al	0.01					0				
Si	0.02					1.63				
P	0					0.09				
14.3-d P-32	0					0	198			
S	0					0.07				
Ti	0.02					0				
Cr	3.66					37.7				
27.8-d Cr-51	0	827	4			0	5,170	1.2		
Mn	0.02					4.36				
312-d Mn-54	0	204	125	23		0	66,000	30,900	5,810	17
Fe	3.74					155				
2.4-y Fe-55	0	2,030	1,730	1,020	157	0	45,300	35,500	20,800	3,220
45-d Fe-59	0	23				0	2,310	13		
Co	0.05					0.22				
71-d Co-58	0	2,250	278			0	136,000	5,250	4	
5.24-y Co-60	0	5,610	5,190	3,990	1,590	0	929	823	632	251
Ni	9.56					17.5				
80,000-y Ni-59	0	4.3	4.3	4.3	4.3	0	2.6	2.6	2.6	2.6
92-y Ni-63	0	632	629	619	588	0	411	408	402	382
Zr	249					0				
65-d Zr-95	0	5,360	541			0				
Nb	0.95					0				

Table 4.8 (continued)

Element or Nuclide		LWR ^a (Zircaloy-4)				LMFBR Mixed Core and Blankets ^b (Type 304 Stainless Steel)					
		Kilograms Charged	Curies Remaining After				Kilograms Charged	Curies Remaining After			
			150 Days Decay	1 Year Decay	3 Years Decay	10 Years Decay		30 Days Decay	1 Year Decay	3 Years Decay	10 Years Decay
35-d	Nb-95	0	9,800	1,130		0					
	Mo	0.56				0					
	Sn	3.76				0					
250-d	Sn-119m	0	20	11	1	0					
2.0-y	Sb-125	0	38	33	20	3					
89-y	Pu-238 ^c	0	1.9	2.0	2.0	1.9	0	3.4	3.4	3.4	3.2
24,360-y	Pu-239 ^c	0	0.3	0.3	0.3	0.3	0	0.11	0.11	0.11	0.11
6,760-y	Pu-240 ^c	0	0.5	0.5	0.5	0.5	0	0.13	0.13	0.13	0.13
13-y	Pu-241 ^c	0	125	121	109	75	0	18.0	17.1	15.4	10.6
Total		271	26,900	9,800	5,790	2,420	219	257,000	72,900	27,700	3,890

^aAverage exposure, 33,000 Mwd/metric ton at 30 Mw/metric ton (see Table 4.1).

^bAverage exposure, 33,000 Mwd/metric ton at 58 Mw/metric ton for mixed core and blankets (see Table 4.1).

^cAssumes Pu losses to cladding of 0.1% and 0.03% for LWR and LMFBR fuels, respectively.

Table 4.9. Minimum Ages for Encapsulation of Selected Solidified LWR, LMFBR, and HTGR Wastes^a

LWR						LMFBR						HTGR									
Case	Solids Volume, ft ³ /metric ton	Conductivity, Btu hr ⁻¹ ft ⁻¹ °F ⁻¹	Container Diameter, in.	Minimum Age, ^b Years	Power Density at Minimum Age, Btu hr ⁻¹ ft ⁻³	Case	Solids Volume, ft ³ /metric ton	Conductivity, Btu hr ⁻¹ ft ⁻¹ °F ⁻¹	Container Diameter, in.	Minimum Age, ^b Years	Power Density at Minimum Age, Btu hr ⁻¹ ft ⁻³	Case	Solids Volume, ft ³ /metric ton	Conductivity, Btu hr ⁻¹ ft ⁻¹ °F ⁻¹	Container Diameter, in.	Minimum Age, Years	Power Density at Minimum Age, Btu hr ⁻¹ ft ⁻³				
1	0.74	0.26	6	2.3	18,000	1	0.81	0.26	6	2.7	18,000	1	2.99	2.27	6	<0.25	54,200				
			12	8.8	5,060				12	5.5	5,060				12	0.36	19,200				
			24	50	1,380				24	46	1,380				24	1.25	6,400				
6	4.8	0.74	6	<0.25	34,700	2	1.84	0.26	6	1.4	18,000	4	21.1	0.26	6	<0.25	18,000				
			12	0.51	10,800				12	3.0	5,060				12	<0.25	5,060				
			24	2.0	3,200				24	13.1	1,380				24	<0.25	1,380				
7	0.48	2.05	6	1.2	52,600	3	1.53	1.02	6	0.76	40,600	5	5.0	1.41	6	<0.25	46,400				
			12	3.3	18,400				12	2.0	13,100				12	<0.25	15,600				
			24	14.3	6,080				24	3.6	4,000				24	0.62	4,920				
8	5.06	0.72	6	<0.25	34,300	4	1.84	1.41	6	0.53	46,400	6	15.6	2.27	6	<0.25	54,200				
			12	0.49	10,600				12	1.5	15,600				12	<0.25	19,200				
			24	2.0	3,130				24	3.0	4,920				24	<0.25	6,400				
						11	4.58	0.78	6	0.21	35,700										
									12	0.93	11,200								12	0.93	11,200
									24	2.6	3,320								24	2.6	3,320
						12	4.89	0.94	6	0.16	39,100										
									12	0.77	12,500								12	0.77	12,500
									24	2.2	3,780								24	2.2	3,780
						13	4.58	0.78	6	0.21	35,700										
									12	0.93	11,200								12	0.93	11,200
									24	2.6	3,320								24	2.6	3,320
						14	4.89	0.94	6	0.16	39,100										
									12	0.77	12,500								12	0.77	12,500
									24	2.2	3,780								24	2.2	3,780

^aBased on a maximum permissible center-line temperature of 900°C when pot is standing in air.

^bAge corresponds to time since discharge of fuel from reactor.

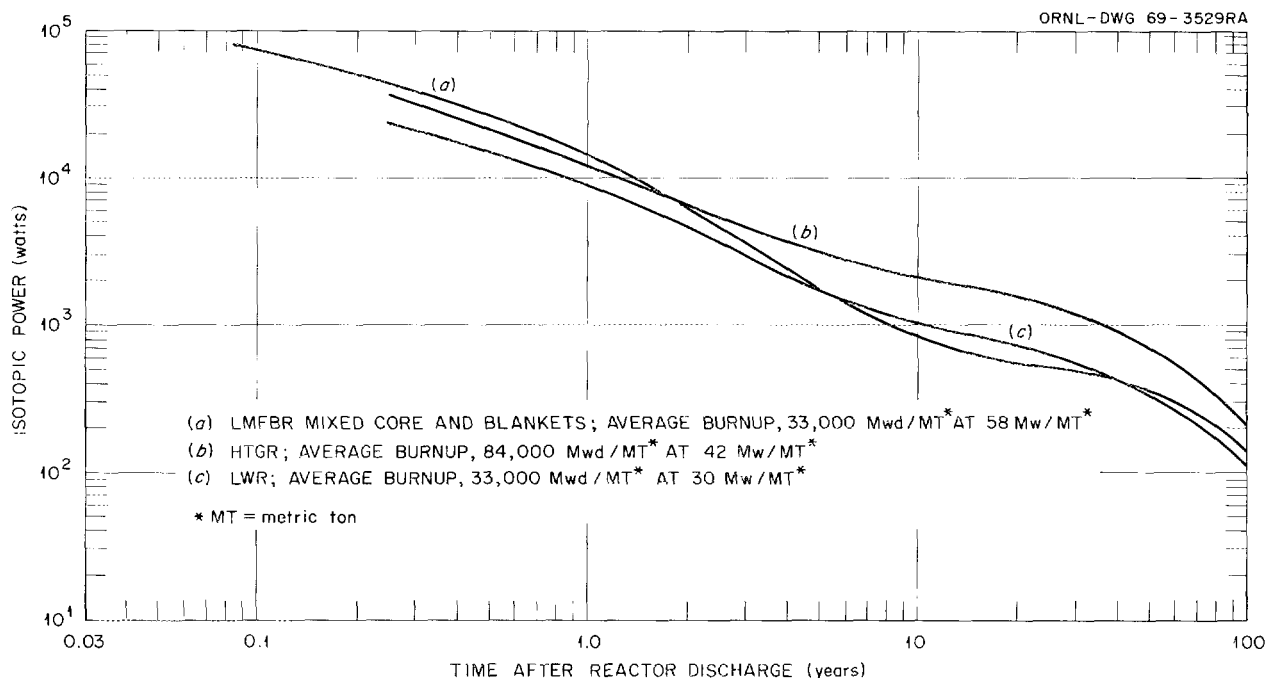


Fig. 4.5. Isotopic Power in the Waste from Processing One Metric Ton of Fuel as a Function of Time After Discharge from the Reactor.

and the overall coefficient of heat transfer between the wall and surroundings was estimated from

$$h = 0.66 \left(\frac{T_w - T_a}{R} \right)^{0.25}$$

In this equation, T_c , T_w , and T_a are the center-line, wall, and ambient temperatures ($^{\circ}\text{F}$); Q is the thermal power density of the waste ($\text{Btu hr}^{-1} \text{ft}^{-3}$); R is the container radius (ft); k_e is the effective thermal conductivity of the wastes ($\text{Btu hr}^{-1} \text{ft}^{-1} \text{ }^{\circ}\text{F}^{-1}$); and h is the overall heat-transfer coefficient to the surroundings ($\text{Btu hr}^{-1} \text{ft}^{-2} \text{ }^{\circ}\text{F}^{-1}$). The constants in the heat-transfer coefficient equation were determined from experimental measurements of containers of waste held vertically in air.⁷

It may be seen from Table 4.9 that even those wastes containing the least amounts of inert diluents (i.e., Case 1 for both LWR and LMFBR) can be encapsulated in 6-in.-diam containers (the

smallest diameter believed to be economically acceptable) after only 2 to 2½ years interim storage. This is not an unreasonable storage time for liquids. In all other cases, encapsulation can take place earlier, in many instances at ages corresponding to the time of their generation (30 to 60 days for the LMFBR, and 120 to 180 days for the LWR and HTGR). However, just as there is a safety incentive to solidify waste as early as possible, there is also an economic incentive to encapsulate the solid waste in a minimum number of containers having the maximum acceptable diameter. In the next phase of this study, the costs of waste management for each of the cases considered thus far will be investigated.

4.2 HIGH-LEVEL RADIOACTIVE WASTE

The safe, economic management and treatment of wastes arising from the processing of fuels from LMFBR's, HTGR's, LWR's, and MSBR's are being studied. Physical and chemical properties of these wastes during various waste treatment steps were determined for use in studies of the economics and safety of alternative treatment methods (see Sect. 4.1).

⁷J. L. McElroy et al., *Pot Calcination Performance During First Radioactive Tests in Waste Solidification Engineering Prototypes: Waste Solidification Program*, vol. 4, BNWL-814 (December 1968).

Chemical Development

A computer program (STORE) was written⁸ to permit more rapid calculation of temperature profiles within cylinders containing uniformly distributed heat sources and materials whose thermal conductivities can be expressed as a tabular function of temperature. Maximum temperature rise calculations were made as a function of thermal conductivity, power density, and cylinder diameter for a fixed surface temperature of 122°F. Results of these calculations have provided incentive for investigation of waste materials with higher thermal conductivities than those of calcines. Such materials with high thermal conductivity have possible application in processes for immediate solidification of wastes following fuel reprocessing to circumvent interim liquid waste storage. Since the thermal conductivity of a given amount of waste solids dispersed in a glass is about twice that of these solids dissolved to form a ceramic product and about three times that of these solids dissolved to form a true glass, primary emphasis in the laboratory has been on efforts to disperse (not dissolve) waste solids in a glassy matrix to yield a two-phase system.

Products with good physical and chemical properties, and containing about 35 wt % solids, from reprocessing LMFBR, HTGR, and LWR fuels were prepared at 800 to 900°C, using small-scale pot calcination equipment. Thus, it appears that the pot calcination process, which has been successfully demonstrated on an engineering scale at Oak Ridge National Laboratory⁹ and Pacific Northwest Laboratory (PNL),¹⁰ can probably be used, with only slight modification, for the preparation of a dispersion of waste oxides in a glassy matrix.

⁸W. Davis, Jr., *Temperature Profiles Within Cylinders Containing Internal Heat Sources and Materials of Temperature-Dependent Thermal Conductivities. Description of Fast Computer Programs as Applied to Solidified Radioactive Wastes*, ORNL-4345 (January 1969).

⁹W. E. Clark, J. C. Suddath, C. W. Hancher, R. E. Blanco, H. W. Godbee, J. M. Holmes, and C. L. Fitzgerald, *Development of Processes for Solidification of High Level Radioactive Waste: Summary for Pot Calcination and Rising Level Potglass Processes*, ORNL-TM-1584 (August 1966).

¹⁰C. R. Cooley, J. L. McElroy, W. V. DeMeir, J. E. Mendel, J. C. Suddath, and J. O. Blomeke, *Pot Calcination Performance During Radioactive Test in Waste Solidification Engineering Prototype. Waste Solidification Program, Vol. 4 (BNWL-814)*.

Liquid-Metal-Cooled Fast Breeder Reactor

(LMFBR) Waste. — The high-level wastes (Table 4.3) arising from the processing of fuels from LMFBR's include fission product wastes (first-cycle raffinates), alpha-active wastes (second-cycle TBP and plutonium purification wastes), solvent cleanup wastes (contaminated with plutonium), and caustic scrubber wastes (possibly contaminated with plutonium). (All wastes containing significant quantities of alpha activity are considered to be high level.) The behavior of the individual wastes (Table 4.3) and various combinations of these wastes (Table 4.6, Nos. 13 and 14) during evaporation, calcination, and melting was studied. The results showed that sodium tetraborate would form a glassy matrix for the stainless steel and fission product oxides in the waste. Thus, in those mixtures, which did not contain boron as a soluble poison (Table 4.6, Nos. 11 and 12), sufficient boron was added to form sodium tetraborate. One objective of laboratory studies is to produce a dispersion at 900°C or less with the fission product waste, using the sodium in caustic scrubber and solvent cleanup wastes and the boron in the fission product waste (plus any additional boron required) to form sodium tetraborate. The addition of other glass formers such as CaO and SiO₂ was used to decrease the corrosiveness of the melts and to make the continuous phase of the products more glassy. The composition of some typical products are given in Table 4.10. Generally, the products appear to have a glassy continuous phase if the ratio of chemical equivalents of boron to sodium is between 2 and 3. Addition of silicon improves the glassy properties of the matrix or continuous phase. The most promising product contains 74.1 wt % waste oxides not including Na₂O (Table 4.10, No. 13). The Na₂O might be considered a waste oxide since it could come from the solvent cleanup or caustic scrubber wastes. A semicontinuous run was made with a waste solution corresponding to the product (Table 4.10, No. 13) in a 2-in.-diam, 12-in.-high type 304 stainless steel pot at 900°C in a 5-kw furnace. The product was a dense glassy solid (Fig. 4.6). On being sectioned, the pot showed no visible signs of corrosion. The thermal conductivity, as well as other physical and chemical properties of this product, will be measured.

Table 4.10. Nominal Composition of Products From Incorporating LMFBR High-Level Aqueous^a Waste in a Glassy Matrix at 900°C

Component	Weight Percent												
	1	2	3	4	5	6	7	8	9	10	11	12	13
<u>Waste Oxides</u>													
B ₂ O ₃	43.6	44.0	44.4	44.8	45.3	43.8	54.1	48.5	50.2	51.1	39.0	42.5	43.9
Fe ₂ O ₃	2.0	2.0	2.0	2.1	2.1	2.0	2.5	2.2	2.3	2.3	2.5	2.9	2.9
Cr ₂ O ₃	0.6	0.6	0.6	0.6	0.6	0.6	0.7	0.6	0.7	0.7	0.6	0.7	0.7
NiO	0.2	0.2	0.2	0.2	0.2	0.2	0.2	0.2	0.2	0.2	0.3	0.3	0.3
La ₂ O ₃	6.9	7.0	7.1	7.1	7.2	7.0	8.6	7.7	8.0	8.1	14.7	16.0	16.5
ZrO ₂	2.5	2.5	2.5	2.5	2.6	2.5	3.1	2.7	2.8	2.9	2.6	2.8	2.9
BaO	1.2	1.2	1.2	1.2	1.2	1.2	1.4	1.3	1.3	1.4	1.4	1.6	1.6
RuO ₂	2.7	2.7	2.7	2.7	2.8	2.7	3.3	3.0	3.1	3.1	2.8	3.1	3.2
Rb ₂ O	1.6	1.7	1.7	1.7	1.7	1.6	2.0	1.8	1.9	1.9	1.9	2.1	2.1
<u>Added Oxides</u>													
Na ₂ O ^b	38.8	29.4	19.8	10.0	-	19.5	24.1	21.6	22.3	22.7	17.4	19.0	19.6
SiO ₂	-	-	-	-	-	18.9	-	10.4	7.2	5.5	16.8	9.2	6.3
CaO	-	8.9	17.9	27.1	36.5	-	-	-	-	-	-	-	-
Waste Oxides (wt %)	61.2	61.7	62.3	62.9	63.5	61.6	75.9	68.0	70.5	71.8	65.8	71.8	74.1
Density ^c (g/cc)	2.29	2.35	2.42	2.50	2.58	2.30	2.29	2.29	2.30	2.30	2.47	2.48	2.49
Comments	crystalline	crystalline	crystalline	crystalline	crystalline	glassy							

^aComposition given in Table 4.3, No. 3.

^bNa₂O might be considered a waste oxide since it could be added from solvent cleanup or caustic scrubber wastes.

^cCalculated pore-free density.

High-Temperature Gas-Cooled Reactor (HTGR) Waste. — The burn-leach treatment for reprocessing HTGR fuels produces high-level fission product, solvent cleanup, and caustic scrubber waste streams (Table 4.4) and a high-level solid waste composed of leached alumina powder (Table 4.7). Such a waste powder (simulated) was dispersed in a lead silicate glass at 800°C to yield a dense, hard, void-free solid containing 35 wt % waste powder and 65 wt % glass. The glass was a commercial fritted product composed of 67.6 wt % PbO, 26.8 wt % SiO₂, and 5.6 wt % CaO. The dispersion process was operated in both a batch and a semi-continuous manner, using the 2-in.-diam, 12-in.-high type 304 stainless steel pot in the 5-kw furnace mentioned above. At 600°C, the measured

thermal conductivity of one product (Fig. 4.7b) was 1.73 Btu hr⁻¹ ft⁻¹ °F⁻¹, which is about a fourfold increase over that of the powder. Simulated HTGR waste powder was also dispersed in soda-lime glasses; however, the products contained many voids and were not homogeneous.

Light-Water Reactor (LWR) Waste. — The high-level wastes (Table 4.2) from the processing of fuels from LWR's are, except for their fission product compositions, similar to those from LMFBR's. Experiments were carried out in the 2-in.-diam by 12-in.-long pot (mentioned above); glass powders were mixed directly with aqueous waste (No. 1 in Table 4.2), and the resulting slurries were pumped to the pot at 900°C as in the pot calcination process. Hard, dense, homoge-

PHOTO 95706



Fig. 4.6. Dispersion Prepared with Simulated Fission Product Aqueous Waste from Processing LMFBR Fuels. The product was prepared at 900°C and contained 74.1 wt % oxides from waste in a sodium tetraborate-silicate matrix.

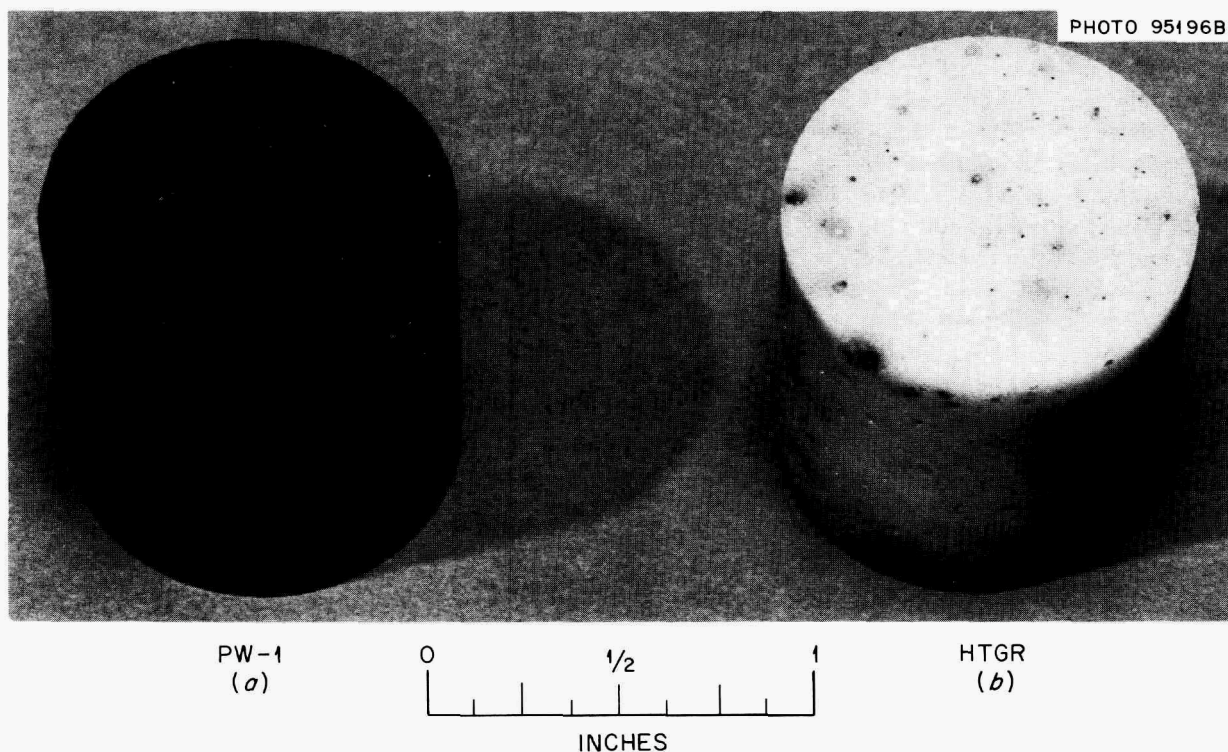


Fig. 4.7. Dispersions Prepared with (a) Simulated Fission Product Aqueous Waste from Processing LWR Fuels and (b) Simulated High-Level Solid Waste from Processing HTGR Fuels. The PW-1 product was prepared at 900°C, while the HTGR product was prepared at 800°C; both contain 35 wt % waste oxides in a lead silicate matrix.

neous products were obtained with the lead silicate glass (Fig. 4.7a), while the products obtained with soda-lime glass contained many voids and were not homogeneous.

Temperature Rise in Cylinders of Waste. — Calculations¹¹ were made of the maximum temperature rise in cylinders containing solidified high-level radioactive wastes. The storage forms considered for these wastes were calcine, phosphate glasses, and calcine dispersed in a glass matrix. These materials have a wide range of thermal conductivities. Maximum temperature rises were calculated as a function of power density and cylinder diameter for long cylinders (length/diameter ≥ 5) at a surface temperature of 122°F; this corresponds to storage under water, at power densities of 2000 to

80,000 Btu hr⁻¹ ft⁻³, and cylinder diameters of 6 to 48 in.

MSBR Waste. — The chemical system being developed for reprocessing the MSBR fuel salt combines reductive extraction, fluorination, and possibly other treatment methods (see Sect. 1). Although reprocessing conditions have not been definitely established, the final waste salt will undoubtedly consist of 67-33 mole % LiF-BeF₂ containing most of the fission products (i.e., 1.38 kg of fission products per 0.49 ft³ of salt per day for the present flowsheet). Developmental work on waste treatment and disposal has been confined to this major waste product. Other less voluminous wastes that will also be produced, such as 0.0086 ft³ of LiF-ZrF₄ salt per day during cleanup of the bismuth extractant, are not being considered at present.

Major problems in managing the MSBR fuel salt waste include: (1) corrosion of the waste containers from the production of fluorine (by radi-

¹¹W. Davis, Jr., C. L. Fitzgerald, and H. F. Soard, *Maximum Temperature Rise in Cylinders Containing Intermediate-Level and High-Level Solidified Radioactive Wastes*, ORNL-4361 (March 1969).

olysis) or hydrofluoric acid (by hydrolysis with traces of moisture); (2) maintenance of an inert atmosphere; (3) control of thermal conductivity and temperature in the waste containers; and (4) volatility and mass transfer of fission products.

A study of the radiolysis of 67-33 mole % LiF-BeF₂ in a ⁶⁰Co source was initiated. A static test at 50°C indicated a maximum fluorine production rate corresponding to a G(F₂) value of 0.005, which is in agreement with values reported by other investigators.¹² Two additional dynamic tests, in which G values were obtained by measuring the amount of nickel fluoride produced on the reaction vessel wall, indicated tentative agreement with these results. No hydrogen, fluorine, or fluoride was detected in the cover gas. Actually, the production of fluorine has not been positively identified since the presence of as little as 1 ppm of water in the gas could produce an equivalent amount of hydrofluoric acid (by hydrolysis of the salt) and a corresponding amount of nickel fluoride. The nickel fluoride was used to indicate the amount of HF or F₂ produced. Either product is of interest in understanding corrosion in the waste container vessel. More precise experiments are in progress.

Liaison with Pacific Northwest Laboratory. — Cooperative work with PNL on the waste solidification program continued in the following areas: (1) preparation of a final report on the first six pot calcination runs in the PNL Waste Solidification Engineering Prototype (WSEP) Pilot Plant,¹⁰ (2) reviewing a PNL status report on waste solidification, and (3) planning of the future program in the WSEP. The solidification of waste types that are representative of advanced light water and fast breeder reactors will be included in the future program.

Encapsulation of Fission Product Gases. — The purpose of this program is to determine the safest and most satisfactory method for permanently disposing of fission product gases, particularly the noble gases, contained in the off-gases from nuclear reactors or fuel reprocessing plants. Other volatile radioactive effluents (e.g., iodine and tritium) can undoubtedly be separated, converted to stable compounds, and stored as stable solids. Compounds of krypton and xenon are known, but

they do not have the thermal stability required for long-term storage.¹³

Present means available for the disposal of noble fission product gases include:

1. controlled discharge to the atmosphere,
2. underground injection in carefully selected geological formations, and
3. containment and storage in pressurized gas cylinders.

Release to the atmosphere within safety limits becomes more difficult as nuclear installations become larger and more numerous. Disadvantages of injection into the ground include: (1) uncertainty regarding eventual contamination of the environment and (2) the probable requirement for disposal of all wastes in a government-owned area. The use of cylinder storage allows close surveillance but involves the possibility of a sudden dangerous discharge in the event of a rupture or a leak in the container. It is believed that modification of cylinder storage, by adding at least one extra stage of containment, represents the safest available method for disposal of gases. This method retains basic advantages of compression to a small volume and storage under carefully controlled conditions.

The isotope of greatest single importance is ⁸⁵Kr (half-life, 10.76 years) since all of the xenon isotopes resulting from fission have half-lives that are sufficiently short to permit release to the atmosphere after storage for only a few months. Separation of krypton from the voluminous inert xenon (Table 4.11) by one of the existing techniques¹⁴⁻¹⁶ may be desirable so that the volume required for long-term storage will be minimized. We assume that separation of ⁸⁵Kr from the nonradioactive iso-

¹⁴R. H. Rainey, W. L. Carter, S. Blumkin, and D. E. Fain, "Separation of Radioactive Xenon and Krypton from Other Gases by Use of Permselective Membranes," paper SM 110/27 presented at the IAEA Symposium on Operating and Developmental Experience in the Treatment of Airborne Radioactive Wastes, New York City, Aug. 26-30, 1968; published in the *Proceedings*, pp. 323-42.

¹⁵J. R. Merriman, J. H. Pashley, K. E. Habiger, M. J. Stephenson, and L. W. Anderson, "Concentration and Collection of Krypton and Xenon from Selective Absorption in Fluorocarbon Solvents," paper SM 110/25 presented at the IAEA Symposium on Operating and Developmental Experience in the Treatment of Airborne Radioactive Wastes, New York City, Aug. 26-30, 1968.

¹⁶C. L. Bendixsen and G. F. Offutt, *Rare Gas Recovery Facility of the Idaho Chemical Reprocessing Plant*, IN-1221 (TID-4500) (April 1969).

¹²*Reactor Chem. Div. Ann. Progr. Rept. Jan. 31, 1965*, ORNL-3789, pp. 49-55.

¹³G. J. Moody and J. D. R. Thomas, *Rev. Pure Appl. Chem.* **16**, 1-24 (1966).

Table 4.11. Estimated Amounts^a of Fission Gases Associated with Spent Fuel Discharged from Various Reactors

Fission Product	Assumed Form	LMFBR ^b		MSRE		PWR-1	
		g-moles	Standard liters	g-moles	Standard liters	g-moles	Standard liters
Tritium ^c	³ HH or ³ HHO	0.00108	0.024	0.0026	0.059	6.9×10^{-4}	0.0155
Krypton	Kr	0.116	2.59	0.299	6.7	0.143	3.20
Xenon	Xe	1.0	22.40	0.933	20.9	1.238	27.72
Iodine	I ₂	0.0572		0.0594		0.029	

^aIn g-moles or standard liters per 1000 Mwd of burnup after a 30-day cooling period.

^bData from RIBDOR Code. Assumes fuel is blended in the following proportions: one-third of the core (80,000 Mwd in 540 days), one-third of the axial blanket (2500 Mwd in 540 days), and three-eighths of the undifferentiated radial blanket (8100 Mwd in 970 days). For a 5-metric ton/day reprocessing plant, 427.1 liters Kr and 3696.1 liters Xe per day would be generated.

^cGenerated by thermal and fast fission of ²³⁵U and Pu in the LMFBR; by fission of ²³³U and the ⁷Li(*n*, T *n*)⁴He and ⁶Li(*n*, α)³H reactions in the MSBR; and by the fission of ²³⁵U in the PWR-1. Tritium produced by the ²H(*n*)³H reaction in cooling water is not included.

topes of krypton will not be economically attractive within the foreseeable future and that we must, consequently, plan for long-term storage of all isotopes of krypton. In the case of the LMFBR, more than 92% of the krypton is present as inactive isotopes one day after the fuel has been removed from the reactor.

The principal possibilities for secondary containment may be classified as follows:

1. simple mechanical containment; that is, a vessel within a vessel (pot),
2. encapsulation of pressurized gas bubbles (foam) or "microampules" containing pressurized or liquefied gases in a suitable matrix such as glass, plastic, or metal, with a pot serving as the exterior container, and
3. entrapment in clathrates or zeolite structures contained within a pot, or encapsulation of the zeolites (loaded with gases) in a matrix as in (2) above.

Neither the compounds of krypton nor its adsorbates are sufficiently stable to serve as long-term storage vehicles for radioactive gas; however, either or both may provide a useful means for separating krypton from xenon, or may possibly serve as intermediates in the formation of foams.

The initial experimental work has been confined to scoping studies at atmospheric pressure to de-

fine the limitations and problems in potentially useful processes. No process can be selected as clearly superior until definitive safety criteria are developed and the mechanical operating problems are evaluated. A comparison of the more obvious possibilities is presented in Table 4.12. Special equipment is being constructed for use in obtaining data at higher temperatures and pressures. Only entrapment in molecular sieves (zeolites¹⁷) is competitive with tank storage on the basis of final storage volume. However, when these zeolites are fully loaded, the heat from radioactive decay could cause the sieve openings to expand and to release the trapped gas, thus pressurizing the containment vessel. Therefore, either provisions must be made for removal of the heat or the pores must be permanently sealed. The data given for clathrates are based on those for the hydroquinone clathrate of krypton.¹⁸ Although the radiation stability of clathrates has not been determined, krypton is known to leak from such material even at ambient temperatures. Possibly more stable inorganic clathrates can be developed. The noble gas output from a plant reprocessing 5 metric tons of fuel per day will generate about 76% of the capacity of one standard pressurized "K" cylinder.

¹⁷L. H. Shaffer and W. J. Sesny, U.S. Patent 3,316,691 (May 2, 1968).

¹⁸H. M. Powell, *J. Chem. Soc. (London)*, 300 (1950).

Table 4.12. Comparison of Methods for Storing Radioactive Noble Gases

Type of Storage	Encapsulation Pressure and Temperature	Standard liters of Gas per liter of Storage Volume	Remarks
Cylinder storage			
Maximum	2640 psi at 21.1°C	167.7	"T" cylinder ^a
Actual	1915 psi at 21.1°C	120.9	Idaho practice ^{a,b} ("K" cylinder)
Foams			
In glass			
20% by volume	14.7 psi at 550°C	0.066	~23% obtained at 700 to 800°C ^c
50% by volume	1470 psi at 550°C	16.59	Estimated
Glass "microampules" encapsulated in glass or other matrix	640 to 2515 psig, 0°C	3.9 to 11.6	Estimated; technology known
In epoxy resins			
67% by volume	14.7 psi at 100°C	0.732	Experimental
Maximum allowed by irradiation and internal heat generation		8.39	Estimated
Entrapment			
In molecular sieves	63,190 psi at 350°C	168	Linde patent (ref. 17)
In clathrates	147 psi at 95°C	57.7	Experimental; impractical because of heat generation and irradiation levels

^aCylinder nomenclature according to G. A. Cook, *Argon, Helium and the Rare Gases*, Interscience, New York, 1961, p. 429. Calculated cylinder volumes are about 51.7 and 44.7 liters for "T" and "K" cylinders respectively. At the temperatures and pressures listed, the "T" cylinder would contain about 8674 liters of gas and the "K" cylinder would contain about 5408 liters of gas, measured at standard conditions.

^bG. F. Offutt, Phillips Petroleum Co., ICPP, personal communication.

^cExperimental data obtained with the higher-melting glass. Glass sufficiently fluid for use at 550°C is commercially available.

The formation of foams in high-viscosity liquids is being studied by correlating bubble formation with agitation in viscous liquids. At present, the use of a Waring Blendor appears to be the most practical method for producing foams. About 21%, by volume, of gas has been incorporated into Polybutene 24 (viscosity, 8600 centistokes at 100°C) and about 23%, by volume, has been incorporated in glass (Table 4.12). Similar experiments will be conducted with other molten glasses in special containers. Radiation and internally generated heat would be minimal problems in a foam glass. The high degree of dispersion of the gas in a

highly viscous fluid should furnish an extra margin of safety in preventing sudden pressurization of the containment vessel, that is, in case the glass matrix should melt during an accidental temperature rise in the shipping or storage area. The 50%, by volume, of gas at 1470 psi shown in Table 4.12 is an estimate of the maximum amount attainable by this method.

The glass "microampule" technique¹⁹ is a variation of the foam glass method. It consists in en-

¹⁹W. W. Shaver and M. Britton, Corning Glass Works, Corning N.Y., private communication.

capsulating pressurized or liquefied gas in tiny glass ampules, which are then incorporated in a low-melting glass or other matrix. The new impervious concretes, which contain organic polymers, will be studied as possible matrices.

Foams have been produced in epoxy resins containing up to 67% by volume of gas. The foam was stable at 150°C, but became increasingly brittle as the temperature increased. Assuming that this same volume percentage of gas could be incorporated at a pressure of 168.5 psig (11.46 atm) and that the foam has the same thermal conductivity as argon gas,²⁰ about 8.4 std liters of gas could be incorporated per liter of foam. Under these conditions, the radiolytic heat could be dissipated from an 8-in.-diam cylinder containing the epoxy-gas mixtures without external cooling, if the center-line temperature were allowed to rise to 150°C. The total radiation dose (infinite time) from the encapsulated ⁸⁵Kr would amount to about 8.3×10^{11} rads, somewhat in excess of doses which epoxy resins have been reported to withstand without serious damage.²¹ Other resins may prove to be more resistant to both temperature and radiation than those studied initially.^{22,23} The value of 8.4 std liters of gas per liter of storage space (5% of that attainable in a "T" cylinder) probably represents about the maximum that we can expect to incorporate in resin or plastic in a practical process.

4.3 INTERMEDIATE-LEVEL RADIOACTIVE WASTE

Nuclear installations routinely produce intermediate-level radioactive wastes (ILW) such as concentrated salt solutions, chemical sludges, and spent organic solvents. Aqueous ILW's are characterized by their modest levels of radioactivity and by their high salt or solids content, which prevent their efficient treatment by a conventional

method such as ion exchange or precipitation. These wastes have generally been stored in tanks or mixed with cement and buried in specially designated land areas above the water table. Both of these methods have limitations. Tank storage is a temporary measure that requires constant surveillance, and the products formed by mixing the waste with cement do not always have low leach rates in ground water. The integrity and the leach rate of cement products decreases and increases, respectively, as the concentration of included salts increases. A low concentration of included salts produces a final volume of product to be stored that is greater than the initial waste volume. Organic ILW's consist of solvents that are used in fuel processing plants and of miscellaneous solid and liquid organic materials that are used in all nuclear installations. These wastes are modest in volume and radionuclide content but are incompatible with disposal systems for low-level aqueous wastes. Presently, such organic wastes are stored in tanks, discharged to the earth in controlled areas, volatilized and discharged to the earth in controlled areas, volatilized and discharged to the atmosphere, buried, or burned in open trays. Many of these current aqueous or organic waste disposal methods are questionable on a long-term basis from the standpoints of immobilization, volume reduction, economics, and pollution control. Under the newer concepts, only wastes containing negligible amounts of long-lived alpha nuclides would be classified as intermediate- or low-level wastes and processed for burial above the water table.

Processes have been developed in the United States,²⁴ Belgium,²⁵ France,²⁶ and the United Kingdom²⁷ for incorporating wastes in asphalt prior to burial. Plants for incorporating ILW's in asphalt

²⁰The thermal conductivity constant, k , for argon gas at 100°C is 1.23×10^{-2} Btu hr⁻¹ ft⁻¹ °F⁻¹, while that for epoxy resin may vary from about 7×10^{-2} to 9.7×10^{-2} Btu hr⁻¹ ft⁻¹ °F⁻¹. The estimate given for the center-line temperature is, therefore, conservative.

²¹W. W. Parkinson, "Radiation-Resistant Polymers," in *Encyclopedia of Polymer Science and Technology*, Interscience, New York (in press).

²²*Chem. Eng. News* 42(15), 55 (1964).

²³*Chem. Eng. News* 43(20), 38 (1965).

²⁴H. W. Godbee, J. H. Goode, and R. E. Blanco, "Development of a Process for Incorporation of Radioactive Waste Solutions and Slurries in Emulsified Asphalt," *Environ. Sci. Technol.* 2, 1034-40 (1968).

²⁵P. Dejonghe, L. Baetsle, N. Van de Voorde, M. Maes, P. Staner, J. Pyck, and J. Souffriau, "Asphalt Conditioning and Underground Storage of Concentrates of Medium Activity," presented at the Third United Nations International Conference on the Peaceful Uses of Atomic Energy, A/CONF.28/P/774 (May 1964).

²⁶J. Rodier, M. Alles, P. Auchapt, and G. Lefillatre, "Solidification of Radioactive Sludges Using Asphalt," SM-71/52, pp. 713-29 in *Practices in the Treatment of Low- and Intermediate-Level Radioactive Wastes*, IAEA, STI/PUB/116 (ORNL-Tr-1432), Vienna, 1966.

²⁷R. H. Burns and G. W. Clare, *Bitumen Incorporation - A.E.R.E. Operational Experiences*, AERE-M2143 (November 1968).

are already in operation at Mol, Belgium; Marcoule, France; and Hatwell, England.

Process Description

The process^{24,28,29} developed at ORNL contains the following steps: (1) wastes are introduced into emulsified asphalt, molten asphalt, or molten polyethylene at any convenient temperature below the boiling point of the solution, (2) water or organic solvent is volatilized by heating, (3) the temperature of the product is increased until the product flows freely, and (4) the product is drained into a steel drum for preliminary storage and shipment to a disposal area. The vapors are condensed, and the inert gases are passed through high-efficiency filters prior to discharge. The condensed organic solvent could be reused and the aqueous condensate could be either reused or combined with other low-level aqueous wastes for further decontamination. Alternatively, all the solvent could be retained in the polyethylene or asphalt matrix by operating at a lower temperature.

Safety Evaluation

The incorporation of inert solids in asphalt does not appear to present any additional hazard to that already present when an organic material with a high flash point is being processed, stored, or shipped. However, results obtained by burning small samples of asphalt products indicated a sharply enhanced burning rate for asphalt containing large amounts of nitrate or nitrite. As part of continuing efforts to evaluate the hazards associated with the organic-nitrate-nitrite system, the burning characteristics of asphalt and polyethylene containing sodium nitrate or sodium nitrite were determined by burning 1- to 2-g samples in a beaker heated on a hot plate in air. The samples contained from 40 to 75 wt % nitrate and/or nitrite salts. The nitrate-asphalt, nitrite-asphalt, and nitrate-polyethylene samples ignited at 330, 275, and 440°C respectively. The asphalt samples

²⁸Chem. Technol. Div. Ann. Progr. Rept. May 31, 1968, ORNL-4272, pp. 74-78.

²⁹C. L. Fitzgerald, R. E. Blanco, H. W. Godbee, and W. Davis, Jr., "The Feasibility of Incorporating Radioactive Wastes in Asphalt or Polyethylene," to be presented at the American Nuclear Society Meeting, Seattle, Wash., June 15-19, 1969.

Table 4.13. Settling of Salts from an Asphalt Product Containing 60 wt % Salts

Temperature (°C)	Time at Temperature (days)	Na Concentration (wt %) in Sampling Zone ^a		
		Top	Middle	Bottom
60	7	8.80	8.36	8.78
100	5	5.83	8.30	9.50
130	1	6.23	8.42	10.53
160	0.2	5.00	6.83	11.08

^aSamples (volume, 200 ml) were held in a standard 250-ml graduated cylinder.

burned vigorously, whereas the polyethylene samples burned slowly. The inorganic salts settled from the organic matrix at these elevated temperatures. Additional tests showed that the salts begin to separate from the asphalt at temperatures above 60°C but that phase separation should not be a problem below this temperature (Table 4.13).

The explosive hazards of the nitrate-asphalt system were studied^{30,31} by detonating blasting jelly in 1- to 2-kg samples of a nitrate-asphalt mixture that was confined in 4-in. sched 80 steel pipes. Only a sample containing 10 wt % asphalt and 90 wt % NaNO₃ (to simulate a condition that might be caused by phase separation), with about 50% voids, could be detonated. Earlier irradiation of similar samples in a ⁶⁰Co source showed that asphalt-nitrate products could reach 50% void volumes at an absorbed dose of about 10⁹ rads; however, polyethylene-nitrate samples showed no signs of voids at this dose.

Asphalt and polyethylene are good media for incorporating ILW's that do not contain oxidizing materials. Asphalt is not recommended for wastes containing oxidants; polyethylene, on the other hand, is probably acceptable for use with such wastes, but further studies will be required to assess the safety of this system. Polyethylene is equal to, or better than, asphalt on most bases. Although it is more expensive than asphalt, the

³⁰C. V. Chester, ORNL, private communication, Sept. 19, 1968.

³¹C. V. Chester, ORNL, private communication, Oct. 8, 1969.

cost of either material is probably not a significant factor in the cost of operating a nuclear installation.

Power Reactor Wastes

Incorporation in asphalt or polyethylene is being studied as a general method for treating nonoxidizing wastes such as evaporator concentrates, spent ion-exchange materials, and other miscellaneous wastes that are generated at power reactor stations. In particular, the concentrate obtained by evaporating coolant letdown from the primary circuit of pressurized-water reactors will contain 5 to 15 wt % boric acid. This solution will be neutralized with either calcium hydroxide or sodium hydroxide before storage or incorporation in polyethylene or asphalt. Asphaltic products containing 50 and 60 wt % NaBO_2 , and 50 and 55 wt % $\text{Ca}(\text{BO}_2)_2$, have been prepared in the laboratory. Polyethylene products containing 20 to 60 wt % NaBO_2 , in increments of 10 wt %, have been prepared with Union Carbide's DYDT and DYLT polyethylenes. The results of leaching the polyethylene products, at the end of about two weeks, expressed as fraction of sodium leached $(\text{cm}^2/\text{g})^{-1} \text{ day}^{-1}$, were 8.1×10^{-5} for the product containing 80% DYLT, 2.9×10^{-4} for 60% DYLT, and 3.6×10^{-3} for 60% DYDT (Fig. 4.8). The leaching values obtained with DYLT polyethylene are comparable to those obtained with similar asphalt products (see section on Engineering Development).

Temperature Rise in Stored Drums

Calculations were made of the maximum temperature rise in cylinders containing radioactive ILW-asphalt products, using a computer program developed for this purpose.³² Maximum center-line temperatures were calculated as a function of power density, cylinder diameter, and cylinder length/diameter ratio for a thermal conductivity of $0.153 \text{ Btu ft}^{-1} \text{ hr}^{-1} \text{ }^\circ\text{F}^{-1}$. The power density was varied from 0.5 to $8 \text{ Btu hr}^{-1} \text{ ft}^{-3}$, and the cylinder diameter was varied from 1 to 14 ft; length/diameter ratios of 1 and 2 were used. The calculations

showed that products with a power density of about $40 \text{ Btu hr}^{-1} \text{ ft}^{-3}$, which is about eight times higher than that of waste concentrates, could be stored in 55-gal drums and still not reach a temperature at which phase separation would become a problem. In general, radiation damage, rather than temperature rise, limits the amount of radionuclides that can be incorporated in asphalt or polyethylene.

Incorporation of Intermediate-Level Radioactive Wastes in Asphalt

A few years ago, hot-cell tests were performed,²⁴ using a 4- by $6\frac{1}{2}$ -in. batch mixer in which three typical aqueous ILW wastes — miscellaneous alkaline evaporator bottoms (ILW), aluminum cladding

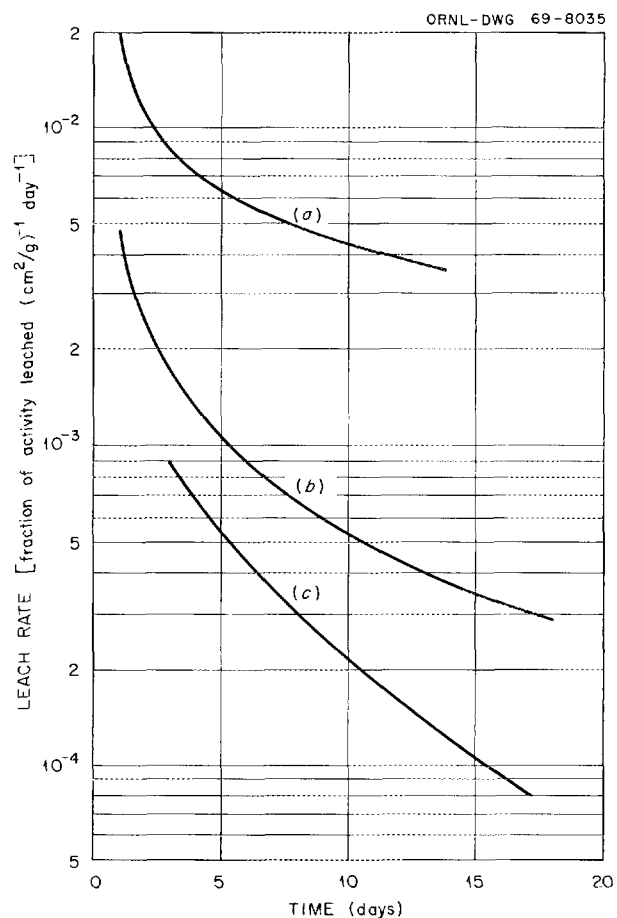


Fig. 4.8. Results of Leaching of Various Elements from Polyethylene Products with Water: (a) Sodium from 40% NaBO_2 -60% DYDT; (b) Sodium from 40% NaBO_2 -60% DYLT; and (c) Sodium from 20% NaBO_2 -80% DYLT.

³²W. Davis, Jr., C. L. Fitzgerald, and H. F. Soard, *Maximum Temperature Rise in Cylinders Containing Intermediate-Level and High-Level Solidified Radioactive Wastes*, ORNL-4361 (March 1969).

solutions (ACS), and neutralized second-cycle solvent extraction raffinates (2CW) – were incorporated into emulsified asphalt to yield products containing about 60 wt % solids (including up to 35 wt % nitrates) and 50 curies of radioactivity per gallon. Static leaching tests of the samples with demineralized water were terminated after 912 to 1013 days, which corresponded to accumulated absorbed radiation doses of 0.87 to 1.5×10^8 rads. This is approximately equivalent to the dose that would be received by a waste product containing 5 curies of ^{137}Cs per liter of asphalt product after ten years of storage. Figure 4.9 shows the fractions of sodium and ^{137}Cs leached from the products as a function of the sample surface area, mass of sample, and time [i.e., fraction leached $(\text{cm}^2/\text{g})^{-1} \text{ day}^{-1}$]. Approximately 1.4, 3.8, and 2.5% of the total sodium in the ILW, 2CW, and ACS samples, respectively, had been leached by the end of the tests. The slight increase in the leach rates of the ACS and 2CW samples late in the leaching period is similar to that observed in long-term

leaching tests with low (tracer) levels of radioactivity. This is attributed to “saturation” of the asphalt by the water.

Engineering Development

The flexibility of the ORNL Waste-Asphalt Process and the capability of the Pfaunder wiped-film evaporator were further demonstrated in a series of 12 runs in which a simulated, nonradioactive borate waste solution was successfully incorporated in asphalt. Pressurized-water reactors use a weak boric acid solution as a primary coolant. The slightly contaminated boric acid solution, which is bled from the system during startup and during normal operation to compensate for fuel burn-up, comprises a low-level waste.

The present method for treating the borate waste solution is to remove the radionuclides from the boric acid by anion exchange and to dispose of the contaminated resin by sluicing it into a drum for final shipment to a disposal site for burial. The

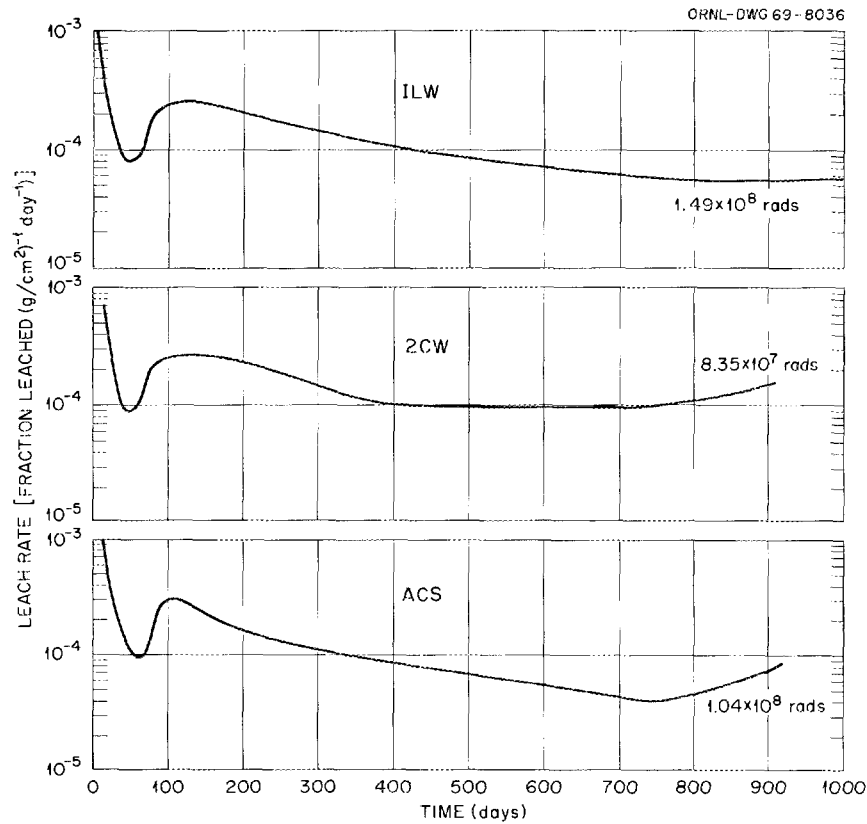


Fig. 4.9. Leaching of Sodium and ^{137}Cs from Intermediate-Level Waste Incorporated into Asphalt (Hot-Cell Tests).

restrictions recently placed on the shipping suggest an alternative procedure, in which the radio-nuclides are immobilized by incorporating the borate waste in asphalt. It is expected that the dilute boric acid solution would undergo a pre-concentration step. The condensate would be recycled to the reactor, and the bottoms, containing about 15 wt % boric acid, would be incorporated in asphalt. The boric acid concentrate would be neutralized with either sodium hydroxide or calcium hydroxide before treatment to prevent decomposition of the asphalt by the acid. The solid product can be shipped safely to a waste disposal site.

In the experimental program, a 20 wt % sodium metaborate solution containing 10% excess caustic was used as simulated waste. The soluble sodium metaborate was selected in preference to the less-soluble calcium metaborate because it imposes a more severe test of the leaching properties of the waste-asphalt product. RS-2, a standard road grade emulsified asphalt, was used in all cases.

Twelve tests were conducted in groups of three and four. In each group of tests, either the solids content of the product or the boilup rate of the evaporator was held constant while other conditions were varied (Table 4.14). Finally, three 10-hr runs were performed to determine if the evaporator could sustain steady-state operation over long periods of time and continue to manufacture a uniform product; results showed that it functioned well over the range investigated. The best products, as defined by minimum residual water content, were obtained at an evaporator boilup rate of 60 to 70 lb of water per hour and a product solids content of 45 to 50 wt %. Under these conditions, about 40 lb of product is manufactured per hour. The behavior of the sodium metaborate-asphalt products in the process was considerably different from that observed in tests with other waste types. In the latter tests, the asphalt products were fluid at temperatures as low as 105°C and flowed freely from the evaporator. Products containing sodium metaborate, on the other hand, did not flow from the evaporator at temperatures less than 110°C; however, they flowed readily at about 120°C and had excellent fluidity at 130°C. Also, a higher temperature is required to prevent the formation of sodium metaborate tetrahydrate, which is stable up to 120°C; this, in part, accounts for the high residual water contents of products in instances where the product temperature did not exceed 120°C (Table 4.14). A plot of the residual water content as a

function of product temperature supports this hypothesis and indicates that product temperatures of 130 to 140°C are required to obtain products with low residual water content (Fig. 4.10). The maintenance of higher temperatures can be accomplished by decreasing the flow of aqueous waste into the evaporator while maintaining a constant flow of asphalt.

Although the residual water content is normally used as a criterion in establishing optimum processing rates, the true test of the product quality is determined by leaching tests. Figure 4.11 shows static leaching data for the products obtained dur-

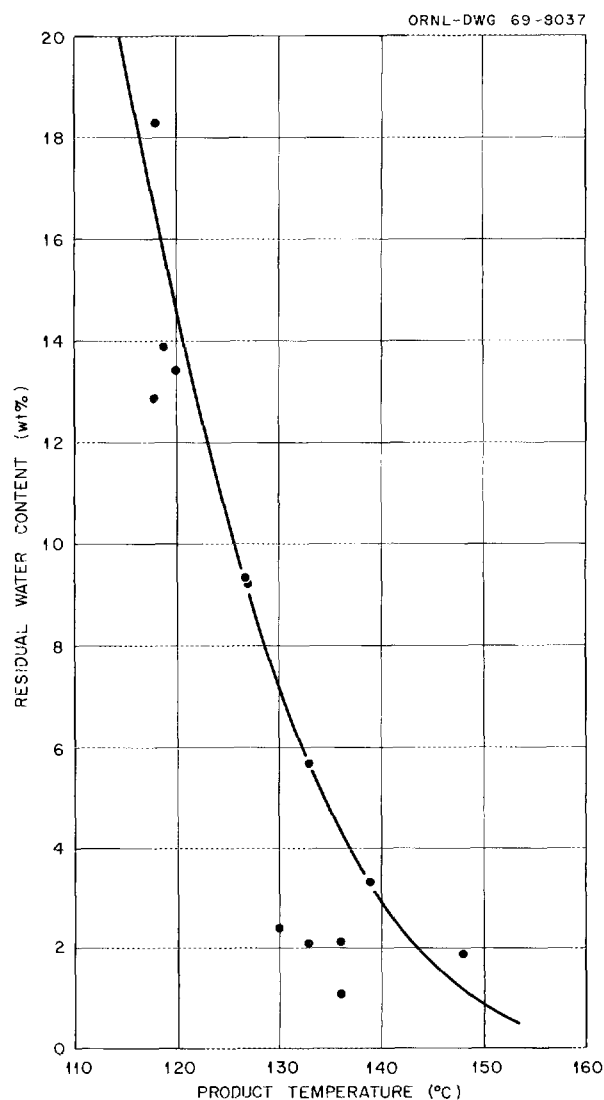


Fig. 4.10. Sodium Metaborate Waste in Asphalt: Residual Water vs Product Temperature.

Table 4.14. Incorporation of Sodium Metaborate Waste in Asphalt

Conditions: evaporator wall temperature, 200°C
 evaporator rotor speed, 295 rpm
 Pfaudler wiped-film evaporator, 4 ft² HTA
 with external condenser

Run No.	Run Time	Design Conditions				Experimental Results				
		Waste Feed (gph)	Asphalt Feed (gph)	Evaporator Boilup (lb/hr)	Solids Content of Product (wt %)	Evaporator Boilup (lb/hr)	Evaporator Decontamination Factor	Solids Content in Product (wt %)	Residual Water in Product (wt %)	Temperature of Product (°C)
1	3.0	8.59	3.31	80	50	77.7	1034	52.3	2.10	133
2	3.0	10.8	4.25	100	50	88.7	365	51.8	18.3	118
3	3.8	6.50	2.54	60	50	58.4	1242	52.0	3.32	139
4	2.5	6.74	2.81	60	50	57.2	1839	46.1	13.4	120
5	3.00	6.85	2.38	60	55	60.0	1973	56.9	5.68	133
6	3.00	7.75	2.74	70	55	65.1	989	50.5	12.86	118
7	2.83	8.80	2.82	80	55	75.0	1855	55.4	9.20	127
8	3.25	7.29	3.55	70	45	67.4	871	45.5	2.37	130
9	3.50	7.26	3.30	70	50	66.9	1764	48.4	1.08	136
10	10.0	7.24	3.62	70	45	62.3	777	39.4	13.9	119
11	10.0	7.19	3.29	65	45	64.0	1564	44.1	1.91	148
12	10.0	7.61	3.33	65	50	69.6	803	47.8	2.05	136

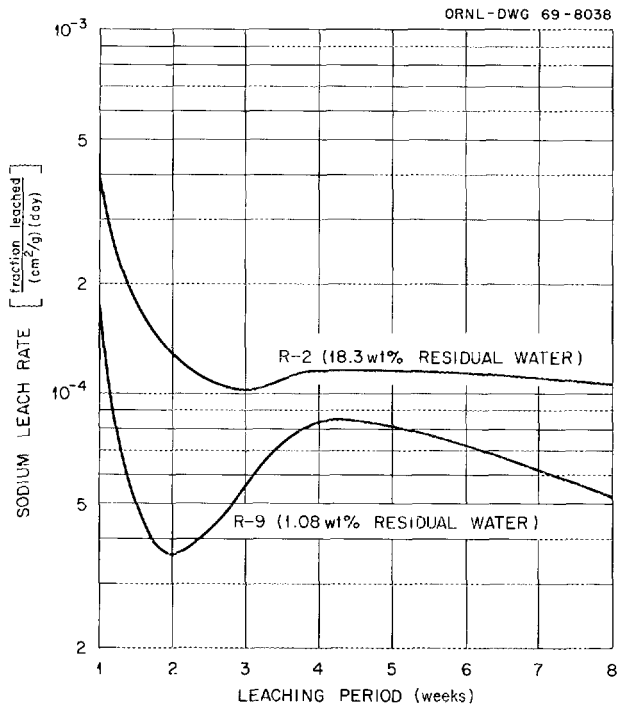


Fig. 4.11. Results Obtained During Static Leaching of Sodium Metaborate-Asphalt Products from Runs R-2 and R-9 with Distilled Water at Room Temperature.

ing runs R-2 and R-9. Leaching tests with the product from run R-2, which had a high water content, approached steady state after 8 weeks and showed a leach rate of approximately 1.0×10^{-4} expressed as fraction of sodium leached $(\text{cm}^2/\text{g})^{-1} (\text{day})^{-1}$. The leach rate for the product from run R-9, with a lower water content, was a factor of 2 lower for the same time period.

The evaporator and auxiliary equipment functioned very well. The decontamination factor for sodium from feed to condensate ranged from 350 to about 2000. The higher value is representative of recommended operating conditions. Solids buildup on the evaporator wall occurred during two runs using low processing rates. The nominal wiper blade wear in the region not affected by solids was less than 0.1 mil/hr, but increased to 2-3 mils/hr in areas where solids collected. Although the deposition of solids is a significant problem, it can be controlled by operating the evaporator at a lower wall temperature.

The 12 runs with simulated sodium metaborate waste conclude the engineering development of the waste-asphalt process. It has been demonstrated

that the process and equipment can be used to satisfactorily incorporate second-cycle Purex waste, aluminum decladding waste, ORNL evaporator concentrate, and sodium metaborate waste. The equipment is now being modified in preparation for demonstrating the incorporation of low- and intermediate-level waste in polyethylene.

4.4 SEPARATION OF RADIOACTIVE XENON AND KRYPTON FROM OTHER GASES BY USING PERMSELECTIVE MEMBRANES

A process is being developed for removing krypton and xenon from other gases by the use of permselective membranes.^{33,34} Separation is based on differences in the solubility of the gases in, and different rates of transport of the gases through, the membrane. Applications of this process to the nuclear industry include the removal of radioactive noble gases from: (1) the air within a reactor containment building after an accidental release of fission products; (2) the off-gas from a processing plant for spent reactor fuels; and (3) the gas that blankets nuclear reactors, such as the molten salt or certain sodium-cooled breeder reactors, which continuously vent volatile fission products.

This method for removing noble gases has process advantages which include: (1) small equipment, (2) operation at ambient temperatures, (3) ease of placement in standby and prompt reactivation, (4) absence of materials that could contaminate coupled systems, (5) absence of explosion and fire hazard, and (6) competitive capital costs.

Gas Transport in Improved Membrane Units

Significantly higher gas transport rates (permeabilities) were obtained by using new units with improved membrane supports. The calculated permeabilities of the gases previously obtained in the work at ORNL³⁵ were about 50% of the permeabili-

³³R. H. Rainey, W. L. Carter, S. Blumkin, and D. E. Fain, "Separation of Radioactive Xenon and Krypton from Other Gases by Use of Permselective Membranes," paper SM 110/27 presented at the IAEA Symposium on Operating and Developmental Experience in the Treatment of Airborne Radioactive Wastes, New York City, Aug. 26-30, 1968; published in the *Proceedings*, pp. 323-42.

³⁴*Nucl. Safety Program Ann. Progr. Rept. Dec. 31, 1968*, ORNL-4374, pp. 150-66.

³⁵*Chem. Technol. Div. Ann. Progr. Rept. May 31, 1968*, ORNL-4272, p. 86.

ties reported by Robb.³⁶ The membranes previously used at ORNL were bonded between two sheets of Dacron and supported on a polyester screen, whereas those used by Robb were unbonded. Recently, Briggs and co-workers at the General Electric Research and Development Center at Schenectady, New York, have developed improved methods for membrane support. Tests with the improved membrane system at ORNL (Fig. 4.12) showed permeabilities about 80% of those reported by Robb. Scientists at General Electric are continuing the development of membrane and expect to decrease the thickness of the membrane to about 1.0 mil from the 1.7 mils now used. A decrease in the thickness would produce a proportional increase in permeability.

The estimated cost of a membrane plant is nearly directly proportional to the membrane area; therefore, an increase in permeability would result in a proportional decrease in the estimated plant cost. On this basis, the separations equipment using the

improved membrane system in a plant for removal of noble gases would cost about 37% less than previous estimates.

Radiation Tolerance of Membrane Units

Calculations and laboratory measurements indicate that irradiation will not seriously limit the use of membranes for removing fission product noble gases in most applications. Irradiation of membrane units to 1×10^8 rads by a ^{60}Co source resulted in less than 10% change in permeability for the test gases (nitrogen, oxygen, and carbon dioxide). More experiments will be required to evaluate the effect of higher irradiation levels. The membranes in the sequential stages of a cascade for removing and concentrating radioactive noble gases would be exposed to a wide range of radiation exposure. The maximum exposure would occur in the top stage, where the gas is most highly concentrated; consequently, the radiation exposure in this stage is used as the limiting case.

The exposure of the membrane in the top stage of a cascade for removing noble gases from a reactor

³⁶W. R. Robb, *Thin Silicone Membranes - Their Permeative Properties and Some Applications*, Report 65-C-031, General Electric Company (October 1965).

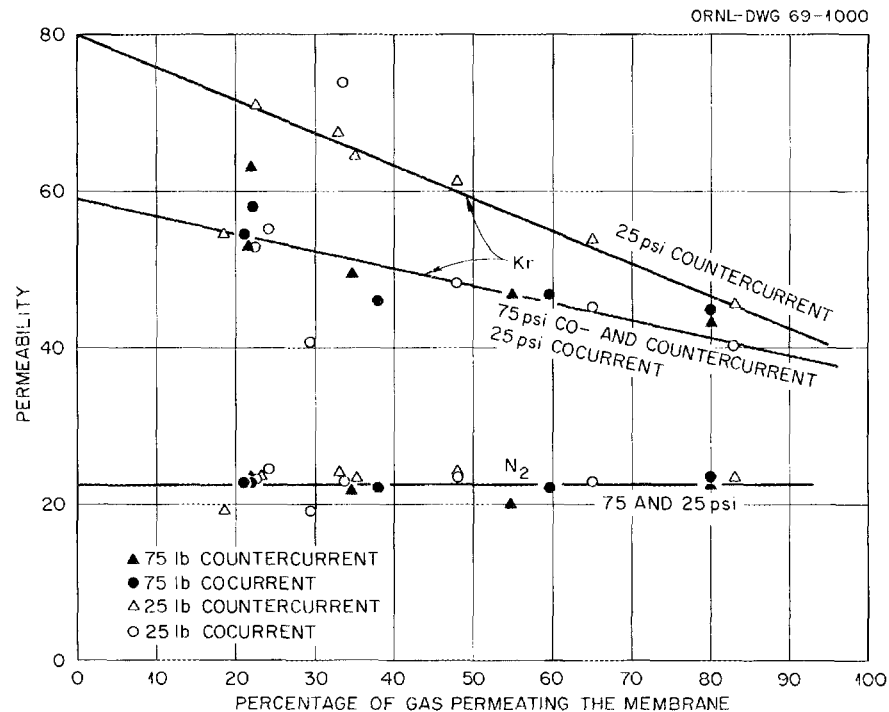


Fig. 4.12. Permeabilities of Krypton and Nitrogen as a Function of the Percentage of Gas Permeating the Membrane and the Pressure Drop Across the Membrane, Using the Improved Membrane Support System.

Table 4.15. Noble Gas Activity in the Shell, and Irradiation Exposure^a of Membrane During Removal of Noble Gases from Nuclear Containment Shell

Basis: Size, 3200 Mw (thermal)
 Flux, 3×10^{13} neutrons $\text{cm}^{-2} \text{sec}^{-1}$
 Fuel life, 625 days
 Fuel load, 100 metric tons
 Fuel enrichment, 2.3% ^{235}U
 Fuel irradiation, 20,000 Mwd/ton
 Containment volume, $3 \times 10^6 \text{ ft}^3$

	Decay Time Before Processing		
	30 Days	60 Days	120 Days
Kr activity in shell, curies	9.0×10^5	8.95×10^5	8.86×10^5
Xe activity in shell, curies	2.0×10^7	8.0×10^5	1.0×10^3
Initial Kr dose rate to membrane, rads/min	2.78×10^2	2.78×10^2	2.71×10^2
Initial Xe dose rate to membrane, rads/min	9.72×10^3	3.82×10^2	4.79×10^{-1}
Initial total dose rate, rads/min	9.99×10^3	6.59×10^2	2.71×10^2
Integrated dose during a 7-day processing period, rads	1.22×10^7	1.07×10^6	5.89×10^5

^aCalculated for the top stage of the cascade, where the noble gas concentration is 100 times higher than that of the feed.

containment building following a nuclear accident was calculated as a function of cooling time (Table 4.15). Assuming that the gases in the containment shell were allowed to decay for 30 days and were removed subsequently by a membrane plant during the next seven days, the integrated exposure to the top stage would be 1.22×10^7 rads. There would be no noticeable loss in membrane efficiency at this exposure. The exposure would increase proportionally with increased processing time.

The corresponding exposure of the top stage in a cascade for removing the noble gases from the off-gas of a facility processing 5 tons of fuel per day, assuming a 30-day cooling period, would be about 4×10^6 rads per day (Table 4.16). If the fuel were cooled 60 days instead of 30 days, the exposure would be about 6×10^5 rads per day.

Based on the above radiation stability limits, membrane replacement would not be required during the removal of noble gases from a reactor containment building after an incident. However, when the noble gases are continuously removed from the off-gas stream from a plant reprocessing 30-day-cooled fuel, replacement of the top stage (7 yd²) may be required after about 25 days (assuming an exposure of 10^8 rads). The membrane life in the second

Table 4.16. Noble Gas Activity in the Off-Gas from a Fuel Reprocessing Plant,^a and Exposure of Membrane

	Decay Time Before Processing	
	30 Days	60 Days
^{85}Kr , curies/ton fuel	3.395×10^4	2.383×10^4
^{131m}Xe , curies/ton fuel	1.477×10^4	3.134×10^3
^{133m}Xe , curies/ton fuel	2.958×10^4	3.503×10^{-3}
^{133}Xe , curies/ton fuel	1.935×10^5	3.742×10^3
Off-gas, ft ³ /min	100	100
Concentration factor, top stage	100	100
Concentration factor, second stage	43.5	43.5
Membrane exposure, top stage, rads/day	3.99×10^6	5.74×10^5
Membrane exposure, second stage, rads/day	1.74×10^6	2.50×10^5

^aPlant processing 5 tons/day of 30-day-cooled LMFBR fuel irradiated to 80,000 Mwd/metric ton in 540 days.

stage would be about twice as long as that of the top stage, and the life of other membrane units would be proportionally longer; about 20 years would be required to give the feed stage an equivalent exposure. As a result, the cost of membrane

replacement due to irradiation effects would not be more than \$4,000 per year. The life of the membrane in a plant processing 60-day-cooled fuel would be about seven times as long as with 30-day-cooled fuel.

5. Transuranium-Element Processing

The Transuranium Processing Plant (TRU) and the High Flux Isotope Reactor (HFIR) were built and are operating at ORNL to produce large quantities of the heavy actinide elements for research. The production for the USAEC Heavy Element Program is centered at these facilities. During this report period, which corresponds to the third year of the operation of these facilities, two major campaigns of processing target rods wholly irradiated in HFIR were conducted. The quantity of actinides produced during this period was more than twice that of the first two years combined. In addition, for the first time, fermium fractions were recovered. The major portions of the recovered elements were provided to research workers in 82 separate shipments. A major effort to study the behavior of iodine in TRU led to the demonstration of a satisfactory retention system on the plant ventilation streams. This will permit the processing of targets that have been cooled only one week.

5.1 TRU OPERATIONS

The major functions of the Transuranium Processing Plant (TRU) are: (1) to process targets that have been irradiated in the High Flux Isotope Reactor (HFIR) and to subsequently isolate and purify the transuranium elements and distribute the transcurium elements to researchers, and (2) to fabricate recycle targets containing americium and curium for additional irradiation in HFIR. TRU is primarily a production facility; however, many of the processes that are routinely employed at this facility are new and are actually being developed at the same time that they are being used to separate and purify the transuranium elements. For the foreseeable future, this development will continue, and, as the processes are proved to be satisfactory in the laboratory, they

will be scaled up and installed for use in main-line processing.

The purpose of this section is to report the production of transuranium materials and to describe recent changes in the equipment and the processes that are being used routinely in TRU.

Status and Progress

This was the third year of operation for TRU. During the first two years, all the processing and recovery steps through the initial partitioning of the transplutonium elements were demonstrated and used in the main-line processing plant in the processing of 27 target rods. The remote target fabrication line was used to fabricate six curium oxide recycle targets from oxides that had been produced in the sol-gel development program. Irradiation of these curium targets was begun in the HFIR.

Two target processing campaigns were completed this year. Fourteen plutonium targets and six curium targets were processed in the first and second campaigns respectively. From these campaigns, a total of 2.0 mg of ^{249}Bk , 14 mg of ^{252}Cf , 91 μg of ^{253}Es , and about 2×10^8 atoms of ^{257}Fm were recovered. The fermium fractions were the first ever recovered in usable amounts in TRU. In a third campaign, the remaining americium and curium was recovered from an SRP raffinate solution. Eighty-two shipments of transuranium elements were made to experimenters at ten laboratories throughout the country.

Permanent metal equipment was installed for the LiCl-based anion exchange process, and the Hepex solvent extraction process, which is an alternative method for partitioning the transplutonium elements, was demonstrated in a single full-scale test. Equipment and procedures for purifying americium-curium solutions (to remove

metal ions) prior to sol-gel processing were perfected, and equipment for forming microspheres of americium-curium oxide was installed and is being placed in operation.

No target failures were observed this year, even though a number of the targets have been irradiated in the HFIR to higher burnups than we had estimated would be required to cause failure.

A major accomplishment was the development of an off-gas treatment system for limiting the release of radioiodine from TRU during the processing of short-cooled HFIR targets. This system, which is composed of a caustic scrubber to remove acidic vapors, a heater, a bed of oxidation catalyst (operated at 350°C) to convert organic vapors to CO₂ and H₂O and protect the charcoal bed from being poisoned, a cooler, and a bed of KI-impregnated charcoal, decontaminated the vessel off-gas from ¹³¹I by a factor as high as 10⁴.

Production and Processing

The amounts of transuranium materials processed this year in the main-line plant are listed in Table 5.1. Campaign 9 completed the processing of the Savannah River Plant (SRP) raffinate solution that resulted from plutonium recovery processing. We recovered about 300 μg of a

special californium product from this SRP solution. Because it contained only 20% ²⁵²Cf (45% ²⁴⁹Cf, 25% ²⁵⁰Cf, and 10% ²⁵¹Cf) it emits much less hazardous radiation per unit mass than our usual californium product (80% ²⁵²Cf). Therefore, experiments can be done with about four times as much of this californium as with our usual californium, with no additional exposure to penetrating radiation.

Each of the 13 targets processed in campaign 11 originally contained 8 g of ²⁴²Pu in the form of calcined oxide. The targets had been irradiated since HFIR first went to full power in September 1966, and had received total exposures of from 37,000 to 41,000 Mwd. Campaign 10 consisted of the dissolution of a single rod and recovery of the plutonium by batch extraction, to test a newly installed iodine retention system. The resultant solutions were combined with the solutions in campaign 11 for complete processing.

Campaign 12 was the first campaign in which recycle curium targets were processed. Prior to irradiation, each of the targets contained 4.4 g of ²⁴⁴Cm, 0.3 g of heavier curium isotopes, and 0.8 g of ²⁴³Am that had been recovered in TRU from irradiated plutonium targets. The six targets had been fabricated in the remote target fabrication equipment in TRU, using americium-curium oxide powder which had been prepared during developmental studies of the curium sol-gel process.

Table 5.1. Amounts of Materials Processed During Major Campaigns in the Transuranium Processing Plant During the Period June 1968 to May 1969

Listed values are measurements or estimates of feed solutions

Campaign No.	9	10 and 11	12
Completion date	December 1968	September 1968	April 1969
Material processed	Remainder of SRP solution	Fourteen HFIR targets	Six curium targets
Amounts processed			
²⁴² Pu, g		17.1	
²⁴³ Am, g ^a	116.8	10.1	0.3
²⁴⁴ Cm, g ^a	129.8	40.6	17
²⁴⁹ Bk, mg		1.4	1.2
²⁵² Cf, mg	b	6.9	9.2
²⁵³ Es, μg		49	68

^aAmericium and curium are not usually separated from each other.

^b275 μg of total californium was recovered (48% ²⁴⁹Cf, 25% ²⁵⁰Cf, 9% ²⁵¹Cf, and 18% ²⁵²Cf).

that this solution had adequate capacity for dissolving aluminum, was less dense, and, most importantly, was much less viscous than the 6 M NaOH-3 M NaNO₃ solution used previously.

First-Cycle Solvent Extraction Process (Tramex)

The transplutonium elements are decontaminated from the lanthanide rare-earth elements and other major fission products by using the Tramex continuous solvent extraction process. In this process, the transplutonium elements are, first, extracted from 11 M LiCl-0.2 M HCl solution into a solution of Adogen 364-HP (a high-purity tertiary amine) in diethylbenzene and, then, are back-extracted into concentrated HCl.

The equipment used for Tramex was replaced during this report period because it was becoming increasingly difficult to operate due to corrosion, wear, and damage. The new equipment is operated with the organic phase continuous (OPC) instead of the aqueous phase continuous (APC). The primary advantage of OPC operation is that the Hepex process (see next section) can be carried out in the same equipment with only minor modifications. In the case of the Tramex process, there was not much difference between the performances of the two modes of operation. It was easier to control the interfaces in the organic-continuous equipment, and we were able to correct the problem with organic overflow to the off-gas header from the columns. However, these operational improvements could have also been designed into new aqueous-continuous equipment.

Partitioning of Actinides

Permanent tantalum equipment was installed for the LiCl-based anion exchange process for separating the transcurium elements from americium and curium. All product fractions were made based on continuous in-line alpha monitoring of the column effluent line and on neutron and gamma scans of the column. Such indications as the green color from nickel during its elution and the red glow from the curium band on the column were clearly not needed.

The Hepex solvent extraction process, which performs basically the same function as the LiCl anion exchange system, was tested in-cell using

the new Tramex equipment (modified slightly) and was demonstrated to be satisfactory for use in TRU. [However, the process, which is quite effective for large batches of americium and curium, will probably not be used very often at TRU because the LiCl-based anion exchange process is better suited for handling our usual batches (10 to 30 g).] About 275 μg of californium was separated from 100 g of curium and 90 g of americium. Material balances for californium and curium were 104 and 100.6% respectively. Two process upsets, which resulted from errors in operation due to our lack of experience, caused the californium product to be contaminated with some curium and americium. However, in the early part of the run, prior to the upsets, the californium decontamination factor was 7000 (the ratio of curium to californium in the feed was 7000 times the ratio in the californium product).

The Hepex flowsheet is given in Fig. 5.2. In this flowsheet, Tramex product solution is adjusted to Hepex feed (0.15 M HCl-1 M LiCl), which is fed to the top of the extraction column. The transcurium actinides are extracted into a solution of 0.8 M di(2-ethylhexyl)phosphoric acid (HDEHP) in Amsco 125-82 diluent, which is fed to the bottom of the extraction column. The americium-curium-bearing aqueous phase flows out the bottom of the extraction column to a product catch tank. The solvent is pumped to the scrub column, where small amounts of americium and curium are removed with 0.5 M HCl; then, in the strip column, the transcurium actinides are stripped into 5 M HCl.

Purification of Americium-Curium Products

Americium-curium product fractions from the actinide partitioning step must be purified (to remove metal ions) prior to sol-gel processing to form oxides for recycle to the HFIR. Equipment and procedures to effect the required purification, using oxalate precipitation, were successfully demonstrated in-cell; the procedures are described below.

Solution containing about 10 g of curium and americium is evaporated to a volume of two to three liters in a process evaporator and transferred by vacuum to a precipitator (glass) on the equipment rack in the cubicle. The HCl concentration of the resulting solution is adjusted to

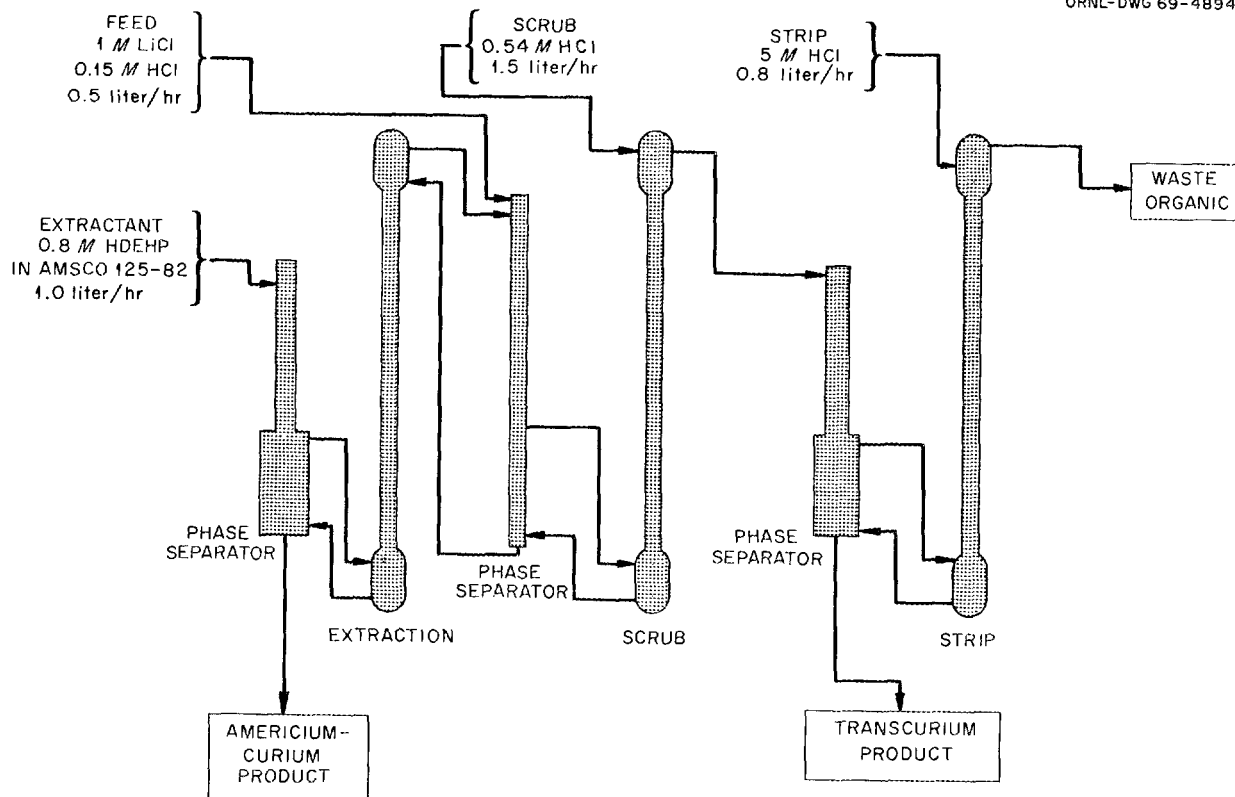


Fig. 5.2. Flowsheet for the Hexpex Process for Partitioning Actinides.

about 0.1 M, using NH_4OH . Then one liter of 0.8 M oxalic acid is added, at about 100 ml/min, to the stirred solution, and water is added to give a final volume of four liters. The resultant slurry, which is about 0.5 M HCl–0.2 M oxalic acid, is digested at 35°C for 20 min. The actinide oxalate precipitate is collected on a medium-frit glass filter, and the precipitator and the filter are flushed three times, using 0.5 liter of 0.5 M HNO_3 –0.2 M oxalic acid. The filter is kept flooded with the latter solution to prevent destruction of the oxalate precipitate by radiation heating. The solids collected on the filter are dissolved with 750 ml of 8 M HNO_3 . If additional purification is required, the product solution is returned to the precipitation tank and the process is repeated as needed (beginning with the partial neutralization using NH_4OH). Recoveries are usually high, but not quantitative; recycle streams result from most runs.

Preparation of Actinide Oxides for HFIR Targets

Most of the americium and curium that is recovered from irradiated targets is incorporated into recycle targets (in the form of americium-curium oxides in pressed aluminum pellets) and irradiated in the HFIR to produce transcurium elements. Last year¹ a sol-gel process for preparing oxides having suitable properties was developed. This year, equipment for use in TRU (Fig. 5.3) was fabricated, tested out-of-cell, using europium as a stand-in for curium, and installed in a TRU processing cell. Testing of procedures and equipment with americium and curium is in progress, using the method described in Section 5.3. The major difficulties encountered

¹Chem. Technol. Div. Ann. Progr. Rept. May 31, 1968, ORNL-4272, p. 110.

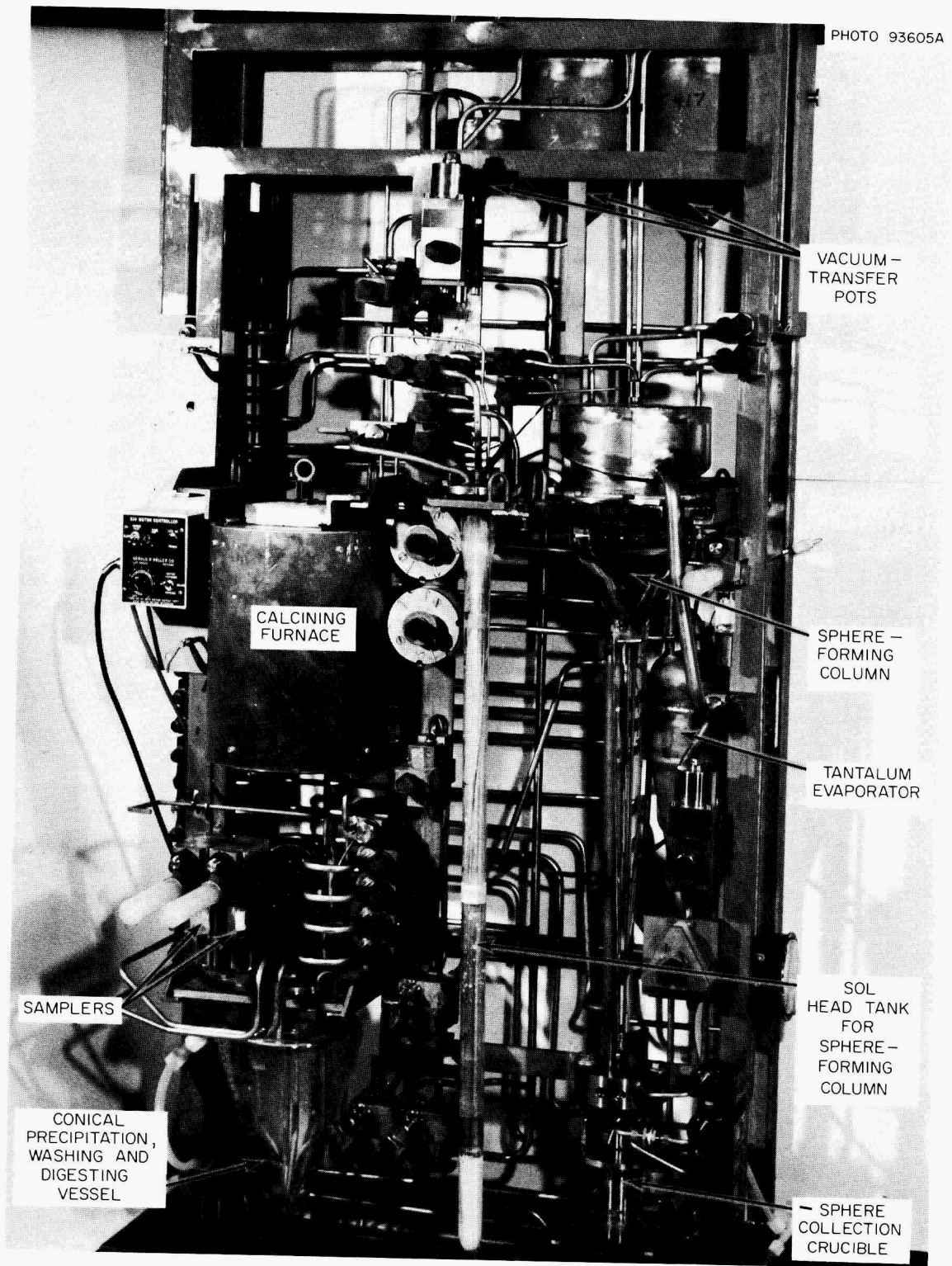


Fig. 5.3. Equipment for Producing Actinide Oxides Using the Sol-Gel Process.

thus far are: (1) high losses (up to 20%) during the washing of the americium-curium hydroxide in the conical washer during sol formation, and (2) clustering in the sphere-forming column.

We routinely produce sols that are stable for as long as 24 hr and are now searching for run conditions, and the combination of drying solvent and additives, that will result in the formation of satisfactory gel microspheres. In the early runs, coalescing and clustering problems have resulted in very low yields in the sphere-forming step.

Target Fabrication

The remote equipment installed in cells 1, 2, and 3 in TRU was used to fabricate three second-cycle curium targets and nine plutonium targets this year. The plutonium targets were fabricated in-cell because this was more convenient than duplicating the fabrication equipment in a glove box.

Fourteen rabbits were fabricated for irradiation in the HFIR hydraulic rabbit facility: one that contained ^{249}Bk , which was irradiated to allow us to search for short-lived neutron emitters; five that contained ^{252}Cf , which was irradiated to produce ^{253}Es ; and eight that contained ^{253}Es , which was irradiated to produce $^{254\text{m}}\text{Es}$ for use at ANL in studying the energy level structure of the alpha-decay product, ^{250}Bk (see Sect. 5.4).

A rabbit for the HFIR (Fig. 5.4) is fabricated from the same extruded, finned aluminum tubing that is used to fabricate TRU-HFIR targets. The material to be irradiated is either deposited (by evaporating a solution) in a quartz vial, which is sealed by melting, or encapsulated in a pellet, similar to a regular target pellet, in which the actinides have been dispersed in some kind of matrix material. One quartz vial and one pellet are shown in Fig. 5.4; however, a given rabbit could contain any combination of vials and pellets.

Details of these activities are reported through the Metals and Ceramics Division.

Irradiation of ^{252}Cf to Produce ^{253}Es

Last year, when special targets containing ^{252}Cf were irradiated for three to five reactor cycles in the HFIR target island in order to produce ^{253}Es , we found that the disappearance cross section of ^{252}Cf was much higher than we had previously estimated.² Thus, the irradiation times that had been used were much too long for optimum einsteinium production, causing a significant fraction of the californium to be consumed in nonproductive reactions.

Two rabbits containing a few micrograms of ^{252}Cf were irradiated in the HFIR hydraulic rabbit facility for three and eight days, respectively, to obtain data on the capture cross section of ^{252}Cf . The activation cross section of ^{252}Cf (to ^{253}Cf) appeared to be about 20 barns, which is in good agreement with the values measured recently in the Oak Ridge Research Reactor (ORR) by Bemis and Halperin.³ We calculated a ^{253}Cf fission cross section of 1300 barns, which indicates that, during irradiation in the HFIR, nearly 90% of the ^{253}Cf fissions instead of decaying to ^{253}Es , the desired product.

These studies showed that the optimum irradiation period for producing ^{253}Es is less than one reactor cycle. Therefore, we experimented with methods for loading significant amounts of ^{252}Cf into pellets for short-term rabbit irradiations (see Sect. 5.3). A method using CeO_2 microspheres as

²Chem. Technol. Div. Ann. Progr. Rept. May 31, 1968, ORNL-4272, p. 113.

³J. Halperin, C. E. Bemis, Jr., and R. Eby, Chem. Div. Ann. Progr. Rept. May 20, 1967, ORNL-4306, p. 31.

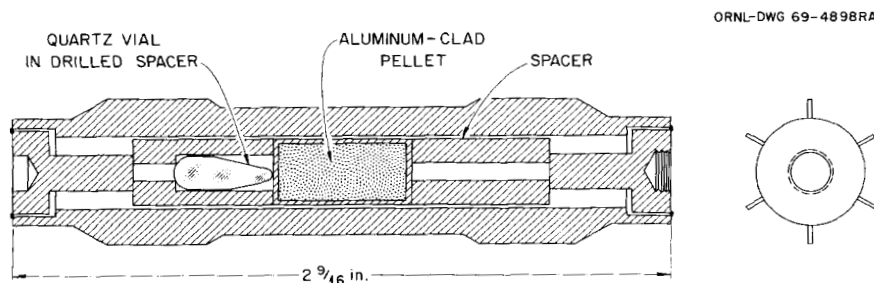


Fig. 5.4. TRU-HFIR Hydraulic Rabbit.

a carrier was developed, and a rabbit containing 10 μg of ^{252}Cf was fabricated and irradiated for a period of 16 days to test this concept. Since processing of the irradiated rabbit revealed no difficulties, we prepared our remaining ^{252}Cf (approximately 2.3 mg) in a similar form.

The four pellets, containing a total of 2.3 mg of ^{252}Cf , were fabricated into two HFIR rabbits. These rabbits were irradiated intermittently in the hydraulic tube for a total of 10 days (four irradiation periods separated by 10 to 18 days for decay). We recovered 12 μg of einsteinium that was rich in ^{254}Es and ^{255}Es . The californium product was stored to permit ^{253}Cf to decay to ^{253}Es ; after a suitable period, 6 μg of ^{253}Es was recovered in a second cycle of processing.

Following the campaign in which six curium targets were processed, all of the available ^{252}Cf (about 7 mg) was incorporated into rabbits. This californium is now being irradiated to produce more einsteinium.

Iodine in TRU

It is desirable to dissolve and process irradiated targets very soon after they are removed from the HFIR in order to recover the maximum possible amount of the short-lived ^{253}Es ($t_{1/2} = 20$ days). A major obstacle to processing after short cooling periods is the presence of about 200 curies of ^{131}I in each target when it is removed from the reactor.

We have made five processing campaigns in which there was a significant amount (20 to 460 curies) of ^{131}I present. In successive campaigns, beginning in 1967 (when we processed three SRP slugs containing 20 to 30 curies of iodine and merely observed the behavior of iodine), we have increased our efforts to study and control iodine in TRU. Before our latest campaign, in which we processed six curium recycle targets, a special group was organized to make a concentrated study of the behavior of iodine in TRU process solutions and of methods for trapping radioiodine from process off-gas streams. In addition to TRU personnel, the study group consisted of personnel from the Chemical Technology Division, the Reactor Chemistry Division, and the Analytical Chemistry Division. The equipment and techniques that evolved from this effort were successful in controlling the release of radioiodine during

the campaign to process six curium targets, which contained a total of 400 curies of ^{131}I ; only 300 mc was released from TRU during seven weeks of processing. The special steps that were made to control the release of radioiodine are discussed below.

Plant piping was modified so that all process and waste solutions that would contain significant amounts of radioiodine would be handled and stored in tanks that were vented through the condensate collection system for the dissolver and the seven process evaporators. Thus, most of the iodine-bearing off-gas was confined to a 3-cfm stream instead of being spread throughout the 350-cfm vessel off-gas (VOG) stream. An experimental iodine-removal system, consisting of a caustic scrubber to remove acidic vapors, a heater, a bed of oxidation catalyst (Hopcalite) to convert organics to CO_2 and H_2O and protect the charcoal trap from organics, a cooler, and a charcoal trap, was placed in the 3-cfm off-gas stream. Hopcalite (a proprietary material of the Mine Safety Appliances Company) is a CuO-MnO_2 mixture that has been treated to give a large surface area. A few tests indicated that it would decompose TRU organics at 300 to 350°C. Previous attempts to trap radioiodine, using beds of KI-impregnated charcoal, had been unsuccessful because organic solvents, which are used in various processing steps, were transported to off-gas streams in amounts that quickly poisoned the beds against iodine retention. We did not study Hopcalite exhaustively; no other catalysts were tested.

The process for removing iodine from the condensate system off-gas is shown in Fig. 5.5. After the gas is scrubbed to remove HCl vapors, it is heated electrically and passed to the bed of catalyst, which is kept at 650°F (350°C). The effluent from the catalyst is cooled, passed through a 7-in.-thick bed of KI-impregnated charcoal, and then added to the main vessel off-gas. The charcoal bed is operated at about 120°F.

Sodium hypochlorite (NaOCl) was added to all waste caustic streams and to the makeup caustic for the scrubber in the iodine treatment system to oxidize the iodine to the nonvolatile iodate or periodate form. In previous campaigns, we had released radioiodine when we transferred radioactive caustic solutions. Apparently, volatile forms of iodine are present in aged radioactive caustic solutions. This is contrary to the behavior in nonradioactive caustic solutions in which

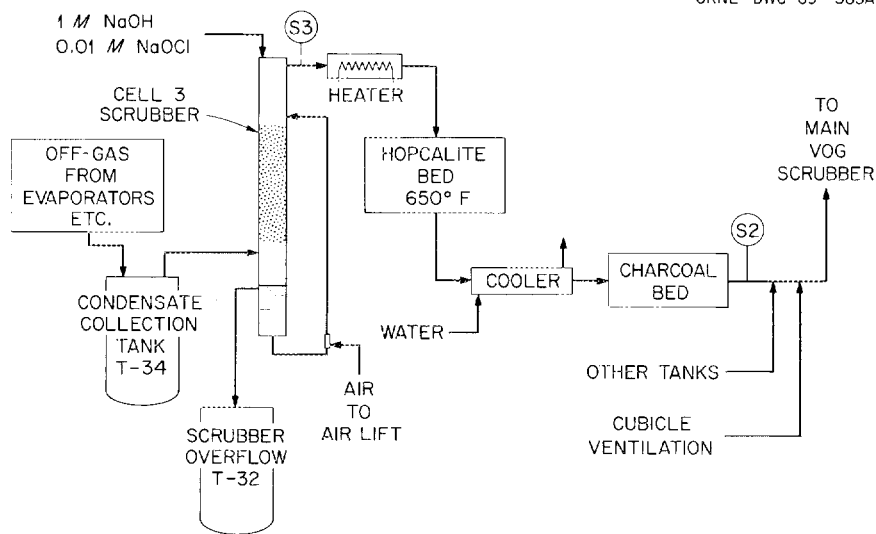


Fig. 5.5. Iodine-Removal Process for the Condensate-Collection System Off-Gas.

iodine is found only in the nonvolatile forms (iodide and iodate).

The Pubex processing step was performed in this campaign merely to remove radioiodine from the feed solution prior to the Tramex processing step; there was no valuable plutonium in the targets. In the Pubex process, iodine reports almost quantitatively to the solvent. Adogen 364-HP (0.1 M) was added to the solvent because laboratory tests had shown that it improved iodine extraction; also, we had hoped that the amine might form stable complexes with the iodine.

Of the 300 mc of ^{131}I released during the campaign, only 6 mc was released from the 3-cfm treatment system; the remainder bypassed the treatment system either from tanks that were not vented through the treatment system or by direct release from the processing cubicles.

Although iodine material balances were poor in many cases, we accounted for about 340 of the 400 curies of ^{131}I we had estimated to be present in the targets; 100 curies was in the caustic de-jacketing waste, 220 curies was in the acid feed for the Pubex process, and 20 curies was in the condensate collection tank at the end of the feed adjustment step.

We did not notice any significant difference between the behavior of iodine in the Pubex steps in this campaign (with amine) and in the previous campaign (without amine). The amount of extracted iodine was the same in each case, and about 0.5 curie was left in the Tramex feed. A small amount

of iodine was volatilized during the stripping step (when we added reductant to the solvent and air sparged).

The NaOCl that was added to the waste caustic streams was effective in keeping the iodine in nonvolatile forms. On one occasion, we tried to release about one curie of iodine from some of the caustic waste by acidifying the waste to 2 M HNO_3 , adding some ferrous sulfamate as a reductant, and air sparging. However, essentially no iodine was evolved. This can be compared with our experience in the previous campaign in which, after about the same one-month aging period, almost 10% of the contained iodine was released from some de-jacketing waste by merely pumping it from one tank to another.

Samples of the 3-cfm VOG stream were taken at two locations: between the scrubber and the heater, and following the charcoal bed. The total VOG stream, which included the 3-cfm condensate-collection system VOG, about 10 cfm of off-gas from other vessels, and 300 cfm of cubicle and shielded cave ventilation, was sampled between the main plant VOG caustic scrubber and the VOG system absolute filters. The gas samplers, which were similar to those described by Bennett, Hinds, and Adams,⁴ were connected to the VOG ducts

⁴R. L. Bennett, W. H. Hinds, and R. E. Adams, *Development of Iodine Characterization Sampler for Application in Humid Environments*, ORNL-TM-2071 (May 1968).

by means of about 50 ft of $\frac{3}{8}$ -in.-diam stainless steel tubing. Although one might expect this much tubing to cause erratic sample results, the daily iodine content, as indicated by the sampler for the 350-cfm stream, agreed closely with the official HFIR stack monitoring results.

The 3-cfm condensate-collection system VOG stream was decontaminated from ^{131}I by a factor (DF) of 4×10^3 to 1×10^4 during the dejacketing and acid dissolution steps. During the Pubex solvent extraction step, the DF appeared to decrease to 30; however, condensate observed in the rotameter on the line sampling the inlet to the system at this time probably introduced errors into the data. For the next week, during Tramex processing, this stream was not sampled. When we returned the sampler to service (during cleanup operations following the Tramex run), the DF had increased to 500. The average DF for the entire campaign (except during Tramex processing) was about 400.

The only significant difficulty we experienced during the test was the tendency of the Hopcalite bed to overheat (from heat of combustion) when we sparged a tank containing organic materials. We had to balance sparging rates and power input to the heater very carefully in order to keep the bed at the proper temperature. This would not be a problem in a larger system in which the concentrations of organics in the off-gas would be lower.

After the campaign was essentially finished, we decided to determine the effects of varying the temperatures of the Hopcalite bed and the charcoal trap. We found that if we increased the temperatures to 800°F and 200°F , respectively, DF's approaching 5×10^3 were obtained and the iodine content in the effluent returned to the very low level (0.006 mc in two days) that we had observed at the beginning of the campaign. When we lowered the temperatures (the Hopcalite to 500°F , and the charcoal to 120°F), the DF decreased to about 100.

When we again increased the temperatures of the Hopcalite and the charcoal to 800 and 200°F , respectively, the DF again increased to about 3×10^3 . Thus, it appears that we can vary the DF by varying these temperatures. Possibly the major effect of varying the Hopcalite and charcoal temperatures is the resulting change in the relative humidity of the off-gas going to the charcoal. Varying the humidity could certainly change the efficiency of the charcoal for methyl iodide retention.

The results obtained during the campaign described above indicate that in future processing we can expect to maintain an iodine DF of 10^3 to 10^4 . This is certainly satisfactory for processing short-cooled targets. We are now investigating a larger system for installation in the total vessel and cubicle off-gas system (350 cfm).

HFIR Target Rod Failures

There have been no target failures since the first group,⁵ which had been irradiated for about one year in a Savannah River Plant reactor and ruptured after additional irradiation in the HFIR.

The engineering model formulated to predict target failures, which was discussed in the previous progress report, indicated that the 13 targets processed in campaign 11 should fail at a burnup of 0.46 fission per original plutonium atom. However, inspection of these targets, after irradiation to burnups of from 0.48 to 0.52 fission per original plutonium atom, disclosed no failures. A similar target has now been irradiated to 0.68 fission per original plutonium atom without failure. We plan to continue irradiating this target until the spring of 1970 (about 0.77 fission per original plutonium atom) or until the cladding ruptures.

Analysis of ^{252}Cf by Neutron Activation of Aluminum

We are developing a nondestructive technique for assaying the ^{252}Cf contents of neutron sources and californium shipping containers. At present, we must depend on the relatively unsatisfactory practice of estimating the amounts of ^{252}Cf in such materials from measurements of product and waste solutions. In the new method, weighed discs of aluminum are activated by the fast-neutron emissions from ^{252}Cf and are then assayed by gamma-ray spectrometry for the activation product, ^{24}Na . Problems that we hope to resolve, or circumvent, by calibration procedures are: (1) uncertainty of the detailed neutron energy spectrum of ^{252}Cf fission, (2) uncertainty in the fine structure of energy dependence of the aluminum activation cross section, and (3) uncertainty of the geometry and efficiency of counting gamma-ray emissions from ^{24}Na .

⁵Chem. Technol. Div. Ann. Progr. Rept. May 31, 1968, ORNL-4272, p. 98.

Four pellets containing ^{252}Cf (which were subsequently made into HFIR rabbits) were measured using the new technique. Six discs were exposed to each pellet, at distances of 1, 2, and 4 in. on either side. Each disc was counted twice. The inferred loading of each pellet (in μg of ^{252}Cf), and the standard deviation of the measurement, are tabulated below:

Pellet No.	First Counting	Second Counting
CE-1	$576 \pm 1.1\%$	$584 \pm 4.7\%$
CE-2	$697 \pm 1.7\%$	$681 \pm 1.5\%$
CE-3	$659 \pm 2.0\%$	$631 \pm 3.0\%$
CE-4	$1038 \pm 1.1\%$	$1019 \pm 1.1\%$
	Total 2970	Total 2915

Subsequent measurements of solutions of the dissolved pellets showed that the actual ^{252}Cf content was somewhat lower; however, the precision is considered to be excellent for sources containing a few hundred micrograms of ^{252}Cf .

5.2 ISOLATION AND PURIFICATION OF TRU PRODUCTS

Product finishing operations and the final purification and isolation of transplutonium elements are accomplished in equipment that is installed in cell 5 in TRU and in supporting shielded-cave facilities.

Special separations and the final processing of main-line products will continue to be performed in the cell 5--shielded cave complex because the equipment and the handling procedures available there are optimum for present program needs. When products reach certain levels of purity, they must be moved to progressively cleaner facilities and, finally, to shielded caves or to glove boxes that are used only for handling products. These operations are the main subject of this section.

Status and Progress

Tramex products are processed routinely in the plant equipment by an LiCl -based anion exchange method to provide additional decontamination and to separate the products into two fractions: an americium-curium fraction and a transcurium frac-

tion. Further processing of these fractions was continued in cell 5 by procedures which have been previously described.⁶ Portions of the americium-curium products were processed to separate the contained elements by selectively precipitating americium as an Am(V) -potassium double carbonate. Berkelium was separated from residual actinides by oxidation to Bk^{4+} by NaBrO_3 and subsequent extraction from 8 M HNO_3 into di(2-ethylhexyl)phosphoric acid (HDEHP). Fermium, einsteinium, and californium were isolated from each other and from other residual actinides by selective elution from cation exchange resin with ammonium α -hydroxyisobutyrate. Purified products from these separations included 40 g of ^{244}Cm , 10 g of ^{243}Am , 1.6 mg of ^{249}Bk , 17 mg of ^{252}Cf , 88 μg of ^{253}Es , and approximately 3×10^8 atoms of ^{257}Fm .

Various special separations were also made; these include: isolation of 24 μg of second-growth ^{253}Es (daughter of ^{253}Cf) and 260 μg of ^{248}Cm , both of which had grown into the purified californium products during storage, and separation of 50 μg of ^{249}Cf that had grown into ^{249}Bk . In other processing, approximately 3 g of curium containing 9% ^{246}Cm was purified from residual americium and converted to the oxide for calutron separation of ^{246}Cm ; approximately 4 g of curium with a high concentration of ^{245}Cm was similarly processed for calutron separation of ^{245}Cm ; and 275 μg of californium rich in the 249, 250, and 251 isotopes, which had been isolated in the full-scale Hepex test from about 100 g of aged Savannah River curium, was purified.

Berkelium-Californium-Einsteinium-Fermium Separations

The results obtained with the high-pressure ion exchange column in separating californium and einsteinium at high activity levels have continued to be very encouraging. In this separation, which involves chromatographic elution from cation exchange resin with α -hydroxyisobutyrate solution, a high-pressure feed pump makes it possible to maintain a constant, rapid flow through a long bed of finely divided resin. The resulting shorter processing time decreases radiation

⁶Chem. Technol. Div. Ann. Progr. Rept. May 31, 1967, ORNL-4145, pp. 136-51.

damage to the resin and suppresses the formation of radiolytic gas during processing. Typical elutions with this system yield product fractions that contain greater than 99% of the desired element with less than 1% cross-contamination, as compared with 80 to 90% yields in the product fraction and 10% cross-contamination for conventional ion exchange column operation.

Using the equipment and process conditions described last year,⁷ numerous separations were made in which the feed typically contained californium and einsteinium at a mass ratio of 200:1, while product fractions contained greater than 99% of the respective elements with substantially less than 1% cross-contamination. The largest quantity of material processed in a single run was approximately 200 mg of ^{244}Cm , 8 mg of ^{252}Cf , and 60 μg of ^{253}Es . The einsteinium fraction contained less than 2 μg of ^{252}Cf , which represents a californium decontamination factor of greater than 1000. A plot of the in-line alpha detector output is shown in Fig. 5.6. The fer-

⁷Chem. Technol. Div. Ann. Progr. Rept. May 31, 1968, ORNL-4272, pp. 100-1.

mium, einsteinium, and californium were eluted with 0.25 M ammonium α -hydroxyisobutyrate (AHIB) at pH 4.20. After the californium was eluted from the column, the berkelium and curium were eluted with 0.4 M AHIB at pH 4.80. The berkelium was subsequently recovered from the curium by oxidation with NaBrO_3 and extraction into HDEHP, as previously described. The recovered berkelium was processed through several cycles to yield an ultrapure product. Typically, the berkelium contained less than 5 at. % metal ion contaminants. The only detectable radioactive contaminant was ^{249}Cf .

Isolation of Second-Growth Isotopes

The isolation of isotopically pure second-growth isotopes such as ^{248}Cm (daughter of ^{252}Cf) and ^{249}Cf (daughter of ^{249}Bk) is becoming an increasingly important part of the transplutonium element production program.

About 300 μg of curium containing 260 μg of ^{248}Cm was recovered from 2.7 mg of ^{252}Cf by high-pressure ion exchange. This material was

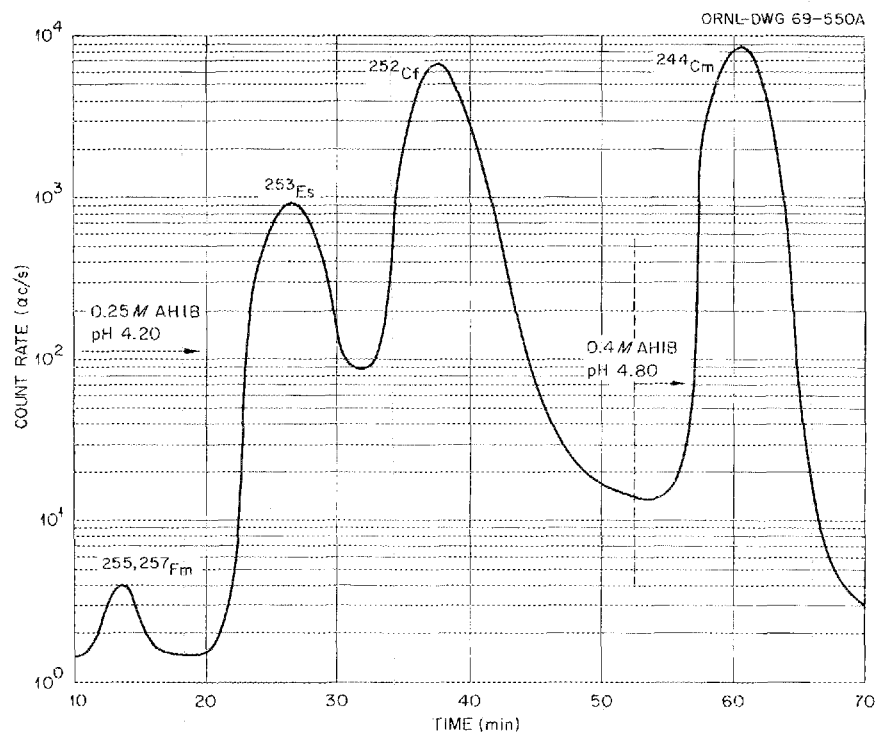


Fig. 5.6. Typical Separation of Actinide Elements on a High-Pressure Column as Indicated by an In-Line Alpha Detector.

about 90 at. % ^{248}Cm (Table 5.2). A small amount of ^{244}Cm was present as the result of either incomplete separation during initial ^{252}Cf isolation or equipment contamination during subsequent processing. This material will be used for cross-section measurements and for irradiation to produce ^{250}Cm .

Although ^{249}Cf is not produced as a main-line TRU product, 50 μg of this isotope was recovered from the ORNL allotment of ^{249}Bk . This material was sent to the University of California at Berkeley and was successfully used as cyclotron target material to produce an isotope of element 104 by the reaction $^{249}\text{Cf}_{98}(^{12}\text{C}_6, 4n)^{257}(104)$.

A special batch of californium (with high ^{249}Cf and ^{250}Cf contents) was recovered from about 100 g of curium that had been produced earlier at Savannah River. The mass analysis of the californium product (275 μg) is given in Table 5.2. Preliminary separations and purifications were done in plant equipment, using the Tramex process for rare-earth decontamination and the Hepex Process (see Sect. 5.1) for separation of californium from the curium. The californium fraction from Hepex processing, along with 600 mg of ^{244}Cm , was isolated and purified by high-pressure ion exchange. This californium will be used for

chemical experiments, for cross-section measurements, and as isotope separator feed to obtain higher mass concentrations of $^{250-251}\text{Cf}$.

5.3 DEVELOPMENT OF CHEMICAL PROCESSES

Laboratory support was provided to investigate chemical problems that arose during high-activity-level processing in TRU. We continued the development of processes to prepare oxides for HFIR targets and special irradiations; also, ^{252}Cf source fabrication methods were developed. In addition, we continued to investigate methods for separating californium, einsteinium, and fermium, recovering plutonium, partitioning actinides, and isolating berkelium.

Status and Progress

The development of the sol-gel method for preparing americium-curium oxide microspheres was continued. Operations in the hot cell demonstrated the feasibility of the process and produced a total of 31 g of mixed oxides, which has since been fabricated into HFIR targets. During the preparation of this material, simplified equipment concepts for sol preparation were demonstrated in which the precipitated metal hydroxide was washed in an inverted-cone fluidized-bed washer.

A technique for incorporating milligram quantities of ^{252}Cf into HFIR target pellets was also developed and demonstrated. This technique consists in adding californium nitrate solution to a rare-earth sol, which is then formed into microspheres and incorporated into pellets. Three additional techniques were developed for preparing alpha-contained sources of ^{252}Cf . These entail: (1) encapsulation of the californium in a small quartz sphere (approximately 3 mm), which can then be welded into a small metal container; (2) adsorption of californium on ion exchange resin in a standard aluminum pellet liner (the resin is subsequently pyrolyzed, and the pellet is pressed); and (3) electrodeposition of californium on platinum or stainless steel plates. Deposition of 400 μg of metal per square centimeter of plate area has been demonstrated.

The laboratory development of high-pressure ion exchange technology was continued. Feed adjustment and column operating procedures for

Table 5.2. Isotopic Compositions of Special TRU Products

Isotope	Abundance (%)	% Alpha Emission	% Neutron Emission
A. Curium			
^{244}Cm	7.86	99.83	2.12
^{245}Cm	0.12		
^{246}Cm	2.71	0.11	0.95
^{247}Cm	0.04		
^{248}Cm	89.27	0.056	96.93
B. Californium			
^{249}Cf	47.23	1.61	
^{250}Cf	24.09	19.45	0.19
^{251}Cf	9.03	0.12	
^{252}Cf	19.63	78.77	99.81
^{253}Cf	0.02		

transcalifornium element separations were optimized and are now considered to be completely reliable. Development emphasis was, therefore, shifted to other chemical systems that may eventually result in improved alternative flowsheets for some of the present existing processes. Studies of the LiCl-based system, using high-pressure technology, have been started. Long-range objectives include providing a one-stage flowsheet for processing a single target that bypasses the Pubex and the Tramex processes. Preliminary studies of fission product behavior were made, and results showed that no individual fission product appears to offer any serious problems in decontamination. Aminopolyacetic acid systems for actinide-lanthanide group separation and actinide partitioning reduce corrosion problems, but they are chemically complex. However, the variety of ligands available for study afford good promise of accomplishing the desired separations.

Laboratory development of the Pubex, Hepex, and modified Berkex processes was continued. These processes are now sufficiently optimized to meet present program needs.

Laboratory studies to assist in minimizing the release of radioiodine during HFIR target processing campaigns were initiated, and minor process changes were suggested. The installation of a new method of trapping in the off-gas system has greatly improved iodine retention; however, the chemistry of iodine in process solutions is not well understood and analytical methods for iodine detection are marginal.

Preparation of Actinide Oxides for HFIR Targets

As reported last year,⁸ the rare-earth sol-gel process⁹ was successfully adapted for the preparation of mixed ²⁴⁴Cm-²⁴³Am sols and used to produce 38 g of americium-curium oxide. During this report period, an additional 31 g of oxide was prepared, and simplified equipment concepts for sol preparation were demonstrated.

⁸Chem. Technol. Div. Ann. Progr. Rept. May 31, 1968, ORNL-4252, pp. 111-13.

⁹C. J. Hardy, S. R. Buxton, and M. H. Lloyd, *Preparation of Lanthanide Oxide Microspheres by Sol-Gel Methods*, ORNL-4000 (1967).

Sol Preparation. — Prior to sol preparation, the feed material was purified by an oxalate precipitation-calcination cycle since previous experiments had indicated that high-purity material is required for optimum sol preparation. Batch sizes in these experiments varied from 8 to 10 g of total metal (16% ²⁴³Am, 78% ²⁴⁴Cm, 6% higher curium isotopes).

Sol preparation requires precipitation of the metal hydroxide by adding a dilute solution of the metal nitrate to a large excess of 8 M NH₄OH, washing the hydroxide to a final pH of about 9, and heating for 1 to 2 hr at 85°C. During heating, the resulting paste is converted to a fluid sol that can be concentrated by evaporation. In previous experiments, the hydroxide precipitate was washed by filtration; however, in five consecutive runs, an inverted-cone fluidized-bed washer was used. This washer appears to be more amenable to remote handling operations.

A fluid sol with good physical characteristics was obtained in each run. The precipitated hydroxide was added to the three-liter wash vessel and was fluidized by introducing wash water at the bottom of the vessel. The behavior of the hydroxide during washing was satisfactory. The bed volume during washing (at a flow rate of 250 ml/min) was approximately 1500 ml; approximately 20 liters of wash water reduced the pH of the wash effluent to a satisfactory level (<9). The bed was not disrupted by radiolytic gas evolution. Curium losses due to peptization were generally about 3%. After being washed, the precipitate was allowed to settle, and was then removed from the washer and digested for 2 hr at 80°C to form the sol.

In the first run, the feed acid concentration was 0.9 M and the NO₃⁻/metal mole ratio of the final sol was 0.65, which is undesirably high. In subsequent runs, feed acid concentrations ranging from 0.05 to 0.28 M were used, and final sols with satisfactory NO₃⁻/metal ratios (0.02-0.17) were obtained. It appears from these data that feed acid concentration is an important variable and that a concentration of about 0.1 M is desirable.

Microsphere Preparation. — Gel microspheres were formed at sol concentrations of 0.11 to 0.13 M, using standard sphere-forming techniques. 2-Ethyl-1-hexanol containing 0.4 vol % Span 80 and 0.6% Amine O was used as the drying alcohol in the sphere-forming column. There was a general tendency for particle clustering to occur late in

a run; however, this effect was not severe when sols with $\text{NO}_3^-/\text{metal}$ ratios of 0.1 or less were used. More severe clustering occurred earlier in the run in which a sol with a $\text{NO}_3^-/\text{metal}$ ratio of 0.17 was used, while the sol with a $\text{NO}_3^-/\text{metal}$ ratio of 0.65 could not be used to form microspheres because of very severe clustering which occurred almost immediately.

The gel microspheres were removed from the column and air dried overnight in an open container prior to calcination in air at 1150°C . The calcined spheres were free flowing, dust-free in appearance, and showed no tendency to crack or disintegrate. Calcined microspheres that have been stored in air for more than a year show no visible sign of alteration or disintegration.

^{252}Cf Target Preparation and Actinide Source Fabrication Methods

In addition to continuing main-line target preparation, we developed a technique for preparing HFIR targets containing milligram quantities of ^{252}Cf , and three methods for preparing alpha-contained actinide sources.

Preparation of ^{252}Cf Targets for HFIR Irradiation. — Four pellets that contained a total of 2.7 mg of ^{252}Cf were prepared. The preparation procedure involves the addition of californium nitrate solution to a cerium hydroxide sol, which is then formed into microspheres, mixed with aluminum powder, and pressed into pellets.

In order to determine the feasibility of this method, a series of experiments were performed, using hydroxide sols of Ce, Ni, Fe, and Zr. These particular metals were chosen because of their low neutron cross sections, the existing technology for the preparation of their sols, and the ease of separation of these metals during postirradiation processing.

The sols of the four metals were prepared by hydroxide precipitation techniques, and the tolerances of the sols to nitrate were investigated. Using europium as a stand-in for californium, it was determined that Ni, Ce, and Zr sols would tolerate up to one equivalent of nitrate per mole of metal, while the iron sol became thixotropic on addition of nitrate. However, during microsphere formation, only the cerium sols formed satisfactory gels that could be calcined to dense

oxide particles; therefore, cerium was chosen as the starting material for the host sol.

The process used to prepare ^{252}Cf targets involved purifying the californium by an ion exchange procedure, which resulted in an ultrapure solution of californium in nitric acid. This solution was evaporated to dryness (to remove the acid), and the residue was dissolved in 1 ml of 1 M HNO_3 . The dissolved ^{252}Cf was added to 5 ml of cerium hydroxide sol (0.8 g of cerium) and thoroughly mixed. The sol was formed into microspheres by injection into a stirred pot of drying alcohol (89% 2-ethyl-1-hexanol, 9.5% 2-octanol, 1% Amine O, and 0.5% Span 80). The microspheres were filtered from the alcohol, air dried, and calcined for 3 hr at 800°C . The resulting oxide had a bulk volume of 0.2 ml.

The calcined Cf-Ce oxide microspheres were then mixed with the proper amount of aluminum core powder and dispensed by manipulator into four target liners, which were pressed into pellets and welded in a rabbit for insertion into the HFIR.

Following irradiation, the targets were processed by dissolving the aluminum matrix in caustic. The Cf-Ce oxide spheres, which had maintained their integrity during irradiation, were easily filtered from the caustic solution. The CeO_2 was dissolved in HNO_3 catalyzed with a trace of HF. The cerium was then removed by oxidation to the tetravalent state with NaBrO_3 and subsequent extraction into HDEHP; the californium was left in the aqueous raffinate. The cerium could also have been separated from the californium by high-pressure ion exchange since cerium elutes much later than einsteinium or californium.

Fabrication of a ^{252}Cf Point Source. — Since ^{252}Cf partially decays by spontaneous fission and emits 2×10^{12} neutrons per second per gram of material, this isotope, encapsulated in a very small volume, would be a valuable neutron source. An encapsulation method was developed by which quartz spheres (i.e., sources) containing up to 20 μg of californium were prepared. These quartz spheres, $\frac{1}{16}$ in. in diameter, completely enclose the highly radioactive californium, thus preventing contamination of the surrounding environment.

The fabrication procedure involved extracting californium from aqueous (acid) solution by an organophosphonic acid extractant, 2-ethylhexyl phenylphosphonic acid, which is adsorbed on

powdered quartz. The powdered quartz was packed into a small-bore quartz capillary tube, and the californium-containing solution was passed through the bed. The organophosphonic acid extracted greater than 99% of the californium from the aqueous solution as it passed through the column. After the californium had been sorbed on the quartz bed, the quartz powder and capillary were dried and then fused into a sphere, which effectively encapsulated the californium. The quartz spheres were then welded into stainless steel capsules about $\frac{1}{8}$ in. in diameter by $\frac{3}{8}$ in. long. This technique was also used to encapsulate 250 μg of ^{244}Cm into a $\frac{1}{16}$ -in.-diam sphere.

The quartz capillary, final sphere, and stainless steel capsule are shown in Fig. 5.7.

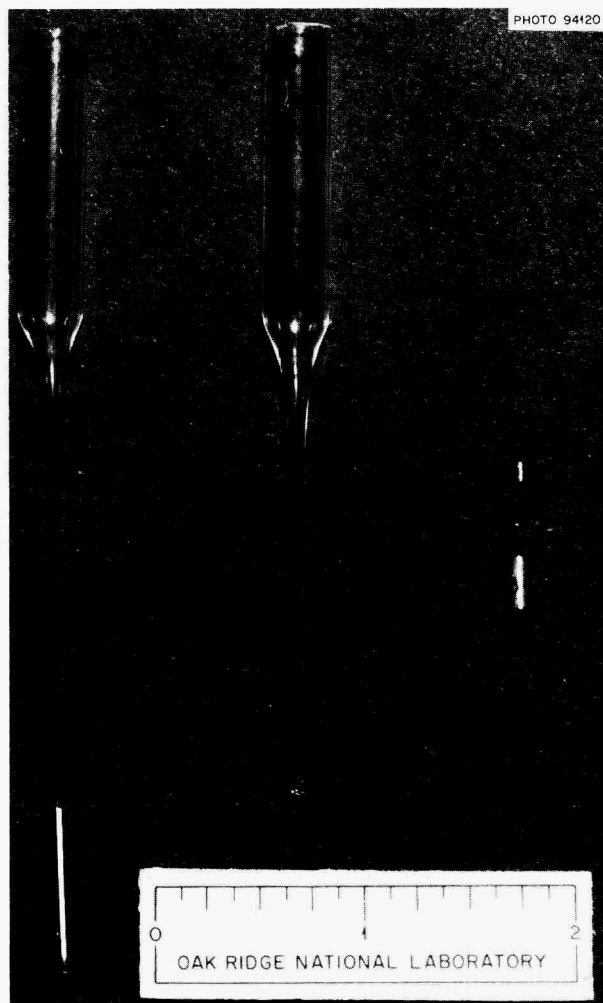


Fig. 5.7. Materials Used in the ^{252}Cf Source Fabrication.

Fabrication of Larger ^{252}Cf Sources.— A 100- μg source pellet was prepared by the following technique. A specially reinforced HFIR target-like pellet liner was filled with 0.2 g of cation exchange resin. The required amount of californium was loaded on this miniature ion exchange column, and then the resin was destroyed by firing to 400°C . The pellet was compacted to minimize the void volume, to reduce the dimensions of the active source region, and to enhance structural integrity; then it was sealed in a $\frac{3}{8}$ -in.-diam stainless steel capsule.

At present, we are attempting to prepare a 1-mg ^{252}Cf neutron source, using the above technique; ultimately, we expect to prepare sources as large as 25 mg.

Source Fabrication by Electrodeposition.— Electrodeposition on metal plates affords a convenient method for preparing sources of transplutonium elements for many types of experiments; however, aqueous-phase electroplating techniques, which require ultrapure solutions to prevent deposition of interfering cations, are very difficult to apply with these elements. We have developed a method for electrodepositing uniformly thin layers of the transplutonium elements from an organic extractant onto platinum, stainless steel, and beryllium plates. In this process, the transplutonium elements are first extracted into di(2-ethylhexyl)phosphoric acid (HDEHP) from dilute mineral or organic acids, while many of the ionic contaminants that normally interfere with aqueous-phase electrodeposition are rejected. The extractant is mixed with a plating solution containing ammonium hydroxide, isopropyl or ethyl alcohol, and 2-ethyl-1-hexanol, and electrolyzed at 300 to 500 v (10–30 ma). The transplutonium elements are deposited at the cathode.

The conditions and results of a typical electrolysis are shown in Table 5.3. In this experiment, 64 μg (90%) of ^{244}Cm was deposited on a platinum cathode, utilizing a platinum anode. The curium feed solution (0.02 M HNO_3) was contacted with 0.8 ml of 0.5 M HDEHP in xylene. After contact, the solutions were centrifuged, and the aqueous phase was discarded. The loaded organic was scrubbed three times with 0.01 M HNO_3 . After each contact, the solutions were centrifuged and the aqueous phase was discarded. The organic extractant was then added to 9 ml of plating solution, which consisted of 0.6 M NH_4OH , 32% isopropyl alcohol, and 64% 2-ethyl-1-hexanol.

Table 5.3. Electrodeposition of ^{244}Cm

Extractant - 0.8 ml of 0.5 M HDEHP in xylene

Plating solution - 0.64 M NH_4OH , 31.9% isopropyl alcohol,
63.8% 2-ethyl-1-hexanol; 9.0 ml

Run Time (min)	v	ma	pH	Amount of Cm in Solution (μg)	% of Curium Remaining in Solution
0	470	16	10.1	70.7	100
15	470	12.5		42.6	60.3
30	470	10.5	8.7	25.7	36.4
45	470	10.0		13.4	18.9
60	470	9.0	8.3	6.6	9.3
Cell solution and flushes				6.3	8.9

This solution was electrolyzed for 1 hr. The spent plating solution was removed from the cell, and the cell was rinsed twice with a few milliliters of isopropanol. After the plate had been allowed to dry for a few hours, the plated deposit was wiped; this removed 5 to 10% of the material on the plate. After the initial wiping, additional material could not readily be removed.

Plating efficiency depends on the quantity of material present in the plating solution. Tracer and 1- to 2- μg , 10- to 50- μg , and 100- μg quantities are deposited with efficiencies of 80%, 60-80%, and 50-60% respectively. Successive depositions can be made on a cathode plate, and deposits of approximately 400 μg of ^{244}Cm on a 1- cm^2 area have been made in this way.

The transplutonium elements that remain in spent plating solution can be readily recovered by adding 6 M HCl to the plating solution until two phases are formed. The aqueous phase containing the transplutonium elements and some ethyl or isopropyl alcohol is evaporated to dryness and then redissolved in dilute nitric acid. The transplutonium elements can then be reextracted and plated.

This technique was used to deposit microgram quantities of various transplutonium elements on platinum, beryllium, and stainless steel plates. Beryllium foils containing 1 to 3 μg of ^{253}Es were prepared for use as cyclotron targets for the production of ^{256}Md . A self-transference source

containing 15 μg of ^{252}Cf was electroplated on platinum. This source is to be used to prepare essentially mass-free californium on thin backing by ^{252}Cf recoil (caused by spontaneous fissioning processes). A 50- μg target of ^{252}Cf was prepared on a 0.1-mil stainless steel disc, and the target area was covered with a 20- μin . nickel deposit. This target is being used for delayed neutron measurements from fission fragments; later, it will be used to obtain the resonance integral for ^{252}Cf by placing the source in a neutron beam. Targets containing about 100- μg quantities of ^{245}Cm and ^{247}Cm were prepared for cross-section measurements.

High-Pressure Ion Exchange Technology

The successful application of a high-pressure ion exchange technique for transcalifornium element separations prompted the investigation of high-pressure techniques for the LiCl-based anion exchange system, which is presently used for actinide partitioning, and a new cation exchange system that utilizes the complexing behavior of various aminopolyacetic acids to provide similar separations.

LiCl-Based Anion Exchange.— Because of the corrosive nature of the LiCl-based anion exchange system and the unavailability of tantalum high-pressure components, it has not been possible to

exhaustively test the high-pressure ion exchange technique with this system; however, several experiments were performed in temporary systems. The results were sufficiently encouraging to warrant procurement of the necessary tantalum components. When compared with results obtained in conventional equipment, the high-pressure technique provided significantly improved actinide separations. Large quantities of rare earths did not affect loading characteristics or recovery of the transplutonium elements. Large volumes of feed solution can be pumped through the column without adverse effects, and high flow rates ($10 \text{ ml cm}^{-2} \text{ min}^{-1}$) can be used.

Actinide elution curves obtained during a laboratory-scale run are shown in Fig. 5.8. The eluting positions of rare earths and the Zr and Ru fission products are also shown. The curium fraction contained 99.4% of the curium and no detectable californium, while the californium fraction contained 98.6% of the californium and 0.03% of the curium. Americium was eluted along with the curium, and einsteinium was eluted along with the californium.

Equipment is being assembled to permit further study of this system. A tantalum head pump with a flow capacity as high as 2 liters/hr has been ordered, and a six-port tantalum valve has been assembled. The final system should have a capacity of approximately one TRU target rod per run.

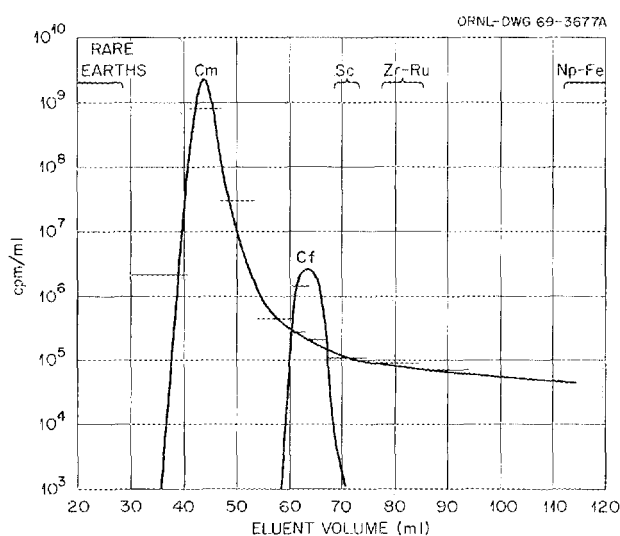


Fig. 5.8. Actinide Elution Curves for LiCl-Based Anion Exchange-High-Pressure Column Run.

Solvent Extraction Process Development

Laboratory development of the Pubex, Hepex, and modified Berkex processes is now essentially complete since the processes have been demonstrated on a scale that is adequate for present program needs.

Plutonium Recovery by Solvent Extraction (Pubex).— Plant operations with the Pubex process have continued to be satisfactory, and parameters have been sufficiently defined to provide latitude in plant processing. In the Pubex process, tetravalent plutonium and zirconium are preferentially extracted from 6 M HCl into 1 M HDEHP in diethylbenzene (DEB). The transplutonium elements remain in the aqueous phase. The solvent is washed with dilute HCl, and the plutonium is reduced to the trivalent form with the organic-soluble reductant 2,5-di-*tert*-butylhydroquinone. This makes it possible to strip the plutonium into 8 M HCl, leaving nearly all of the zirconium in the waste solvent, which is discarded.

Extraction coefficients (E_a^o) were obtained for additional elements between 1 M HDEHP in DEB and various concentrations of HCl. Extraction coefficients for Al(III), Cr(III), Ce(III), and Ni(III) were less than 0.005 in the acid concentration range 2 to 10 M. Extraction curves for Cf(III) and Cm(III) had similar shapes;¹⁰ however, the californium extraction was a factor of 30 higher.

Because it is frequently desirable to strip zirconium from HDEHP for analytical purposes, several complexing agents were evaluated for zirconium and plutonium stripping. Oxalic acid was found to be quite effective and superior to either citric acid or sodium carbonate. A zirconium stripping coefficient, S_o^a , of greater than 700 was obtained between 1 M HDEHP-DEB and 0.5 M oxalic acid, while the S_o^a for plutonium was 115.

Water-soluble reductants have not been highly effective in selectively stripping plutonium from HDEHP-DEP; however, it was found that their effectiveness is greatly increased at elevated temperatures. The most promising results were obtained with 0.2 M hydroquinone in 10 M HCl; a plutonium stripping coefficient of 36 was obtained.

Heavy-Element Partitioning (Hepex).— Continued laboratory studies of the Hepex process led to a

¹⁰Chem. Technol. Div. Ann. Progr. Rept. May 31, 1968, ORNL-4272, pp. 103-6.

successful plant demonstration (see Sect. 5.1) in which about 140 μg of californium was isolated from multigram quantities of ^{243}Am and ^{244}Cm . In this process, the transcurium elements are separated from americium and curium by extraction into HDEHP.

In laboratory-scale experiments, berkelium was separated from curium by continuous countercurrent extraction with 0.8 M HDEHP in kerosene from 0.5 N HCl. Single-stage berkelium-curium separation factors averaged about 14, while overall factors up to 10,000 were obtained with only six stages. Plant feeds are expected to contain LiCl, which reduces distribution coefficients; however, it was found that reduction of the HCl concentration of the feed to approximately 0.15 N will compensate for the presence of 1 M LiCl.

A crucial step in the Hepex process is solvent pretreatment; however, various lots of solvent have not reacted similarly to treatment procedures. One method of purification involved repeated treatments of kerosene solutions of HDEHP with NaOH and then with ethylene glycol. This increased the californium-curium separation factor obtainable from an existing supply of HDEHP from 10 to 37, which compares favorably with results obtained with the purest HDEHP available. Similar performance was obtained by simple treatment of this particular batch of HDEHP with either equal-volume mixtures of ethylene glycol and 0.05 M Na_5DTPA in 1 M carboxylic acid (acetic, glycolic, or lactic) or with 0.05 M Na_5DTPA alone, adjusted to pH 4 with HCl.

These results could not be duplicated with a new supply of HDEHP. Without treatment, the new HDEHP gave a californium-curium separation factor of 16; in the laboratory, separation factors up to 30 were obtained by various treatment methods, some of which are not applicable in the plant. Solvent which had been treated in the plant with DTPA and which provided a separation factor of 25 was used in the production runs.

Berkelium Isolation by Solvent Extraction (Berkex). -- We continued the laboratory development of a modification of the process for isolating berkelium as Bk(IV) by extraction with HDEHP, using chromate instead of bromate for the oxidation. Separation factors of greater than 10^4 between berkelium and curium, as indicated by separate measurements of the extraction coefficients, have been reported;¹¹ they were confirmed by extraction from 4 N HNO_3 solution

(0.08 M CrO_3) containing both actinides. The berkelium can be stripped with either 4 N HNO_3 –1 M H_2O_2 or 4 N HCl–1 M H_2O_2 , depending on how the product is to be handled subsequently.

Laboratory investigations of the bromate oxidation of berkelium were also continued. It was found that Ce(III) and Bk(III) can be quantitatively oxidized to Ce(IV) and Bk(IV) and extracted by HDEHP from aqueous solutions containing much lower concentrations of nitric acid (e.g., 2 N) and bromate than were previously considered necessary. The major requirement is excellent contact of the two phases. Initial partial oxidation (varying with the nitric acid and bromate concentrations) is rapid, as is the extraction of the resulting Ce(IV) or Bk(IV), but completion of this approach to the final equilibrium can be slow. The required time (from minutes to several hours) depends on the efficiency of mixing of the phases as well as on the nitric acid and bromate concentrations.

Berkelium is highly extractable by HDEHP from nitric acid solutions containing ceric ammonium nitrate because the oxidation potential of the Ce(IV)/Ce(III) couple is higher than that of the Bk(IV)/Bk(III) couple (cf. Sect. 10.9). Berkelium, but not cerium, can be oxidized by persulfate in moderate concentrations of nitric acid for extraction by HDEHP.

HFIR Target Dejacketing Solution

Laboratory studies were conducted to modify the caustic solution (NaOH-NaNO_3) that is used to dissolve the aluminum jackets and matrices of HFIR targets during processing, in an effort to improve pumping and filtration characteristics. It was found that reduced concentrations of NaOH and NaNO_3 resulted in improved filtration rates without promoting the formation of objectionable precipitates.

The plant dissolver solution, 6 M NaOH–3 M NaNO_3 , was found to have a specific gravity of 1.365 and a relative viscosity of 10.64 at room temperature. In redetermining these measurements, while gradually reducing the hydroxide and the nitrate concentrations but keeping the aluminum concentration constant, no precipitate formation

¹¹J. B. Knauer and Boyd Weaver, *Separation of Berkelium from Trivalent Actinides by Chromate Oxidation and HDEHP Extraction*, ORNL-TM-2428 (Nov. 14, 1968).

was observed until concentrations of less than 3 M NaOH and 1.5 M NaNO₃ were reached. Solutions of the composition 3 M NaOH–1.5 M NaNO₃, in which 1.2 M aluminum is dissolved, have a specific gravity of 1.216 and a relative viscosity of 3.45. No precipitation was noted when such solutions were diluted with water in any proportion. Thus, caustic dissolver solution with this composition was used in the latest campaign in TRU, and a marked decrease in time required for filtration was observed.

5.4 SPECIAL PROJECTS

An increasingly important phase of the program at TRU involves making the excellent resources of this facility available to other groups, not only at ORNL but also at locations elsewhere. We can provide a number of useful services, such as canning alpha-active material in irradiation capsules. Sometimes we provide assistance in the planning and execution of projects primarily under the direction of others. Such projects are reported in this section. Although the end results of the research are not described, some general background information concerning these projects is presented, along with somewhat more detailed reports of the specific work done in TRU. Efforts in the past year have been centered on the preparation of rabbits containing ²⁵³Es for irradiation in the HFIR hydraulic rabbit facility and on the preparation of ²⁵²Cf neutron sources. In addition, several lots of curium were prepared for isotope separation in a calutron, and assistance was provided for an experiment in which the production and identification of ²⁵⁸Fm were attempted.

Einsteinium Rabbits

Six rabbits containing initially from 0.04 to 2.5 μg of ²⁵³Es were prepared for the HFIR hydraulic rabbit facility for H. Diamond at ANL. The desired product was the 39.3-hr ^{254m}Es. Diamond has studied the energy level structure of the alpha-decay product, ²⁵⁰Bk, and is doing some molecular beam studies with ²⁵⁴Fm, the beta-decay product. The rabbits were irradiated for 2 to 3 days in the HFIR, moved to TRU, dejected, and repackaged for air freight shipment to Chicago. Diamond received most of the shipments

in less than 24 hr after discharge. The shipments were spaced at least 2 weeks apart to allow time for data analysis between runs.

Fabrication of Neutron Sources

One of the major uses for ²⁵²Cf is as a neutron source. We have been developing methods for preparing pellets containing ²⁵²Cf for encapsulation as neutron sources (see Sect. 5.3). The first procedure, described last year, involved making a miniature filter funnel out of a standard HFIR target pellet liner and filtering a slurry of aluminum powder and californium hydroxide. After being calcined, the liner was loaded into a die, filled with pure aluminum cap powder, and compacted to approximately 90% of theoretical density by pressing at 20 tsi. We have made a number of pellets by this technique, both as targets for irradiation and for neutron sources. The technique seems to be limited to about 750 μg of ²⁵²Cf in one pellet.

A neutron source of this type, containing 309 μg of ²⁵²Cf, was built for John Auxier of the Health Physics Division during this report period. The source was in the form of a doubly encapsulated 1/4-in. pellet, the first encapsulation being a 3/8-in.-diam aluminum tube and the second a 5/8-in.-diam stainless steel capsule.

The ²⁵²Cf source was used for measuring the gamma radiation and neutron leakage from duplicates of the atomic bombs exploded in World War II. For years, health physicists have desired such information. By using the ²⁵²Cf source, it was obtained without actually detonating the bombs.

Two other techniques were developed, with the objective of reducing material losses during source fabrication. One of these methods involved the use of a micro extraction-chromatography column (see Sect. 5.3). A source containing 20 μg of ²⁵²Cf was prepared in this manner, yielding a 1/16-in.-diam sphere which was, in turn, sealed in a 1/8-in.-diam stainless steel capsule. This source has been shipped to PNL. A larger source, containing 100 μg, was prepared by a technique in which the californium was adsorbed on a small ion exchange column in the form of a specially reinforced HFIR target-like pellet liner filled with 0.2 g of cation exchange resin. This source was delivered to Oak Ridge Associated Universities to be used for instructional purposes.

At present, we are preparing a 1-mg ^{252}Cf neutron source, using the latter technique. The source that we made for the Transuranium Research Laboratory last year has been returned from the original experimenter, and has been made available to a group at PNL for neutron radiography studies.

Curium for Isotope Separation

Portions of two batches of curium, CMP-10B and CMP-11 (See Table 5.4 for composition), were set aside for separation of isotopes in the calutrons at the Y-12 Plant. The source of CMP-10B was the curium recovered at PNL from the blanket of the Shippingport Reactor. The curium in CMP-11 was recovered at TRU during campaign 11 (see Sect. 5.1). These materials were purified by carbonate precipitation (to separate the americium from the curium), followed by three successive oxalate precipitations to purify the curium from most metallic contaminants. The oxalate was fired to oxide (believed to be $\text{CmO}_{1.72}$) at 800°C for 4 hr and was then loaded into graphite charging bottles preparatory to insertion into the calutron. The high ^{243}Cm content of batch CMP-10B increased the gamma dose rate for this batch significantly, thus preventing us from loading more than about 200 mg of curium per bottle (vs 500 mg of batch CMP-11). About 3 mg of 70% ^{245}Cm was recovered from 1.1 g of batch CMP-10B by the isotope separation group. The 2.6 g of batch CMP-11 yielded about 11 mg of 95% ^{246}Cm plus small amounts of material enhanced in ^{247}Cm , ^{248}Cm , and ^{250}Cm .

Table 5.4. Isotopic Compositions of Two Special Batches of Curium

	CMP-10B	CMP-11
^{242}Cm	0.001	
^{243}Cm	1.48	
^{244}Cm	93.48	88.69
^{245}Cm	3.94	0.724
^{246}Cm	1.07	9.89
^{247}Cm	0.019	0.227
^{248}Cm	0.016	0.413

The Search for Fermium-258

An excellent example of a cooperative effort between ORNL and other transuranium facilities is the recent experiment in which the production and identification of ^{258}Fm was attempted at ORNL. A team of scientists at Lawrence Radiation Laboratory, headed by E. K. Hulet, had previously made six attempts, all unsuccessful, to produce and identify this isotope, which is believed to have a short half-life and to decay by spontaneous fission. ORNL was the logical site for the next attempt because of the availability of the HFIR with its very high flux, plus the availability of increased amounts of ^{257}Fm feed material from the ORNL transplutonium element production program.

Hulet joined with C. E. Bemis, of the Transuranium Research Laboratory staff, in planning and carrying out the experiment. A pneumatic rabbit based on ideas developed in a similar previous attempt was designed at ORNL. The experiment was first attempted unsuccessfully in October 1968, when the rabbit transfer system failed. The system was disassembled, and a portion of the in-pile section was brought to TRU, where the flight tube was cut open and the rabbit was recovered.

On the basis of information gained from this attempt, a revised flight tube was designed and installed, with some engineering assistance from TRU personnel.

From the six curium targets processed in February 1969, a fermium product was recovered and a rabbit containing about 6×10^7 atoms of ^{257}Fm (300 dis/min) was prepared. The standard hydraulic rabbit facility, along with the transplutonium targets, was removed from the HFIR, and the special pneumatic rabbit facility was installed. The calculated flux at the location of the fermium sample was 4.2×10^{15} neutrons $\text{cm}^{-2} \text{sec}^{-1}$. The experiment consisted of dropping the rabbit into the heart of the reactor and irradiating it for 5 sec. The rabbit was then blown, by using helium gas, about 33 ft up into the catcher. The catcher is a turret-like device that positions the rabbit in front of a solid-state fission fragment detector, which counts the rabbit for several seconds. The experiment was adjusted so that only 350 msec elapsed between irradiation and the beginning of the counting period. Although this experiment was repeated nearly a thousand

times, not one fission event that could be attributed to ^{258}Fm was recorded. The absence of fission events means that ^{258}Fm has a half-life of less than 100 msec if the cross section for production from ^{257}Fm is 1 barn. If the cross section were 10 barns, the half-life would have to be less than 30 msec for ^{258}Fm to remain unobserved. This highly sophisticated experiment did not succeed in identifying ^{258}Fm ; nevertheless, it was very useful in further circumscribing the range of half-lives that this isotope might have — a result which will affect interpretation of experiments to produce still heavier nuclides.

5.5 TRANSPLUTONIUM ELEMENT RESEARCH

As significant quantities of new isotopes become available, a systematic study of actinide element chemistry and of comparative lanthanide chemistry will be carried out. Such a study materially increases our basic understanding of actinide systems. This part of the transplutonium element program includes work on problems involving solution chemistry, with particular emphasis on complex formation, and the preparation of solid actinide compounds that will be characterized by x-ray diffraction, electron microscopy, thermogravimetry, differential thermal analysis, and metallographic examination.

Status and Progress

The investigation of lanthanide sulfate complexes by amine extraction was extended to americium. As expected, the americium complexes and their formation constants proved to be very similar to those found for europium. The species and their thermodynamic (zero ionic strength) constants for formation from the uncomplexed species Am^{3+} were: AmSO_4^+ , $K_{01} = 6.24 \times 10^3$; $\text{Am}(\text{SO}_4)_2^-$, $K_{02} = 4.43 \times 10^5$; and $\text{Am}(\text{SO}_4)_3^{3-}$, $K_{03} = 2.27 \times 10^5$. The existence of a dinuclear complex $\text{Am}_2(\text{SO}_4)_3$ was suggested, as was $\text{EuAm}(\text{SO}_4)_3$ when both elements were present. No evidence for a higher sulfate complex $\text{Am}(\text{SO}_4)_4^{5-}$ was found. Ancillary computer programs were improved, particularly to allow calculation of the fractional distribution of all species at each sulfate ion concentration. Experimental difficulties causing scatter of data were largely resolved, and improved methods of

sampling and of counting by using an extractive liquid scintillator were developed.

Anhydrous chlorides of the heavy elements are of interest per se, and as intermediates for preparing other compounds. Laboratory efforts were, therefore, initiated to study methods for preparing anhydrous chlorides of the lanthanides as standards for trivalent actinides. The best results have been obtained with $\text{NH}_4\text{Cl} + \text{HCl}$ in conjunction with a programmed temperature rise from 200 to 500°C. However, phosgene gas in a fluidized bed at 500°C offers some operational advantages and shows enough promise to warrant further study. Thus far, no method that has been tested has provided effective chlorination of Yb_2O_3 (which represents the heaviest lanthanides).

Based on electron microscopy, x-ray diffraction, and thermogravimetry, the study of trends and differences in the crystallization behavior of lanthanide hydroxide preparations was extended to the entire series. This study showed that the lanthanides can be divided into two groups, based on crystallizing times and the microstructure obtained for the hydroxides. The diffraction patterns obtained for the first group indicate that the structures are hexagonal; however, the second group gave diffraction patterns that are much more complex. In parallel studies of the actinide elements, hydroxide preparations of curium, berkelium, and californium were examined. Crystalline forms of these materials were observed; however, it has not been possible, as yet, to unambiguously characterize the crystal structure from the diffraction patterns obtained. The original actinide preparations were examined microscopically at Baylor University in collaboration with Dr. W. O. Milligan. An electron microscope now being used at TRU in studies of the transplutonium elements is expected to greatly facilitate this research.

Thermal analyses (which consist of thermogravimetric and differential thermal analyses), in conjunction with x-ray analyses, were made of plutonium carbides, particularly those prepared by dispersing carbon in colloiddally stabilized plutonia (see Sect. 7.5). Construction of a microthermogravimetric balance was completed and tested with lanthanide compounds.

Several research projects were conducted in collaboration with the Transuranium Element Laboratory (TRL). These include: (1) studies of the berkelium fluorides and metal systems (low-

and high-temperature forms of BkF_3 , were characterized by x-ray diffraction), (2) determination of the formal potential for Bk(III)-Bk(IV) oxidation, and (3) development of a method for determining the II-III oxidation potentials of the transplutonium elements.

Lanthanide and Actinide Sulfate Complexes

In continued investigations of the sulfate complexes of the lanthanides and higher actinides,¹² americium sulfate complexes were examined by equilibration of aqueous phases of various sulfate concentrations with an americium-loaded extractant (1-nonyldecylamine sulfate in xylene) of constant composition. As expected, the complexes of americium were found to be very similar to those reported earlier for europium.¹² The known mono- and disulfate complexes of americium were confirmed. A previously unknown trisulfate species was found, and its formation constant was measured. Some data also suggest that a small amount of a dinuclear neutral species exists in the aqueous phase; however, no evidence was found for a tetrasulfate species even at 1.5 M sulfate.

In the investigation of americium complexes, excessive scattering of data was encountered in analyzing the aqueous phases that had been equilibrated with the americium-loaded organic phase (see Sect. 10.9). Attempts to relieve this problem by using 10^{-4} M europium as a carrier resulted in a drastic change in the shape of the curve showing the aqueous americium concentration vs the aqueous sulfate ion concentration. A broader minimum was observed, indicating a higher neutral species concentration at intermediate aqueous sulfate levels and a lower anionic complex concentration at higher aqueous sulfate levels. This result suggests the formation of a dinuclear species $\text{EuAm}(\text{SO}_4)_3$, but no additional work has yet been done to confirm its existence.

The cause of the scatter in the data was determined to be a combination of microdispersions of the americium-loaded organic phase in the aqueous phase and adsorption of aqueous americium species on the sampling glassware. When these interferences were alleviated (see following

subsection), the scatter of the data dropped to a level comparable to that experienced with europium.

Figure 5.9 shows the experimental points, together with the smooth curve obtained with the formation constants, fitted as previously described.¹² Table 5.5 compares the experimentally determined formation constants with values from the literature. The latter values, taken at ionic strengths of 1 and 2 M, have been adjusted to zero ionic strength by the Debye-Hückel expression.

An extension of the computer treatment of the data now allows computation and plotting of the mole fraction of the metal in each complex species at each aqueous sulfate ion concentration. Such a plot for the americium sulfate complexes is shown in Fig. 5.10.

Improvement of Experimental Precision.—As noted above, excessive scattering of the data was attributed to (1) adsorption on the sampling glassware, and (2) microdispersions of the loaded organic phase in the low-concentration aqueous phase. Adsorption was minimized by rinsing the

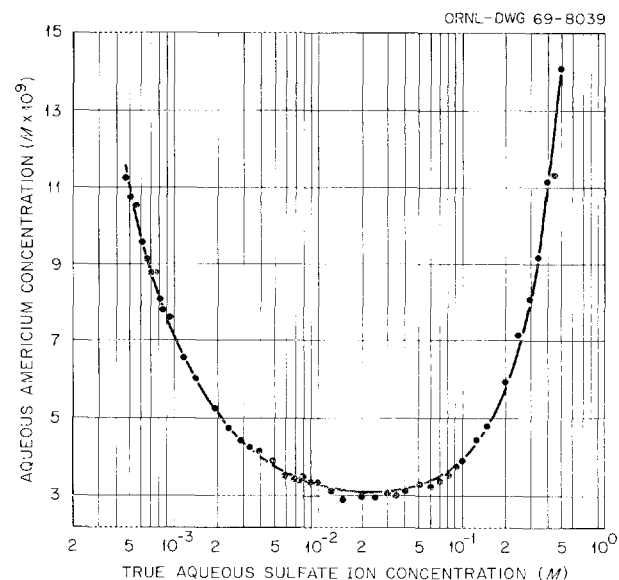


Fig. 5.9. Aqueous Americium Concentration as a Function of Aqueous Sulfate Ion Concentration at Constant $a_{\text{H}_2\text{SO}_4} = 3.58 \times 10^{-10}$ M (pH = ~ 3.0). The points are experimental observations. The curve is a least-squares fit, using a model which sums the concentrations of the various species.

¹²Chem. Technol. Div. Ann. Progr. Rept. May 31, 1968. ORNL-4272, pp. 116-18.

Table 5.5. Formation Constants for Americium Sulfate Complexes

Complex	Constant	Value of Constant		
		This Work	Sekine ^a	De Carvalho and Choppin ^b
AmSO_4^+	K_{01}	6.24×10^3	1.03×10^4	1.55×10^4
$\text{Am}(\text{SO}_4)_2^-$	K_{02}	4.43×10^5	8.28×10^5	3.47×10^5
$\text{Am}(\text{SO}_4)_3^{3-}$	K_{03}	2.27×10^5		
	K_{12}	70.9	80.4	22.5

^aTatsuya Sekine, *Acta. Chem. Scand.* **19**, 1465 (1965).

^bR. G. De Carvalho and G. R. Choppin, *J. Inorg. Nucl. Chem.* **29**, 725 (1967).

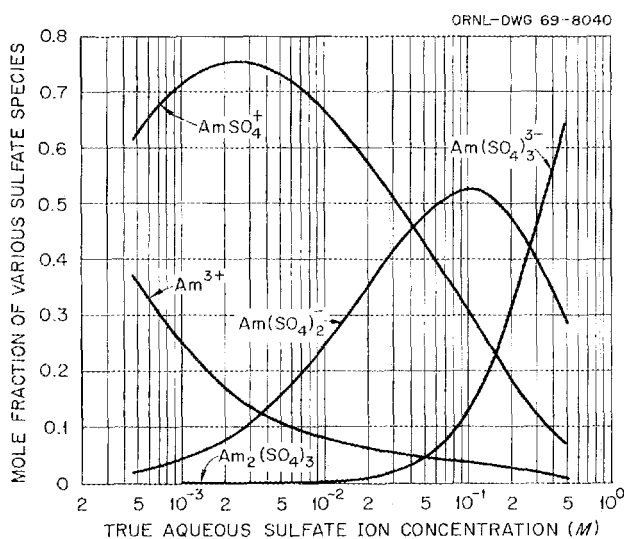


Fig. 5.10. Mole Fraction of Aqueous Americium Species as a Function of Aqueous Sulfate Ion Concentration. The sulfuric acid activity is constant, but the total ionic strength of the solution varies directly with the sulfate ion concentration ($I \approx 3 \times [\text{SO}_4^{2-}]$).

sampling pipet with an extractive scintillator,¹³ and microdispersions were prevented by quiescent-interface equilibration. The new procedure used is discussed below.

(1) *Adsorption of Tracer.* — Adsorption of the carrier-free tracer on the walls of the sampling micropipet (and the walls of any intervening vessels used in sampling) was suspected of causing

¹³Although use of liquid scintillation for alpha counting is not widespread, it is used in this work because it combines ease of sample preparation, high counting reproducibility, and 100% counting efficiency.

difficulties early in the investigations. Two steps were introduced to eliminate these difficulties: (a) sampling was done via an unwetted Teflon tube extending through the lighter organic phase, thus eliminating contact of any additional vessel with the low-concentration aqueous sample, and (b) a method was developed by which the pipet could be rinsed with the scintillator liquid.

The scintillator that was originally used contained large concentrations of a wetting agent to allow the aqueous sample to mix with the toluene-based scintillator. These solutions were too viscous to be used to rinse a pipet. An extractive scintillator was developed containing no wetting agent but containing 0.005 M 1-nonyldecylamine sulfate. Pipets can be rinsed with this low-viscosity mixture; and although the aqueous sample does not mix with this scintillator, essentially all of the actinide is extracted into the scintillator ($E > 1000$) when gentle agitation is employed. The separate water phase produces no effect on the count rate.

(2) *Microdispersions.* — The report of experience in another laboratory¹⁴ of similar excessive scatter of data in counting carrier-free tracers, and of subsequent improvement by high-speed centrifugation of the samples, suggested that at least a part of the difficulty might be due to persistence of very small organic droplets, or "microdispersions." This was supported by the finding that a marked decrease of scatter was obtained

¹⁴G. K. Schweitzer, University of Tennessee, private communication (Mar. 6, 1969).

when stirring with quiescent interface¹⁵ was used instead of shaking as the method for achieving equilibration.

Preparation of Anhydrous Chlorides

Methods are being investigated to improve the efficiency and simplicity of preparation of anhydrous chlorides of the heavy elements. Study has started with lanthanides, both as stand-ins for the trivalent actinides and to provide for subsequent comparisons. Table 5.6 summarizes, qualitatively, the results obtained thus far. Although much successful work on the chlorination of oxides of the light lanthanides has been reported, considerably less work with less successful results has been reported for the heaviest lanthanides. For example, no method tried to date has resulted in satisfactory chlorination of ytterbium.

The best results have been obtained with ammonium chloride under a stream of anhydrous hydrogen chloride, in conjunction with a gradual increase in temperature from about 200 to about 500°C; further improvement may be possible through adjustment of the programmed temperature rise. In addition, the method of passing phosgene (COCl₂) through a fluidized bed in a vertical filter tube at constant temperature offers operational advantages and shows enough promise to warrant further study.

Investigation of Lanthanides and Actinides by Electron Microscopy

Electron microscopy and electron diffraction have been employed for investigating the hydrous oxides and hydroxides of lanthanides and actinides. The interest in these materials arises from their use in several sol-gel programs at ORNL. Previous investigations of thorium, uranium, plutonium, americium, curium, and some of the light lanthanides have already been reported.^{16,17} Some of the more recent work on lanthanides and actinides is discussed here.

¹⁵K. A. Allen and W. J. McDowell, *J. Phys. Chem.* **64**, 877 (1960).

¹⁶*Chem. Technol. Div. Ann. Progr. Rept. May 31, 1968*, ORNL-4272, pp. 123-25.

¹⁷C. J. Hardy, S. R. Buxton, and M. H. Lloyd, *Preparation of Lanthanide Oxide Microspheres by Sol-Gel Methods*, ORNL-4000 (August 1967).

Table 5.6. Chlorination of Lanthanide Oxides

Chlorinating Agent(s)	Temperature Schedule (°C)	Quality of Results for:			
		La	Eu	Gd	Yb
HCl	300 → 500 ^a	Poor			
NH ₄ Cl + HCl	200 → 500 ^a	Good	Good	Good	Poor
COCl ₂	500				
Boat		Fair	Fair		Poor
Fluidized bed		Fair			
		Good ^b		Good ^b	
CCl ₄	600				Poor

^aArrow indicates gradual increase in temperature to the higher value.

^bLow-fired La₂O₃ and Gd₂O₃.

In the case of the lanthanides as well as the transplutonium elements, the procedure¹⁶ for preparing the hydrous oxides or hydroxides of the metals consists of precipitation from dilute nitric acid solution with ammonium hydroxide, followed by extensive washing and then digestion at ambient or elevated temperatures. During the latter step, the material is converted to a crystalline form. Electron microscopy and electron diffraction were used to follow the changes that took place in the material from the initial precipitation to the final crystalline form.

As a result of the continued interest in hydroxides of the actinide elements, it was necessary to investigate the behavior of the lanthanide hydroxides. This study¹⁸ extended earlier work¹⁷ and included all of the lanthanides and yttrium. It was found that the lanthanides could be divided into two groups, based on the crystallizing times and the microstructures obtained for the hydroxides. Examination of the initial precipitates of each group showed that the material consisted of amorphous-like 20- to 50-A particles. For the elements lanthanum through dysprosium, the crystallizing time was relatively short and the crystalline material appeared as rod- or needle-like structures. With these elements, there appeared to be a trend in the size of the crystal-

¹⁸R. G. Haire and T. E. Willmarth, *Trends and Differences in the Crystallization Behavior of Lanthanide Hydroxide Preparations*, ORNL-TM-2387 (October 1968).

line needles or rods obtained under the same conditions, with larger rods forming for the heavier members. A comparison of the rods or needles for lanthanum, samarium, and dysprosium is shown in Fig. 5.11. The lanthanum needles

were approximately 50 by 1000 Å; for samarium, needles of 500 by 6000 Å were observed; and for dysprosium, the rods were 0.2 by 2 μ. With this group of lanthanide elements, the time for crystallization also increased with increasing



Fig. 5.11. Electron Micrographs of Lanthanum, Samarium, and Dysprosium Preparations (24°C).

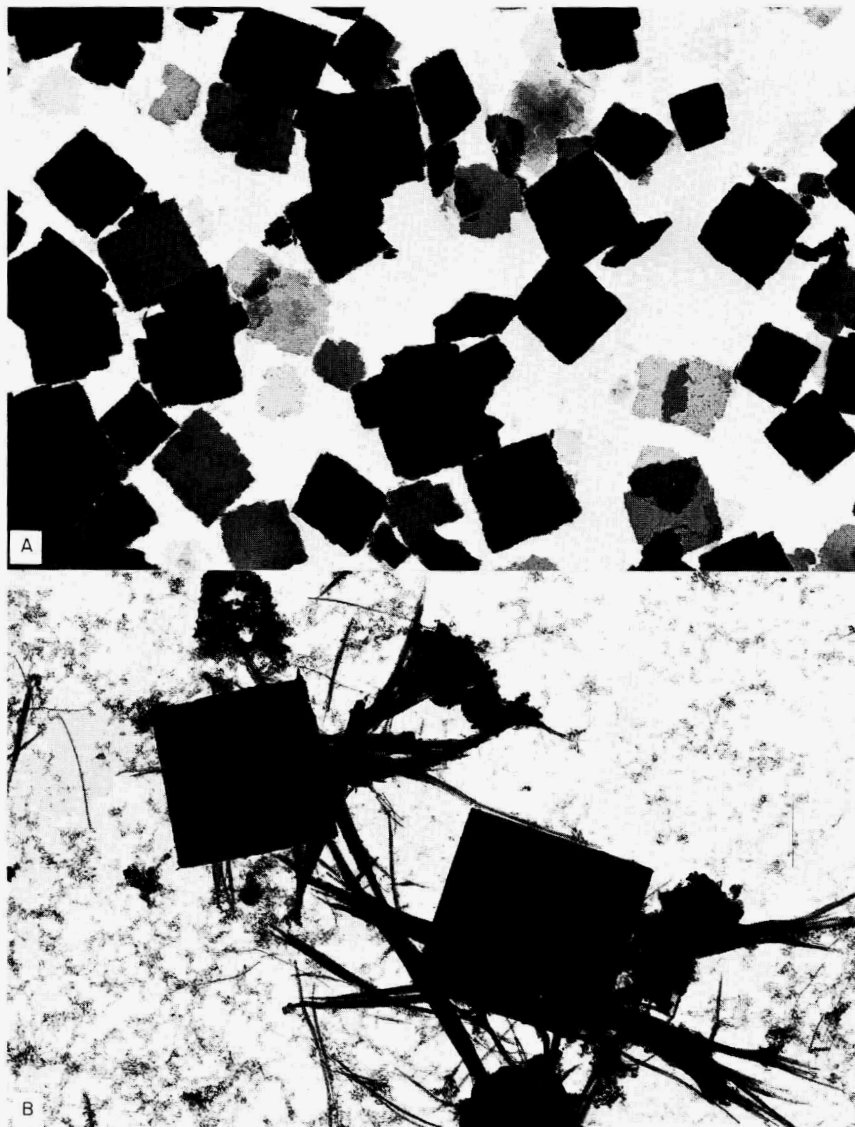
molecular weight. At 24°C, the crystallizing times for the three elements above were 1 hr, 12 hr, and 8 days respectively. The diffraction patterns for this group of the lanthanides indicate that the structures are hexagonal.

The second group of the lanthanides and yttrium had much longer crystallizing times, and the material formed fiber-like rods and platelets instead of the rods or needles previously observed. At 24°C, the crystallizing time for holmium was

2 to 3 months, while that for lutetium extended to 9 months. Figure 5.12 shows electron micrographs of some platelets and fibrous rods observed for preparations of ytterbium and lutetium. The diffraction patterns for members of this second group are more complex than those for the first group and are still under study.

In studies of americium and curium reported last year,¹⁶ it was shown that the behavior of americium and curium preparations was very simi-

PHOTO 93158R

SCALE \longleftarrow 1450 Å

A-YTTERBIUM AGED AT 80°C

B-LUTETIUM AGED AT °C

Fig. 5.12. Electron Micrographs of Ytterbium and Lutetium Preparations Converted at 80°C.

lar to that of the lighter lanthanides. The initial precipitates consisted of 15- to 20-Å amorphous-like particles, which converted to crystalline needles or rods after a period of aging in solution. The diffraction pattern for americium hydroxide was isomorphous with $\text{Nd}(\text{OH})_3$, indicating that the product was $\text{Am}(\text{OH})_3$. In more recent work, x-ray diffraction has been used to confirm the electron diffraction results, and the conversion time for forming crystalline $\text{Am}(\text{OH})_3$ has been established at 12 to 24 hr at 25°C . A similar crystallization sequence has been observed for curium preparations, with slightly larger needle structures being obtained under the same experimental conditions. A striking change in the crystalline forms was observed with aging; the effect is believed to be due to self-radiation damage. Figure 5.13 shows needles of curium near completion of crystallization (1 hr at 75°) and after an additional 3 hr in solution. The large symmetrical particles in the first sample are colloidal gold particles, which are used as a

focusing aid. The smaller particles are unconverted curium particles. The film that appears around the needles in the 4-hr sample probably arises from the forms of degraded curium. The time required for complete degradation appears to be dependent on several factors; the concentration and curium purity are two important variables. Diffraction patterns have been obtained for crystalline forms of curium, but analysis of these patterns is complicated by damage to the crystal lattice due to radiation. Further work is planned to resolve the patterns.

Experiments with berkelium, californium, and einsteinium hydroxide preparations have been initiated. Interest in these elements arises from their potential use in mixed sol-gel systems for target applications. Also, it would be interesting to compare their chemistry with that of the lanthanides and lighter actinides. For the experiments, high-purity solutions of each element were used, with ^{249}Bk , ^{249}Cf , and ^{253}Es being the major isotopes present in each sample. The prep-

PHOTO 93149R

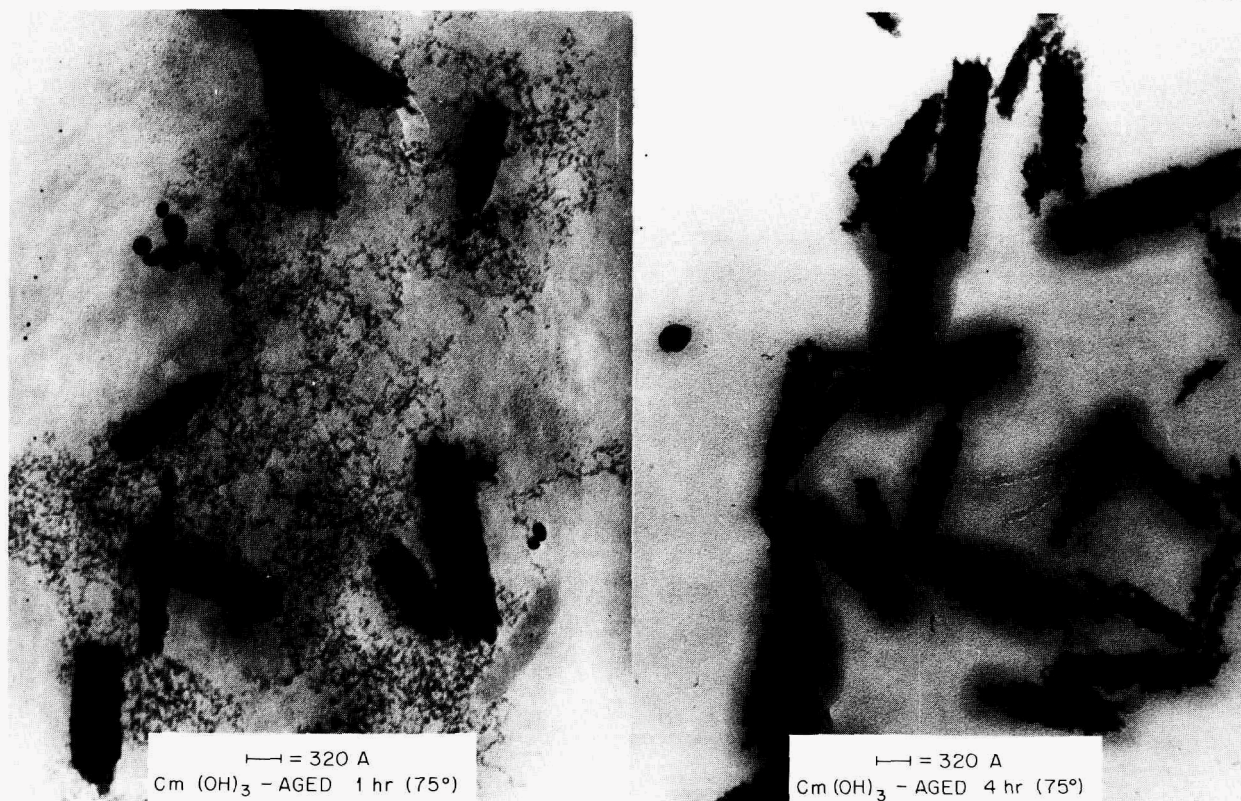


Fig. 5.13. Electron Micrographs of Curium Hydroxide Preparation.

arations were made on the microgram level, and the general procedure was essentially the same as outlined for preparing the hydroxides of americium and the lanthanides.¹⁶ From previous work on the lanthanides, we expected the crystallization time to increase as the heavier actinides were prepared. As the half-life of the heavier actinides became shorter, it was anticipated that the crystalline hydroxides of these elements would become more difficult to prepare and, once prepared, they would have a limited lifetime. Experiments to date have supported these assumptions. In addition, there is the added difficulty of preparing samples from the very small quantities of starting material. Although crystalline berkelium, californium, and einsteinium products have been prepared and observed, additional work is required for verification of the compositions of these products and elucidation of their chemistry. Future work will include examination of other preparatory techniques, using the lighter actinides and lanthanides as stand-ins for the heavier actinides.

Collaborative Research with the Transuranium Element Laboratory

Several research projects are being carried out in collaboration with personnel at the Transuranium Element Laboratory (TRL). Data obtained in two cooperative experiments have recently been published.^{19,20}

Studies of the fundamental chemistry of berkelium were extended to include the berkelium fluoride and metal systems. Low- and high-temperature forms of BkF_3 were prepared and characterized

by x-ray diffraction as orthorhombic and trigonal respectively. The transition temperature is approximately 600°C. Berkelium metal samples were prepared and characterized as a double hexagonal close-packed structure with a metallic valence of about 3.2. A secondary metal phase was identified as a fcc structure, which is the high-temperature form of the metal. Similar studies with californium fluoride and metal systems are in progress.

The formal potential for Bk(III-IV) oxidation in 1.1 *N* H_2SO_4 was determined by controlled potential coulometry to be 1.37 v vs the H_2 electrode.

A method of determining the II-III oxidation potentials of the transplutonium elements was developed by determining the electron transfer spectra of reducible lanthanides and using this calibration curve to estimate the II-III potentials for actinides. It was possible to estimate the II-III standard oxidation potentials for this series by utilizing Jorgansen's refined spin-pairing electronic energy theory, using the recently determined mendelevium and nobelium II-III oxidation potentials and our measurements of the electron transfer absorption bands of the transplutonium elements. A value of 1.9 v was obtained for the II-III standard oxidation potential for californium.

¹⁹L. J. Nugent, R. D. Baybarz, and J. L. Burnett, *J. Phys. Chem.* **73**(4), 1177 (1969).

²⁰L. J. Nugent, J. L. Burnett, R. D. Baybarz, G. K. Werner, S. P. Tanner, J. R. Tarrant, and O. L. Keller, Jr., "Intramolecular Energy Transfer and Sensitized Luminescence in Actinide (III) β -Diketone Chelates," *J. Phys. Chem.* (in press).

6. Development of the Thorium Fuel Cycle

During this report period we have successfully demonstrated most of the steps of the fuel particle preparation portion of the thorium fuel cycle. Fuel particle preparation is based on the sol-gel process, which employs solvent extraction to prepare a sol (colloid) from thorium and uranyl nitrate solutions, followed by the formation of microspheres by gelation of sol droplets in an immiscible alcohol. The gel microspheres are then dried and fired to yield a product that is about 350 μ in diameter, has a Th/U atom ratio of about 4, a density greater than 95% of theoretical, and is sufficiently strong to undergo coating with pyrolytically deposited carbon in fluidized beds.

Sol preparation has been demonstrated on an engineering scale, and no significant problems are anticipated in adapting this procedure for use with ^{233}U in the remotely operable equipment that is being designed and built for the Thorium-Uranium Recycle Facility (TURF) at ORNL.

Future studies will be concerned with investigating the recycle and cleanup of the alcohol used in sphere forming in an effort to find ways to minimize the likelihood of gel product deterioration that could result from long-term changes in column behavior.

Further developmental efforts on the drying and firing steps are also needed. The directions that these efforts should follow are clear; additional equipment development and testing should be carried out before establishing the final design of the drying and firing equipment that is to be installed in TURF.

The preparation of ThO_2 - $^{233}\text{UO}_2$ fuel for use in the High-Temperature Lattice Test Reactor (HTLTR) tests has considerably extended our experience and confidence in handling ^{233}U in sol-gel processes. In addition, our continued operation as a national distribution center for ^{233}U has enlarged our capability for receiving, storing, and purifying ^{233}U at ORNL.

6.1 PREPARATION OF ThO_2 - $^{233}\text{UO}_2$ FUEL FOR HTLTR

The High-Temperature Gas Cooled Reactor (HTGR) being developed by Gulf General Atomics, Inc., is a very promising thermal reactor for the conversion of thorium to ^{233}U and the economical production of electrical energy. The HTGR operates at temperatures to 1200°C or higher, which will affect the reactor reactivity, that is, the extent of the Doppler broadening. Doppler broadening studies will be made in a reactor assembly at the Pacific Northwest Laboratory (PNL), Richland, Washington. This reactor, called the High-Temperature Lattice Test Reactor (HTLTR), requires the use of fuel closely simulating actual HTGR fuel in order to make these studies meaningful. The HTGR fuel consists of approximately 400- μ -diam ThO_2 - UO_2 microspheres coated with pyrolytically deposited carbon. A total of 32 kg of 75% ThO_2 -25% $^{233}\text{UO}_2$ microspheres have been prepared by the sol-gel process at ORNL for use in these tests. These microspheres were coated with carbon by the ORNL Metals and Ceramics Division and shipped to PNL, where they were loaded into graphite blocks for use in preparing the test assemblies.

The sol-gel process utilized thorium nitrate solution and freshly separated ^{233}U solution¹ (containing 6 ppm of ^{232}U); these solutions were blended to give a Th/ ^{233}U atom ratio of 3.

Sol Preparation

The Solux Development Laboratory, which was designed to produce hydrosols of high-specific-

¹J. R. Parrott and R. E. Brooksbank, "The Handling of Kilogram Quantities of ^{233}U by Direct and Remote Methods at the ORNL Central Dispensing Facility," *Proceedings of 15th Conference on Remote Systems Technology, American Nuclear Society, 1967.*

alpha materials by the amine extraction process, has been utilized to produce 1 M thoria-urania (75% Th-25% ^{233}U) hydrosols containing 55 kg of metal. These hydrosols were produced in 1-kg batches over a period of eight months. In general, equipment operation was very satisfactory during this time; the only difficulty encountered involved the failure of two pumps.

The initial operation of the Solex Development Laboratory consisted of scrubbing three batches of organic, 0.75 M Amberlite LA-2 in an *n*-paraffin diluent through seven complete cycles to remove undesirable impurities. The acid concentration of the contact solution was decreased stepwise between cycles.

Because we needed to produce the most highly concentrated hydrosol possible for microsphere for-

mation, we initially attempted to use the Solex cocurrent flowsheet (Fig. 6.1). The hydrosols produced by this flowsheet contained about 0.14 mole of nitrate per mole of heavy metal and could be concentrated to about 2 M in total metal (Th + ^{233}U).

Difficulty was encountered in forming microspheres from such concentrated hydrosol. Eight runs were made in which contact times, interstage digestion times, and postextraction digestion times were varied. Despite the use of different combinations of conditions, the improvement in microsphere forming properties was very slight. Thus, we decided to use the Solex countercurrent flowsheet (Fig. 6.1) instead.

The hydrosols produced by the Solex countercurrent flowsheet contained about 0.10 mole of nitrate per mole of heavy metal and could be concen-

ORNL-DWG 69-62RA

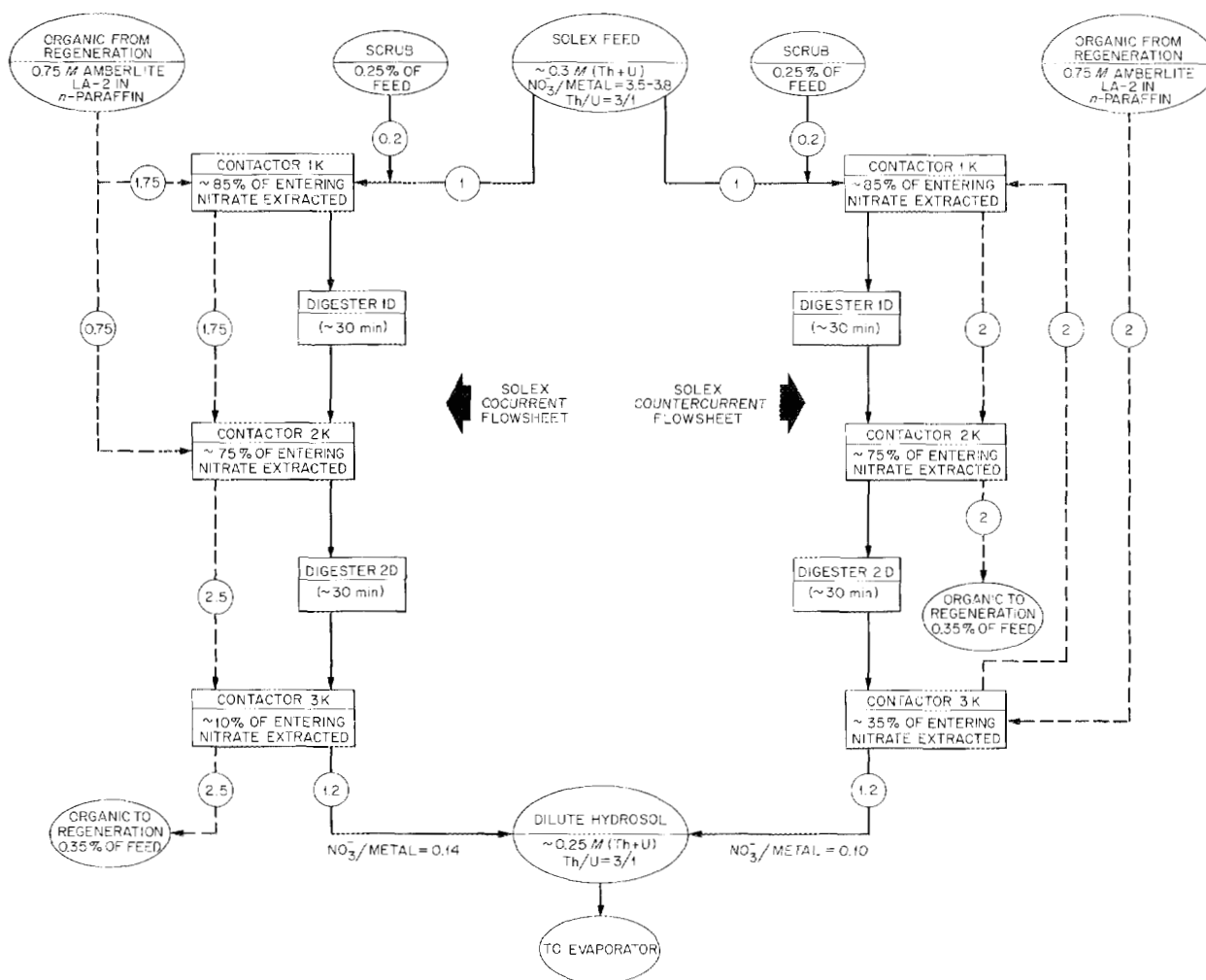


Fig. 6.1. Solex Cocurrent and Countercurrent Flowsheets.

trated to 1 M in Th + ^{233}U . The electrical conductivity of these sols was 2.20 ± 0.2 millimhos/cm.

The inherent stability of the Solex countercurrent flowsheet operation has been demonstrated previously. During these production runs the equipment was operated in a manner that would amplify any non-steady-state characteristics. The batches of feed used were so small that only about one-half of each was recovered in the corresponding product; the other half was held up in the extractors and digesters. Thus, each product was made up of material (~50%) from the run being made at that particular time as well as material (~50%) used in the prior run. Yet, analysis of the mixed evaporator batches and of the heel left in the last contactor showed no differences in composition.

Microsphere Preparation

The microsphere forming operation was carried out in the remotely operated, neutron-shielded

facility² in cell 4, Building 3019 (Fig. 6.2). Microspheres were formed from hydrosol (from the Solex Development Laboratory) by using a two-fluid nozzle to form sol droplets and 2-ethyl-1-hexanol in a tapered glass column to extract the water.³ The sol feed rate was maintained at the rate of 31 g (Th + U)/hr, or 0.5 kg per 16-hr day. A photograph of the column in operation is shown in Fig. 6.3. The wet microspheres (500-g batches) were steam dried to 200°C to remove traces of organic, then calcined in 2-kg (Th + U) batches to 1150°C, using argon-4% hydrogen in the final reduction step.

It was necessary to process approximately 55 kg of metal (Th + U) in order to provide the 32 kg of oxide needed to fulfill the HTLTR commitment.

²Chem. Technol. Div. Ann. Progr. Rept. May 31, 1968, ORNL-4272, pp. 168-70.

³Chem. Technol. Div. Ann. Progr. Rept. May 31, 1968, ORNL-4272, pp. 146-62.



Fig. 6.2. View of Remotely Operated Sphere-Forming Facility.

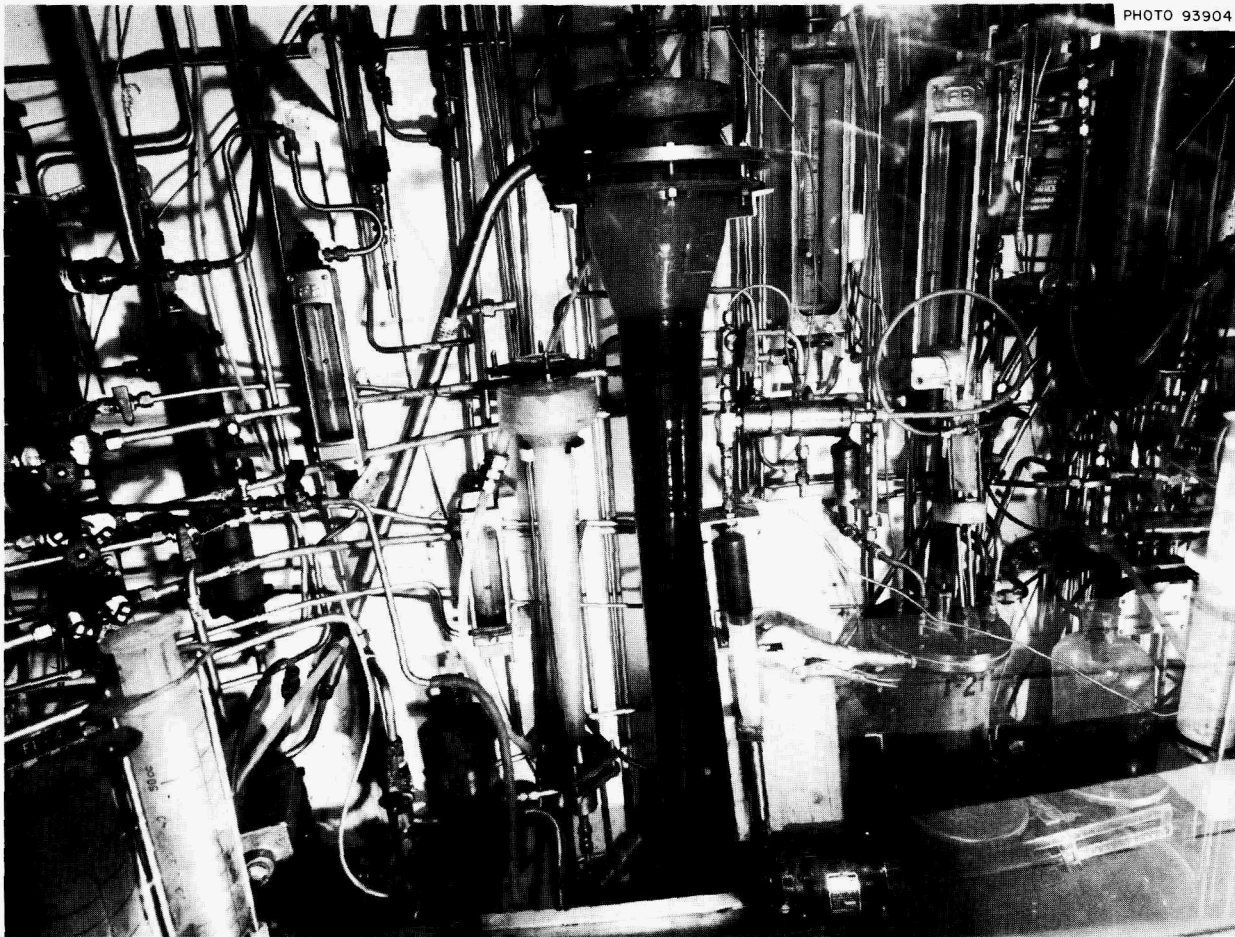


Fig. 6.3. Photograph of the Mixed Oxide Sphere-Forming Column in Operation.

This yield reflects reject rates of approximately 5% from the sphere-forming system (principally fines $<200 \mu$ diam) and 5% from the carbon coating system (principally due to failure of the microspheres to pass the roundness test). The specifications called for the diameters of the bare microspheres (kernels) to be in the range of 250 to 420 μ , the density of the final product to be greater than 95% of theoretical, and the porosity to be less than 1%. Approximately 90% of the product was in the 250- to 350- μ size range, whereas all of the product met the requirements for density and porosity.

Initial operation of the sphere-forming equipment with a $\text{ThO}_2\text{-}^{233}\text{UO}_3$ hydrosol having a $\text{NO}_3^-/\text{metal}$ mole ratio above 0.11 was unsuccessful. Immediately after formation the microspheres disintegrated into minute, nonround fragments. After experimenting with $\text{ThO}_2\text{-}^{238}\text{UO}_3$ sols, which gave

the same results, we operated the Solex system to produce a hydrosol with a lower $\text{NO}_3^-/\text{metal}$ ratio. This hydrosol was formed into microspheres that remained intact.

Although initially an overall yield of the process of only about 60% was realized, improvements made to the latter resulted in yields during the final batches (based on feed to the sphere-forming system and product to the carbon coater) of 95%. A photograph of a typical product is shown in Fig. 6.4.

The increase in yields can be attributed to: (1) installation of a parallel two-fluid nozzle and a resulting decrease in the sol feed rate to the nozzles from 3 to 1.5 cc/min, (2) installation of a superior sol metering pump, and (3) a change in the surfactant content of the 2-ethyl-1-hexanol (2EH); that is, use of Span 80 was discontinued, and the Ethomeen S/15 concentration was adjusted to 0.1% each day.

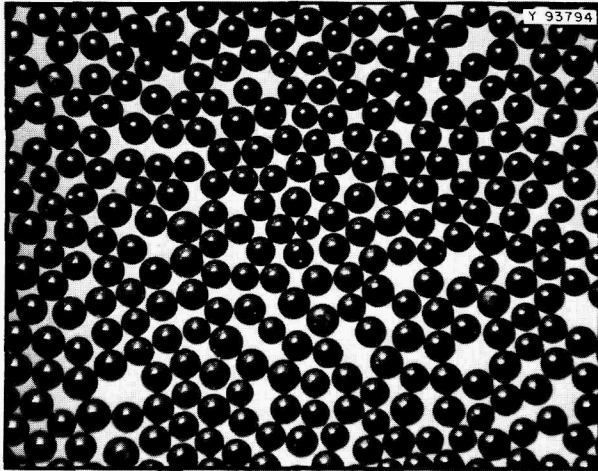


Fig. 6.4. Calcined 75% ThO_2 -25% $^{233}\text{UO}_2$ Microspheres. Diameters, 250 to 350 μ .

It is interesting to note that clustering did not occur in the absence of Span 80.

The calcined product from the sphere-forming system was transferred to the Metals and Ceramics Division for coating with pyrolytic carbon prior to shipment to PNL.

6.2 DEMONSTRATION OF THE ENGINEERING-SCALE PRODUCTION OF ThO_2 - UO_2 MICROSPHERES

The present emphasis is on the demonstration of the procedures and equipment to be used in the Thorium-Uranium Recycle Facility (TURF). The reference material is 300- to 500- μ -diam ThO_2 - UO_2 microspheres with a Th/U atom ratio of 4.25, as required for one HTGR recycle fuel composition. The ThO_2 - UO_3 sol was prepared by amine solvent extraction and was converted into oxide microspheres in equipment having a design capacity of 10 kg/day. The process flowsheets were demonstrated during short (less than 8-hr) periods of operation. Continuous operation for more than 100 hr was planned: (1) to determine the reliability and behavior of both the processes and equipment for extended operating periods; (2) to adapt the equipment to remote operation; and (3) to provide ThO_2 - UO_2 microspheres for fabrication and reprocessing studies.

Preparation of ThO_2 - UO_3 Sol by Amine Solvent Extraction

The engineering-scale amine solvent extraction equipment described in a previous report⁴ was operated continuously for a 10-day period to produce sol containing about 120 kg of 81% ThO_2 -19% UO_3 and to demonstrate the feasibility and consistency of operation of the amine solvent extraction process. The Th/U atom ratio of 4.25 is representative of the Gulf General Atomic (PSC) reference recycle fuel; however, slightly depleted uranium was used in place of the ^{233}U .

The ThO_2 - UO_3 sols were produced by extraction of the nitrate from the $\text{Th}(\text{NO}_3)_4$ - $\text{UO}_2(\text{NO}_3)_2$ [0.3 M in (Th + U); 1.37 M in NO_3^-] feed with 35% excess 0.75 M Amberlite LA-2 (a secondary amine) in *n*-paraffin. Three nitrate extraction stages and two amine regeneration stages – a water scrub followed by a carbonate scrub – were used. The water scrub was combined with the nitrate feed, and the carbonate scrub was routed to waste. We used the countercurrent flowsheet in which fresh amine enters the third nitrate extraction stage and the nitrate feed enters the first stage; however, the liquid flow in the six compartments of each extractor is cocurrent, with the aqueous and organic streams entering at the top and leaving at the bottom. The aqueous phase was digested at approximately 100°C for 30 min between the first and second extractors to promote crystallite formation and, concomitantly, to release additional nitrate for extraction. The dilute sol (forty-three 33.16-liter batches), which was about 0.315 M in (Th + U) and had a NO_3^- /total metal mole ratio of about 0.12, was concentrated in the forced-circulation vertical-tube evaporator⁴ to 1.64 M (Th + U) and subsequently used to form 300- to 500- μ -diam microspheres.

Analyses of periodic samples showed that there was very little fluctuation in the flowing streams during the run, and the equipment operated very satisfactorily with no interruptions during the entire run. The overall material balances (see Table 6.1) for (Th + U) were 100.2 and 100.4% for the solvent extraction equipment and the evaporator respectively. Typical flow rates and analyses of the aqueous and organic streams are presented in Table 6.2. There was an overall 0.04% loss of (Th + U)

⁴Chem. Technol. Div. Ann. Progr. Rept. May 31, 1968, ORNL-4272, pp. 156-59.

Table 6.1. Overall Material Balances for 10-Day Continuous Operation of Amine Solvent Extraction Equipment Producing Approximately 120 kg of 81% ThO₂-19% UO₃ Sol

Sol Preparation by Solvent Extraction ^a	
Entering System:	
Dilute feed	465.3
Leaving System:	
5 liters leaking out pump seal	1.90
50 liters remaining in feed tank at conclusion of run	18.15
Sol product, forty-three 33.16-liter batches	443.46
4.6 liters in sol product drum at conclusion of run	1.43
2.15 liters of samples	0.70
1.18 liters of sample purges	0.32
Carbonate scrub (waste)	0.20
Total	466.2
Overall Material Balance	100.2%
Sol Concentration by Forced-Circulation Evaporation ^a	
Entering System:	
Dilute sol feed, forty-three 33.16-liter batches	443.46
Leaving System:	
Concentrated sol product, forty-three ~6.4-liter batches	445.2
Overall Material Balance	100.4%

^aAll values except material balances are given in g-mole (Th + U).

to the carbonate waste stream, and a loss of 1 to 5 ppm of (Th + U) to the condensate during evaporation of the sol; the entrainment of organic in the sol product was approximately 0.02 vol %.

Microsphere Preparation Pilot Plant

In the Coated Particle Development Laboratory (CPDL), microspheres of the oxides of thorium and of mixtures of uranium and thorium were prepared. The steps in the CPDL operation are: (1) dispersing a sol into droplets of desired size; (2) suspending the droplets in an alcohol to remove water and to effect gelation of the sol droplets; (3) collecting the gelled, spherical particles and drying them to 200°C; and (4) firing the gel microspheres to 1150°C to sinter and densify the product. We operate the CPDL at rates of 10 to 25 kg of oxide microspheres per 24 hr of operation.

A five-day, round-the-clock run that included all the above steps was attempted, using a ThO₂-UO₃ sol with a Th/U atom ratio of 4.25 (see previous section). This was the first operation of this type attempted with the CPDL system. The objectives were to identify problems arising from sustained operation and to produce microspheres for coating and fabrication studies. The sol molarity was 1.64 M (total metal), and the feed rate was equivalent to 10 kg of metal oxides per 24-hr day.

In general, the operation of the column and its auxiliaries was satisfactory for the entire 5-day period. Some difficulty was encountered in surfactant control during the startup period, but this was corrected by adding 50 ml of Span 80 and 5 ml of Ethomeen S/15 at 2-hr intervals. Another problem, the accumulation of an undesirable quantity of oxide fines in the column, was also corrected by replacing a malfunctioning two-fluid nozzle disperser with a new one. Following these

Table 6.2. Typical Flow Rates and Analyses Obtained During 10-day Continuous Run
Producing 81% ThO₂-19% UO₃ Sol by Amine Solvent Extraction

	Flow Rate (liters/hr)	Th Conc. (M)	U Conc. (M)	(Th + U) (M)	NO ₃ ⁻ (M)	NO ₃ ⁻ /Metal Mole Ratio	Free Amine (M)	pH	Conductivity (millimhos/cm)	CO ₃ ⁻ (M)	OH ⁻ (M)	Density at 22°C	Viscosity (centistokes at 25°C)
Nitrate Feed	5.031	0.29	0.07	0.36	1.37								
First Extractor													
Aqueous phase					0.219			4.12	6.8 × 10 ⁻³				
Organic phase													
Digester													
Aqueous phase					0.219			3.24	9.48 × 10 ⁻³				
Second Extractor													
Aqueous phase					0.088			3.85	2.43 × 10 ⁻³				
Organic phase					0.55		0.147						
Third Extractor													
Aqueous phase	6.0	0.253		0.311	0.038	0.122		4.7	5.46 × 10 ⁻⁴				
Organic phase	11.76						0.73						
Water Scrub													
Aqueous phase	1.337	0.0065	0.0019										
Organic phase		1-7 ppm	0.5-5 ppm							1	1		
Carbonate Regen- eration													
Aqueous (in)	3.82												
(out)		20-33 ppm	17-25 ppm		1.62	0.112							
Organic					0.026		0.73						
Composite Con- centrated Sol		1.32	0.32	1.65	0.184			5.07	2.72 × 10 ⁻³			1.403	1.37

two adjustments, column operation was satisfactory in all respects.

Operation of the two batch dryers (batch size, 10 to 20 kg of oxide) was unsatisfactory because of deleterious temperature excursions. The mixed oxide sols used in this run were more sensitive to such excursions than any feed material encountered thus far in the sol-gel program. These excursions were the result of localized overheating and were "triggered" at temperatures around 130°C. A temperature excursion occurred during the drying of each batch (total, 4) processed during the 5-day campaign. The results ranged from complete destruction of the product in one instance to a 50% yield of good-quality microspheres in the desired size range for the best batch. The inadequate performance of the dryer was apparently caused by uneven peripheral distribution of heat. The dryers have been rebuilt to circumvent this problem.

Furnace operation was satisfactory. Microspheres that remained intact after drying met all chemical and physical specifications.

6.3 MICROSPHERE FORMING, DRYING, AND FIRING STUDIES

Microsphere-Forming Column Design and Operating Parameters

The basic process and equipment flowsheets for the sol-gel preparation of microspheres are the same for the thorium fuel cycle, the uranium fuel cycle, and special sol-gel processes. A primary objective of the thorium fuel cycle studies is to adapt these procedures and equipment for use in fuel preparation by remote methods in the Thorium-Uranium Recycle Facility (TURF). The procedures and equipment have been demonstrated for ThO₂-UO₃ sol in directly maintained equipment, as reported in Sect. 6.2. The chemical conditions required for sphere forming, drying, and firing depend, in part, on the sol; results obtained, using various conditions, for ThO₂ and ThO₂-UO₃ sols are presented in Sect. 7.4. Microspheres having diameters less than 100 μ were prepared from these sols by procedures described in Sect. 9.5.

Column Capacities. — Geometrically similar microsphere-forming columns with recommended configurations can be characterized by a single dimension: the minimum inside diameter (i.e., the

diameter at the bottom of the fluidized bed). Thus, the dimensions of a standard tapered column might be as follows:

- D_B = the minimum diameter,
- $2D_B$ = the diameter at the top of the taper,
- $15D_B$ = the length of taper,
- $10D_B$ = a reasonable length of the cylindrical section having a diameter of $2D_B$.

Then the volume of the taper would be $27D_B^3$, and the volume of the cylinder would be $31D_B^3$. The total volumes would be $58D_B^3$, or 950, 3200, 7600, and 25,000 cc for 1-, 1.5-, 2-, and 3-in.-diam columns respectively.

Average bed loadings of 10 to 20 vol % seem desirable. In instances where the microspheres are small, lower loadings must be used to reduce clustering and sticking; on the other hand, higher loadings are possible for the larger, uniform spheres. The sol droplets undergoing gelation constitute most of the volume loading, since the gel microspheres have volumes only one-sixth to one-sixteenth of those of the sol droplets. From these limits, the approximate capacities for several sol molarities and droplet sizes can be calculated (Table 6.3). About one-half of the volume of the bed is located in the cylindrical section; therefore, columns without such a section would have smaller capacities.

The capacity of the column increases as the cube of the diameter, as would be expected. In terms of sol volume per unit time, it varies only slightly with sol molarity or droplet size; the shorter gelation times for smaller drops are offset by the smaller bed loadings that are recommended for the smaller spheres. Columns that have 2-in. (and probably 3-in.) minimum diameters could be made critically safe by using boron-loaded baffles in the larger-diameter top sections. The allowable column sizes for low-enrichment fuels would depend on the actual fuel compositions.

The capacities in Table 6.3 can be thought of as being bracketed by lower and upper limits that are about one-half and twice those listed. The 1.5- and 2-in.-diam columns were operated for long periods at about half the capacities shown in Table 6.3 without any visible signs of overloading. Higher capacities have been demonstrated for short periods only. The top and the bottom of the bed accommodate lower loadings than the middle of the

bed. To achieve capacities twice as high as those given in Table 6.3 would require that the most heavily loaded parts of the bed approach fixed-bed loadings; this would correspond to fixed-bed loadings without fluidization. Operating problems are almost certain to occur at such loadings; therefore, the capacities listed in Table 6.3 are unlikely to be in error by as much as a factor of 2.

Minimum Diameter for Products. — Although the fluidized-bed systems for the preparation of microspheres have no inherent lower limit on diameters, there are several good reasons to avoid fluidization of small droplets if the sol droplets can be gelled without it: (1) The elimination of fluidizing flows would simplify the forming process. (2) The surfactants required to control sticking or clustering

during fluidization would not be needed in an unfluidized system. This would be advantageous since surfactants may contribute to cracking and shape distortions of the microspheres and tend to yield a product having a high carbon content. (3) Continuous operation of a fluidized bed requires the formation of uniformly sized sol drops, while an unfluidized bed does not, and disperser operation would be simplified if less-uniform drops, which are acceptable in some cases, could be gelled in the column.

Small microspheres can be prepared without fluidization if the sol droplets are completely gelled before they fall to the bottom of the vessel. This type of operation has been studied (see Sect. 9.5). Both the settling velocity and the gelation time

Table 6.3. Estimated Capacities of Microsphere-Forming Columns of Various Sizes

Basis: Arithmetic average volume for gelation time, θ_G . Additional average holdup after gelation, $3\theta_G$. 10 vol % loading for 200- μ -diam product; 20 vol % loading for 400- to 500- μ -diam product.

Product Diameter, D_c , μ	200	200	400	400	500	500
Sol molarity, M_I	1.0	2.4	1.0	2.4	1.0	2.4
Sol drop diameter, D_I	675	500	1350	1000	1700	1250
Gelation time, θ_G , min	19	10	38	19	48	23
Bed loading, vol %	10	10	20	20	20	20
(Holdup volume/sol feed rate)						
During gelation, min	10	6	20	11	25	13
As gel spheres, min	4	5	7	10	10	12
Volume ratio of capacities or:						
(sol feed rate/bed volume), cc/hr	0.43	0.55	0.44	0.57	0.34	0.48
(product rate/bed volume), g of gel/hr	0.11	0.35	0.12	0.36	0.09	0.30
Column capacities, cc sol/hr, for:						
1-in.-diam column	410	520	420	540	320	460
1.5-in.-diam column	1,400	1,800	1,400	1,800	1,100	1,500
2-in.-diam column	3,300	4,200	3,300	4,300	2,600	3,600
3-in.-diam column	11,000	14,000	11,000	14,000	8,500	12,000
Column capacities, g of gel/hr, for:						
1-in.-diam column	100	330	110	340	90	280
1.5-in.-diam column	350	1,100	380	1,100	290	1,000
2-in.-diam column	850	2,700	900	2,700	700	2,700
3-in.-diam column	2,700	9,000	3,000	9,000	2,300	7,500

increase as the sol droplet diameter increases so that the distance which a particle will settle increases very rapidly with diameter (i.e., it is approximately proportional to the cube of the diameter). Of the several concatenated or staged devices tested, none offered any advantages over a simple, single-stage "fall through" column. An alcohol with a high capacity for dissolved water would give proportionately shorter gelation times; however, rapid gelation usually increases distortion and cracking problems. The settling velocity would be greater if the alcohol also had a lower viscosity.

The sizes of spheres that could be prepared without fluidization depend, among other things, on the column height (or allowable headroom). For the usual range of sol molarities, the column height required for gelation varies principally with the initial droplet diameter, D_1 , and only slightly with the initial sol molarity, M_1 . A droplet of a less-concentrated sol has a longer gelation time, but the average settling velocity is smaller. As a first approximation, the maximum droplet sizes of 1.2 to 2.5 M sols that will gel in 2EH containing 0.5 to 1 vol % water, without fluidization, are:

Column Height (ft)	Maximum Initial Drop Size for Gelation, D_1 (μ)
2	230
8	360
16	450
32	600

These sol droplets can be gelled in one-half to one-third of the column heights indicated if isoamyl alcohol is used instead of 2EH; however, distortions and cracking in the product would be expected for sol droplets having initial diameters larger than 300 μ .

Laboratory Studies of Microsphere Forming

Gel microspheres are formed from aqueous hydrosol droplets as the water is extracted by the column solvent (2EH). Addition of surfactants to the 2EH is usually required to stabilize the droplets during the water extraction. A combination of a nonionic surfactant, Span 80,⁵ and a cationic surfactant, Ethomeen S/15,⁶ is most commonly used. The 2EH is recycled, after water is removed

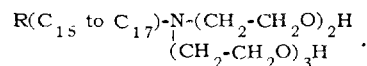
by continuous distillation at temperatures of 140 to 160°C, for use in column operations.

Previous studies have shown that the pH (nitric acid content), the surfactant concentration, and the water content of the 2EH are important variables in the sphere-forming process.^{7,8} These studies showed also that nitric acid reacted with the surfactants and 2EH during the removal of water by distillation. Since the surfactants are destroyed in this process, satisfactory long-term operation requires periodic addition of surfactants to the solvent, and the use of a sol that is not sensitive to surfactant degradation products or to changes in nitric acid content of the 2EH. The concentrations of nitric acid, water, and surfactants that are used in the 2EH to form microspheres would depend on the particular hydrosol that is selected for starting material.

Our present studies are concerned with determining the effects of variations in the 2EH composition on sphere forming and with seeking means for controlling this composition during long-term column and 2EH recycle operations. The effects on the formation of microspheres from $\text{ThO}_2\text{-UO}_3$ sols was studied by a factorial experiment. This type of experiment permits estimations of interactions (i.e., cross effects) among the variables, as well as primary, or first-order, effects. Also, the factorial experiment was carried out in batch sphere-forming tests, using fresh solvent to eliminate any effects due to distillation. We are examining two methods for controlling 2EH composition during long-term column operation. In one, nitric acid is eliminated prior to the removal of water (by distillation) by scrubbing the 2EH with an aqueous sodium carbonate solution. After distillation, the nitric acid concentration is readjusted before the 2EH is recycled to the forming column. In the other method, a total 2EH purification is used; that is, the 2EH is recovered by distillation, and the used surfactants

⁵Product of Atlas Chemical Co.; trade name for sorbitan monooleate.

⁶Product of Armour Industrial Chemical Co.; trade name for a polyoxyethylenated tertiary amine of composition:



⁷*Chem. Technol. Div. Ann. Progr. Rept. May 31, 1967, ORNL-4145, pp. 167-69.*

⁸*Chem. Technol. Div. Ann. Progr. Rept. May 31, 1968, ORNL-4272, pp. 133-36.*

and other still pot residues are discarded. The 2EH is recycled to the forming column after appropriate amounts of surfactants, water, and nitric acid have been added. One or both of these methods will allow us to more effectively control 2EH composition during the continuous, long-term operation of microsphere-forming columns.

Effect of Solvent Composition on the Formation of Microspheres from $\text{ThO}_2\text{-UO}_3$ Sols

The effects of water, nitric acid, and Ethomeen S/15 concentrations in 2EH on microsphere forming were studied in a factorial experiment.⁹ The concentration of the surfactant Span 80 was also known to be significant, and studies of its effect are being completed at this time. The design of the experiment included the use of two levels of concentration for water, nitric acid, and Ethomeen S/15; this gave 2³, or eight, 2EH compositions (Table 6.4) for each sol tested. These particular levels were chosen because they represent the concentration limits within which forming columns can usually be operated. The nitric acid concentration was selected so that chemical equivalence for forming the amine-nitrate salt occurred in solvents, 1, 2, 7, and 8.

⁹K. J. Notz and A. B. Meservey, *Microsphere Forming Conditions for $\text{ThO}_2\text{-UO}_3$ Sols: A Factorial Experiment*, ORNL-TM-2516 (July 1969).

We selected $\text{ThO}_2\text{-UO}_3$ sols for this study because $\text{ThO}_2\text{-UO}_3$ sols having a wide range of properties in regard to sphere-forming behavior and product cracking were available from early experimental runs in the engineering-scale development of the amine extraction process. These sols afforded a very sensitive measure of the effect of 2EH composition on sphere properties such as cracking, clustering, and deformation. Included were four sols of high nitrate content, typical of those from the cocurrent extraction preparation method, and one of low nitrate content, made by the countercurrent method (Table 6.5). The sols selected from those prepared by cocurrent extraction consisted of both digested and undigested sols.

Two laboratory columns, A-13 and B-13, that were essentially the same in design and had nearly identical taper angles (2.87° vs 3.10°) were used to conduct the sphere-forming tests. (However, the turbulence of one column was greater than that of the other because of a slight difference in the placement of the bottom horizontal inlet tube.) Each sol was used to form microspheres in each 2EH composition in each column so that any effects of seemingly small differences in the designs of the columns could be observed. Two columns were used because it had been noted previously that superficially identical conditions in different columns sometimes gave widely varying results.

Table 6.4. 2-Ethyl-1-hexanol Solvent Compositions Used in Factorial Experiment

Solvent No.	H ₂ O Content ^a	HNO ₃ Concentration ^b	Ethomeen S/15 Concentration ^c	Apparent pH
1	+	+	+	2.0
2	--	+	+	1.8
3	+	--	+	7.3
4	--	--	+	6.7
5	+	+	--	1.0
6	--	+	--	0.8
7	+	--	--	3.8
8	--	--	--	3.7

^aHigh value (+): 1.6 vol %; low value (--): 0.4 vol %.

^bHigh value (+): 0.01 N; low value (--): 0.001 N.

^cHigh value (+): 0.01 N or 0.5 vol %; low value (--): 0.001 N or 0.05 vol %.

Table 6.5. Summary of Data for ThO₂-UO₃ Sols Used in Factorial Experiment

Sol No. ^a	C	1(A)	2(B)	B	3(E)
Sol Preparation No.	EV-29B	EV-30A	EV-30A-RV3	EV-30B-D1	ASP-15-AE1
Digestion, hr	0	0	2	2	0 ^b
Analyses:					
(Th + U), M	2.81	2.30	c	2.11	1.37
$\frac{U}{(Th + U)}$, %	24.9	25.7	c	26.0	24.8
$\frac{NO_3^-}{(Th + U)}$, mole ratio	0.14	0.12	c	0.12	0.073
Apparent pH ^d	4.4, 4.4	4.5, 4.8	4.4, 4.8	4.1, 4.8	5.2, 5.4
Conductivity, micromhos/cm ^d	7200, 7100	6700, 5900	6700, 6100	6100, 5400	1800, 2300
Zeta potential, mv	39	31	56	44	48
Crystallite size, A	60	56	60	60	65
Relative crystallinity ^e	1160	1520	1780	2390	2800

^aAll sols were prepared by cocurrent extraction except 3(E), which was prepared by countercurrent extraction.

^bDilute sol was concentrated at 1 atm, which provided some digestion.

^cValues were assumed to be the same as for sol 1(A) since the only difference in preparation was the 2-hr digestion.

^dThe two values are measurements made when the sol was first produced and at a later date respectively.

^eIn arbitrary units per mole of contained oxide. Determined by x-ray-diffraction peak heights above background.

After the microspheres were produced they were examined microscopically and photographed; then, the percentage yields of good-quality, cracked, and deformed product were recorded. Representative micrographs of microspheres prepared from two of the sols in all eight solvent compositions are shown in Figs. 6.5 and 6.6. The percentage yields were used in a statistical evaluation of the solvent compositions.

Statistical analysis of the data showed that, of the three variables related to the solvent, the Ethomeen S/15 concentration was most important. A low Ethomeen S/15 content favored a product with desirable characteristics (including minimal cracking) (Table 6.6). Two cross effects, or interactions of solvent variables, were also noted. A high yield of good-quality spheres was obtained when the nitric acid \times Ethomeen S/15 cross product was positive and when the water \times Ethomeen S/15 cross product was negative. A positive cross product results when both of the variables are high or when both are low, and a negative cross product occurs

when one variable is high and the other is low. In the case of Ethomeen S/15 and nitric acid, the positive cross effect occurs when equivalent quantities of the compounds are present. The highest-quality microspheres were obtained with solvents 7 and 5 (which had low Ethomeen S/15 concentrations), high water concentrations, and an acid concentration at either level. Low-quality product microspheres were obtained with solvents 3 and 4 (which had high Ethomeen concentrations), low concentrations of acid, and a water concentration at either level. Solvent 5 was singular in behavior in that it promoted the formation of microspheres that were granular in appearance but had no cracks. Solvent 6 always gave products characterized by a large dimple (i.e., cherry-pitted). No prominent column operating problems with regard to coalescence, clustering, or wall wetting resulted with any of the solvents or sols that were used.

Cracking of microspheres by a "gel-layering" mechanism was observed frequently (Figs. 6.7 and 6.8). Although uneven gelation has been observed

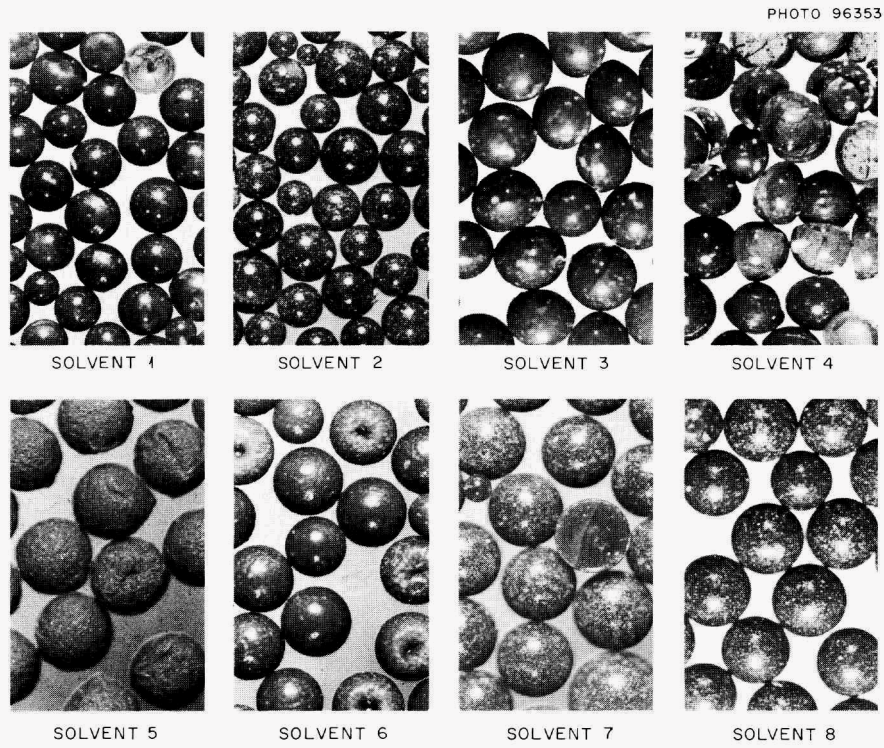


Fig. 6.5. Microspheres Produced from Sol 3(E). Size of microspheres, 300 to 600 μ .

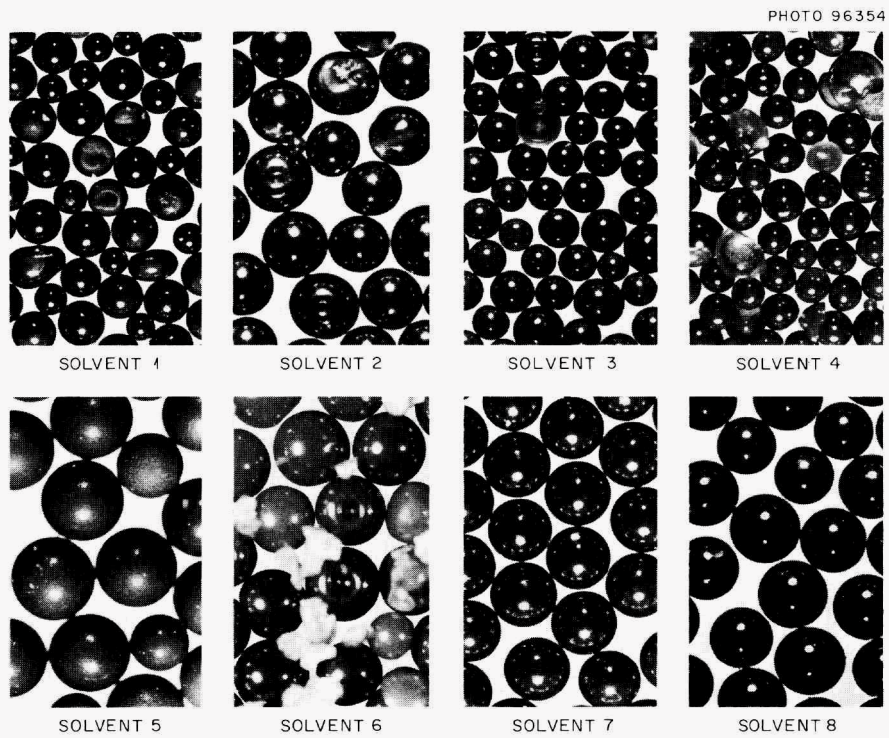


Fig. 6.6. Microspheres Produced from Sol D. Size of microspheres, 300 to 600 μ .

Table 6.6. Summary of Solvent Ratings

Rating	Defects ^c	Solvent ^a				Statistical Effect ^b			
		No.	H ₂ O Content	Acid Content	Ethomeen S/15 Content	Apparent pH	Ethomeen S/15	Acid x Ethomeen S/15	Water x Ethomeen S/15
Superior		7	+	-	-	3.8	F	F	F
Excellent ^d	D ^d	5	+	+	-	1.0	F	Un	F
Good	C	8	-	-	-	3.7	F	F	Un
Fair	C	2	-	+	+	1.8	Un	F	F
Poor ^e	C,D	6	-	+	-	0.8	F	Un	Un
Poor	C,D	1	+	+	+	2.0	Un	F	Un
Poor	C,D	3	+	-	+	7.3	Un	Un	Un
Unsatisfactory	C,D	4	-	-	+	6.7	Un	Un	F

^aSolvent numbers and composition levels are taken from Table 6.4; “+” means high and “-” means low.

^bThe statistical effect is calculated from the solvent composition. F = favorable; Un = unfavorable.

^cD = deformed; C = cracked.

^dProducts characterized by granularity and absence of cracking.

^eProducts characterized by almost 100% cherry-pitting.

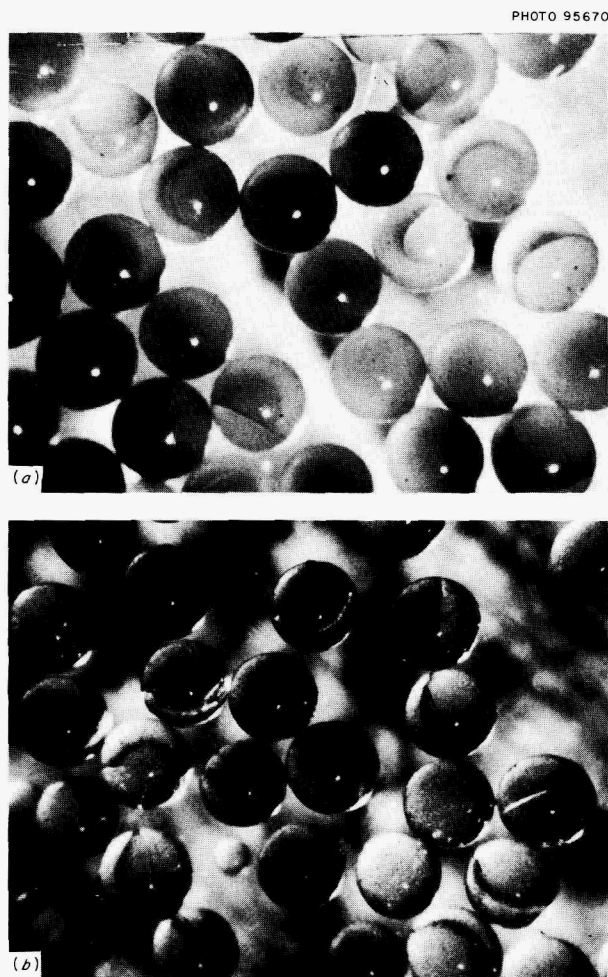


Fig. 6.7. Translucent Microspheres (Undried), Showing Gel Layering and Internal Cracking. (a) Solvent 8, Sol 2(B); (b) Solvent 3, Sol 3(E).

and discussed by Clinton previously,¹⁰ the resultant cracking was first clearly noted in products that were formed from the sols described in this report. In mild, or borderline cases, these cracks could be fused during subsequent firing.

The performance of the sols prepared by cocurrent solvent extraction was as expected; that is, the digested sols gave the best-quality products. The sol prepared by countercurrent extraction performed satisfactorily, giving a product relatively free of cracking. Chemical analyses of these sols showed very few differences, except for the lower NO_3^- /

¹⁰S. D. Clinton, *Mass Transfer of Water from Single Thoria Sol Droplets Fluidized in 2-Ethyl-1-hexanol*, M.S. thesis, University of Tennessee, Knoxville; also issued as ORNL-TM-2163 (June 1968).

(Th + U) mole ratio in the sol prepared by the countercurrent method. X-ray-diffraction measurements indicated identical crystallite sizes in these sols but also suggested that differences in crystallinity or amorphous content might exist. It is interesting to note that all of the sols could be formed into good-quality microspheres under some of the solvent conditions. However, the better-quality sols gave more desirable results for a wider range of solvent compositions.

Although considerable effort was made to operate the two sphere-forming columns (A-13 and B-13) in an identical manner, large differences in corresponding products occurred occasionally (Fig. 6.9). The available evidence indicates that small differences in solvent turbulence in the columns were responsible for such deviations, and that the effect was greatly magnified by the nature of the defects (i.e., cracking or deformation either occur or do not occur). With a borderline sol, a small change in forming conditions was sufficient to take it from a condition where defects were almost occurring to a condition where they did occur.

Studies of 2EH Purification

The removal of nitric acid from 2EH prior to distillation and the recovery of 2EH by distillation were examined in laboratory-scale experiments. Removal of nitric acid prior to distillation prohibits rapid surfactant depletion (due to reaction with nitric acid) during distillation. In addition to the destruction that occurs during distillation, small amounts of these surfactants react with nitric acid in the forming column as evidenced by a slow discoloration of the solvent when the column is operated without a distillation system. Nonetheless, surfactant losses would be significantly reduced by eliminating losses due to distillation.

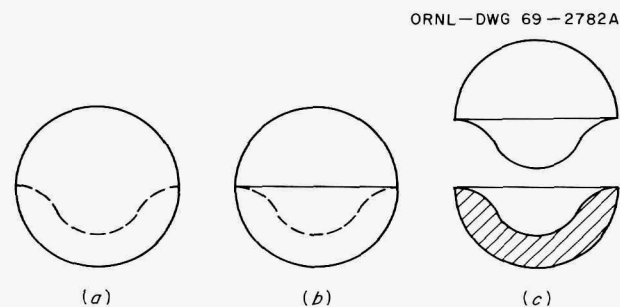


Fig. 6.8. Sequence of (a) Gel Layering, (b) Internal Cracking, and (c) Separation.

The recovery of 2EH by distillation is also being studied as a 2EH recycle method based on total purification of the solvent. Total purification would permit better control over the 2EH composition and eliminate any effects due to buildup of reaction products of surfactants and 2EH with ni-

tric acid. This would be followed by reintroduction of nitric acid, surfactant, and water by infusion.

Samples of 2EH containing known amounts of surfactants were tested without pretreatment, by washing with water and with sodium carbonate solution (Table 6.7) prior to distillation. The depletion of

ORNL DWG 69-2784R

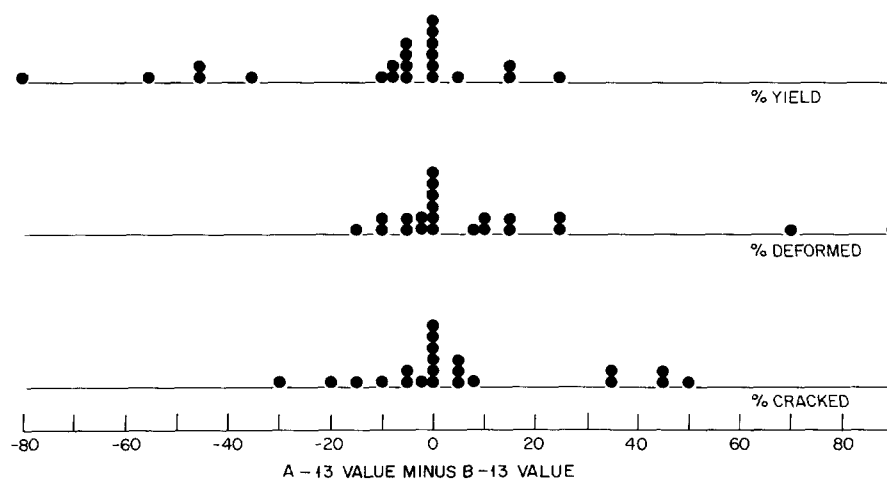


Fig. 6.9. Distribution of Differences Between Columns A-13 and B-13 with Regard to Percentage Yields of Good Product, Deformed Product, and Cracked Product.

Table 6.7. Decomposition of Surfactants During Refluxing with 2EH-0.01 M-HNO₃-2 vol % H₂O

Sample No.	Initial Surfactant Concentration (vol %) ^a		Pretreatment Before Reflux	Refluxing Time (hr)	Post-Refluxing Surfactant Concentration (vol %)	
	Span 80	Ethomeen S/15			Span 80 ^b	Ethomeen S/15
1	0.45	0.55	None	3.5	0.47	0.24
2	0.45	0.00	None	1.2	0.40	
3	0.45	0.00	None	1.2	0.44	0.57 ^c
4	0.00	0.55	None	6.0		0.15
5	0.00	0.55	None	6.0	0.51 ^d	0.26
6	0.45	0.55	H ₂ O wash	2.0	0.54	0.35
7	0.45	0.55	Na ₂ CO ₃ wash; H ₂ O wash	1.3	0.46	0.56

^a0.5 vol % is ~0.01 M for either Span 80 or Ethomeen S/15.

^bAs measured by infrared analysis for the carbonyl group. The measurement does not necessarily reflect the true concentration of sorbitan monooleate (Span 80).

^c0.55 vol % added after the refluxing period.

^d0.45 vol % added after the refluxing period.

surfactants was prevented when the solvent was prewashed with an equal volume of 1 M Na₂CO₃ solution. However, washing with an equal volume of water did not deter decomposition. No discoloration of the solvent that had been washed with Na₂CO₃ was observed during distillation as it was in the case of untreated 2EH. These encouraging results prompted us to install a sodium carbonate washing column in the Unit Operations Section continuous sphere-forming facility. The performance and usefulness of this washing column will be evaluated during the next report period.

The separation factors for the distillation recovery of 2EH are quite good (Table 6.8). Decomposition of the surfactants occurred at temperatures in excess of 200°C in instances where the total surfactant composition in the distilling pot was 50 vol %. In separate tests, the decomposition of Ethomeen S/15 began at about 220°C, at which temperature its concentration was 65 vol %, while there was no apparent decomposition of Span 80 at 226°C, at which temperature its concentration was 78 vol %. The data indicate that 98 to 99% of the 2EH can be recovered from the combined surfactants by distillation at 200°C. Generally, the combined concentration of the surfactants totals 0.1 to 1.0 vol % in used solvent, and distillation at 200°C increases this concentration to about 50 vol %. Further distillation at higher temperatures would probably increase alcohol recovery but would require more rectification of vapor to purify it from surfactant decomposition products. At present, we

plan to discard the still pot liquid after distillation at 200°C. The recovery of alcohol by a continuous side stream distillation system for possible incorporation into the continuous operation of a microsphere-forming column will be studied during the next report period.

6.4 ²³³U STORAGE AND DISTRIBUTION

ORNL serves as a national distribution center for ²³³U. The ²³³U facility, which contains a small batch leacher, a batch dissolver, and a single-cycle solvent extraction system, is capable of purifying ²³³U at the rate of 25 kg per week. The recovery of ²³³U from scrap is limited only by the compatibility of the dissolvent with the stainless steel equipment.

The facility includes systems for storing (1) liquids, (2) solids, and (3) shipping containers that hold solids or liquids; capacities for ²³³U are 500 kg (at concentrations as high as 250 g/liter), 120, and 70 kg respectively. The facility can supply ²³³U with isotopic contents ranging between 90 and 97%, and ²³²U concentrations ranging from 6 to 250 ppm. The average inventory of ²³³U in the plant for the past year has been 234 kg. (This does not include material in the TRUST facility, which will be described later.)

Activities for 1968 are summarized in Table 6.9.

Receipts and shipments of ²³³U for calendar years 1960 through 1968 are shown in Fig. 6.10. The ²³³U received in 1968 amounted to 50 kg (not including the 34 kg of ²³³U received for the TRUST facility), or 41% of that received in 1967. The weight of ²³³U shipped in 1968 was 52 kg, or 87% of that shipped in 1967.

The TRUST (Thorium Reactor Uranium Storage Tank) facility was built to store a metric ton of highly enriched uranium (76.5% ²³⁵U, 9.7% ²³³U) in the form of a uranyl nitrate solution. This solution is the uranium product from the Indian Point Reactor fuel; it was purified by solvent extraction at the Nuclear Fuel Services (NFS) plant in West Valley, New York. The solution will be stored indefinitely since the ²³²U content (120 ppm) prohibits its direct refabrication into fuel elements, and the low ²³³U content makes it of little interest for reactors demonstrating the thorium fuel cycle.

The uranyl nitrate solution (a total of 527 "safe" 10-liter plastic bottles in drum-type containers) was received in 24 shipments during the period from December 16, 1968, to February 6, 1969. The

Table 6.8. Distillation of 2-Ethyl-1-hexanol Containing Span 80 and Ethomeen S/15

Temperature (°C) ^a	Liquid (vol %)		Vapor Distillate (vol %)	
	Ethomeen S/15	Span 80	Ethomeen S/15	Span 80
185	2.4	2.4	<0.05	<0.02
187	7.3	7.7	<0.05	<0.02
188	11.8	10.5	<0.05	<0.02
193	16.7	18.1	<0.05	<0.02
204	23.9		0.08	<0.02
230	29.3		<0.05	<0.02

^aAt 753 mm Hg.

Table 6.9. Summary of Operations in ^{233}U Facility for 1968

Activity	No. of Transactions	Wt. of ^{233}U (g)	Wt. of ^{235}U (g)
Receipts	22	20,055	
	24 ^a	101,642	799,755
Shipments	84	50,126	
Dissolutions	53	20,285	
Solvent Extractions	3	27,174	
Repackaging	18	11,372	

^aTRUST facility material.

procedure used for transferring it to the TRUST facility consisted in:

1. moving the shipping containers from the trailer to the penthouse (a contained area of Building 3019), using a forklift and the building crane;
2. opening the containers, with surveillance by Health Physics personnel;
3. manually transferring the bottles of solution (one at a time) from the container into the charging glove box;
4. lowering the bottles to the transfer cubicle in cell 4, using a motorized winch;
5. weighing the contents of each bottle, using a Toroid load cell (model 36-133-BDC) and a Daytronic digital indicator (model 700-1);
6. sampling the contents of selected bottles, using a syringe;
7. transferring the solution to storage tank P-25, using a steam jet;
8. rinsing the bottle and jetting the rinse solution to P-25;
9. bagging out the empty bottles;
10. hauling the bottles to the burial ground; and
11. returning the closed, empty shipping containers to the trailer.

The transfer operations at ORNL were completed in 22 days. A total of 25 people worked full- or part-time on the project; an average of 9.4 operating people and 2.2 Health Physics people were required each operating day. The number of containers and bottles that were handled varied from 10 to 48 in an

8-hr day. On one occasion, when three shipments arrived during a weekend, 56 units were handled in 12 hr.

The radiation intensities at the surfaces of the filled shipping containers, as received, ranged from 30 to 140 mrad/hr. The intensities at the surfaces of the filled plastic bottles varied from 50 to 600 mrad/hr.

Personnel radiation exposure data were as follows:

Average for all	21 mrem/man-day
Maximum for a single day	160 mrem
Maximum for entire period	650 mrem
Average for various work areas:	
Outside (loading and unloading shipping containers)	9 mrem/man-day
Penthouse (transporting bottles to cell 4)	26 mrem/man-day
Cell 4 (transferring solution to tank P-25)	19 mrem/man-day

During the entire transfer operation, no uranyl nitrate solution or vapor escaped from the sealed plastic sleeves that contained the solution bottles, even though four shipping containers were tipped over (one on the trailer during transit, and three at ORNL during unloading). Leaks of small amounts of solution from the bottle to the sleeve were detected in 14 units; in each instance, the rubber O-ring sealing the bottle cap to the bottle was not in its proper position.

Measurements of the amount of material received at ORNL agreed very well with those reported by NFS; the data are compared in Table 6.10.

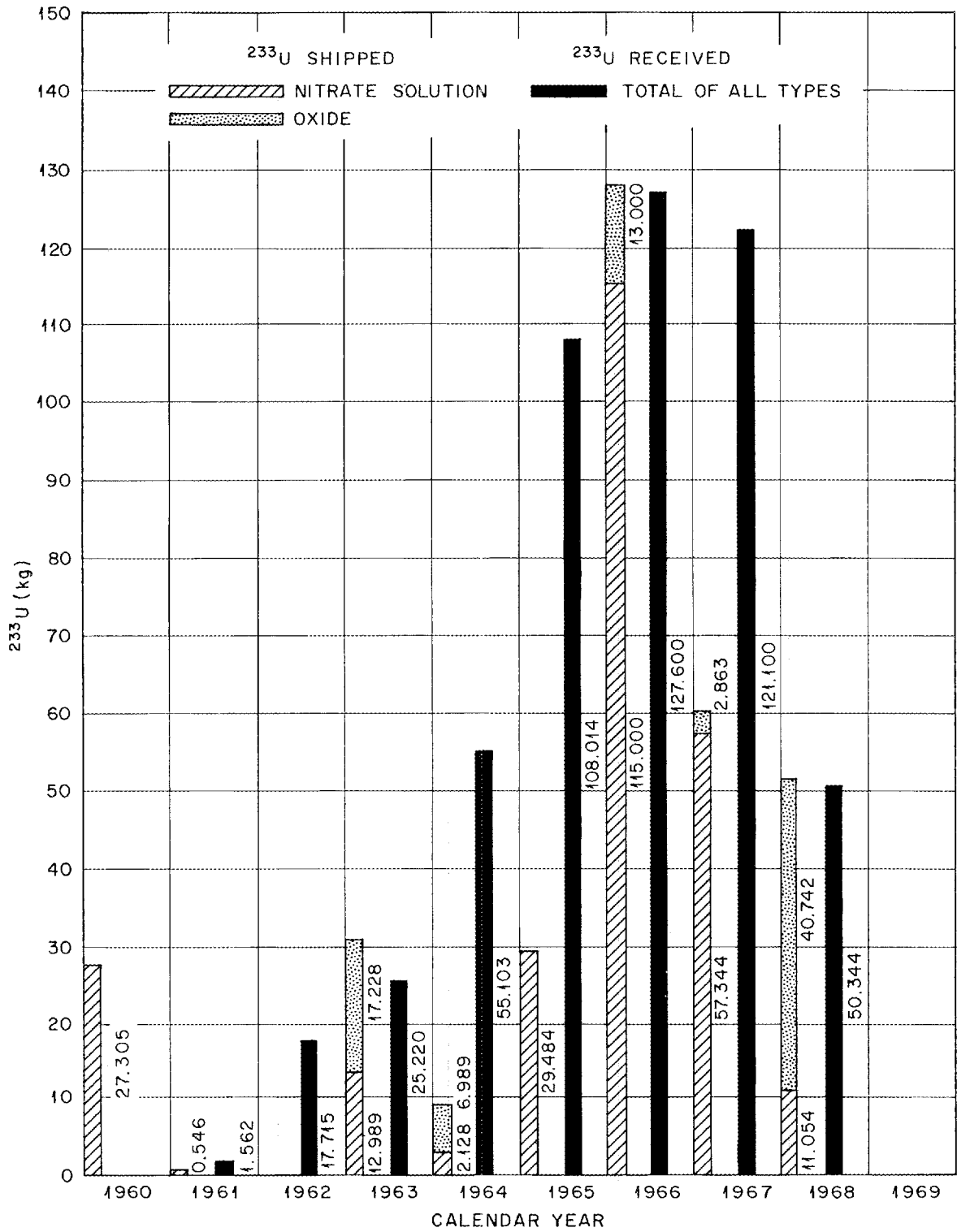


Fig. 6.10. ^{233}U Receipts and Shipments, Bldg. 3019 Dispensing Facility.

Table 6.10. Weight Measurements of TRUST Material

Item	NFS Shipping Wt. (g)	ORNL Receiving Wt. (g)	Difference (%)	ORNL Tank Composite (%)	Difference (%)
Uranyl nitrate solution	6,950,774	6,944,862	-0.09		
Total U	1,038,866	1,047,185	+0.80	1,034,441	-0.43
²³³ U	100,766	101,642	+0.87	101,247	+0.48
²³⁵ U	794,325	799,755	+0.68	791,129	-0.40

The solution weights were obtained by using a load cell with a digital indicator and a recorder. (The load cell was located inside the solution transfer cubicle, and the indicator and recorder were situated in the operating area at the third level of cell 4.) The uranium content of the solution was determined from coulometric and isotopic analyses. The volume of solution in the storage tank was determined from a tank liquid level recorder, the specific gravity of the solution, and the tank calibration.

The TRUST storage system was designed to maintain the uranyl nitrate solution in a subcritical condition. The storage tank was filled with boron-glass Raschig rings, and the solution was mixed with both cadmium nitrate and gadolinium nitrate solutions that had previously been placed in the tank. Each of the three poisons will independently render the solution subcritical.

The Raschig rings will constitute the primary source of criticality control during the first year that the solution is stored; during this period, the stability of the soluble poisons will be determined. After one year, the soluble poisons will become the main criticality control; the rings would be of no value if a leak should develop in the tank, allowing solution to drain to the pit, or if the rings should disintegrate, leaving a portion of the tank unprotected because of settling of the glass fragments.

The solution in the tank will be maintained at the following concentration at all times:

Uranium	150 ± 50 g/liter
Cadmium	0.313 mole/mole U (minimum)
Gadolinium	0.0263 mole/mole U (minimum)
H ⁺	~2 M

Samples of solution will be analyzed each month during the first year, and subsequently at greater intervals, to determine any changes in the above concentrations so that corrective measures may be taken.

Measurements of liquid level and of density in the storage tank and pit sump are made daily. The emergency air compressor, which supplies instrument purge gas to the storage tank during an air and power failure, is checked once each month. Also, monthly radiation checks are made at the pit area, south of Building 3019. Radiation intensities measured in this area immediately after the transfer of the uranyl nitrate solution were:

Pit surfaces	<0.1 mrad/hr
In the street	<0.1 mrad/hr
At the vessel off-gas control valve	
Normal	15 mrad/hr
During solution sparging before sampling	40 rad/hr
One week after sparging	15 mrad/hr

7. Sol-Gel Processes for the Uranium Fuel Cycle

7.1 PREPARATION OF UO_2 SOLS BY SOLVENT EXTRACTION

A new process, known as the CUSP (Concentrated Urania Sol Preparation) process, for the preparation of concentrated ($\geq 1 M$) urania sols directly by solvent extraction has been developed in the laboratory and tested in engineering-scale equipment. Suitability of the resulting sols for the preparation of microspheres has also been demonstrated. In the process, nitrate ion is extracted continuously at a controlled rate from a U(IV) nitrate-formate solution by an organic solution of Amberlite LA-2 (a high-molecular-weight secondary amine). By following a prescribed conductivity-temperature-time schedule, concentrated urania sols characterized by a high degree of crystallinity, stability, and a high U(IV) content are produced. The new process assures a means of process control and reproducibility of product properties that are difficult, or impossible, to attain by using previous sol preparation processes (i.e., the precipitation-peptization and dilute solvent extraction processes).¹⁻⁴

Laboratory Development

In the laboratory development and demonstration of the CUSP process, 1 to 1.3 M U(IV) solutions with a NO_3^-/U mole ratio of 2.0 and a $HCOOH^-/U$ mole ratio of 0.5 were prepared by reducing the corresponding uranyl nitrate-formate solutions with

hydrogen, using a PtO_2 catalyst. Nitrate was extracted from the resulting solutions by a 0.25 M solution of Amberlite LA-2 in 75% diethylbenzene-25% *n*-paraffin. The amine was bubbled through the U(IV) solutions, then regenerated by a continuous method, and recycled back through the uranium solution. Nitrate was extracted at 35°C until the conductivity of the U(IV) solution indicated a free acid concentration just high enough to prevent gelling (point one, Fig. 7.1). At this point, the solution was heated to 58–63°C (the crystallization temperature), and the nitrate extraction was controlled at a rate that maintained the conductivity just above the "gel line." At the crystallization temperature, nitrate extraction was continued, or accelerated, to promote crystallization (point two, Fig. 7.1). Crystallization of the U(IV) polymer was indicated by a change in color from green to black, by off-gassing of the solution, and by a conductivity excursion. Nitrate extraction during the crystallization process was regulated in such a manner that the conductivity excursion was minimized. When crystallization was complete, as indicated by the cessation of nitrate release (i.e., as shown by conductivity measurement), nitrate extraction was continued at about 62°C until a specified conductivity was reached (point three, Fig. 7.1); then the solution was cooled to room temperature. At room temperature, the conductivity was adjusted to yield the optimum NO_3^-/U mole ratio (0.12 ± 0.02) by further extraction of NO_3^- . Optimum final conductivities were about 6.0 and 4.0 millimhos/cm for 1.3 M and 1.0 M solutions respectively.

The success of the process depends on controlling the extraction of nitrate at a rate that allows the system to remain essentially at equilibrium at all times, and on following a temperature-conductivity schedule that prevents gelling, minimizes oxidation of the U(IV), allows complete crystallization of the U(IV) polymer, and produces a sol with

¹J. P. McBride *et al.*, *Preparation of UO_2 Microspheres by a Sol-Gel Technique*, ORNL-3874 (February 1966).

²*Chem. Technol. Div. Ann. Progr. Rept. May 31, 1966*, ORNL-3945, p. 157.

³*Chem. Technol. Div. Ann. Progr. Rept. May 31, 1967*, ORNL-4145, p. 180.

⁴*Chem. Technol. Div. Ann. Progr. Rept. May 31, 1968*, ORNL-4272, p. 142.

a conductivity (free acid content) and a NO_3^-/U mole ratio that are consistent with sol stability. The process concept arose, in part, from digestion studies which had showed that: (1) U(IV) polymer crystallization is inhibited by the presence of excess nitrate and excess U(VI), (2) nitrate must be extracted at the crystallization temperature in order to promote complete crystallization, and (3) the free acid concentration should be minimal during all stages of the process to minimize oxidation.

In general, sols prepared in the laboratory by the CUSP process contained a large fraction of crys-

talline solids (80 to 100%) having an average crystallite size of $40 \pm 1 \text{ \AA}$, whereas all of the sols prepared in processing equipment under an optimized mode of operation were 100% crystalline (see subsection on "Determination of the Average Crystallite Size and the Fraction of Crystalline Solids in Urania Sols"). Each sol was very stable, with a shelf life (i.e., the period of time during which it remained fluid) of several months, and could be readily concentrated under vacuum to 3 M or higher. Properties of the laboratory-prepared sols are listed in Table 7.1. It should be recognized that

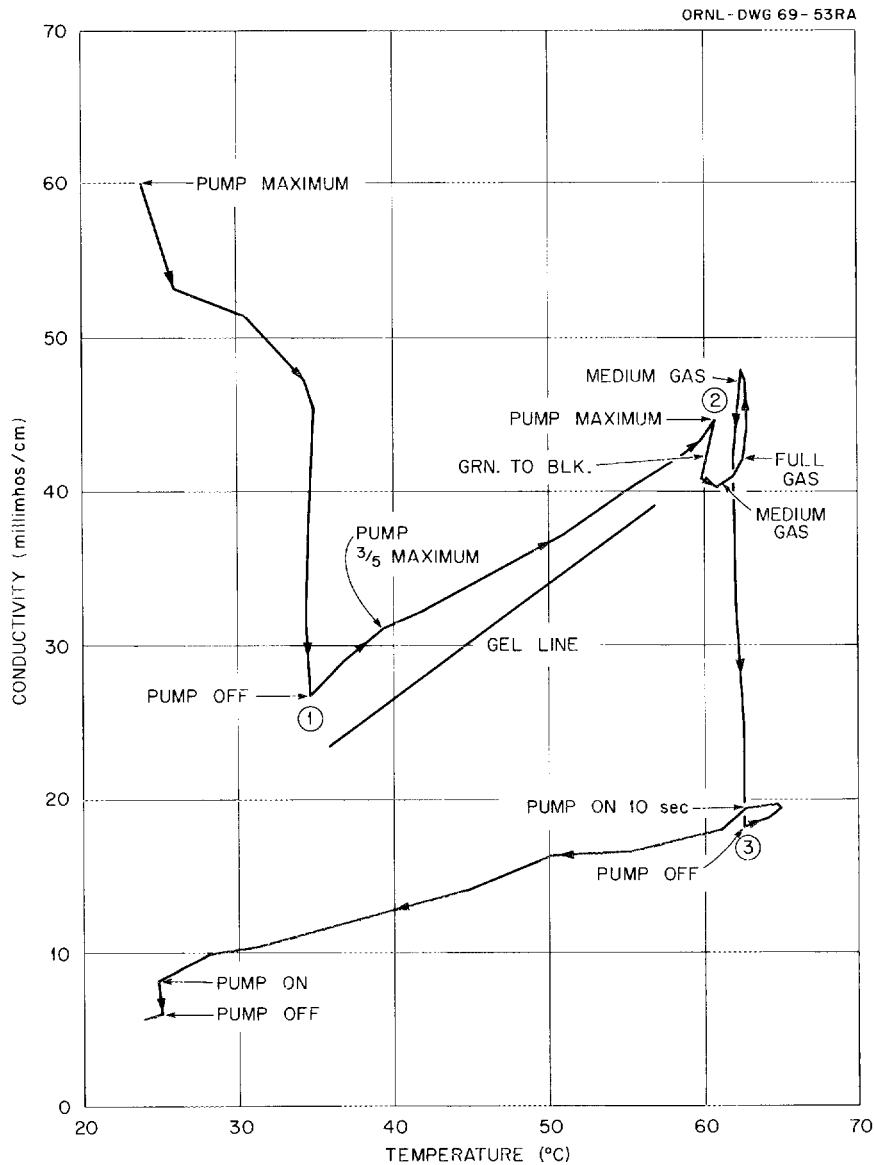


Fig. 7.1. Typical CUSP Operating Curve.

the listed variations in properties result from deliberate variations in operating parameters made to study the effect of process variables. Thus, the sols designated as CUSP-4 through CUSP-7 represent attempts to reproduce a given operating procedure, while the sols designated as CUSP-8 and higher were prepared with deliberate parameter variations (i.e., CUSP-8 and -9, variable crystallizing temperature; CUSP-10 and -11, variable time of initial nitrate extraction; CUSP-12, variable uranium feed concentration).

Analyses of the conductivity-temperature-time curves and of the sols indicated the following:

1. The NO_3^-/U mole ratios in polymer solutions (having the same conductivity) prior to heating to the crystallization temperature are functions of the initial extraction time (Table 7.2).

2. An initial extraction that is too rapid produces a urania sol with a high nitrate content. Such a sol appears to release its nitrate less rapidly than sols prepared by slower extractions.

3. The most effective crystallization temperature appears to be about 62°C.

4. The current estimates of operating time are: 90 min for the initial extraction; a heatup rate of 1°C/min; 90 min at the crystallization temperature, with the extraction rate adjusted to give about 60 min at a conductivity of about 40 to 45 millimhos/cm.

5. It is difficult to adjust the conductivity of the sol (i.e., by extraction of excess nitrate ion) while it is at 62°C to ensure that, on cooling to room temperature, the optimum conductivity for stability will be achieved; thus far, "polishing" of each sol

Table 7.1. Properties of Urania Sols Prepared in the Laboratory by the CUSP Process

Sol (CUSP-)	U Conc. (M)	U(IV) Content (% U)	NO_3^-/U Mole Ratio	HCOO^-/U Mole Ratio	Crystallinity ^a (% U)
4	1.34	82	0.14	0.47	
5	1.39	84	0.14	0.44	
5 and 6	1.39	82	0.12	0.36	
7	1.38	89	0.11	0.48	100
8	1.32	85	0.15	0.41	79
9	1.42	82	0.19	0.35	46
10	1.39	81	0.14	0.42	33
11	1.47	84	0.21	0.36	77
12	0.93	89	0.13	0.43	81

^aAverage crystallite size: 39 ± 1 Å.

Table 7.2. Effect of Initial Extraction Time on NO_3^- Content of Urania Polymer

Preparation (CUSP-)	U Conc. (M)	Volume (liters)	Extraction Time (min)	Conductivity (millimhos/cm)	NO_3^-/U Mole Ratio
3	1.25	1.5	197	24	0.48
9	1.25	1.5	86	26	0.68
10	1.25	1.5	62	27	0.58
11	1.25	2.0	50	25.5	0.89
12	0.92	~2.0	139		0.60

preparation at room temperature has been required to obtain the optimum NO_3^-/U ratio.

Figure 7.2 shows a relationship between the U(IV) content of the final sol and the fraction of crystalline solids. The fraction of crystalline solids is seen to vary from about 30 to 100% as the U(IV) content of the final sol increases from 80 to about 90%. It should be noted that this increase in U(IV) content represents a decrease of 100% in the U(VI) content.

Table 7.3 shows the effect of aging on the conductivity of sols prepared by the CUSP process. Sols become thixotropic when their conductivity values become greater than about 11 millimhos/cm.

Figure 7.3 shows the effect of off-gassing temperature on the surface area of dried gels that were prepared by drying CUSP-produced sols at room temperature under argon. The maximum surface area is obtained at an off-gassing temperature of 85 to 100°C. A sharp decrease in surface area is seen at off-gassing temperatures just above 100°C; a plateau appears between 300 and 400°C, and then another sharp decrease occurs above 400°C. The decrease between 100 and 400°C could be the result of chemical bonding between the individual crystallites, whereas that occurring above 400°C may be related to actual sintering. The experimentally determined surface area of the CUSP-7 gel is 136 m²/g, which is very close to the theoretical value (139 m²/g) that was calculated from the average crystallite size (39 Å) of the CUSP-7 sol. The CUSP-8 and -10 sols had significant amorphous fractions (67 and 21%, respectively), and hence showed lower surface areas.

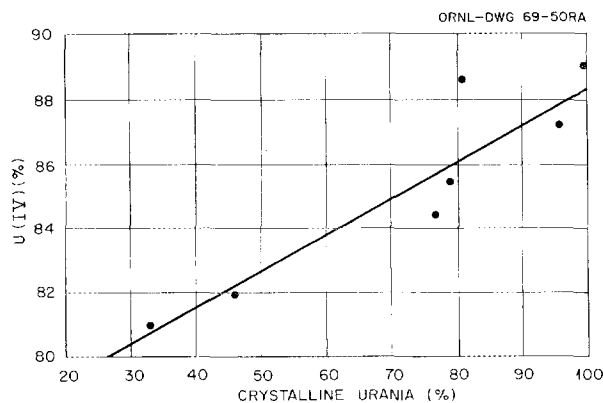


Fig. 7.2. Effect of U(IV) Content on Crystallinity of Urania Sols Prepared by the CUSP Process.

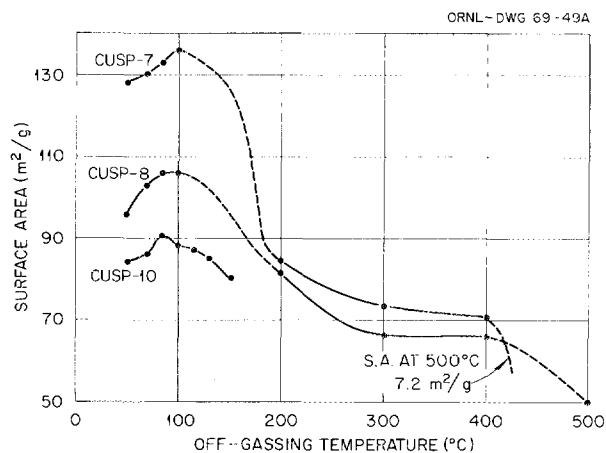


Fig. 7.3. Surface Areas of Urania Gels Prepared from Sols Produced by the CUSP Process.

Only limited microsphere forming studies have been carried out with the laboratory-prepared sols. However, the high crystallinity and reproducible characteristics of the sols prepared in engineering equipment suggest that microsphere forming will not be a problem, and should, in fact, be easier than with sols prepared by previous methods. Some properties of fired microspheres made from laboratory-prepared sols are given in Table 7.4.

Demonstration of the CUSP Process on an Engineering Scale

Existing equipment for the continuous production of dilute urania and dilute $\text{ThO}_2\text{-UO}_3$ sols by a multistage extraction-digestion process⁵ was adapted for the engineering-scale demonstration of the CUSP process. The major changes in the equipment were confined to one of the three extraction stages of the original system. The aqueous surge tank, pump, conductivity instrumentation, and piping for aqueous recycle to the extraction column were the principal new items added (see Fig. 7.4). Operating time of the extraction equipment was about 5 hr per batch of 16 liters of 1 M urania sol; the production rate was approximately 18 kg of UO_2 per 24-hr day.

⁵R. G. Wymer, "Laboratory and Engineering Studies of Sol-Gel Processes at Oak Ridge National Laboratory," in *Sol-Gel Processes for Ceramic Nuclear Fuels*, IAEA, Vienna, 1968; see also ORNL-TM-2205 (May 1968).

Table 7.3. Effect of Aging on the Conductivity of Sols Prepared in the Laboratory by the CUSP Process

Sol (CUSP-)	As Prepared		Aging Time (months)	After Aging	
	Temperature (°C)	Conductivity (millimhos/cm)		Temperature (°C)	Conductivity (millimhos/cm)
7 ^a	25.1	7.7	5.3	23.2	9.0
8 ^b	27.6	6.2	3.7	23.8	9.6
9 ^c	22.7	4.7	2.0	25.0	11.2
10 ^b	24.0	5.9	1.6	25.8	9.5
11 ^c	33.1	8.5	1.3	24.0	11.7
12 ^b	24.1	4.3	1.0	25.0	6.4

^a100% crystalline.

^bLow NO_3^-/U mole ratio.

^cHigh NO_3^-/U mole ratio.

Table 7.4. Properties of Fired Microspheres Made from Laboratory-Prepared CUSP Sols

Sol (CUSP-)	O/U Atom Ratio	BET Surface Area (m^2/g)	Hg Porosity (%)	Hg Density (% of theoretical)
4	2.02	0.0059	0.96	97.3
5	2.01	0.0074	0.84	97.3
6	2.01	0.0053	0.33	96.9

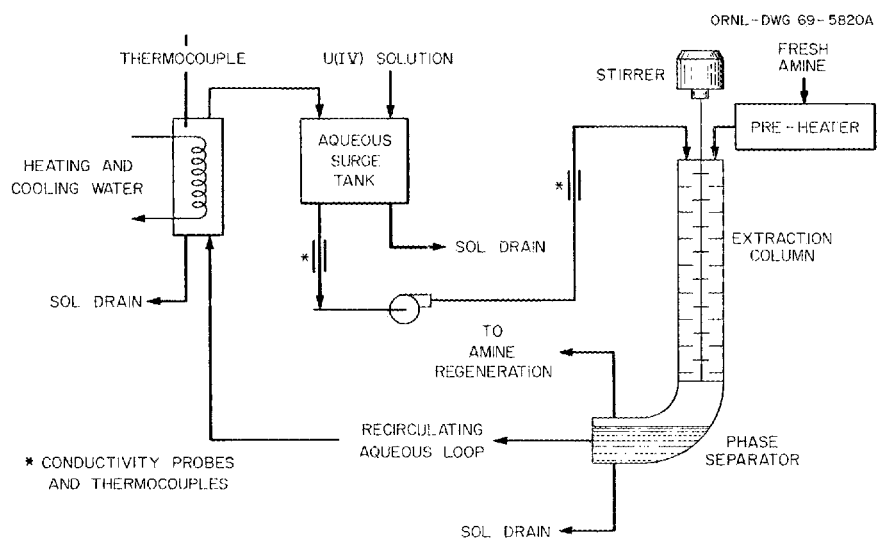


Fig. 7.4. Diagram of Engineering-Scale Equipment for Preparing Concentrated Urania Sol by the CUSP Process.

Six runs (i.e., five developmental runs and one special product run) were required to establish reasonably routine operation. When the conductivity probes were properly located (i.e., after run 1), control of the process via conductivity measurement became straightforward and reproducible. Chemical data relevant to the sols prepared in these six runs are summarized in Table 7.5.

Sols characterized by excellent fluidity, long shelf lives, and ease of concentration to fluid 3 *M* sols were produced in runs 2, 3, and 4. In run 1 the conductivity probes were located in stagnant areas of the system, and gelation occurred during the initial nitrate extraction. Due to an extended hold time prior to heating to the crystallization temperature, an inferior sol product was eventually prepared. The feed for run 5 was prepared in a different reduction apparatus than that used for preparing feed for the other runs, and the product sol was definitely inferior (e.g., some thickening at 1 *M* occurred after 6 weeks; gelling occurred at a concentration of 2.3 *M*). The apparent cause was insufficient agitation during the reduction step and the subsequent production of undesirable side-reaction products. Overreduction of the U(IV) feed for run 6 because of instrument difficulties (i.e., the flow of hydrogen was allowed to continue after the reduction of U(VI) to U(IV) was complete) produced sufficient ammonia to cause gelation during the final NO₃⁻ extraction step, after crystallization was complete (see Table 7.5). Thus, failure to

make a satisfactory product sol was clearly the result of gross equipment failure or inadequacy of equipment performance.

Figure 7.5 is an electron photomicrograph of a 1 *M* sol that was prepared in engineering-scale equipment. This photomicrograph shows that, although x-ray diffraction indicates an average crystallite size of 40 Å, the actual micelles are very uniform spherical agglomerates that are 250 to 300 Å in diameter and composed of many small crystallites. X-ray diffractometry measurements showed this sol to be 100% crystalline. An electron diffraction pattern of the sol particles is shown in Fig. 7.6.

Microspheres were prepared from the product sol from run 2 by gelation in a drying solvent and subsequent drying and firing. The 1 *M* sol, as prepared, and a sol prepared by concentrating the 1 *M* sol to 3 *M* were used. Conditions during the forming step were not optimized, but were based on previous experience with UO₂ sols. Properties of the fired microspheres are given in Table 7.6.

Determination of the Average Crystallite Size and the Fraction of Crystalline Solids in Urania Sols

The average size of urania sol crystallites was calculated from the x-ray diffractometer line-broadening data, using the Jones B instrument correction

Table 7.5. Properties of UO₂ Sols Prepared on an Engineering Scale by the CUSP Process

Run No.	Feed Solution		Sol Properties				
	U(IV) Content (%)	NH ₃ /U Mole Ratio	U(IV) Content (%)	NO ₃ ⁻ /U Mole Ratio	Conductivity at 25°C (millimhos/cm)	% Crystallinity	Shelf Life ^a
1			82	0.14	6.6	100	<5 weeks at 1 <i>M</i>
2	99	0.0017	86	0.09	3.5	100	≤3 months at 3 <i>M</i>
3	94		90	0.11	2.25	100	≤2 months at 1 <i>M</i>
4	95		86	0.14	4.25		≤2 months at 1 <i>M</i>
5	91		83	0.08	3.75		≤6 weeks at 1 <i>M</i>
6	95	0.029		0.08	5.0 ^b		

^aTime prior to gelation.

^bGelled because of high NH₃ content of feed solution.

method.⁶ Copper k_{α} radiation and the broadening of the (111), (220), and (311) lines were used. When these three lines did not give the same apparent size, the values were averaged; however, differences were seldom greater than that due to experimental error.

⁶H. P. King and L. E. Alexander, *X-Ray Diffraction Procedures*, Wiley, New York, 1954; H. S. Peiser, H. P. Rookby, and A. J. C. Wilson, *X-Ray Diffraction of Polycrystalline Materials*, Reinhold, New York, 1960.

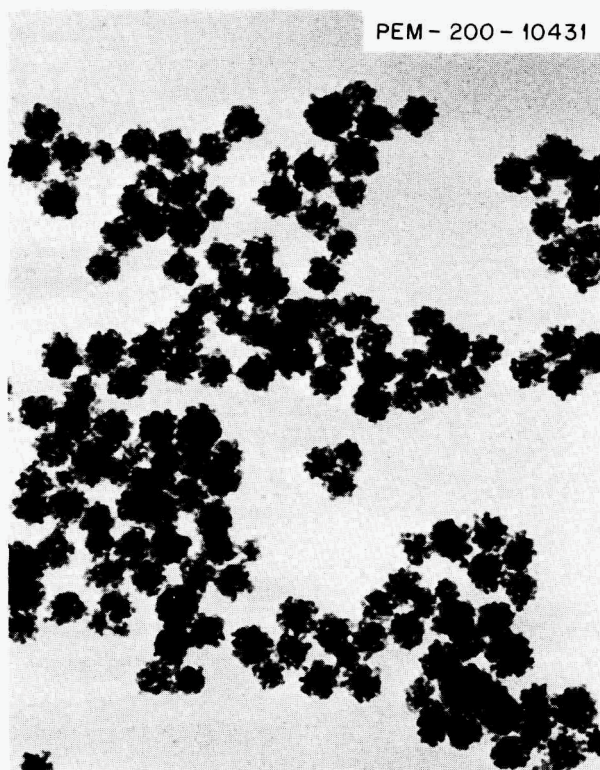


Fig. 7.5. Electron Photomicrograph of Fully Crystalline UO_2 Sol Prepared in Engineering-Scale Equipment by the CUSP Process. The sol is composed of 40-A crystallites and uniform micelles 250 to 300 Å in diameter. 183,000 \times .

The percentage of urania in crystalline form (rather than amorphous or dissolved) was determined by two methods:

1. Comparison of the x-ray diffractometer trace (111) line of the sample with a diffractometer trace for the (111) line of a urania sol that had been shown to be crystalline by agreement between the particle size determined by x-ray diffraction line broadening and that calculated from the BET gas adsorption area of dried gel prepared from the sol by means of the equation:

$$A = \frac{6}{\rho D},$$

where

ρ is the density of the particle,

D is the average particle diameter,

A is the specific surface area.

2. Comparison of the x-ray diffractometer trace for the (111) line of the sample with a diffractometer trace for the (111) line of a thoria sol that had been shown to be fully crystalline by the method above. The contribution of amorphous or soluble metal species to the (111) line pattern is negligible in the concentration ranges encountered.

The particular parameter chosen for comparison was the net peak height of the diffraction line, divided by the background level at lower angles than the line. By rigidly standardizing all sample handling and diffractometer operation procedures, it was possible to get a monotonic calibration function of this parameter vs the U(IV) or Th(IV) molarity of the standard to about the $\pm 5\%$ level of reproducibility. The same parameter was determined for the sample, and the molarity of crystalline metal oxide in the sample was interpolated in the above function. A correction factor, empirically determined, is applied to the calibration function when

Table 7.6. Properties of Microspheres Formed from Sol Produced in Run 2

Sol (M)	Final O/U Atom Ratio	C Content (%)	Hg Density (g/cc)		Bead Size (μ)	Average Crush Strength (g)
			15 psi	15,000 psi		
1	2.005	0.003	10.53	10.60	350-400	746
3	2.003	>0.002	10.78	10.81	300-350	614

thoria is used for comparison. A urania standard can be used directly if its crystallite size is the same as that of the sample (which was the case for all sols discussed here). The thoria standard is not air-sensitive, and is therefore more convenient to use, despite the correction factor that is required in the calibration function. Figure 7.7 shows a crystallinity calibration curve obtained for a typical

urania sol. The calibration curve is an empirical curve related to the particular equipment and sample handling procedures used. In each case in which crystallinity is to be determined, a standard is analyzed along with the sol in order that slight variations from the calibration curves as the result of sample handling, equipment parameters, etc. may be detected and proper corrections may be made.



Fig. 7.6. Electron Diffraction Pattern of 1 M UO_2 Sol Prepared in Engineering-Scale Equipment by the CUSP Process.

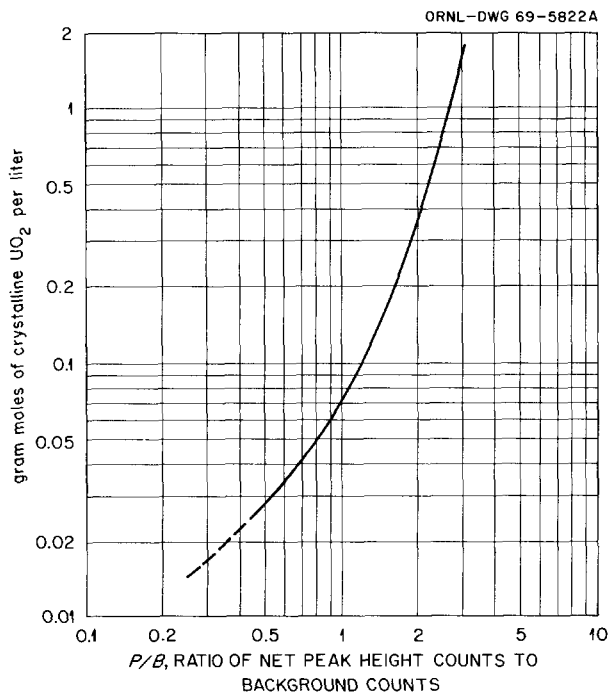


Fig. 7.7. Crystallinity Calibration Curve for Typical Urania Sol.

7.2 UO₂-PuO₂ AND PuO₂ SOL-GEL PROCESS DEVELOPMENT⁷

Preparation of Mixed Urania-Plutonia Sols by Solvent Extraction

Interest in mixed UO₂-PuO₂ fuels for fast breeder reactors, the ease of operation of solvent extraction processes, and the previously demonstrated success in preparing UO₂ sols by solvent extraction techniques provided the impetus for laboratory studies to develop a solvent extraction process for preparing mixed UO₂-PuO₂ sols. In initial experiments, incompatibilities between uranium and plutonium components were more severe than anticipated. Although oxidation of ionic U(IV) by ionic Pu(IV) was expected, this reaction remained troublesome even when significant quantities of the uranium were hydrolyzed prior to mixing the uranium and plutonium components. An additional difficulty arose from an apparent adverse effect of formic acid

⁷This section includes work on the preparation of ²³³UO₂-ZrO₂ microspheres.

(present in the urania sols) on the mixed UO₂-PuO₂ sols.

We have developed several procedures that greatly improve mixed sol stability, and mixed sols can now be prepared by methods which yield microspheres with good physical characteristics. These procedures include: (1) addition of high-nitrate plutonia sols (i.e., sols having a NO₃⁻/Pu mole ratio of about 1.3), instead of ionic Pu(NO₃)₄ solutions, to urania sol, and (2) digestion at temperatures higher than normally used for urania sols to produce larger, more chemically stable crystallites. Most significant of all, however, is the observation that urania sols prepared by the CUSP process can be mixed with high-nitrate plutonia sols and successfully formed into microspheres if the mixing and forming are carried out within a 24-hr period.

Dilute mixed sols prepared by the procedure shown in Fig. 7.8 were stable indefinitely; however, sediment collected in sols that were concentrated to more than 1 M in total metal. Microspheres prepared from the 1 M sols showed no tendency to crack, and the average crushing strength for a 250- μ -diam microsphere was 560 g.

The need to use high-nitrate plutonia sol to obtain a satisfactory mixed sol feed prompted the development of the amine extraction procedure shown in Fig. 7.9. Recent work indicates that *n*-hexanol extraction may be superior to amine extraction in this procedure.

In a later development, improved mixed sols were prepared using highly crystalline urania sol prepared by the CUSP process and a plutonia sol prepared by *n*-hexanol extraction. When mixed, these feed sols showed no indication of physical instability at a total metal concentration of 1 M and formed microspheres with improved properties.

An observed increase in stability of mixed urania-plutonia sols that had been digested at 100°C prompted studies of the effects of particle crystallinity and crystallite size in mixed sols. Urania crystallites formed and grew as large as 100 Å at temperatures less than 100°C, whereas plutonia crystallites (in separate experiments) formed but did not grow any larger than 5 to 15 Å at such temperatures.

An outline of treatment given to dilute urania sols in urania crystallite growth studies is shown in Fig. 7.10. Urania crystallites grew from an initial size of 35 to 100 Å in 3 hr at 100°C. The rate of growth was essentially linear after the first hour. A release of anions from the dispersed solid phase

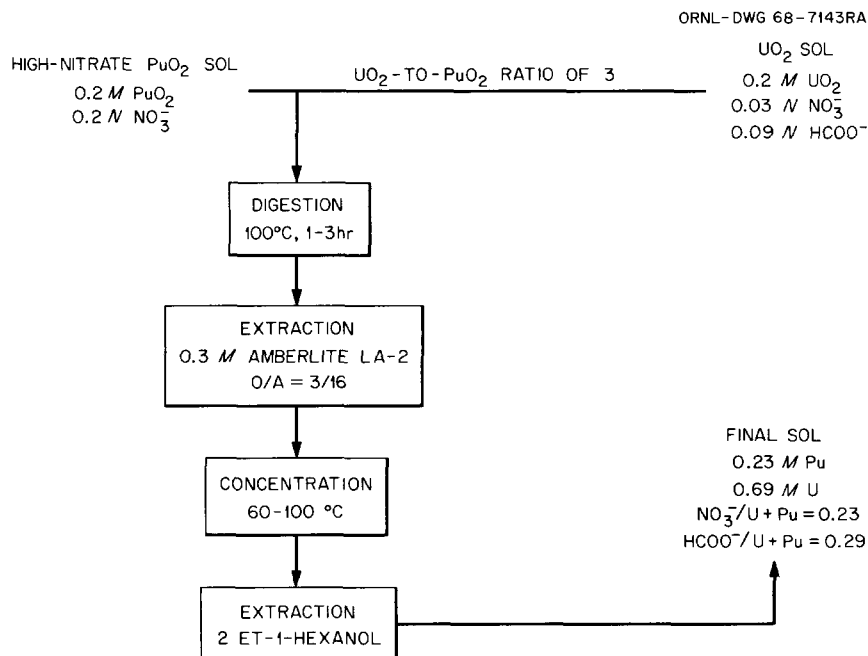


Fig. 7.8. Flowsheet for the Laboratory Preparation of Mixed Plutonia-Urania Sols.

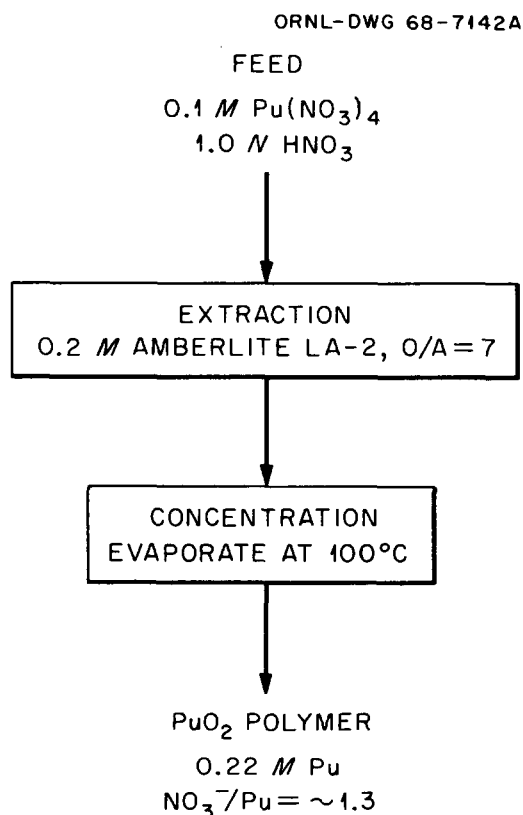


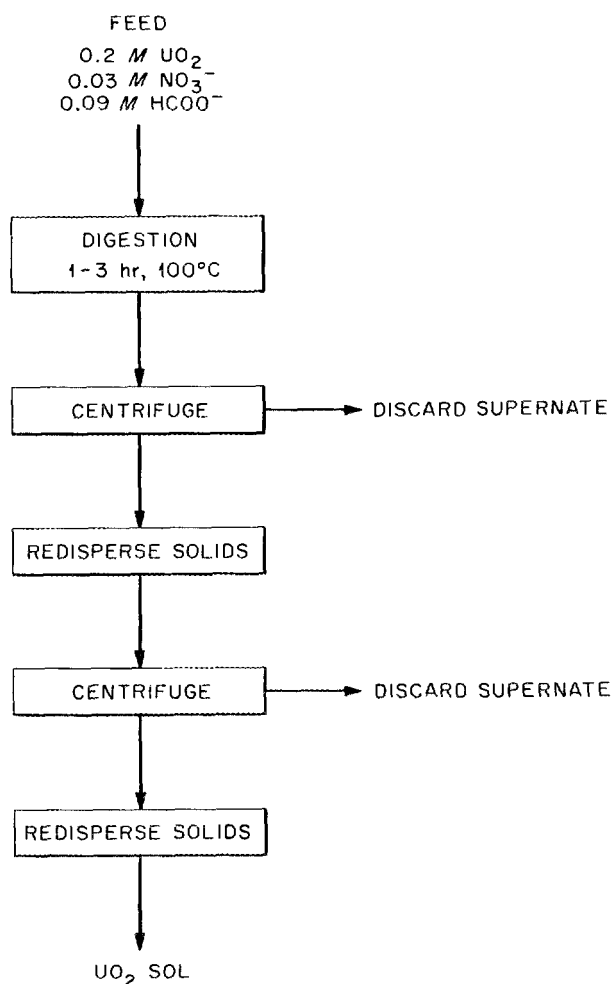
Fig. 7.9. Flowsheet for Preparing High-Nitrate Plutonia Sol by Solvent Extraction.

to the aqueous phase accompanied crystallite growth. The concentration of anions remaining with the dispersed solid phase of the sol was a function of the solid-phase surface area. The surface area (calculated from crystallite size based on cubic geometry) per gram of urania decreased from 114 to 57 m²/g in 3½ hr of digestion at 100°C. Anion concentration per unit area of crystallite surface remained relatively constant with increasing crystallite size (approximately 20 micromoles of anion per square meter of urania surface).

When mixed 75% urania-25% plutonia sols were digested 3 hr at 100°C, the average crystallite size was only 68 Å. This indicated, as expected, that the plutonia crystallites did not grow and that, in addition, they retarded urania crystallite growth. In conjunction with centrifugation studies, these results indicate that the urania and plutonia were associated in a single solid phase. One explanation for slow urania crystallite growth is that part of the urania surface may be covered by adsorbed plutonia, which inhibits growth.

Formic acid is used to stabilize U(IV) in the urania sol preparation process. However, it was found that after formation and growth of crystallites the formic acid is no longer needed, and its presence in mixed sols promotes pseudoplastic and thixotropic properties. These effects are elimi-

ORNL-DWG 68-7144A

Fig. 7.10. Postextraction Treatment of UO_2 Sols.

nated by extracting the formic acid into aliphatic alcohols. A study made with formate-free mixed urania-plutonia sols indicated that formate is not the major factor in mixed sol concentration problems since sols without formic acid began to exhibit solid formation at a total metal concentration of about 1.3 M. The study demonstrated that in the absence of formic acid stable mixed sols containing up to 25% U(VI) can be prepared. Crack-free microspheres calcined at 1150°C were prepared from these sols. The average crushing strength for a 250- μ -diam microsphere was 550 g.

PuO_2 Sol-Gel Development

The method described last year⁸ is still our most reliable and efficient way of preparing a pure PuO_2

sol. Sols made by this method may be formed into microspheres, or may be mixed with UO_2 sols to make a feed sol for use in preparing mixed UO_2 - PuO_2 microspheres or shards. Results of laboratory studies of the PuO_2 sol-gel process (see Sect. 8.1) have indicated that two minor process changes will result in an improved product in large-scale glove-box operations (150 g). These modifications require decreasing the HNO_3/Pu mole ratios from 2.5 to 1.2 when nitric acid is added to peptize the washed hydroxide, and increasing the plutonium concentration from 0.1–0.2 M to 0.4–0.45 M during peptization.

Preparation of $^{233}\text{UO}_2$ - ZrO_2 Microspheres

Microspheres of $^{233}\text{UO}_2$ - ZrO_2 were formed from mixed urania-zirconia sols (prepared by blending urania and zirconia sols) by standard ORNL techniques.⁹ The zirconia sols (4 M) that had low nitrate contents had been produced by autoclaving zirconyl nitrate.¹⁰ The urania sols (1 M) had been prepared according to the standard urania precipitation flowsheet. The U(IV)/U and the HCOOH/U mole ratios in the urania sol varied from 0.80 to 0.85 and from 0.3 to 0.5 respectively. The $\text{NO}_3^-/\text{metal}$ mole ratios for the mixed sols varied from 0.15 to 0.20. Microspheres of $^{233}\text{UO}_2$ - ZrO_2 with an 8 wt % uranium composition were made from the mixed sols and were fired at 1150°C under Ar-H_2 according to the accepted procedure for pure uranium.¹¹ During the year, 233 g of the calcined $^{233}\text{UO}_2$ - ZrO_2 microspheres were coated with pyrocarbon by the ORNL Metals and Ceramics Division and were then sent to the Pacific Northwest Laboratory for use in physics experiments.

One difficulty encountered in this work was that of preparing the $^{233}\text{U(IV)}$ solutions for making the UO_2 sols. The procedure used for preparing $^{238}\text{U(IV)}$ solutions consists of contacting 0.2 M $\text{UO}_2(\text{NO}_3)_2$ -0.1 M HCOOH with hydrogen, using platinumized Al_2O_3 powder as a catalyst. Preparation of the $^{233}\text{U(IV)}$ solutions was found to require 20

⁸ Chem. Technol. Div. Ann. Progr. Rept. May 31, 1968, ORNL-4272, pp. 161–70.

⁹ Chem. Technol. Div. Ann. Progr. Rept. May 31, 1968, ORNL-4272, p. 149.

¹⁰ Chem. Technol. Div. Ann. Progr. Rept. May 31, 1967, ORNL-4145, p. 195.

¹¹ Chem. Technol. Div. Ann. Progr. Rept. May 31, 1967, ORNL-4145, p. 180.

times as much catalyst as preparation of the $^{238}\text{U(IV)}$ solutions. Similar difficulties have been reported for $^{235}\text{U(IV)}$ solutions.¹² The reason for the difference in catalyst requirements is not understood at the present time.

7.3 PREPARATION OF $\text{UO}_2\text{-PuO}_2$ AND PuO_2 MATERIALS

In a cooperative effort with the Metals and Ceramics Division, the Chemical Technology Division is providing fast reactor fuel materials for fuel fabrication development and for irradiation specimen loading. Concurrently with providing these fuel materials in the desired form, sol-gel technology has been extended, with emphasis on the development of techniques for producing improved UO_2 sols (i.e., sols that are more stable and more compatible with PuO_2 sols). In developmental work on techniques for forming microspheres, we have found that the use of systems with low surfactant concentrations may circumvent many of the undesirable results (surface wrinkling and dimpling) that were associated with earlier systems (using high surfactant concentrations). During this report period, we prepared about 3.8 kg of dense 80% $\text{UO}_2\text{-20% PuO}_2$ microspheres (Table 7.7), of which 25% contained enriched uranium. Urania and plutonia sols were also prepared.

Preparation of Sols

Plutonia Sol. — A total of 5.1 kg of plutonium was converted into stable PuO_2 sol by using the flowsheet¹³ reported previously. Of this total, 3.8 kg was converted into dense PuO_2 microspheres (Sect. 7.2); the remainder was either blended with UO_2 sol for forming 80% $\text{UO}_2\text{-20% PuO}_2$ microspheres (0.75 kg of plutonium) or transferred to the Metals and Ceramics Division for conversion into shards for pelletization studies.

Urania Sols. — Natural urania sols were prepared according to (1) the precipitation-peptization method and (2) the solvent extraction method.¹⁴

Urania sols containing enriched uranium were prepared according to the laboratory precipitation flowsheet.¹⁵ A modification of the flowsheet, which consisted in increasing the digestion period at 65°C (after peptization) to 3 hr, resulted in very fluid sols that could be filtered; this characteristic would be important in normal production operations. These sols were stable on standing; their physical characteristics were similar to those of sols prepared earlier [U(IV) content, >90%; NO_3^-/U mole ratio, ~ 0.12 ; uranium concentration, $\sim 0.9\text{ M}$].

Compatibility of UO_2 Sols with PuO_2 Sols. — Dense $\text{UO}_2\text{-PuO}_2$ microspheres have exhibited a decided tendency to crack upon sintering, even when the component sols individually yield crack-free microspheres. Studies aimed at eliminating this tendency and developing UO_2 sols that are compatible with PuO_2 sols are still in progress (Sect. 7.2). The results of these studies indicate that the "free formate" remaining in the UO_2 sols from the U(VI)-U(IV) reduction step is an important factor in the cracking of the mixed oxide microspheres. When the formate/U mole ratio was reduced to approximately 0.2, there was a marked decrease in the cracking. The formate content of up to about 0.2 mole per mole of uranium appears to be, in some manner, more strongly bound to the crystallite surfaces and is not readily removed by solvent extraction unless it is displaced with a stronger acid such as HNO_3 .

Initial studies were conducted with the mixed sols. Each sol mixture was digested for 0.5 hr at 95°C and then contacted with two volumes of 2-ethyl-1-hexanol (2EH), which extracts formic acid and some water. Although this approach gives a higher yield of crack-free microspheres, it has a serious drawback; the product sol is unstable and, upon standing, deposits solids. This makes it difficult to ensure a constant Pu/U atom ratio. A modification to this approach, in which the UO_2 sol is independently digested and extracted prior to blending with the PuO_2 sol, offered no advantage.

A significant improvement was realized by extracting undigested UO_2 sol with 2EH or *n*-hexanol at room temperature and then blending it with the PuO_2 sol (Fig. 7.11). Microspheres obtained from an 80% $\text{UO}_2\text{-20% PuO}_2$ sol feed, whose urania sol component had been previously extracted at room

¹²J. P. McBride, *Preparation of UO_2 Microspheres by a Sol-Gel Technique*, ORNL-3874 (February 1966), p. 3.

¹³*Chem. Technol. Div. Ann. Progr. Rept. May 31, 1967*, ORNL-4145, pp. 195-99.

¹⁴*Chem. Technol. Div. Ann. Progr. Rept. May 31, 1968*, ORNL-4272, pp. 142-45.

¹⁵*Chem. Technol. Div. Ann. Progr. Rept. May 31, 1966*, ORNL-3945, p. 157.

Table 7.7. Production and Distribution of Dense PuO₂-UO₂ Microspheres

Run No.	Pu/(U + Pu) Mole Ratio	U Enrichment (%)	Product (g of oxide)			Density (% of theoretical)	C (ppm)	Condition of Product	Final Use of Product
			Total	Size Specified (420 to 595 μ)	Fines (<44 μ)				
4, 4F	0.198		750	515	200	98	<40	Mild cracking	TREAT Expt.
4F1	0.206		166		150	96	<80	Acceptable	TREAT Expt.
4A, 4AF	0.195		830	None	177			Severe cracking; malformation	TREAT Expt.
4B, 4BF	0.215		720	123	177	>99	<70	Severe cracking; malformation	TREAT Expt.
5	0.198	93	599	289	193	>96	<50	Mild cracking	EBR-II
6	0.208	93	a						Experimental
7	0.209	93	a			>96	150	Cracking	Experimental
8	0.20	20	675	450	200	>96	<50	Minor cracking	Babcock and Wilcox Co.

^aThese experimental runs were conducted to develop feed preparation and sphere-forming techniques that would be applicable to extracted sols; little satisfactory product was recovered.

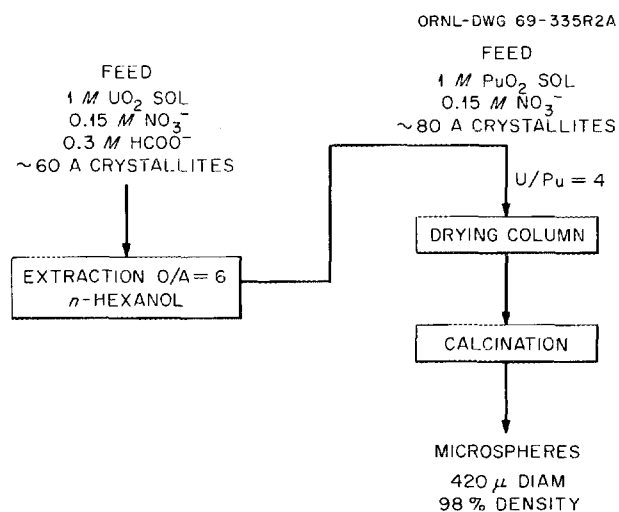


Fig. 7.11. Improved Method for Preparing 80% UO_2 -20% PuO_2 Microspheres.

temperature with *n*-hexanol, contained less than 5% of cracked product.

In this series of experiments, aging of the mixed sols was found to have a deleterious effect on the characteristics of the product. However, microspheres that were formed immediately from freshly mixed blends of UO_2 and PuO_2 sols had satisfactory properties (i.e., very few of the microspheres were cracked). This effect, evaluated over a period of 0.5 to 100 hr, is noticeable even with blends of extracted UO_2 sol and PuO_2 sol, although to a much lower degree. It appears to offer a valid explanation for the variation in previous results: the longer the sols aged, the smaller the yield of crack-free dense microspheres.

Microsphere Preparation

Microsphere Forming. — We studied the behavior of various mixed UO_2 - PuO_2 sols during microsphere formation. A marked difference was noted between untreated UO_2 sols and UO_2 sols that had been extracted with an aliphatic alcohol to remove excess formate. When the latter type of sols was used, the sol droplets coalesced severely and stuck to the walls of the column after about 15 min. The droplets that survived long enough to gel began to cluster; this ultimately resulted in large agglomerates, which, in the extreme cases, plugged the column. Adjustment of the surfactant content over a relatively large range (Span 80, 0.2 to 2 vol %;

and Ethomeen S/15 or Amine O, 0.2 to 0.6 vol %) was unsuccessful. Adjustment of the pH to approximately 3.2 with HNO_3 (added to the 2EH drying solvent over the range 0.001 to 0.05 *M*) also was unsuccessful. However, when Pluronic L-92 was used instead of Amine O and/or Ethomeen S/15, the Span 80 content could be reduced to 0.2 to 0.4 vol %, provided the 2EH drying solvent was acidified to 0.001 *M* HNO_3 ; under these conditions, clustering, sticking, and coalescence of sol droplets did not occur. A low surfactant concentration (which appears to be highly dependent on the acidification step) is desirable in order to avoid the “dimpling” and “wrinkling” that are associated with the fired product obtained by using a high surfactant concentration.

Firing Conditions. — During the past year, both the microsphere firing equipment and the procedures were modified. Installation of an Inconel furnace tube allowed us to hold the dried gel microspheres in a steam atmosphere during the firing step. The additional organic material is steam-pyrolyzed from the gel beads during the early stages of the firing procedure (up to 300°C); the organic material is nitrogen free. A further advantage of steaming is that it reduces the yield of cracked microspheres. Best results were obtained when the heatup rate was held at 25 to 50°C/hr in steam-argon atmospheres until the temperature reached 600°C, with 2- to 4-hr hold periods at 200, 400, and 600°C. The heatup rate was increased to 300°C/hr after the 600°C period; the atmosphere was changed to argon-4% hydrogen at 900°C, and was maintained for 4 hr at a final temperature of 1150°C.

7.4 MICROSPHERE FORMING, DRYING, AND FIRING STUDIES

Microsphere Forming Studies

The microsphere forming equipment flowsheets and the pilot plant used for preparing ThO_2 and ThO_2 - UO_3 spheres can also be used for preparing UO_2 spheres, if an inert gas atmosphere is provided. (The continuing equipment development studies are reported in Sect. 6.3.) However, the chemical conditions in the sphere-forming column and in the gel drying and firing steps are different for UO_2 as compared with ThO_2 or ThO_2 - UO_3 . The major emphasis for the UO_2 sphere forming studies has been on determining optimum chemical condi-

tions. The UO_2 spheres with diameters of less than 100μ are prepared by procedures discussed in Sect. 9.5.

Column Operating Conditions

When a specified sol is used to form gel spheres, the composition of the organic fluidizing medium is the principal operating variable. Problems such as sticking, clustering, coalescence, cracking, or distortions can be effectively controlled by varying the types or the concentrations of the surfactants, the water content of the alcohol, the type of alcohol, or the pH. With respect to selecting the composition of the organic fluidizing medium, the properties of the sol are very important. With a new sol, the usual procedure is to start with a commonly used alcohol composition and then to vary the composition to solve any operating problems.

The strategies for controlling the alcohol compositions during extended periods of operation can be logically grouped into four classes, according to the method of control of chemical additives. Each composition depends on the rates of additive input and removal, and each of these rates can either be "uncontrolled" or controlled (or modified) by process conditions. An uncontrolled composition is one that results essentially from other process conditions (i.e., no significant attempt has been made to modify the process to control additive input or removal). The four strategies for each composition variable, with respect to additives, are denoted as follows:

- UU – uncontrolled input, uncontrolled removal
- CU – controlled input, uncontrolled removal
- UC – uncontrolled input, controlled removal
- CC – controlled input, controlled removal

In each case, the strategies used for ThO_2 , $\text{ThO}_2\text{-UO}_2$, $\text{ThO}_2\text{-UO}_3$, and UO_2 sols were CU for surfactant, UC for water, UU for nitrate, and UU for surfactant and alcohol degradation products. The UU combination, of course, provides no control of composition, whereas any of the other three can, in theory, provide any composition desired. The CU and UC strategies require only one control operation; however, the CC strategy may be easier.

The desired values for surfactants, water, and nitrate fall in ranges having minimum and maximum values; the degradation products, on the other hand,

probably have only a maximum limit, with zero as the desired value. Neglecting the startup with virgin (new) alcohol, the optimum operation usually requires removal of water, addition of surfactants, removal of degradation products, and either removal or addition of nitrate, depending on the sol. Each control operation, except for degradation products (where complete removal is preferred), requires a measurement to maintain a satisfactory value.

Promising methods for controlling the input and/or removal of additives and for making measurements are tabulated (Table 7.8). The water and surfactant control procedures listed in this table were used for all our sphere forming studies, except for some small-scale operations in which alcohol was discarded to remove water.

The successful continuous operation of a sphere forming column requires that the alcohol composition be controlled within satisfactory ranges. If the initial conditions are not satisfactory, this will become apparent by the time the first particles are completely gelled. After 1 hr, the sphere forming behavior may begin to change slowly as surfactants are depleted or degraded. Normally these changes are tolerable for at least 10 hr, and sometimes as long as 100 hr; however, we are convinced that satisfactory long-term operation requires periodic additions of surfactants to the 2EH. While continuous additions would be ideal, additions every 2 to 12 hr appear to be adequate.

To demonstrate satisfactory column operating conditions employing the system and procedures described above, the following steps are required:

1. Demonstration of satisfactory initial operation. This will require more than 1 hr of operation and a sol feed volume greater than 5% of the fluidized-bed volume.
2. Demonstration of a surfactant addition schedule that prevents unsatisfactory depletion of surfactant. This will require more than 50 hr of cumulative operation and a sol feed/2EH inventory volume ratio greater than 0.5.
3. Demonstration of a satisfactory long-term operation without excessive accumulation of surfactants or degradation products. We consider a time period of more than 200 hr and a sol feed/2EH inventory volume ratio greater than 2 to be significant.

The tendency for distortions and cracking to occur can be observed by using only a few par-

Table 7.8. Methods for Measuring and Controlling Alcohol Compositions for Sol-Gel Sphere-Forming Systems

Components (other than alcohol)	Input Control		Removal Control	
	Possible Input Procedure	Measurement or Control of Input	Possible Removal Procedure	Measurement or Control of Output
Water	Not required, but would be by volume for virgin alcohol.		Distillation	Alcohol exit temperature and pressure from still.
Surfactants	By measured volume.	Visual observation of poor operation or by a preset schedule.	Not required.	Not required.
Nitrate	By measured volume.	Preset schedule or by pH measurements.	By caustic scrub (or perhaps ion exchange).	Use complete removal and controlled input.
Sol components other than nitrate	Not ordinarily required, but might be by control of sol composition.		Probably replacement of alcohol with new charge.	
Degradation products of surfactants and alcohol	Minimize input by minimizing degradation reactions; reduce still temperature and/or nitrate concentration in alcohol.		Replacement of used alcohol with pure alcohol.	Not required.

ticles. However, sticking, clustering, and coalescence depend on the inventory of sol drops, the extent of loading of the fluidized bed, and, in part, on the quantity of gelled spheres present. For this reason, the requirements listed in step 1 are necessary to fully demonstrate satisfactory initial conditions.

Our limited surfactant depletion data seem to indicate that the effective life of the surfactants is two to four days, depending on the sol and on the temperature of the still. This rate of depletion is in agreement with the surfactant addition schedules that we use. No visible effects of long-term accumulations of surfactants or degradation products have been observed after 200 hr of operation using ThO₂ sol. Thus, operating periods of greater than 200 hr, using the same organic fluidizing medium, would probably be feasible with ThO₂ sol. Of course, the 2EH could be completely reprocessed or replaced after more than 200 hr if necessary.

The water content of the 2EH in the column is controlled by controlling the flow of 2EH through, and the temperature in, a single-stage distillation. Calculations made using material balances show that from 75 to 90% of the water in the sol is extracted into the 2EH under steady-state conditions. At steady state, the water content in the column is constant, and the water input from the sol is the product of the 2EH flow rate through the still and the difference in water content in the 2EH flowing to, and that in the 2EH flowing from, the still. The water content in the 2EH returning to the column from the still is determined by the temperature of the still. Values we use for our still temperatures are:

Temperature of 2EH (°C)	Volume Percent H ₂ O
140	0.7
150	0.5
160	0.35

Some loss of surfactants from the 2EH occurs during operation of the still, and it increases as the temperature of the still is increased. Thus the amounts of surfactants needed and the accumulation of degradation products are dependent on the temperature of the still. We believe that 2EH temperatures above 155°C are definitely undesirable since degradation products are formed more rapidly at these temperatures. If temperatures below 140°C

are used, either a vacuum still must be used or the flow rate of the 2EH to the still must be greatly increased. The use of an upper temperature limit requires that the still be designed and operated to avoid localized overheating.

The water content of 2EH can be measured by an in-line determination of boiling point. This was demonstrated by an apparatus in which a small, metered stream of 2EH was heated by an electrical heater of sufficient heat input to heat dry 2EH to its boiling point (183°C). The vapors were completely condensed and returned to the heated pot by an oversize, close-coupled condenser. The pot temperatures remained at approximately the inlet 2EH boiling point independent of moderate changes in heat input or 2EH flow rates. The relatively large, regular change of boiling point from 183°C for dry 2EH to 99°C for 2EH saturated with water can thus be easily measured and a temperature-water content relationship can be established.

Most of the problems associated with the operation of the column can be solved by varying the Span 80, Ethomeen S/15, and H₂O contents in the 2EH. The initial surfactant compositions and the surfactant addition schedules for the most frequently used sols are listed in Table 7.9. The schedule for ThO₂ sols has been demonstrated for more than 200 hr, while other schedules have not undergone long-term evaluation. Low water contents (<0.7 vol %) in the 2EH sometimes cause cracking of products, while high water contents (~2 vol %) result in slower gelation and sometimes cause clustering. In most of the demonstration runs, the 2EH contained 1.2 to 1.5 vol % water (the normal range); changes in water content within this range are rarely a controlling variable.

Microsphere Drying and Firing

Work during the past year was concerned with experiments that were aimed at understanding the reactions which occur during the sintering of UO₂ microspheres in a steam atmosphere, and with studies of the firing of <50-μ-diam microspheres that were formed in isoamyl alcohol (rather than 2-ethyl-1-hexanol, which is used for preparation of larger microspheres).

It is well known that the excess oxygen content, x , in UO_{2+x} is an important variable in sinter-

Table 7.9. Initial Surfactant Concentrations and Addition Schedules for 2EH in Fluidized-Bed Columns

Other conditions: about 1.2 vol % H₂O in 2EH; temperature of 2EH in still, 155°C

Type of Sol	Method of Preparation	Initial Concentration (vol %)		Additions per 6-8 hr				Demonstrated for	
		Span 80	Ethomeen S/15	Based on 2EH Volume (vol %)		Based on Sol Fed (cc/liter sol)		Step No.	Period (hr)
				Span 80	Ethomeen S/15	Span 80	Ethomeen S/15		
ThO ₂	Hydrothermal denitration	0.05	0.2	0.01	0.05	2	10	3	>200
UO ₂	Precipitation, pH = 9	0.8	0.1	0.1	0.02	20	5	2	50
UO ₂	Precipitation, pH = 7.5	0.4	0.05	0.02	0.01	5	2	2	50
ThO ₂ -UO ₃	Solvent extraction, Th/U = 3	0.2	0.05	0.02	0.01	5	2	2	50
ThO ₂ -UO ₃	Solvent extraction, Th/U = 4.25	0.4	0.05	0.05	0.01	10	1	2	50
UO ₂	Solvent extraction, ~0.2 M U feed	0.2	0.05	0.02	0.01	5	2	2	30
UO ₂	Solvent extraction, >1 M U feed (CUSP)	0.4	0.05	0.03	0.01	8	2	1	1

ing.^{16,17} Experiments were performed to ascertain how the O/U atom ratio varies with heat treatment, sphere shrinkage (as determined by density measurements), and removal of volatile organics from gel (as determined by carbon analysis) (Table 7.10). These experiments showed that gel microspheres of UO_{2+x} are more easily freed of the organic materials sorbed on the spheres when the spheres are heated in steam than when they are heated in argon. Significant U(VI) reduction and carbon removal occurred at temperatures of 550°C in steam, whereas higher temperatures were required with argon. These results were obtained both with ~600- μ -diam gel spheres that had been formed in 2-ethyl-1-hexanol and with <50- μ -diam gel spheres that had been formed in isoamyl alcohol. Gel shards, which contain no sorbed organic from the sphere-forming column but do contain formic acid, exhibit a change in O/U ratio on heat treatment; however, this change is not as great as that seen in the microspheres. Thus, both the formic acid and the sorbed alcohol are apparently responsible for U(VI) reduction.

Urania must contain excess oxygen in order to have optimum sintering properties; results showing the reduction of UO_{2+x} on heatup explain many of the results we have obtained with other gel preparations. Since the sols contain different amounts of formic acid and the gel microspheres contain both differing amounts of formic acid and of sorbed organics, the extent of reduction during heatup will vary. Therefore, the "soaking" (i.e., heating) times had to be adjusted for both carbon removal and oxidation of the UO_2 by steam. When trace amounts of hydrocarbon or CO are present in the steam, the steam cannot oxidize UO_{2+x} ; however, after all the reducing gases have been evolved, the atmosphere, which then consists of steam alone, becomes oxidizing. The oxidizing effect of the steam is demonstrated by the differences in the O/U ratios of the <50- μ -diam spheres when heated in steam to 1000°C and when heated to 1150°C. The sample heated to 1150°C was oxidized to approximately U_4O_9 , which has an O/U ratio of 2.25, and closely approached the theoretical density for

U_4O_9 (11.2 g/cc). Empirically, we had previously determined that a dense UO_2 product could be obtained by using a hydrocarbon analysis to adjust the soaking time (in steam) required to reach 650°C; this analysis helped us to determine when all of the hydrocarbons had been evolved. When the evolution of hydrocarbons had been completed, the temperature was increased to 1150°C, where the UO_2 microspheres were fired for densification. Thus, in this cycle, we take advantage of the enhanced removal of the organic materials by use of steam before the sintering process begins, and then, after carbon removal, we adjust the O/U ratio to a suitable value to obtain optimum sintering by the oxidizing effect of the steam. We noted in these studies that some gel samples would densify at temperatures as low as 850°C, whereas others required a much higher temperature (1100°C). These differences probably occurred because, after the hydrocarbon analyses had indicated removal of all of the organics, the O/U atom ratios were too low in some instances to permit the samples to be sufficiently oxidized by the time a temperature of 850°C was attained.

Our work on the drying and firing of <50- μ -diam UO_2 microspheres showed that practically no hydrocarbons were evolved from the spheres during firing in steam when the spheres had been dried in steam to 180–225°C prior to firing. This was not the case with larger-diameter (>150- μ) spheres. The difference in behavior appears to be the difference between the sorption characteristics of isoamyl alcohol and 2-ethyl-1-hexanol. (The small spheres are formed in isoamyl alcohol, whereas the larger spheres are formed in 2-ethyl-1-hexanol.) Since the smaller spheres were essentially free of sorbed organics after the low-temperature drying, studies were made to determine if firing under a steam atmosphere was necessary for attaining product specifications on <50- μ -diam spheres.

Three firing schedules were tested using four different preparations of <50- μ -diam gel microspheres (see Table 7.11). The gels had been dried in steam to temperatures of 180–225°C prior to firing. There was essentially no differences in the densities of products obtained by firing in an argon atmosphere vs those obtained in a steam atmosphere. The long firing cycle in steam, which included an overnight soaking at 650°C, was no more effective than the much shorter cycle in steam. The carbon contents of products obtained by the argon firing were slightly higher but were accept-

¹⁶N. Fuhman, L. D. Hower, Jr., and R. B. Holden, "Low-Temperature Sintering of Uranium Dioxide," *J. Am. Ceram. Soc.* **46**, 114–20 (1963).

¹⁷J. Williams, E. Barnes, R. Scott, and A. Hall, "Sintering of Uranium Oxides of Composition UO_2 to U_3O_8 in Various Atmospheres," *J. Nucl. Mater.* **1**, 23–38 (1959).

Table 7.10. Effect of H₂O Atmosphere on O/U Atom Ratio and Carbon Content During Sintering

Conditions: Dried gels of composition shown were heated under conditions shown at 100°C/hr. Temperature rise rates other than 100°C/hr are indicated.

Gel Code	Gel Diameter (μ)	Heat Treatment	O/U Atom Ratio	Total C (%)	HCOO ⁻ (%)	Density Measurements			
						By Hg Displacement (g/cc)			By He Displacement (g/cc)
						15 psi	210 psi	15,000 psi	
MS-6-20-1610 Spheres	<50	Dried gel	2.44	0.60	2.50 ^a				
		Ar to 550°C	2.38	0.054		4.46	4.60	7.31	
		H ₂ O to 550°C	2.26	0.022		4.49	4.70	7.79	
		H ₂ O to 1000°C	2.06	<0.002		9.46	9.46	10.4	10.97
		H ₂ O to 1150°C; hold 12 hr	2.21	<0.002		10.56	11.04	11.11	
P-6-15-1545 Spheres	~600	Dried gel	2.28	2.16	4.66 ^a				
		Ar to 550°C	2.33	0.611		6.23	6.25	6.35	
		H ₂ O to 550°C	2.09	0.009		7.47	7.49	7.68	
		H ₂ O to 850°C	2.00 ^c	0.001		10.54	10.49	10.61	
		Ar to 1000°C ^b	2.00	0.346		9.58	9.63	9.70	
Shards		Dried gel	2.28	1.60	5.34 ^a				
		H ₂ O to 750°C	2.14	0.003					

^aThe contributions to total carbon from formic acid in MS-6-20-1610 and P-6-15-1545 are 0.67% and 1.24% respectively.

^bTemperature rise rates of 300°C/hr were used instead of the nominal 100°C/hr.

^cReduced for 2 hr at 850°C in Ar-4% H₂.

Table 7.11. Firing of $<50\text{-}\mu\text{-diam}$ UO_2 Gel Spheres in Steam and Argon

Gel Preparation No.	Firing Schedule ^a	Carbon (ppm)	Hg Density (g/cc)			
			15 psi	210 psi	1000 psi	15,000 psi
MS-9-3-1245	A	50	10.36	10.51	10.65	10.69
	B	<20	10.15	10.59	10.73	10.74
	C	<20	9.68	10.50	10.59	10.60
MS-9-3-1616	A	50	10.46	10.65	10.76	10.74
	B	<20	10.05	10.58	10.65	10.66
	C	<20	10.16	10.66	10.71	10.72
MS-9-4-1200	A	40	9.55	10.41	10.56	10.58
	B	20	9.72	10.65	10.79	10.86
	C	40	9.46	10.56	10.68	10.70
MS-9-4-1520	A	<20	9.58	10.42	10.55	10.57
	B	40	9.46	10.29	10.39	10.41
	C	<20	9.61	10.46	10.53	10.54

^aA -- Argon to 1000°C and hold 1 hr.

B -- Steam to 1000°C and hold 1 hr.

C -- Steam to 650°C at 100°C/hr and hold overnight; steam to 1000°C at 300°C/hr and hold 1 hr. Steam to 1150°C.

able. In each case, the small, fired spheres sintered into a loosely bound mass; however, the material could be separated into individual spheres and screened.

7.5 DEVELOPMENT OF HIGH-PERFORMANCE FUEL MATERIALS

Preparation of UC Microspheres

We have previously shown that a UO_2 sol acts as a protective colloid toward carbon black, thus giving a stable, codispersed sol when the two are blended intimately (e.g., by ultrasonic agitation).^{18,19} Microspheres can be formed from these mixed sols by the standard ORNL technique, then dried and prefired to 1000°C under argon to remove volatile material. This series of steps also re-

duces any UO_{2+x} that is present to UO_2 by reaction with the carbon. The microspheres, consisting of $\text{UO}_2 + \text{C}$, are then reacted to give carbide (with evolution of CO) at 1600 to 2000°C, either under argon or vacuum. We have shown previously in experiments with ThC_2 and $(\text{Th,U})\text{C}_2$ microspheres prepared by this procedure that proper control of temperature, atmosphere, and heating rate is required in order to obtain dense products by reaction sintering.^{19,20} A suitable firing cycle for obtaining dense UC is comprised of a fairly fast heatup under argon ($\sim 50^\circ\text{C}/\text{min}$), holding for 2 to 4 hr at 1900°C under argon or at 1600°C under a vacuum (which is gradually increased from ~ 10 to ~ 0.1 torr), and then completing the firing under a vacuum of 15 μ or lower.

Obtaining single-phase UC is difficult, and, even if UC is fabricated as a single-phase material, it will not remain as such in a reactor after some

¹⁸K. J. Notz, *J. Phys. Chem.* **71**, 1965 (1967).

¹⁹*Chem. Technol. Div. Ann. Progr. Rept. May 31, 1968*, ORNL-4272, pp. 157-60.

²⁰*Chem. Technol. Div. Ann. Progr. Rept. May 31, 1967*, ORNL-4145, pp. 159-65.

burnup occurs. Therefore, from a practical point of view, a phase adjustment of UC must be made. Three possibilities have been considered in recent years: (1) to prepare a hypostoichiometric product and have some uranium metal present, (2) to prepare a hyperstoichiometric product and have some UC_2 present, and (3) to prepare hyperstoichiometric product with an added third component (such as chromium or vanadium carbide), thereby creating a ternary phase field of which UC is one phase. Thus far we have made both carbon-rich and carbon-poor UC by our method, and there is no reason why the sol-gel procedure should not be amenable to the addition of a third component.

Figures 7.12 and 7.13 show etched cross sections of hyper- and hypostoichiometric UC microspheres respectively. Both show typical UC grain structure. Traces of free metal are present as small droplets, both within grains and at grain boundaries, in the hypostoichiometric structure. The hyper-

stoichiometric sample contains UC_2 , which apparently precipitated during cooling. Each of these samples has a high density (>13.0 g/cc), greater than 95% of theoretical. We consistently obtain densities greater than 90% of theoretical, usually greater than 93%.

Chemical analysis of the UC products shows that the C/U atom ratios are near unity, usually between 0.94 and 1.06. The oxygen contents are low: 100 to 300 ppm for the hyperstoichiometric and approximately 1000 ppm for the hypostoichiometric material. We usually do not analyze for nitrogen since there is no source of it in our process, other than accidental contamination; two samples that were analyzed were found to contain only 150 and 260 ppm. Our free carbon analyses usually are about 300 ppm, but we feel that this represents an extreme upper limit. The true free carbon content is probably lower than this since the analyzed value includes traces of carbon generated during hydro-

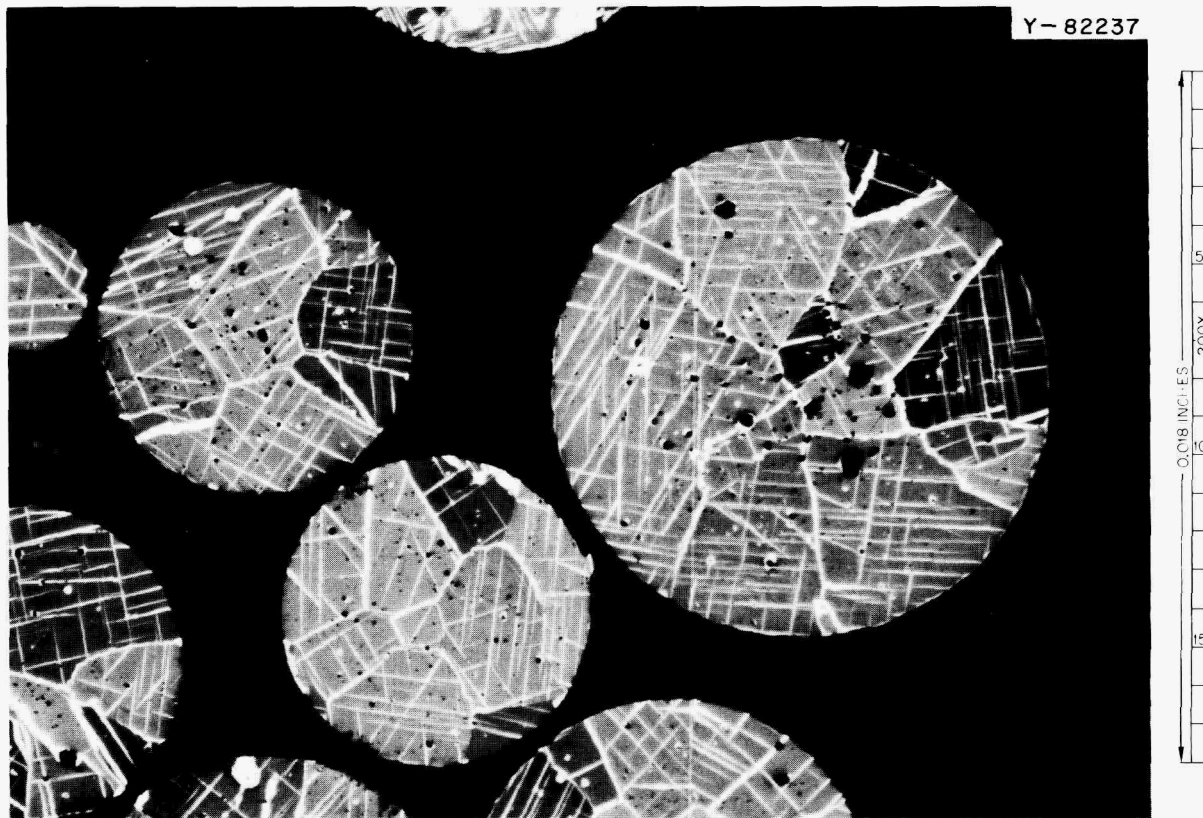


Fig. 7.12. Hyperstoichiometric UC. Large grains are UC. White streaks are UC_2 , both at grain boundaries and within the grains. Black spots are pores.

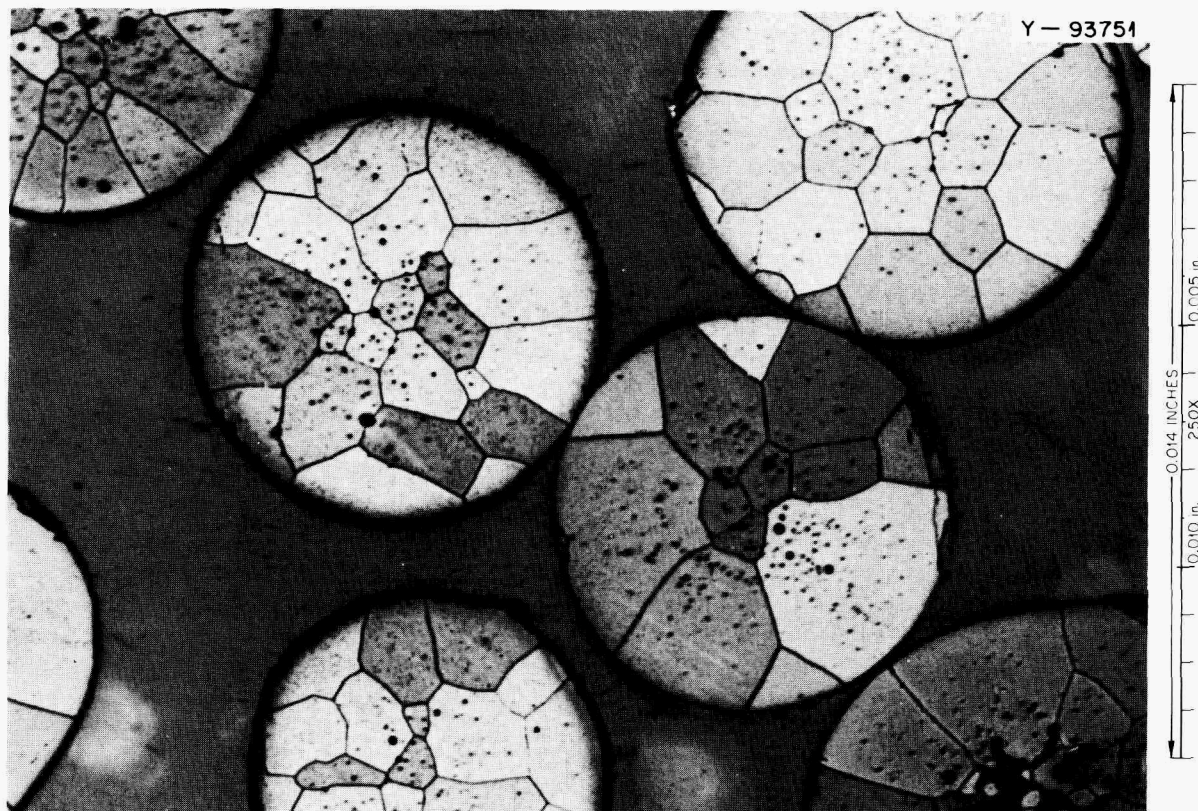


Fig. 7.13. Hypostoichiometric UC. Large grains are UC. Traces of free uranium metal appear as shiny spots, both within the grains and at grain boundaries. Black spots are pores.

lytic dissolution. Lattice parameters determined from x-ray diffraction patterns are 4.9577 Å for a hypostoichiometric composition and 4.960 Å for a hyperstoichiometric sample; these values are in good agreement with the literature.²¹

Preparation of Plutonium and Uranium-Plutonium Carbides

The plutonia sols routinely produced at ORNL (see Sect. 7.2) show little variation in surface area, crystallite size, and NO_3^-/Pu mole ratio; all of the plutonium is in the tetravalent state. These properties make plutonia sols ideal for blending with carbon black. Although our main effort has involved the preparation of the monocarbide, stable plutonia-carbon sols have been prepared with suf-

ficient carbon to produce the monocarbide, the sesquicarbide, or the dicarbide (C/Pu atom ratios of 3.0, 3.5, and 4.0 respectively). More carbon can probably be incorporated if desired.

According to the phase diagram for the plutonium-carbon system,²² single-phase monocarbide can exist from $\text{PuC}_{0.5}$ to $\text{PuC}_{0.9}$. Since the carbothermic reaction requires two carbon atoms to reduce one molecule of PuO_2 , C/Pu atom ratios of 2.5 to 3.0 were used for the monocarbide preparations. Examination by electron microscopy has shown that the carbon-plutonia sols are intimate mixtures of carbon and plutonia particles, with each retaining approximately the same structures as observed for unmixed materials. The plutonia sols examined were made up of essentially symmetrical

²¹E. K. Storms, *The Refractory Carbides*, Academic, New York, 1967.

²²R. N. R. Mulford, F. H. Ellinger, G. S. Hendrix, and E. D. Albrecht, p. 303 in *Plutonium 1960*, ed. by E. Grison, W. B. H. Lord, and R. B. Fowler, Cleaver-Hume Press, Ltd., London, 1961.

particles about 80 Å in diameter, while the carbon consisted primarily of 300-Å particles.

Microspheres were made from carbon-plutonia sols by extraction of water from sol droplets, using typical ORNL microsphere forming columns. Powder samples were obtained by vacuum freeze-drying the sols. Prior to the carbothermic reaction, the material was heated to 900°C in flowing argon at a controlled rate, in order to gradually remove the volatile materials present. Thermogravimetric analyses in argon showed that a powdered plutonia gel without carbon lost water and nitrate in two steps; the loss was complete at 700°C. Pure plutonia microspheres showed two additional changes when heated in argon: (1) a loss of residual drying alcohol between 200 and 250°C, and (2) a gradual loss in weight from small amounts of carbonaceous residue (from decomposition of the residual organic material). The latter reaction started at about 850°C and increased in rate above 1000°C until the carbon was gone. Similar weight losses were found for the respective materials obtained from plutonia-carbon sols. After pre-firing at 850°C in argon, products from plutonia-carbon sols were examined by x-ray and chemical analysis and were found to contain PuO_2 and C (with only a slight change in the C/Pu atom ratio). Above 1000°C, the rate of the reaction between plutonia and carbon in an argon atmosphere increased. The reaction appeared to occur in two overlapping steps, with the rate becoming very rapid above 1350°C.

Although the reactants are often melted in the usual metallurgical preparation of carbides, the microspheres cannot be heated above the melting point of the carbide. For plutonium monocarbide, this necessitates working at temperatures below 1650°C, which is the peritectic point for PuC. The procedure used in these experiments was to heat the pre-fired material in argon at a moderate rate (10 to 15°C/min) to the final reaction temperature, which was usually 1450 to 1550°C. After this temperature had been maintained for one or more hours, the system was evacuated and heating was continued under vacuum. It was hoped that these conditions would afford the best balance between sintering, grain growth, and chemical conversion to the carbide.

A summary of the work to date is shown in Table 7.12. The main purpose of preparing the powdered samples was to determine if the particle sizes of the blended material influenced the final composition. With both forms it was found that, when the

C/Pu atom ratio became greater than 3.0 (<3.5) in the original sols, a mixture of carbides was obtained, the sesquicarbide being the major component in each mixture. Even when the C/Pu atom ratio was 2.5 to 3.0 some sesquicarbide was present in addition to the monocarbide. The oxygen content of the carbide products was high, ranging from 0.5 to 3.0 wt %. Although higher C/Pu atom ratios may tend to give lower oxygen contents, there is a greater tendency for the formation of some sesquicarbide. Lower oxygen contents were found for products that underwent prolonged heating; however, analyses indicated a loss of plutonium, thereby providing carbon for the formation of sesquicarbide. These results suggest that plutonium or a lower oxide of plutonium may be volatilized during the extended heating periods. It appears that, for preparation of the monocarbide, a C/Pu atom ratio of 2.8 to 3.0 is most suitable, although in the experiments to date the oxygen content has remained high under these conditions. In instances where x-ray analysis indicated that the monocarbide was the product (or major component), it is interesting to note that (Table 7.12) the C/Pu ratio in the product was approximately 0.6, and the sum of the O/metal and C/metal ratios in the product was 0.83 to 1.0. These data are in agreement with the literature,²³ which reports that plutonium monocarbide forms a PuC_xO_y product with a wide composition range, even when an oxide phase is absent.

Uranium-plutonium carbides are also being prepared. Sols of urania, plutonia, and carbon were prepared by first mixing urania and plutonia sols in the desired ratio and then ultrasonically dispersing carbon black in the mixed sols. Stable sols of the three components were obtained, but the inherent sensitivity of urania sols to air oxidation was retained; therefore, the mixtures must be protected from exposure to air. Preliminary firing results indicated that higher temperatures can be used with the uranium-plutonium mixtures, as compared with plutonium preparations, without the occurrence of melting. Additional experiments with the mixed system are presently in progress.

²³F. Anselin, G. Dean, R. Lorenzelli, and R. Pascord, "Carbides in Nuclear Energy," Vol. I, *Physical and Chemical Properties/Phase Diagrams*, ed. by L. E. Russell, et al., p. 113, Macmillan, New York, 1964.

Table 7.12. Summary of Data for Plutonium Carbide Preparations

Run No.	C/Pu Atom Ratio in Sol	Form Used	X-Ray Analysis ^a	% Pu	% C	% O	O/Pu Atom Ratio	C/Pu Atom Ratio	(O + C)/Pu Ratio	Material Balance (%)	Remarks
9-2A	3.1	Microspheres	PuC, <u>Pu₂C₃</u>	93.6	5.8	0.65	0.10	1.24	1.34	100.5	Heated at 1550°C in argon
9-2B	3.1	Microspheres	PuC, <u>Pu₂C₃</u>	94.0	5.1	0.73	0.12	1.23	1.35	99.8	Heated at 1550°C in argon
9-2D	3.1	Microspheres	PuC, <u>Pu₂C₃</u>	94.3	4.8	0.73	0.12	1.02	1.14	99.7	Heated at 1550°C in argon
9-3A	2.5	Microspheres	PuC, <u>Pu₂C₃</u> (other lines)	97.1	2.07	0.84	0.13	0.363	0.49	100.0	Heated at 1450°C in argon, then at 1450°C in vacuum
9-3C	2.8	Microspheres	PuC, <u>Pu₂C₃</u>	95.0	3.00	1.73	0.27	0.63	0.90	99.7	Heated at 1450°C in argon, then at 1450°C in vacuum
9-3D	3.0	Powder	<u>PuC</u>	95.0	2.80	2.75	0.43	0.59	1.02	100.6	Heated at 1450°C in argon, then at 1450°C in vacuum
9-3E	3.5	Microspheres	PuC, <u>Pu₂C₃</u>	90.2	6.50	2.96	0.49	1.43	1.92	99.7	Heated at 1450°C in argon, then at 1450°C in vacuum
9-28	2.8	Powder	<u>PuC</u> , <u>Pu₂C₃</u>	95.4	2.90	1.39	0.22	0.61	0.83	99.6	Heated at 1450°C in argon, then at 1450°C in vacuum
9-25	2.5	Powder	<u>PuC</u>	95.1	3.50	1.30	0.20	0.73	0.93	100.0	Heated at 1350°C in argon, then at 1450°C in vacuum
9-33	3.3	Powder	PuC, <u>Pu₂C₃</u>	93.2	6.20	0.51	0.082	1.35	1.43	99.9	Heated at 1350°C in argon, then at 1450°C in vacuum
9-30	3.1	Powder	<u>PuC</u> , <u>Pu₂C₃</u>	95.1	2.80	2.14	0.34	0.58	0.92	99.0	Heated at 1420°C in vacuum
9-29	2.9	Microspheres	PuC, <u>Pu₂C₃</u>	93.7	6.40	0.47	0.075	1.36	1.44	100.6	Heated at 1450°C in argon for 4.5 hr, then at 1500°C in vacuum for 10 hr (vs 2-4 hr for above runs)

^aUnderlined material is the major component.

Kinetic Studies of the Carbothermic Synthesis of Carbides, Nitrides, and Carbonitrides²⁴

We have studied the reactions that take place in the carbothermic synthesis of uranium dicarbide from dense, sol-gel UO_2 spheres and graphite. The general experimental method used a new, quantitative metallographic technique to measure the rate of reaction of the dense oxide microspheres.²⁵ The experimental data were then used to determine the rate-controlling mechanism by the fit of the data to thoroughly tested models that exist in the literature for solid-state reactions in spheres in which the reactants and products are spherically symmetrical.

The study of 97% dense, 500- μ -diam UO_2 microspheres with graphite over a temperature range of 1400 to 1756°C showed that the rate-controlling mechanism was the diffusion of oxygen through the UC_2 product layer when a spherically symmetrical layer of carbide was produced around the UO_2 core.²⁶ The Arrhenius relation for this reaction was:

$$k_d = 21.0 \times 10^{-8} e^{-90,000/RT} \text{ (in cm}^2\text{/sec) .}$$

The reaction of a nonsymmetrical configuration of UO_2 and UC_2 with graphite was also studied.²⁶ Different geometric configurations could be effected by changing the heating rate used to attain the reaction temperature of the UO_2 and the graphite. When heating rates of less than 25°C/min were used, the spherically symmetrical configuration resulted; with heating rates in excess of 50 to 100°C/min, however, the nonsymmetrical configuration was obtained. A comparison of the reactions in the symmetrical and nonsymmetrical systems demonstrated that the kinetic behavior of the two systems is quite different; that is, the reaction in the nonsymmetrical system was two to five times faster.

Studies have also been made of the reaction of 98% dense, 500- μ -diam UC_2 spheres with nitrogen in the temperature range of 1500 to 1700°C. The

UC_2 initially contained about 1 vol % free carbon as a fine uniform distribution in the UC_2 . These carbon particles and the surface of the sphere act as nuclei for the precipitation of the carbon that is released by the $\text{UC}_2\text{-N}_2$ reaction. The latter reaction produced a uniform layer of U(C,N) -carbon mixture, which surrounded the UC_2 core. This reaction was controlled by the diffusion of carbon from the $\text{UC}_2\text{-U(C,N)}$ interface to the nearest free carbon site and was described by the relationship

$$r_0 - r = 85.9te^{(-77,700 \pm 3,660)/RT} ,$$

where r_0 is the initial radius of the sphere in centimeters and r is the UC_2 radius at time t (in seconds). We have also determined that the reaction rate increases as the initial free carbon in the UC_2 increases, and that the rate appears to be independent of the nitrogen gas pressure between 180 and 580 torr.

7.6 PLUTONIUM STORAGE FACILITY

A critically safe, contained storage and handling facility for plutonium has been constructed in Building 3019 to meet the needs for development of the sol-gel flowsheet for fast reactor fuels. It is located in the basement adjacent to the Metals and Ceramics alpha laboratory and has a capacity of 100 kg of plutonium in solid (fluoride) or liquid (nitrate) form.

The liquid-handling portion of the facility consists of a doubly contained, 150-gal tank filled with borosilicate glass Raschig rings (as a fixed neutron poison). The outer shell of the tank is a part of the storage glove box. Other parts of the system are: a charging glove box for introducing $\text{Pu(NO}_3)_4$ to the storage tank and a shipping glove box for removing $\text{Pu(NO}_3)_4$ from the storage tank. An equipment flowsheet for the facility is shown in Fig. 7.14.

The liquid-handling storage facility has provisions for vacuum transfer, weighing, sampling, and storing of solution; vessel and glove box pressure control; and remote alarm instrumentation.

The room is air conditioned, and the inlet and exhaust air passes through absolute filters.

Construction of the liquid-handling portion of the facility was completed during the year. The checking of instrumentation and the calibration of vessels are in progress.

²⁴This work was done by T. B. Lindemer of the ORNL Metals and Ceramics Division.

²⁵T. B. Lindemer and M. D. Allen, "Technical Note: A Metallographic Method for Studying Reaction Kinetics in Spheres," *Trans. Am. Soc. Metals* (in press).

²⁶T. B. Lindemer, M. D. Allen, and J. M. Leitmaker, "Kinetics of the Graphite-Uranium Dioxide Reaction from 1400 to 1756°C," *J. Am. Ceram. Soc.* **52**, 233-37 (1969).

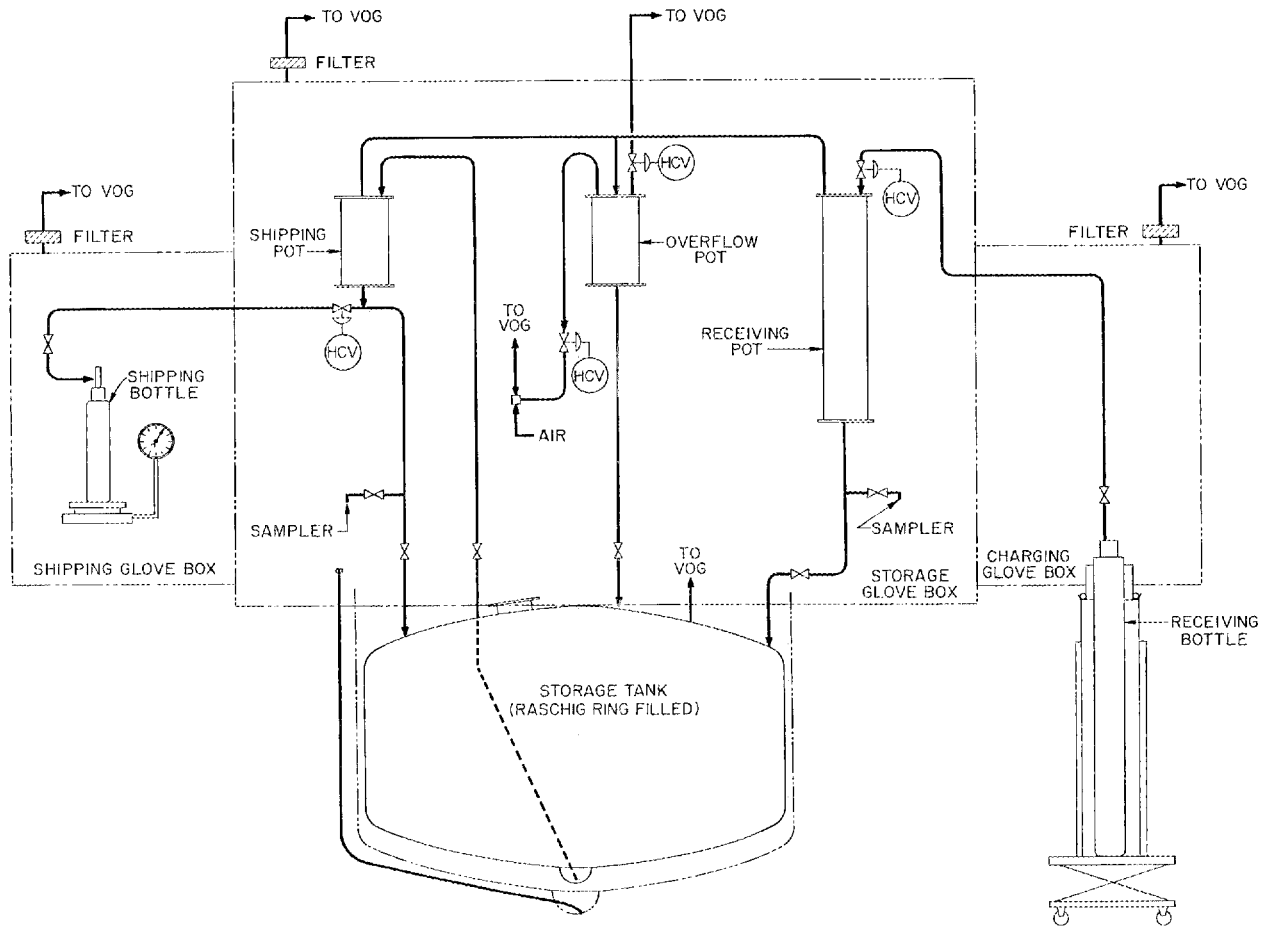


Fig. 7.14. Equipment Flowsheet for Plutonium Nitrate Solution Storage Facility.

8. Sol-Gel Processes for Isotopic Heat Sources

Plutonium-238, with its 86-year half-life and its heat generation rate of greater than 0.5 w/g, is potentially an important isotopic power source. Its possible applications include: auxiliary power for space missions, pacemakers for heart patients, and an artificial heart that can be surgically implanted in a patient. The preparation and the use of ^{238}Pu have been studied at several locations. Because scientists and engineers at Oak Ridge National Laboratory had made significant progress in applying sol-gel technology to the production of reactor fuel containing ^{239}Pu and had produced high-quality $^{239}\text{PuO}_2$ microspheres, they were asked to extend their developmental effort to ^{238}Pu for the Isotopic Power Program. Much of the work with ^{239}Pu was found to be applicable to ^{238}Pu .

Sol-gel developmental work with curium, which has already proved useful for isotopic power sources, was also carried out during this report period.

8.1 LABORATORY STUDIES OF $^{238}\text{PuO}_2$ SOL-GEL PROCESS

The successful preparation of $^{238}\text{PuO}_2$ sols and microspheres on a laboratory scale (10 g of ^{238}Pu) was reported last year.¹ During the current report period, difficulties were encountered in scaleup experiments that were conducted at Mound Laboratory. Therefore, in addition to the small-scale experiments, which were continued, data that had been generated at Mound Laboratory were analyzed, and electron microscopy was introduced as a diagnostic tool to evaluate larger-scale (50 g of ^{238}Pu) sol preparations. The principal problem areas in the large-scale process were isolated; recognition of these difficulties led to minor process changes

which, in turn, resulted in the successful preparation of $^{238}\text{PuO}_2$ sols and microspheres in batches containing up to 50 g of ^{238}Pu .

Investigation of Process Variables

It was recognized from previous investigations² that the formation and the retention of highly crystalline plutonium polymer are required for successful sol preparation. Primary efforts were, therefore, directed at determining the effects of process variables on polymer formation and degradation.

Effects of Initial HNO_3/Pu Mole Ratio During Peptization. – When the high-nitrate sol is evaporated to dryness, the plutonium polymer is exposed to high HNO_3 concentrations at an elevated temperature. Depolymerization could occur during this operation; in fact, in the case of ^{238}Pu , its self-heating and radiolytic properties would be expected to increase the degradation. Since the nitrate that is present in the system is determined by the amount of HNO_3 that is used to peptize the aged precipitate, the effect of acid on depolymerization was evaluated as a function of the HNO_3/Pu mole ratio employed during peptization. High-nitrate sols of both ^{238}Pu and ^{239}Pu were examined immediately after peptization (approximately 0.1 M Pu) and after evaporation to dryness.

It was shown that maximum degradation occurred during evaporation, especially as dryness was approached ($>5\text{ M NO}_3^-$). Freshly peptized $^{238}\text{PuO}_2$ sol contained 1 to 2% ionic species (mainly Pu^{6+}), while less than 1% of such species was observed for $^{239}\text{PuO}_2$ sols. The initial HNO_3/Pu ratio had little effect on these values; on the other hand, the effect was significant in samples that had been evaporated to dryness. With ^{239}Pu preparations

¹*Chem. Technol. Div. Ann. Progr. Rept. May 31, 1968, ORNL-4272, pp. 161–65.*

²*Chem. Technol. Div. Ann. Progr. Rept. May 31, 1968, ORNL-4272, pp. 125–26.*

that had been peptized at NO_3^-/Pu mole ratios of 3 or less, the maximum amount of ionic species amounted to 2% of the plutonium; at a ratio of 1, only 0.1 to 0.2% ionic species were observed, whereas at a ratio of 4 more than 10% was found. Under similar conditions, the amount of ^{238}Pu polymer that decomposed was substantially higher than that of ^{239}Pu polymer. For example, when an initial NO_3^-/Pu ratio of 2.5 was used, about 6% ionic plutonium was found in ^{238}Pu preparations. Other ratios were not investigated for ^{238}Pu in this series of experiments; however, less degradation had been noted in previous experiments in which a NO_3^-/Pu ratio of 1.4 was used.

These experiments demonstrate the adverse effect of HNO_3 on plutonium polymer. However, since depolymerization also depends on the length of time of contact with a given acid, as well as the acid concentration and the temperature, the exact amount of degradation to be expected at a given acid concentration will vary with process conditions and batch size.

Variation of Peptization Time with Initial NO_3^-/Pu Ratio. — It was thought that the use of low NO_3^-/Pu peptizing ratios (1 to 1.2) might necessitate longer digestion times to accomplish peptization at a given plutonium concentration. However, in experiments with ^{238}Pu and ^{239}Pu we found that lower ratios could be used without an appreciable extension of the peptization time if higher plutonium concentrations were employed. Subsequent experiments showed that plutonium concentrations up to 0.45 M could be used without the formation of a solid phase. Thus, in using a lower $\text{NO}_3^-/\text{metal}$ ratio (1 to 1.2), we would gain the advantage of a reduced volume of liquid to be evaporated (i.e., 22% of that required when a plutonium concentration of 0.1 M is used).

Investigation of the Solid Phase. — When high-nitrate sols (prepared from aged precipitates) are concentrated by evaporation, a solid phase appears at a nitrate concentration between 0.5 and 5 M . This effect reflects an unstable electrolyte condition, but the exact mechanism causing the formation of solids is not known. When the nitrate concentration exceeds 5 M , a stable colloidal solution is produced again. Thus the reaction is reversible; that is, the addition of water to a 5 M solution will produce two phases, and the addition of water to the solid phase after its separation from the supernate will produce a stable colloidal solution. We investigated this phenomenon because of con-

cern over inadvertent thermal denitration of the solid phase when low aqueous volumes are attained in process equipment.

It was found that the solid phase consists of crystalline polymer that can be separated from the liquid by filtration, dried, denitrated, and formed into excellent-quality sol. Analysis of the liquid phase provided a sensitive measurement of the ionic plutonium species present. It appears that both ionic species and degraded polymer concentrate in the liquid phase. In some cases, 30 to 40% of the plutonium in this phase was hexavalent. Attempts to form sols from solids obtained by evaporating the liquid phases to dryness were unsuccessful. Denitration was very rapid, and the solids obtained would not resuspend. These results confirmed that degradation of the polymer increases as the HNO_3 concentration increases.

Effects of Iron and Fluoride Impurities. — Experiments were performed to determine whether the presence of small amounts of fluoride (from the dissolution of PuO_2) or iron (a contaminant) would create difficulties in the preparation of plutonia sols. Plutonium nitrate feed solutions containing about 3 wt % iron (based on plutonium weight) and/or 0.1 M in HF were prepared. These solutions were processed in the usual manner to form sols. No detrimental effects were observed in any of the preparations. Fluoride was removed during precipitation and washing of the plutonium, while iron was carried through the entire process, resulting in a final sol with a slightly different color.

Self-Denitration of ^{238}Pu High-Nitrate Sol. — The denitration, by self-heating effects, of $^{238}\text{PuO}_2$ solids made by evaporating high-nitrate sols was studied at two batch sizes. The sols were prepared in the normal manner (using a NO_3^-/Pu peptizing ratio of 1.5). A 5-g portion was spread to a 1/16-in. bed depth, and a 15-g portion was arranged to a depth of 1/4 in. Nitrate was lost in both samples, and the NO_3^-/Pu mole ratio, which was checked periodically, decreased to about 0.18 in one week (rates were not appreciably different for the two samples). The apparent temperature (measured by a thermocouple placed in the solids) did not exceed 120°C in either case. However, after one week, approximately one-half of each sample would not resuspend to form a sol. These results cannot be extrapolated directly to larger batches of ^{238}Pu ; however, it must be inferred that, since denitration does occur in the solid state (even with small quantities of material) at

temperatures at least 100°C less than the normal processing temperature for ^{239}Pu , the effect will be more pronounced with larger batches where the increased internal heat generation will be sufficient to sustain even higher temperatures. Since the resulting solids were not satisfactory for use in sol formation, any holding of $^{238}\text{PuO}_2$ high-nitrate solids prior to thermal denitration is probably undesirable.

Electron Microscopic Studies of $^{238}\text{PuO}_2$ Sols

Because of difficulties experienced at Mound Laboratory during the preparation of $^{238}\text{PuO}_2$ sols in 50-g batch sizes, we decided to use electron microscopy as a diagnostic tool to evaluate sol preparations. These studies were carried out in close collaboration with Mound personnel. The results substantiated previous findings, which indicated that problems encountered during scaleup experiments resulted from the failure to produce crystalline polymer or the degradation of the crystalline polymer, if produced.

The crystallinity of $^{238}\text{PuO}_2$ sols was evaluated at various stages in the sol preparation process,

for example, before evaporation, after drying, and after denitration, by examining electron diffraction patterns obtained at each stage. Subsequent to these experiments, photomicrographs of high-nitrate and product (denitrated) $^{238}\text{PuO}_2$ sols were obtained. These photomicrographs demonstrated that there are no fundamental differences between $^{238}\text{PuO}_2$ sols and $^{239}\text{PuO}_2$ sols as to crystallinity or particle size.

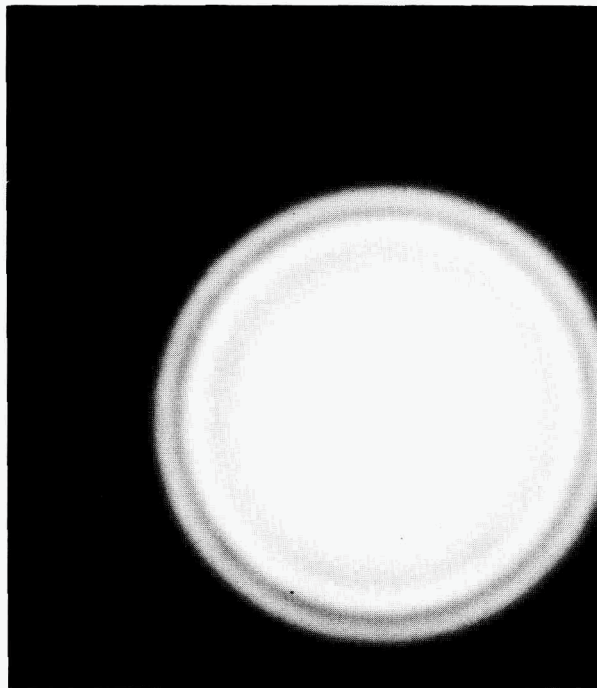
Results of the first 50-g run showed that, immediately after peptization, the high-nitrate sol was amorphous rather than crystalline, the desired form. Electron diffraction patterns that demonstrate this difference are shown in Fig. 8.1. The final sol that was prepared from this material was characteristic of sols prepared from amorphous polymer.

A second 50-g experiment was designed to determine if longer aging times of the washed hydroxides would produce crystalline polymer. The washed hydroxide was boiled for 6 hr and examined by electron diffraction after each 2-hr period of aging. The polymer was found to be crystalline after 2 hr of aging, which suggests that amorphous polymer at this stage could result from hydrolysis (or partial hydrolysis) of the plutonium that occurs

PHOTO 96356



AMORPHOUS POLYMER



CRYSTALLINE POLYMER

Fig. 8.1. Diffraction Patterns of High-Nitrate $^{238}\text{PuO}_2$ Sols.

during feed adjustment. Hydrolysis has probably been responsible for some of the difficulties experienced during scaleup experiments, thus making feed adjustment a critical area in the flowsheet.

In the run made with a hydroxide that had been aged for 6 hr, a satisfactory final sol was not formed, although the polymer in the original high-nitrate sol was highly crystalline. Electron diffraction patterns for this sol are compared with a 10-g control batch in Fig. 8.2. It is interesting to note the loss of pattern in the dried high-nitrate sol in the case of the 50-g batch. This indicates that the crystalline polymer was partially degraded to

ionic forms of plutonium by contact with HNO_3 of increasing concentration as the material was evaporated to dryness, and suggests that this degradation is probably the principal cause of the difficulties encountered during scaleup. Increased crystallinity is obtained in the baked material for two reasons: (1) crystallite size increases during baking, and (2) ionic forms of plutonium present in the dry material are converted to PuO_2 at the baking temperature.

The formation of solids during the evaporation of a high-nitrate sol provides a means of avoiding contact with strong acid; that is, the polymer solids

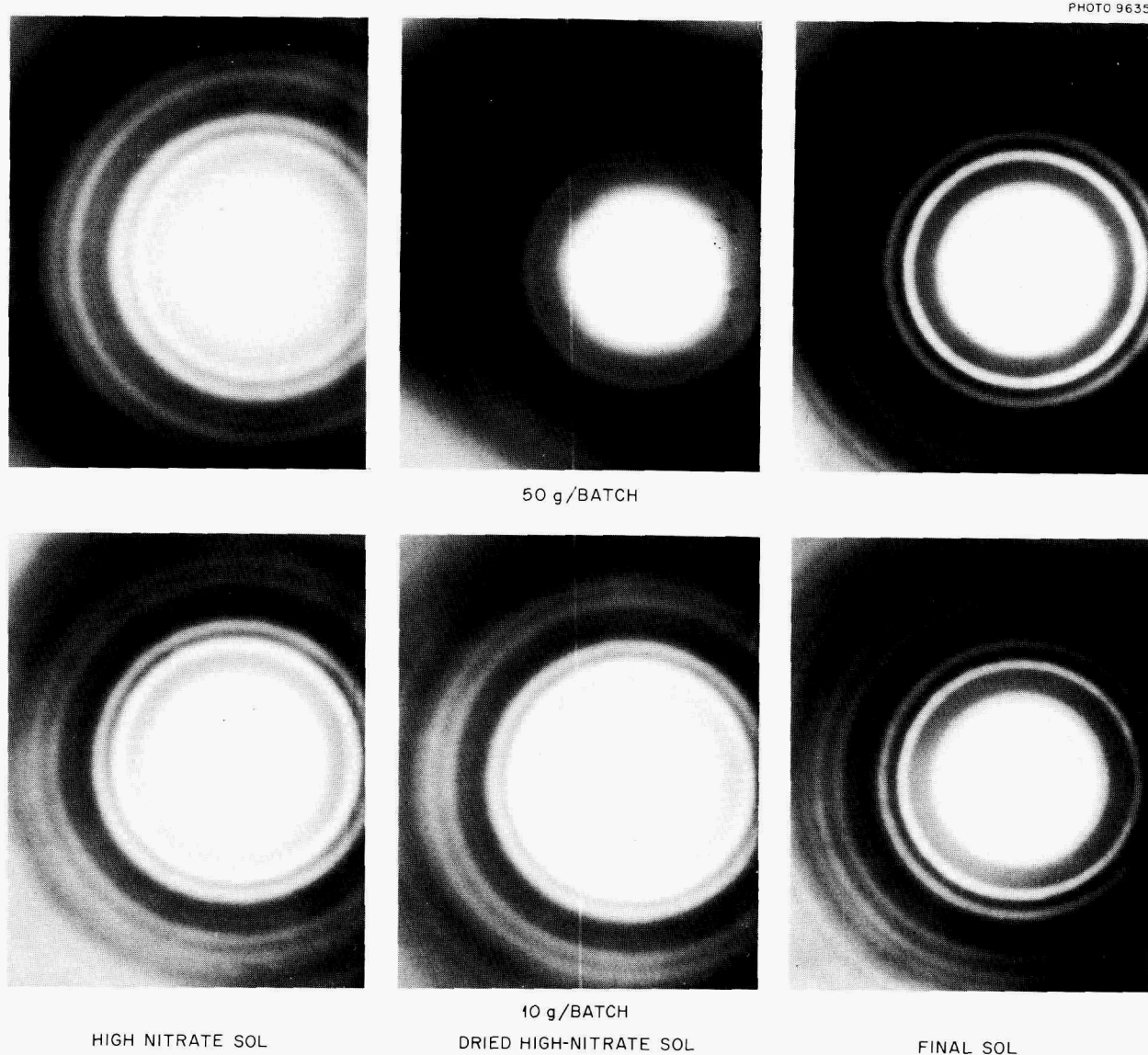


Fig. 8.2. Diffraction Patterns for Sol Preparations.

can be separated by filtration when precipitation occurs. This technique was investigated by chemists at Mound Laboratory, who used both 10- and 50-g batches of ^{238}Pu . Their results correlate very well with those obtained in the small-scale experiments described above. They found that, for both batch sizes, maximum precipitation occurs at a nitrate concentration of about 2 *M*, and that as much as 80% of the plutonia can be recovered by filtration. The filtered precipitate, which readily disperses in water, can be dried and baked in the usual manner. In their experiments, they attempted to form sols from both the precipitate and the filtrate. The precipitate formed excellent final sol (100% yield) with a low nitrate content, from which good-quality microspheres were readily produced. The filtrate contained a high percentage of ionic plutonium, however, and did not produce sol; solids obtained upon drying denitrated very rapidly and would not resuspend after a very short denitration time.

These results substantiate that the primary difficulty in scaleup experiments is degradation of the polymer by HNO_3 during the period in which the polymer is evaporated to dryness. The fact that degradation is more pronounced in 50-g runs than in 10-g runs indicates that contact time between polymer and HNO_3 is also an important variable. For example, in these experiments, the time required for evaporation to dryness increased as the batch size increased, and it is likely that the temperature also increased due to radiolytic self-heating effects. In general, the data indicate that depolymerization is similar to simple dissolution of PuO_2 and is, therefore, a function of time, temperature, and acid concentration.

8.2 DEVELOPMENTAL STUDIES IN A GLOVE-BOX SYSTEM

Because of its chemical and mechanical stability at high temperatures, dense plutonia is an attractive material for application in reactor fuels and isotopic heat sources. The glove-box facility at ORNL, originally built for use in the development of a PuO_2 sol-gel process flowsheet, was operated to supply PuO_2 as sol or as dense microspheres needed in isotopic and reactor fuel fabrication development studies. Its capacity is 150 g of plutonium per day. The PuO_2 sol-gel flowsheet, de-

scribed previously,³ was used to produce PuO_2 sols, from which a total of 2.5 kg of dense $^{239}\text{PuO}_2$ microspheres was prepared for use as a stand-in for $^{238}\text{PuO}_2$ in the development of fuel forms for isotopic power sources. Flowsheet development studies included a demonstration of the peptization of the hydrous plutonia precipitate at 70% of the usual NO_3^-/Pu mole ratio (i.e., 1.4 instead of 2) and at a slurry concentration twice that normally used. Other developmental work included demonstrating the operation of a drying column with a minimum of turbulence in the fluidized bed and developing a firing technique to produce plutonia of near theoretical density.

Preparation of PuO_2 Sol

A "low-acid" flowsheet, which reduces the volume of dilute sol that must be evaporated, was used successfully to produce $^{239}\text{PuO}_2$ sol. The washed, hydrous $^{239}\text{PuO}_2$ was slurried in the usual volume of water, resulting in a nominal plutonium concentration of 0.19 *M*. After the slurry had been digested at 95 to 97°C, one-half of the water previously added was removed by filtration, and 6.6 *M* HNO_3 was added to the remaining slurry (now about 0.4 *M* in plutonium) to adjust the NO_3^-/Pu mole ratio to 1.4. The HNO_3 concentration in the slurry, however, was the same as that in the original flowsheet. Peptization was complete within 1 hr of digestion at 95 to 97°C, the period specified by the flowsheet. After evaporation to dryness and denitration at 240°C, the solids were resuspended in water to produce a $^{239}\text{PuO}_2$ sol identical with those prepared at a NO_3^-/Pu mole ratio of 2 in a slurry concentration of 0.19 *M*. Thus, by using the low-acid flowsheet, the volume of water that must be evaporated is reduced, which, in turn, results in savings in both the evaporator size and the operating time.

Development of Firing Schedules

Previously, $^{239}\text{PuO}_2$ in the form of dried shards or gel microspheres was fired in moist air to 1200°C to obtain a product with a density 95 to 98% of theoretical. Metallographic examination of the fired microspheres, however, showed that some

³*Chem. Technol. Div. Ann. Progr. Rept. May 31, 1967, ORNL-4145, pp. 195-99.*

Table 8.1. Characteristics of Dense PuO₂ Microspheres

Firing Schedule ^a	Density ^b (g/cc)		Surface Area (m ² /g)	Pore Volume (cc/g)	Carbon (ppm)	O/Pu Atom Ratio	Crush Strength ^c (g)
	Bulk	Pressure					
A	11.13	11.27	0.023	0.001	<20		575
B	10.65	10.85	0.023	0.002	25		490
C	11.34	11.44	0.002	0.001	<20	2.00	460

^aFiring Schedule:

A. Heatup to 1200°C at 300°C/hr in humidified air; hold 1 hr at 1200°C.

B. Heatup to 1150°C at 300°C/hr in steam-argon, with 2-hr hold at 500°C; hold in argon for 2 hr at 1150°C.

C. Heatup to 1050°C at 300°C/hr in steam-argon, with 1-hr holds at 250 and 400°C; change atmosphere to argon-4% hydrogen at 1050°C, and hold 6 hr.

^bTheoretical density = 11.45 g/cc.^cParticle size: 105 to 250 μ in diameter.

undesirable microporosity remained. The micropores in dense ²³⁹PuO₂ microspheres held at 1800°C in high vacuum over a 0.5-hr period apparently migrated to the grain boundaries, resulting in distortion and cracking of the microspheres. Several firing schedules were evaluated in an effort to reduce the microporosity and to increase both the density and the dimensional stability of the ²³⁹PuO₂ microspheres at high temperatures. The first schedule required the atmosphere maintained in the furnace to be replaced by a mixture of argon and steam. To permit the use of a steam-argon atmosphere, the ceramic furnace tube was replaced with an Inconel pipe to eliminate the danger of breakage; however, the softening point of Inconel (~1390°C) limited the working temperature in the microsphere bed to about 1150°C. Plutonia gel microspheres heated to 1150°C (2-hr hold at 500°C) in steam-argon and held for 2 hr in argon had lower densities (93 to 95% of theoretical) and more open porosity (Table 8.1) than those fired in moist air (97 to 98% of theoretical density). When the schedule included heating in steam-argon to 1050°C (with 1-hr holds at 250 and 400°C), followed by a 6-hr hold in argon-4% hydrogen at 1050°C, the bulk density increased to 99% of theoretical and the surface area was 10% of that obtained with a steam-argon atmosphere in the absence of the 6-hr hold period in argon-4% hydrogen. The oxygen-to-metal atom ratio of this product was 2.00. The evaluation of typical microspheres fired according to these schedules after being heated to 1800°C is not complete.

8.3 ASSISTANCE TO MOUND LABORATORY

The installation at Mound Laboratory of equipment (designed and fabricated at ORNL, described last year⁴) to produce 150-g batches of ²³⁸PuO₂ microspheres was completed, and a program of extensive checking-out and modification was carried out. Developmental work associated with the formation of sols and microspheres was continued during the fabrication and installation of the system, and several equipment improvements that should enable the facility to take advantage of the most recent advances in technology were made. Further work with the ORNL system is awaiting the outcome of large-scale (>50 g of plutonium/batch) development work being conducted by Mound Laboratory personnel, using ²³⁸Pu in similar equipment in shielded glove boxes.

Check-Out and Modification

The cubicle containing the ORNL equipment was installed, shielding was erected, and utilities and instrumentation were connected by Mound personnel. Instrumentation and operational check-outs were then accomplished with the assistance of ORNL personnel. The cubicle was closed and leak checked at this point, and was then reopened for additional checking and equipment modification.

⁴Chem. Technol. Div. Ann. Progr. Rept. May 31, 1968, ORNL-4272, pp. 170-71.

In the sol-forming equipment, a vacuum regulator was installed on the filtrate tank, and a means to permit the continuous addition of water was provided for the precipitator-filter (so that continuous washing of the hydrous plutonia precipitate can be accomplished). The design of the evaporator bottom was changed to a 45° cone to allow concentration to smaller volumes. Also, the substitution of resistance heating for steam and the addition of vacuum capability to the condensate tank made vacuum distillation in the evaporator possible. The mounts and shaft connectors of agitator motors were modified to facilitate remote replacement and alignment.

Preliminary tests of the microsphere-forming equipment by Mound personnel, using ThO₂ sol, showed the need for a filter to remove fine sol droplets entrained in the solvent before the solvent reaches the recirculating pump; this assembly was supplied by ORNL. Upon the recommendation of Mound personnel, all the components for handling wet gel spheres were replaced with similar units having larger flow passages ($\frac{9}{16}$ in. in diameter instead of $\frac{5}{16}$ in.). Also, an "abort" valve was added at the bottom of the sphere-forming column to allow the removal of off-specification material for easier recycle. Capability for steam treating the gel spheres was incorporated by adding a water addition rotameter and a steam generator to the

purge-gas line for the dryer, and by modifying the dryer basket to ensure passage of steam through the bed of spheres.

Sustained Operation with ThO₂ Sol

After the new and modified components supplied by ORNL had been installed by Mound personnel, a series of five runs was made by ORNL personnel to check the capability of the system for sustained operation. In each run, 136.6 g of ThO₂ in the form of approximately 1.5 M sol was pumped to the column at the rate of approximately 2 cc/min. After 3 to 4 hr of continuous column operation, the gel spheres were transferred, as a batch, into the dryer, where they were contacted with superheated steam ($\cong 4$ g of H₂O per gram of ThO₂) up to 200°C. They were then transferred to the furnace, where they were heated to 1200°C over a period of 8 hr and then held at that temperature for 3 hr.

The data for these runs are presented in Table 8.2. A total of 80 to 128 g of essentially theoretically dense product ThO₂ was recovered after each run. Of these microspheres, more than 94% were round (determined by the Mound shake table), and about 88% were in the 74- to 250- μ -diam size range. A partial clean-out of the system revealed the presence of 110.3 g of ThO₂ gel fines in the over-

Table 8.2. Product Characterization and Material Balances for ThO₂ Runs at Mound Laboratory

	Run No.					Partial Clean-Out
	TX-13	TX-14	TX-15	TX-16	TX-17	
Input						
ThO ₂ as sol, g	136.6	136.6	136.6	136.6	136.6	0
Product						
Dense ThO ₂ , g	100.1	128.5	82.4	96.2	80.4	0
Round, %	97.8	99.6	89.0	94.6	86.1	
Size range, %						
>250 μ	2.5	9.2	22.5	18.1	Not separated	
177-250 μ	32.3	82.7	25.6	24.1		
125-177 μ	59.2	6.5	37.9	37.4		
74-125 μ	6.0	1.6	14.3	20.4		
Other ThO ₂ recovered, g	8.4	0	6.3	6.3	13.3	110.3
ThO ₂ not recovered, g	28.1	8.1	47.9	34.1	42.9	-110.3
Cumulative unrecovered, g	28.1	36.2	84.1	118.2	161.1	50.8

flow filter. All the equipment will be cleaned thoroughly prior to operation with $^{238}\text{PuO}_2$; this will prevent contamination of the $^{238}\text{PuO}_2$ with ThO_2 and, hopefully, will reveal the location of the 51 g of ThO_2 presently unaccounted for.

The problem involving the entrainment of fines was solved by expanding the disengaging section at the top of the forming column. The bottom and fluidizing sections were not changed; however, an increase of less than 4 in. in overall height allowed us to more than double the cross-sectional area at the point of solvent overflow and to almost triple the distance from the top of the fluidizing section to the overflow point. Two of the modified columns and improved two-fluid nozzles were supplied by ORNL.

Development Program at Mound Laboratory

As the size of $^{238}\text{PuO}_2$ sol batches was increased stepwise from 5 to 50 g Pu at Mound Laboratory, satisfactory results became increasingly difficult to achieve. Processing of larger batches in laboratory facilities was not permissible; it was decided to continue the studies in shielded, glove-box facilities rather than in the manipulator-operated ORNL equipment. The developmental sol-forming facility utilizes an existing precipitation vessel, a porous stainless steel filter funnel, and an 8-in.-diam denitration vessel that was supplied by ORNL and used earlier in the smaller-scale laboratory studies.

The microsphere-forming equipment used at Mound Laboratory is patterned after that in the ORNL cubicle. It incorporates one of the improved forming columns (supplied by ORNL), and a solvent still and pump tank that were fabricated at Mound Laboratory from ORNL prints. A furnace normally used in another process will be utilized for firing the dried gel spheres. Initial attempts to form $^{238}\text{PuO}_2$ microspheres (by both Mound and ORNL personnel) in this facility, using the conventional Span 80-Ethomeen S/15 surfactant system, were singularly unsuccessful. However, the use of another surfactant, Pluronic L-92, supplied by ORNL, gave both good column operation and acceptable product quality, enabling the production of multigram quantities of $^{238}\text{PuO}_2$ microspheres by the sol-gel method.

8.4 CURIUM SOL-GEL STUDIES⁵

Curium is one of the elements that has already proved to be useful in the Isotopic Power Program. Hence, it is appropriate to summarize the ORNL sol-gel work on curium here.

Previously, the rare-earth sol-gel process was successfully adapted for use in preparing mixed ^{244}Cm - ^{243}Am sols and was used to obtain 38 g of dense americium-curium oxide.⁶ During this report period, an additional 31 g of oxide was prepared, simplified equipment concepts for sol preparation were demonstrated, and a permanent sol-gel equipment rack was designed and installed in the Transuranium Processing Plant.

Sol Preparation

Since high-purity feed material is required for the preparation of good-quality sols, an oxalate precipitation-calcination cycle was used for purification prior to feed adjustment. Batch sizes in these experiments varied from 8 to 10 g of total metal (16% ^{243}Am , 78% ^{244}Cm , and 6% higher curium isotopes). Preparation of the sol requires precipitation, by adding the dilute metal nitrate feed solution to a large excess of 8 M NH_4OH , washing the hydroxide to a final pH of less than 9, and heating for 1 to 2 hr at 85°C. This converts the resulting paste to a fluid sol that can be concentrated by evaporation.

A sol with good physical characteristics was obtained in each of the five runs made. In these runs an inverted-cone, fluidized-bed washer was shown to be superior to filtration as remote handling operations were simplified. Recoverable curium losses due to peptization during washing were generally about 3%. In the four runs in which feed acid concentrations ranged from 0.05 to 0.28 M, final sols with satisfactory NO_3^- /metal mole ratios (0.02 to 0.17) were obtained. This suggests that the feed acid concentration is an important variable and that a concentration of about 0.1 M would be desirable.

⁵This topic is covered in greater detail in Sect. 5.3.

⁶Chem. Technol. Div. Ann. Progr. Rept. May 31, 1968, ORNL-4272, pp. 170-73.

Preparation of Microspheres

Gel microspheres were formed at sol concentrations of 0.11 to 0.13 *M*, using standard sphere-forming techniques. The drying medium was 2-ethyl-1-hexanol containing 0.4 vol % Span 80 and 0.6% Amine O. There was a general tendency for particles to cluster late in a run; however, this effect was not severe with sols having $\text{NO}_3^-/\text{metal}$

mole ratios of 0.1 or less. (More severe clustering had occurred earlier in runs with sols having higher $\text{NO}_3^-/\text{metal}$ ratios.) The gel microspheres were air-dried overnight prior to firing in air to 1150°C. The fired microspheres were free-flowing and dust-free, and showed no tendency to crack or disintegrate. Similar microspheres were examined after being stored in air for more than a year; no alteration or disintegration was visible.

9. Special Sol-Gel Processes

The versatility of the sol-gel process and the ease with which it can be adapted to form a variety of ceramic bodies of different shapes and sizes has led to its use in preparing materials for special applications. Sol-gel methods for the preparation of such materials (i.e., materials to be used for purposes other than nuclear fuel or isotopic heat sources (Sects. 6–8) are reported here. A variety of sols were produced by the precipitation-washing-peptization method that was originally developed for preparing lanthanide hydroxide sols, and the preparation of titania sols was demonstrated on a 100-g scale. Mixed oxide materials were usually prepared starting with mixed sols; in some cases, soluble salts were added to the feed solutions used in sol preparation. Techniques of adding carbon to urania and thoria sols were extended to include the addition of carbon to many special sols, both for the purpose of forming metal carbides and for the purpose of preparing porous oxides. Porous oxides were prepared from sols to which carbon had been added by forming the codispersed sols into gels of the desired shapes and then burning out the carbon; they were also formed by controlling the temperature and time during the sintering of oxide gels. Investigations were made to develop techniques for producing $100\text{-}\mu\text{-diam}$ microspheres in closely controlled size ranges.

9.1 SOL PREPARATION

Several metal hydroxide and/or hydrous oxide sols have been prepared to satisfy numerous requests for sol-gel-derived materials. The precipitation-washing-peptization procedure that was previously developed for preparing rare earth sols has been used to prepare hydroxide sols of all the rare earths (except promethium), several trivalent actinides, Y, Fe, Zr, Hf, Al, and Ti. The success achieved with this procedure indicates that it can be used, with minor modifications in some cases,

to prepare sols of most metals that form insoluble hydroxides. Various methods have been used to prepare zirconia sols with different properties, and some special materials have been made by mixing sols and by the addition of soluble salts to the nitrate feed solutions.

Preparation of Metal Hydroxide Sols by the Precipitation-Peptization Process

The process that was previously developed for the preparation of rare earth sols¹ has been found to be useful in preparing a wide variety of metal hydroxide and/or hydrous metal oxide sols. This process consists in precipitating the metal hydroxide by adding a dilute solution of the metal nitrate or chloride to a large excess of 8 to 10 M NH_4OH , washing the hydroxide with distilled water to a final pH of 9 to 9.5, dewatering by filtration (or centrifugation), and digesting the filter cake at 60 to 80°C. During digestion, the gelatinous precipitate is converted to a fluid sol that can be concentrated and formed into microspheres. In each case, the original precipitate consists of small amorphous particles from 20 to 50 Å in diameter. During digestion, this material is converted to crystalline forms that are peptized by residual chloride or nitrate anions to form a fluid sol. The digestion time and temperature required to convert the paste-like solids to a fluid sol varied widely for the different metals. In some instances, it was advantageous to modify the procedure for materials that required digestion times of days or months. It was found that a fluid sol can also be obtained by vigorously agitating the washed precipitate, and that sols produced in this way can also be successfully formed into microspheres. Usually, these

¹C. J. Hardy, S. R. Buxton, and M. H. Lloyd, *Preparation of Lanthanide Oxide Microspheres by Sol-Gel Methods*, ORNL-4000 (August 1967).

sols retain their amorphous characteristics for long periods of time; although they thicken with age, they can be refluidized by agitation.

Vigorous agitation of the gelatinous precipitate has been a very useful technique for preparing sols from the heavier rare earths because the times required for conversion to a crystalline product increase with increasing molecular weight in the series and involve many days to months for the heaviest elements.²

The precipitation-washing-peptization method has been satisfactory for preparing sols from all metals tested to date, including Y, Fe, Zr, Hf, Al, Ti, Am, Cm, Bk, and Cf, as well as the rare earths. With the exception of titania and hafnia sols, which were prepared from chloride salts, the sols were prepared in nitrate media. The flowsheet developed to prepare titania sol is shown in Fig. 9.1.

The signs of the electrical charges on these sols were determined with a streaming current detector (see Sect. 16.2) and were found to be positive in most cases; however, several negatively charged sols have also been prepared. Yttrium and rare earth hydroxide sols were positively charged.

These colloids are stabilized by nitrate ion; NO_3^- /metal mole ratios typically varied from 0.05 to 0.15. Zirconia, hafnia, and titania sols were negatively charged, and anion (Cl^- or NO_3^-)-to-metal mole ratios of these sols were very low (<0.001 to 0.01). Alumina sol appears to be slightly positively charged, although the anion/metal ratio is also very low (0.004). Microspheres can be prepared from negatively charged sols; however, it was found that such sols can be made positively charged by the addition of small amounts of HNO_3 . Nitric acid generally increases the fluidity of the sol and improves sphere-forming capabilities.

The primary operational difficulty was encountered in washing the precipitated hydroxide. Because filtration is usually difficult, washing in initial small-scale experiments was accomplished by centrifugation and decantation. To scale up the process we developed an inverted cone fluidized-bed washer in which the precipitated hydroxide is fluidized by introducing wash water at the bottom of the vessel and allowing it to overflow at the top. This equipment has performed very well in laboratory experiments and appears to be amenable to scaleup (see Sect. 9.2). The inverted cone washer was used for most of the above-mentioned metal hydroxides. However, it is not suitable for the lighter rare earths (lanthanum through neodymium)

²R. G. Haire and T. E. Willmarth, *Trends and Differences in the Crystallization Behavior of Lanthanide Hydroxide Preparations*, ORNL-TM-2387 (October 1968).

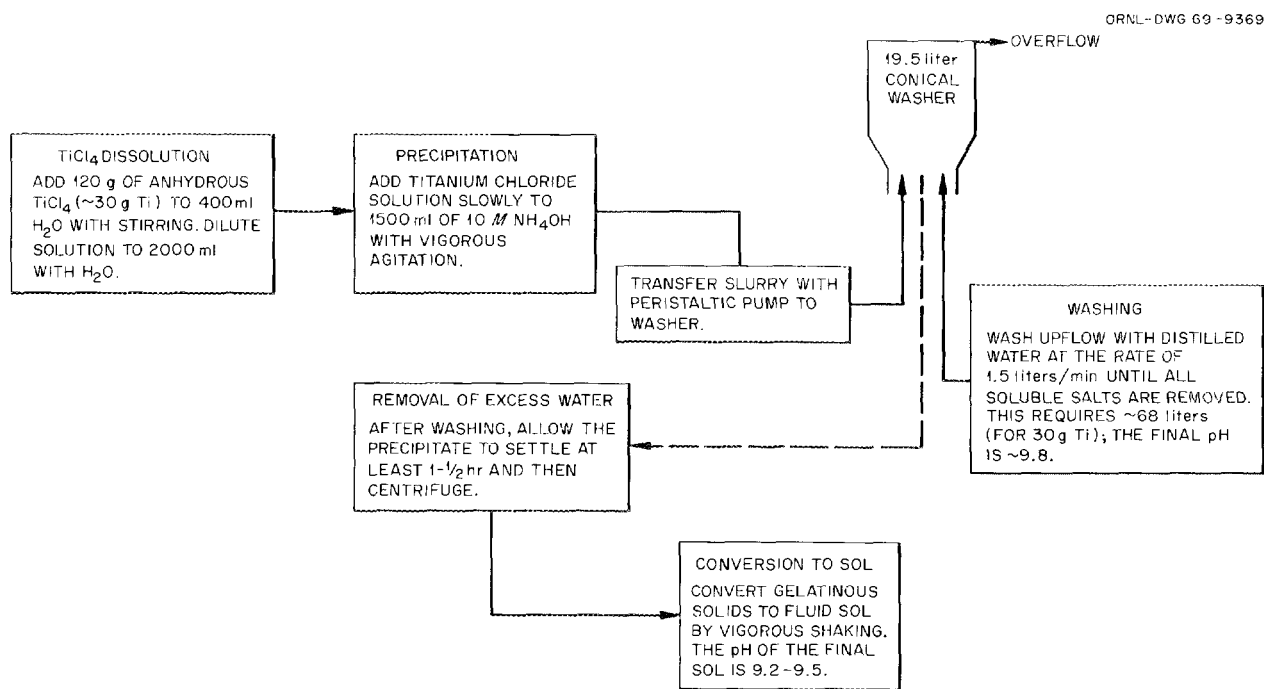


Fig. 9.1. Flowsheet for the Preparation of Titania Sol. Basis: 120 g of TiCl_4 (~30 g of Ti).

because these hydroxides are converted from amorphous solids to crystalline forms in only a few minutes, and, as a result, excessive peptization occurs before adequate washing can be accomplished.

Preparation of Zirconia Sols

Zirconia sols have been prepared by several methods other than the one described above. The preparation of large-crystallite, low-nitrate ZrO_2 sols by autoclaving zirconyl nitrate solutions at $200^\circ C$ has been described previously.³ The procedure used for preparing PuO_2 sols⁴ has also been used for the preparation of zirconia sols. This procedure consists of precipitation, washing, peptization at a high nitrate/metal ratio, heating to decrease the nitrate/metal ratio, and re-peptizing in water. A high-nitrate zirconia sol can also be produced by starting with a dilute zirconyl nitrate solution, evaporating to dryness, heating, and re-dispersing in water.

With the modified plutonia sol method, zirconyl nitrate (or chloride) is precipitated with excess NH_4OH , and the hydroxide precipitate is washed to remove contaminant ions. Next, the precipitate is peptized by digestion with sufficient HNO_3 to provide a NO_3^-/Zr mole ratio of 2.0. The resulting sol is then evaporated to dryness and heated to remove excess nitrate. The final sol is formed by resuspending the solids in water. The NO_3^-/Zr mole ratio of the final sol varies from 0.8 to 1.2. While a zirconia sol with a nitrate concentration of this magnitude would normally be undesirable, especially for blending with UO_2 sol, such sols have been readily formed into microspheres in laboratory experiments.

When zirconyl nitrate is used as the starting material for zirconia sol, the precipitation step may be eliminated; that is, a dilute solution of zirconyl nitrate is simply refluxed for several hours, boiled to dryness, and then heated to $130-140^\circ C$. The friable product is readily dispersed into water to give an acidic sol as concentrated as 2 M in zirconium with a NO_3^-/Zr mole ratio of about 1. Sols prepared in this manner are especially suitable for

codispersing carbon and, in turn, for the preparation of zirconium carbide microspheres (see Sect. 9.3).

Mixed Sol Preparations

A number of special materials have been produced from mixed sols. Zirconia-yttria microspheres were prepared in this manner. Yttrium hydroxide sol produced by the rare earth sol preparation method was added to zirconia sol that had been prepared by the autoclave method to yield a mixed sol containing 10% yttria. This mixture was used to form microspheres under the same conditions used with pure zirconia sol. Mixtures of plutonia and thoria sols have been used to prepare PuO_2-ThO_2 microspheres containing 85, 90, and 95% PuO_2 .

Calcined neodymia microspheres containing 1.2 wt % boron were prepared for the Isotopes Division for use in the investigation of helium release during neutron irradiation. These microspheres were formed from a neodymium hydroxide sol that had been prepared by adding boric acid to a neodymium nitrate solution prior to hydroxide precipitation.

9.2 SCALEUP OF THE PRECIPITATION-WASHING-PEPTIZATION SOL PROCESS

Equipment was built and used to prepare 100- to 200-g batches of sol by the general precipitation-washing-peptization process that was originally developed for the preparation of rare earth sols. The following description of the preparation of titania sol, using this equipment and the process outlined in Fig. 9.1, is an example of how the larger-scale operations are carried out.

One pint of anhydrous $TiCl_4$ (203 g of Ti) was added over a 40-min period to about 2.5 liters of water in the 6-liter Pyrex dissolver shown in Fig. 9.2. The titanium chloride solution was then diluted to 6 liters and fed, over a period of 40 min with thorough agitation, into approximately 12 liters of 10 M NH_4OH contained in a 13-in.-diam by 18-in.-deep steel tank (Fig. 9.3). The slurry of titanium hydroxide was then pumped through plastic tubing, by means of a peristaltic pump, into the wash tank. Actually, there were two large wash tanks operated in series; demineralized water

³Chem. Technol. Div. Ann. Progr. Rept. May 31, 1967, ORNL-4145, p. 195.

⁴M. H. Lloyd and R. G. Haire, "A Sol-Gel Process for Preparing Dense Forms of PuO_2 ," *Nucl. Appl.* 5, 114-22 (1968).

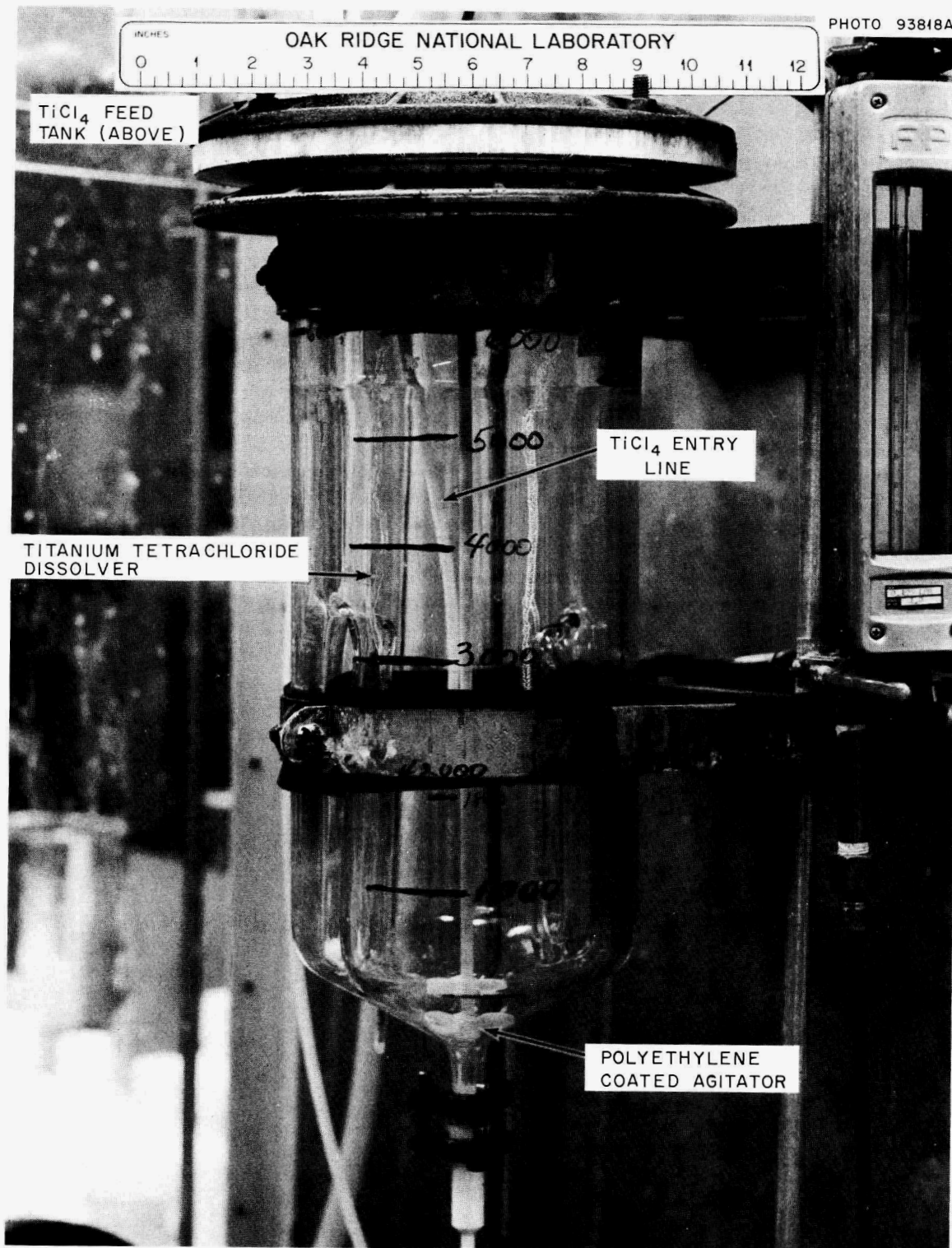


Fig. 9.2. Six-Liter Glass and Plastic Tank for Dissolving TiCl₄ in Water.

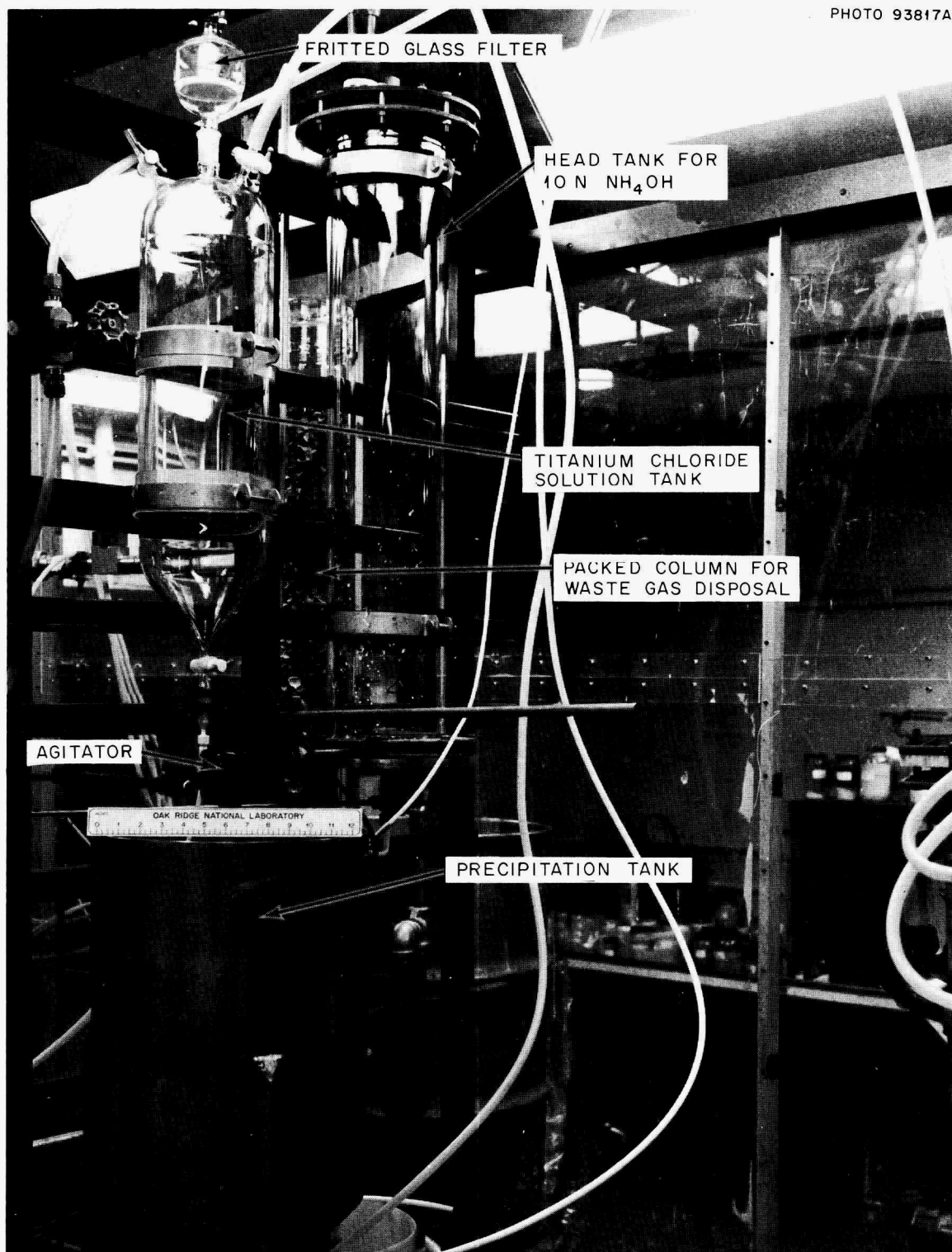


Fig. 9.3. Precipitation Equipment Used in Preparing Titania Sol.

entered the bottom of the tank that contained the precipitate, and the overflow was fed to the bottom of the second tank. These tanks were made from 55-gal stainless steel drums with 30° inverted cones welded to the bottoms. The precipitate was washed with about 1000 liters of water over a 4½-hr period. After thorough washing, as indicated by the pH of the effluent wash, the precipitate was allowed to settle overnight; it was then dewatered in a 12-in. basket centrifuge (Fig. 9.4). The wet cake was transferred to plastic bags contained in ½-gal paint cans; there it was transformed to fluid sol by thorough agitation with a paint shaker.

Since the principal purpose of these runs was to demonstrate the preparation of sol, only slight attention was given to process losses – that were sometimes as high as 50%. The principal losses were from slow-settling solids or from premature peptization during washing. These losses can be decreased by use of optimum washing conditions. Any material in the effluent wash stream can be recovered for recycle.

9.3 INCORPORATION OF CARBON INTO METAL OXIDE SOLS

The dispersion of carbon black into metal oxide (or hydroxide) sols is an essential step in the preparation of carbides and of porous oxides by the sol-gel process (see Sect. 7.5). Previous studies of various mixed oxide-carbon sols have shown that positively charged oxide sols (such as UO_2 , ThO_2 , $\text{ThO}_2\text{-UO}_3$) that are composed of small crystallites act as protective colloids toward carbon black, forming very stable and fluid codispersed sols at C/metal mole ratios as high as 15.⁵ Other oxides, in the form of large-crystallite, positively charged sols [such as $\text{Eu}(\text{OH})_3$ or autoclaved ZrO_2] or negatively charged sols (e.g., SiO_2) do not exhibit this protective, stabilizing action on carbon black.⁵ Additional oxide sol-carbon black systems, including sols of ZrO_2 , TiO_2 , HfO_2 , and CeO_2 , have been examined. Tests were made in which Spheron 9, an acidic channel black, was added to each sol.

In order to utilize oxide sols for the preparation of carbides by carbothermic reduction, or porous oxides by carbon burnout, it is necessary to be able to disperse several moles of carbon per mole

of oxide. The large-crystallite, low-nitrate ZrO_2 sols prepared by autoclaving will not accept large amounts of carbon black; instead, these mixtures become very viscous at a relatively low carbon concentration. The high-nitrate, small-crystallite ZrO_2 sol that is prepared by refluxing zirconyl nitrate solution and then boiling to dryness (see Sect. 9.1) will accept at least six moles of carbon per mole of zirconium. This sol was positively charged and acted as a protective colloid toward carbon; it was analogous to UO_2 , ThO_2 , and $\text{ThO}_2\text{-UO}_3$ but was clearly different from large-crystallite ZrO_2 sol. This codispersed sol was readily formed into microspheres. Drying of these microspheres must be done carefully since an exothermic reaction occurs at a temperature between 100 and 200°C, and the large amount of heat that is liberated must be dissipated to prevent temperature excursions.

On cursory examination, ceria sol, which was prepared by a precipitation-peptization process similar to that used for the preparation of PuO_2 sols, appeared to act as a protective colloid in the manner of other positively charged small-crystallite sols. Positively charged, small-crystallite HfO_2 sol was prepared by precipitation with NH_4OH , followed by peptization with HNO_3 . This sol also behaved as a protective colloid toward carbon black, dispersing and stabilizing 15 moles of Spheron 9 carbon black per mole of oxide.

The TiO_2 sol contained small crystallites, but was negatively charged. It was not directly compatible with Spheron 9; however, by adding Marsperse CB⁶ in the amount of 3 wt % (carbon basis), carbon black was dispersed to form a negatively charged sol that could be mixed with the negatively charged TiO_2 sol in all proportions.

9.4 PREPARATION OF POROUS OXIDES

Sol-gel techniques have been developed for preparing small, porous microspheres of ZrO_2 and porous shards of U_3O_8 . Porous microspheres of ZrO_2 , or of some other inorganic oxide, are of interest as packing support in chromatographic columns.⁷ Fine-grained, porous U_3O_8 is being con-

⁶Product of American Can Co.; a lignosulfonate.

⁷C. D. Scott, *Body Fluids Analyses Program Progress Report for the Period March 1 to August 31, 1968*, ORNL-TM-2372 (April 1969).

⁵*Chem. Technol. Div. Ann. Progr. Rept. May 31, 1968*, ORNL-4272, pp. 157–58.

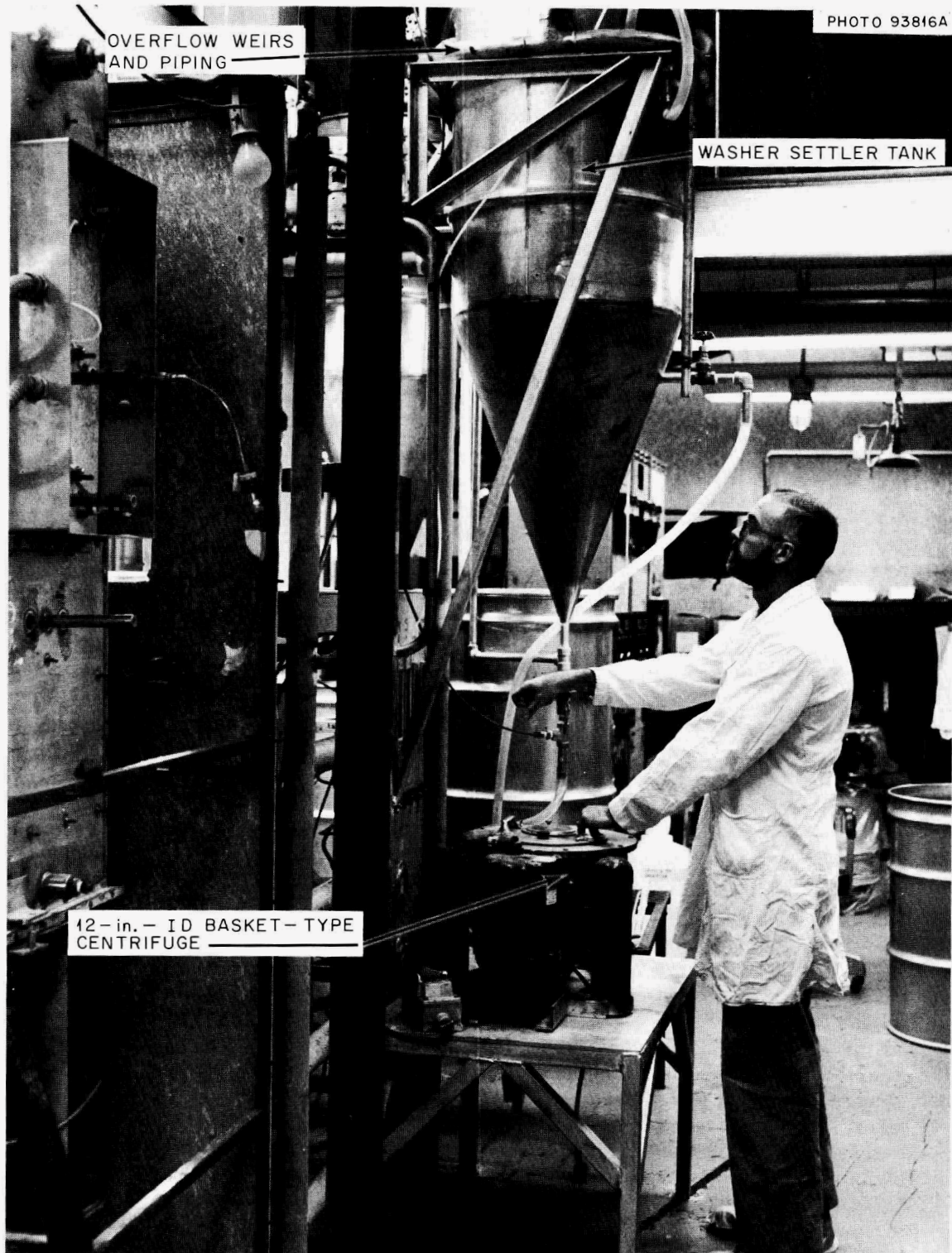


Fig. 9.4. Equipment for Washing and Centrifuging $Ti(OH)_4$.

sidered for use in fuel elements of the High Flux Isotope Reactor (HFIR).

Porous ZrO_2 Microspheres

Porous ZrO_2 microspheres in the 2- to 20- μ -diam range were prepared by two methods: (1) by burning carbon out of ZrO_2 -C gel spheres, and (2) by controlling sintering conditions (temperature and time) to limit the densification of ZrO_2 gel spheres. In two separate preparations, porosities of 61 and 70% were obtained in ZrO_2 -C spheres by burning out carbon which had been added in amounts of about four moles per mole of ZrO_2 . In another experiment the temperature and the time of sintering were regulated to prepare ZrO_2 spheres with 25% porosity by air firing ZrO_2 gel spheres at 400°C. The low-fired, porous material was desired because it had maximum surface activity.

High-nitrate ZrO_2 sol that had been made by evaporating zirconyl nitrate to dryness and dispersing the solids in water (see Sect. 9.1) was used. Stable, codispersed sols of ZrO_2 and C were prepared by ultrasonically blending carbon black into the ZrO_2 sol (see Sect. 9.3). A two-fluid nozzle was used to disperse the sol droplets into isoamyl alcohol containing 0.1% Span 80. The ZrO_2 -C gels were first fired to 1000 to 1200°C in argon to densify the oxide to a temperature-stable form, and then the carbon was burned out by heating the spheres in air at 800°C.

Two different carbon blacks having particle sizes of 140 and 300 A, respectively, were used in an unsuccessful effort to produce pores of about the same size as the carbon black. With both carbon blacks, the final products had pores with diameters in the 400- to 1200-A range, as determined by Hg porosimetry. The surface-connected porosities measured in this way were 50 and 66%. Additional closed porosities of 11 and 4%, respectively, were calculated from the measured densities of the two samples. The measured porosities were greater than the values calculated from the volume of carbon contained in the gel spheres and indicate that densification of the oxide may not have been completed in the firing at 1000 to 1200°C.

When porous oxides are produced by the controlled sintering of gel spheres, maximum porosity and maximum surface area (and activity) are obtained at the lowest firing temperature that can be used to remove water and organic material. Ther-

mogravimetry and x-ray diffraction were used to determine this minimum temperature for firing ZrO_2 gel spheres. Thermogravimetry of gel microspheres showed a large weight loss in air between room temperature and 400°C, followed by a small weight loss between 500 and 600°C. The material dried at 400°C was identified by x-ray diffraction as crystalline ZrO_2 . The densities of the 400°C product indicated porosities of 21 to 27%. The pore size was not determined; however, the BET surface area of 16 m²/g indicated a large internal surface.

Porous U_3O_8 Shards

Porous U_3O_8 is of interest for use in HFIR fuel elements. It is believed that an improved physical form of U_3O_8 will permit a longer fuel element life-time. We have produced a form of U_3O_8 that is characterized by high porosity and a fine-grained structure. This U_3O_8 was obtained by oxidation of UO_2 gel shards and by partial densification, which was controlled by regulating sintering conditions. Samples of U_3O_8 with closed porosities of 6 to 19% and open porosities of 1 to 19% have been made by this method. A test fabrication and an irradiation of enriched U_3O_8 that was made by this method are being conducted by the Metals and Ceramics Division. The addition of materials that volatilize during the oxidation-densification step, such as carbon or sulfate, gave open porosities up to 28%; however, the closed porosity was less.

A UO_2 sol was converted to gel shards by air drying at 110 to 150°C. The shards were then fired in air at the temperature rise rate of 200°C/hr until the temperature necessary to achieve the desired sintered density (Table 9.1) was attained. Samples were removed from the furnace when the final temperature listed in the table was reached. The open, or surface-connected, porosity decreased and the pore size increased as the firing temperature increased. Closed porosity appeared to be independent of the firing temperature. Early, complete oxidation at lower temperatures was necessary in order to prevent sintering and to retain porosity upon firing. The sample of $UO_{2.25}$ shards that was heated to 1000°C in argon and then oxidized in air at 800°C had a much lower porosity than shards fired in air to 1000°C.

The U_3O_8 that was sintered in air at 1000°C was sent to the Metals and Ceramics Division for further

Table 9.1. Porosities of U_3O_8 Shards Prepared by Oxidation of UO_2 Gel Shards and by Controlling the Degree of Densification via Temperature and Time of Sintering

Final Temperature (°C)	Open Porosity ^a		Closed Porosity (%)	Total Porosity (%)
	%	Average Pore Diameter (A)		
550	22	<170	2	24
650	19	~400	15	34
750	19	~500	16	35
850	16	~700	15	31
950	14	~1400	18	32
1000	12 ^b	~2000	11 ^b	23 ^b
1100	13	~2500	19	32
1200	10	~4000	19	29
1300	10	~7000	17	27
1000/800 ^c	1		6	7

^aMeasured by mercury porosimetry to 10,000 psi.

^bThis sample was fired to 1000°C twice, which probably accounts for its lower porosity.

^cGel shards of about the composition $UO_{2.25}$; fired to 1000°C in argon and then in air at 800°C.

examination. This examination showed that it had uniform porous microstructures (Fig. 9.5) and a high crushing strength (87 g, as compared with a value of 4 g for the standard high-fired U_3O_8 that is normally used as fuel particles). Pore diameter sizes of this material are estimated to be 3000 to 7000 A from the metallographic cross section. The diameter of the open pores was estimated to be 2000 A by Hg porosimetry and was calculated to be 3400 A from the BET surface area (0.49 m²/g); this is reasonable agreement for the two methods.

Materials that subsequently volatilized during oxidation and firing of the gel were added to urania sol as a means of producing porosity in the U_3O_8 product. The three materials tested were carbon black, chloride, and sulfate. All three are known to produce porosity in fired oxides under the proper conditions. The carbon black is burned out, as discussed previously, and the chloride produces porosity by virtue of the volume of HCl evolved;⁸ on the other hand, the mechanism by which sulfate produces porosity is not known.⁹ In these tests, chloride did not give additional porosity, but both sulfate and carbon black doubled the open porosity

(Table 9.2). However, closed porosity decreased, and the total porosity was virtually unchanged.

9.5 MICROSPHERE FORMING

Microsphere forming techniques that were developed for the Thorium Fuel Cycle (Sect. 6.3) and for the Uranium Fuel Cycle (Sect. 7.4) can also be applied to the preparation of microspheres from sols other than thoria or urania. Use of these techniques in conjunction with two dispersion devices, the two-fluid nozzle (at turbulent flows) and a hypodermic needle (for electrostatic dispersion), has been investigated for the production of <100- μ -diam microspheres. Microspheres of this size are of interest for the Uranium Fuel Cycle, and the capability of producing closely controlled sizes in this range will increase the versatility of sol-gel methods for other applications.

⁸T. A. Gens, *Préparation of Uranium and Thorium Oxide Microspheres with Controlled Porosity by a Sol-Gel Process*, ORNL-TM-1530 (May 1966).

⁹F. P. Treadwell and W. T. Hall, *Analytical Chemistry*, p. 557, Wiley, New York, 1937.



Fig. 9.5. Microscopic Cross Section of Porous U_3O_8 Prepared by Oxidation and Controlled Sintering of UO_2 Gel Shards in Air. Air fired to $1000^\circ C$. Open porosity, 12%; closed porosity, 11%.

Two-Fluid Nozzle Operation to Produce <100- μ -Diam Spheres

When two-fluid nozzle dispersers are operated at high organic drive fluid flow rates, sols are dispersed into small droplets.¹⁰ This is in contrast to normal operation in which low drive fluid flow rates cause a varicose dispersion of the sol to form large drops. Recent studies have been made over a wide range of variable and with a variety of sols. The data have been correlated with a dimensionless expression that relates sol-drop diameter to operating variables:

$$\left(\frac{D_{sol}}{ID}\right) = 1630 \left(\frac{G}{F}\right)^{0.1} Re^{-1.5},$$

¹⁰Chem. Technol. Div. Ann. Progr. Rept. May 31, 1968, ORNL-4272, pp. 151-52.

where

D_{sol} is the sol droplet diameter,

ID is the alcohol flow channel diameter,

G is the alcohol flow rate,

F is the sol flow rate,

Re is the Reynolds number of the alcohol.

The relationship in dimensional units commonly used is:

$$D_{sol} = 7.0 \cdot 10^6 \frac{ID^{2.5} \mu^{1.5}}{G^{1.4} F^{0.1}},$$

where

D_{sol} is given in μ ,

ID is in cm,

G is in cm^3/min ,

F is in cm^3/min ,

μ is the viscosity of the alcohol in centipoises.

In the case of the two-fluid nozzle, the most important variable (and the one used primarily to control the sol drop size) is the turbulence of the organic fluid in the nozzle. In addition to the organic fluid flow rate, the sol inlet configuration also promotes turbulence; therefore, different nozzle arrangements will produce different droplet sizes.

In a simple pipe, the transition from laminar to turbulent flow commonly occurs at Reynolds numbers of about 2000. For the two-fluid nozzle configuration in which the sol inlet capillary is perpendicular to the axis of the alcohol channel, the relationships given above were valid for Re greater than 600, perhaps due to promoted turbulence for Re greater than 600 but less than 2000. This promoted turbulence depends on the nozzle configuration and does not appear at the same Reynolds number for all nozzles. Terms for ratios of the viscosities and densities of the alcohol and

sol were omitted from the equation since sufficient data are not available to determine their effects. The variables for which the correlation was evaluated (and the ranges involved) were: ID , 0.15 to 0.38 cm; G , 210 to 860 cc/min; μ , 2.0 to 5.7 centipoises; F , 1.5 to 15 cc/min; and Re , 600 to 4000.

An important feature of the two-fluid nozzle (with turbulent flow of alcohol) is that only a small fraction of product has a diameter considerably smaller than the mean diameter. About 60 wt % of the spheres are between $0.7 d_{50}$ and $1.4 d_{50}$ (where d_{50} is the mean diameter). Data for products of the same mean size for a paddle agitator¹¹ and the two-fluid nozzle are given in Table 9.3. From visual observations, the differences are even

¹¹M. E. Whatley *et al.*, *Unit Operations Section Quarterly Progress Report, July–September 1965*, ORNL-3916, pp. 44–50.

Table 9.2. Porosities of U_3O_8 Shards Prepared by Oxidation and by Controlled Sintering of Sol-Gel-Derived UO_2 Shards Containing Volatile Additives

Additive	Amount of Additive (moles/mole of U)	Open Porosity ^a		Closed Porosity (%)	Total Porosity (%)
		%	Average Pore Diameter (A)		
Carbon black	3	28	~2500	2	30
Chloride ^b	0.04	11	~2000	7	18
Sulfate ^b	0.045	24	~2000	7	31

^aBy mercury porosimetry.

^bAdded as HCl or H_2SO_4 to the original UO_2 sol.

Table 9.3. Size of Product Obtained with the Paddle Agitator and the Two-Fluid Nozzle with Turbulent Flow

	Comparison 1		Comparison 2	
	Paddle Agitator	Two-Fluid Nozzle	Paddle Agitator	Two-Fluid Nozzle
Mean diameter, d_{50} , μ	92	90	78	76
wt % smaller than: $0.8 d_{50}$	42	30	38	28
$0.6 d_{50}$	30	13	26	11
$0.5 d_{50}$	24	7	~19	~4
$0.4 d_{50}$	~18	~3	~14	<2

greater at $0.2 d_{50}$; however, we do not have numerical measurements at the small diameters.

Most of the metal oxide-carbon sols (Sect. 9.3) were made into $<100\text{-}\mu$ -diam products by dispersing small sol droplets from a two-fluid nozzle into isoamyl alcohol. Drying was rapid enough to eliminate the need for fluidizing the gel spheres. This system was designed to take advantage of the easier separation of gel spheres and the more rapid gelation that is possible with isoamyl alcohol. Only one pump and one storage-settler tank (Fig. 9.6) are needed. An 18-in.-diam cone, which is used as the tank bottom, has a much larger volume than an inclined slab settler of the same efficiency; however, this tank also serves as a surge vessel. The lower boiling point and the higher water solubility of the isoamyl alcohol, as compared with 2-ethyl-1-hexanol (2EH) make it possible to use low-pressure (22-psig) steam, lower flow rates

through the still, and smaller heat exchangers. The system is usually operated with sol feed rates of 3.8 to 15 cc/min and surfactant concentrations of <0.2 vol %. About 200 liters of $\text{UO}_2\text{-C}$, $\text{TiO}_2\text{-C}$, $\text{ZrO}_2\text{-C}$, UO_2 , ThO_2 , and ZrO_2 sols were formed into gel spheres in this equipment.

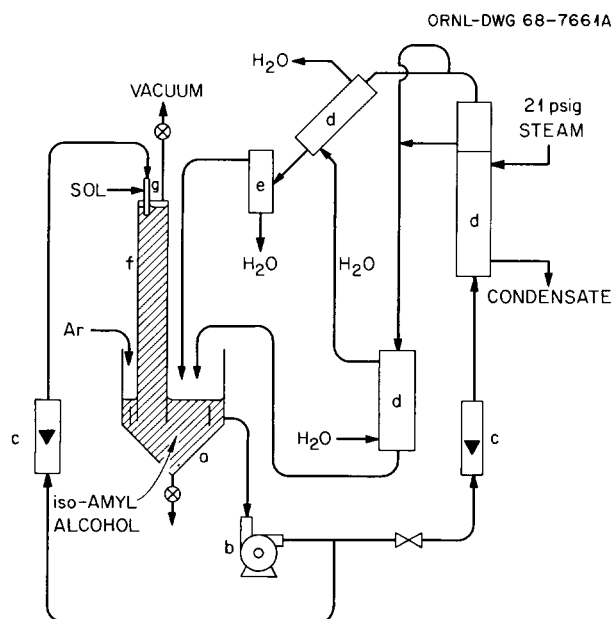
Electrostatic Dispersion to Produce $<100\text{-}\mu$ -Diam Microspheres¹²

The effect of an applied electrical potential on the formation of uniformly sized microspheres was reexamined. Previous work¹³ had shown that this method could be used to obtain ThO_2 microspheres of sizes greater than $250\ \mu$. In this study, the uniformity of spheres in the 50- to $100\text{-}\mu$ -diam range was of interest.

Microspheres were formed by injecting a $1.6\ M$ $\text{ThO}_2\text{-UO}_3$ sol through a single hypodermic needle (10 mil ID) into a column through which 2EH was circulated to fluidize and gel the droplets. A positive potential was placed on the needle, and the voltage was varied to control the droplet size. The voltage was applied by connecting the tip of the 10-mil-diam hypodermic needle to the positive electrode of a 600- to 1800-v dc power supply. The negative electrode used was a 1-cm-diam ring centered about the tip of the needle. The experiments were of a factorial design, and a linear regression analysis of the data indicated that flow rate and voltage were the important variables while the sol concentration had a relatively minor effect. Increasing the voltage or decreasing the sol flow rate had the effect of decreasing particle size.

Variables in the factorial experiment were as follows: potential between the needle and ring, 822, 748, and 655 v; sol concentrations, 1.6, 1.2, and $0.8\ M$; and sol flow rates, 0.153, 0.109, and $0.0553\ \text{ml/min}$. Correlation of the resulting data by linear regression analysis produced the following equation:

$$d = 136.7 + 3298F - 0.469C - 0.0397V - 3.37FV,$$



- a SETTLER-SURGE TANK
- b CENTRIFUGAL PUMP
- c ROTAMETERS
- d HEAT EXCHANGERS
- e PHASE SEPARATOR
- f METHACRYLATE PLASTIC PIPE, 3.5 in. ID
- g TWO-FLUID NOZZLE

Fig. 9.6. Settler-Still System for Preparation of Small Gel Spheres Using Isoamyl Alcohol.

¹²This work was performed by R. P. Wilcox and R. Farooki, MIT, School of Chemical Engineering Practice.

¹³D. M. Helton, *Dispersion of a Liquid Stream by an Electrical Potential: Applications to the Preparation of Thoria Microspheres*, ORNL-TM-1395 (Jan. 17, 1966).

where

d = particle diameter, μ ,

F = sol flow rate, cc/min,

C = sol concentration, % of 1.6 M sol,

V = applied potential, v.

This equation was then used to set the conditions of flow rate and voltage in order to produce 75- μ -diam particles from 1.6 M sol. The results in Fig. 9.7 show that 80 wt % of the microspheres were in the 50- to 100- μ -diam range.

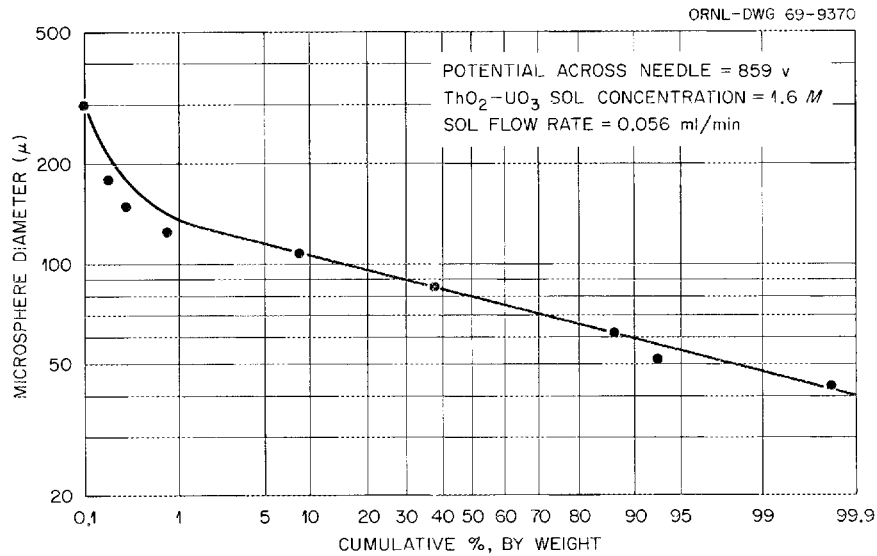


Fig. 9.7. Size Distribution of Microspheres Produced by Electrostatic Dispersion of Sol at Conditions Preset to Produce 75- μ -diam Microspheres.

10. Separations Chemistry Research

10.1 EXTRACTION OF METAL SULFATES AND NITRATES BY AMINES

In view of the potential for increased use of amine extractants, a systematic survey is being made of the extraction of metals from various acid and salt solutions with representative amines. The study of metal chloride extractions from hydrochloric acid and acidified lithium chloride solutions has been completed and reported.¹ Results of the extraction of 15 metals from acidified lithium sulfate solutions and from acidified lithium nitrate solutions have also been reported.^{2,3} Extraction data for additional metals have now been obtained for the sulfate and nitrate systems.

Figure 10.1 shows curves for the extraction of 16 metals from Li_2SO_4 -0.2 *N* H_2SO_4 solutions (ranging from 0.3 to 5 *N* sulfate) with 0.1 *N* solutions of representative primary, secondary, tertiary, and quaternary amines in diethylbenzene. Extraction coefficients higher than 1 were obtained only for V(V), Zr(IV), Nb(V), Mo(VI), Pd(II), and U(VI). In most cases the extraction coefficients were higher for the primary amine than for the other amines and were not greatly affected by a change in sulfate concentration over the range studied.

In the LiNO_3 -0.2 *N* HNO_3 system (0.5 to 10 *N* nitrate), the highest extraction coefficients were usually obtained with the quaternary amine. The coefficients showed a stronger dependence on salt concentration in this system than in the sulfate system. Extraction coefficients higher than

1 were obtained for Zr(IV), Mo(VI), Pd(II), Eu(III), Hg(II), and U(VI), as shown in Fig. 10.2. Data for Cr(III), Mn(II), Ni(II), and Cu(II) are not included since the extraction coefficients for these metals were less than 0.01 in all tests.

10.2 NEW SEPARATIONS AGENTS

We are continuing to investigate, for potential utility in solvent extraction, chromatography, or other separations methods, compounds that are (1) newly available commercially, (2) submitted by manufacturers for testing, or (3) specially procured for testing of class or structure.

Tetraalkylphosphonium Salts

We obtained samples of three phosphonium salts from Carlisle Chemical Works, Reading, Ohio. Two of them, triphenyl(benzyl)phosphonium chloride and 1,2-ethylenebis(triphenylphosphonium) dibromide, were excessively soluble in the aqueous solutions of usual interest in solvent extraction and extraction chromatography, but might be compatible with solutions of higher ionic strength. The third, methyltrioctylphosphonium (MTO) dimethylphosphate, has very low solubility in aqueous 1 *M* HCl or 1 *M* Na_2CO_3 solution. Its nominal purity is greater than 95%, and its neutral equivalent is within 99% of theoretical. Samples of MTO dimethylphosphate in diethylbenzene solution were readily converted to the chloride and the carbonate forms by contact with 1 *M* HCl and 1 *M* Na_2CO_3 solutions. This compound proved to be similar to the quaternary ammonium Adogen 464 ($\text{R}_3(\text{CH}_3)\text{N}^+$, where R = mixed *n*-octyl and *n*-decyl) in preliminary tests of the extraction of cobalt from acid chloride solution, the extraction of beryllium from sodium carbonate solution,

¹F. G. Seeley and D. J. Crouse, *J. Chem. Eng. Data* 11(3), 424 (1966).

²*Chem. Technol. Div. Ann. Progr. Rept. May 31, 1967*, ORNL-4145, pp. 208-9.

³*Chem. Technol. Div. Ann. Progr. Rept. May 31, 1968*, ORNL-4272, p. 174.

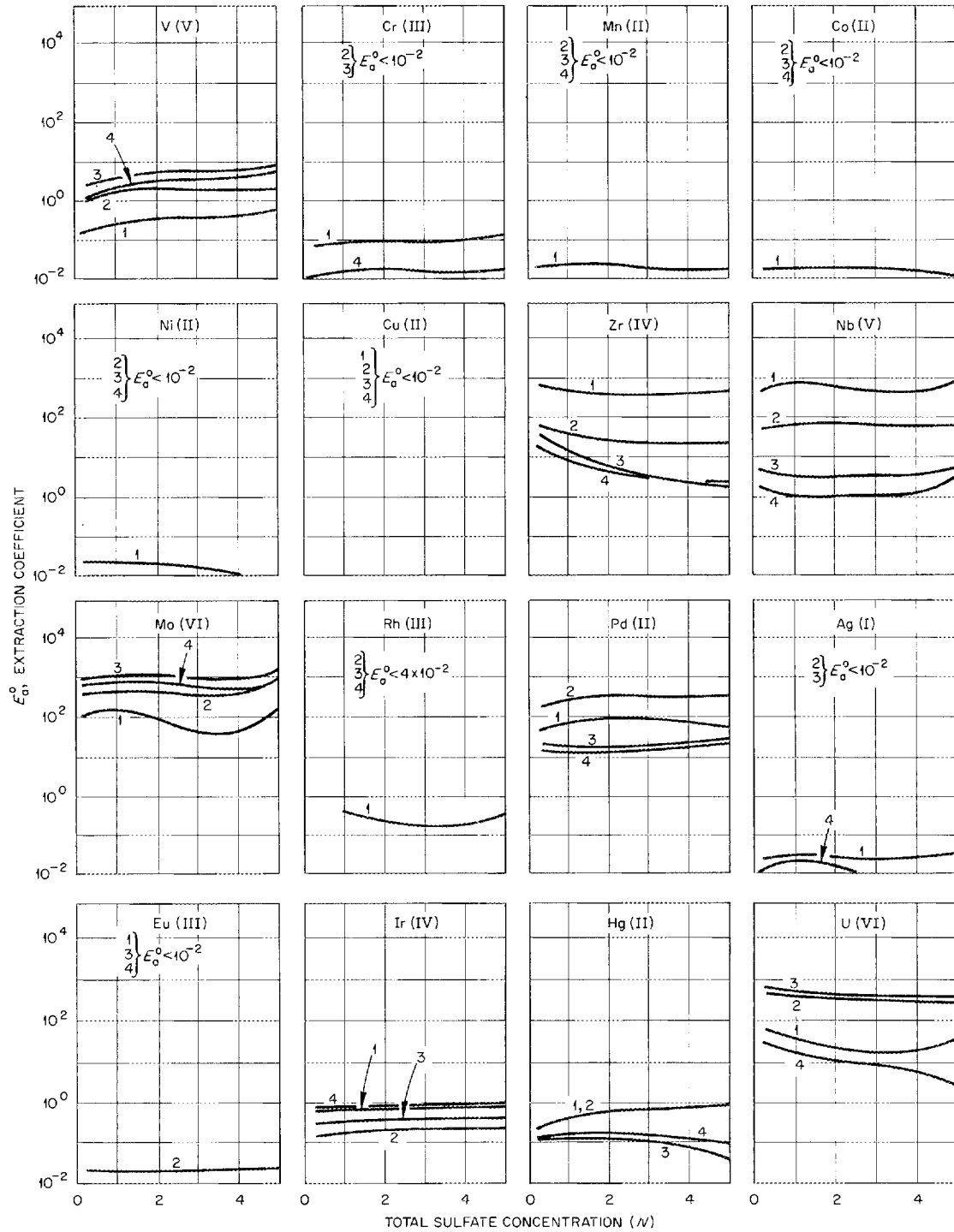


Fig. 10.1. Extraction of Metals from Sulfate Solutions with Amines. Organic phase: 0.1 M solutions of (1) Primene JM ($RR'R''CNH_2$, 18 to 22 carbon atoms), (2) Amberlite LA-1 ($RR'R''CNHC_{12}H_{23}$, 24 to 27 carbon atoms), (3) Adogen 364 (R_3N , $R = n$ -octyl, n -decyl mixture), (4) Adogen 464 [$R_3(CH_3)N^+$, $R = n$ -octyl, n -decyl mixture] in diethylbenzene. With Adogen 464, 3 vol % of tridecanol was added to the solvent to prevent the formation of a third phase. Amines were in the sulfate form. Aqueous phase: 0.01 M metal ion in Li_2SO_4 -0.2 N H_2SO_4 . Contact: 10 min at a phase ratio of 1:1.

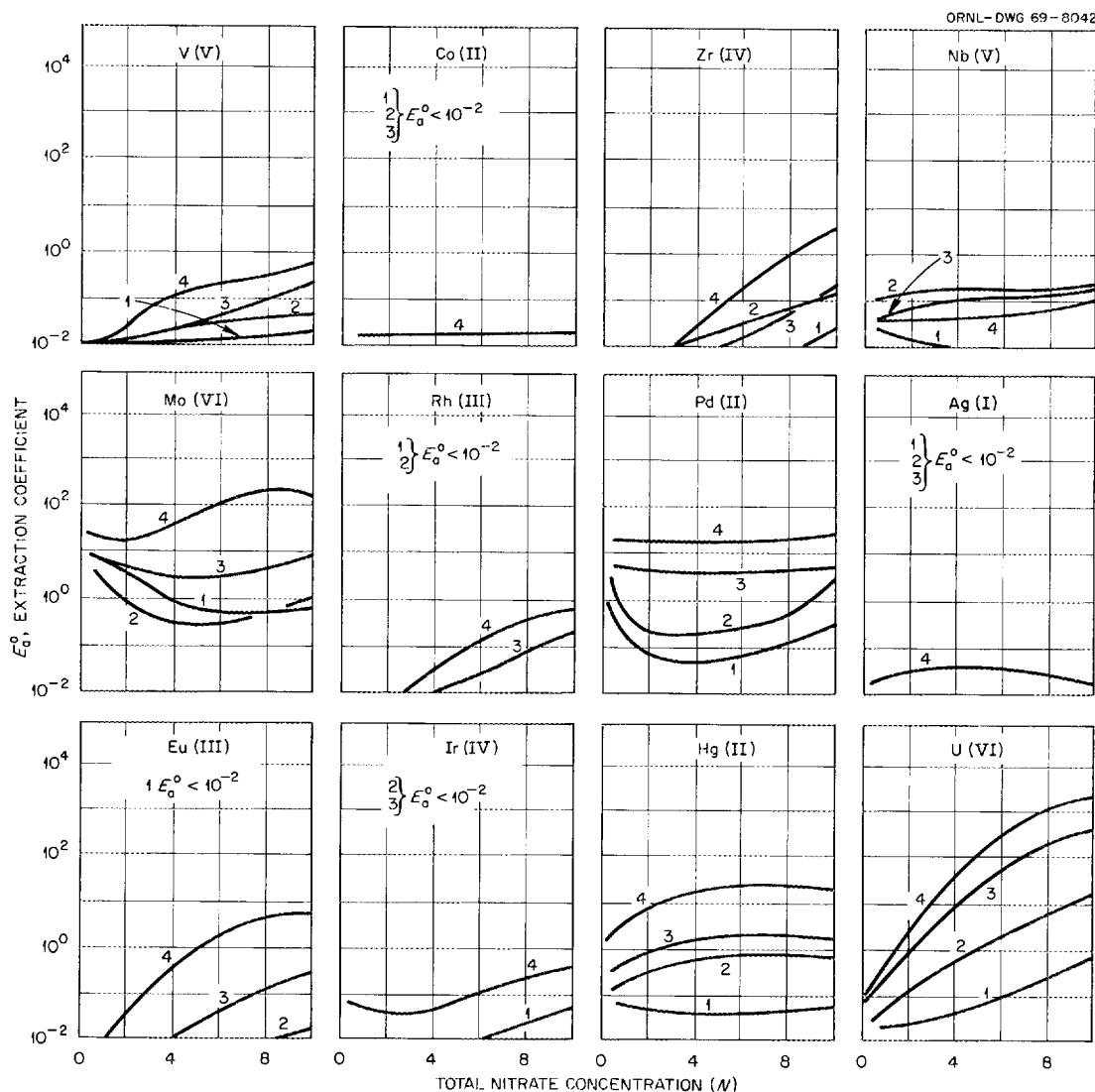


Fig. 10.2. Extraction of Metals from Nitrate Solutions with Amines. Organic phase: 0.1 M solutions of (1) Primene JM, (2) Amberlite LA-1, (3) Adogen 364, (4) Adogen 464 in diethylbenzene. With Adogen 464, 3 vol % of tridecanol was added to the solvent to prevent the formation of a third phase. Amines were converted to the nitrate form just prior to use in the extraction tests. Aqueous phase: 0.01 M metal ion in LiNO_3 -0.2 N HNO_3 . Contact: 10 min at a phase ratio of 1:1.

and the chromatographic separation of transfer ribonucleic acids by elution with a sodium chloride gradient.

Unsymmetrical Sulfoxides

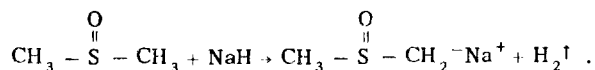
We previously found⁴ that the unsymmetrical methyl(2-ethylhexyl)sulfoxide extracts a different group of elements from those extracted by sym-

metrical dialkylsulfoxides, suggesting that bonding occurs through the oxygen of the unsymmetrical, but through the sulfur of the symmetrical, compounds. A series of symmetrical dialkylsulfoxides was synthesized and examined;⁴ however, attempts to make additional unsymmetrical

⁴Chem. Technol. Div. Ann. Progr. Rept. May 31, 1967, ORNL-4145, p. 211.

sulfoxides at that time were not successful since their preparation by preparing and oxidizing the required sulfide produced too many side reactions when one or both alkyl groups were extensively branched.

A procedure recently developed by Lyness and others⁵ has allowed us to synthesize several sulfoxides having structures of interest. In this preparation, dimethylsulfoxide is converted to a reactive sulfinyl carbanion by reaction with a strong base, such as sodium hydride,



The carbanion is then reacted with a suitable branched alkyl bromide,



The compounds prepared were: methyl-3-ethylheptylsulfoxide (Me-3EHSO), methyl-4,8-dimethylnonylsulfoxide (Me-4,8-DMNSO), and methylpentadecylsulfoxide (Me-PDSO). Each of these sulfoxides was a clear-to-yellowish liquid. Elemental analysis showed them to be better than 97 mole % pure, based on the largest deviation from theoretical for any of the elements. All three compounds showed the good organic-phase miscibility and the low aqueous-phase distribution that are desirable in a solvent extraction reagent.

All three compounds, 0.1 M in *p*-xylene solution, extracted iron(III) from hydrochloric acid solutions. At low hydrochloric acid concentrations, the iron extraction coefficients increased by a factor of about 10 for each 1 M increase in HCl concentration, up to 1.2 with Me-3-EHSP, 1.5 with Me-4,8-DMNSO (cf. Sect. 10.8), and 33 with Me-PDSO at 4 M HCl. Extraction coefficients with the first two rose to maxima of about 100 at 8 M HCl; Me-PDSO precipitated at hydrochloric acid concentrations above 4 M. Extraction coefficients for cobalt, manganese, calcium, sodium, and europium were very low; for example, the maximum coefficients for these elements, at 8 to 10 M HCl, were mostly below 0.1.

⁵W. I. Lyness, D. E. O'Conner, and J. S. Berry, U.S. Patent 3,288,860 (Cl. 260-607), Nov. 26, 1966; W. I. Lyness and D. E. O'Conner, U.S. Patent 3,355,494 (Cl. 260-586), Nov. 28, 1967.

Further preparation and screening of sulfoxides are planned as time and available manpower permit. Structures that appear promising are: (1) other branched alkyls opposite methyl, (2) branched alkyls opposite ethyl, and (3) ring structures. Plans include the investigation of a much broader range of elements and systems.

10.3 BERYLLIUM PURIFICATION BY SOLVENT EXTRACTION

New and potentially less-expensive methods are being investigated for preparing high-purity beryllium compounds for reactor use, starting with beryllium concentrates such as those obtained by amine extraction or di(2-ethylhexyl)phosphoric acid extraction of low-grade beryllium ore leach liquors. Major emphasis has been on the development of a purification process^{6,7} that uses quaternary ammonium extractants to recover beryllium from a carbonate solution of the beryllium concentrate. The beryllium is stripped from the solvent with 2 to 2.5 M NH_4HCO_3 and is precipitated as the hydroxide from this solution by heating.

Status and Progress

The development of the quaternary ammonium extraction process is essentially complete. Some additional tests were made recently to more accurately define the product purity that is obtainable, particularly when EDTA is added to the system to complex metal impurities. A product containing 60 ppm total detectable metal contaminants was prepared. A study of methods for decreasing the boron contamination (20 to 30 parts per million parts of BeO) of the products was begun.

Effect of EDTA Addition

Direct precipitation of beryllium from an ammonium carbonate feed solution by heating to volatilize ammonia and carbon dioxide gave a $\text{Be}(\text{OH})_2$ product containing 3500 parts of total

⁶Chem. Technol. Div. Ann. Progr. Rept. May 31, 1967, ORNL-4145, pp. 215-17.

⁷Chem. Technol. Div. Ann. Progr. Rept. May 31, 1968, ORNL-4272, pp. 175-77.

metal impurities per million parts of BeO (Table 10.1). This level of contamination was about a factor of 5 lower than that in the original feed solution. The addition of sufficient EDTA to give a concentration of 0.02 M in the feed solution prior to precipitation decreased the total metal impurities by an additional factor of 3. The solvent extraction process yielded a product with 860 ppm of total metal impurities when EDTA was not used in the process flowsheet. The purest product was obtained by using the solvent extraction process and by including small concentrations of EDTA in the scrub solution, the strip solution, and the solution used to wash the Be(OH)₂ precipitate. In this case, the product contained only 140 ppm of sulfur and 60 ppm of total detectable metal impurities. About one-third of the latter impurity concentration was due to boron in spite of the fact that the solvent extraction and product preparation steps were conducted in plastic or Teflon-lined glass equipment.

Extraction of Boron

We made some preliminary tests to determine if the solvent extraction process gives effective

Table 10.1. Effect of EDTA on Purity of Beryllium Product

	Product Analysis (Parts per 10 ⁶ Parts BeO)	
	Total Metal Impurities	Sulfur
Direct precipitation of Be(OH) ₂ from carbonate feed solution ^a	3500	
Direct precipitation of Be(OH) ₂ from carbonate feed solution (EDTA present)	1170	2100
Solvent extraction process product (No EDTA)	860	
Solvent extraction process product (EDTA present in scrub, strip, and product wash solutions)	60	140

^aAmmonium carbonate feed solution had 16,000 parts of total metal impurities and 120,000 parts of sulfur per 10⁶ parts of BeO.

separation of beryllium from boron. In extractions from 1 M (NH₄)₂CO₃ solution with 0.5 M Adogen 464, the boron extraction coefficient was about 0.5 in the pH range of 9.4 to 10. This coefficient is sufficiently high to allow an appreciable fraction of any boron in the feed solution to follow the beryllium through the solvent extraction process. Use of a complexing agent to decrease the amount of extracted boron is being studied.

Precipitation of Be(OH)₂ from the Strip Solution

A series of precipitation tests was made to obtain a better understanding of the factors affecting the precipitation of beryllium from the strip solution. These tests showed that essentially all of the NH₃ and CO₂ are volatilized from the solution by the time beryllium precipitation is complete. In one test with a strip solution that was 2 M in total carbonate and contained 6.4 g of beryllium per liter, the solution was slowly heated (at the rate of ~0.6°C/min) to 95°C in a flask connected to a condenser. At 50°C, CO₂ began to evolve and, at about 80°C, Be(OH)₂ began to precipitate. At this point, about 40% of the CO₂ had evolved. When the temperature reached 95°C, 99.97% of the beryllium had precipitated and only 0.4% of the carbonate remained in solution. The process flowsheet calls for recovery of the NH₃ and CO₂ from the off-gas for recycle.

10.4 RECOVERY OF URANIUM FROM COMMERCIAL PHOSPHORIC ACID

A promising solvent extraction process⁸ for recovering uranium from commercial wet-process phosphoric acid was developed and demonstrated successfully in small-scale batch tests. In this process, the uranium is extracted from the acid with the synergistic reagent combination of di(2-ethylhexyl)phosphoric acid (D2EHPA) plus tri-octylphosphine oxide (TOPO) in a kerosene diluent. (This extractant was selected for process studies following extraction screening

⁸F. J. Hurst, D. J. Crouse, and K. B. Brown, *Solvent Extraction of Uranium from Wet-Process Phosphoric Acid*, ORNL-TM-2522 (April 1969).

tests^{8,9} of a wide variety of extractants of different types and structures.) After the extract is scrubbed with water to remove phosphoric acid, the uranium is stripped with ammonium hydroxide--ammonium carbonate solution and precipitated from the strip solution by heating. Commercial phosphoric acid produced from Florida phosphate rock contains 0.1 to 0.2 g of uranium per liter and by 1970 is expected to represent a potential source of about 2000 tons of U_3O_8 per year.

Extraction Tests

Samples of wet-process acid were obtained from two Florida phosphate plants (identified as Company A and Company B) for testing. The samples were about 6 M in H_3PO_4 and contained about 0.17 g of uranium per liter plus the following impurities (concentration in g/liter): 6 to 9 Fe, 2.5 to 3.5 Al, 0.5 to 1 Ca, 20 to 30 SO_4 , and 0.5 to 1.7 F.

Uranium must be in the hexavalent form to be effectively extracted from H_3PO_4 with D2EHPA--TOPO. Essentially all of the Fe(II) in the phosphoric acid must be oxidized to Fe(III) to ensure complete oxidation of the uranium. Based on limited information, the concentration of Fe(II) in fresh wet-process acid is usually in the range of 0.3 to 0.5 g per liter, while about 50% of the uranium is present as U(IV). Tests have shown that the addition of about one-sixth mole of $NaClO_3$ per mole of Fe(II) to the acid liquor is sufficient to oxidize essentially all of the uranium to U(VI). Also, preliminary tests have indicated that the uranium can be oxidized readily by bubbling air through the liquor at 60 to 70°C.

Coefficients for the extraction of uranium from the oxidized commercial acid samples were about 25% higher than the coefficients obtained for the extraction of U(VI) from "pure" acid of equivalent phosphoric acid concentration. The diluent used in most tests was *n*-dodecane. However, approximately the same extraction performance and phase separation characteristics are obtained by using low-cost aliphatic diluents such as refined kerosene.

Increasing the temperature has a strong adverse effect on uranium extractions. For example, in tests with one of the acid samples, increasing the temperature from 20 to 50°C decreased the uranium extraction coefficient by about a factor of 5. Without cooling, the wet-process phosphoric acid feed to solvent extraction would normally be at a temperature of about 60°C. Industrial representatives have indicated that the acid can be cooled easily and inexpensively to about 40°C but that cooling below this temperature would be relatively expensive.

The phosphoric acid concentration of the commercial wet-process acid that is produced in the United States is typically in the range of 5.3 to 6 M. At the highest acid concentration in the range, particularly if extraction occurs at temperatures above 50°C, the extraction power of the D2EHPA--TOPO extractant is barely high enough to provide good uranium recoveries at favorable solvent loadings in a reasonable number of stages. The extraction efficiency can be increased by increasing the extractant concentration, but only at the expense of higher solvent costs. Tests have shown that the dependence of the uranium extraction coefficient on the D2EHPA concentration in this system is about 1.5 power.

Data for the extraction of uranium by 0.5 M D2EHPA--0.125 M TOPO--*n*-dodecane from Company A acid at 43°C and from Company B acid at 38°C were about equivalent; therefore, they are plotted in Fig. 10.3 as a single isotherm. These data indicate that about 90% of the uranium could be recovered in four ideal extraction stages when operation is carried out at an aqueous/organic feed ratio of 3/1. Under these conditions and assuming a uranium concentration of 0.17 g/liter in the feed liquor, the solvent would contain about 0.46 g of uranium per liter.

Significant amounts of H_3PO_4 are extracted by the D2EHPA--TOPO solvent. Most of this H_3PO_4 is easily removed by scrubbing the extract with water. For example, about 92% of the phosphate was removed from an extract containing 3.8 g of PO_4 per liter by a single batch contact with water at an organic/aqueous phase ratio of 10/1.

Uranium Stripping and Product Recovery

Uranium is effectively stripped from D2EHPA--TOPO by contact with ammonium hydroxide--ammonium carbonate solutions to give the soluble

⁹Chem. Technol. Div. Ann. Progr. Rept. May 31, 1968, ORNL-4272, pp. 177-79.

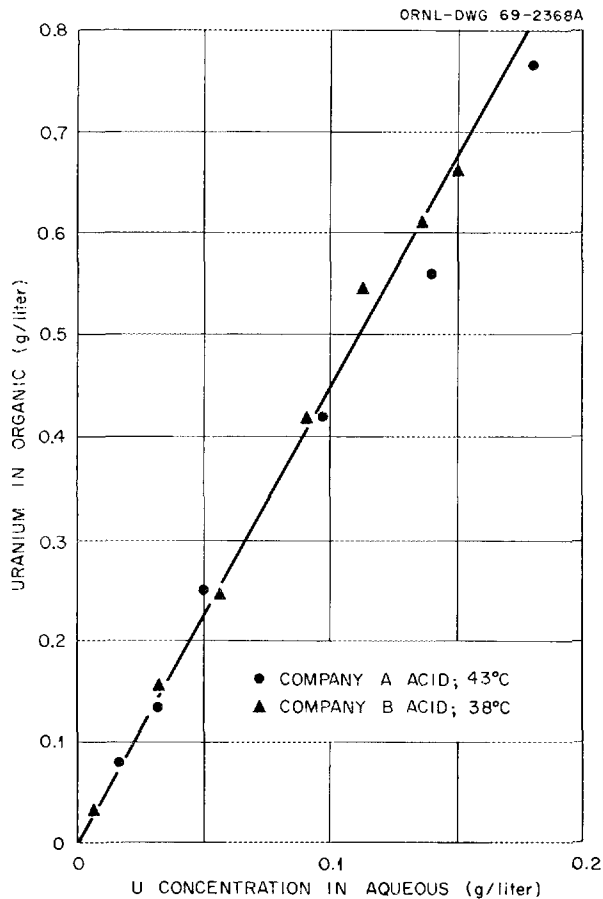


Fig. 10.3. Isotherm for the Extraction of Uranium from Wet-Process Phosphoric Acid with 0.5 M D2EHPA-0.125 M TOPO-*n*-dodecane.

uranyl tricarbonate complex in the aqueous phase. Any extracted iron precipitates during stripping and is filtered off from the strip solution prior to uranium recovery. The uranium is precipitated by heating (or steam stripping) the solution to volatilize ammonia and carbon dioxide. A uranium product prepared in this manner contained (after calcination) 87% U_3O_8 and 8.7% PO_4 . Although the high phosphate content is somewhat objectionable, it could be decreased by more extensive water scrubbing of the solvent extract prior to stripping.

Alternative methods for recovering uranium from the strip solution, including the extraction of uranium with a quaternary ammonium compound or adsorption on a strong-base anion exchange resin, have shown promise and are being evaluated further.

Batch Countercurrent Test

A batch countercurrent demonstration of the process flowsheet was made, using 0.5 M D2EHPA-0.125 M TOPO-*n*-dodecane, to recover uranium from Company B acid. Figure 10.4 shows the relative solution flows and the distribution of uranium in the system at steady state. About 88% of the uranium was extracted, using an aqueous/organic phase ratio of 2.7/1. Two extraction stages, two scrub stages, and two stripping stages were used at room temperature; additional extraction stages would be needed to

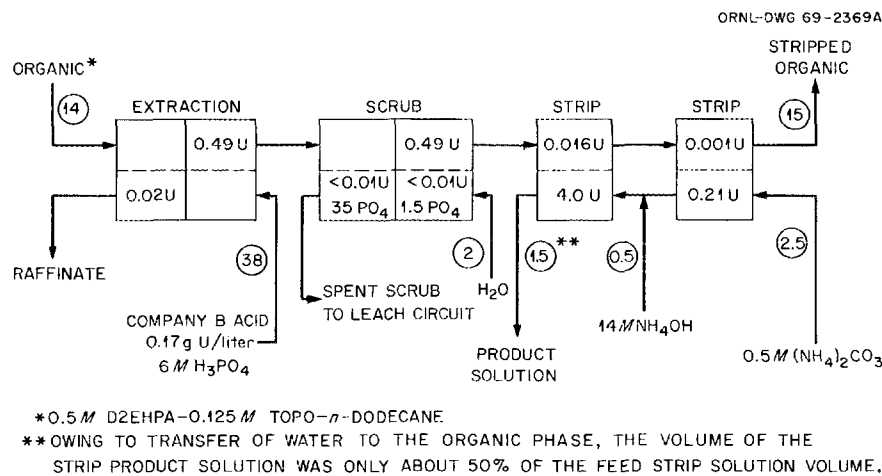


Fig. 10.4. Batch Countercurrent Test Demonstrating Uranium Recovery from Phosphoric Acid. Numbers in the circles show the relative volume flows. Numbers in blocks show concentrations in grams per liter.

achieve equivalent recovery at elevated temperatures. The extract was scrubbed with one-seventh volume of water to remove extracted phosphoric acid and was then stripped with $\text{NH}_4\text{OH}-(\text{NH}_4)_2\text{CO}_3$ solution. Greater than 99% of the uranium was recovered from the solvent.

A mixer-settler system is being assembled so that the process can be demonstrated on a continuous basis and at elevated temperatures.

Reagent Costs

We have made some rough estimates of chemical reagent costs for the process for use in guiding future work. These estimates indicate that the total reagent costs would be in the range of \$0.89 to \$2.78 per pound of recovered U_3O_8 . Variations within the range would depend, principally, on the magnitude of the solvent loss, which is estimated to be in the range of \$0.20 to \$1.65 per pound of recovered U_3O_8 .

10.5 RAPID HIGH-RESOLUTION CHROMATOGRAPHY

We are studying the use of high-pressure ion exchange to obtain more rapid chromatographic separations on tracer and near-tracer scales. Since rates of ion exchange processes are often diffusion controlled, the use of very finely divided resin and high flow rates may reduce the time required for the development of good chromatographic elution bands. Recently, it has been shown that elution bands may be broadened significantly if the eluate simply flows through a tube (i.e., the column effluent tube). This effect, which can probably be attributed to the nonuniform flow velocity in the tube, may be greatly diminished by injecting bubbles into the flowing stream.

Last year it was reported that widths of elution bands increased with flow rate, but that the low-level tailing was substantially independent of flow rate. Generally, even with low flow rates, the right (final) side of the elution band was less steep than the left (initial) side, and, in fact, much of the right side could be represented by a straight line on the semilog plots used to display data. Numerous experiments with ^{142}Pr tracer were carried out to study the effect of various parameters on band shape. The α -hydroxyisobutyric acid-vs-Dowex 50 resin system was used.

The experimental setup consisted of a Beckman pump to force the solutions through a six-port valve used for sample injection, to a 1-ml-capacity ($\frac{1}{4}$ -in.-OD) column, and finally through an effluent tube from which one-drop samples were collected. The effluent tube provided most of the exposed surface area. Several different materials used for the effluent tube, including Teflon, polyethylene, and stainless steel, had no significant effect on either band shape or tailing.

Several experiments were done with a column from which the resin was removed in order to study the effects of solution flow alone; later, a new column was placed in the system so that no trace of resin was present. Praseodymium-142 tracer (ca. 0.25 ml in 0.1 M HNO_3) was introduced either into the sample injection loop or into the bottom of the empty column. Subsequently, the column was removed from the system, and several runs were made in which a sample was pumped directly from the sample injection loop through one tubing fitting and a 12-cm length of $\frac{1}{8}$ -in.-OD stainless steel effluent tube. In all cases the "elution" curves were similar, showing a very sharp rise, a more or less Gaussian top with a half-width of 0.4 to 0.5 ml, followed by a linear decrease in the log of the concentration; the volume required to reduce the concentration by a factor of 2 was 0.2 to 0.3 ml. This decrease continued for three to four orders of magnitude until the usual tailing was observed at very low concentrations. Variations in flow rate had little effect on these curves, and the addition of stable rare earths to the tracer (to minimize any effects from adsorption) had no effect.

In order to study the simplest system possible, and to eliminate mixing which may occur in fittings, a longer effluent tube (a 33-cm stainless steel tube with a volume of 0.46 ml) was connected to the six-port valve. Samples with a volume of 0.25 ml were drawn into this tube by suction. Thus, the tracer was located only in the downstream end of the effluent tube. These samples were pumped out with 0.1 M HNO_3 . A typical result is shown on curve *a* (left side) of Fig. 10.5. The volume of the sample amounted to about seven drops, but the effluent concentration decreased continuously, even while the sample was being displaced. More than 3 ml of solution was required to wash this 0.25-ml sample from the tube.

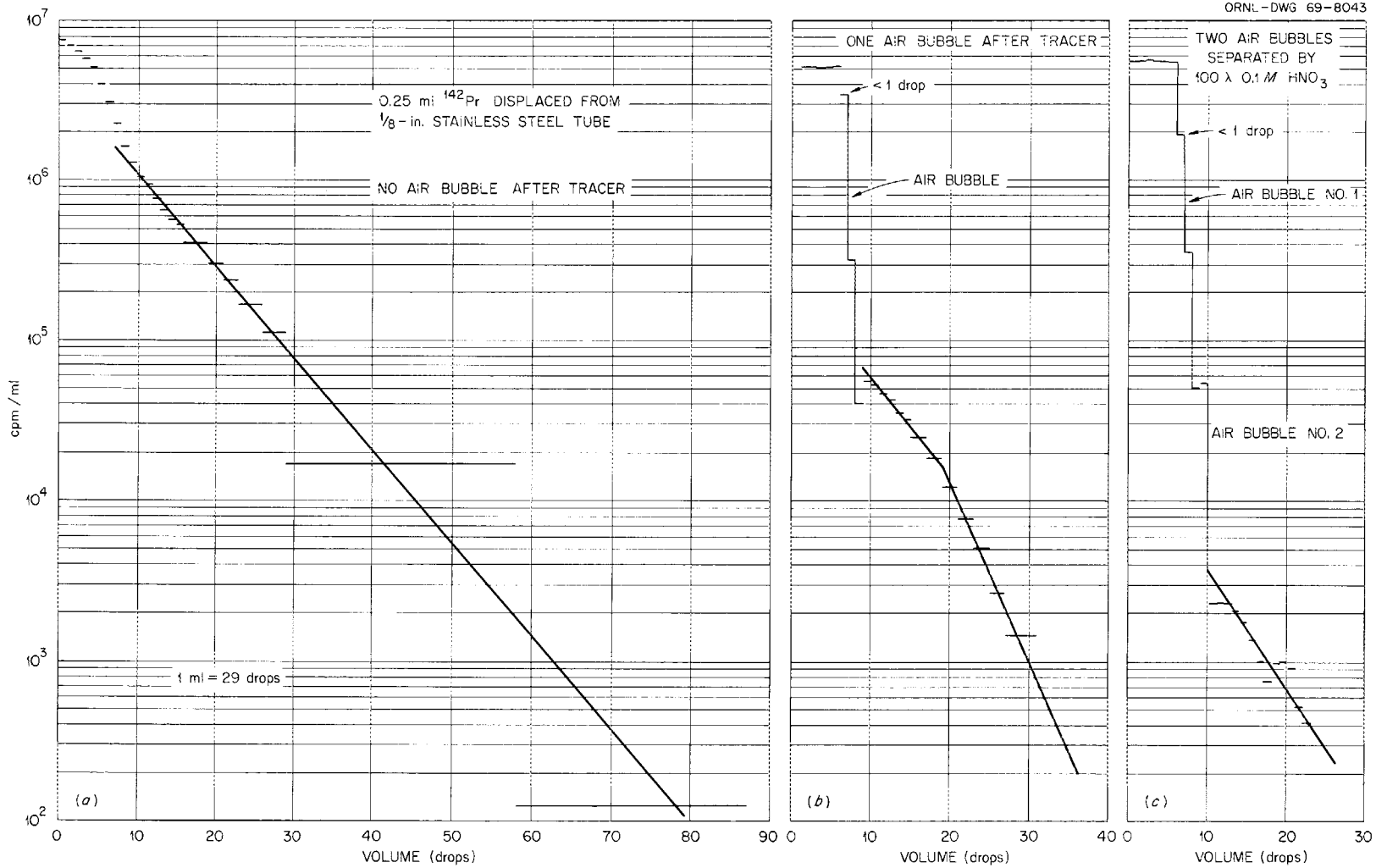


Fig. 10.5. Effect of Air Bubbles on Gradient Broadening in Effluent Tubes.

The other two curves in Fig. 10.5 differ from curve *a* only in that the sample, drawn into the effluent tube, was separated from the eluent by one (curve *b*) or two (curve *c*) air bubbles. The air bubbles, which followed the sample, caused two very significant changes. The first few drops, representing the original sample, were of essentially constant concentration (instead of decreasing as in curve *a*). The last point shown before the bubble emerged represents a volume of less than one drop emerging; it, therefore, contained less activity than the preceding full drops. The air bubble followed, and the concentration decreased by a factor of about 100 by the time the second drop after the air bubble had emerged (curve *b*). Subsequently, the concentration showed a decrease similar to that of curve *a*. In the case of curve *c*, there were two air bubbles separated by 0.1 ml of 0.1 M HNO₃. The first bubble caused the same effect as shown in curve *b*, while the second caused a somewhat smaller decrease in concentration, for an overall decrease by a factor of about 2000.

It is clear from these results that the bubbles significantly decrease the volume of solution required to wash out this simple tube. A corollary observation is that flow through a simple effluent tube may significantly broaden a sharp concentration gradient. With tracer or small-scale elutions, and probably even with larger-scale operations if there is enough plumbing downstream from the column, the observed elution band may be substantially broadened as compared with the actual band leaving the column itself. This broadening is probably caused by the presence of material in the boundary layer (near the tube wall), which flows along the tube very slowly, or not at all, and thus must diffuse into the flowing stream. A discontinuity in the surface (for example, a fitting) could cause an even greater effect.

The introduction of bubbles causes turbulence, which promotes mixing of the material in the boundary layer into the bulk of the solution. However, one disadvantage of such bubbles is that they interfere seriously with the usual method for collecting small samples, namely drop collection. Possibly, droplets of an immiscible liquid could be used instead of air bubbles. It is interesting, in this connection, to note that at least one commercial chromatographic system injects air bubbles into the line downstream from the column. Very simple laboratory columns generally do not

have any associated lines and, therefore, the broadening effect should be minimal; however, in radioactive systems, which usually require lines and sometimes more complex equipment such as valves and monitors, the effect may be significant.

The effect discussed above is separate and distinct from the "tailing" generally observed in these elutions. Tailing did occur in the experiments just described, at a low concentration level (ca. 10 to 100 counts min⁻¹ ml⁻¹); however, the bubbles appeared to have little effect on it. The counting system is presently being modified to permit a wider range of activity levels to be handled. The new system should make observation of both the peak and the tailing for the same run practical.

This work is being carried out in cooperation with B. H. Ketelle of the Chemistry Division.

10.6 ACTINIDE AND LANTHANIDE INTRAGROUP SEPARATIONS BY DISPLACEMENT ELUTION FROM ION EXCHANGE RESINS

Preliminary investigation at Pacific Northwest Laboratory¹⁰ has shown that it may be possible to separate the transplutonium elements from fission product rare earths by displacement elution from H⁺-form resin (e.g., Dowex 50) with aminopolyacetic acids such as diethylenetriaminepentaacetic acid (DTPA) and nitrilotriacetic acid (NTA). We have begun work using aminopolyacetic acids to improve the separations of lanthanides and actinides and to enable the transcurium elements to be eluted ahead of the main Am-Cm elution band. Spectrophotometric analysis has indicated that americium forms complexes with several of the aminopolyacetic acids,¹¹ and also that biligand complexes are formed between americium and EDTA-HEDTA, and between americium and IDA-NTA.

In an initial investigation in which neodymium and praseodymium were used as stand-ins for the actinides, the following chelating agents were compared at various molarities and pH ranges:

1. hydroxyethylethylenediaminetriacetic acid (HEDTA),

¹⁰E. J. Wheelwright, F. P. Roberts, L. A. Bray, R. G. Ritter, and A. L. Bolt, BNWL-SA-1492.

¹¹Chem. Technol. Div. Ann. Progr. Rept. May 31, 1968, ORNL-4272, pp. 115-20.

2. 1,2-diaminocyclohexanetetraacetic acid (DCTA),
3. iminodiacetic acid (IDA),
4. nitrilotriacetic acid (NTA),
5. diethylenetriaminepentaacetic acid (DTPA),
6. ethylenediaminetetraacetic acid (EDTA),
7. HEDTA + NTA,
8. HEDTA + hydroxyethyliminodiacetic acid (HIMDA),
9. HEDTA + DTPA,
10. HEDTA + IDA,
11. HEDTA + EDTA,
12. EDTA + DCTA.

Excellent separation of Nd and Pr was achieved with either DCTA or EDTA when the resin was loaded to about one-third of the column capacity; however, both DCTA and EDTA required a barrier metal ion, such as Zn or Cu, to prevent the precipitation of the free acid on the H^+ -form resin. This would make the application of these two chelating agents to transplutonium element separations at TRU somewhat questionable. Ion diffusion rates with DCTA were slower than with EDTA, and a heated column was necessary during operation with DCTA.

The ligands IDA, NTA, HEDTA, and DTPA can be used on a H^+ -form resin without precipitating. Good resolution of the Nd and Pr bands were obtained with HEDTA and DTPA. The HEDTA ligand caused the two rare-earth elements to be eluted as very concentrated bands, and the interface between them was relatively sharp. DTPA provided the best separation and yielded an elution band with a somewhat lower metal ion concentration. IDA is an unsatisfactory eluting agent, and the rare earths moved exceedingly slowly, showing poor band resolution. NTA gave fair separation of the Nd and Pr and did not precipitate in the heated ion exchange column; however, precipitation did occur in the cooled column eluate. A barrier metal ion would probably have to be used with this ligand in separations that are carried out in a remotely operated cell where plugged lines could occur.

Absorption spectroscopic analysis had shown the formation of additional americium complexes when pair combinations of HEDTA and IDA, NTA, or HIMDA were present. Ion exchange separations of Nd and Pr were, therefore, made using different ratios of HEDTA + IDA, HEDTA + NTA, and HEDTA + HIMDA to determine the effect of such combinations on elution and resolution. In each

case, it was found that the second ligand tended to enhance the separation of the two elements by lengthening the resolved bands so that the concentration of the metal ion in the interface was quite low. Also, the presence of the second ligand made it possible to move the Nd band out of the loading mixture and leave a Pr band behind, a condition not seen with single ligand elution. Very good separations were obtained in relatively short runs. Mixtures of HEDTA + DTPA, HEDTA + EDTA, and HEDTA + DCTA, on the other hand, behaved essentially as the second ligand alone; that is, no enhancement in separation of the two elements was noted. Investigations with the foregoing promising pairs (and others) are continuing.

The ion exchange behavior of transplutonium elements was investigated with the following ligands: HEDTA, NTA, IDA, 2-hydroxypropane-1,3-diaminetetraacetic acid (HPDTA), and various combinations of these. Ion exchange runs were made in hot-cell facilities that contained a high-pressure stainless steel column ($\frac{1}{4}$ in. OD, 36 in. long). This column was filled with 20 ml of Dowex 50-X8 resin and equipped with a water jacket that permitted operation at 80°C. The experimental feed solution contained 80 mg of ^{241}Am , 80 mg of ^{244}Cm , 10 μg of ^{252}Cf , and approximately 0.2 μg of ^{253}Es , and was adjusted to a final HNO_3 concentration of 0.25 M before loading. After loading, the column was eluted with one, or a combination of two, of the ligands just mentioned.

HEDTA alone (10 g/liter at pH 8.5) gave poor resolution; all the actinides were eluted from the column essentially as one fraction. Similar results were obtained in elutions with HEDTA (8 g/liter)-IDA (8 g/liter) at pH 6.5, and with HEDTA (3.5 g/liter)-NTA (1.0 g/liter) at pH 6.5. HPDTA alone (10 g/liter at pH 8.0) gave excellent separation of the actinides into four fractions. Fraction 1 consisted of about 20 column volumes containing essentially all of the ^{253}Es , about 30% of the ^{252}Cf , and <0.1% of the Cm; fraction 2 consisted of 25 column volumes containing 70% of the Cf and about 0.2% of the Cm; fraction 3 consisted of about 10 column volumes containing approximately 80% of the Cm, no Es or Cf, and only a trace of Am; the final fraction consisted of 13 column volumes containing more than 99% of the Am, about 19% of the Cm, and none of the transcurium elements.

It should be pointed out that, when the amino-polyacetic acid chelating agents are used as eluents for metals loaded on hydrogen-form resin, displacement elutions, rather than chromatographic elutions, are obtained. Displacement elution requires that relatively large quantities of the actinides be present before separation can become completely effective. The poor resolutions obtained in some of these experiments were probably due, at least in part, to insufficient quantities of the actinides on the column. However, even under these conditions, HPDTA gave relatively good separation of the actinides; thus plans have been made for further investigations concerning its use as an eluent in combination with other chelating agents. Additional work is in progress with the actinides and with mixtures of lanthanides to fully resolve the displacement elution technique as a method of actinide-lanthanide intergroup and actinide intragroup separations.

10.7 SEPARATIONS BY PRECIPITATION

Precipitation of Berkelium(IV) Iodate from Homogeneous Solution

Many procedures for the separation and analysis of metals have been improved by application of the technique of precipitation from homogeneous solution, following methods initiated by Willard.¹² An outstanding example is the Willard-Yu¹³ method of precipitation of ceric iodate by formation of cerium(IV) ions from cerium(III) in a solution containing an excess of iodate ions. Berkelium, still a very scarce element, has oxidation-reduction properties very similar to those of cerium. A study of tracer-level berkelium in the presence of cerium confirmed the expectation of coprecipitation from the homogeneous solution. The results of this study have been published in *Analytical Chemistry*;¹⁴ the abstract follows:

"The Willard-Yu method of precipitation of ceric iodate from homogeneous solution is even more effective for separating berkelium from other elements. In hot, dilute nitric acid solutions

containing iodic acid, Bk(III) and Ce(III) are oxidized homogeneously to Bk(IV) and Ce(IV) by bromate and coprecipitated as iodates. Coprecipitation of tracer berkelium with ceric is highly quantitative (>99%) from HNO₃ solutions up to 2 N containing 0.1 mg Ce/ml and up to 0.5 N containing only 0.01 mg Ce/ml. Removal of >99% of trivalent lanthanides and actinides may be accomplished simultaneously. Separations are obtained from most other metals. The procedure requires less than two hours. Results indicate that microgram quantities of berkelium can be precipitated without carrier. The method is useful for recovery of berkelium, purification of analytical samples, and milking of ²⁴⁹Bk."

Mechanisms in the Coprecipitation of Berkelium(IV) with Cerium(IV) Iodates from Homogeneous Solution

There are two well-known models for coprecipitation of a trace element with another precipitating element. Henderson and Kracek¹⁵ showed that, when the whole precipitate is continually in equilibrium with the solution, the trace element, B, distributes between the crystals of A and the solution according to the relationship

$$\left(\frac{B}{A}\right)_{\text{crystal}} = D \left(\frac{B}{A}\right)_{\text{solution}}$$

The model of Doerner and Hoskins¹⁶ for the case where only the surface of the crystal is in equilibrium with the solution is given by

$$\log \left(\frac{B_{\text{initial}}}{B_{\text{final}}}\right)_{\text{solution}} = \lambda \log \left(\frac{A_{\text{initial}}}{A_{\text{final}}}\right)_{\text{solution}}$$

Which of the two models prevails can be important when decontamination is being accomplished by carrier precipitation; in many examples studied, precipitation from homogeneous solution tended to follow the latter model. We found this to be true for berkelium iodate that was carried on cerium iodate over a considerable range of conditions. A paper has been submitted to *Analytical*

¹²L. Gordon, M. L. Salutsky, and H. H. Willard, *Precipitation from Homogeneous Solution*, Wiley, New York, 1959.

¹³H. H. Willard and S. T'S. Yu, *Anal. Chem.* **25**, 1754 (1953).

¹⁴Boyd Weaver, *Anal. Chem.* **40**, 1894 (1968).

¹⁵L. M. Henderson and F. C. Kracek, *J. Am. Chem. Soc.* **49**, 738 (1927).

¹⁶H. H. Doerner and W. M. Hoskins, *J. Am. Chem. Soc.* **47**, 662 (1925).

Chemistry: "Mechanisms in the Coprecipitation of Berkelium(IV) with Cerium(IV) Iodate from Homogeneous Solution," by Boyd Weaver and John J. Fardy.¹⁷ *Abstract.* "Ce(III) in HNO₃ containing iodate is homogeneously oxidized by bromate to Ce(IV), which is precipitated as Ce(IO₃)₄ with a second-order rate relation. Precipitation occurs at room temperature, and the rate increases with concentrations of bromate and iodate, but decreases as concentration of acid increases. Bk(III) is oxidized and coprecipitated with Ce(IV). Under conditions where precipitation is not too rapid, concentrations of the two elements in solution decrease with precipitation according to the equation

$$\log \frac{[\Sigma \text{Bk}]_i}{[\Sigma \text{Bk}]_f} = k\lambda \log \frac{[\Sigma \text{Ce}]_i}{[\Sigma \text{Ce}]_f},$$

where

$$k = \frac{[\text{Bk}^{4+}]}{[\text{Bk}^{3+}]} \bigg/ \frac{[\text{Ce}^{4+}]}{[\text{Ce}^{3+}]}$$

and has a value of ~ 10 , and $k\lambda$ is nearly 3."

The distribution equation cited in this abstract differs from that of Doerner and Hoskins by the factor k , which enters because the concentrations analyzed are $[\Sigma \text{Bk}] \approx [\text{Bk}^{3+}]$ and $[\Sigma \text{Ce}] \approx [\text{Ce}^{3+}]$, whereas the precipitation rates involve the concentrations $[\text{Bk}^{4+}]$ and $[\text{Ce}^{4+}]$. (For the evaluation $k \approx 10$, see Sect. 10.9.) Since $k\lambda$ is greater than 1, berkelium is depleted from the solution

more rapidly than is cerium. However, since $k \approx 10$, λ itself is less than 1 ($\lambda \approx 0.3$), which suggests that cerium would be depleted more rapidly than berkelium if the precipitation were not controlled by the redox reaction.

Solubility of Ceric Iodate

As a part of the foregoing study, the solubility of ceric iodate was measured in nitric acid solutions (plus holding oxidant), with and without added iodate. The results are summarized in Table 10.2.

Physical Properties of Ceric Iodate

The examination of precipitated ceric iodate produced some surprising results. One of the frequently reported advantages of precipitation from homogeneous solution is that it produces precipitates which are more crystalline than those obtained from ordinary precipitation. The fact that coprecipitations from homogeneous solution follow a logarithmic law also indicates the formation of crystals in which the internal material is unavailable for re-equilibration with the solution. In the present instance, even the precipitates from hot solutions were considered to be crystalline, as reported by Willard and Yu.¹³ Settling characteristics and the apparent density of our precipitates suggested that crystallinity increased as the rate of precipitation was decreased. However, observation by microscope did not reveal any definite crystal forms. Attempts to obtain x-ray diffraction patterns from powdered precipitates were unsuccessful, as were attempts to obtain

¹⁷ Guest scientist from Australia. Present address: Australian Atomic Energy Commission; Lucas Heights, Sydney, Australia.

Table 10.2. Solubility of Ceric Iodate in Nitric Acid Solutions

HNO ₃ Concentration (N)	Solubility of Ce(IO ₃) ₄ (M)		Solubility Product [Ce ⁴⁺][IO ₃ ⁻] ⁴
	a	a,b	
1	3.13 × 10 ⁻⁴	7.3 × 10 ⁻¹¹	7.7 × 10 ⁻¹⁶
2	8.10 × 10 ⁻⁴	8.1 × 10 ⁻⁹	8.5 × 10 ⁻¹⁴
3	1.68 × 10 ⁻³	3.2 × 10 ⁻⁷	3.4 × 10 ⁻¹²

^aNaBrO₃ added at 3 mg/ml to inhibit reduction of Ce(IV).

^bAdditional iodate present, 0.057 M HIO₃.

crystals by moderate aging and digestion of precipitates. Finally, definite x-ray patterns were obtained from precipitated ceric iodate that had been digested at 80°C for two weeks. This behavior indicates that coprecipitation can follow a logarithmic law even though the precipitate is amorphous, and casts considerable doubt about the crystallinity of many reported precipitates, which may have been simply dense forms of amorphous material.

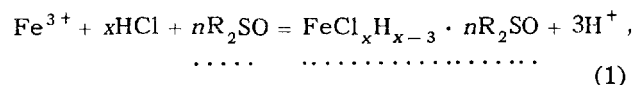
10.8 EQUILIBRIA AND MECHANISMS OF EXTRACTION

Extraction of Iron(III) Chloride by Methyl-4,8-dimethylnonylsulfoxide

Iron(III) is extracted from chloride solution by all of the unsymmetrical methylalkylsulfoxides (Sect. 10.2 and ref. 18), but not by any of the symmetrical dialkylsulfoxides, that we have tested.¹⁸ We have started a detailed examination of the extraction of iron from hydrochloric acid solutions by one of the unsymmetrical sulfoxides, methyl-4,8-dimethylnonylsulfoxide, in order to elucidate this difference and to characterize, in general, the extractions by this promising class of new extractants.

Effect of Sulfoxide Concentration. — Extraction coefficients, $E = [\Sigma\text{Fe}]_o / [\Sigma\text{Fe}]_a$, were measured by the back-extraction of iron, traced with ⁵⁵Fe, into 8 M HCl solution from a series of *p*-xylene solutions containing both sulfoxide and iron at a constant iron/sulfoxide mole ratio of 0.05. The sulfoxide concentration was varied between 10⁻³ and 10⁻¹ M.

A general equation expressing the reaction may be written as follows (omitting hydration):



where dotted underlines indicate the organic phase. The assumption in this equation that the iron is monomeric in both phases is reasonable for the low iron concentrations used, and the assumption that the sulfoxide is monomeric is supported by osmometric measurements thus far completed (Sect.

10.11). The concentration quotient for Eq. (1) is:

$$Q = \frac{[\text{FeCl}_x\text{H}_{x-3} \cdot n\text{R}_2\text{SO}][\text{H}^+]^3}{[\text{Fe}^{3+}][\text{HCl}]^x[\text{R}_2\text{SO}]^n} = E \frac{[\text{H}^+]^3}{[\text{HCl}]^x[\text{R}_2\text{SO}]^n} \quad (2)$$

At constant HCl concentration,

$$E = Q' [\text{R}_2\text{SO}]^n,$$

$$\log E = \log Q' + n \log [\text{R}_2\text{SO}]. \quad (3)$$

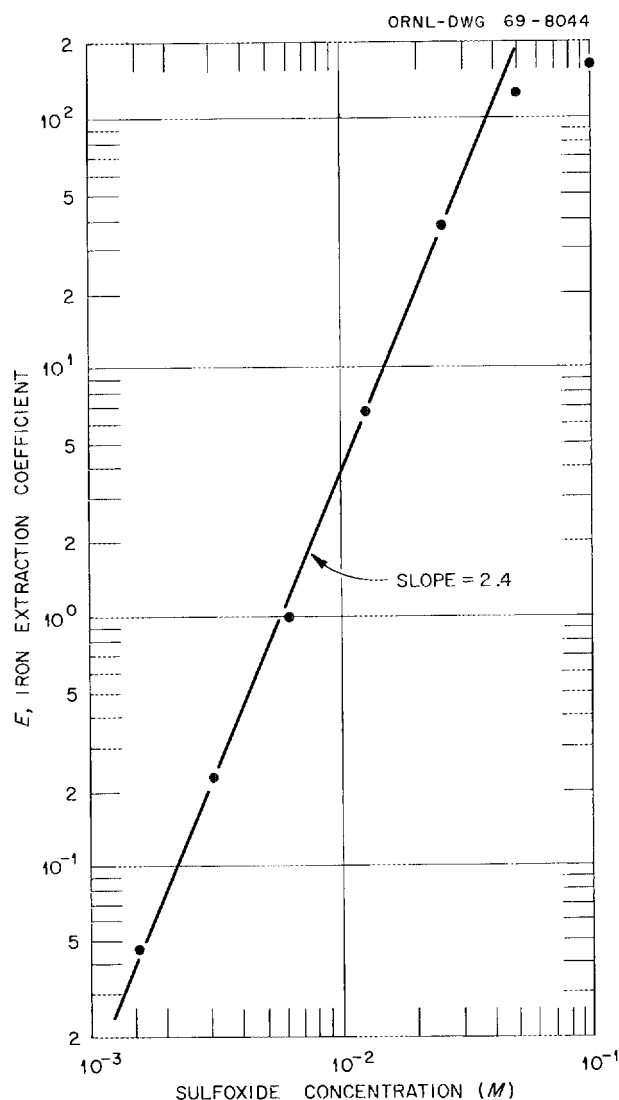


Fig. 10.6. Extraction of Iron(III) Chloride by Methyl-4,8-dimethylnonylsulfoxide in *p*-Xylene. Dependence of extraction coefficient on sulfoxide concentration in extraction from 8 M HCl.

¹⁸Chem. Technol. Div. Ann. Progr. Rept. May 31, 1967, ORNL-4145, p. 211.

If the concentration quotient is reasonably constant, a plot of $\log E$ vs $\log [R_2SO]$ should give a straight line of slope n . The experimental results (Fig. 10.6) conform, up to a sulfoxide concentration of 0.025 M , to a straight line with a slope of 2.4, suggesting the formation of a mixture of $FeCl_xH_{x-3} \cdot 2R_2SO$ and $FeCl_xH_{x-3} \cdot 3R_2SO$.

Effect of Hydrochloric Acid Concentration. — Extraction coefficients were measured between a 0.1 M sulfoxide solution in *p*-xylene and a series of 1 to 11 M HCl solutions. The results (Fig. 10.7) show a strong dependence on hydrochloric acid concentration, which is linear on a log-log scale between 2 and 6 M HCl with a slope of about 9 (i.e., $E \propto [HCl]^9$).

We have not yet varied the chloride ion concentration independently of the total acid con-

centration in order to estimate the chloride ratio x [Eq. (1)] in the extracted complex. (In principle, this ratio could be obtained from our present data, but only if we had information on the hydrogen ion activity separate from the hydrochloric acid activity, as well as the water activity, over the range of hydrochloric acid concentrations used.) In earlier work¹⁹ on iron complexing in, and ether extraction of iron from, hydrochloric acid solutions, Friedman found that the anion $FeCl_4^-$ is an important species and is extracted as an ether- $HFeCl_4$ adduct. Analogous species $HFeCl_4 \cdot 2R_2SO$ and $HFeCl_4 \cdot 3R_2SO$ in the sulfoxide extraction are not inconsistent with the results obtained thus far.

10.9 RELATIVE POTENTIALS OF THE Bk(IV)/Bk(III) AND Ce(IV)/Ce(III) COUPLES

The difference between the formal potentials of the Bk(IV)/Bk(III) and Ce(IV)/Ce(III) couples at 25°C in nitric acid solutions was measured by determining the relative concentrations of the oxidized and reduced species of berkelium and cerium in equilibrium in aqueous solutions.

The potential difference (in volts) is given by a form of the Nernst equation,

$$E_{Ce} - E_{Bk} = 0.059 \log \frac{[Bk(IV)]}{[Bk(III)]} - 0.059 \log_{10} \frac{[Ce(IV)]}{[Ce(III)]}$$

The ratios of the concentrations of Ce(IV) and Ce(III) were fixed experimentally by mixing solutions of $(NH_4)_2Ce(NO_3)_6$ and $Ce(NO_3)_3$ and were not significantly altered by the addition of tracer ^{249}Bk . The equilibrium ratios of concentrations of Bk(IV) and Bk(III) were determined by essentially quantitative extraction ($E_a^0 > 100$) of the Bk(IV), along with the Ce(IV), but without significant extraction of Bk(III) or Ce(III), into an equal volume of an organic phase, and subsequent measurement of the relative concentrations of ^{249}Bk in the two phases. The extractant was di(2-ethylhexyl)phosphoric acid (HDEHP) in *n*-dodecane that had been thoroughly scrubbed with

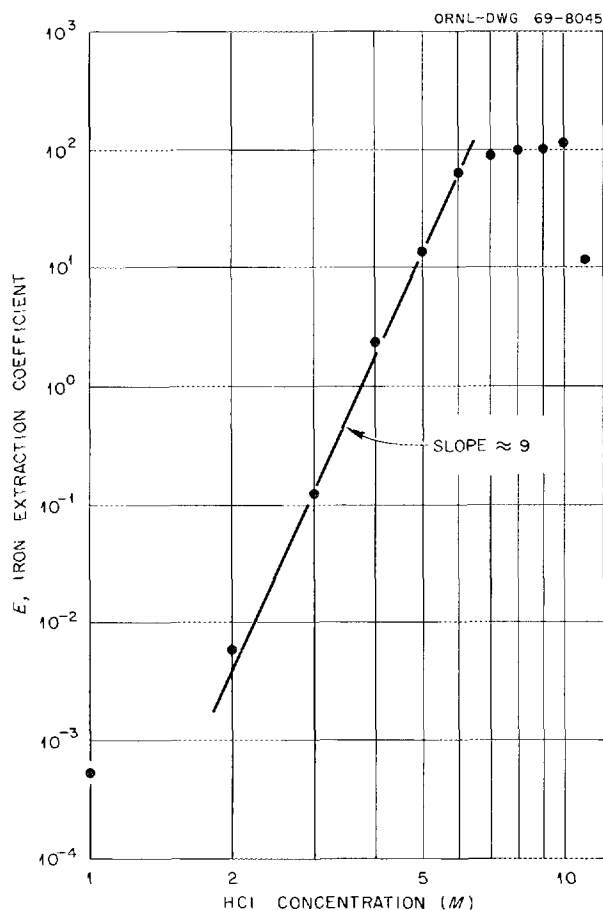


Fig. 10.7. Extraction of Iron(III) Chloride by Methyl-4,8-dimethylnonylsulfoxide in *p*-Xylene. Dependence of extraction coefficient on HCl concentration in extraction by 0.1 M sulfoxide.

¹⁹H. L. Friedman, *J. Am. Chem. Soc.* **74**, 5 (1952), and references therein.

concentrated H_2SO_4 . Satisfactory separations of trivalent and tetravalent species were obtained with 0.1 M HDEHP at all acid concentrations higher than 1 N and with 0.2 M or 0.5 M HDEHP when the acid concentration was 4 N or greater. Total aqueous concentrations of 0.01 M and 0.1 M cerium gave concordant results; with only 0.001 M cerium, however, there was apparently some extraneous reduction. Extractions were performed within a few minutes after the aqueous solutions were prepared, in order to minimize the extraneous reduction of the cerium.

This method and the results obtained differ from those of Musikas and Berger,²⁰ who applied the Nernst equation to aqueous concentrations of the four species, after both redox and extraction equilibration, with organic phases that allowed significant concentrations of the tetravalent species to remain in the aqueous solutions. Also, they used much lower cerium concentrations.

In all experiments, Ce(IV) was found to be a stronger oxidizing agent than Bk(IV). In one series of experiments with 4 N HNO_3 , varying the Ce(IV)/Ce(III) concentration ratio from 1/9 to 9/1 gave values for $E_{\text{Ce}} - E_{\text{Bk}}$ varying only from 0.054 to 0.063 v. In another series, with Ce(IV)/Ce(III) concentrations fixed at 1/1, values of 0.061, 0.072, 0.064, 0.044, and 0.019 v were obtained with 1, 2, 4, 6, and 7.5 N HNO_3 respectively. The values above 4 N HNO_3 were not consistently reproducible, but they did indicate a sharp decrease as the acid concentration was increased. There is a need for a further study of this region and the behavior of cerium and berkelium in sulfuric and perchloric acids since uncertain results were also obtained in these media in preliminary experiments.

The potential of the Bk(IV)/Bk(III) couple is approximately 0.06 v lower than that of the Ce(IV)/Ce(III) couple in 1 to 4 N HNO_3 . No absolute value is assigned to the potential of the Bk(IV)/Bk(III) couple because of uncertainty about the value of the Ce(IV)/Ce(III) couple.

10.10 KINETICS OF METAL ION EXTRACTIONS BY ORGANOPHOSPHORUS ACIDS

The experimental technique for measuring extraction kinetics was improved by substituting continuous closed-loop flow sampling and automatic counting, summed over equal intervals, for

the previous intermittent manual sampling and subsequent counting. Other experimental details are as previously described.²¹ The revised system can run unattended. In addition to improved convenience and efficiency, this system has proved to give several important advantages: it yields a maximum amount of data per run, the analytical precision is markedly improved, and runs without information gaps are no longer limited to an approximate 8-hr period. The improved precision has permitted refinement of the rate constants reported last year for iron extraction by di(2-ethylhexyl)phosphoric acid (HDEHP or HA) and a significant start in the analysis of the much more complicated behavior encountered in the extraction of beryllium by HDEHP.

Iron Extraction

As previously described,²² the overall rate of iron extraction by HDEHP from acid perchlorate solutions results from the combination of two parallel steps for introduction of the first ionic ligand, in series with two or more parallel steps for introduction of the second ionic ligand, of the three ionic and three molecular ligands in the final complex $\text{FeA}_3(\text{HA})_3$. The best fit to the experimental data (Fig. 10.8) is given by

$$\frac{\text{rate}}{[\text{Fe}]} = r = \frac{(r_{1m} + r_{1d})(r_{2s} + r_{2d} + r_{2df})}{r_{1m} + r_{1d} + r_{2s} + r_{2d} + r_{2df}}, \quad (1)$$

where

$$\begin{aligned} r_{1m} &= 5.5 \times 10^{-4} [\Sigma\text{HA}]^{0.5} / [\text{H}^+], \\ r_{1d} &= 1.8 \times 10^{-3} [\Sigma\text{HA}] / [\text{H}^+], \\ r_{2s} &= 1.5 \times 10^{-7} / [\text{H}^+][\text{Fe}], \\ r_{2d} &= 9.0 \times 10^{-6} [\Sigma\text{HA}]^{1.5} / [\text{H}^+]^2, \\ r_{2df} &= 1.2 \times 10^{-5} [\Sigma\text{HA}]^2 / [\text{H}^+]^2, \\ \sigma &= 9.5 \times 10^{-5} \text{ (standard deviation of fitting)}. \end{aligned}$$

The fit is not improved by including a sixth parameter, r_{2m} , which would correspond to the one additional reaction step that appears plausible. The equations for the six different reaction steps

²⁰C. Musikas and R. Berger, p. 296, *Lanthanide/Actinide Chemistry*, Advances in Chemistry Series, American Chemical Society, Washington, D.C., 1967.

²¹*Chem. Technol. Div. Ann. Progr. Rept. May 31, 1967*, ORNL-4145, p. 230.

²²*Chem. Technol. Div. Ann. Progr. Rept. May 31, 1968*, ORNL-4272, p. 182.

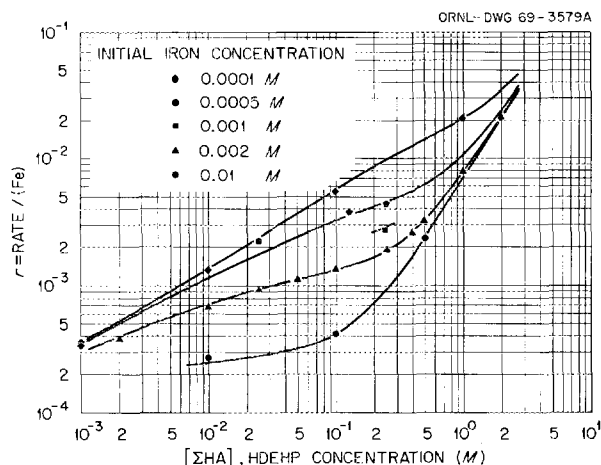


Fig. 10.8. Kinetics of Iron(III) Extraction from Acid Perchlorate Solution by HDEHP (HA) in *n*-Octane. Initial acid concentration = 0.052 *M*. Points: experimental; curves: calculated from Eq. (1).

are given in ref. 22. In the subscripts, 1 refers to the first and 2 to the second ionic ligand A^- ; m refers to the monomer HA, d to the dimer $(HA)_2$, and s to saturation of the interface with the monoligand intermediate.

Beryllium Extraction

As previously noted,²¹ the data for the extraction of beryllium by HDEHP from acid perchlorate solutions do not fit well to the standard plot for any order. In a plot corresponding to first-order rate control ($-d[Be]/dt = k[Be]$; slope of $\ln [Be]_i/[Be]_f$ vs t giving k), the slope increases gradually for several hours before becoming constant. However, plots corresponding to other orders do not show any constant slope. With the improvement in precision and length of runs, as described above, it has now become possible to discern more detailed structure in these curves. This structure suggests the occurrence of at least three different regions, as illustrated in Fig. 10.9. The extraction appears to be moderately slow at the start (commensurate with iron extraction rates), and decreases in 1 to 3 hr to a lower rate. In the second region, the rate gradually increases again over a period of 10 to 15 hr to a considerably higher level. In the third region, it becomes

proportional to the beryllium concentration (i.e., first order). The induction period and final constant ($\text{rate}/[Be]$) are almost independent of stirrer speed over a wide range, indicating (as in iron extraction) control by a reaction at the interface. Because Fig. 10.9b is a differential plot, it greatly magnifies the experimental and analytical scatter of the data, in contrast to the smooth appearance of the same data in Fig. 10.9a. In spite of the scatter, the marked differences of the three regions are emphasized. The sudden increase of scatter in the third region is striking and may give some clue to the nature of the successive controlling reactions.

10.11 AGGREGATION AND ACTIVITY COEFFICIENTS IN SOLVENT PHASES

Techniques for Measuring Vapor Pressure Depression

We previously reported²³ the testing of a commercial diaphragm manometer²⁴ for measuring small vapor pressure differences between solution and pure solvent. Although it showed good sensitivity and precision, satisfactory use was prevented by a persistent real or virtual leak in the indicator head. Subsequently, we obtained two indicator heads (ranges, 3 mm and 100 mm Hg) of a newer design.²⁵ These heads have a welded construction and can be heated to 400–450°C for outgassing. The use of these new units in a redesigned vapor pressure apparatus, constructed of stainless steel and brass tubing and with decreased internal area, has yielded the most accurate vapor pressure data that we have obtained thus far.

Reference Solutes for Isopiestic and Dynamic Vapor Pressure Osmometry in Organic Solutions

Previously reported²⁶ osmotic coefficients of benzene solutions of triphenylmethane (TPM)

²³Chem. Technol. Div. Ann. Progr. Rept. May 31, 1966, ORNL-3945, p. 188.

²⁴MKS Baratron Electronic Pressure Meter, Bulletin 77, MKS Instruments, Inc., Burlington, Mass.

²⁵MKS Baratron Electronic Pressure Meter, Bulletin 90, MKS Instruments, Inc., Burlington, Mass.

²⁶K. B. Brown et al., Chem. Technol. Div. Sect. C Progress Report, ORNL-3785 (April 1965), pp. 155–67.

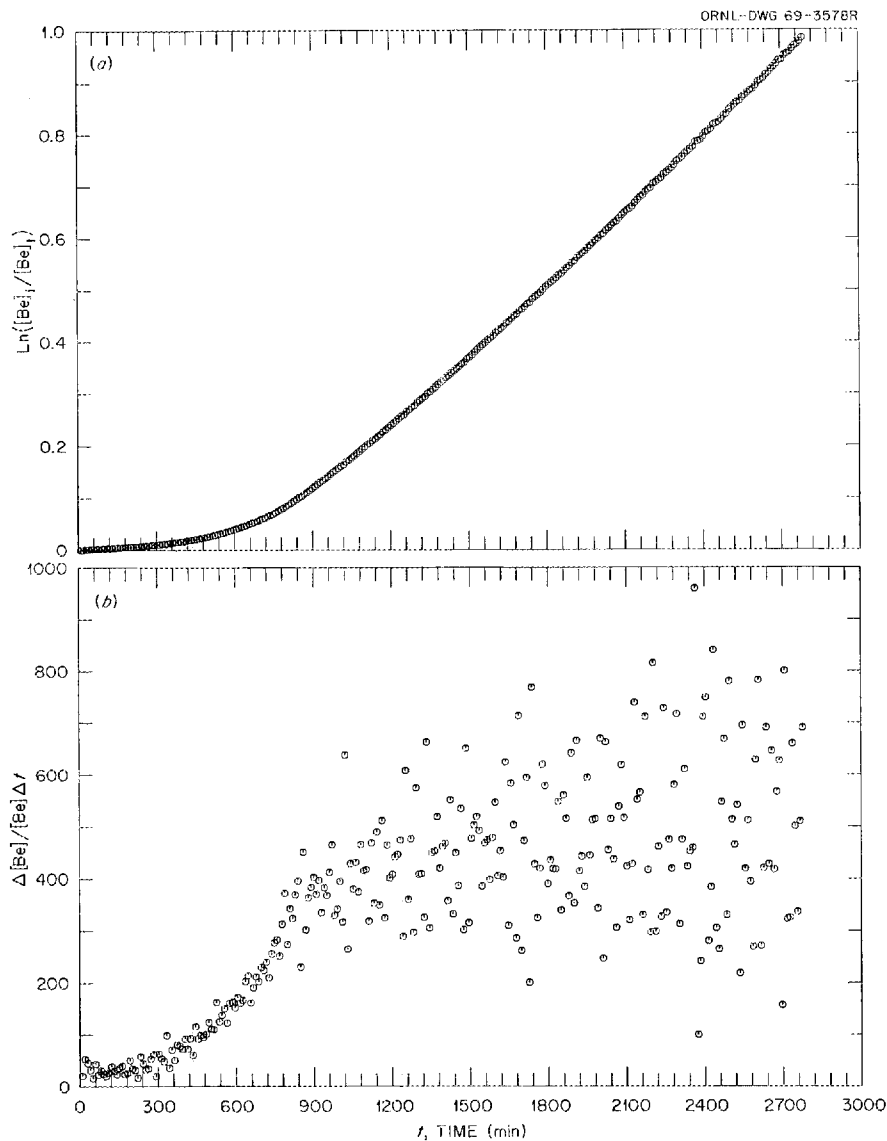


Fig. 10.9. Kinetics of Beryllium Extraction by HDEHP, Showing Change of Rate with Time. (a) Plot according to first-order kinetics. (b) Incremental difference plot. Slope in (a) and ordinate in (b) correspond to first-order rate constant.

and azobenzene (AZO) showed some discrepancy (<2%) between direct measurements and isopiestic comparisons. These solutions, together with benzene solutions of a third common reference solute, benzil (BZL), were reexamined with the improved vapor pressure system. The results (Table 10.3) are well-fitted by an empirical three-parameter equation. They do not conform to regular solution theory, nor can they be accounted for by assuming dimeric association.

We obtained this empirical equation by combining the line $y = a - bm$ with the hyperbola $y =$

$k/(m + c)$ so as to match the shape of the curve for triphenylmethane. It also gave a better fit to the AZO and BZL data than that obtained with a fifth-degree polynomial. A further test was available in von Gierke's BP data (in benzene),²⁷ which had been converted to osmotic coefficients vs molarity and fitted to a sixth-degree polynomial

²⁷O-M. H. von Gierke, Dissertation, Johannes Gutenberg Univ., Mainz, West Germany, 1957.

by Harris and Dunlop.²⁸ We fitted the tabulated data²⁸ to our three-parameter equation with a standard deviation of fitting of 4.2×10^{-3} (Table 10.3), which is as good as the fit Harris and Dunlop obtained (4.7×10^{-3}) with their six-parameter equation. These results suggest that the form of this equation may be particularly suitable for a considerable range of such solutes.

The solution densities required for calculating the solute concentrations in the differential vapor pressure measurements were measured with the Hennion modification²⁹ of the Sprengel-Ostwald pycnometer. The results (Table 10.4) were fitted to a polynomial equation of the form $d = d_0 + k_1 m + k_2 m^2$. Attempts to fit them to the Root equation³⁰ $d = d_0 + k_1 m + k_2 m^{3/2}$ were not successful.

Dialkylsulfoxide

A dynamic (matched thermistor) osmometer was used to determine whether significant aggregation occurs in benzene solutions of methyl-4,8-dimethylnonylsulfoxide (cf. Sect. 10.8). The results show only a small amount of association:

Analytical M	Apparent M	Indicated \bar{n}
0.100	0.0925	1.08
0.050	0.0478	1.05
0.025	0.0235	1.06
0.0125	0.0122	1.02
0.00625	0.0060	1.04
0.003125	0.0030	1.04

Triphenylmethane in benzene was used as the reference standard. Sample solutions, triphenylmethane solutions, and the solvent benzene were saturated with water. Readings, made at $25 \pm 0.1^\circ\text{C}$, were taken 2 min after each sample drop was placed on the thermistor bead.

It is interesting to note that attempts to obtain the apparent molecular weight of the same sulfoxide in benzene solutions equilibrated with aqueous HCl solutions, and of lithium di(2-ethylhexyl)phosphate in benzene solutions, by

²⁸K. R. Harris and P. J. Dunlop, *J. Phys. Chem.* 71, 483 (1967).

²⁹G. F. Hennion, *Ind. Eng. Chem., Anal. Ed.* 9, 479 (1937).

³⁰W. C. Root, *J. Am. Chem. Soc.* 55, 850 (1933).

Table 10.3. Osmotic Coefficients of Benzene Solutions of Reference Solutes Triphenylmethane, Azobenzene, Benzil, and Biphenyl

$$\phi = A + B m + C(1 - A)/(m + C)$$

Solute	Range (m)	A	B	C	Std. Dev. of Fitting
TPM	0-0.3	0.9847	-0.1120	0.0504	5.8×10^{-4}
AZO	0-1.8	0.8795	-0.0530	0.4313	8.0×10^{-4}
BZL	0-1.9	0.7713	-0.0112	0.5247	8.2×10^{-4}
BP ^a	0-18	0.6547	-0.0082	5.419	4.2×10^{-3}

^aData of von Gierke,²⁷ at 20°C and 50°C combined, quoted and fitted to polynomial by Harris and Dunlop²⁸: $1 - 7.726 \times 10^{-2} m + 1.470 \times 10^{-2} m^2 - 2.294 \times 10^{-3} m^3 + 2.018 \times 10^{-4} m^4 - 8.805 \times 10^{-6} m^5 + 1.484 \times 10^{-7} m^6, \pm 4.7 \times 10^{-3}$.

Table 10.4. Densities^a of Benzene Solutions of Reference Solutes Triphenylmethane, Azobenzene, and Benzil

$$d = d_0 + D m + E m^2$$

Solute	d_0	D	E	Std. Dev. of Fitting
TPM	0.8790	0.0469	-0.0022	3.9×10^{-4}
AZO	0.8790	0.0304	-0.0031	3.9×10^{-4}
BZL	0.8789	0.0454	-0.0054	3.7×10^{-4}

^aIn g/cc.

means of the matched thermistor osmometer were not successful. The resistance bridge could not be balanced and often drifted in a direction opposite to that normally observed. Attempts to examine these systems by isopiestic methods are in progress.

Water in Extractant Phases

Last year³¹ we reported initial measurements of water extraction by tri-*n*-octylamine salts. This work has now been completed and is summarized

³¹*Chem. Technol. Div. Ann. Progr. Rept. May 31, 1967, ORNL-4272, p. 185.*

in a paper that has been accepted for publication in the *Journal of Inorganic and Nuclear Chemistry*. The conclusions reported are as follows:

“Solutions of TOA and its salts extract more water than do the diluents (benzene and phenylcyclohexane) alone. All of the salts tested extract more water than does the free-base TOA, varying in the order acetate < perchlorate < nitrate < chloride < bisulfate < sulfate.

“Infrared spectra show evidence of direct interaction between the water and the sulfate ion, but not between the water and the alkyl ammonium ion, even though the organic species to which the water molecules are attached are ion pairs.

“Details of both the extraction equilibria and the spectra suggest that the extracted water is held both as definite hydrates and in simple solution. That is, the organic phase appears to contain two kinds of attachment for water differing in bond strength, one where it is rather strongly bonded to the amine salt and the water:amine ratio is little affected by variations in the amine concentration, the other where it forms rather weak hydrogen bonds and the water:amine ratio shows considerable dependence upon amine salt concentration. The normal TOA sulfate forms both mono- and trihydrates (and perhaps higher

hydrates). The other salts tested did not show hydrates higher than the monohydrate.”

The anomalous results previously reported in water extraction by tri-*n*-octylamine perchlorate,³¹ which appeared to indicate an extremely stable hydrate and also to contradict the aggregation measurements, were traced to impurities containing replaceable hydrogen. Tritium exchange with this hydrogen caused a constant additive error in the tritium-traced water analysis. The corrected water contents conform to Henry's law over the entire range of water activities.

Quaternary Ammonium Salts. — Water solubility ($a_w = 1$) increased nearly linearly from zero to 1.4 *M* and 0.75 *M* as the concentrations of tetra-*n*-heptylammonium chloride (THACl) and tetra-*n*-heptylammonium bromide (THABr), respectively, in benzene increased from zero to 0.5 *M*. The water content of a 0.1 *M* THABr solution varied linearly with water activity, $[H_2O]_{org} = 0.135 a_w$ (Henry's law constant = 0.135). However, the water content of a 0.1 *M* THACl solution varied with a power of the water activity between 2 and 3, $[H_2O]_{org} = 0.285 a_w^{2.3}$.

Both salts in (dry) benzene solution showed considerable aggregation, measured both isopiastically and by dynamic (matched thermistor) osmometer. The aggregation numbers rose nearly linearly to around 10 at 0.1 to 0.2 *M* salt, then fell gradually to around 5 at 0.6 *M* salt.

11. Chemical Applications of Nuclear Explosions

The purpose of this program is to provide research and development in selected areas of the Plowshare Program, especially those areas requiring knowledge of chemistry or metallurgical engineering to determine feasibility. Areas in which research was performed during the past year included:

1. studies of the behavior of radionuclides derived from the use of nuclear devices in the recovery of copper from ore deposits,
2. studies of the behavior of radionuclides derived from the use of nuclear devices in the recovery of oil from shales.

Knowledge of the thermal stability and the high-temperature reactions of actinide compounds is pertinent to the possible production of these compounds through the use of thermonuclear devices. A description of related studies to determine some of these data by differential thermal analysis and thermogravimetric analysis techniques appears in Sect. 5 of this report.

11.1 COPPER ORES

Fracturing of copper ore deposits with nuclear explosives, followed by leaching in place, is being studied by the Division of Peaceful Nuclear Explosives of the USAEC and by associated contractors. The Oak Ridge National Laboratory is cooperating in this program by studying potential problems that might arise from the presence of radioactive contaminants in the processing cycle. The proposed flowsheet for recovering copper includes percolating a leaching solution of dilute sulfuric acid down through the nuclear-broken ore to dissolve the copper, collecting the leach liquor at the bottom of the ore body and pumping it to the surface, recovering a copper concentrate from the solution by cementation on iron, and recycling the barren solution, after fortifying it with acid, for

use in the leaching step. The cement copper is then smelted into a consumable anode and purified by electrolysis.

Status and Progress

Previous studies^{1,2} indicated that ^{106}Ru is probably the only isotope of importance with respect to possible radioactive contamination of the copper product. The ruthenium forms volatile compounds, which are deposited on the chimney rubble upon collapse of the cavity formed by the nuclear detonation. Some of the ruthenium is dissolved by the leaching solution and cements with the copper on sheet iron. Fortunately, most of this ruthenium is rejected during the final purification of the copper by electrolysis. In recent tests simulating the conditions of an expected copper recovery system, the behavior of the radionuclides present in a sample of test-shot debris taken from high up in the chimney of broken rock was similar to that observed earlier with a sample of debris taken from near the bottom of the chimney. Ruthenium-106 was again the dominant radionuclide contaminating the cement copper. Less ruthenium contamination of the cement copper and more efficient copper cementation were obtained in batch tests by increasing the copper concentration of the leach liquors and by decreasing the amount of excess sheet iron used for cementation.

Leaching of Test-Shot Debris

A sample of nuclear-broken rock was obtained from a medium that did not contain copper; it was taken from near the center of the broken-rock chim-

¹*Chem. Technol. Div. Ann. Progr. Rept. May 31, 1966, ORNL-3945, p. 189.*

²*Chem. Technol. Div. Ann. Progr. Rept. May 31, 1967, ORNL-4145, p. 234.*

ney, about 200 ft above the detonation level. The gross gamma activity of this sample, which was measured about two years after the detonation, was about 10^4 counts $\text{min}^{-1} \text{g}^{-1}$. The activity was principally due to ^{106}Ru and ^{137}Cs ; however, small concentrations of ^{125}Sb , ^{90}Sr , and ^{144}Ce were also detected. In leaching this debris with simulated copper ore leach liquors, we found that about 50% of the ^{90}Sr and 30 to 35% of the ^{106}Ru were dissolved in the pH range 1 to 2. The amounts of dissolved ^{125}Sb and ^{137}Cs decreased from about 12% at pH 1 to 2–4% at pH 2. No ^{144}Ce was detected in the leachates.

Cementation Tests

In batch cementation tests in which samples of leach liquors from the above tests were contacted with sheet iron (detinned cans), 60 to 70% of the copper was cemented. About 8 and 14% of the ruthenium cemented with the copper at pH 2 and at pH 1 respectively. Less than 2% of the ^{90}Sr , ^{137}Cs , or ^{125}Sb cemented with the copper at these pH levels. With the exception of the ^{125}Sb results, these data agree with those obtained earlier. In the prior tests with simulated leach liquors traced with ^{125}Sb , about 14% of the antimony cemented with the copper from the liquor at pH 2.

Copper cementation efficiency increased as the copper concentration of the liquor increased in the range of 2 to 10 g per liter. In addition, the ruthenium concentrations in copper products cemented from the liquor containing 10 g of copper per liter were lower by factors of 4 to 10 than in the products obtained from the liquor containing 2 g of copper per liter.

11.2 RECOVERY OF OIL FROM SHALE

The feasibility of recovering oil from Green River oil shales by using a nuclear device to fracture the shale and then retorting the oil in place is being studied by several government agencies and commercial companies. The Oak Ridge National Laboratory is participating in this program by studying the oil recovery system with regard to the behavior of the radioactive contaminants that would be formed in the nuclear detonation.

Status and Progress

Recent studies confirmed the earlier observation³ that tritium is a major potential contaminant

of the shale oil product. Oil that was retorted from shale after extended exposure to tritiated water vapor at elevated temperature in a sealed flask was found to contain tritium; the contamination of the oil increased as the exposure temperature increased and as the shale particle size increased, but did not change significantly when the exposure time at 85°C was extended from 30 to 106 days. Treatment of contaminated shale with hot, moist air removed most of the tritium; however, when large shale pieces were treated, a portion of the tritium was driven from the outer layers more deeply into the shale. Attempts to scrub tritium from contaminated oil were unsuccessful.

Behavior of Tritium

Earlier test results² showed that exposure of oil shale at elevated temperatures to tritiated water causes the shale, as well as the oil that is subsequently retorted from the shale, to be contaminated with tritium. Studies of the variables that affect the tritium contamination were continued. Water containing 100 μC of tritium per milliliter and shale (4.8- to 8.0-mm particles), at a ratio of 1 ml/100 g, were heated in sealed flasks. Before being retorted, the shale was washed thoroughly with water and dried to remove entrained water.

The tritium contamination of oil that was retorted from shale after 25 days of exposure to tritiated water vapor was directly dependent on the temperature in the sealed reaction flask (Fig. 11.1). The oil contained 0.48, 0.67, 0.92, and 1.0 μC of tritium per gram of oil when the exposure temperatures were 45°C, 65°C, 85°C, and 97°C respectively. Increasing the exposure time at 85°C to 106 days increased the tritium concentration of the oil to only 0.93 $\mu\text{C}/\text{g}$. In tests with shale fractions both coarser and finer than the 4.8- to 8.0-mm fractions, the tritium contamination of the shale and the retorted oil increased as the shale particle size increased (Table 11.1). The surface area and the porosity of the shale samples increased as the shale size decreased, possible as the result of fractures introduced by crushing the shale. Most of the pores in the coarsest fraction were less than 1 μ in diameter, while the

³Chem. Technol. Div. Ann. Progr. Rept. May 31, 1968, ORNL-4272, p. 187.

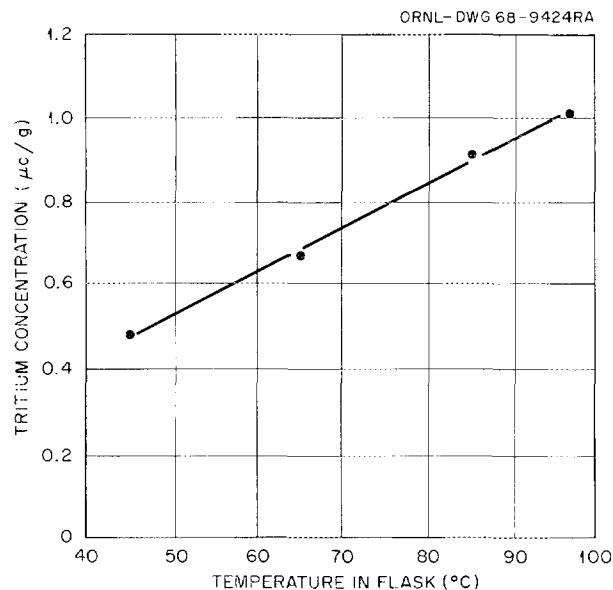


Fig. 11.1. Effect of Reaction Temperature on Tritium Contamination of Oil. Procedure: 120 g of Green River oil shale and 1.2 ml H₂O containing 120 μc of tritiated water were heated in a sealed flask for 25 days at the indicated temperatures. Oil was retorted from the washed and dried shale.

Table 11.1. Effect of Shale Particle Size on Tritium Contamination of Shale and Retorted Oil

Procedure: 120-g samples of Green River oil shale were heated at 85°C for 25 days in sealed 1-liter flasks with 1.20 ml of water containing about 115 μc of tritiated water. Oil was retorted from 100 g of the washed and dried shale samples.

Range of Shale Particle Sizes (mm)	Surface Area ^a (m ² /g)	Porosity ^a (%)	Tritium in Shale (μc/g)	Tritium in Retorted Oil (μc/g)
1.2-2.0	0.165	4.7	0.14	0.52
2.0-4.8	0.127	3.2	0.17	0.51
4.8-8.0	0.092	1.7	0.32	0.92
8.0-26	0.004	0.5	0.36	1.42

^aMeasurements made by the ORNL Analytical Chemistry Division.

other three fractions contained pores or fractures up to 17 μ in diameter.

Tritiated water penetrated to the center of a shale cube that measured about 28 mm on a side when the shale was heated with tritiated water for 25 days at 85°C. The tritium concentration decreased with depth, from 0.46 μc/g in the outer 4-mm layer to 0.13 μc/g in the center 10-mm cube.

Removal of Tritium from Shale and Oil

Although the mechanism by which tritium is held in contaminated shale is not known at this time, recent test results indicate that the reaction is reversible. Almost 92% of the tritium was removed from a sample of contaminated shale (4.8- to 8-mm particle size) by treating it for 15 days, at a shale temperature of 200°C, with a gas stream that had been saturated with water at 38°C (Fig. 11.2). About 40% of the tritium was removed from the shale in the 4 hr required to heat the shale from room temperature to 200°C, and 70% of it was re-

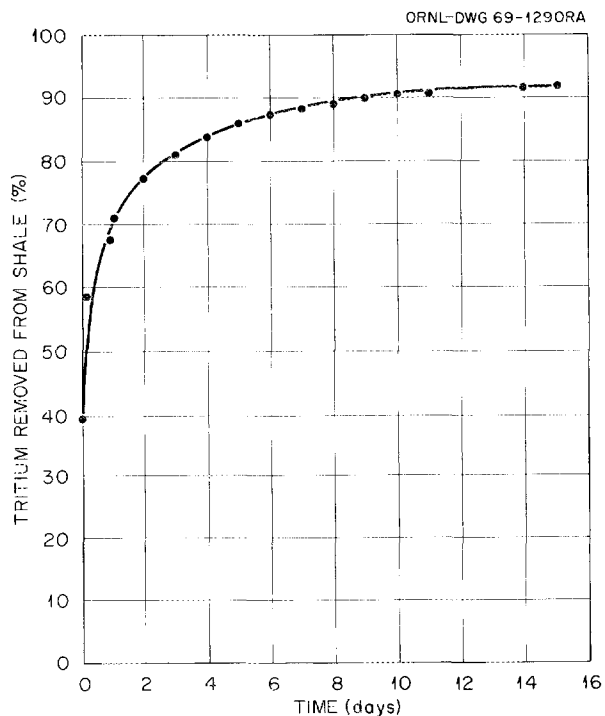


Fig. 11.2. Removal of Tritium from Shale at 200°C. Procedure: 100 g of tritiated shale (0.3 μc/g) was heated to 200°C for 15 days in a gas stream that had been saturated with water at 38°C.

moved in 24 hr at 200°C. The oil retorted from the shale after 15 days of treatment contained 0.12 μC of tritium per gram, which is equivalent to slightly more than 1% of the tritium that was added to the reaction flask at the beginning of the test. Similar results were obtained with a shale sample that was exposed to tritiated water vapor for 108 days. In this case, about 90% of the tritium was removed from the shale in 15 days of treatment at 200°C, and the oil that was retorted from the shale after this treatment contained 0.20 μC of tritium per gram.

Removing tritium by this method was less efficient for a relatively large shale cube (28 mm on a side). The cube, which had been contaminated by being heated with tritiated water vapor for 25 days at 85°C, was heated for 10 days in a sealed flask at 95°C. For 2 hr each day, water-saturated air at 95°C was passed through the flask. This treatment removed about 20% of the tritium from

the shale. Part of the remaining tritium was driven further into the shale cube; the outer 4-mm layer contained 0.39 μC of tritium per gram, and the center 10-mm cube contained 0.43 $\mu\text{C}/\text{g}$.

Tritium was also removed from contaminated shale by submerging it in hot water. Two one-week treatments at 95°C with 1 ml of water per gram of shale removed 85% of the tritium from the shale (initially 0.3 $\mu\text{C}/\text{g}$).

In contrast to the above results, tritium was not easily removed from contaminated shale oil. Refluxing the oil with water, 0.1 *N* NaOH, or 0.1 *N* H₂SO₄ for 24 hr removed only a few percent of the tritium. Failure to remove more of the tritium from the oil under these conditions tends to confirm the conclusion that the tritium is present in the oil as a part of the hydrocarbon structure rather than as tightly bound water. When the oil was distilled, the tritium concentrations in the distillate fractions were approximately equal.

12. Biochemical Separations

Macromolecular Separations

12.1 DEVELOPMENT OF REVERSED-PHASE CHROMATOGRAPHY SYSTEMS FOR SEPARATING TRANSFER RIBONUCLEIC ACIDS

The continuing search for new ion exchange materials that are capable of being incorporated into reversed-phase chromatography (RPC) systems has led to the investigation of a series of phosphonium analogs of the quaternary ammonium salts currently employed in existing RPC systems. Of the three compounds studied, one, trioctylmethylphosphonium dimethylphosphate, has proved to be useful. The other two in this series, triphenylbenzylphosphonium chloride and 1,2-ethylenebis-(triphenylphosphonium) dibromide, were found to be soluble in NaCl solutions and thus were not applicable for use in RPC systems.

Successful results have been obtained with an RPC system employing 6.5 wt % trioctylmethylphosphonium dimethylphosphate on acid-washed, dimethyldichlorosilane-treated, 100- to 120-mesh Chromosorb W. The packing was prepared by evaporative deposition of the ion exchanger from chloroform solution and poured into a 1- by 240-cm jacketed column. It was then equilibrated with NaCl solution in order to exchange the dimethylphosphate anion for chloride. Chromatograms were developed by the NaCl gradient elution technique described in previous progress reports. A typical chromatogram of *E. coli* tRNAs obtained by using this system is shown in Fig. 12.1. The capacity of this phosphonium system for resolving tRNAs is as high as that for the quaternary ammonium RPC systems, and the tRNA elution sequence is similar to that obtained on RPC-3 columns employing trioctylpropylammonium bromide. Good resolution of tRNAs by the system is demonstrated by the multiplicity of peaks present for certain tRNAs (e.g., leucine tRNA and arginine tRNA). An unusual feature is the wide separation of the two alanine tRNAs. A total of six chromatograms

were run on one column. In the last two runs the chromatographic resolution tended to decrease, probably as the result of a progressive loss of ion exchanger from the column.

12.2 ENGINEERING SCALEUP OF BIOLOGICAL MACROMOLECULAR SEPARATIONS TECHNIQUES

Purification of Formylmethionine and Valine tRNAs from *E. coli* B

In the first campaign for the production of purified tRNAs from *E. coli* B described last year,¹ approximately 0.5 ton of cells was grown in a fermenter in a minimal media and processed to yield about 500 g of crude tRNA. This mixture was fractionated by RPC-1 reversed-phase chromatography (dimethyldilaurylammonium chloride in isopentyl acetate on Chromosorb G, AW-DMCS) to yield purified phenylalanine tRNA. Most of the tRNAs were eluted from the RPC-1 column ahead of the phenylalanine tRNA; they were collected, precipitated with ethanol, recovered by centrifugation, and stored at -20°C for further processing.

A previously described procedure¹ for the recovery of formylmethionine and valine tRNAs was successfully scaled up, and the tRNA₁^{fMet}, tRNA₂^{fMet}, and tRNA^{Val} were recovered from the remaining *E. coli* B tRNAs on hand. The tRNAs were first separated on an RPC-3 column (trioctylpropylammonium bromide on Chromosorb G, AW-DMCS) to yield purified tRNA₁^{fMet} and a tRNA₂^{fMet}-tRNA^{Val} mixed pool. The major part of the processing was done on a 10- by 100-cm column. As shown in Fig. 12.2, the resolution obtained was equal to, or better than, that obtained

¹Chem. Technol. Div. Ann. Progr. Rept. May 31, 1969, ORNL-4272, pp. 194-97.

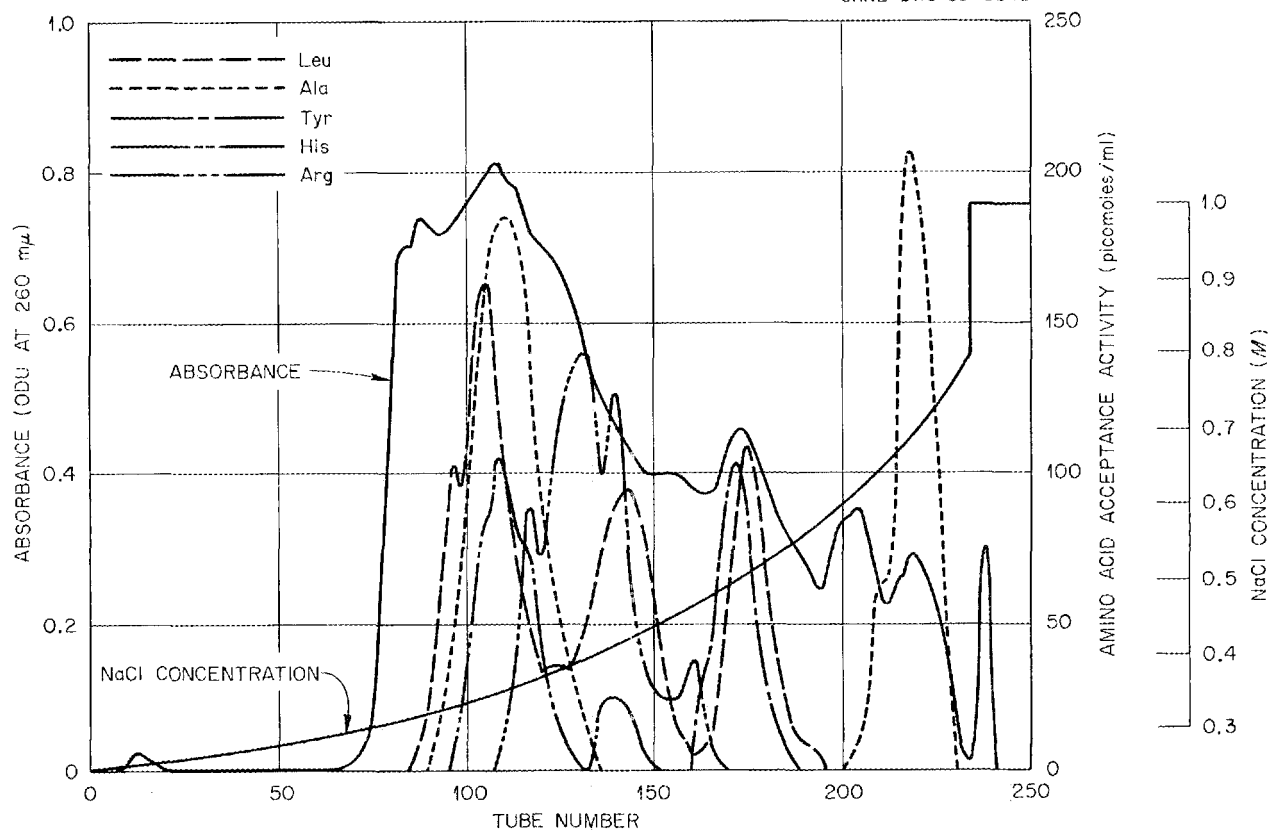


Fig. 12.1. Chromatogram Showing Separation of *E. coli* B tRNAs on Trioctylmethylphosphonium Dimethylphosphate Reversed-Phase System. Twelve hundred A_{260} units of crude *E. coli* B tRNA in 50 ml of 0.25 M NaCl solution were applied to a 1- by 240-cm column at 37°C. Three liters of a gradient solution having a NaCl concentration that increased from 0.25 M to 0.80 M was used to elute the column at the rate of 1.5 ml/min. All solutions were 0.01 M in $MgCl_2$, 0.01 M in Tris-HCl buffer (pH 7.0), and 0.002 M in $Na_2S_2O_3$. Fifteen-milliliter fractions were collected. The eluate was monitored at 260 mμ, and the activities of the indicated amino acid accepting tRNAs were assayed under standard conditions.

with smaller experimental columns. A number of runs were made with feed consisting of the mixed tRNAs as stored, while about an equal number were made with feed that had been upgraded by DEAE-cellulose column chromatography to concentrate the methionine and valine tRNAs. In early processing runs, the separation obtained between $tRNA_1^{fMet}$ and $tRNA_2^{fMet}$ was very sharp, and the ratio of peak heights of $tRNA_1^{fMet}$ to $tRNA_2^{fMet}$ was about 1.5. About midway through the processing, however, the separation markedly deteriorated and the ratio decreased to about 0.8; the time at which these changes occurred can be correlated with changes in the batches of mixed tRNA feed. Apparently,

$tRNA_2^{fMet}$ is a degradation product of $tRNA_1^{fMet}$, other evidence suggests damage to the 4-thiouridine nucleotide in $tRNA_1^{fMet}$.

The bulk of the $tRNA_1^{fMet}$ was of product grade after being processed on the RPC-3 column; however, the $tRNA_2^{fMet}$ - $tRNA^{Val}$ mixture and some lower-grade $tRNA_1^{fMet}$ were further purified by rechromatography on RPC-4 columns (dimethyldilaurylammonium chloride on Chromosorb G, AW-DMCS). The final products were 860 mg of $tRNA_1^{fMet}$ at essentially 100% activity, 550 mg of $tRNA_2^{fMet}$ at 93% activity, and 700 mg of $tRNA^{Val}$ at 89% activity. (Activity is the amino acid acceptance divided by the terminal adenosine content.)

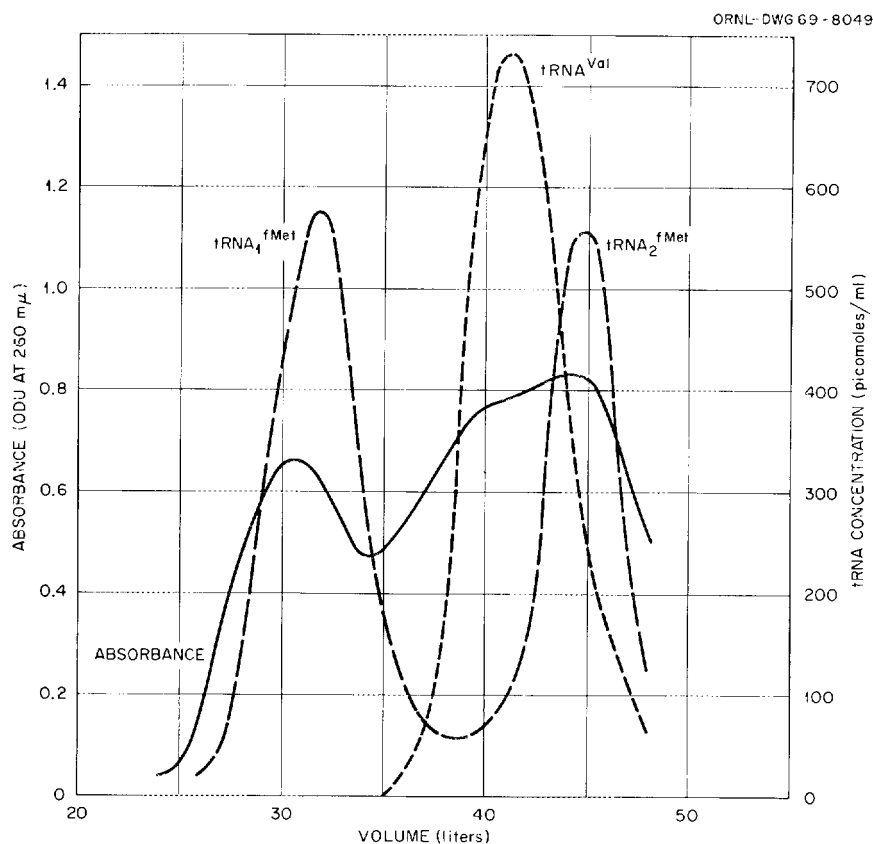


Fig. 12.2. Separation of Formylmethionine and Valine tRNAs on an RPC-3 Column. Column was 10×100 cm and maintained at 37°C . 71,000 A_{260} units of tRNA were loaded and then eluted with a 50-liter gradient from 0.250 M NaCl to 0.281 M NaCl at 16 ml/min flow rate. The eluents were also 0.01 M in MgCl_2 and 0.01 M in Tris-HCl buffer, pH 7.0.

Preparation of Crude tRNAs from *E. coli* K-12 M07

An improved flowsheet, shown in Fig. 12.3, was evaluated for the recovery of crude tRNA. The procedure involves (1) semicontinuous growth in a 350-liter fermenter, (2) phenol extraction of the harvested cells, (3) ethanol precipitation, and (4) DEAE-cellulose chromatography to yield three pools of partially purified tRNAs. The phenol extraction was carried out with mild agitation on a less-concentrated cell slurry from which the aqueous phase containing the tRNAs separated by gravity, thus eliminating a troublesome centrifugation step. Further, DNA contamination was reduced, and the fractional precipitation with isopropanol, with concomitant loss of tRNAs, was

eliminated. All solutions contained 0.002 M sodium thiosulfate to minimize oxidation of labile sulfur-containing nucleotides in tRNAs. The size of the DEAE-cellulose column was increased to 6×30 in., which permitted as much as 70 g of crude tRNA per run to be partially purified by sodium chloride gradient elution. The eluted fractions were pooled to optimize the concentration of methionine tRNAs in pool A, phenylalanine tRNAs in pool B, and tyrosine tRNAs in pool C.

Typical results for the processing of 77 kg of *E. coli* K-12 M07 cells and the recovery of tRNAs after the DEAE-cellulose chromatographic step are shown in Table 12.1. The overall yield of crude tRNAs was about fourfold greater than that obtained with the previous flowsheet. The recovery of tRNAs across the DEAE-cellulose

column was about 80%, and, except for pool C, the DNA contamination was reduced to less than 1%. The specific activities of the methionine and phenylalanine tRNAs in their respective pools were more than doubled.

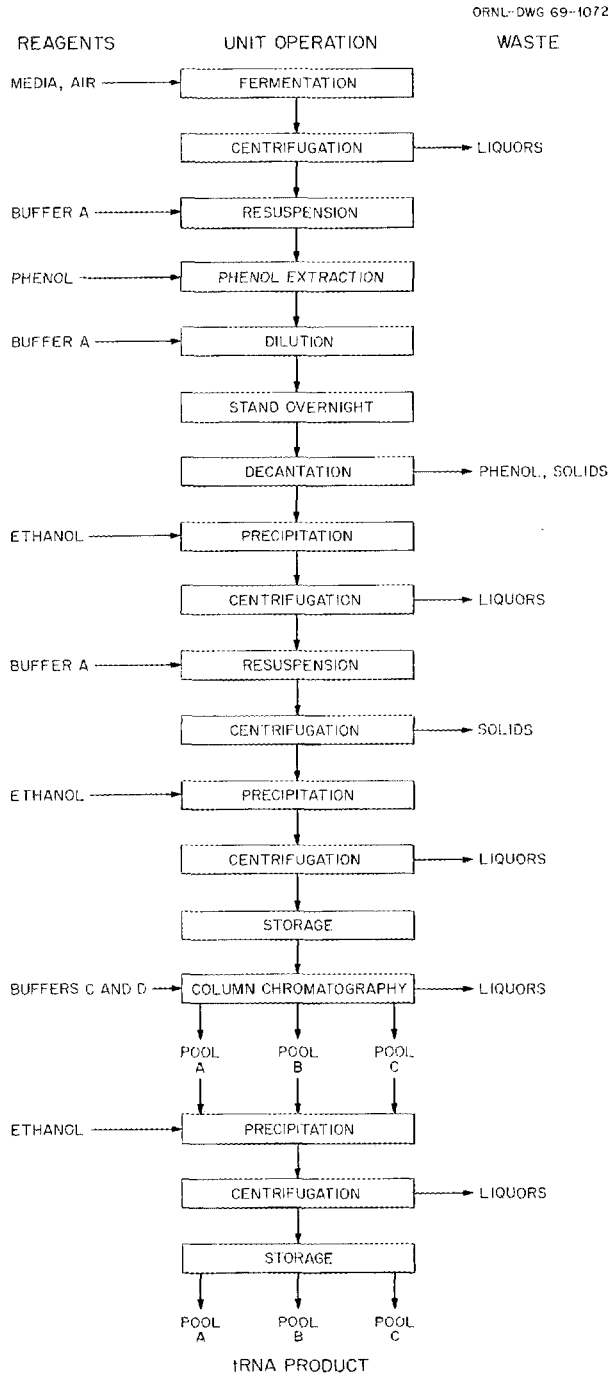
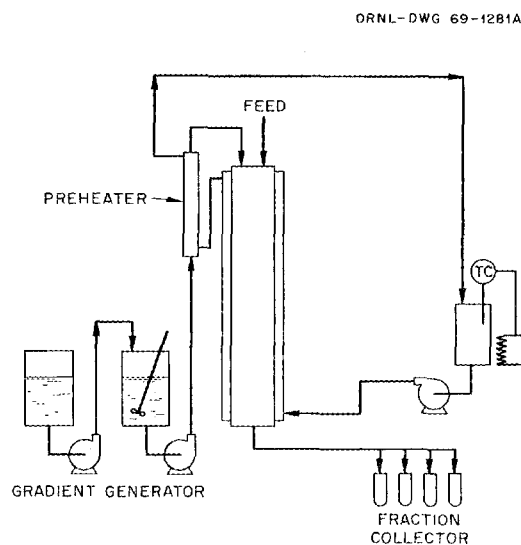


Fig. 12.3. Improved Process Flowsheet for the Recovery of tRNAs.

Recovery and Purification of Two Phenylalanine tRNAs from *E. coli* K-12 M07

After DEAE-cellulose chromatography, the phenylalanine-tRNA-enriched fractions from pool B (see previous subsection), were concentrated by ethanol precipitation and stored at -20°C until they could be used as feed for the recovery of phenylalanine tRNA by reversed-phase chromatography on the RPC-4 system. A schematic of the RPC-4 system used is shown in Fig. 12.4. The column is a length of jacketed glass pipe, 2 in. \times 8 ft, maintained at 37°C . In order to obtain good resolution, a preheater was added to heat the eluents to 37°C before they entered the column. In a typical run, 5 to 8 g of pool B feed in a solution having a low sodium chloride concentration was pumped onto the column, and the chromatogram was then developed by sodium chloride gradient elution.

Early tests of the RPC-4 column had been made with pool B phenylalanine tRNAs obtained from two batches of *E. coli* K-12 M0 cells. These feeds yielded a single phenylalanine tRNA peak with a maximum specific activity as high as 1800 picomoles phenylalanine accepted per A_{260} unit, a value far higher than values previously obtained.



COLUMN—2 in. \times 8 ft—0 in.
 FEED—150,000 ODU OF MIXED tRNA IN 500 ml 0.52 M NaCl SOLUTION.
 FLOW RATE—32 ml/min
 GRADIENT—8 hr WASH AT 0.52 M NaCl, THEN 70 μ TO 0.62 M NaCl.

Fig. 12.4. Flowsheet for the Separation of Phenylalanine tRNAs on a Large RPC-4 Column.

Table 12.1. Typical Data for Purification of tRNAs on a Large DEAE-Cellulose Column

	Feed	Pool A	Pool B	Pool C	Total (A + B + C)
A_{260} units, total	109×10^4	41×10^4	40×10^4	13×10^4	93×10^4
A_{260} units, %	100	38	36	11	85
RNA/DNA ratio	5.3	120	270	20	
Amino acid accepting activity, picomoles/ A_{260}					
Methionine	93	213	0	0	
Valine	134	186	56	0	
Phenylalanine	39	0	86	0	
Tyrosine	27	0	45	78	
Distribution of tRNAs, %					
Methionine	100	87	0	0	87
Valine	100	59	9	0	68
Phenylalanine	100	0	81	0	81
Tyrosine	100	0	62	13	75

However, later batches of pool B feed, prepared from *E. coli* K-12 M07 cells grown in a somewhat different fermentation media, yielded lower specific activities and showed two phenylalanine tRNA peaks. Peak activities of a maximum of 1000 to 1400 picomoles/ A_{260} were obtained in several runs.

The phenylalanine tRNAs from the pool B feed obtained from 77 kg of *E. coli* K-12 M07 (see previous subsection) were recovered in a total of 12 runs on the large RPC-4 column. Figure 12.5 shows that the two phenylalanine tRNA peaks were clearly resolved. The specific activities of the two peaks were about 950 and 1100 picomoles/ A_{260} respectively. The two phenylalanine tRNA peaks and the tyrosine tRNA peak were pooled separately. A total of 920 mg of tRNA₂^{Phe} with an activity of 78% and 400 mg of tRNA₁^{Phe} with an activity of 43% were obtained.

Basic Separation Data Using DEAE-Cellulose

Although DEAE-cellulose has been used for a number of years as an ion exchange material in column chromatography to separate various types of materials in addition to tRNAs, little fundamental information is available about its basic equilibria and kinetics. The distribution of tRNAs

between DEAE-cellulose and buffered NaCl solution has been determined both by batch elution and by continuous flow elution² from a column, using a NaCl solution of constant concentration. Normally, gradient elution is used in which the NaCl concentration is increased as the elution proceeds. Since the entire spectrum of tRNAs can be eluted at a constant NaCl concentration,

²P. B. Hamilton *et al.*, *Anal Chem.* **32**, 1782 (1960).

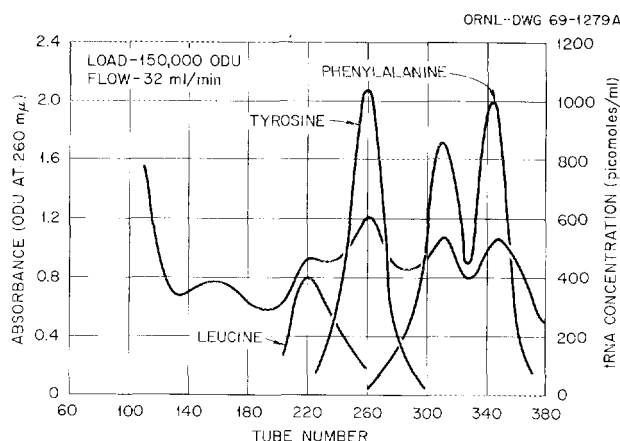


Fig. 12.5. Separation of Two Phenylalanine tRNAs from *E. coli* K-12 M07 on an RPC-4 Column. The column was 2 in. \times 8 ft, and was maintained at 37°C.

Table 12.2. Data for Separation of tRNAs on DEAE-Cellulose

Elution Method	NaCl Concentration (M)	Distribution Coefficient, ($\frac{\text{Concentration in Packing}}{\text{Concentration in Solution}}$)			Single Stage Separation Factor, (Ratio of Distribution Coefficients)		
		Met	Val	Phe	Met/Val	Met/Phe	Val/Phe
		Batch	0.25	3.9	7.8	10.0	2.1
Batch	0.30	2.1	3.5	7.1	1.8	3.4	2.0
Column, 25 cm	0.30	7.5	13.4		1.8		
Column, 25 cm	0.32	3.0	5.0	10.9	1.7	3.6	2.2
Column, 210 cm	0.32	3.5	5.5	9.3	1.6	2.7	1.7

although at increased volumes, the process can be considered to be multistage. Our data (Table 12.2) show that the distribution coefficients decrease with increasing NaCl concentration, which is consistent with the chromatograms produced by gradient elution. The coefficients from the column elutions are consistently higher than those from the batch experiments because of kinetic effects. Coefficients calculated from data obtained in 25- and 210-cm-long columns were in good agreement. The separation factors (ratio of distribution coefficients) for pairs of tRNAs were relatively insensitive to NaCl concentration, column length, or method of elution (batch vs continuous). The height of a theoretical stage, slightly less than 1 cm, was nearly the same for different tRNAs. This value is much larger than that usually experienced in ion exchange chromatography, indicating that diffusion is the limiting exchange rate for large molecules such as tRNAs.

12.3 SEPARATION OF TRANSFER RIBONUCLEIC ACIDS FROM *B. subtilis* A-12

It would be of considerable interest to compare the chemical, physical, and biological properties of samples of purified tRNAs for a given amino acid obtained from different organisms. Phenylalanine tRNA from *E. coli* B and from *E. coli* K-12 M07 has previously been separated and purified by RPC-1 and RPC-4 chromatography; thus, the isolation of phenylalanine tRNA from other microorganisms is now being investigated. Crude tRNA has been prepared from *B. subtilis* A-12, using

the improved recovery method described in Sect. 12.2. This method is a general one that can be used, without modification, to isolate tRNAs from most microorganisms. About $900 \times 10^3 A_{260}$ units of crude tRNA were obtained from approximately 4 kg of *B. subtilis* A-12 cells. The chromatographic separation of this crude tRNA on an RPC-4 column is shown in Fig. 12.6. Sharp peaks were obtained for five tRNAs, three of which showed multiple peaks. Experiments are now under way to define conditions for isolating purified phenylalanine and tyrosine tRNAs.

12.4 SEPARATION OF AMINOACYL-RNA SYNTHETASES

During the past year, a program to isolate the 20 aminoacyl-RNA synthetases from *E. coli* was begun. The synthetases, which are companions to the tRNAs that have already been purified and to some of the tRNAs that will be purified in the future, are of particular interest. They will be used as tools in helping to isolate the tRNAs and as components in the biochemical studies of the synthetase-tRNA complexes.

Flowsheets that had been used for the separation of several of the individual aminoacyl-RNA synthetases were reviewed, and their steps were combined to form a general flowsheet that would permit any one, or a small group, of the synthetases to be isolated. The resulting flowsheet (see Fig. 12.7) can be scaled up so that any size batch of *E. coli* can be processed.

In order to evaluate the flowsheet, a 300-g batch of *E. coli* cells was slurried in 1 liter of 0.01 M

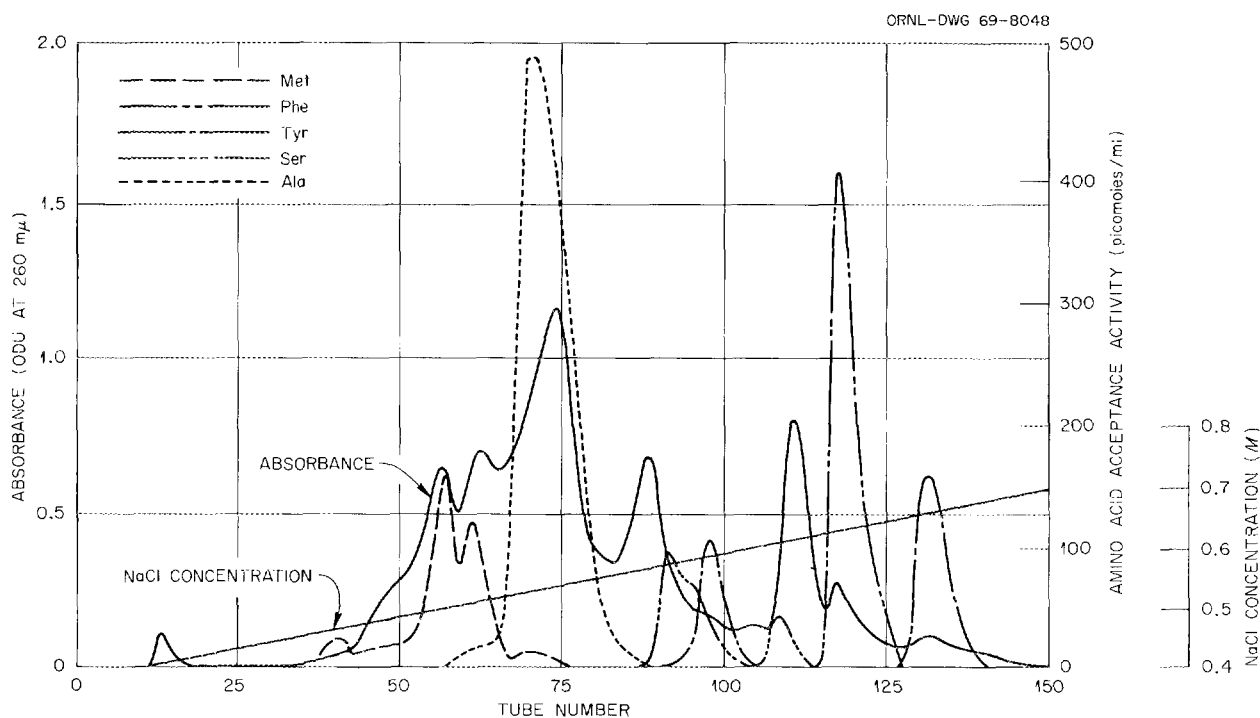


Fig. 12.6. Chromatogram Showing Separation of *B. subtilis* tRNAs on an RPC-4 Column. One thousand A_{260} units of *B. subtilis* A-12 crude tRNA in 0.45 M NaCl solution were applied to a 1- by 240-cm RPC-4 column at 37°C. Three liters of a gradient solution having a NaCl concentration that increased from 0.45 M to 0.80 M was used to elute the column at the rate of 2.5 ml/min. All solutions were 0.01 M in $MgCl_2$, 0.01 M in Tris-HCl buffer (pH 7.0), and 0.002 M in $Na_2S_2O_3$. Fifteen-milliliter fractions were collected. The eluate was continuously monitored at 260 $m\mu$, and the amino acid accepting activities of selected fractions were subsequently assayed.

Tris-HCl buffer (pH 7.5) containing 10% glycerol. The slurry was extruded through a Gaulin press under a pressure of 10,000 psi, which ruptured the cells. The cell debris was then removed by low-speed centrifugation. The DNA and the RNA in the cell extract were precipitated by the addition of a solution of streptomycin sulfate, and were removed by centrifugation. The synthetases were separated from the bulk of the other proteins by fractional precipitation with ammonium sulfate, and by fractional adsorption and elution on hydroxylapatite. Further purification and separation into individual synthetases or small groups of synthetases were accomplished by elution chromatography on columns of DEAE-cellulose, followed by rechromatography on hydroxylapatite.

Efforts to isolate and purify leucyl-RNA synthetase have been only partially successful. Although the enzyme has been isolated, it has been shown to be extremely labile. Its activity

after these purification steps showed only an eightfold increase. Methionyl-RNA synthetase, one of the other desired synthetases, is more stable. Its activity was increased 50-fold; however, complete isolation from the tyrosyl-RNA and the phenylalanyl-RNA synthetases has not been accomplished.

12.5 SEPARATION OF RIBOSOMAL RIBONUCLEIC ACIDS

A program to develop methods for separating ribosomal ribonucleic acids (rRNAs) was started. The major rRNA components are identified from their sedimentation behavior as 16S and 23S molecules. The three major aspects of the program involve preparation of the bulk rRNA from the cells, separation of the component rRNAs, and development of the necessary analytical techniques and methods.

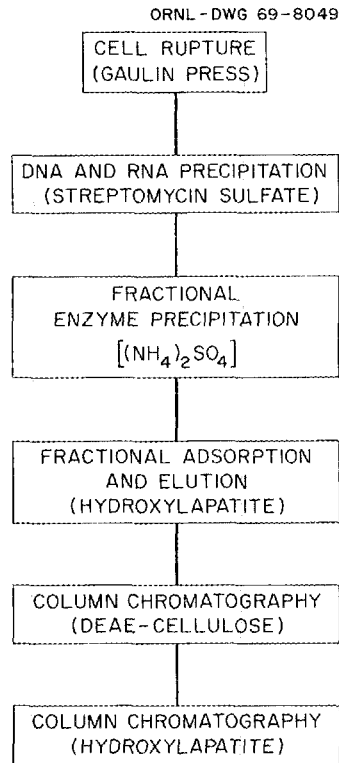


Fig. 12.7. General Flowsheet for Separating Aminoacyl-RNA Synthetases from *E. coli*.

Gram quantities of rRNA were prepared from *E. coli* cells. Initially, *E. coli* strain B was used. More recently, a nuclease-deficient strain, Q-13, was used to reduce any enzymatic degradation of the rRNA. After growth, the cells were ruptured with a Gaulin press, and the cell debris was removed by centrifugation. The ribosomes were recovered from the supernate by high-speed centrifugation ($80,000$ to $100,000 \times g$) for 3 to 4 hr. In one run, in which a model K-II zonal ultracentrifuge was used for the ribosome recovery, approximately 250 g of wet ribosomes was prepared.

The total ribosomal RNA was obtained from the ribosomes by utilizing a phenol extraction procedure. In this procedure, the ribosomes were suspended in a buffer solution and deproteinated with 0.5 to 2% sodium dodecyl sulfate. Macaloid was added to reduce nuclease activity, and then the solution was stirred with an equal volume of 88% phenol. Phase separation was enhanced by centrifugation. After the aqueous phase had been reextracted with fresh phenol, the total RNA was precipitated from this phase by the addition of

three volumes of cold ethanol. The solid obtained on centrifugation was dissolved in 0.1 M sodium acetate solution; then enough sodium acetate was added to the solution to increase its concentration to 2 M. This procedure precipitates primarily rRNA, leaving most of the lower-molecular-weight material (tRNA and 5S RNA) in solution. The precipitate was washed with ethanol, partially dried, and stored at -20°C as a moist solid.

Separation methods that have been studied include gel permeation chromatography and reversed-phase chromatography. Dextran gels (Sephadex), beaded agarose, and porous glass beads were evaluated in the gel permeation studies. Sephadex G-100 was found to be useful in separating low-molecular-weight components from the rRNA preparation. Using this medium, the 16S and 23S rRNAs were eluted in a column void volume, while lower-molecular-weight components permeated the gel and were eluted later. Partial separation of rRNAs was obtained on beaded agarose; best results were obtained on a 6% (nominal) agarose column (Bio-Rad A-5m).

Reversed-phase chromatographic systems that previously proved to be useful for tRNA separations have been studied for possible application to rRNA separations. Generally, these systems consist of a quaternary ammonium salt supported on an inert packing. Compounds which have been tried include dimethyldilaurylammonium chloride (Aliquat 204), trioctylpropylammonium bromide, and tricaprylylmethylammonium chloride (Adogen 464). The system that has been studied most extensively, and appears to be the most promising, is designated RPC-2; it uses tricaprylylethylammonium chloride dissolved in Freon 214 and supported on acid-washed, dimethyldichlorosilane-treated, 100- to 120-mesh Chromosorb W. A typical chromatogram obtained, at 5°C , on a 1×240 cm column is shown in Fig. 12.8. The eluent consisted of a 0.05 M Tris-HCl buffer (pH 7.5) that was 0.01 M in MgCl_2 and 3 M in urea, and had an NaCl concentration that increased from 0.35 M to 0.65 M.

A polyacrylamide gel electrophoresis technique has been adapted for rRNA separation and identification on an analytical scale. Density gradient centrifugation, which has been used as an analytical technique, is also being considered as a possible separation technique. Figure 12.9(a) shows a chromatogram obtained by reversed-phase chromatography, and Fig. 12.9(b) shows the elec-

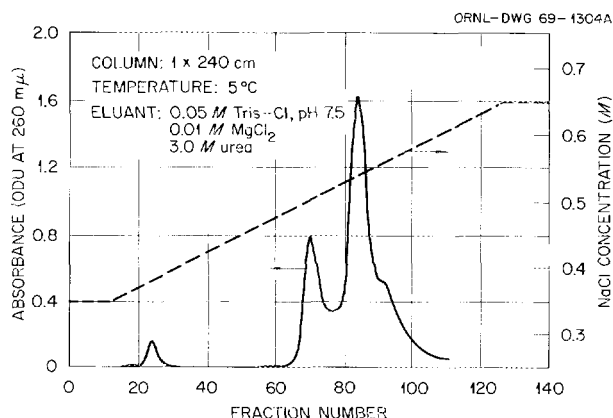


Fig. 12.8. Chromatogram Showing Separation of rRNA on an RPC-2 Column. Column size, 1 by 240 cm; temperature, 5°C; eluent: 0.05 M Tris-HCl buffer (pH 7.5), 0.01 M MgCl₂, 3.0 M urea, and 0.35 M to 0.65 M NaCl.

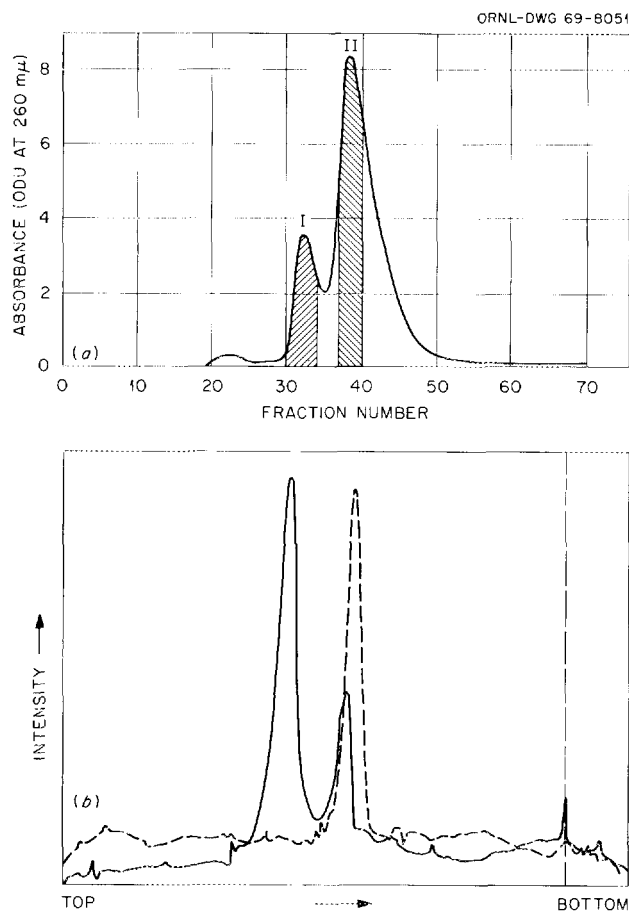


Fig. 12.9. (a) Reversed-Phase Chromatogram of rRNA; (b) Analysis of Pooled Fractions I and II by Gel Electrophoresis; Pool I, -----; Pool II, —————.

trophoresis patterns obtained for pooled fractions I and II, using a 2% acrylamide–0.5% agarose gel. Fraction I (i.e., the material corresponding to the peak near the front of the chromatogram) gave a single peak on electrophoresis, as shown by the dashed line. Fraction II contained a higher-molecular-weight component along with a significant amount of the lower-molecular-weight material associated with the first peak. It appears, therefore, that the rRNAs are eluted from the reversed-phase column according to size, the lower-molecular-weight component being eluted first.

Body Fluids Analysis

In order to take advantage of recent advancements in the medical sciences, the supporting clinical laboratory must have more-selective and more-sensitive analytical techniques. Increasing demands for medical services will also require that these techniques and other laboratory procedures be highly automated, accurate, and as rapid as is practical. The development of instrumentation to meet these needs is the objective of the Body Fluids Analysis Program.

At present, our efforts are directed toward the development of high-resolution automated analyzers for clinical application; emphasis is on techniques that result in the determination of a large number of constituents. The initial effort has involved the determination of low-molecular-weight constituents of body fluids and has resulted in the development of two separate analytical systems: an analyzer for ultraviolet (uv)-absorbing constituents and an analyzer for carbohydrates.

12.6 PROTOTYPE ANALYZERS

Prototype systems for both the uv analyzer³ and the carbohydrate analyzer,⁴ each of which is designated model Mark II, have been designed. The designs have been documented, and three uv ana-

³Prints available as CAPE-1753 from the Clearinghouse for Federal Scientific and Technical Information, U.S. Department of Commerce, 5285 Port Royal Road, Springfield, Va. 22151.

⁴Prints available as CAPE-1779 from the Clearinghouse for Federal Scientific and Technical Information, U.S. Department of Commerce, 5285 Port Royal Road, Springfield, Va. 22151.

lyzer prototypes and one carbohydrate analyzer prototype have been built for evaluation in other laboratories (see Figs. 12.10 and 12.11).⁵⁻⁸

Both analytical systems use heated high-pressure (up to 4000 psi) anion exchange columns for separation, elution with a buffer whose concentration

increases with time for separating and transporting the constituents of the sample, and a recording photometer for detection. Samples are introduced

⁷Chem. Technol. Div. Ann. Progr. Rept. May 31, 1968, ORNL-4272, pp. 201-17.

⁸C. D. Scott, R. L. Jolley, W. Wilson Pitt, and Wayne F. Johnson, "Prototype Systems for the Automated, High-Resolution Analyses of UV-Absorbing Constituents and Carbohydrates in Body Fluids," presented at the First Annual Symposium on Automated, High-Resolution Analyses in the Clinical Laboratory, held at Oak Ridge National Laboratory, March 13-14, 1969; to be published in the *American Journal of Clinical Pathology*.

⁵C. D. Scott et al., *Body Fluids Analyses Program Progress Report for the Period March 1 to August 31, 1968*, ORNL-TM-2372 (April 1969).

⁶C. D. Scott et al., *Body Fluids Analyses Program Progress Report for the Period September 1, 1968, to February 28, 1969*, ORNL-TM-2551 (July 1969).

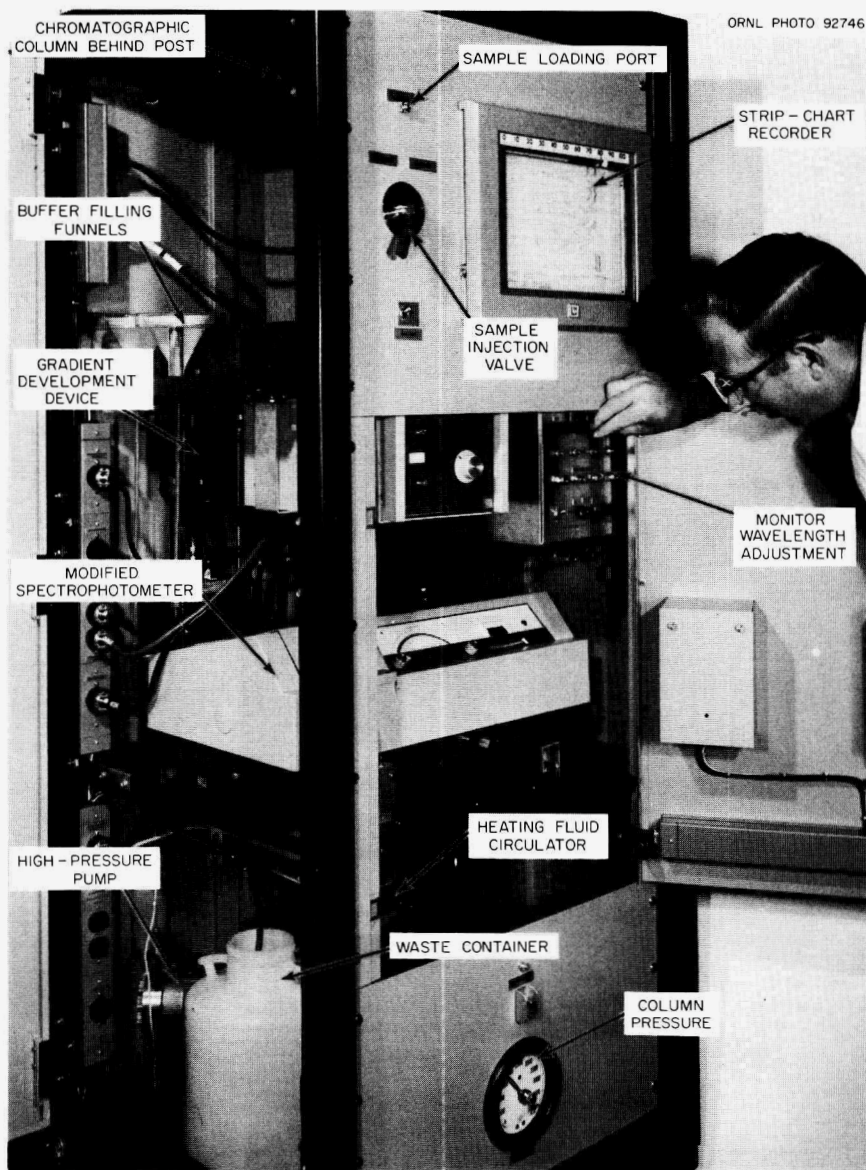


Fig. 12.10. UV-Analyzer Prototype Model Mark II.

into each system by injecting a measured volume (0.5 to 2.0 ml) of the sample, via an automatic six-port injection valve, into the high-pressure eluent stream just ahead of the separation column.

One uv analyzer prototype system is being evaluated by the Department of Medicine, Duke University Medical Center, where it is being used in their investigation of inborn errors of metabolism. Another uv analyzer prototype will be used at the Clinical Center, NIH, for in-depth analysis of urine from hospital patients, and the third will be

used in the Department of Pediatrics at Johns Hopkins University Medical Center.

At the Clinical Center, NIH, where a carbohydrate analyzer prototype was installed to analyze urine from hospital patients, over 1000 hr of satisfactory operation has been achieved.

The first assembled model of a new advanced uv analyzer, designated model Mark III, which incorporates new design and operating features that have been developed during the past year, is now undergoing initial testing at ORNL (Fig. 12.12).

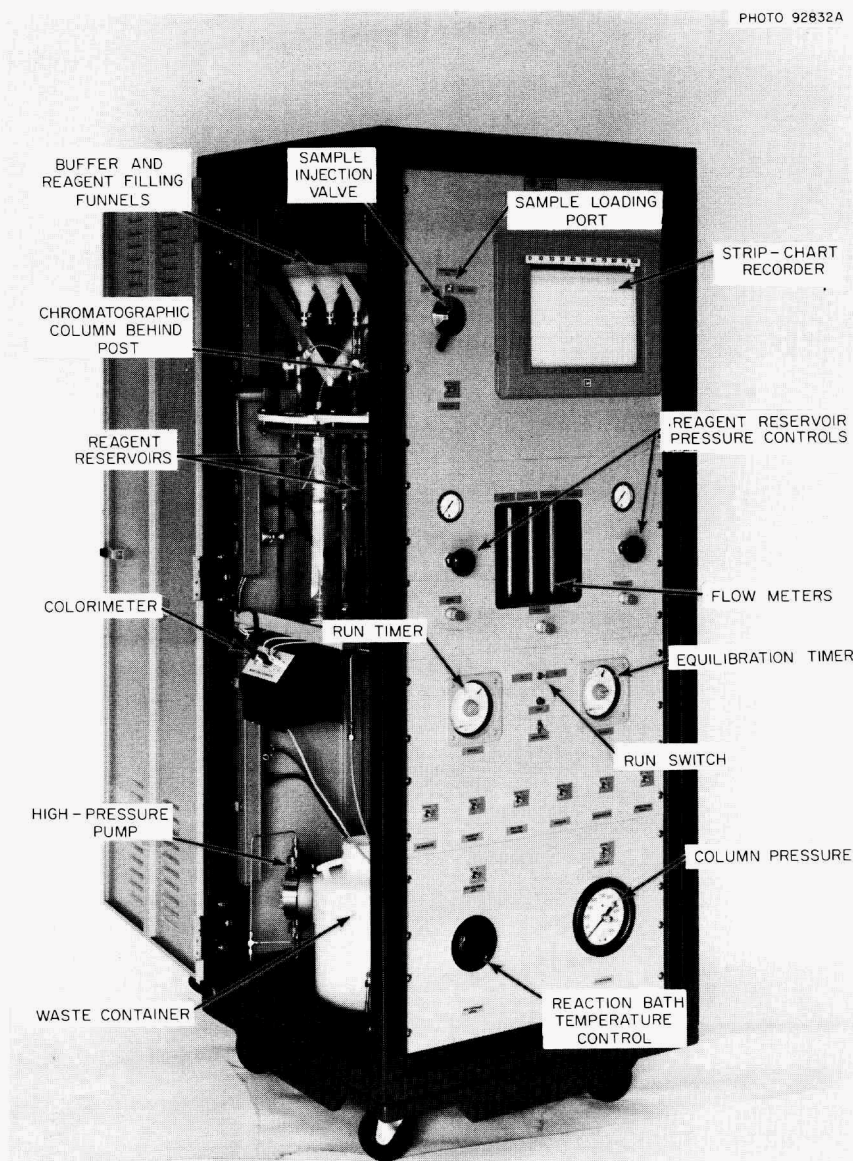


Fig. 12.11. Carbohydrate Analyzer Prototype Model Mark II.

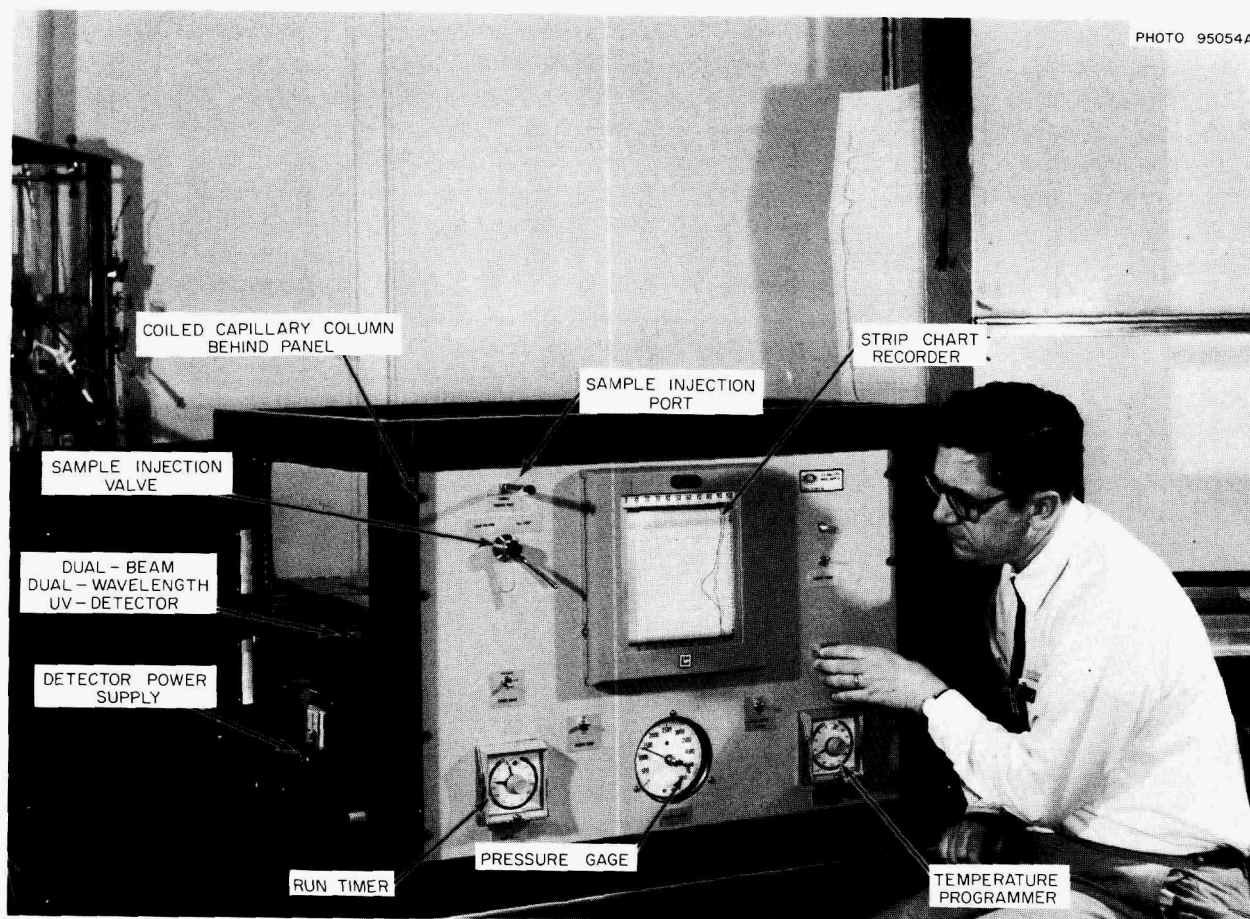


Fig. 12.12. Advanced UV-Analyzer Model Mark III.

Unique features are an electrically heated, coiled capillary column, a sample injection valve that is capable of operation at a pressure of 5000 psi, and a miniaturized uv detector.

of ammonium acetate for sodium acetate in the eluent used with the uv analyzer has resulted in more effective resolution (Fig. 12.13).

12.7 SEPARATION SYSTEMS

Ion Exchange Resin

Additional batches of type 1 anion exchange resin have been obtained from Bio-Rad Laboratories. This resin, designated as Aminex A-15 (by Bio-Rad), is now available to the general public. We have processed the new batches of resin, which had been sized to less than 10μ in diameter by the manufacturer, to remove the less than $5\text{-}\mu$ -diam fraction by elutriation.⁹

The Aminex A-15 resin with an average particle diameter of 7μ in a 0.62-cm -diam by 150-cm -long column now constitutes the standard separations system for both the uv and the carbohydrate analyzers. The use of this resin and the substitution

Dynamic Packing of Ion Exchange Columns

When finely divided ion exchange resin ($<10 \mu$ diam) is used, nonhomogeneous packing of the ion exchange column can be a problem. To circumvent this problem, we have developed a technique of dynamic packing in which the ion exchange particles are forced into the packed bed in a flowing fluid at a velocity much greater than the settling velocity of the particles.¹⁰

⁹C. D. Scott, "Continuous Separation of Ion-Exchange Resin into Size Fractions by Elutriation with Water," *Anal. Biochem.* **24**, 292 (1968).

¹⁰C. D. Scott and N. E. Lee, "Dynamic Packing of Ion Exchange Chromatographic Columns," *J. Chromatog.* (in press).

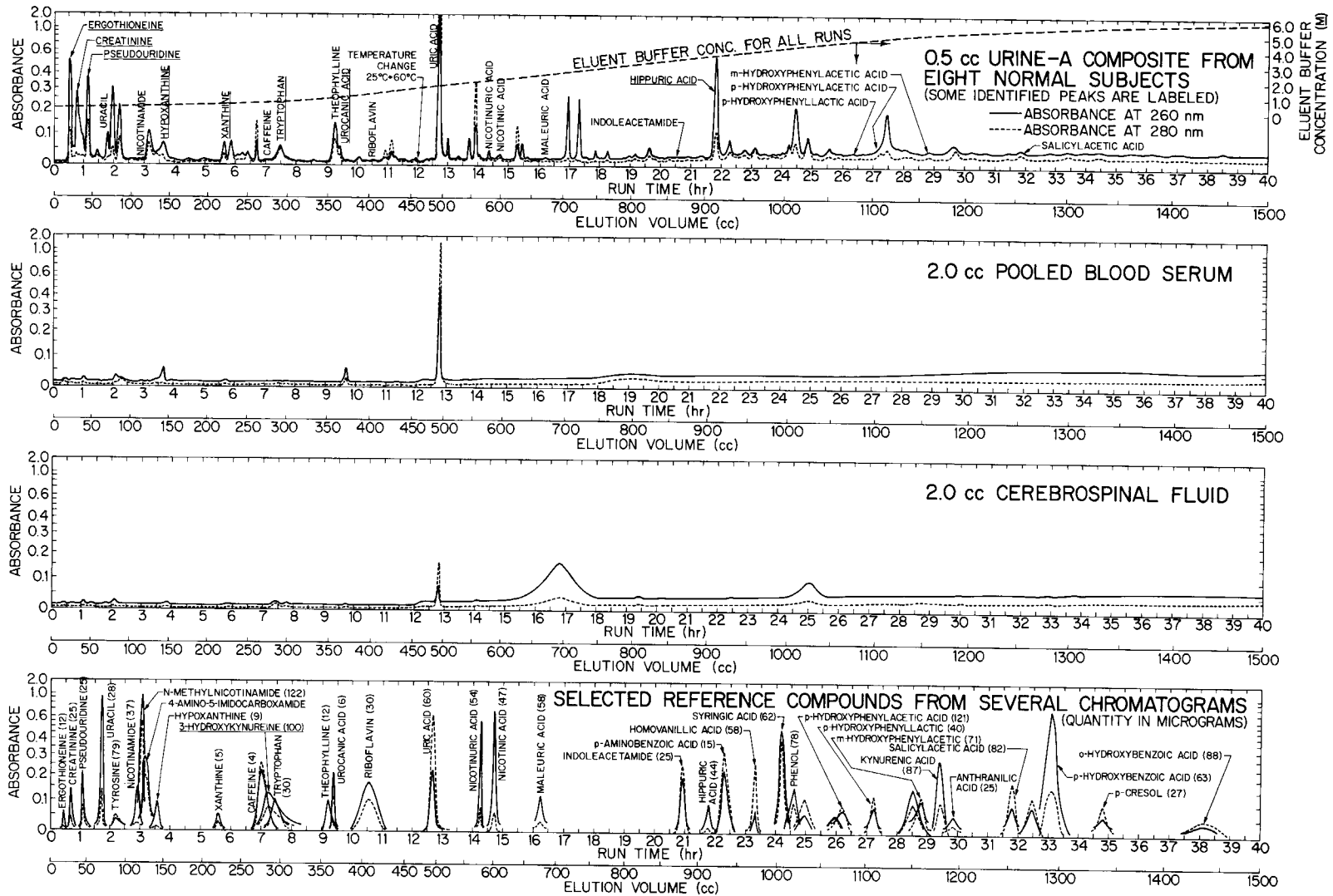


Fig. 12.13. Typical Chromatograms from the UV-Analyzer Showing the Difference Between Urine and Other Body Fluids and the Identification of Some Chromatographic Peaks.

Chromatographic columns using ion exchange resin can be packed dynamically either by displacing a thick slurry or by extruding a prepacked bed.

Dynamic packing with a slurry is accomplished by connecting a chamber or reservoir to the chromatographic column, filling the chamber with a thick slurry of the ion exchange resin, and then displacing the slurry into the column with a liquid that is pumped into the top of the slurry chamber (see Fig. 12.14). If the linear velocity of the displacement fluid in the slurry chamber is substantially greater than the settling velocity of the largest particle, the resin particles will be distributed uniformly throughout the resulting packed bed.

In dynamic packing, a slurry of 25 to 50 vol % solids is used. Usually, the slurry chamber is sufficiently large to hold enough slurry to pack the column without refilling. In the event that the volume of the column is larger than the volume

of the slurry chamber, the following procedure is used: (1) one chamber volume of slurry is packed into the column; (2) the supernatant liquid in the slurry chamber is removed by siphoning; (3) another batch of slurry is added; and (4) the previous three steps are repeated as needed.

In packing small-diameter columns of appreciable length (e.g., a 0.45-cm-diam \times 200-cm-long column) with small ion exchange resin particles (5 to 10 μ diam), we have found it difficult to pump a liquid through the slurry chamber and into the column at a sufficiently rapid rate to prevent size segregation. This difficulty is caused by a high pressure drop (in the long column), which prevents rapid displacement of the slurry from the slurry chamber into the column. However, as an alternative, one can first pack a fixed bed into a large-diameter reservoir (or cartridge) and then extrude that bed into the small-diameter chromatographic column by displacing it with liquid. This extrusion technique can also be used to pack a coiled column that has constant packing properties and no void spaces.

ORNL-DWG 68-9506A

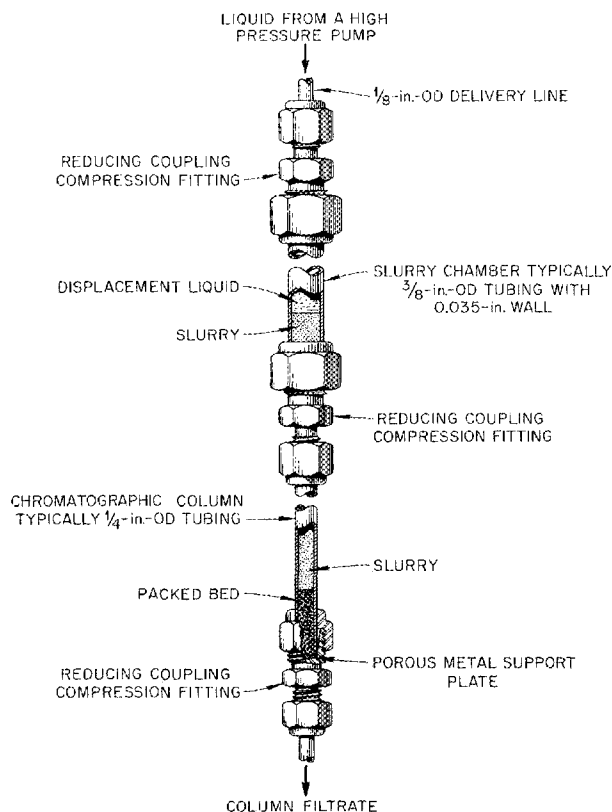


Fig. 12.14. Experimental Setup for Dynamic Packing of a High-Pressure Chromatographic Column.

Effects of pH on Chromatographic Separation

In the uv analyzer the elution of certain chromatographic peaks appears to be a function of the pH of the column eluate. A large number of compounds are known to elute early in the chromatographic run (in the first 50 ml) with resulting poor resolution. The possibility of improving the resolution by changing the pH of the eluate has been evaluated, and methods for adjusting the pH have been developed. Results of tests in which the pH was varied between 4.4 and 10 showed that, at higher pH's, peaks were generally displaced farther from the column volume breakthrough point, thus yielding more effective separation at the beginning of the chromatogram. A pH of about 9.0 seems to be optimum.

Fundamental Studies

We have begun a fundamental study of column chromatography with gradient elution, with the objective of optimizing separation system parameters. A mathematical analysis has been made, and the resulting mathematical solution, coupled with results of experimental studies, will make the prediction of optimum column conditions possible.^{5,6}

The fundamental criterion of a chromatographic column is its resolution, or ability to separate two or more constituents of a mixture. Two chromatographic peaks are said to be resolved when the distance between them is greater than half the sum of their widths. Thus the variables of primary concern are peak width (or dispersion) and peak position of the individual constituents. The purpose of the mathematical analysis is to establish a means of predicting the effects that changing operating conditions would have on these variables.

A modified uv analyzer was used to determine the dispersion of the chromatographic peaks of seven reference compounds, known to be constituents of body fluids, that were eluted with 0.015 *M* sodium acetate-acetic acid buffer (pH 4.4) over a range of flow rates at temperatures of 34.5, 44.0, and 54.1°C. The elution volumes, and hence the distribution coefficients, of the seven reference compounds were also determined over the temperature range of 26.6 to 65°C with 0.015 *M* acetate buffer, and over a range of buffer concentrations 0.0 to 0.06 *M* at 55°C. (Use of a computer program will depend on knowledge of distribution coefficients as a function of column parameters.) No dependence of distribution coefficients on

superficial flow velocity was found up to 0.9 mm/sec, indicating that the distribution coefficients are not affected by interphase mass transport. These experimental data will be used in the computer optimization of operating conditions.

12.8 SYSTEM COMPONENTS

UV Photometry

A developmental model of a small uv photometer, designed and built at ORNL, is now being used in the advanced uv analyzer model Mark III. This photometer (Fig. 12.15) operates at 254 and 280 nm.

The detector head is approximately 2 in. in diameter by 5 in. long. Reference and sample streams flow upward through two vertical quartz tube cells (3 mm ID). The 254-nm channel is activated directly by a low-pressure mercury lamp, and the 280-nm radiation is obtained by absorbing excess 254-nm radiation in a pair of phosphor rods that emit at 280 nm. Interference filters are used to remove light of other wavelengths.

Tests of this detector and its associated electronics have shown very high peak resolution, with 0.1 absorbance unit being equal to full scale on a

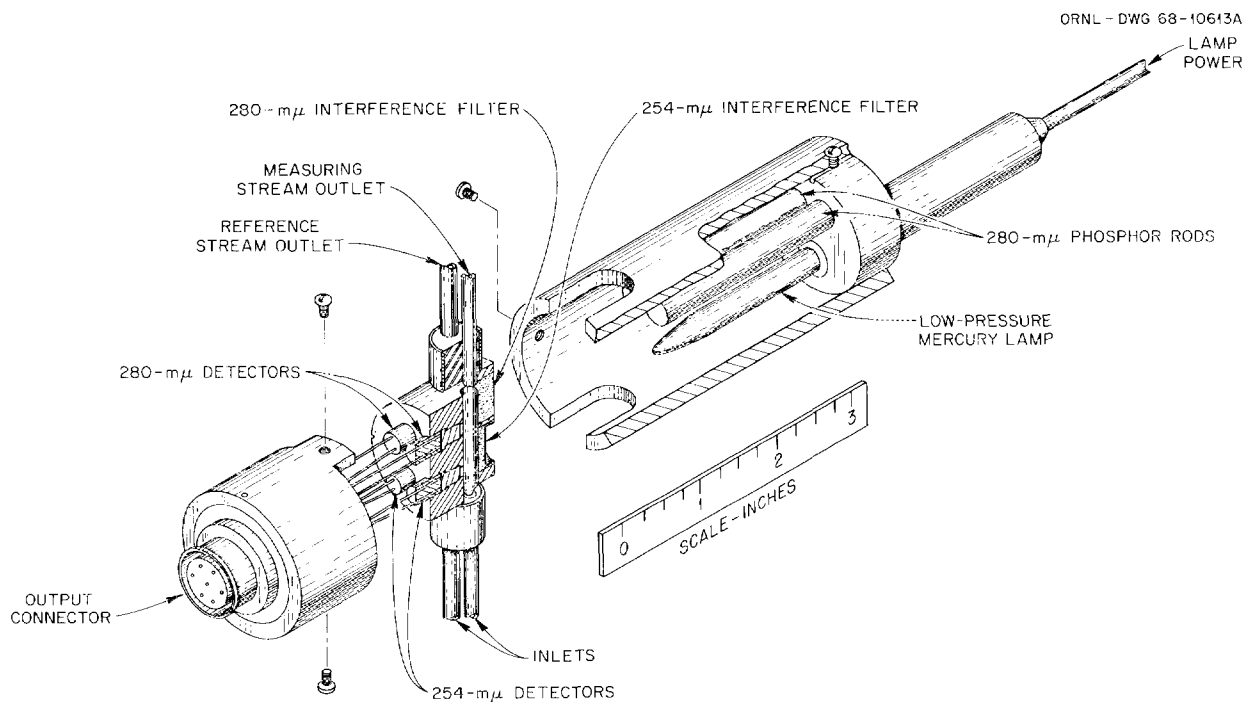


Fig. 12.15. Dual-Beam, Dual-Wavelength Ultraviolet Flow Photometer.

strip-chart recorder. There was no tendency for gas bubbles to become suspended in the cells, and excellent base-line compensation was found with the gradient elution systems. However, some difficulty has been encountered in obtaining a filter with a sufficiently narrow bandwidth for the 280-nm channel.

Sample Injection Valve

One way of introducing a sample directly into the high-pressure eluent stream of a chromatograph is to use a sample injection valve that provides a means for switching a prefilled sample loop into the column eluent line. The contents of the loop, then, are swept into the column by the eluent. A six-port valve with provisions for switching the connections between ports will allow this type of operation. Figure 12.16 shows how such a valve works. In position *A*, the eluent stream flows through the valve and then directly into the chromatographic column. The remaining four ports can be used to fill the sample loop at ambient pressure. In position *B*, the ports in the valve are reconnected, and the eluent successively enters the valve, flows through the sample loop, and passes into the column.

We have recently designed and successfully tested a new sample injection valve that will operate at liquid pressures up to 5000 psi for extended periods of time. This valve has six ports,

with attached tubing, spaced equidistantly around a metal cylindrical sleeve (Fig. 12.17). Each of the three pairs of ports is connected by small slots machined in the plastic cylindrical sleeve that rotates inside the metal sleeve. Rotation of the inner sleeve allows the slots to move and connect different ports. This permits the valve to operate in the two positions shown in Fig. 12.16.

A unique feature of this valve is the special type of seal used to separate the high-pressure side of the valve from ambient pressure. The inner plastic sleeve is held on a tapered metal shaft that has a fixed restraint on one side and a movable metal washer on the other side. The washer is forced against the plastic by a nut located on the threaded end of the metal shaft. This action drives the plastic sleeve up the shaft and against the outer metal sleeve, thereby providing a seal between each port. The metal restraints on each end of the shaft, as well as the outer metal sleeve, prevent the plastic from deforming.

The new valve has been tested for more than 2000 hr at pressures up to 5000 psi on a prototype uv analyzer; no leaks occurred during this period. The valve can be operated satisfactorily either by simple hand pressure or by a motorized control.

A complete set of construction prints for this valve is available as CAPE-1853 from the Clearinghouse for Federal Scientific and Technical Information, U.S. Department of Commerce, 5285 Port Royal Road, Springfield, Virginia 22151.

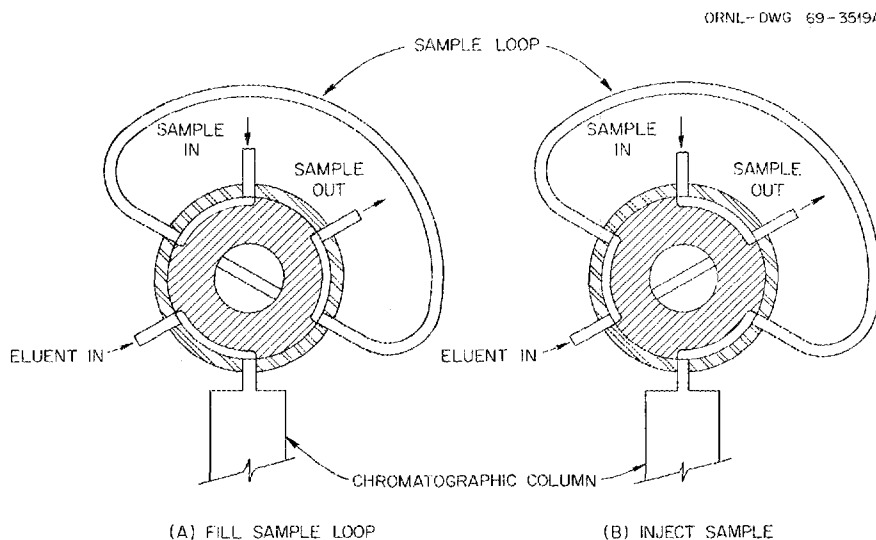


Fig. 12.16. A Six-Port Sample Injection Valve for Introduction of a Sample into a Liquid Chromatograph.

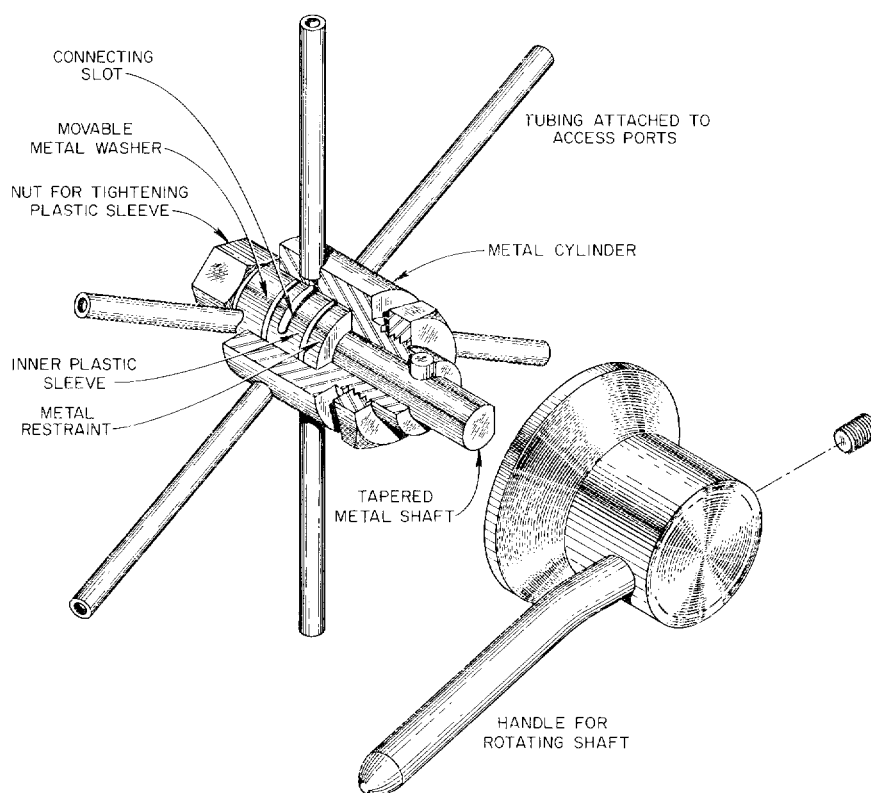


Fig. 12.17. A Small, Six-Port Sample Injection Valve Capable of Operation up to 5000 psi.

12.9 IDENTIFICATION OF BODY FLUID CONSTITUENTS

Two types of identification of chromatographically separated body fluid constituents are being made: (1) tentative identification by chromatographic properties; and (2) confirmative, or definite, identification by spectrometry, gas chromatography, and chemical analysis of isolated constituents.

To date, 21 specific uv-absorbing chromatographic peaks from body fluids have been definitely identified by the techniques of mass spectrometry, nuclear magnetic resonance, infrared spectroscopy, uv spectrophotometry, and chemical testing of separated fractions; an additional 18 compounds have been tentatively identified. (Many of these are shown in Fig. 12.13.) Three carbohydrate chromatographic peaks have been definitely identified, and an additional 13 peaks have been tentatively identified. The chromatographic positions of 143 and 48 reference compounds have been established on the uv analyzer and the carbohydrate analyzer respectively.

Effect of Chemical Structure

The work done with regard to identifying chromatographic positions has allowed us to begin to establish the relationship between elution position and chemical structure, especially for uv-absorbing constituents.¹¹ This relationship will be useful in helping to establish the identities of eluted compounds.

In general, compounds elute in the order: basic > neutral > acidic. The carboxyl group is the only functional group that, alone, contributes substantially to retention on the column. This effect is altered by the presence of an α -amine group (amino acids, etc.). Other functional groups strongly affect retention on the column, but only when they are combined with some other structural feature. Amine and enol components and the carbonyl group located next to an α -hydrogen are effective when

¹¹S. Katz and C. A. Burtis, "The Relationship Between Chemical Structure and Elution Position in an Anion Exchange System," *J. Chromatog.* 40, 270 (1969).

positioned on aromatic structures. Conjugated double bonds in the side chain increase the effect of the carboxyl group.

The contribution of the aromatic structure to retention volume appears to be dependent on the attached functional groups. Basic groups on any of the aromatic structures cause little or no retention. With weakly acid and acid functional groups, however, the contribution of the aromatic structure becomes more evident; for example, with the functional group of carboxyl plus an α -hydrogen, the pyrimidine structure contributes less to retention volume than the purine structure does. In general, the order of contribution to retention appears to be: imidazole > purine > pyrimidine > indole > quinaldic structures > benzoic structures.

The regularities noted have been useful in predicting the elution positions of known compounds and in identifying compounds that are responsible for peaks. The accuracy of predictions of peak positions has been highest in instances where related members of the same family have been tested.

Gas Chromatography

Mass spectral analysis of urinary compounds that have been separated by either the uv analyzer or the carbohydrate analyzer is frequently difficult because many biochemicals have insufficient volatility for such an analysis. In addition, the eluate fraction may contain more than one urinary compound, thus resulting in a complex and uninterpretable spectrum.

The volatility of many of the urinary compounds can be increased, and the compounds can be further purified, by using gas chromatography (GC). Elution position in the gas chromatograph can also be used for confirmative identification. Elution positions have been determined for many known urinary constituents.^{5,6}

After the buffer salt has been removed, the biochemicals in the column fraction can be converted to volatile compounds by forming their trimethylsilyl derivatives. These derivatives are separated by GC, and the separated compounds are then analyzed by mass spectrography.

The ammonium acetate-acetic acid buffer used in the uv analyzer can be removed from the column eluate fraction by lyophilization, while the sodium borate-boric acid buffer used in the carbohydrate analyzer can be removed by cation exchange (for

the sodium ion), methylation (with methanol), and flash distillation (for removal of the methylated boric acid).

12.10 ANALYTICAL RESULTS

Concurrent with progress in the development of improvements in the uv and the carbohydrate analyzers, a program to evaluate these instruments in their present states is under way. A large number of analyses have been made to establish base-line chromatograms of eight "normal" male subjects. In these tests, urine and blood serum samples from the normal subjects were analyzed by both of the analytical systems.

A limited number of analyses are also being made in cooperative research projects. In addition, a few pathologic urine samples have been analyzed. Some of these will be discussed briefly, since they have been useful in our identification program.

Normal Body Fluids Program

In order to differentiate between the normal and the pathologic states by analyses of body fluids, it will be necessary to establish either normal excretion rates of body fluid constituents or normal chromatographic patterns for the two high-resolution analytical systems under development. Of the several individuals that were clinically screened, eight males were chosen as "normal" subjects. (Normal subjects were defined as males between the ages of 25 and 40, having no clinical manifestations of disease or physical abnormality.) Blood and urine samples obtained from these subjects were analyzed by both analytical systems.

Two complete series of urine and blood serum samples were obtained from the eight normal subjects. In each series, composite urine samples were collected from each subject in two 12-hr fractions (a day sample from about 7:00 AM to 7:00 PM, and a night sample from about 7:00 PM to 7:00 AM the following day). The two series of collections were made several weeks apart.

Carbohydrate analyses of a total of 56 urine and blood serum samples have been completed, and the data have been evaluated. Ultraviolet analyses of the samples are also complete; however, due to the complexity of the uv chromatograms, these results have not been entirely evaluated.

Analyses of Blood Serum

Carbohydrate chromatograms for fasting blood serum samples from the eight normal subjects indicate the presence of as many as 17 carbohydrate components, of which 7 were common to all subjects.¹²

The mean concentrations, expressed as milligrams per 100 milliliters, of six sugars that have been tentatively identified in the blood serum samples are given in Table 12.3. There were significant variations in the amounts of many of the sugars; however, the sugars that were present in relatively large amounts were found in fairly narrow ranges of concentration. Glucose was notable in that it had a standard deviation of only 16.49%.

Analyses of Urine

A total of 48 urine samples were collected from the eight normal subjects during the two sampling periods. In each period, two 12-hr urine composites were collected, and samples were taken from each of these composites, as well as from the total 24-hr composite.

UV Analyses. — As previously reported,⁷ the uv chromatograms of urine have as many as 100 peaks, of which 50 to 60 are common to each subject and 70 to 80 are common to most. Day and night excretion patterns for the individual uv-absorbing constituents appear to differ in that the night excretion rate (ER) is generally higher. The excretion volume of the night sample is also greater. The average ER's for the two major components are compared below:

	Average Diurnal ER [mg(24 hr) ⁻¹ kg ⁻¹]	Average Nocturnal ER [mg(24 hr) ⁻¹ kg ⁻¹]	Apparent % Increase in ER at night
Hippuric acid	2.12	3.75	77
Uric acid	5.11	6.27	23

¹²R. L. Jolley, K. S. Warren, C. D. Scott, and M. L. Freeman, "Carbohydrates in Normal Urine and Blood Serum as Determined by High-Resolution Column Chromatography," presented at the First Annual Symposium on Automated, High-Resolution Analyses in the Clinical Laboratory, held at Oak Ridge National Laboratory, March 13-14, 1969; to be published in the *American Journal of Clinical Pathology*.

Table 12.3. Mean Sugar Concentrations for Eight Carbohydrate Chromatograms of Blood Serum Samples in the Normal Body Fluids Program

Peak Designation	Mean Sugar Concentration (mg/100 ml)	Standard Deviation	
		mg/100 ml	%
Sucrose	0.06	0.04	67
Raffinose	0.24	0.27	112
Mannose	1.15	0.22	19
Fructose	0.87	0.28	32
Galactose	0.70	0.22	32
Glucose	74.9	12.3	16.4

These data indicate that the daily excretion of hippuric acid and uric acid totals about 0.5 and 0.8 g respectively; these values are in fair agreement with values cited in the literature.

Carbohydrate Analyses. — Forty-eight urine samples, representing two sample series, from the eight normal subjects were analyzed with the carbohydrate analyzer. In each series sampling period, two 12-hr urine composites (designated day and night) were collected by each subject; samples of these composites, as well as samples of the 24-hr composite (prepared by proportionally mixing the two 12-hr composites), were analyzed.

Carbohydrate chromatograms of 24-hr composites (Fig. 12.18) of the urine samples indicated the presence of as many as 48 carbohydrate components, of which 23 were common to all.

The mean excretion rates (and standard deviations) of the major sugars present in the 24-hr composite samples are given in Table 12.4. These values were calculated by combining the results of both series of urine analyses for the eight normal subjects. The determined concentrations are in agreement with handbook values, with the fol-

SAMPLE SIZE

N-1 THRU. N-7 16 ml.
N-8 12.5 ml.

NORMAL BODY FLUID PROGRAM
URINE CARBOHYDRATES

490 m μ

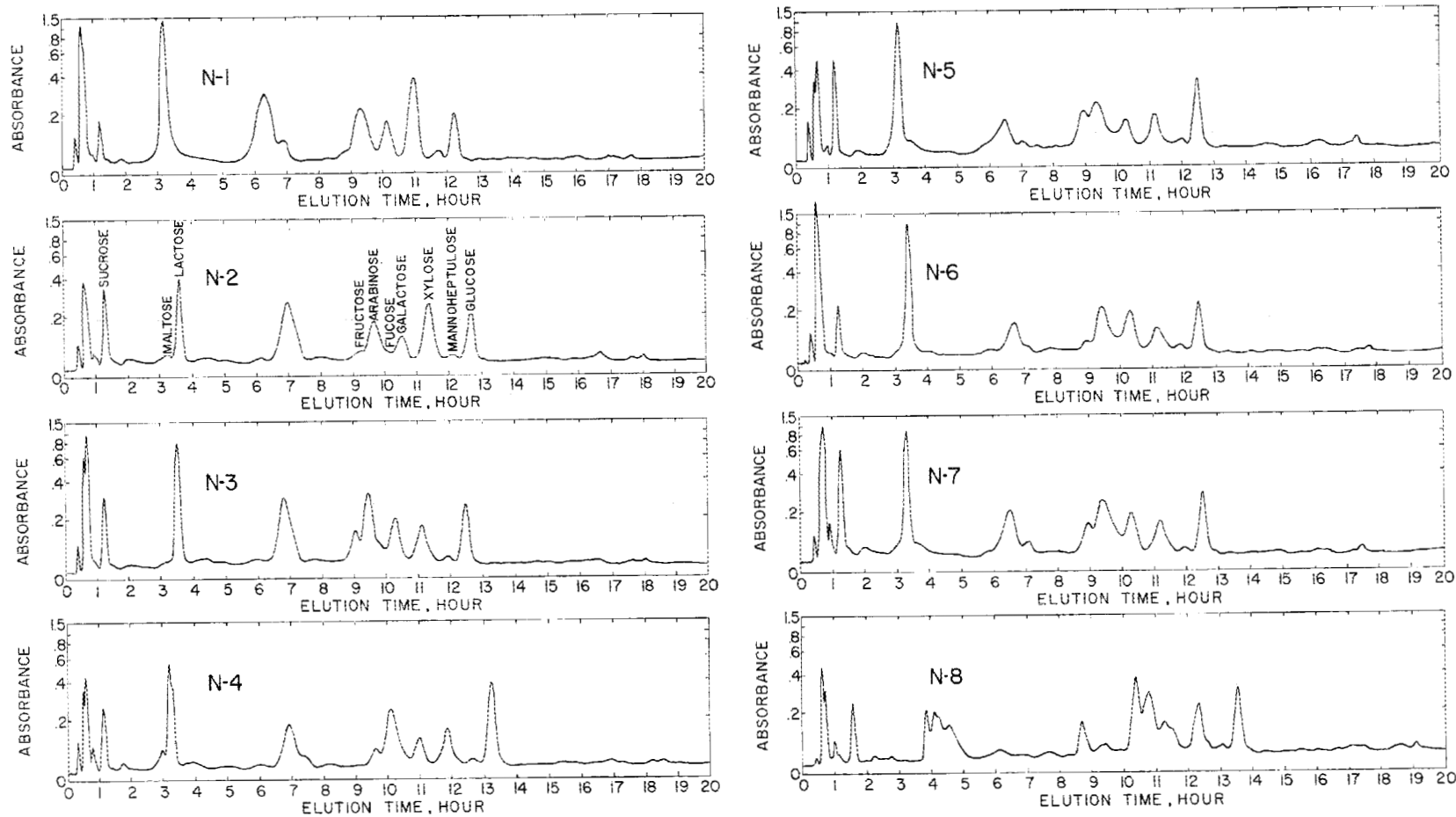


Fig. 12.18. Urine Carbohydrate Chromatograms of the First Series of 24-hr Composite Samples.

lowing exceptions: arabinose and galactose, for which our values are high, and raffinose, rhamnose, maltose, and mannoheptulose, for which normal values were not found.

Excretion of the more abundant sugars is reasonably uniform, as judged from the standard deviations. This is particularly true in the case of glucose, the fundamental sugar in many metabolic processes.

Table 12.5 compares the relative changes in the 24-hr sugar excretion rates from the earlier collection period (first series) to those from the later collection period (second series). The relative change for a given sugar is defined as the second series excretion rate minus the first series excretion rate, divided by the standard deviation from both series. In only one case does the relative change differ by more than three times the standard

Table 12.4. Mean Excretion Rates (with Standard Deviations) and Mean Concentrations of Major Sugars in 24-hr Urine Samples of Both Series in the Normal Urine Program

Sugar	Excretion Rate		Mean Concentration (mg/100 ml)
	Mean [mg (24 hr) ⁻¹ kg ⁻¹]	Standard Deviation (%)	
Sucrose	0.292	43	2.2
Raffinose	0.056	43	0.42
Maltose	0.229	38	1.8
Lactose	1.29	49	9.5
Rhamnose	0.038	197	0.38
Ribose	0.055	185	0.24
Fructose	0.260	55	2.1
Arabinose	0.644	45	6.9
Galactose	0.545	36	4.0
Xylose	0.385	57	2.8
Mannoheptulose	0.060	42	0.46
Glucose	0.662	18	5.2

Table 12.5. Relative Change in 24-hr Composite Excretion Rates for Subjects in Normal Urine Program

$$\text{Relative change} = \frac{(\text{second series rate} - \text{first series rate})}{\text{standard deviation from both series}}$$

Sugars	Subjects							
	N-1	N-2	N-3	N-4	N-5	N-6	N-7	N-8
Sucrose	-0.2	0.4	-1.1	-0.08	-1.3	-1.0	-0.8	0.9
Raffinose	-0.5	1.4	1.5	1.6	0.8	0.4	2.7	2.1
Maltose	1.7	-0.17	0	0.26	-0.17	-0.7	1.3	-0.5
Lactose	-2.5	0.6	0.5	1.1	-1.8	-0.5	-0.3	-1.6
Rhamnose				-1.0	2.9		3.0	-1.2
Ribose	-3.8				-1.2		-0.6	-1.8
Fructose	0.5	1.6	-1.4	0.8	-0.14	1.1	-0.8	-0.6
Arabinose	-2.5	-0.6	-2.9	-1.4	-1.5	-2.2	-0.5	-1.5
Galactose	-0.3	1.0	-1.1	-0.4	-1.0	-1.2	0.05	1.2
Xylose	-1.3	-0.7	-0.5	0.18	-0.14	-0.18	0.4	0.4
Mannoheptulose	0.12	-0.12	0.02	0.04	-0.18	-0.11	0.04	0.09
Glucose	1.8	-0.6	0.7	-0.3	-0.2	-0.2	0.6	2.7

deviation. This type of data may prove useful in defining pathologic states. For example, an abnormal state might be defined as that in which the relative change in the excretion rate of a particular urinary constituent differs from the mean established for normals by greater than five standard deviations.

The 12-hr urine composites (day and night fractions) were also analyzed by the carbohydrate analyzer. The resulting chromatographic patterns were similar to those for the 24-hr composites. No general conclusion could be drawn as to whether carbohydrate excretion rates were higher for day or night samples, although two major sugars (galactose and glucose) had slightly higher daytime excretion rates.

Ethylation of Rat RNA

In the study of the *in vivo* ethylation of rat RNA, which is in progress in the Biology Division, rats are being fed diethylnitrosamine to determine if the ethylation of tRNA affects enzyme levels and activities.

The tRNA from some of these animals has been isolated and hydrolyzed with acid to yield free purine bases and pyrimidine nucleotides. The tRNA hydrolysates, along with reference solutions of methylated and ethylated guanines and adenines, were analyzed by the uv analyzer. Comparison of the results with the elution volumes that have been established for 29 reference compounds indicated the presence of 7-ethylguanine in these hydrolysates. Ethylated compounds are very unusual in biological systems.

Patient with Neuroblastoma

Urine from a patient with a neuroblastoma was obtained from the University of Tennessee Memorial Hospital, Knoxville, Tenn. This patient had received 6-mercaptopurine, steroids, and phenacetin, as well as 100 r of cranial radiation. Homovanillic acid was positively identified in the urine chromatogram. Excretion of large amounts of homovanillic acid has been shown to be associated with a neuroblastoma. Other chromatographic peaks identified from uv chromatograms of this urine were 3-methoxy-4-hydroxymandelic acid, 6-mercaptopurine (an ingested drug), and two compounds, 4-hydroxyacetanilide and 3-methoxy-4-hydroxyacetanilide, which are metabolites of phenacetin.¹³

12.11 DATA ACQUISITION AND ANALYSIS

A small digital computer has been purchased and is being prepared for use as an on-line computer for acquiring and analyzing the information from two or more chromatographs. A computer programming technique for this purpose is also being developed. The computer program will have the capability of stripping individual peaks from an envelope of interfering peaks by use of a nonlinear least-squares procedure. Such a technique has been used effectively to evaluate complex spectral curves.¹⁴

We have written and tested a computer program (Fig. 12.19) for the real-time analysis of complex chromatographic data.¹⁵ The program was evaluated on a large off-line computer; however, results showed that it is capable of analyzing complex chromatographic data and that it should be applicable for use with small on-line computers.

In the evaluation, the program was used to analyze synthetic data containing single and interfering Gaussian peaks. We found that it was capable of analyzing envelopes of up to three Gaussian peaks with an error of less than 1% (based on peak areas).

Actual experimental data (e.g., chromatographic data containing an envelope of two interfering peaks, uracil and nicotinamide, from the uv analyzer) were also analyzed by the program. The Gaussian peaks that were stripped out of the envelope were compared with the single peaks that had also been obtained experimentally. The area of the major peak (nicotinamide) and the area of the minor peak (uracil) were determined to

¹³C. A. Burtis, W. C. Butts, and W. T. Rainey, Jr., "Separation of the Metabolites of Phenacetin in Urine by High-Resolution Anion Exchange Chromatography," presented at the First Annual Symposium on Automated, High-Resolution Analyses in the Clinical Laboratory, held at Oak Ridge National Laboratory, March 13-14, 1969; to be published in the *American Journal of Clinical Pathology*.

¹⁴R. E. Buggers, J. T. Bell, E. C. Long, and O. W. Russ, *Mathematical Resolution of Complex Overlapping Spectra and Spectral Fine Structure with Nonlinear Least-Squares Computer Techniques*, ORNL-3834 (in preparation).

¹⁵C. D. Scott, J. M. Jansen, Jr., and W. W. Pitt, "A Computer Technique for On-Line Analyses of Complex Column Chromatographic Data," presented at the First Annual Symposium on Automated, High-Resolution Analyses in the Clinical Laboratory, held at Oak Ridge National Laboratory, March 13-14, 1969; to be published in the *American Journal of Clinical Pathology*.

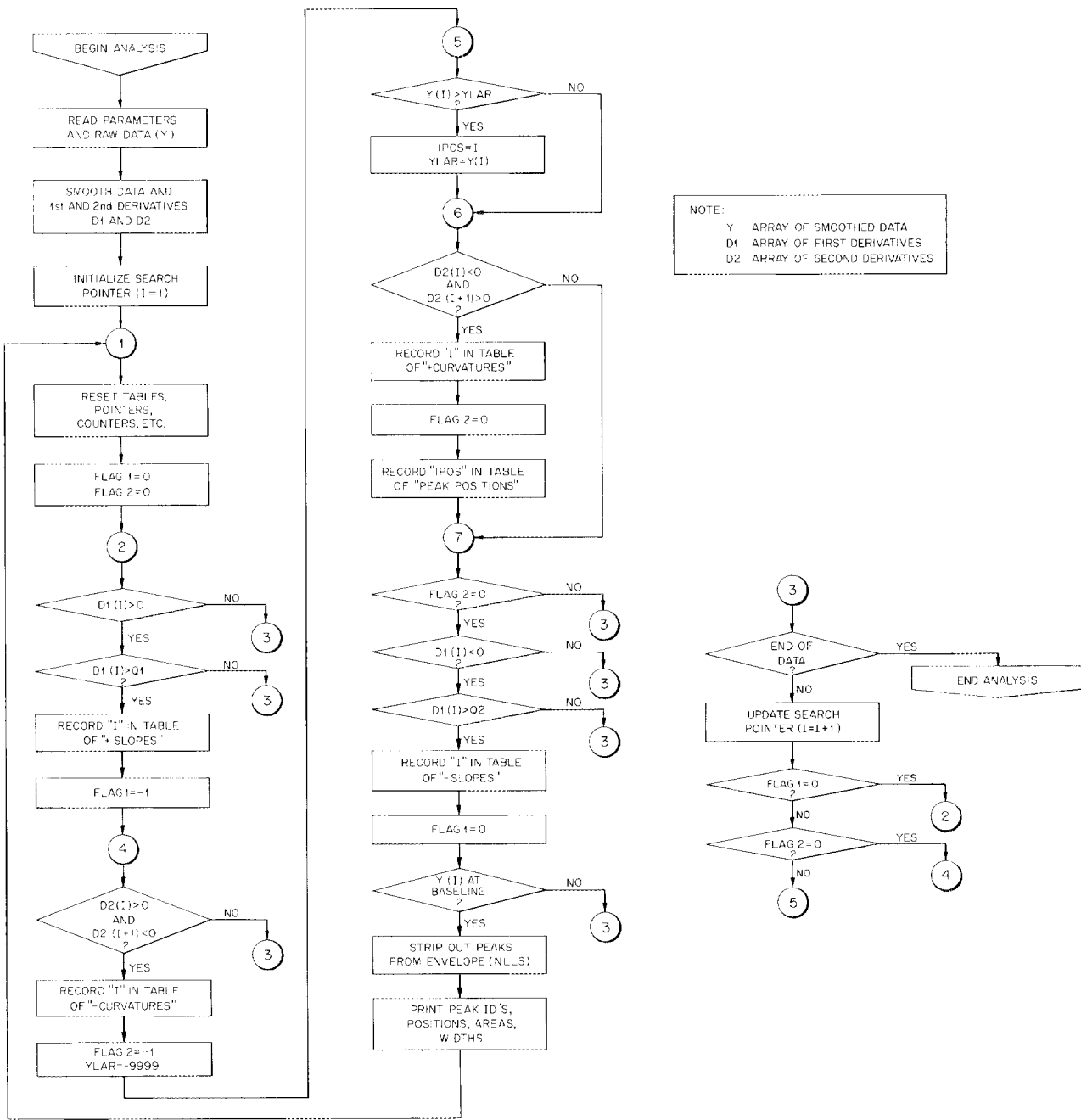


Fig. 12.19. Flow Chart of Computer Program for Analyzing Chromatographic Data.

within 3.6 and 6.3%, respectively, of their actual values.

The present computer program, after addition of provisions for acquiring and discarding small blocks of data, will be used on the small on-line computer.

12.12 LITERATURE SURVEY

An annotated collection of 3079 literature references that are concerned with the determination of low-molecular-weight organic constituents in normal and pathologic human urines has been completed.¹⁶ The references were collected from volumes 59–65 of *Chemical Abstracts* (July 1963 through December 1966), *Biological Abstracts* for

the years 1964–66, *Index Medicus* for the year 1965, and by an automated search by the MEDLARS system for the year 1966. The references are listed alphabetically by the first author, and key words have been added in instances where the title itself did not contain all information relating to ingested materials, excreted compounds, analytical techniques, and health relationships. Indexes keyed to each of the above categories are included.

References to more than 1000 molecular constituents were found. The majority of these were associated with a pathologic state or with an ingested drug.

¹⁶S. Katz *et al.*, *An Annotated Bibliography of Low-Molecular-Weight Constituents of Human Urine*, ORNL-TM-2394 (Oct. 11, 1968).

13. Irradiation Effects on Heterogeneous Systems

Several types of heterogeneous systems have been investigated and reported under this program: the dehydration of cyclohexanol over radioactive sulfate catalysts, the decomposition of formic acid on irradiated oxide catalysts, and the radiolysis of water adsorbed on various solids. Recent studies have been devoted to the behavior of inorganic aquasols upon exposure to ^{60}Co gamma rays.

13.1 EFFECTS ON AQUEOUS SOLS

Methods

A variety of aqueous inorganic sols were exposed to ^{60}Co gamma radiation, and the effects on pH, electrical conductivity, and streaming current were determined. The streaming current, which is proportional to the zeta potential of the sol particles, was measured with a Waters streaming current detector. Static tests were made by irradiating sol samples in glass-stopped bottles and removing them periodically from the radiation field for measurements. In dynamic tests, the sol was pumped in a stainless steel loop through the ^{60}Co source and into the streaming current detector; the measurements were continuously recorded.

Variations in dose rate were achieved by changing the relative positions of the radiation source and the sol sample, and by placing lead shielding between the source and the sample.

Gold Sols

One of the most interesting, and as yet unexplained, effects of radiation on sols was reported by Crowther *et al.*, prior to World War II.¹⁻⁸ With low doses of x or gamma radiation, they observed cyclical variations in the zeta potential

for a number of sols, including gold sols. In an attempt to learn more about this phenomenon, we prepared several gold sols, which ranged in color from blue to red, by the reaction of AuCl_3 with H_2O_2 in basic solution at 85°C . Electrophoretic mobilities were measured with the Beckman model H electrophoresis apparatus, and streaming currents were measured with the Waters streaming current detector. Neither cyclical variations in zeta potential nor color changes, such as those reported by Oreshko *et al.*,⁹ were observed. Table 13.1 shows the results from a series of tests at low doses comparable with those used by Crowther. Although there is some decline in the zeta potential, no regular variation pattern is evident. Changes in pH and electrical conductivity reflect, primarily, aging of the sol rather than radiation effects. Irradiation of a blue sol at higher dose rates produced a marked decline in the zeta potential, as is shown by the decline in streaming current (Fig. 13.1). Because streaming current measurements can be made much faster than electrophoretic measurements, sol aging effects are negligible. When a red-colored gold sol was irradiated at the higher dose rate to a total of $7.5 \times$

¹J. A. Crowther, H. Liebmann, and C. C. Mills, *Brit. J. Radiology* **9**, 631 (1936).

²J. A. Crowther, H. Liebmann, and T. B. Lane, *Phil. Mag.* **24**, 654 (1937).

³J. A. Crowther and H. Liebmann, *Nature* **140**, 28 (1937).

⁴J. A. Crowther, H. Liebmann, and R. Jones, *Phil. Mag.* **26**, 120 (1938).

⁵J. A. Crowther, *Nature* **142**, 569 (1938).

⁶J. A. Crowther, H. Liebmann, and R. Jones, *Phil. Mag.* **28**, 64 (1939).

⁷J. A. Crowther and H. Liebmann, *Nature* **143**, 598 (1939).

⁸J. A. Crowther, H. Liebmann, and R. Jones, *Phil. Mag.* **29**, 391 (1940).

⁹V. F. Oreshko, N. G. Serebryakov, and E. K. Sakseev, *Colloid J. (USSR) (English Transl.)* **17**, 361 (1955).

10^{18} ev/g, no effect on the streaming current was found. It therefore appears that the blue-colored, large-particle-size gold sols suffer a decrease in zeta potential with irradiation, whereas the more-stable, small-particle-size red sols are not measurably affected.

Table 13.1. Effect of Low-Level Radiation on a Gold Sol^a

Dose (ev/g)	Zeta Potential ^b (mv)	pH	Conductivity (micromhos/cm)
$\times 10^{14}$			
0 ^c	-36.8	10.8	220
	-33.7	10.7	217
	-35.4	10.5	216
	-36.4	10.3	195
1.33	-36.2	10.9	263
3.30	-36.6	10.9	258
5.70	-28.7	10.4	198
	-31.6	10.4	196
	-32.6	10.3	192
7.48	-33.6	10.3	192
8.85	-25.2	10.5	192
10.8	-21.5	10.4	197
12.0	-31.2	10.3	195
16.1	-31.4	10.4	197
48.2	-31.1	10.7	214
144.6	-30.5	10.6	206

^aPreparation DMH-3; red-colored.

^bUsing Beckman model H electrophoresis-diffusion apparatus.

^cDecline in pH and conductivity represents aging effects for two months.

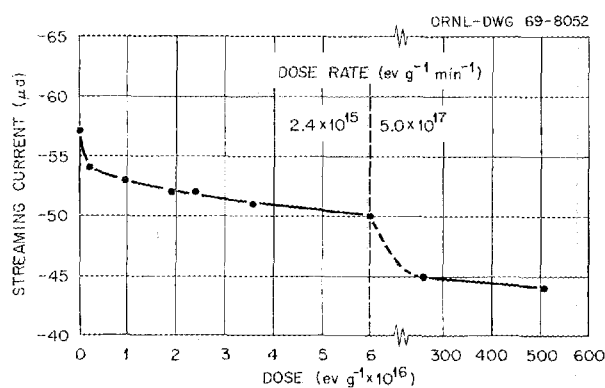


Fig. 13.1. Effect of Irradiation on a Gold Sol (Preparation Au-C; Blue-Colored).

Lanthanide Hydroxide Sols

Since sols of several of the lanthanide and actinide elements are of interest to the sol-gel process, a study of the effects of irradiation on them was undertaken. The sols were prepared by adding 0.2 M metal nitrate solution to a twenty-fold excess of NH_4OH with stirring. The precipitates were then washed five to ten times with distilled water, which resulted in peptization. It has been shown (see Sect. 16.2) that the pH, electrical conductivity, and zeta potential of such preparations change rather drastically initially, requiring about seven days to reach steady state. However, once the sols attained steady-state conditions, they were essentially unaffected by irradiation (see Table 13.2).

In one test, a freshly prepared europium hydroxide sol was pumped through the ^{60}Co source, and the streaming current was measured continuously. The average dose rate estimated from the portion of the total sol volume in the irradiation field was 9.6×10^{18} $\text{ev g}^{-1} \text{hr}^{-1}$. Simultaneously, the streaming current of a second portion of the sol was measured in the laboratory, using the No. 2 streaming current detector. The results are shown in Fig. 13.2.

The two streaming current detectors do not give equivalent readings; therefore, the ordinates in Fig. 13.2 were arbitrarily scaled to match at the first point taken 4.5 hr after precipitation of the hydroxide and prior to any irradiation. Results indicate that, although irradiation slows down the aging process somewhat, it has little effect on the

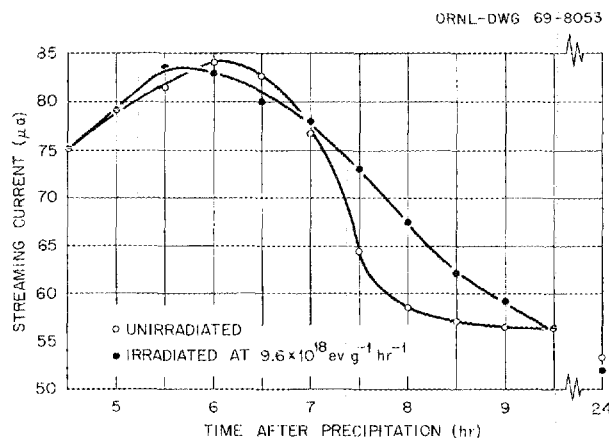


Fig. 13.2. Effect of Irradiation on the Aging of a $\text{Eu}(\text{OH})_3$ Sol.

Table 13.2. Effect of Irradiation on Aged Lanthanide Hydroxide Sols

Lanthanide	Unirradiated Sols			Irradiated ^a Sols		
	pH	Electrical Conductivity (micromhos/cm)	Streaming Current (μ amp)	pH	Electrical Conductivity (micromhos/cm)	Streaming Current (μ amp)
La	8.1	3650	14.6	8.0	3700	15.2
Pr	7.4	3250	12.8	7.3	3400	12.8
Sm	7.0	2800	18.0	6.9	2800	18.2
Gd	6.9	5200	12.4	6.7	5100	11.6
Tm	7.3	640	35.5	7.2	670	36.0
Yb	7.0	680	34.0	6.9	750	34.0

^aIrradiated with 2.2×10^{21} ev/g ^{60}Co gamma rays.

final value of the streaming current. There was a marked difference in the electrical conductivity values of the irradiated sol and the unirradiated sol; that is, 1260 micromhos/cm vs 2150 micromhos/cm.

Irradiation of the $\text{Eu}(\text{OH})_3$ sol was continued under static conditions to a total dose of 1.36×10^{20} ev/g. During this time, the pH decreased from 7.4 to 7.3, the streaming current decreased from 52 to 32 μ amp, and the electrical conductivity increased to 1500 micromhos/cm. In the case of the unirradiated sol, the pH decreased from 7.4 to 7.2, the streaming current decreased from 53 to 26 μ amp, and the conductivity increased to 2260 micromhos/cm during the same period of time (~19 days). Although changes continue to take place at a slow rate, both sols are still stable after five months. It thus appears that, while the irradiation of freshly prepared lanthanide sols causes some changes in aging behavior, these changes are not deleterious to the stability of the sols.

Other Inorganic Sols

The effects of irradiation on other inorganic sols were briefly examined, using suspensions of

Alon-C¹⁰ and bentonite. Alon-C, which is finely divided $\gamma\text{-Al}_2\text{O}_3$, was easily suspended in water by shaking. The bentonite, a 325-mesh material supplied by E. H. Sargent and Company, was mixed with water in a Waring Blender; the coarse material was allowed to settle, and the "supernate" was withdrawn for the experiments. The Alon-C and bentonite suspensions were irradiated for 18 and 40.4 hr, respectively, in a modified pump loop (installed in the ^{60}Co source) at an average dose rate of 2.6×10^{18} ev g^{-1} hr^{-1} , and the streaming current was monitored continuously. In each case, a continuous decrease in the absolute value of the streaming current was found; a decrease from +16 to +11 μ amp was observed for the Alon-C, whereas a decrease from -31.5 to -17.8 μ amp was observed for the bentonite. Streaming current values for unirradiated suspensions remained constant. The pH of the irradiated Alon-C sol increased from 5.1 to 7.0, and the electrical conductivity increased from 11.8 to 110 micromhos/cm; corresponding changes for the unirradiated sol were 5.1 to 5.35 and 11.8 to 19.7. Somewhat different behavior was noted for the bentonite; the pH and the electrical conductivity of the irradiated

¹⁰Registered trademark, Cabot Corporation.

sol decreased from 7.7 to 6.6 and increased from 69 to 112 micromhos/cm, respectively. In the case of the bentonite, the pH of the unirradiated sol only decreased 0.1 unit; however, the conductivity increase to 136 micromhos/cm was similar to the increase observed for the irradiated sample. Some inconclusive work on the effects of irradiation on bentonite suspensions has indicated that

cyclical changes in particle charge might be observed under the conditions of our experiment;¹¹ however, to date, we have not observed such changes.

¹¹*The Effect of Ionizing Radiation on Colloids*, Research Dept., Unidynamics, Phoenix, Ariz., COO-1653-15 (November 1967).

14. Spectrophotometric Studies of Solutions of Lanthanides and Actinides

The major objective of this program is to develop and exploit spectrophotometric techniques for studying the chemical properties of aqueous solutions, especially of the lanthanide, actinide, and transition elements, over wide ranges of experimental conditions. Studies of the non- or low-alpha-active elements, which are of initial interest, are being accomplished with the usual spectrophotometric techniques. Preliminary investigations of the uranyl ion and the correlation of its spectra with those of penta- and hexavalent transuranium elements have been completed and published.¹⁻⁴ A specially modified Cary model 14 spectrophotometer system^{5,6} for studying the more highly alpha-active actinides has been built, and is presently installed in a standard laboratory where it is being used to study non- and low-alpha-active solutions. This modified system, which is designed to provide safe containment for all alpha-active materials, is capable of operating at temperatures up to the critical point of water (373°C) and pressures up to 10,000 psi. In conjunction with the spectrophotometric studies, the densities of aqueous solutions of the lanthanides and actinides are being studied over the temperature range of 25 to 400°C to determine the effects of temperature on concentration and structure.

¹J. T. Bell and R. E. Biggers, *J. Mol. Spectry.* **18**, 247 (1965).

²J. T. Bell and R. E. Biggers, *J. Mol. Spectry.* **22**, 262 (1967).

³J. T. Bell and R. E. Biggers, *J. Mol. Spectry.* **25**, 312-29 (1968).

⁴J. T. Bell, *J. Inorg. Nucl. Chem.* **31**, 703 (1969).

⁵*Chem. Technol. Div. Ann. Progr. Rept. May 31, 1966*, ORNL-3945, pp. 221-27.

⁶*Chem. Technol. Div. Ann. Progr. Rept. May 31, 1965*, ORNL-3830, pp. 236-47.

14.1 SPECTRA OF AQUEOUS $\text{Pr}(\text{NO}_3)_3$ AND $\text{Nd}(\text{NO}_3)_3$ TO 356°C

The visible spectra of aqueous $\text{Pr}(\text{NO}_3)_3$ and $\text{Nd}(\text{NO}_3)_3$ were recorded to 356°C. The integrated areas of the absorption bands have been analyzed with respect to changes caused by temperature and hydrolysis, and similarities to corresponding spectra from organic solutions have been observed.⁷ The areas of the two Pr^{3+} spectral band groups decrease by 40 and 60%, but the transition energies remain constant, when the temperature is increased to 356°C. The temperature effects on the Nd^{3+} spectral bands are more dramatic. One new band observed above 290°C results from the thermal population of an energy level above the usual ground state. Also, the area of the Nd^{3+} hypersensitive band at 5754 Å increases by a factor of about 5 when the temperature is increased from 25 to 356°C. This increase in area appears to be the result of a change in the vibration effects on the Nd^{3+} ion as the ion is dehydrated. The changes in the area and the position of the hypersensitive band are essentially linear functions of temperature. However, changes in slope occur at 90°C and at 240°C, which appear to be the temperatures at which specific changes occur in the hydration number of the Nd^{3+} .

14.2 TEMPERATURE EFFECTS ON AQUEOUS Am^{3+} COMPLEXES

A preliminary examination of the temperature effects (15 to 90°C) on the spectrum of an aqueous

⁷J. T. Bell, C. C. Thompson, and D. M. Helton, "The High Temperature Spectra of Aqueous Transition Metal Salts. Part I. Praseodymium and Neodymium Nitrate to 356°C," *J. Phys. Chem.* (in press).

solution of Am^{3+} and iminodiacetic acid indicates that the formation of the americium-carboxylic acid complex is highly endothermic; ΔH was found to be approximately 8 kcal. This is a large ΔH for a reaction which was not expected to be endothermic, and it encourages more intensive investigations of the thermodynamic quantities for such reactions.

14.3 EMISSION SPECTRA OF THE TRANSURANIUM ELEMENTS

The emission spectrum of 1 at. % of Am_2O_3 embedded in crystalline calcium tungstate (CaWO_4) was found to have a strong emission band at 7984 Å, which is approximately 50 Å higher than the wavelength of the ruby laser light. Other emission bands that will aid in establishing the energy levels for the electronic transitions in trivalent americium were also observed. The quantum efficiencies of the Am_2O_3 emission transitions are now of interest in determining the feasibility of an americium laser.

14.4 DENSITIES OF AQUEOUS KCl AND UO_2SO_4 TO 374°C

The titanium dilatometer and the techniques developed for measuring the densities of liquids and solutions from room temperature to 400°C have been described.⁸ The densities of three KCl solutions and one UO_2SO_4 solution were measured at temperatures between 25 and 374°C.⁹ The change

in the densities of the KCl solutions at 25°C is a linear function of the KCl concentration, but this linear relationship disappears at higher temperatures. At the higher temperatures, the greatest change in the solution density per unit of KCl concentration occurs between 0 and 0.1 M, whereas between 0.1 and 1.0 M KCl the density change is a linear function of the KCl concentration. The change in the density of the UO_2SO_4 solution over any temperature range is greater than the density changes for the KCl solutions over the same range, and is most notable at temperatures above 250°C.

At low temperatures, the density of pure water is greater than the density of water containing KCl or UO_2SO_4 .¹⁰ At temperatures near 250°C these two densities are nearly equal; however, at higher temperatures the density of pure water is less than the density of water containing the electrolytes. This supports the theory that dissolved electrolytes induce specific structures in the solution and hold the solvent molecules together as the temperature increases.

⁸J. T. Bell, R. E. Biggers, T. G. Rogers, and A. M. Rom, "A Dilatometer Method for the Precision Measurement of the Densities of Liquids to 400°C and 5000 psi," *Rev. Sci. Instr.* (in press).

⁹J. T. Bell, D. M. Helton, and T. G. Rogers, "The Densities of Aqueous KCl and UO_2SO_4 from 25°C to 374°C," submitted to the *Journal of Chemical and Engineering Data*.

¹⁰J. T. Bell and D. M. Helton, "Some Qualitative Deductions About Solution Structure Based on the Densities of 'Solution Water' and Pure Water from 25 to 374°C," submitted to the *Journal of Physical Chemistry*.

15. Reactor Evaluation Studies

This program, which is a joint effort with other ORNL Divisions, especially the Reactor Division and the Metals and Ceramics Division, has the primary purpose of assisting the USAEC in evaluating the technical feasibility and economics of various nuclear power concepts being developed, or being considered for development, under the U.S. civilian power program. Work in this Division during the past year was devoted primarily to the development of linear programming models for use in the planning of optimal nuclear power systems in the United States. Other work in the Division included principal responsibility for preparation of the report of the Fuel Recycle Task Force,¹ assistance in preparation of the report of the Systems Analyses Task Force,² evaluation of fuel cycle costs for metallic uranium-fueled pressurized-water reactors (PWR's),³ estimation of costs for on-site vs off-site fuel cycle facilities and shipping associated with liquid-metal-cooled fast breeder reactors (LMFBR's), and initiation of studies to develop a dynamic programming model for the optimization of nuclear power systems.

15.1 OPTIMIZATION STUDIES OF THE REPROCESSING INDUSTRY IN AN EXPANDING NUCLEAR ECONOMY

Last year's report⁴ described early results from linear programming studies of the optimal growth

¹Reactor Fuel Cycle Costs for Nuclear Power Evaluation, USAEC Civilian Nuclear Power Series, WASH-1099 (in preparation).

²Potential Nuclear Power Growth Patterns, USAEC Civilian Nuclear Power Series, WASH-1100 (in preparation).

³F. G. Welfare and J. E. Jones, *Physics, Thermal Hydraulic, and Fuel Cycle Cost Analyses of a Metallic Uranium Direct Replacement Core for PWR's*, ORNL-TM-2943 (April 1969).

⁴Chem. Technol. Div. Ann. Progr. Rept. May 31, 1968, ORNL-4272, pp. 234-36.

of the fuel reprocessing industry in the United States. Emphasis was centered on the effects of shipping and inventorying of fuel and the economics associated with large plant sizes. In these studies the regional spent fuel reprocessing loads are based on projections of nuclear power generation throughout the period 1970 to 2020 in each of the eight Federal Power Commission regions (Table 15.1). Costs are present-worthed using a discount rate of 12%/year, which is estimated to be applicable to common ownership of the fuel, the backlogging facility, and the reprocessing plant by a corporation with a "medium" cost of money. Maximum fuel reprocessing plant sizes are prescribed for each year throughout the period of study, based on projected limits of technology. The linear programming solution, obtained with the MPS/360 mathematical programming system on an IBM 360/75 computer, provides estimates of the optimal degree of inventorying and the size and startup schedule of new reprocessing plants in each region and time period.

Other data assumed for the study are as follows:

Plant life	= 15 years
Plant capital cost	= $(\$9 \times 10^6)$ (metric tons capacity/year) ^{0.35}
Plant operating cost	= \$500/metric ton fuel
Inventorying cost	= \$10,600/metric ton fuel

Shipping costs, \$/metric ton fuel:

Between Region	and Region						
	I	II	III	IV	V	VI/VII	VIII
I	1600	3200	4100	4300	6700	8400	10700
II		1600	3000	3200	4800	7000	8900
III			2000	4300	4500	7700	9200
IV				1800	4000	5100	7200
V					2200	5300	6100
VI/VII						3000	4200
VIII							2000

The nonlinearity of the plant capacity-capital relationship (which is handled in the MPS/360 system by using separable programming procedures) creates a multiplicity of local extremals on the system response surface, and the linear program is not assured of finding the global extremal among these. The study led to eight different solutions from the same set of input data. A

solution that is more accurate than the solutions described last year is presented in Table 15.2. The present-worth-levelized reprocessing cost for the solution shown is \$10.84 per kilogram of fuel. This cost consists of 70% for new plant capital, 22% for shipping, 4.5% for plant operation and maintenance, and 3.5% for inventorying. A solution in which no limits were placed on plant

Table 15.1. Projected Geographical Distribution of Spent-Fuel Discharges

Units are "equivalent" metric tons^a discharged during year

Year	FPC ^b Region Designation								Total in U.S.A.
	I	II	III	IV	V	VI	VII	VIII	
1970	94	3	0	21	0	0	24	15	157
1971	127	9	13	72	0	0	25	16	262
1972	228	21	86	163	0	0	33	21	553
1973	308	28	202	182	0	11	31	19	782
1974	370	78	285	224	0	36	30	54	1,078
1975	426	105	348	260	15	43	46	108	1,351
1976	529	125	455	303	25	50	75	150	1,711
1977	633	141	545	347	24	53	102	198	2,042
1978	781	175	684	414	39	55	134	273	2,556
1979	889	192	803	458	47	67	159	336	2,950
1980	1,204	258	1,090	606	54	88	219	481	4,001
1982	1,694	397	1,589	819	115	140	315	738	5,807
1984	2,079	554	2,002	995	187	177	400	971	7,365
1986	2,694	808	2,674	1,301	316	238	539	1,344	9,914
1988	3,525	1,195	3,602	1,747	540	327	742	1,866	13,544
1990	4,358	1,672	4,633	2,253	896	429	981	2,474	17,697
1992	4,847	2,113	5,349	2,629	1,339	508	1,174	2,947	20,907
1994	5,362	2,640	6,074	3,061	1,940	599	1,420	3,475	24,571
1996	5,923	3,262	6,855	3,544	2,598	701	1,696	4,043	28,623
1998	6,414	3,897	7,556	4,001	3,305	799	2,006	4,586	32,564
2000	7,376	4,840	8,735	4,739	4,277	955	2,484	5,437	38,842
2002	8,301	5,791	9,896	5,446	5,289	1,109	3,049	6,233	45,114
2004	9,343	6,832	11,135	6,187	6,360	1,270	3,600	7,063	51,791
2006	11,115	8,461	13,282	7,467	7,953	1,543	4,490	8,398	62,708
2008	12,200	9,617	14,564	8,291	9,098	1,720	5,131	9,190	69,812
2010	13,791	11,168	16,481	9,456	10,640	1,970	5,999	10,284	79,789
2012	15,214	12,585	18,181	10,474	12,071	2,203	6,799	11,176	88,703
2014	16,550	13,899	19,732	11,428	13,369	2,417	7,552	11,955	96,902
2016	18,605	15,843	22,111	12,878	15,298	2,736	8,648	13,245	109,365
2018	19,557	16,868	23,246	13,602	16,291	2,905	9,237	13,775	115,480
2020	20,419	17,822	24,274	14,274	17,278	3,056	9,778	14,214	121,116

^aOne metric ton of (mixed core and blanket) FBR fuel is assumed to be equivalent to two metric tons of LWR fuel for reprocessing purposes.

^bFederal Power Commission.

Table 15.2. Minimum-Cost Schedule for Construction of New Reprocessing Plants and
Inventorying and Reprocessing of Spent Fuel

(all values in metric tons)

Year	Plant Size Limit	Total Fuel Inventoryed	Total Fuel Processed	New Plants Constructed [size (region)]
1970	520	160		
71	650	420		
72	910	60	910	910(I)
73	1,200		840	
74	1,300	170	910	
75	1,400	610	910	
76	1,700	1,400	910	
77	1,800	220	3,200	970(II); 1,300(IV)
78	2,000		2,800	
79	2,200		3,000	
80	2,500		4,000	1,200(VIII)
81	2,700	260	4,400	
82	3,000		6,100	2,000(III)
83	3,200		6,500	
84	3,400		7,400	1,600(I)
85	3,500		8,100	
86	3,900		9,900	3,700(III)
87	4,000	330	10,500	
88	4,700		13,900	3,400(VIII)
89	4,900		15,400	4,900(I)
90	5,200		17,700	
91	5,500		19,200	
92	5,700		20,900	2,700(IV); 3,000(VI/VII)
93	6,000		22,400	4,000(II)
94	6,200		24,600	3,300(IV)
95	6,500		26,500	
96	6,800		28,600	
97	6,900		30,400	6,900(III)
98	7,200		32,600	
99	7,400	2,600	31,900	
2000	7,800		41,400	5,700(V); 6,800(VIII)
1	8,200		42,000	5,000(I)
2	8,400		45,100	6,400(III)
3	8,700		48,200	
4	9,100		51,800	7,500(IV); 8,500(VI/VII)
5	9,400		55,300	
6	10,000		62,700	10,000(II)
7	10,300		66,500	9,900(I)
8	10,400		69,800	
9	10,400		73,300	7,800(V); 5,400(VIII)
10	10,400		79,800	
11	10,400		84,000	10,400(III); 6,000(IV)
12	10,400		88,700	
13	10,400		92,700	8,800(I)

Table 15.2 (continued)

Year	Plant Size Limit	Total Fuel Inventoried	Total Fuel Processed	New Plants Constructed [size (region)]
14	10,000		96,900	
15	10,400		101,700	10,400(III); 10,400(V)
16	10,400		109,400	10,400(VIII)
17	10,400		111,800	10,400(II)
18	10,400		115,500	10,400(I)
19	10,400		117,900	10,400(IV); 10,400(VI/VIII)
20	10,400		121,100	

size (and which led to plants of capacity up to 62,000 metric tons of fuel per year) indicated a present-worth-levelized reprocessing cost of \$9.43 per kilogram of fuel. The major conclusion of the study is that there is considerable economic incentive toward acquiring the capability to build and operate large plants.

15.2 THE OAK RIDGE SYSTEMS ANALYSIS CODE

A nuclear power systems linear programming model, designated the Oak Ridge Systems Analysis Code (ORSAC), was developed this year for use in planning optimal nuclear electric power systems in the United States. This model is similar to the one that was developed by the USAEC Systems Analysis Task Force (SATF) and programmed for a Univac 1108 computer at the Pacific Northwest Laboratory. By comparison, the ORSAC model is applicable to problems having greater detail and dimensionality because it exploits the capabilities of the IBM 360/91 computer and the IBM proprietary linear programming package, MPS/360.

In the ORSAC model the United States is divided into a maximum of 36 power cost regions based on the regional cost of fossil fuel. Individual nuclear and fossil plants are permitted to assume one of two or more characteristic functions that prescribe the plant capacity factor as a function of the age of the plant. Available forecasts of the electrical generating capacity demands for each region, capacity factor type, and time period are supplied as input to the code. The amounts of U_3O_8 available at 11 price levels are also established as input. Availability and requirements of other fissile and fertile materials and

commodities are balanced throughout the period of study. Startup rate restraints are imposed on new reactor types based on forecasted technology. The linear program (LP) is then used to determine the regional startup and operating schedule, of both nuclear and fossil power plants, that represents the minimum present-worth cost of electric energy. This cost includes the purchase of U_3O_8 and other materials, construction and operation of fuel cycle plants, separative work in existing and new gaseous diffusion plants, and the installation and operation of the power plants throughout the period of the study. Nonlinear costs, such as fuel cycle costs that may vary exponentially with plant size, are treated by iteration of the LP results.

A simplified flow diagram of the ORSAC package is shown in Fig. 15.1. The main program of the package, SYSCO, has the primary functions of generating magnetic tapes for input to the linear program MPS/360, providing for the iteration of LP results, guiding the selection of subprograms, and storing data that are common to the various subprograms. This program may also be used independently of the LP to calculate complete material balances and costs for a system of power plants with a prescribed startup and operating schedule.

The first step in implementation of the package involves the selection of the types of nuclear plants for the study. A permanent data tape containing the transient nuclear materials loading and charge-discharge history (in full power years) of 70 types and/or versions of conceptual 1000-Mw (electrical) nuclear reactors has been prepared by using tabulated data from SATF exhibits or by direct generation using either the zero dimensional

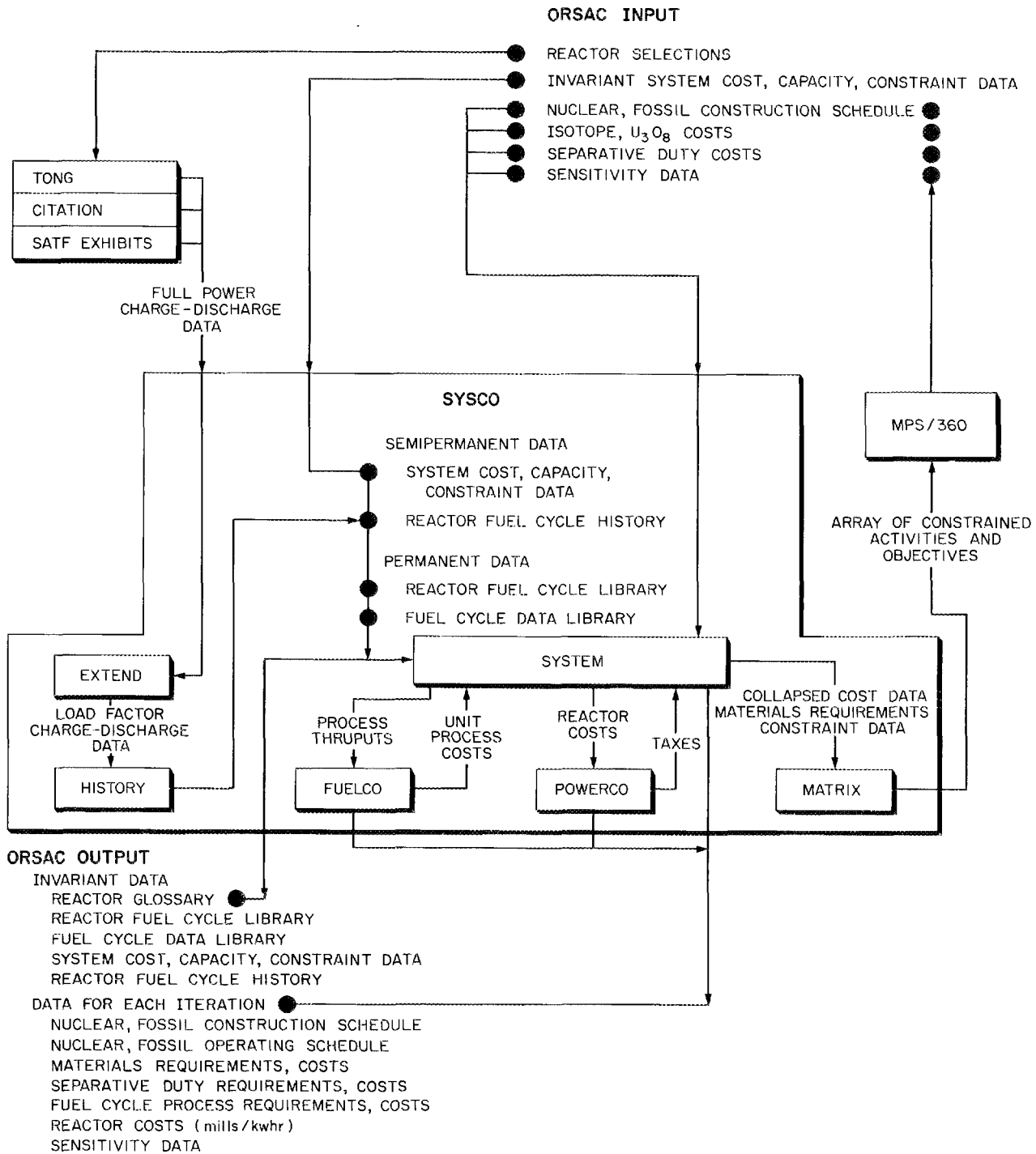


Fig. 15.1. Flow Diagram of the Oak Ridge Systems Analysis Code.

reactor depletion code TONG or the multidimensional depletion code CITATION. The reactor full power operating history is described in terms of the beginning-of-cycle loading, end-of-cycle loading, fresh-fuel charge, recycle fuel charge, and discharge of each of 12 actinide isotopes in a maximum of four refueling zones for as many as 200 refueling events plus those for steady-state cycles. The SYSCO program also contains a built-in library of cost and auxiliary data for these 70 types of nuclear plants, as well as for a variety of types of fossil-fueled plants.

The execution of the ORSAC program begins with the reading (by SYSCO) of input data that specify such items as the time horizon, types of power plants to be included, economic ground rules (e.g., interest, tax, and insurance rates) for power and fuel cycle plants, U_3O_8 availability as a function of cost, existing separative duty capacity, electrical power demands, and constants for the analytical capacity factor functions. A subprogram, EXTEND, then begins to read the full-power charge-discharge data for the appropriate reactors and, using the analytical capacity factor functions, to generate charge-discharge data in calendar years and provide for the complete discharge of the reactor at the end of its operating life.

The charge-discharge data for each refueling event in the operating history of a reactor are read by the HISTORY subprogram as they are generated by EXTEND. The HISTORY subprogram then makes use of two other permanent data libraries, the "fuel cycle data library" and the "reactor fuel cycle library," that are built into SYSCO to generate an array of annual material throughputs for each of the operations that characterize the fuel cycle of the reactor. These calculations are repeated for each date in the charge-discharge history of the reactor and for each reactor in the study. The resulting reactor fuel cycle material history data are stored in SYSCO and written out as part of a report of the calculation.

The fuel cycle data library contains information that characterizes 200 types of fuel cycle operations. These data include constants for cost equations, incremental time required for the operation, the fractional loss of fuel, the fractional recycle of fuel, and the base enrichment of fuel. The processes and other fuel cycle operations include conversion, gaseous diffusion, preparation, fabrication, reprocessing, reconversion, and shipments.

The reactor fuel cycle library provides an itemization of the chains of fuel cycle events that

are used by each type of reactor. The data include lag times for plant inventory and decay, indexes that refer to the appropriate fuel cycle operations, and other indexes that denote either withdrawal from or generation of material stockpiles.

After the fuel cycle history of each reactor has been generated, the SYSTEM subprogram of SYSCO is supplied with estimates of the optimal startup schedules of nuclear and fossil plants and certain other data that will be recalculated by iteration through the linear program. The SYSTEM subprogram uses the startup schedules of the nuclear plants to deduce the operating schedules; from these schedules, it then calculates the throughputs for each of the fuel cycle processes by considering that many of these processes are shared by several types of reactors. The FUELCO subprogram uses the throughputs to calculate the unit process cost for each of the years of the horizon under study. For each reactor type and startup period, a progressive weighted vector multiplication of these process costs with the fuel cycle throughputs generated by HISTORY permits the calculation of annual fuel cycle costs. Fuel cycle costs for fossil plants are calculated by using analytical functions of unit cost as a function of cumulative usage.

The annual fuel cycle and operating costs, together with the capital cost that is associated with the startup of each nuclear or fossil plant in each period of the horizon, are used by the POWERCO subprogram to calculate the total annual expenses including taxes, insurance, and interim replacements. The POWERCO results are present-worthed to derive a single cost coefficient that represents all of the cost (except U_3O_8 and separative duty, which are treated separately) that is associated with the startup of a 1000-Mw (electrical) power plant having a characteristic capacity factor history for each period in which the plant type may enter the solution.

The array of collapsed cost coefficients, annual materials requirements, and other constraints from each possible power plant startup is used by the MATRIX subprogram to generate an array of constrained activities and objectives for use by the linear program. The MPS/360 programming system is then employed to generate new construction schedules for nuclear and fossil plants, marginal costs of various isotopes and separative duty, and sensitivity information. These data are then used to generate new fuel cycle costs for the next iteration.

16. Preparation and Properties of Actinide Oxides

16.1 ELECTROPHORETIC STUDIES OF URANIA AND THORIA-URANIA SOLS

UO₂ Sols

Studies of the electrokinetic properties of urania and thoria-urania sols were continued, using both the Beckman model H electrophoresis instrument and the Waters streaming current detector.

We previously reported that the U(VI) in a partially oxidized chloride-stabilized UO₂ sol was not uniformly distributed and, further, that the particles with the higher U(VI) concentrations had the higher electrophoretic mobility.¹ This means that the charge on the oxidized particles is higher and, consequently, the stability of the sol containing such particles should be enhanced. In the case of nitrate-stabilized sols, such a situation would be contrary to the general observation that the oxidation of these sols causes coagulation. Therefore, electrophoretic measurements were made using a nitrate-stabilized UO₂ sol that had been prepared by the amine extraction process to clarify this point. Here, as in previous work, two moving boundaries were observed, indicating two differently charged species. Upon completion of the electrophoresis experiment, the Tiselius cell arms were isolated and sampled. Analyses of the faster-moving, more highly charged material that was found in the ascending branch of the cell showed a U(VI)/U(IV) ratio of 0.192, as compared with 0.287 for the slower-moving material that was removed from the descending branch of the cell. (The ratio was 0.239 in the starting material.) Thus, in the case of nitrate-stabilized sols, the more highly charged material is that with the lower concentration of U(VI). We conclude, then,

¹Chem. Technol. Div. Ann. Progr. Rept. May 31, 1968, ORNL-4272, pp. 238-39.

that oxidation of a nitrate-stabilized UO₂ sol decreases the zeta potential, thus rendering the sol less stable, and leads to coagulation, in agreement with previous observations. Calculations based on material balance and the geometry of the electrophoresis cell showed that about 17% of the total uranium in the sol was associated with the faster-moving material.

In studies using the Waters streaming current detector, we attempted to determine what effect digesting a UO₂ sol at 80°C would have on the zeta potential. The results, which are summarized in Table 16.1, show that a sharp drop occurs in the streaming current in the first 1.5 hr, followed by a much slower decrease. The pH was found to increase from 2.40 to 2.65 during digestion.

ThO₂-UO₃ Sols

The electrokinetic properties of several ThO₂-UO₃ sols were investigated, using, for the most part, the same sols that were used in the micro-

Table 16.1. Effect of Digestion of a UO₂ Sol^a at 80°C on Its Zeta Potential

Digestion Period (hr)	Streaming Current (μamp ^b)	Zeta Potential (mv ^c)
0	+27	+64
0.5	+24	+57
1.0	+20	+47
1.5	+18	+43
24	+16	+38

^aBatch code ASPU-6.

^bMeasured after quenching to room temperature.

^cEstimated by using the empirical conversion factor for Waters streaming current detector No. 1.

sphere-forming studies reported in Sect. 6.3. When these sols were subjected to moving-boundary electrophoresis, two boundaries were again seen; however, chemical analysis of the separated fast- and slow-moving fractions showed no differences in composition. It is likely that the second boundary was caused by the presence of Th^{4+} in the system, since it had been noted previously that a Th^{4+} concentration as low as $10^{-4} M$ in ThO_2 sols caused an observable boundary.² The electrophoretic mobilities that were calculated from the velocities of the major descending sol boundaries are given in Table 16.2. The electrical conductivities and the pH values measured at the time of electrophoresis are also included. As shown in Table 16.3, all of these properties change with time.

The pH decreases and the electrical conductivity increases, while the streaming current changes in an unpredictable manner. As with pure ThO_2 sols, the streaming current values for these materials correlated poorly with zeta potentials that were calculated from electrophoretic mobilities. An interesting phenomenon observed during the electrophoresis of these red-colored ThO_2 - UO_3 sols was the formation of a very thin layer of yellow material at the interface between the ascending sol boundary and the supporting electrolyte, which was an aqueous HNO_3 - NH_4NO_3 solution with a pH and a conductivity approximately equal to those of the sol. Although attempts to recover and analyze this layer were unsuccessful, we believe that it is the result of an electrochemical reaction occurring between the sol and HNO_3 . (Addition of a drop of HNO_3 to such a sol has been noted to give an instantaneous yellow color.) This phenomenon was not observed at the interface between the supporting electrolyte and the descending sol boundary.

Adsorption of CO_2 by UO_2 Sols

The rapid, reversible adsorption of CO_2 on chloride-stabilized UO_2 and nitrate-stabilized ThO_2 sols has been reported.¹ Recently, this reaction has also been noted for nitrate-stabilized UO_2 sols; specifically, the CO_2 was found to displace nitrate ions associated with the sol

particles. By extracting the freed nitrate with an amine, essentially quantitative replacement was achieved. The sol was converted to a gel in the process, but could be readily reconverted to a sol by the addition of either HNO_3 or HCl . Thus,

Table 16.2. Electrophoretic Mobilities of ThO_2 - UO_3 Sols

Sol Code	Electrophoretic Mobility ($\text{cm}^2 \text{v}^{-1} \text{sec}^{-1}$)	Electrical Conductivity (micromhos/cm)	pH
	$\times 10^{-4}$		
EV-30A	1.16	5900	4.75
EV-30A-RV3	1.23	6100	4.8
ASP-15-AEI	1.26	2300	5.4
ASP-9-RT ^a	0.73	525	4.5
ASP-9-ID-96 ^a	0.74	2700	3.6

^aDiluted 1:5 with distilled water; $\sim 0.016 M$ in uranium, $0.04 M$ in thorium.

Table 16.3. Effect of Time on the Properties of ThO_2 - UO_3 Sols

Sol Code	Streaming Current (μamp^a)	pH	Electrical Conductivity (micromhos/cm)
EV-29B			
Initially ^b	+39	4.42	7100
31 days later	+52	4.25	7250
EV-30A			
Initially ^b	+31	4.75	5900
31 days later	+27	4.15	6000
EV-30A-RV3			
Initially ^b	+56	4.84	6100
31 days later	+48	4.20	6400
EV-30-BD-1			
Initially ^b	+44	4.82	5400
26 days later	+54	4.42	5800
ASP-15-AEI			
Initially ^b	+48	5.38	2300
26 days later	+76	4.90	2500

^aUsing Waters streaming current detector No. 2. This detector reads about 85% higher than the No. 1 detector.

^bAt the time of initial streaming current measurement.

²Chem. Technol. Div. Ann. Progr. Rept. May 31, 1967, ORNL-4145, pp. 282-84.

CO₂ adsorption could be used as a simple method for changing a sol from one stabilizing ion form to another.

16.2 INVESTIGATION OF LANTHANIDE SOLS

The study of the hydroxide (or hydrous oxide) sols of the lanthanides was continued. Emphasis was centered on aging phenomena as observed by changes in the streaming current, electrical conductivity, and pH. The sols were prepared by adding, with vigorous stirring, 0.2 *N* lanthanide nitrate solutions to a 20-fold excess of 8 *N* NH₄OH. Each precipitate was washed with distilled water five to ten times by slurring and then centrifuging. When the pH of the wash water decreased to less than 9, washing was stopped, and the cake was liquefied by shaking it on a vortex mixer. In most cases, water was then added to give 0.1 to 0.2 *M* sols; however, sols of higher concentrations (0.8 to 1.0 *M*) were also prepared in a few instances. These sols tended to be very thixotropic, and reliable measurements of their properties, especially streaming current, were difficult to make.

Aging Effects

Figure 16.1 shows the behavior of the streaming current for some freshly prepared sols. These changes were accompanied by an increase in electrical conductivity and a decrease in pH. In the case of the sols of the three lightest lanthanides, the streaming current slowly declined with time after precipitation; the streaming currents of the sols of four heavier lanthanides, on the other hand, showed a large initial increase, followed by a fairly sharp decline. This behavior may be related to the times required for crystallization of the originally amorphous precipitates. Haire and Willmarth³ have reported the following crystallization times at 24°C: 1 hr for La, Ce, and Pr; 4 hr for Nd; 12 hr for Sm; 24 hr for Eu; and 40 hr for Gd. Since La, Ce, and Pr would have completed the crystallization process before the streaming current measurements were taken, no effect would be observed. The times at which the decline in

streaming current were noted for Nd and Sm sols, but not those for Eu and Gd sols, are in good agreement with Haire's values.

Changes in the streaming current and the pH continued for seven to ten days, until steady-state conditions were reached. In most cases, changes in the electrical conductivity continued for a similar period of time; however, the electrical conductivities of Eu and Gd sols continued to increase significantly for more than two months.

Temperature Effects

One of the most interesting observations made previously on lanthanide hydrous oxide sols was the reversal of the sign of the charge (from positive to negative) upon digestion of the sols at 80°C for two to four weeks.¹ However, in attempts to study the rate of this process, we were unable to duplicate these results. Hydrous oxide sols of ytterbium and thulium were prepared and placed in an 80°C constant-temperature bath. Samples were removed periodically and cooled to room temperature; then the streaming current was measured. Both sols showed normal aging behavior for the first several days. Then, after four days in the case of thulium and five days in the case of ytterbium, it was noted that the sols had separated into two fluid phases and the streaming current (measured after the sol was shaken) had increased by about 10 μamp. In a few more days, however, the sols essentially reached steady

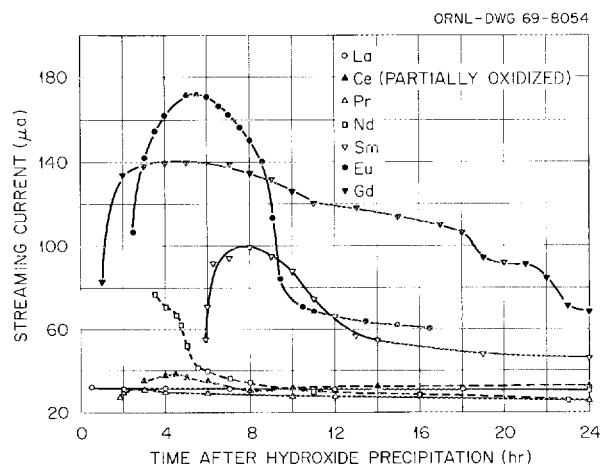


Fig. 16.1. Changes of Streaming Current in Freshly Prepared Lanthanide Hydrous Oxide Sols as a Function of Time After Precipitation.

³R. G. Haire and T. E. Willmarth, *Trends and Differences in the Crystallization Behavior of Lanthanide Hydroxide Preparations*, ORNL-TM-2387 (October 1968), p. 7.

state, and continued digestion for three months did not produce any further change. Charge reversal did not occur in the digested sols; in fact, the sols were more highly charged than the controls, which had been aged at room temperature. The digested sols also had higher electrical conductivities. When the two phases of the ytterbium sol were separated and examined by an electron microscope, the light phase was found to be essentially amorphous, while the denser phase consisted mainly of square platelets about 0.4μ on a side.

Later, a gadolinium sol that had been standing at room temperature for eight months was observed to have formed two phases similar to those found in the 80°C digested sols. Further investigations of the differences in preparative and experimental techniques will be made in an effort to determine why some sols undergo reversal of the sign of the charge upon digestion and others do not.

16.3 MATHEMATICAL MODELS OF COLLOIDAL SYSTEMS

The theoretical study of colloidal particles was continued. Two projects, a study of the flocculation process and a statistical study of the double layer, are in progress.

Flocculation

In many sols, the colloidal particles aggregate to form strings. In order to explain this type of flocculation, the Verwey-Overbeek attractive and repulsive potentials for the interaction between two particles were used. It was assumed that the attractive and repulsive potentials of a string were a linear sum of the attractive and repulsive potentials of the individual particles. Thus

$$V_{AS} = \sum_i V_{Ai},$$

$$V_{RS} = \sum_i V_{Ri},$$

and

$$V_{TS} = V_{AS} + V_{RS} = \sum_i (V_{Ai} + V_{Ri}),$$

where V_{Ai} is the attractive potential of the i th particle, V_{Ri} is the repulsive potential of the i th particle, V_{AS} is the attractive potential of the string, V_{RS} is the repulsive potential of the string, and V_{TS} is the total potential of the string.

Calculations have been made for 80-Å-diam particles and singly charged $0.08 M$ electrolyte. The number of particles has been varied from two to seven. In each case, the repulsive potential is at a minimum and the attractive potential is at a maximum at the end of the string. Currently, we are studying a larger number of particles, particles of larger radii, variations in electrolyte concentration, and variations in the charge of the electrolyte. We also hope to consider nonspherical particles in the future.

Double Layer

In the study of the double layer, we are attempting to create a mathematical model using Monte Carlo techniques. Adsorption sites on the surface and ions in the adjacent solution are represented by locations in the computer core storage, and energies are assigned to the ions, using kinetic theory. A random number is generated, which corresponds to the storage location representing an ion, and the selected ion is then considered to absorb, desorb, or remain unaffected, depending upon its energy and its state when selected.

Future work will include the correlation of the results of this study to isotherms and to results of experimental rate studies. The purpose of such a correlation will be to test the assumptions that are used in double-layer theory and to eventually study the effects of temperature, charge, and concentrations on the formation of the double layer.

17. Chemistry of Carbides, Nitrides, and Carbonitrides

The basic chemistry of the carbides, nitrides, and carbonitrides of uranium and thorium is being investigated, with emphasis on reactions in aqueous systems. This work has application to the processing of power reactor fuels, reactor safety, and high-temperature materials development. Previous studies were concerned primarily with the reactions of the uranium and thorium carbides with water and aqueous solutions of nitric, hydrochloric, and sulfuric acids, sodium hydroxide, and ammonium fluoride. During the past year, attention was focused on the reactions of uranium mononitride and carbonitrides with nitric acid.

Reaction of UN with Nitric Acid

Uranium mononitride, like uranium monocarbide, shows promise as a potential fuel for fast breeder power reactors. It has been reported that a fast reactor fueled with UN could have a breeding ratio of 1.40 (vs ~ 1.43 for carbide and 1.25 for oxide-fueled reactors).¹ In comparison with uranium monocarbide, the mononitride has better compatibility with claddings, a higher thermal conductivity, a higher melting point, and a lower thermal-expansion coefficient. Also, limited irradiation data for the mononitride indicate that it swells less during irradiation and has a higher "break-away swelling" temperature.¹ In addition, the U-N system is simpler than the U-C system since the higher nitrides can be destroyed by simple thermal decomposition, thereby making the production of stoichiometric mononitride easier than that of monocarbide. One step in the chemical processing of nitride reactor fuels may be the dissolu-

tion of the nitride in the nitric acid; consequently, this reaction was studied in some detail.

A preliminary investigation at this laboratory² showed that uranium mononitride reacts with 0.5 to 15.8 *M* HNO₃, giving yellow uranyl nitrate solutions and gaseous mixtures of N₂, N₂O, NO, and NO₂ (when the acid concentration was 6 *M* or higher). More complete studies have shown that significant quantities of nitrous acid and, in some cases, ammonium ions, are produced in the reaction of uranium mononitride with 0.5 to 15.8 *M* HNO₃; in addition, the off-gas contains elemental nitrogen and gaseous nitrogen oxides (Table 17.1). The quantities of the various nitrogen-containing products were found to be functions of the acid concentration, reaction temperature, and time of the reaction. For convenience, the nitrogen oxide gases have been reported as N₂O, NO, and NO₂, which were the species detected by the gas chromatographic analysis. In experiments 19 and 21, which were run at 25°C (i.e., the temperature at which the total volume of the system is known), the actual gaseous products must have been N₂, N₂O, N₂O₃ (NO + NO₂), and N₂O₄ (NO₂ + NO₂) in order to relate the experimentally observed gas expansion with the gas volume as calculated from the known volume of the system and the gas chromatographic analysis. Experiments 17, 18, 20, and 22 were calculated by assuming that the products were N₂, N₂O, N₂O₃, and N₂O₄, since only the gas expansion in the system could be determined for experiments carried out above room temperature (i.e., where there was a temperature gradient across the apparatus). Oxidation-reduction balances for these experiments agreed within $\pm 10\%$, which is the accuracy of the gas chromatographic technique.

¹Liquid Metal Fast Breeder Reactor Program Plan, Volume 7, Fuels and Materials, WASH-1107 (August 1968), pp. 7-399-7-402, 7-415.

²L. M. Ferris, *J. Inorg. Nucl. Chem.* **30**, 2661 (1968).

Table 17.1. Data for the Reaction of UN^a with HNO₃

Expt. No.	HNO ₃ Concentration (M)	Temperature (°C)	Volume of Gas Evolved [milliliters (STP) per gram of nitride]	Gaseous Products (millimoles/g)				Species in Solutions (millimoles/g)		Time Required to Dissolve All Solids	Time ^b Allowed for Reaction	Atom Ratio of N ₂ Formed to Nitride Nitrogen Oxidized Above NH ₄ ⁺
				N ₂	NO	N ₂ O	NO ₂	NH ₄ ⁺	NO ₂ ⁻			
1	0.5	80	122	3.8	1.4	0.2		0.3	0.6	1 day 5 hr	2 days	2.1
2	0.5	80	120	4.2	1.0	0.1		0.01	0.4	1 day < t < 2 days	8 days	2.2
3	1	80	110	2.4	2.1	0.4		1.2	0.5	5 hr	5 hr	1.8
4	1	80	117	3.8	1.0	0.3		0.03	0.3	5 hr	7 days	1.9
5	2	25	72	1.4	1.0	0.8		1.6	2.0	1 day 6 hr	2 days	1.2
6	2	25	78	1.8	0.8	0.9		1.2	2.0	1 day < t < 7 days	7 days	1.3
7	2	80	110	2.5	1.7	0.8		0.8	1.1	2 hr	2 hr	1.6
8	2	80	127	3.3	1.3	0.9		0.02	0.8	< 2½ hr	2 days	1.7
9	4	25	79	1.8	0.5	1.3		0.9	2.6	6 hr	23 hr	1.2
10	4	25	82	1.9	0.2	1.6		0.7	2.3	4 < t < 21 hr	7 days	1.2
11	4	35	82	1.5	0.6	1.6		0.8	2.5	2¾ hr	2¾ hr	1.0
12	4	35	95	2.5	0.2	1.5		0.2	2.1	3½ hr	7 days	1.4
13	4	80	120	2.4	1.3	1.5		0.3	1.3	13 min	1 hr	1.3
14	4	80	124	2.9	0.9	1.8		< 0.05	0.7	16 min	1 day	1.5
15	8	25	83	1.5	0.1	1.9	0.2	0.5	3.1	1 hr < t < 2 hr	2 hr	0.9
16	8	25	91	1.7	0.2	2.2		0.2	2.6	30 min	3 days	0.9
17	8	35	111	1.5 ^c	1.2 ^c	2.3 ^c	0.2 ^c	0.4	1.9	27 min	2½ hr	0.9
18	8	80	125	2.4 ^c	1.3 ^c	1.9 ^c	0.7 ^c	0.01	1.4	3 min	1 hr	0.9
19	12	25	119	1.6	0.5 ^d	2.6	1.5 ^d	0.2	2.0	12 min	2½ hr	0.9
20	12	35	129	1.7 ^c	1.0 ^c	2.8 ^c	1.5 ^c	0.1	1.3	4 min	3½ hr	0.9
21	15.8	25	115	1.5	0.3 ^d	2.6	1.9 ^d	0.2	2.2	8 min	1 hr	0.8
22	15.8	35	126	1.5 ^c	0.7 ^c	3.0 ^c	1.7 ^c	0.2	1.5	3 min	3 hr	0.8

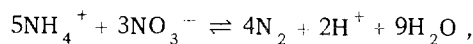
^aElemental analysis: U, 3.96 mg-atoms per gram of nitride; N, 3.90 mg-atoms/g; O, 0.11 mg-atom/g; C, 0.03 mg-atom/g.

^bAll the solids were dissolved but not necessarily all of the gas was evolved.

^cCalculated, assuming N₂, N₂O, N₂O₃, and N₂O₄ were actual products.

^dActual products were N₂, N₂O, N₂O₃ (NO + NO₂), and N₂O₄ (2NO₂).

Ammonium ion was an intermediate in the oxidation of nitride nitrogen to free nitrogen. At low acid concentrations and low temperatures, nitrogen, resulting from the oxidation of the ammonium ion, was evolved slowly (over a period of weeks, in some cases) after all the uranium mononitride had dissolved. This would not be a problem in fuel processing since the ammonium ion is readily destroyed by increasing the acid concentration and/or temperature. For example, less than 0.3% of the nitride nitrogen was found in the form of ammonium ion after an 8 M HNO₃ solution was heated for 1 hr at 80°C. The stoichiometry did not follow the simple equation



which was reported for the reaction of UC_{0.23}N_{0.77} with 1 to 8 M HNO₃.³ At high acid concentrations (8 to 16 M), the total amount of elemental nitrogen formed did not account for all the nitride nitrogen oxidized to a state higher than it has in NH₄⁺, while at very low acid concentrations (0.5 to 1 M), much more nitrogen was formed than was expected from the above equation (see Table 17.1). Although nitrate is obviously the principal oxidizing agent, the nitrite and NO formed in the initial dissolution of the mononitride can also oxidize the ammonium ion in 0.5 to 4 M HNO₃. This is most obvious in experiments 3 and 4 with 1 M HNO₃. When the reaction in experiment 3 was terminated at the end of 5 hr after all the mononitride had dissolved, the products (in millimoles per gram of mononitride) were: 2.4 of N₂, 2.1 of NO, 0.4 of N₂O, 0.5 of NO₂⁻, and 1.2 of NH₄⁺. In experiment 4, the reaction was continued for seven days; at the end of this time, the amount of nitrogen had increased to 3.8 millimoles per gram, while the amount of NH₄⁺ was negligible and the amounts of NO and NO₂⁻ had decreased to 1.0 and 0.3 millimole respectively. No significant change in the amount of N₂O was observed.

Reactions of Uranium Carbonitride with Aqueous Reagents

Uranium carbonitrides (solid solutions of UC and UN) are also of interest as possible fuels for

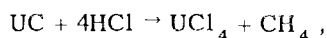
nuclear reactors. Last year the chemical properties of a UC_{0.23}N_{0.77} specimen were discussed.³

A second carbonitride specimen was prepared for us by R. A. Potter of the Metals and Ceramics Division by the reaction:



The product had the composition UC_{0.57}N_{0.38}O_{0.02} and contained less than 0.01% unreacted carbon. It was single-phase by x-ray diffraction analyses and had a lattice constant of 4.945 Å. While no UN was detected in the powder pattern, unreacted UN was recovered in HCl dissolution experiments. Therefore, the material was probably a mixture of a UC_{0.61}N_{0.34}O_{0.02} phase and about 5.6 wt % UN. Under the microscope the material appeared to be quite porous, containing perhaps 50% voids. The specimen was broken to a -10 +100 mesh powder for chemical studies. In preliminary qualitative tests made with various solutions, the uranium carbonitride was found to be inert both in water and in 6 M NaOH at 80°C (2-hr tests); reaction occurred with 6 M HCl, 6 M H₂SO₄, and nitric acid solutions.

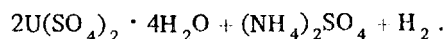
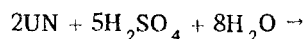
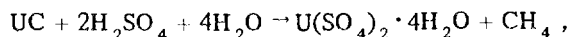
The reaction of this uranium carbonitride powder (U, 3.99 mg-atoms per gram of carbonitride; C, 2.29 mg-atoms/g; N, 1.51 mg-atoms/g) with 6 M HCl at 25°C exhibited an induction period of about 50 min during which no visible attack occurred. After this period, the reaction proceeded at a moderate rate, with 98% of the gaseous products being evolved within 4 hr. The primary products were: CH₄ (2.00 millimoles per gram of specimen), H₂ (0.90 millimole/g), NH₄⁺ (1.36 meq/g), and U⁴⁺ (3.75 mg-atoms/g) in accordance with the equations:



Some unreacted UN (0.22 millimole/g) was recovered as an insoluble black residue at the conclusion of the experiment. A small quantity of ethane (0.02 millimole/g) was detected in the gas. At 80°C, the reaction of this uranium carbonitride with 6 M HCl was quite rapid; 98% of the gas was evolved within the first 10 min. The products were similar to those obtained at 25°C except that all of the specimen, including the UN, reacted.

³Chem. Technol. Div. Ann. Progr. Rept. May 31, 1968, ORNL-4272, pp. 244-48.

In the reaction of the $UC_{0.57}N_{0.38}$ with 6 M H_2SO_4 at 80°C, 95% of the gas was evolved within 3 hr. The primary products were: CH_4 (2.04 millimoles per gram of specimen), H_2 (1.15 millimoles/g), NH_4^+ (1.47 meq/g), $U(SO_4)_2 \cdot 4H_2O$ (2.78 millimoles/g), and U^{4+} (0.88 millimole/g) in accordance with the equations:



Small quantities of ethane, ethene, propane, propene, and butane (totaling 5% of the carbon) were also detected in the gas. Three percent of the carbon was found in the sulfuric acid solution, and 3% was found in the uranous sulfate precipitate.

The uranium carbonitride reacted exothermally with nitric acid solutions to produce a yellow uranyl nitrate solution, carbon dioxide, nitrogen oxides, nitrous acid, unidentified nitric acid-soluble organic compound(s), and, in some cases, NH_4^+ and insoluble organic compound(s) (Table 17.2). Each reaction was arbitrarily terminated before all the gas had been evolved since previous experience had shown that this type of system requires days, or even weeks, to reach steady state. The amount of carbonitride carbon found as carbon dioxide varied with the acid concentration, temperature, and time allowed for the reaction. For example, with 4 M HNO_3 at 80°C, 30 and 70% of the carbon was found as CO_2 at the end of 1 and 24 hr respectively. There was not enough of the nitric acid-soluble organic compound(s) to permit their isolation or identification. The colors of the solutions varied from deep orange to a very dark wine, similar to those obtained from the reaction of uranium carbides with nitric acid. Small quantities (4 to 13% of the carbon) of insoluble organic compound(s) were found in the reactions with 1 to 8 M HNO_3 . These precipitates were insoluble in water, acetone, ether, and tetrahydrofurane, but dissolved readily in concentrated nitric acid, yielding very dark-colored solutions. Less than 0.1% of the uranium was associated with these precipitates. The quantities of the nitrogen-containing compounds produced by the reaction

also varied with the acid concentration, temperature, and time. Ammonium ion appeared to be an intermediate in the oxidation of the carbonitride nitrogen to elemental nitrogen. Somewhat more elemental nitrogen was found than would be expected from the experiments with pure UN. No nitrogen was found in the reactions of UC with nitric acid.⁴

Studies Relating to the U-C and Th-C Constitutional Diagrams

The carbide specimens prepared for the chemical studies covered a wide range of compositions and heat treatments, and had been carefully characterized by chemical, x-ray diffraction, and metallographic techniques. These specimens were used to obtain some information on the U-C system.⁵ Uranium sesquicarbide was found to have a line composition very close to $UC_{1.50}$ and an upper stability limit of about 1800°C. Below 1800°C, the uranium monocarbide lattice accommodated a maximum of about 1.02 carbon atoms per uranium atom. The dicarbide phase existed over a much wider composition range, from about $UC_{1.7}$ to $UC_{1.9}$ at 1765°C; this range narrowed as the temperature decreased. The maximum carbon content of the cubic dicarbide phase decreased with temperature from 1.89 carbon atoms per uranium atom at the melting point to a minimum of 1.85 at about the cubic-to-tetragonal transformation temperature. Combined-carbon/uranium atom ratios above 1.85 could be obtained at room temperature only by quenching specimens containing less than 0.2% free carbon because the free carbon acted as precipitation centers in the metastable solutions. When cooled from the cubic to the tetragonal region, the dicarbide disproportionated into monocarbide and a tetragonal dicarbide that had an estimated composition of $UC_{1.89}$ at room temperature. No thermal decomposition of the tetragonal uranium dicarbide was observed after heat treatment at 1260 to 1600°C.

The microstructures of the arc-cast thorium carbide specimens with C/Th atom ratios varying from

⁴L. M. Ferris and M. J. Bradley, *J. Am. Chem. Soc.* 87, 1710 (1965).

⁵M. B. Sears and L. M. Ferris, "Studies on the U-C Constitutional Diagram Between UC and UC_2 ," to be published in the *Journal of Nuclear Materials*.

Table 17.2. Data for the Reaction of $UC_{0.57}N_{0.38}O_{0.02}^a$ with HNO_3

Expt. No.	HNO_3 Concentration (M)	Temperature ($^{\circ}C$)	Volume of Gas Evolved [milliliters (STP) per gram of carbonitride]	Gaseous Products (millimoles/g)						Species in Solution			Precipitate C (mg-atoms/g)	Time ^b Allowed for Reaction	Atom Ratio of N_2 Formed to Nitride Nitrogen Oxidized Above NH_4^+
				N_2	NO	N_2O	NO_2	CO	CO_2	NH_4^+ (millimoles/g)	NO_2^- (millimoles/g)	C (mg-atoms/g)			
23	0.5	80	177	2.0	4.6	0.1	0.04		1.1	0.01	1.4	1.2	0.1	2 days	2.7
24	1	80	172	1.4	5.6				0.7	0.3	1.2	1.1	0.2	5 hr	2.3
25	1	80	198	1.9	5.0	0.3		0.03	1.7	0.02	0.8	0.7	0.1	2 days	2.5
26	2	25	95	0.9	2.9				0.5	0.6	3.9	1.2	0.3	1 day	2.0
27	2	80	144	1.1	4.8		0.1		0.5	0.3	1.8	1.3	0.2	1 hr	1.8
28	2	80	180	1.8	4.4	0.1	0.2	0.06	1.6	0.01	2.3	0.6	0.1	1 day	2.4
29	4	25	72	0.9	1.9				0.4	0.6	5.2	1.4	0.3	4 $\frac{1}{2}$ hr	2.0
30	4	25	79	0.8	1.9	0.1		0.04	0.6	0.6	5.4	1.0	0.1	1 day	1.8
31	4	80	123	1.4	3.0	0.1	0.2		0.8	0.04	2.4	1.9		1 hr	1.6
32	4	80	147	1.6	3.3	0.2	0.2	0.08	1.4	0.01	2.7	0.6		1 day	2.1
33	8	25	92	0.7	2.8 ^c	0.1	0.5 ^c		0.4	0.4	5.2	1.5	0.1	1 hr	1.3
34	8	25	114	1.2	2.8 ^c	0.2	0.5 ^c	0.08	0.8	0.1	4.1	1.4		1 day	2.2
35	12	25	98	0.8	2.1 ^c	0.2	2.4 ^c	0.02	0.4	0.3	4.9	1.4		1 $\frac{1}{4}$ hr	1.3
36	15.8	25	80	0.8	0.2 ^c	0.2	2.8 ^c	0.05	0.2	0.2	5.0	1.7		1 hr	1.1
37	15.8	25	110	1.1	0.9 ^c	0.1	3.2 ^c	0.05	0.6	0.1	5.3	1.3		1 day	1.6

^aElemental analysis: U, 3.99 mg-atoms/g; N, 1.51 mg-atoms/g; C, 2.29 mg-atoms/g; O, 0.08 mg-atom/g.

^bSolutions were usually too dark colored to tell visually when solids dissolved. In addition, solid products were often formed.

^cActual products were primarily N_2O_3 (NO + NO_2) and N_2O_4 ($2NO_2$).

0.8 to 2.1 (4.0 to 10.0 wt % carbon) were correlated with the chemical analyses, the x-ray diffraction analyses, and the products of hydrolysis.⁶ The thorium monocarbide phase was found to exist over a range of composition from about $\text{ThC}_{0.94}$ to at least as low as $\text{ThC}_{0.81}$. Specimens with compositions from $\text{ThC}_{0.99}$ to $\text{ThC}_{1.88}$ were two-phase mixtures of the mono- and dicarbides at room temperature. The maximum combined-C/Th atom

ratio obtained by arc-melting with graphite electrodes was 1.96. There was no evidence for any significant range of composition for the dicarbide at room temperature.

⁶M. B. Sears, T. M. Kegley, Jr., Leslie M. Ferris, and B. C. Leslie, *Metallographic Preparation of Arc-Cast Thorium Carbides and Correlation of Their Microstructures with Composition*, ORNL-4354 (March 1969).

18. Safety Studies of Fuel Transport

This program was organized in early 1966 to identify and resolve problems involving the transport of irradiated fuel elements from a reactor to a reprocessing site and to develop an *Irradiated Fuel Shipping Cask Guide* (originally designated as an *Irradiated Fuel Shipping Cask Criteria*¹) for the Division of Reactor Development and Technology.

The *Guide* was completed during this reporting period and is available as ORNL-TM-2410. It establishes suitable engineering standards for the design, fabrication, and inspection of irradiated fuel shipping casks by providing information on structural integrity, shielding, heat transfer, criticality, and materials of construction. A considerable amount of emphasis is placed on quality control during the fabrication of a cask.

The *Guide* is presently being revised to incorporate newly developed data, as well as comments that have been received from recipients of the report.

18.1 RESEARCH

The *Guide* was based, for the most part, on experimental results that were obtained by subjecting casks to the accident conditions that are stipulated in the Federal regulations.^{2,3} Results indicate that the application of a specified static force will not produce damage similar to that produced by the impact of a 30-ft drop. However, damage may be assessed by analytical methods based on the conservation of energy principle, as outlined in the *Guide*. In several cases this method has been correlated with experimental results.

At the present time we do not have sufficient data to predict with confidence the best weld joint design. Some limited information, based on observations of static tests and personal contacts with first-hand observers of cask impacts, leads us to believe that certain joint designs will withstand the 30-ft free fall more effectively than others.

A series of $\frac{3}{8}$ -in.-thick, 2-in.-wide coupons representing six different weld designs commonly accepted in present-day technology have been tested. These coupons, some of A516 carbon steel and some of 304L stainless steel, were backed with lead and placed in a holding fixture. A 300-lb weight was then dropped onto each specimen from a height of 30 ft, and the resulting deformation was noted. Results were found to be similar to those observed in tests conducted on full-scale lead-shielded shipping containers.

Figure 18.1 shows the results of the 30-ft drop test on five types of weld joint designs, three of which were accepted and two of which were rejected. The tests, which will include specimens up to 1 in. thick, are being continued.

Although the loss of shielding from a cask can present a problem, the primary hazard associated with the 30-ft free fall is breach of containment; for this reason it is necessary to protect closure regions from impact. Energy absorbers that may be useful for such a purpose are being investigated both at ORNL and the University of Tennessee. Fins show considerable promise in this respect, even for large casks, and, in addition, are useful for dissipating heat. A toroidal shell welded to the edge of a cylindrical cask also appears to have potential merit and has been evaluated in several preliminary impact tests.⁴

¹Chem. Technol. Div. Ann. Progr. Rept. May 31, 1968, ORNL-4272, p. 249.

²Code of Federal Regulations, Title 49, Parts 171-178, Federal Register 33 No. 194, Part II (Oct. 4, 1968).

³Code of Federal Regulations, Title 10, Part 71.

⁴A. Estep et al., *Energy Absorption Parameters in Steel Rings*, Report EM 69-1 Dept. of Engineering Mechanics, Univ. of Tenn., Knoxville, March 1969.

ORNL-DWG 69-4896A

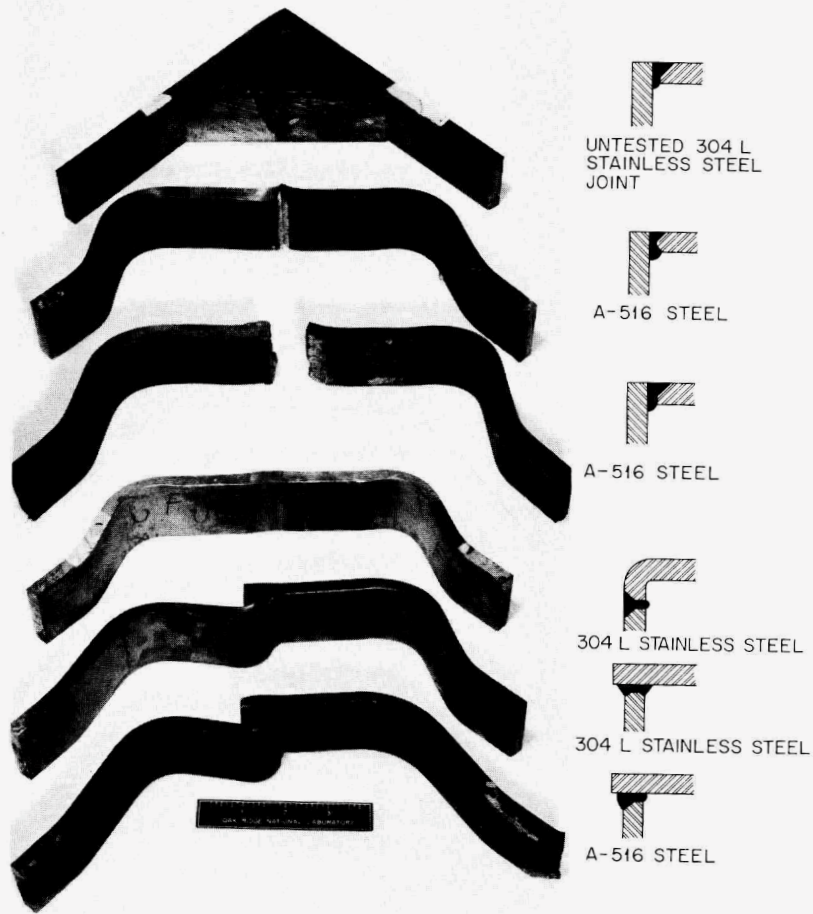


Fig. 18.1. Weld Joint Designs Tested Under a 300-lb Weight Dropped 30 ft.

ORNL-DWG 69-3563A

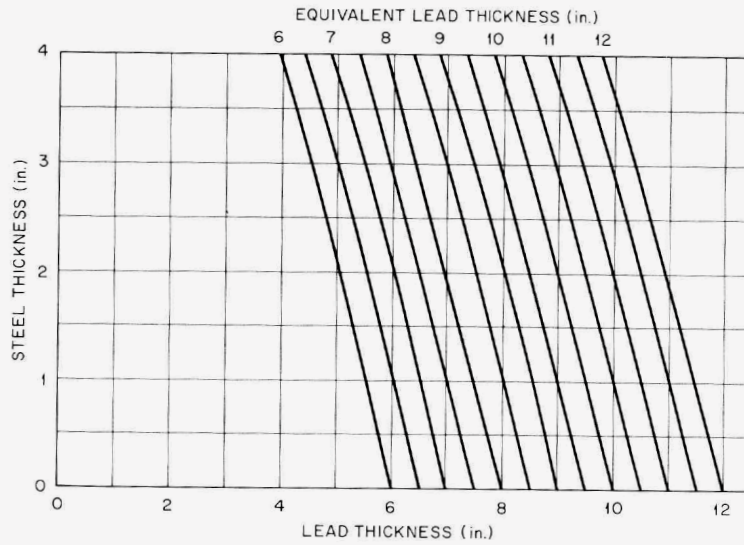


Fig. 18.2. Actual Steel and Lead Shielding Thicknesses as a Function of Equivalent Lead Thickness.

In many cases, shielding calculations for gamma sources are used to indicate required thicknesses of one shielding material, such as lead; however, in actual practice lead shields are encased in steel shells for ease of handling and for impact and fire protection. Optimization of such a composite shield can be a difficult problem.

Figure 18.2 is the result of a machine calculation⁵ which presents the actual steel and lead thicknesses that would be equivalent to a specified lead thickness. The code used for the calculation takes the buildup factors in lead and steel into account.

18.2 CONTACTS WITH PRIVATE INDUSTRY

It is apparent that, as the number of nuclear plants increases, an increased number of shielded shipping casks will be required to service the plants. During the past year we were contacted or visited by a total of six private industrial organizations – either companies just entering the reprocessing business or firms interested in building and leasing equipment to the operators of reactors – for the purpose of obtaining information about fuel shipment. Fuel shipment and handling should represent a potentially profitable field, since utility companies usually prefer to purchase such services.

18.3 CTD CASK EVALUATION PROGRAM

The Department of Transportation (DOT) requires that all radioactive material shipping containers in interstate commerce meet its regulations (CFR

Title 49, Part 173). These regulations are concerned, primarily, with ensuring that a given cask is capable of adequately containing and shielding its contents under both normal and accident conditions.

During this report period, a program was initiated to evaluate and to obtain approval from the AEC and the DOT for all fissile and radioactive material shipping containers that are used by the Chemical Technology Division in interplant shipments. Special DOT permits have already been issued for, or have been requested for, the following containers:

Container Name	DOT Number	Status
TRU Curium Shipping Container	5461	In service; increased source limits are being requested.
TRU Ten Ton Californium Shipping Container	5740	In service.
Uranium Shielded Cask, D-38	5787	In service.
Vermiculite Shipping Container	5765	In service; changes in container dimensions have been requested.
Foamglas Shipping Container	5795	In service.
Dry Hole Charger	5936	In service.
Hot Garden Carrier No. 2		Analysis is complete; application for AEC and DOT approval is being prepared.
Sodium Fluoride Absorber Shipping Container		Application submitted to AEC and DOT.

⁵M. Solomito and H. C. Claiborne, *A Simple Method for Determining a Combined Lead-Steel Shield for Shipping Casks That Is Equivalent to a Lead Shield*, ORNL-TM-2591 (May 29, 1969).

19. Nuclear-Powered Agro-Industrial Complexes: Special Studies

Work by the Chemical Technology Division on studies of Nuclear-Powered Agro-Industrial Complexes is described in detail in monthly reports issued by the Nuclear Desalination Program [(1)

Nuclear Desalination Program Report on Activities of Interest to the Atomic Energy Commission, and (2) Middle East Study]; consequently, only an abstract appears in this report (see the Summary).

20. Siting of Fuel Reprocessing Plants and Waste Management Facilities

The Chemical Technology Division participated in a study of long-range considerations involved in the siting of commercial fuel reprocessing plants and waste management facilities. Other participants in the study included representatives of the Pacific Northwest Laboratory, Idaho Nuclear Corporation, Savannah River Laboratory, Atlantic Richfield Hanford Company, and the Health Physics Division, Operations Division, and Civil Defense Research Project of ORNL. The objectives of the study were: (1) to identify factors that will influence growth patterns of the commercial fuel reprocessing and waste management industry, and (2) to explore the need, and recommend bases for, a national siting policy that would present minimum impediment to the growth of economic nuclear power while fully satisfying the requirements of public health and safety. The information developed in the study is to be published as an ORNL report.¹

The principal conclusions of the study are concerned with: (1) the need for standards or regulations, (2) factors that influence the sizes of sites, (3) the safety and economics of large fuel reprocessing plants, (4) alternative schemes for the management of high-level wastes, (5) the effects of shipping radioactive materials, and (6) the question of whether reprocessing and waste facilities should be located on private lands.

These conclusions can be summarized as follows:

1. Standards or regulations are needed that establish: (1) acceptable chronic and acute radiation exposure of each of the organs of men, women, and children, both in individuals and in critical population groups, and (2) performance criteria

for engineered safety features. Sufficient technical information is presently available to allow substantial progress toward these goals through revision of existing Federal regulations (e.g., 10CFR20, 10CFR50, and 10CFR100).² Any revisions should attempt to provide an appropriate balance of risk vs benefit in view of current technological alternatives, should be subject to periodic upgrading, and, preferably, should be sufficiently inclusive to apply to all nuclear installations including reactors, fuel reprocessing plants, waste storage and disposal facilities, and fuel fabrication plants.

The criteria for chronic exposure of the public (perhaps a revision of 10CFR20, Sect. 20.106) would preferably establish maximum acceptable dose rates to body organs rather than allowable concentrations of radioactive effluents in air and water. These latter values do not explicitly consider perhaps more limiting pathways for radiation exposure than those caused by submergence in (or inhalation of) air and ingestion of water. It may be desirable, however, to retain the "maximum allowable" concentrations in air and water as point-of-departure reference values to facilitate monitoring and inspection.

The criteria for acute or emergency exposure of the public surrounding a nuclear facility (perhaps a revision of 10CFR100) should provide guidelines for acceptable dose commitments to all organs and should be developed in conformance with the recommendations of authoritative agencies such as the Federal Radiation Council and the National Council on Radiation Protection and Measurement.

¹Oak Ridge National Laboratory Staff *et al.*, *Siting of Fuel Reprocessing Plants and Waste Management Facilities*, ORNL-4451 (to be published).

²*Title 10, Code of Federal Regulations, Parts 20, 50, and 100.*

The performance criteria for engineered safety features in fuel reprocessing plants and waste management facilities would presumably be similar to those prescribed for nuclear power reactors in the proposed Appendix A of 10CFR50 entitled "General Design Criteria for Nuclear Power Plant Construction Permits."

2. Based on the current and projected technology of systems for cleaning off-gas streams from fuel reprocessing plants, routine releases, rather than potential releases from accidents, will tend to determine the site boundary distances. It is estimated that on-site waste storage facilities do not materially increase either the rate of routine release of radioactivity or the potential release of radioactivity following accidents, provided the facilities are designed to ensure containment following exposure to internal and external forces. For plants with capacities of more than a few tons of fuel per day, it is estimated that economic considerations will favor the installation of equipment for partially removing noble fission product gases from effluent gas streams. The development of off-gas systems that will achieve an iodine decontamination factor of about 10^8 will be necessary if fast breeder fuels are to be processed after decay periods approximating only 30 days.

In the year 2000 the worldwide distribution of ^{85}Kr and ^3H (assuming their complete release during fuel processing) will result in dose equivalents to man that are small (<1%) as compared with current guidelines for population exposure. Worldwide pollution hazards are avoided and on-site personnel are protected by the necessary expedient of ensuring appropriately low exposures of the public near the site boundary.

3. In the plant capacity range of interest (1 to 40 tons of fuel per day), the confinement barriers of fuel reprocessing plants, including their waste storage facilities, can be designed to maintain their confinement potential following exposure to credible internal or external forces (excluding acts of war or sabotage). Regardless of size, plants that are sited and constructed according to a given set of acceptable criteria for chronic and probable acute exposure of the public at the site boundary are considered to be equivalently safe. The costs of

preventive measures and the relatively expensive confinement systems are estimated to scale in such a way that larger plants will be favored, while the costs of off-gas treatment facilities required to achieve practical site sizes for large plants are estimated to be modest. In general, when the costs associated with shipping are also considered, it is concluded that economic factors will favor the installation of a relatively small number of large multipurpose reprocessing plants instead of a larger number of smaller plants for specific types of fuel.

4. The shipping of spent fuel elements, solidified fissile products for recycle, and solidified fission product wastes can be conducted safely and economically regardless of the number and duration of the shipments. The shipment of high-level liquid wastes is not considered feasible because of considerations of steam-pressure buildup within casks in the event of a loss-of-cooling incident.
5. High-level liquid wastes can be stored safely in tanks that have been provided with properly designed safety features and are maintained under active surveillance. Because of the requirements for continuous removal of heat, maintenance of a nonexplosive vapor phase, and prompt detection of leakage, the effectiveness of the containment system will depend on an active program of monitoring, inspection, and maintenance. Liquid waste storage can be condoned only as long as the waste management facility remains on a fully active status. In this context, "storage" does not constitute disposal, and "perpetual tank storage," even under government auspices, is not an acceptable substitute for disposal.

The application of properly engineered safety features, together with a high degree of surveillance, will, in principle, result in a low risk to the health and safety of the public, regardless of whether the waste is stored as a solid or liquid. Environmental and geographic characteristics of the site are of secondary importance.

6. Solidification followed by burial in deep geologic formations is the method currently favored for disposal of high-level fission product wastes. Typical sequential unit opera-

tions in this method -- interim liquid waste storage, solidification, interim solid waste storage, solid waste shipment, and emplacement in underground salt formations -- have been shown to be technologically feasible and are estimated to contribute relatively little expense to the nuclear fuel cycle.

7. Considerations of the long-term hazard of the wastes and the nearly prohibitive costs for reclaiming large areas of contaminated land surface militate against any disposal (or burial) of wastes on privately owned land. All radioactive wastes should be maintained in a retrievable condition as long as they are retained on-site.

Government ownership must extend to any subsurface geological formation that is used for disposal, as well as to the land areas above those formations. Control of the land surface must be maintained to prevent unauthorized penetrations of the formations utilized for dis-

posal, although the surface itself can be put to unrestricted agricultural or recreational use.

8. Plants and storage facilities that are built with proper forethought can be decontaminated and/or made sufficiently inaccessible that they do not represent hazards to public health and safety. With the stipulation that all contaminated equipment and materials outside the massively shielded concrete canyons and vaults be removed from the premises before abandonment of the site, government ownership is not required.

In a continuation of this study, the U.S. Atomic Energy Commission has considered adopting a statement of policy concerning the siting of commercial fuel reprocessing plants and related waste management facilities.³

³U. S. Atomic Energy Commission, "Siting of Commercial Fuel Reprocessing Plants and Related Waste Management Facilities; Statement of Proposed Policy," *Federal Register* 34(105), 8712 (1969).

21. Chemical Engineering Research

21.1 DEVELOPMENT OF THE STACKED-CLONE CONTACTOR

The stacked-clone contactor is a multistage, countercurrent solvent extraction device that is capable of performing liquid-liquid mass transfer operations with good efficiency and high throughput.¹ One of its principal advantages is its low ratio of stage inventory to throughput. This low ratio provides rapid response and facilitates process control. Thus, attainment of steady-state operating conditions after startup or after a process interruption is very rapid. Since the process can operate most of the time at steady state, the quantity of off-specification solutions that must be reworked is minimized. Radiation and chemical degradation of the organic solvent is also minimized.² Other attractive features of the stacked-clone contactor are its compact size (i.e., the contactor occupies less physical space in a shielded facility than any other contactor known) and its capability of operating in almost any attitude.

One possible application of the stacked-clone contactor is the reprocessing of high-burnup, short-cooled LMFBR fuels, which are characterized by high-specific-activity aqueous feed solutions and high plutonium:uranium ratios.

Probably the two most important questions yet to be answered regarding the application of the stacked-clone contactor to LMFBR or other short-cooled fuel processing involve operating experience in a remotely operated shielded facility and the

ability to scale the device up to significant processing capacities. To date, remote operation with radioactive solutions has not been scheduled, although a stainless steel prototype unit is now available for such tests.

A new miniature solvent extraction device, a pulsed stacked-clone contactor for use in bench-scale solvent extraction experiments, has been designed, and a first model has been built and tested. A model small enough to fit in a glove box is being designed. This device should be useful for applications where only small amounts of feed are available and for in-cell tests at full activity levels.

Efforts during the past year were directed principally toward scaleup. Subsequent to the establishment of an optimized geometry and tests with a variety of chemical systems, experimental stacked-clone contactors were operated to determine the effects of hydroclone size. Units that were 0.5 and 1.4 times the size of the standard device provided flow capacities that were 41 and 119%, respectively, of those obtained with the standard-sized contactor.³ (It had been expected that flow capacities would vary as the square of the scale factor.) Thus, the smaller hydroclones gave the higher specific flow capacity (flow per unit cross section).

On the strength of this information, we fabricated a contactor having nine hydroclones, in parallel, per stage (known as the Multiclone contactor), as shown in Fig. 21.1. Each clone was 0.375 times the standard size, and all the clones in a given stage were driven by the same pump. (A concept for scaling up stacked-clone contactors to multiton-per-day capacities also involves the manifolding of hydroclones in each stage. The machine shown in Fig. 21.1 is based on this concept.) The flow

¹W. S. Groenier and M. E. Whatley, *The Stacked-Clone Contactor: A High Performance Solvent Extraction Machine Having Potential for Use in the Processing of Highly Radioactive Nuclear Fuels*, ORNL-4267 (July 1968).

²W. S. Groenier, *Some Factors Affecting the Choice of a Solvent Extraction Contactor for the First Cycle Reprocessing of LMFBR Fuels*, ORNL-TM-2290 (September 1968).

³L. O. Finsterwalder, *Geometric Scaling of Stacked-Clone Contactors*, ORNL-4088 (April 1967).

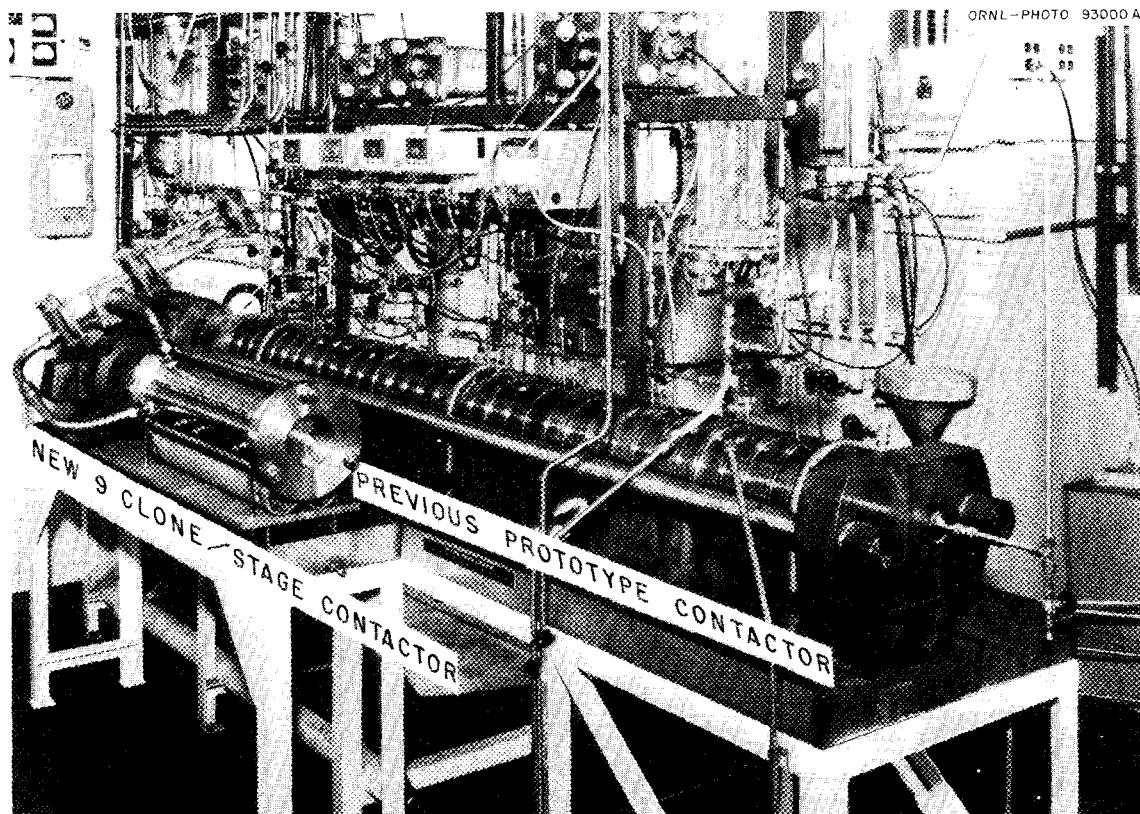


Fig. 21.1. Stacked-Clone Contactor Having Nine Clones per Stage.

capacity of this device was found to be equal to that of the standard-size contactor; that is, the flow capacity of each of the nine hydroclones was 0.11 times that of the standard clone. However, we had anticipated a comparative value of 0.30. Several tests were made to determine the cause of this difference. The concept of manifolding hydroclones in each stage was proved to be valid by plugging eight of the nine hydroclones in each stage and verifying the flow capacity of the remaining hydroclone to be one-ninth of that of all hydroclones. A check of the validity of the hydroclone size extrapolation to 0.375 scale was made using a new experimental 0.375-scale contactor. Recent operation of the Multiclone contactor at shaft speeds near 5500 rpm showed that surpassing the design speed (4800 rpm) did not offer enhanced performance. The next operation will be to modify the stage recycle pumps to decrease mixing. This will be done in a manner to produce less shearing action on, and shock to, the fluid.

It was shown that additional mixing in the stage recycle loop does decrease hydroclone performance.

Tests made with the Multiclone contactor at about half the design speed produced about 30% less throughput; this was caused by 60% less pressure and 40% less flow from the stage pump. In an experimental contactor, orifices were placed in pump discharge lines to promote mixing. While these orifices decreased pressure and flow by only 30 and 10%, respectively, the throughput was also decreased by 30%.

Results of tests made using the new 0.375-scale experimental stacked-clone contactor showed that our prediction of a 0.30 relative flow capacity was somewhat high. In fact, the relative flow capacity was only 0.206.

The relationship between scale factor and relative flow capacity is shown in Fig. 21.2. It is obvious that the actual function is not parabolic. By knowing that the stage volume varies as the cube of the scale factor (omitting nonlinearities in pump and duct design) and approximating the left-hand portion of the actual function of Fig. 21.2 with a straight line, it is possible to optimize hydroclone size with respect to a minimum resi-

dence time. It was found that 0.34- to 0.37-scale hydroclones would give the least residence time. However, a thorough optimization study for stacked-clone contactors would have to take other factors, including fabrication costs, into consider-

ation. A processing plant design requiring perhaps several thousands of hydroclones with complex manifolding would probably compromise somewhat on residence time and use 0.6-scale or larger hydroclones.

It has been estimated that the use of 0.375-scale hydroclones in the first TBP extraction cycle of a typical LMFBR reprocessing scheme would involve as many as 12,000 hydroclones, or 640 per stage.² The use of 0.6-scale hydroclones would require 272 per stage for the same operation. A conceptual design for a 300-hydroclone-per-stage contactor appears in Fig. 21.3. The duct and conduit volumes have been minimized through the use of an annular or turbine pump design that would rotate at only a few hundred revolutions per minute. Overall size of the contactor would be about 2 ft in diameter by 8 ft long for 28 stages. Fabrication techniques used for a contactor of this type would likely be quite different from those used in the past. Automated methods of producing the many parts would offer substantial reductions in the cost per hydroclone.

Solvent extraction via the stacked-clone contactor continues to be a major contender for the

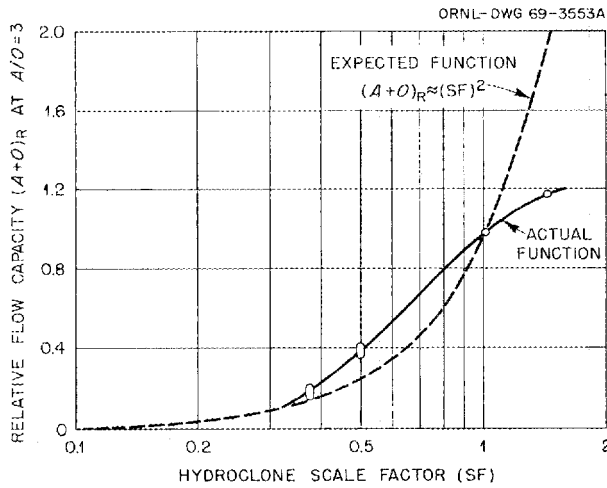


Fig. 21.2. Effect of Hydroclone Size on Relative Flow Capacity.

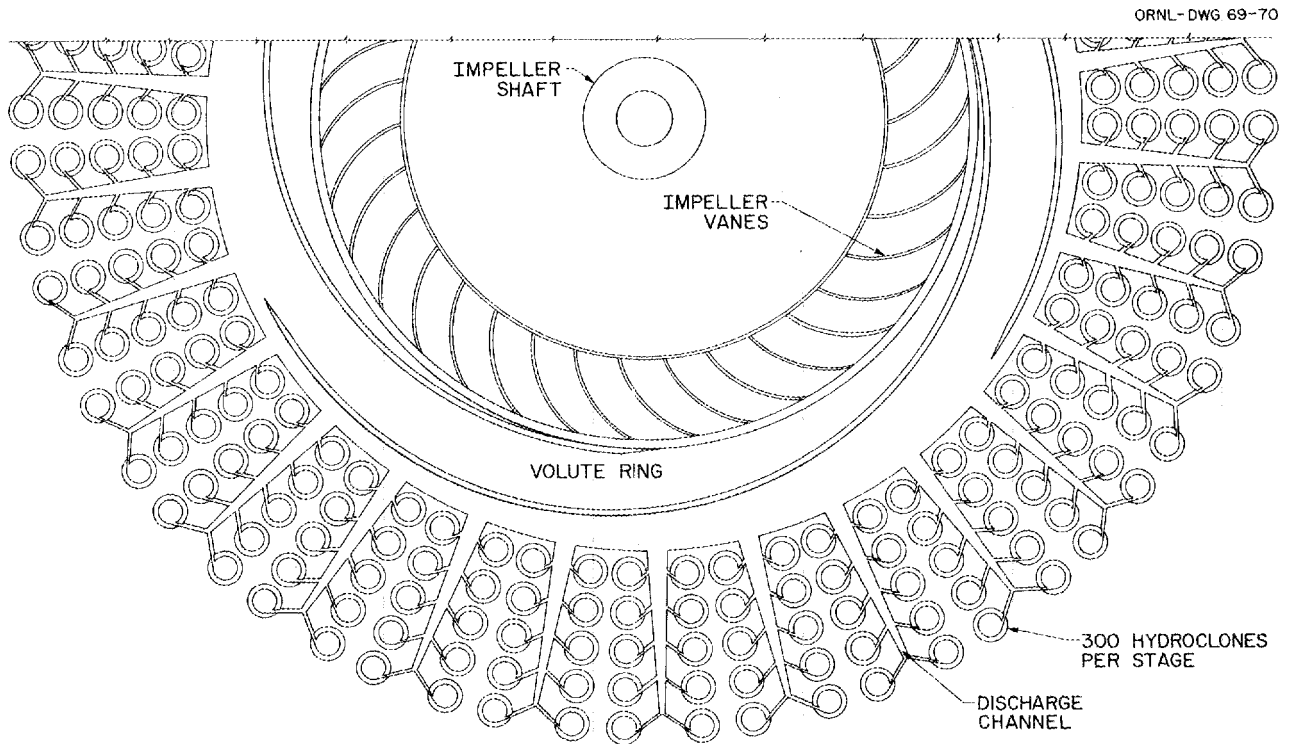


Fig. 21.3. Conceptual Design for a Stacked-Clone Contactor Containing 300 Hydroclones per Stage.

method of processing short-cooled fuels. Continued advances in contactor technology are being made. Application of the key features of the stacked-clone contactor -- rapid response, low

inventory, and small space requirements -- to an integrated solvent extraction processing facility would represent a decided advance in the technology.

22. Assistance Programs

The Division provided assistance to others on several projects, principally the Eurochemic Assistance Program and a program in which the radiation resistance of several protective coatings is being determined.

22.1 EUROCHEMIC ASSISTANCE PROGRAM

The Laboratory has continued to coordinate the Eurochemic Assistance Program, which originated in 1958, to provide an exchange of information between Eurochemic and the several AEC sites included in the program. During the construction and early operational phases of the plant, the Laboratory supplied the services of a U.S. technical advisor, E. M. Shank, who was stationed at Mol, Belgium. The plant is now in successful operation, and the residence of the U.S. Technical Advisor was terminated in January 1969. However, the Eurochemic Assistance Program will continue to serve as the medium for the exchange and dissemination of technical information.

Eurochemic has successfully processed a total of 19.5 metric tons of natural and low-enriched uranium and 259.1 kg of highly enriched uranium in four campaigns (two of each type). About 25.9 kg of plutonium was separated. Research and development activities have been restricted to neptunium distribution in the process, preparation of UF_4 , use of uranous nitrate as a plutonium reductant, waste solidification, and analytical development of methods and equipment. Special studies have been made of in-plant blending, processing of uranium-zirconium fuels, plant capacity, modifications of extraction cycles, shear head-end methods, waste solidification, and processing of special fuels.

During the year about 24 USAEC-originated reports were sent to Eurochemic, and 32 Eurochemic-originated reports were received, reproduced, and distributed by the Laboratory.

22.2 EVALUATION OF RADIATION RESISTANCE OF SELECTED PROTECTIVE COATINGS (PAINTS)

Tests to evaluate commercial protective coatings have been continued, using samples that were supplied principally by manufacturers with a recent or renewed interest in marketing their products in the nuclear field. Eighty coatings (seven generic types), supplied by nine manufacturers, are being tested by exposure to a ^{60}Co gamma source with an intensity of 6×10^5 r/hr and a temperature range of 40 to 50°C. Current exposure data are presented in Table 22.1. Tests of these coatings will be continued until they have failed or until they have received an accumulated exposure of 1×10^{10} rads. The epoxies and phenolics that were continuously exposed until failure occurred were found to exhibit the greatest resistance at an average of 3.7×10^9 rads in air and 1×10^9 rads in deionized water. The polyurethanes maintain good resistance up to an exposure of approximately 4×10^9 rads in air but to only about 3.7×10^8 rads in deionized water.

A summary chart of the comparative radiation tolerances of four generic types of coatings is presented in Fig. 22.1. The epoxies and phenolics showed highest resistance to exposures in both air and deionized water.

A United States of America Standards Institute paint standard, "Protective Coatings (Paints) for Light Water Nuclear Reactor Containment Facilities," has been written and is now being reviewed. It is scheduled for completion by June 1969. The committee that is responsible for the standard is comprised of reactor designers, protective coatings manufacturers, USAEC site contractors, architect-engineers, private consultants, and representatives from TVA and the Northern States Power Company.

Table 22.1. Gamma Radiation Resistance of Several Protective Coatings

Radiation Source: ^{60}Co at 6×10^5 r/hr and 40 to 50°C temperature

Coating	Generic Type	Manufacturer ^a	Substrate	Exposure ^b in Demineralized Water		Exposure ^b in Air	
				Dose (rads)	Effect ^c	Dose (rads)	Effect ^c
Epolon, 68-122A	Epoxy ^d	1	Concrete	8×10^8	B	2.4×10^9	C, D
Epolon, 68-121A	Epoxy	1	Steel	8×10^8	B	$>4.6 \times 10^9$	
Epolon, 68-121B	Epoxy	1	Steel	1.9×10^9	B	$>4.6 \times 10^9$	
Vinyloid, 68-121D	Vinyl	1	Steel	1×10^8	B	8×10^8	B
Vinyloid, 68-122C	Vinyl	1	Concrete	1×10^8	B	1.2×10^9	C, D
Vinyloid, 68-121C	Vinyl	1	Steel	1×10^8	B	8×10^8	B
Vinyloid, 68-122B	Vinyl	1	Concrete	1×10^8	B	1.2×10^9	C, D
Absorption process topping	Epoxy ^e	2	Concrete	5×10^8 ^f	A	5×10^9	C
Topping No. 285	Epoxy ^d	2	Concrete	1.8×10^9 ^f	B	5.6×10^9	C
Topping No. 2036	Epoxy ^d	2	Concrete	1.8×10^9 ^f	B	5.6×10^9	C
High Build (HB) stainless steel (SS) flake enamel (No. 1)	Epoxy ^g	3	Concrete	4×10^8 ^f	B	$>8 \times 10^9$	
No. 7230 HB SS flake enamel	Phenolic	3	Concrete	2.3×10^9 ^f	A	$>8 \times 10^9$	
No. 7239 catalyzed SS flake enamel	Urethane	3	Concrete	4×10^8 ^f	B	4.5×10^9	A
No. 4130 epoxy	Epoxy ^g	3	Concrete	1×10^9 ^f	B	2.3×10^9	B
HB SS flake enamel (No. 5)	Epoxy ^g	3	Concrete	1×10^9 ^f	B	4.5×10^9	A
No. 4130 top coat HB primer (No. 6)	Epoxy		Steel	1×10^9 ^f	B	2.3×10^9	D
Epoxy white enamel, RC1 (No. 7)	Epoxy ^g	3	Steel	1×10^9 ^f	A, B	4.5×10^9	A
HB SS flake on enamel (No. 8)	Epoxy ^g	3	Steel	1×10^9 ^f	B	$>8 \times 10^9$	
No. 7230 HB enamel (No. 9)	Phenolic	3	Steel	4×10^8 ^f	B	$>8 \times 10^9$	
No. 7230 HB white with Zn-chlorinated rubber primer (No. 11)	Phenolic	3	Steel	4×10^8 ^f	B	$>8 \times 10^9$	
No. 7230 over 6040 oxidized alkyd primer (No. 12)	Phenolic	3	Steel	4×10^8 ^f	B	$>8 \times 10^9$	
No. 2952, chlorinated rubber, over No. 6040, oxidized alkyd primer (No. 13)	Chlorinated rubber	3	Steel	4×10^8 ^f	B, D	2.8×10^9	B
Epoxy enamel, white (No. 14)	Epoxy ^g	3	Steel	1×10^9 ^f	A	4.5×10^9	A
No. 6002, oxidized alkyd (No. 15)	Alkyd	3	Steel	4×10^8 ^f	B	4.5×10^9	A
No. 6002 over No. 6040 (No. 16)	Alkyd	3	Steel	4×10^8 ^f	B	4.5×10^9	A
Alkyd enamel over No. 6040 (No. 17)	Alkyd	3	Steel	4×10^8 ^f	B	4.5×10^9	A
No. 4130 epoxy over HB primer (No. 18)	Epoxy ^g	3	Concrete	1.5×10^9 ^f	A	4.5×10^9	A
Epoxy enamel, RC1 over HB (No. 19)	Epoxy ^g	3	Concrete	1.5×10^9 ^f	A	4.5×10^9	A

Table 22.1 (continued)

Coating	Generic Type	Manufacturer ^a	Substrate	Exposure ^b in Demineralized Water		Exposure ^b in Air	
				Dose (rads)	Effect ^c	Dose (rads)	Effect ^c
84-F-15/89-F-34 and Zinc 7 (No. 1)	Epoxy ^d	4	Steel	1.6×10^9	C	$>4 \times 10^9$	
84-F-15/89-F-34 (No. 7)	Epoxy ^d	4	Steel	1.6×10^9	C	$>4 \times 10^9$	
78-D-7/Zinc-7 (No. 3)	Epoxy ^e	4	Steel	1.6×10^9	C	$>4 \times 10^9$	
78-D-7 (No. 15)	Epoxy ^e	4	Steel	1.6×10^9	C	$>4 \times 10^9$	
80-F-15/83-F-34 and Zinc-7 (No. 5)	Vinyl	4	Steel	3.8×10^8	B	$>4 \times 10^9$	
80-F-15-83-F-34 (No. 11)	Vinyl	4	Steel	1.1×10^8	B	$>4 \times 10^9$	
28-F-15/27-F-34 and Zinc-7 (No. 6)	Chlorinated rubber	4	Steel	3.8×10^8	B	$>4 \times 10^9$	
28-F-15/27-F-34 (No. 9)	Chlorinated rubber	4	Steel	3.8×10^8	B	$>4 \times 10^9$	
Val-Chem/89-F-34 (No. 17)	Polyurethane	4	Steel	$>4 \times 10^9$		$>4 \times 10^9$	
89-F-15/84-F-15 (No. 19)	Epoxy ^d	4	Concrete	3.8×10^8	B	$>4 \times 10^9$	
84-F-15/89-F-34 W/latex filler (No. 19-1)	Epoxy ^d	4	Concrete	1.1×10^8	B	1.9×10^9	C
28-F-15/27-F-34 (No. 20)	Chlorinated rubber	4	Concrete	3.8×10^8	B	$>4 \times 10^9$	
80-F-15/83-F-34 (No. 21)	Vinyl	4	Concrete	3.8×10^8	B	$>4 \times 10^9$	
78-D-7 (No. 23)	Epoxy	4	Concrete	5.9×10^8	B	$>4 \times 10^9$	
Val-Chem/89-F-34 (No. 24)	Polyurethane	4	Concrete	3.1×10^8	B	$>4 \times 10^9$	
No. 5671, thixopoxy ^h	Epoxy	5	Steel	1×10^9	B	$>2.4 \times 10^9$	
No. 5671, thixopoxy ⁱ	Epoxy	5	Steel	1×10^9	A, B	$>2.4 \times 10^9$	
No. 5671, thixopoxy	Epoxy	5	Concrete	1.4×10^9	A, B, C	$>2.4 \times 10^9$	
No. 5697 ^d	Epoxy	5	Concrete	$>2.4 \times 10^9$		$>2.4 \times 10^9$	
No. 5673 ^h	Epoxy	5	Steel	1×10^9	A, C	$>2.4 \times 10^9$	
No. 5673 ⁱ	Epoxy	5	Steel	1×10^9	A, C	$>2.4 \times 10^9$	
No. 5673	Epoxy	5	Concrete	1×10^9	B	1.8×10^9	B, C
No. 1371 ^h	Inorganic zinc	5	Steel	1×10^9	E	$>2.4 \times 10^9$	
No. 5627 ^h	Epoxy	5	Steel	1×10^9	B	$>2.4 \times 10^9$	
No. 1357 ^h	Inorganic zinc	5	Steel	$>2.4 \times 10^9$		$>2.4 \times 10^9$	
No. 1357 ⁱ	Inorganic zinc	5	Steel	$>2.4 \times 10^9$		$>2.4 \times 10^9$	
No. 5697 ^{d,h}	Epoxy	5	Steel	$>2.4 \times 10^9$		$>2.4 \times 10^9$	
No. 5697 ^{d,i}	Epoxy	5	Steel	1×10^9	A, C	$>2.4 \times 10^9$	
No. 5627 ^h	Epoxy	5	Steel	1×10^9	A, C	$>2.4 \times 10^9$	
No. 5627 ⁱ	Epoxy	5	Steel	1×10^9	A, B, C	$>2.4 \times 10^9$	
B69-W36 (ME-1022)	Epoxy	6	Steel	$>1.3 \times 10^9$		$>1.3 \times 10^9$	
B69-W56 (ME-1023)	Urethane	6	Steel	$>1.3 \times 10^9$		$>1.3 \times 10^9$	
B69-W36 (ME-1024)	Epoxy	6	Steel	8×10^8	B	$>1.3 \times 10^9$	

Table 22.1 (continued)

Coating	Generic Type	Manufacturer ^a	Substrate	Exposure ^b in		Exposure ^b in Air	
				Demineralized Water		Dose (rads)	Effect ^c
				Dose (rads)	Effect ^c		
B69-W56 (ME-1025)	Urethane	6	Steel	3×10^8	B	$>1.3 \times 10^9$	
B69-W56 (ME-1026)	Urethane	6	Concrete	5×10^8	B	$>1.3 \times 10^9$	
B69-W56 (ME-1027)	Urethane	6	Concrete	5×10^8	D	$>1.3 \times 10^9$	
Capox EP (X-430A)	Epoxy phenolic	7	Steel	1.2×10^9	A, C	$>3.7 \times 10^9$	
Capox A (X-430B)	Epoxy	7	Steel	1.5×10^9	B	$>3.7 \times 10^9$	
Subox (X-430C)	Vinyl	7	Steel	3×10^8	B	$\sim 5 \times 10^8$	B
Capox EP (X-430D)	Epoxy phenolic	7	Steel	1.2×10^9	A, C	$>3.7 \times 10^9$	
Capox EP (X-430E)	Epoxy phenolic	7	Concrete	1.2×10^9	A, C	3.5×10^9	C, D
Capox A (X-430F)	Epoxy	7	Concrete	1.2×10^9	B	$>3.7 \times 10^9$	
No. 92 Theme-Zinc	Inorganic zinc	8	Steel	3×10^8	E	$>2.1 \times 10^9$	
No. 53-1235 Vinoline	Vinyl	8	Steel	$\sim 1 \times 10^8$	B	$>2.1 \times 10^9$	
No. 66-1235	Epoxy	8	Steel	3×10^8	B	$>2.1 \times 10^9$	
No. 66-1235 ^d	Epoxy	8	Steel	$>2.1 \times 10^9$		$>2.1 \times 10^9$	
No. 35-1235	Vinyl	8	Steel	$\sim 1 \times 10^8$	B	$>2.1 \times 10^9$	
No. 368	Polyurethane	8	Concrete	$>1.3 \times 10^9$		$>2.1 \times 10^9$	
No. 66-1241 ^d	Epoxy	8	Concrete	$>1.3 \times 10^9$		$>2.1 \times 10^9$	
Plasite 1100/1120 (No. A)	Inorganic zinc	9	Steel	$>6.9 \times 10^9$		$>6.9 \times 10^9$	
Plasite 1100/1120 (No. 1)	Inorganic zinc	9	Steel	$>4.6 \times 10^9$		$>4.6 \times 10^9$	
Plasite 1100/1120 (No. 2)	Inorganic zinc	9	Steel	$>4.6 \times 10^9$		$>4.6 \times 10^9$	

^aManufacturers: 1, Con-Lux Paint Products, Inc.; 2, Kaiman Floor Co., Inc.; 3, Keeler and Long, Inc.; 4, Mobil Chemical Co.; 5, NAPCO, Inc.; 6, Sherwin-Williams Co., Inc.; 7, Wyandotte Chemical Corp., Subox Division; 8, TNEMEC Co.; 9, Wisconsin Protective Coating Co.

^bThe coatings were inspected for radiation damage at various exposure levels: $\sim 1 \times 10^8$, 3×10^8 , 5×10^8 , and each additional 5×10^8 rads exposure thereafter. The values listed represent the cumulative dose that had been received at the time adverse effects were observed. If no effects are entered, the exposure test is continuing.

^cRadiation Effects: A, chalked; B, blistered; C, embrittled; D, loss of adhesion; E, "sweating."

^dPolyamid-cured epoxy.

^eInorganic fillers, epoxy sealer.

^fReported previously in ORNL-4272.

^gAmine-cured epoxy.

^hSandblasted steel.

ⁱPickled steel.

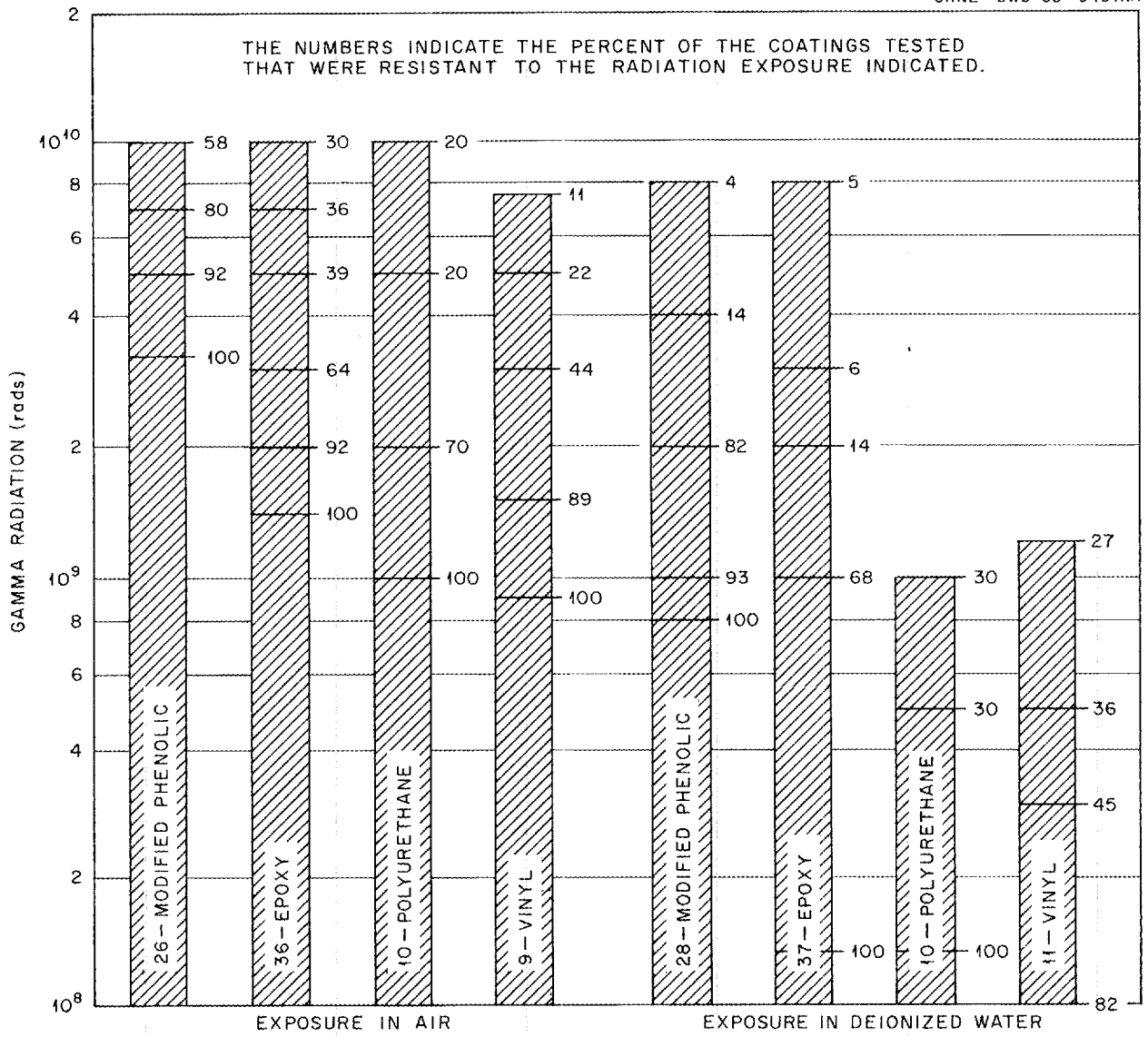


Fig. 22.1. Comparative Radiation Tolerances of Some Generic Types of Protective Coatings.

Publications, Speeches, and Seminars

ASSISTANCE PROGRAMS

Shank, E. M., W. E. Unger, and R. A. Miller, *List of Information Sent to and Received from the Eurochemic Company, January 1, 1968 Through January 31, 1969 (Categorized)*, ORNL-TM-685, suppl. 9 (March 28, 1969).

BIOCHEMICAL SEPARATIONS

Burtis, C. A.,¹ "Fractionation of Urine by Gel Filtration Chromatography," presented at the 20th National Meeting of the American Association of Clinical Chemists, Washington, D.C., Aug. 18-23, 1968.

Burtis, C. A., W. C. Butts,² S. Katz, and C. D. Scott, "Chemical Identification of Urinary Constituents Isolated by Anion Exchange Chromatography," presented at the Southeast Section Meeting of the American Association of Clinical Chemists, Birmingham, Ala., Oct. 11-12, 1968.

Burtis, C. A.,¹ W. C. Butts,² W. T. Rainey,² and C. D. Scott, "Separation of Drug Metabolites by High-Resolution Anion Exchange Chromatography," presented at the First Annual Symposium on Automated, High-Resolution Analyses in the Clinical Laboratory, ORNL, Mar. 13-14, 1969.

Egan, B. Z., R. W. Rhear, and A. D. Kelmers, "Behavior of Transfer Ribonucleic Acids on Polyacrylamide Gels," presented at the Southeastern Regional Meeting of the ACS, Florida State University, Dec. 4-7, 1968.

Egan, B. Z., R. W. Rhear, and A. D. Kelmers, "Behavior of Transfer Ribonucleic Acids on Polyacrylamide Gel Columns," *Biochim. Biophys. Acta* **174**, 23-31 (1969).

Hancher, C. W., and H. O. Weeren, "A Fraction Collector for Large-Volume Chromatographic Separations" (communication to editor), *Biotechnology and Bioengineering* **10**(5), 681-83 (1968).

Jolley, R. L., W. F. Johnson,³ and C. D. Scott, *The Mark II Prototype Carbohydrate Analyzer: Description and Operation*, ORNL-TM-2530 (April 1969).

Jolley, R. L., and H. V. Malling,⁴ "Man or Mouse? A Comparison of Urinary Carbohydrate Constituents Using High Resolution Column Chromatography," presented at the 1968 Southeastern Regional Meeting of ACS, Florida State University, Dec. 4-7, 1968.

Jolley, R. L., W. W. Pitt, Jr., and C. D. Scott, "Non-Pulsing Reagent Metering for Continuous Colorimetric Detection Systems," *Anal. Biochem.* **28**, 300 (1969).

¹Present address: Varian Aerograph, Walnut Creek, Calif.

²Analytical Chemistry Division.

³Instrumentation and Controls Division.

⁴Biology Division.

- Jolley, R. L., K. S. Warren, C. D. Scott, J. L. Jainchill,⁵ and M. L. Freeman, "Carbohydrate Concentrations in Normal Body Fluids as Determined by High-Resolution Column Chromatography," presented at the First Annual Symposium on Automated, High-Resolution Analyses in the Clinical Laboratory, ORNL, March 13-14, 1969.
- Jolley, R. L., K. S. Warren, E. Schonfeld, C. D. Scott, and M. L. Freeman, "High-Resolution Column Chromatography of Carbohydrates in Normal Body Fluids," presented at the 20th National Meeting of the American Association of Clinical Chemists, Washington, D.C., Aug. 18-23, 1968.
- Jolley, R. L., K. S. Warren, E. Schonfeld, C. D. Scott, and M. L. Freeman, "High-Resolution Column Chromatography of Carbohydrates in Normal Body Fluids," presented at the 78th Annual Meeting of the Tennessee Academy of Science, Clarksville, Tenn., Nov. 22-23, 1968.
- Katz, S., and C. A. Burtis,¹ "The Relationship Between Chemical Structure and Elution Position in an Anion Exchange System," *J. Chromatog.* **40**, 270 (1969).
- Katz, S., A. Confer,⁶ C. D. Scott, C. A. Burtis,¹ R. L. Jolley, N. Lee, S. McKee,⁶ B. E. Maryanoff,⁶ W. W. Pitt, and K. S. Warren, *An Annotated Bibliography of Low-Molecular-Weight Constituents of Human Urine*, ORNL-TM-2394 (Oct. 11, 1968).
- Katz, S., and C. D. Scott, "The Limits of Detection of Over 60 Compounds and Methods of Quantification of a High-Resolution Analyzer for UV-Absorbing Constituents of Body Fluids," presented at the Southeast Section Meeting of the American Association of Clinical Chemists, Memphis, Tenn., Mar. 28-29, 1969.
- Kelmers, A. D., "Reversed-Phase Chromatographic Separations of Transfer Ribonucleic Acids," presented at a meeting of the Naval Reserve, Oak Ridge, Tenn., Nov. 13, 1968.
- Kelmers, A. D., "Reversed-Phase Chromatographic Separations of Transfer Ribonucleic Acids," presented at a seminar at St. Louis University, St. Louis, Mo., Dec. 4, 1968.
- Kelmers, A. D., "The Experimental Method in Developing Better Separation Methods," presented at the 65th National Meeting of the American Institute of Chemical Engineers, Cleveland, Ohio, Mar. 7, 1969.
- Kelmers, A. D., "Separations Technology," presented at the Conference on Engineering at ORNL, April 28, 1969.
- Scott, C. D., "Automatic, High-Resolution Analyses of Body Fluids," *Clin. Chem.* **14**, 521 (1968).
- Scott, C. D., "Continuous Separation of Ion Exchange Resin into Size Fractions by Elutriation with Water," *Anal. Biochem.* **24**, 292 (1968).
- Scott, C. D., "Techniques in High-Pressure Ion Exchange Chromatography," presented at the 20th National Meeting of the American Association of Clinical Chemists, Washington, D.C., Aug. 18-23, 1968.
- Scott, C. D., "Techniques in High-Pressure Ion Exchange Chromatography," presented at the 7th Annual Meeting of the American Society for Testing Materials, Cincinnati, Ohio, Sept. 24-27, 1968.
- Scott, C. D., "Techniques in High-Pressure Ion Exchange Chromatography," presented at the 4th Middle Atlantic Regional Meeting of the ACS, Washington, D.C., Feb. 12-15, 1969.
- Scott, C. D., J. M. Jansen, Jr.,³ and W. Wilson Pitt, "A Computer Technique for On-Line Analysis of Complex Column Chromatographic Data," presented at the First Annual Symposium on Automated, High-Resolution Analyses in the Clinical Laboratory, ORNL, Mar. 13-14, 1969.

⁵National Cancer Institute, Bethesda, Md.

⁶Co-op Student.

Scott, C. D., R. L. Jolley, W. W. Pitt, and W. F. Johnson,³ "Prototype Systems for the Automated, High-Resolution Analyses of UV-Absorbing Constituents and Carbohydrates in Body Fluids," presented at the First Annual Symposium on Automated, High-Resolution Analyses in the Clinical Laboratory, ORNL, Mar. 13-14, 1969.

Weiss, J. F., R. L. Pearson, and A. D. Kelmers, "Two Additional Reversed-Phase Chromatographic Systems for the Separation of Transfer Ribonucleic Acids and Their Application to the Preparation of Two Formylmethionine and a Valine Transfer Ribonucleic Acids from *E. Coli* B," *Biochemistry* **7**, 3479-87 (1968).

CHEMICAL PROCESSING FOR MOLTEN-SALT BREEDER REACTORS

Carter, W. L., R. B. Lindauer, and L. E. McNeese, *Design of an Engineering-Scale, Vacuum Distillation Experiment for Molten-Salt Reactor Fuel*, ORNL-TM-2213 (November 1968).

Chandler, J. M., and S. E. Bolt,⁷ *Preparation of Enriching Salt ${}^7\text{LiF}\cdot{}^{233}\text{UF}_4$ for Refueling the Molten Salt Reactor*, ORNL-4371 (March 1969).

Ferris, L. M., *Some Aspects of the Thermodynamics of the Extraction of Uranium, Thorium, and Rare Earths from Molten $\text{LiF}\text{-BeF}_2$ into Liquid $\text{Li}\text{-Bi}$ Solutions*, ORNL-TM-2486 (March 1969).

Ferris, L. M., J. C. Mailen, F. J. Smith, E. D. Nogueira,⁸ J. H. Shaffer,⁹ D. M. Moulton,⁹ C. J. Barton,⁹ and R. G. Ross,⁹ "Isolation of Protactinium from Single-Fluid Molten-Salt Breeder Reactor Fuels by Selective Extraction into $\text{Li}\text{-Th}\text{-Bi}$ Solutions," presented at the Third International Protactinium Conference, Mittenwald, Germany, Apr. 14-19, 1969.

Hightower, J. R., "Distillation as a Tool for Fission Product Removal from Molten Salt Reactor Fuels," presented at Oak Ridge Naval Reserve Unit, Oak Ridge, Tenn., Dec. 18, 1968.

DEVELOPMENT OF THE THORIUM FUEL CYCLE

Cordiner, J. B.,¹⁰ and O. C. Dean,¹¹ *A Study of Gas Evolution from Sol-Gel Thoria and Thoria-Urania*, ORNL-TM-2268 (July 15, 1968).

Haws, C. C., and J. W. Snider, *A Vertical Tube Furnace for Continuously Calcining Sol-Gel-Derived $\text{ThO}_2\text{-UO}_2$ at a Rate of 35 Kilograms Per Day*, ORNL-3894 (January 1969).

FLUORIDE VOLATILITY PROCESSING

Katz, S., and G. I. Cathers, "A Gas Sorption-Desorption Method for Separating the Hexafluorides of Neptunium and Uranium," *Nucl. Appl.* **5**, 206 (1968).

Katz, S., and G. I. Cathers, "A Gas Sorption-Desorption Method for Recovering Plutonium Hexafluoride," *Nucl. Appl.* **5**, 5 (1968).

Mailen, J. C., and G. I. Cathers, *Fluorination of Falling Droplets of Molten Fluoride Salt as a Means of Recovering Uranium and Plutonium*, ORNL-4224 (November 1968).

Mailen, J. C., and G. I. Cathers, *Hot-Cell Studies of the Fluidized-Bed Fluoride Volatility Process for Recovering Uranium and Plutonium from Spent UO_2 Fuels*, ORNL-TM-2170 (April 1969).

⁷Reactor Division.

⁸Junta de Energia Nuclear, Madrid, Spain.

⁹Reactor Chemistry Division.

¹⁰Louisiana State University, Baton Rouge.

¹¹Deceased.

Matson, L. K.,¹² E. F. Stephan,¹² P. D. Miller,¹² W. K. Boyd,¹² and R. P. Milford, "Cathodic Protection in Molten Fluoride Salts at 1200°F," *Corrosion* **22**, 194-97 (1966).

Nogueira, E. D.,⁸ and G. I. Cathers, *Sorption of Fission Product (Niobium, Ruthenium) Fluorides on Sodium Fluoride*, ORNL-TM-2169 (April 1969).

MISCELLANEOUS

Arnold, E. D., "Neutron Sources," Sect. 2.1.2, pp. 30-35 in *Engineering Compendium on Radiation Shielding*, Vol. 1, Springer-Verlag, 1968.

Arnold, E. D., "Prompt Fission Neutrons," Sect. 2.3.1.1, pp. 68-72 in *Engineering Compendium on Radiation Shielding*, Vol. 1, Springer-Verlag, 1968.

Bell, J. T., "Continuities in the Spectra and Structure of the Actinyl Ions," presented at the 1968 South-eastern Regional Meeting of ACS, Florida State University, Dec. 4-7, 1968.

Bell, J. T., "Continuities in the Spectra and Structure of the Actinyl Ions," *J. Inorg. Nucl. Chem.* **31**, 703 (1969).

Brooksbank, R. E., and J. R. Parrott, "The ²³³U Storage and Dispensing Facility," presented at the Research Materials Meeting, Gatlinburg, Tenn., Apr. 30-May 1, 1969.

Campbell, D. O., "Studies of the Behavior of Protactinium in Sulfuric Acid," *Colloq. Intern. Centre Natl. Rech. Sci.* **154**, 209-24 (1966).

Carr, W. H., "Policies and Procedures Used in the U.S. for Decontaminating Hot Cells," *Nucl. Safety* **7**, 212-14 (1966).

Clark, W. E., "Principles of Scientific Education: Some Remarks on U.S. Practices and Recommendations for Nepal," *J. Tribhuvan Univ. (Nepal)* **4**, 1-5 (1968).

Ferguson, D. E., Introduction to the section on "Nuclear Reactors," pp. 74-75 in the *Kirk-Othmer Encyclopedia of Chemical Technology*, Vol. 14, 2d ed. (A. Standen, executive ed.), Interscience (Wiley), New York, 1967.

Ferris, Leslie M., "Reactions of Uranium Mononitride, Thorium Monocarbide and Uranium Monocarbide with Nitric Acid and Other Aqueous Reagents," *J. Inorg. Nucl. Chem.* **30**(10), 2661-69 (1968).

Graham, H. B., "The Effect of Nuclear Standards on the Nuclear Industry," presented at the 10th Annual Meeting of the Institute of Nuclear Materials, Las Vegas, Nev., Apr. 29, 1969.

Gresky, A. T., "Chemical Reprocessing," a subsection of "Nuclear Reactors," pp. 91-102 in the *Kirk-Othmer Encyclopedia of Chemical Technology*, Vol. 14, 2d ed. (A. Standen, executive ed.), Interscience (Wiley), New York, 1967.

Guthrie, C. E.,¹³ "Safety in Nuclear Facilities," a subsection of "Nuclear Reactors," pp. 108-15 in the *Kirk-Othmer Encyclopedia of Chemical Technology*, Vol. 14, 2d ed. (A. Standen, executive ed.), Interscience (Wiley), New York, 1967.

Haire, R. G., and T. E. Willmarth, *Trends and Differences in the Crystallization Behavior of Lanthanide Hydroxide Preparations*, ORNL-TM-2387 (Oct. 8, 1968).

Haire, R. G., and T. E. Willmarth, "The Systematic Trends and Differences in Crystallization Behavior of the Lanthanide Hydroxides," presented at the 7th Rare Earth Research Conference, Coronado, Calif., Oct. 28-30, 1968; published in the *Proceedings*, Vol. 1, p. 282.

¹²Battelle Memorial Institute, Columbus, Ohio.

¹³Now at Westinghouse Corporation, Pittsburgh, Pa.

- Harrell, J. E., Jr.,¹⁴ and J. J. Perona, "Mixing of Fluids in Tanks of Large Length-to-Diameter Ratio by Recirculation," *Ind. Eng. Chem., Process Design Develop.* **7**, 464 (1968).
- Holmes, J. M., "Energy and Heat Intensive Processes for a Nuclear Energy Center," presented at the Conference on Abundant Nuclear Energy, Gatlinburg, Tenn., Aug. 26-29, 1968.
- Holmes, J. M., R. Salmon, R. E. Blanco, and J. W. Ullmann, *The Production of Ammonium Nitrate Fertilizer by Using Low-Cost Energy from a Nuclear Desalination Reactor*, ORNL-TM-2202 (Apr. 30, 1968).
- Johnson, J. S., Jr.,¹⁵ K. A. Kraus,¹⁶ S. M. Fleming,¹⁷ H. D. Cochran, Jr.,¹⁷ and J. J. Perona, "Hyperfiltration Studies XIV. Porous Tubes Precoated with Filteraids as Supports for Dynamically Formed Membranes," *Desalination* **5**, 359-69 (1968).
- Kibbey, A. H., and W. Davis, Jr., *Methylation and Gas Chromatographic Analysis of the Decomposition Products of Tributyl Phosphate*, ORNL-TM-2289 (Aug. 1, 1968).
- Klima, B. B., *Reusable Radioactive and Fissile Material Shipping Containers in Use by, or Owned by, the Chemical Technology Division*, ORNL-TM-2509 (Feb. 19, 1969).
- Klima, B. B., and E. L. Youngblood, "Poor Man's Model," *Chemical Engineering -- Plant Notebook* (Feb. 24, 1969).
- Landry, J. W., "From Swords into Mighty Plowshares," presented to Oak Ridge Rotary Club, Oak Ridge, Tenn., July 11, 1968.
- Landry, J. W., "Man's Most Powerful Tool, the Peaceful Nuclear Explosion," presented to the Exhibit Managers of "This Atomic World," American Museum of Atomic Energy, Oak Ridge, Tenn., July 23, 1968.
- Landry, J. W., "Canals, Gas, Copper, and Water from Peaceful Nuclear Explosives," presented to United States Naval Research Reserve Seminar, Oak Ridge, Tenn., Aug. 30, 1968.
- Landry, J. W., "Industrial and Scientific Application of Nuclear Explosives," presented in Seminar-Lecture Program at Tennessee Technological University, Cookeville, Mar. 24, 1969.
- Landry, J. W., "Engineering with Nuclear Explosives," presented to Carolina Section of American Society of Mechanical Engineers, Greensboro, N.C., Apr. 1, 1969.
- Mrochek, J. E., "The Economics of Hydrogen and Oxygen Production by Water Electrolysis and Competitive Processes," presented at the Conference on Abundant Nuclear Energy, Gatlinburg, Tenn., Aug. 26-29, 1968.
- Mrochek, J. E., "Nuclear Energy Centers: Economic Help for Developing Nations," presented at the National Youth Conference on the Atom, Chicago, Ill., Nov. 21-23, 1968.
- Scott, C. D., "Analysis of the Combustion of Graphite-Uranium Fuels in a Fixed Bed or Moving Bed," *Ind. Eng. Chem., Process Design Develop.* **5**, 223-33 (1966).
- Scott, C. D., "Removal of Water and Carbon Dioxide from Helium Coolants by Molecular Sieves," *Nucl. Sci. Eng.* **34**, 314-23 (1968).
- Scott, C. D., "Oxidation of Hydrogen in a Helium Stream by Copper Oxide: Analysis of Combined Film and Pore Diffusion with Rapid Irreversible Reaction in a Fixed-Bed Process," *A.I.Ch.E. J.* **15**, 116 (1969).
- Sears, M. B., T. M. Kegley, Jr.,¹⁸ L. M. Ferris, and B. C. Leslie,¹⁸ *Metallographic Preparation of Arc-Cast Thorium Carbides and Correlation of Their Microstructures with Composition*, ORNL-4354 (March 1969).

¹⁴Air Products and Chemicals, Inc.

¹⁵Chemistry Division.

¹⁶Director's Division.

¹⁷Oak Ridge Station, MIT School of Chemical Engineering Practice.

¹⁸Metals and Ceramics Division.

- Shappert, L. B., "Highlights of the Second International Symposium on Packaging and Transportation of Radioactive Materials," presented at the 16th Conference on Remote Systems Technology, Idaho Falls, Idaho, Mar. 11-13, 1969.
- Thomas, I. L., "The Protonic Structure of Methane, Ammonia, Water, and Hydrogen Fluoride," presented at: the University of Pennsylvania, Philadelphia, May 13, 1969; Princeton University, Princeton, N.J., May 15, 1969; Bell Laboratories, Murray Hill, N.J., May 16, 1969; New York University, New York City, May 19, 1969.
- Unger, W. E., "Special Engineering for Radiochemical Plants," a subsection of "Nuclear Reactors," pp. 115-21 in the *Kirk-Othmer Encyclopedia of Chemical Technology*, Vol. 14, 2d ed. (A. Standen, executive ed.), Interscience (Wiley), New York, 1967.
- Vissers, D. R.,¹⁹ "The Sorption of Orthophosphate on Crystalline Metal Oxides," *J. Phys. Chem.* **72**, 3236-44 (1968).
- Watson, C. D., "Status of Standard on Reactor Containment Coatings," presented at the Spray Technology Program Meeting, Toronto, Canada, June 11, 1968.
- Watson, C. D., and G. A. West, "Protective Coatings Standards and the Nuclear Industry," presented at the Southeast Regional Meeting of the National Association of Corrosion Engineers, Protective Coatings Symposium, Atlanta, Ga., Sept. 20, 1968.
- Yee, W. C., "Marine Chemical Recovery," presented at the Conference on Abundant Nuclear Energy, Gatlinburg, Tenn., Aug. 26-29, 1968.
- Yee, W. C., "Nuclear-Powered Agro-Industrial Complex," presented at "High School Science Night," Carson-Newman College, Jefferson City, Tenn., Nov. 4, 1968.
- Yee, W. C., "Economic Implications of Nuclear Desalination on Seawater Chemicals Recovery," presented at the Third Symposium on Salt, Cleveland, Ohio, Apr. 21-24, 1969.

PATENTS FOR 1967 AND 1968

- Bennett, M. R., and G. I. Cathers, "Method of Separating UF_6 from Bromine Fluorides," U.S. Pat. 3,328,132 (June 27, 1967).
- Clinton, S. D., and P. A. Haas, "Method for Preparing Metal Oxide Microspheres," U.S. Pat. 3,331,898 (July 18, 1967).
- Crouse, D. J., Jr., and F. G. Seeley, "Process for Separating Beryllium Values from Aqueous Solutions," U.S. Pat. 3,359,064 (Dec. 19, 1967).
- Frederick, E. J., H. W. Godbee, J. M. Holmes, and G. D. Davis, "Concentration and Containment of Radioactivity from Radioactive Waste Solutions in Asphalt," U.S. Pat. 3,298,961 (Jan. 17, 1967).
- Lloyd, M. H., "Preparation of Plutonium Oxide Sol and Calcined Microspheres," U.S. Pat. 3,310,386 (1967).
- McBride, J. P., and W. L. Pattison, "Urania Sol Forming Method in the Presence of Formic Acid and a Palladium-on-Thoria Catalyst," U.S. Pat. 3,361,676 (Jan. 2, 1968).
- Meservey, A. B., J. D. Sease,¹⁸ and R. B. Fitts,¹⁸ "Method of Fabricating Ceramic Nuclear Fuel Product," U.S. Pat. 3,356,776 (Dec. 5, 1967).
- Moore, J. G., "Preparation of Actinide Sols by Amine Extraction," U.S. Pat. 3,335,095 (Aug. 8, 1967).
- Morse, L. E., "Extraction Method for Preparing UO_2 Microspheres," U.S. Pat. 3,367,881 (Feb. 6, 1968).

¹⁹Present address: Argonne National Laboratory, Chemical Engineering Division.

- Notz, K. J., Jr., "Ammonium Nitrate Explosive Compositions Containing (Metal-Excess Chloride) Combustion Catalyst," U.S. Pat. 3,336,171 (August 1967).
- Ryon, A. D., "Apparatus for Separation of Immiscible Liquid Pairs Including Remote Interface Control," U.S. Pat. 3,362,791 (Jan. 9, 1968).
- Wymer, R. G., and D. M. Helton, "Electrical Potential Method for Dispersion of Metal Oxide Microspheres," U.S. Pat. 3,352,950 (Nov. 14, 1967).

POWER REACTOR FUEL PROCESSING

- Davis, W., Jr., and H. F. Soard, *A Computer Program for Handling and Comparing Fission Product Data from RIBDOR for Mixtures of Reactor Fuels Irradiated Under Different Conditions: Application to Atomics International LMFBR Fuel*, ORNL-TM-2393 (November 1968).
- Ferguson, D. E., and R. E. Blanco, "General Survey of Reprocessing of Thermal Reactor Fuels," presented at the 1968 American Nuclear Society International Meeting, Washington, D.C., Nov. 10-15, 1968; to be published in the Proceedings.
- Groenier, W. S., *Some Factors Affecting the Choice of a Solvent Extraction Contactor for the First Cycle Reprocessing of LMFBR Fuels*, ORNL-TM-2290 (September 1968).
- Irvine, A. R., "Fast-Breeder-Reactor Fuel Shipment," presented at the 16th Conference on Remote Systems Technology, Idaho Falls, Idaho, Mar. 11-13, 1969.
- Shappert, L. B., "Development of an Engineering Design Guide for Irradiated Fuel Shipping Casks," presented at the Second International Symposium on Packaging and Transportation of Radioactive Materials, Gatlinburg, Tenn., Oct. 14-18, 1968.
- Shappert, L. B., *Irradiated Fuel Shipping Cask Design Guide*, ORNL-TM-2410 (January 1969).
- Vaughen, V. C. A., *Head-End Studies of SiC-Coated HTGR Fuels: Unirradiated Dragon Compact No. 8232*, ORNL-TM-2389 (February 1969).
- Watson, C. D., R. S. Lowrie, W. S. Groenier, G. A. West, and S. D. Clinton, "Head-End Processing of Spent LMFBR Fuel," presented at the ANS Topical Meeting, Remote Handling and Examination in the Fast Reactor Fields, at the 16th Conference on Remote Systems Technology, Idaho Falls, Idaho, Mar. 11-13, 1969.
- Witte, Hartmut O.,²⁰ "Fluidized-Bed Combustion of Graphite-Base Nuclear Reactor Fuels," *Ind. Eng. Chem., Process Design Develop.* 8(2), 145-49 (1969).

PROGRESS REPORTS

- Arnold, W. D., C. A. Blake, Jr., and D. J. Crouse, *Chemical Applications of Nuclear Explosions (CANE): Progress Report for April 1 to June 30, 1968*, ORNL-TM-2298 (July 24, 1968).
- Arnold, W. D., and D. J. Crouse, *Chemical Applications of Nuclear Explosions (CANE): Progress Report for July 1 to September 30, 1968*, ORNL-TM-2399 (Oct. 29, 1968).
- Arnold, W. D., and D. J. Crouse, *Chemical Applications of Nuclear Explosions (CANE): Progress Report for October 1 to December 31, 1968*, ORNL-TM-2502 (Apr. 8, 1969).
- Arnold, W. D., and D. J. Crouse, *Chemical Applications of Nuclear Explosions (CANE): Progress Report for January 1 to March 31, 1969*, ORNL-TM-2567 (Apr. 24, 1969).
- Blanco, R. E., and K. E. Cowser, *Waste Treatment and Disposal Semiannual Progress Report July-December 1967*, ORNL-TM-2294.

²⁰Guest scientist from Germany. Present address: KFA-heisse Zellen, Juelich, Germany.

- Burch, W. D., J. E. Bigelow, and L. J. King, *Transuranium Processing Plant Semiannual Report of Production, Status, and Plans for Period Ending June 30, 1968*, ORNL-4376 (April 1969).
- Ferguson, D. E., and staff, *Chemical Technology Division Annual Progress Report for Period Ending May 31, 1968*, ORNL-4272 (September 1968).
- Scott, C. D., *Body Fluids Analyses Program Progress Report for the Period March 1 to August 31, 1968*, ORNL-TM-2372 (April 1969).
- Unger, W. E., R. E. Blanco, C. D. Watson, D. J. Crouse, and A. R. Irvine (compilers), *Aqueous Processing of LMFBR Fuels, Progress Report, March 1969, No. 1*, ORNL-TM-2552 (April 1969).
- Unger, W. E., R. E. Blanco, C. D. Watson, D. J. Crouse, and A. R. Irvine (compilers), *Aqueous Processing of LMFBR Fuels, Progress Report, April 1969, No. 2*, ORNL-TM-2585 (May 1969).
- Wymer, R. G., and A. L. Lotts, *Status and Progress Report for Thorium Fuel Cycle Development for Period Ending Dec. 31, 1966*, ORNL-4275 (January 1969).

SEPARATIONS CHEMISTRY RESEARCH

- Chilton, J. M., and J. J. Fardy,²¹ "Isolation of Plutonium in Chloride Media I. Anion Exchange Resin Studies," *J. Inorg. Nucl. Chem.* **31**(4), 1171-77 (1969).
- Davis, W., Jr., and D. O. Rester, "Kinetics of Precipitation of Ferric Dibutylphosphate from Aqueous HNO₃ Solutions," *J. Inorg. Nucl. Chem.* **30**, 3317 (1968).
- McDowell, W. J., "Synergistic and Solvent Effects in the Extraction of Strontium and Sodium by Di(2-Ethyl-Hexyl)Phosphate," *J. Inorg. Nucl. Chem.* **30**, 1037-49 (1968).
- McDowell, W. J., and H. D. Harmon, "Sodium and Strontium Extraction from Sodium Nitrate Solutions by *n*-Octane Solutions of a Branched Aliphatic Monocarboxylic Acid: Mechanism and Equilibria," presented at the Southeastern Regional Meeting of the American Chemical Society, Tallahassee, Fla., Dec. 4-7, 1968.
- McDowell, W. J., and H. D. Harmon, "Sodium and Strontium Extraction from Sodium Nitrate Solutions by *n*-Octane Solutions of a Branched Aliphatic Monocarboxylic Acid: Mechanism and Equilibria," *J. Inorg. Nucl. Chem.* **31**, 1473-85 (1969).
- Roddy, J. W., and C. F. Coleman, "Solubility of Water in Hydrocarbons as a Function of Water Activity," *Talanta* **15**, 1281-86 (1968).
- Roddy, J. W., and C. F. Coleman, "Diluents of Low Volatility for Studies in the Tri-*n*-Octylamine Sulfuric Acid System," published as a Note, *J. Inorg. Nucl. Chem.* **30**, 1975-79 (1968).
- Roddy, J. W., and C. F. Coleman, "Reference Solutes for Isopiestic and Dynamic Vapor Pressure Osmometry in Organic Solvents: I. Triphenylmethane, Azobenzene, and Benzil in Dry Benzene," presented at the 157th American Chemical Society Meeting, Minneapolis, Minn., Apr. 13-18, 1969.
- Weaver, Boyd, "Precipitation of Berkelium(IV) Iodate from Homogeneous Solution," *Anal. Chem.* **40**, 1894-96 (1968).
- Weaver, Boyd, and J. J. Fardy,²¹ "Comparison of Electric Potentials of the Bk(IV)-Bk(III) and Ce(IV)-Ce(III) Couples," *Inorg. Nucl. Chem. Letters* **5**, 145 (1969).

SEPARATIONS PROCESS DEVELOPMENT

- Horner, D. E., *The Use of Ferrous Nitrate as a Plutonium Reductant for Partitioning Plutonium and Uranium in Purex Processes*, ORNL-4383 (April 1969).

²¹Australian Atomic Energy Commission; Lucas Heights, Sydney, Australia.

- Hurst, F. J., D. J. Crouse, and K. B. Brown, *Solvent Extraction of Uranium from Wet-Process Phosphoric Acid*, ORNL-TM-2522 (April 1969).
- Lee, W. A.,¹⁵ W. L. Taylor,²² W. J. McDowell, and J. S. Drury,¹⁵ "Solvent Extraction of Lithium," *J. Inorg. Nucl. Chem.* **30**(10), 2807-21 (1968).
- Moore, J. G., *The Extraction of Pu(VI) from Nitric Acid-Uranyl Nitrate Solutions with Tri-n-Butyl Phosphate*, ORNL-4348 (January 1969).

SOL-GEL STUDIES

- Bond, W. D., "Preparation of Porous Oxides and Carbides," presented at the 14th AEC Coated-Particle Fuels Working Group Meeting, ORNL, Nov. 20-21, 1968.
- Brooksbank, R. E., and M. H. Lloyd, "Status of ORNL Sol-Gel Work Sponsored by SNS," presented at the ²³⁸Pu Isotopic Fuels and Heat Source Conference, Germantown, Md., Oct. 29-30, 1968.
- Haws, C. C., "Microsphere Preparation: A Status Report," presented at the 14th AEC Coated-Particle Fuels Working Group Meeting, ORNL, Nov. 20-21, 1968.
- Lloyd, M. H., and R. G. Haire, "Development of a Sol-Gel Process for the Preparation of Dense Oxide Forms of PuO₂," *Nucl. Appl.* **5**, 114-22 (1968).
- Notz, K. J., *Preparation of Porous Thoria by Incorporation of Carbon in Sols*, ORNL-TM-1780 (December 1968).
- Notz, K. J., and W. D. Bond, "Preparation of Dense UC Microspheres by a Sol-Gel Method," presented at the 71st Annual Meeting of the American Ceramic Society, Washington, D.C., May 3-8, 1969.
- Smith, F. J., and N. A. Krohn, *The Preparation of Iron-Thoria and Iron-Alumina Cermets by a Sol-Gel Method*, ORNL-TM-2518 (Feb. 25, 1969).

THESIS

- Snider, J. W., *Effects of Gas Flow Rate on the Mass Transfer Coefficient, Measured Across the Liquid-Solid Interface, in a Packed-Bed Catalytic Reactor Using Cocurrent Upflow*, M.S. thesis, University of Tennessee, Knoxville; also published as ORNL-TM-2320 (February 1969).

TRANSURANIUM ELEMENT PROCESSING

- Baybarz, R. D., and A. Delle Site, "An Absorption Spectrophotometric Study of the Complexing of Americium with Aminopolyacetic Acids," presented at the International Conference on Coordination Chemistry, Haifa, Israel, Sept. 8-12, 1968.
- Baybarz, R. D., "Chemical Properties of ²⁵²Cf," presented at the ANS ²⁵²Cf Symposium, New York City, Oct. 22, 1968; to be published in the *Proceedings*.
- Baybarz, R. D., "The Berkelium Oxide System," *J. Inorg. Nucl. Chem.* **30**, 1769-73 (1968).
- Baybarz, R. D., "High Pressure Ion Exchange I: The Rapid Separation of Californium, Einsteinium and Fermium," presented at the Nuclear Applications Award Symposium, ACS, Minneapolis, Minn., Apr. 14-16, 1969.
- Bigelow, J. E., "²⁵²Cf Production at ORNL," presented at ANS ²⁵²Cf Symposium, New York City, Oct. 22, 1968.
- Burch, W. D., "Transuranium Program," presented at Mound Laboratory, Cincinnati, Ohio, Dec. 6, 1968.

²²Summer Participant at ORNL, 1966; Mount Vernon Nazarene College, Mount Vernon, Ohio.

- Ferguson, Don E., and John Ealy Bigelow, "Production of ^{252}Cf and Other Transplutonium Isotopes in the United States of America," *Actinides Rev.* 1, 213-21 (1969).
- King, L. J., and E. D. Collins, *Summary of the Campaign to Process Six SRP Reactor Slugs in the Transuranium Processing Plant*, ORNL-TM-1939 (April 1969).
- Knauer, J. B., and Boyd Weaver, *Separation of Berkelium from Trivalent Actinides by Chromate Oxidation and HDEHP Extraction*, ORNL-TM-2428 (Nov. 14, 1968).
- Milligan, W. O.,²³ M. L. Beasley,²³ M. H. Lloyd, and R. G. Haire, "Crystalline Americium Trihydroxide," *Acta Cryst.* B24, 979-81 (1968).
- Nugent, L. I.,²⁴ J. R. Tarrant,²⁴ J. L. Burnett,²⁴ R. D. Baybarz, G. K. Werner,²⁴ and O. L. Keller, Jr.,²⁴ "Intra-Molecular, Energy Transfer in Actinide Beta-Diketones. Exchange of Lanthanide and Actinide Ions in a Convenient Method of Scanning Actinide Complexes for Application to Liquid Lasers," presented at the 155th American Chemical Society Meeting, San Francisco, Calif., June 1968.
- Nugent, L. J.,²⁴ R. D. Baybarz, and J. L. Burnett,²⁴ "Electron-Transfer Spectra and the II-III Oxidation Potentials of Some Lanthanide and Actinide Halides in Solution," presented at the Seventh Rare Earth Conference, Coronado, Calif., Oct. 28-30, 1968.
- Nugent, L. J.,²⁴ R. D. Baybarz, and J. L. Burnett,²⁴ "Electron-Transfer Spectra and the II-III Oxidation Potentials of Some Lanthanide and Actinide Halides in Solution," *J. Phys. Chem.* 73(4), 1177 (1969).

URANIUM FUEL CYCLE SOL-GEL PROCESSES

- Haas, P. A., *Engineering Development of Continuous Sol-Gel Equipment for Preparing UO_2 Sols by Precipitation-Peptization Processes*, ORNL-TM-2227 (July 1968).
- Snider, J. W., *The Design of Engineering-Scale Sol-gel Equipment*, ORNL-4256 (April 1969).

WASTE TREATMENT AND DISPOSAL

- Blanco, R. E., "Proposed Definition of Radioactive Waste Categories: A Summary of a USASI Standard," *Nucl. Safety* 9, 515-18 (1968).
- Blanco, R. E., "Treatment of Low- and Intermediate-Level Liquid and Gaseous Wastes from Fuel Reprocessing Plants," presented to the National Academy of Science Committee on Radioactive Waste Disposal, ORNL, Oct. 17-18, 1968.
- Blomeke, J. O., "Waste Management," a subsection of "Nuclear Reactors," pp. 102-8 in the *Kirk-Othmer Encyclopedia of Chemical Technology*, Vol. 14, 2d ed. (A. Standen, executive ed.), Interscience (Wiley), New York, 1967.
- Blomeke, J. O., "Waste Management Experience at Nuclear Power Stations and Economic Evaluations of Fuel Processing Waste Management," presented to the National Academy of Science Committee on Radioactive Waste Disposal, ORNL, Oct. 17-18, 1968.
- Blomeke, J. O., "Sources, Characteristics, and Management of Wastes from the Nuclear Power Industry," presented to the American Association for the Advancement of Science, Rockefeller University, New York City, Feb. 8, 1969.
- Davis, W., Jr., *Effects of Fission Product Heat on the Production Capacity of the Fingal Process*, AERE-R-5268 (September 1967).

²³Baylor University, Waco, Tex.

²⁴Transuranium Research Laboratory, ORNL.

- Davis, W., Jr., *Temperature Profiles Within Cylinders Containing Internal Heat Sources and Materials of Temperature-Dependent Thermal Conductivities. Description of Fast Computer Programs as Applied to Solidified Radioactive Wastes*, ORNL-4345 (January 1969).
- Davis, W., Jr., C. L. Fitzgerald, and H. F. Soard, *Maximum Temperature Rise in Cylinders Containing Intermediate-Level and High-Level Solidified Radioactive Wastes*, ORNL-4361 (March 1969).
- Godbee, H. W., J. H. Goode, and R. E. Blanco, "The Development of a Process for Incorporation of Radioactive Waste Solutions and Slurries in Emulsified Asphalt," presented at the American Chemical Society meeting, Atlantic City, N.J., September 8-13, 1968.
- Godbee, H. W., J. H. Goode, and Raymond E. Blanco, "Development of a Process for Incorporation of Radioactive Waste Solutions and Slurries in Emulsified Asphalt," *Environ. Sci. Technol.* **2**, 1034-40 (1968).
- Nichols, J. P., "Summary of Considerations Related to Siting Fuel Processing Plants and Waste Management Facilities," presented to the National Academy of Science Committee on Radioactive Waste Disposal, ORNL, Oct. 17-18, 1968.
- Rainey, R. H., "Separation of Radioactive Xenon and Krypton from Other Gases by Use of Permselective Membranes," paper SM 110/27 presented at the IAEA Symposium on Operating and Developmental Experience in the Treatment of Airborne Radioactive Waste, New York City, Aug. 26-28, 1968; published in the *Proceedings*, pp. 323-42.
- Rainey, R. H., "Separation of Radioactive Xenon and Krypton from Other Gases by Use of Permselective Membranes," presented at the Nuclear Safety Annual Information Meeting, ORNL, Feb. 17, 1969.
- Schonfeld, E., and W. Davis, Jr., "Softening and Decontaminating Waste Water by Caustic Carbonate Precipitants in a Slowly Stirred Sludge Blanket Column," *Health Phys.* **12**, 407-15 (1966).
- Suddath, J. C., "Treatment of High-Level Liquid Wastes from Fuel Reprocessing Plants," presented to the National Academy of Science Committee on Radioactive Waste Disposal, ORNL, Oct. 17-18, 1968.
- Weeren, H. O., "Disposal of Radioactive Wastes by Hydraulic Fracturing: Part III, Design of ORNL's Shale Fracturing Plant," *Nucl. Eng. Design* **4**, 108-17 (1966).

SEMINARS

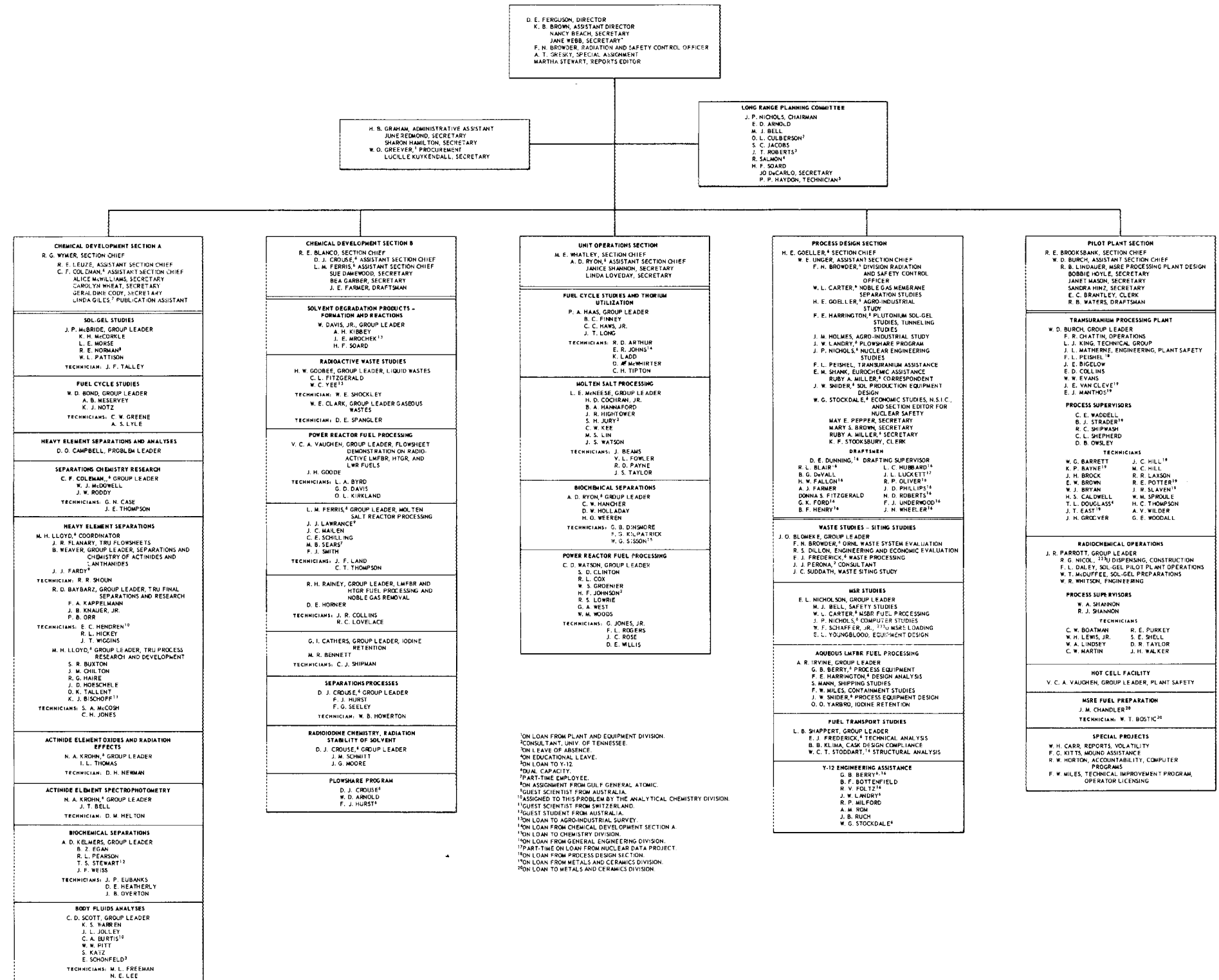
1968

October 16	Introduction to Nepal	W. E. Clark
October 23	Packaged Glass Equipment for the Chemical Process Industry	H. C. Travers (Corning Glass Works)
October 30	Zirconium Organophosphorus Superextractants	B. Weaver
November 6	Sodium and Strontium Extraction by an Aliphatic Monocarboxylic Acid	W. J. McDowell
November 20	High Temperature Spectrophotometry of Aqueous Solutions	J. T. Bell
November 27	Performance of the High-Level Waste Disposal Pilot Plant at Hanford	J. C. Suddath
	Disposal of High-Level Waste as High-Thermal-Conductivity Solids	W. Davis, Jr.
December 4	Bk(IV) Iodate Precipitation from Homogeneous Solution	J. J. Fardy
December 11	Status of Mound Sol-Gel Assistance Program: Engineering Chemistry	F. G. Kitts M. H. Lloyd

December 18	Disposal of Intermediate-Level Wastes in Asphalt or Polyethylene: Incorporation and Safety Studies Pilot Plant Tests	C. L. Fitzgerald J. C. Suddath
1969		
January 8	Sol-Gel Engineering Development Studies Sol-Gel Laboratory Development Studies	P. A. Haas W. D. Bond
January 15	Electrokinetic Studies of Sols Adsorption of CO ₂ by Sols	N. A. Krohn I. L. Thomas
January 22	Project Plowshare: Radionuclide (particularly ³ H) Contamination of Nuclear-Broken Shale and Shale Oil	W. D. Arnold
January 29	Fast Reactor Fuel Material Preparation Important Developments in the Preparation of Urania Sols	O. K. Tallent J. P. McBride
February 5	Recovery of Uranium from Wet-Process Phosphoric Acid	F. J. Hurst
February 12	Separation of Bk from Trivalent Actinides by Chromate Oxidation and HDEHP Extraction	J. B. Knauer
February 26	Preparation of ²³³ UO ₂ -ThO ₂ Microspheres for the HTL/TR	J. W. Snider J. R. Parrott J. Furman (M&C Div.)
March 5	Recovery of tRNA's from <i>E. Coli</i> Scale-Up of the Separation of tRNA's on Chromatographic Columns	C. W. Hancher H. O. Weeren
March 12	Separation of Ribosomal RNA's Recovery and Purification of Certain <i>E. Coli</i> Enzymes	B. Z. Egan R. L. Pearson
March 19	Removal of Noble Gases from Off-Gas Streams, Using Permeable Membranes	R. H. Rainey W. L. Carter
March 26	Chemical Development of Reductive Extraction Processes for MSBR Fuels Protactinium Isolation Separation of Rare Earths from Thorium	J. C. Mailen L. M. Ferris
April 2	Measurement of Flooding, Pressure Drops and Hold-Up in Packed Columns Using Water and Mercury Electrolytic Oxidizer-Reducer Development	J. S. Watson M. S. Lin
April 16	Status of TRU Processing of Six Irradiated Curium Targets Iodine in TRU - Past, Present, and Future	W. D. Burch E. D. Collins L. J. King
April 23	Special TRU Projects	R. D. Baybarz F. A. Kappelmann
May 1	Development of Nondestructive Assay Techniques	Dr. Howard Menlove Los Alamos Scientific Laboratory

May 14	LMFBR Fuel Reprocessing	
	Mechanical Handling	G. A. West
	Hot Cell Studies: Fission Gas Removal and Dissolution	J. H. Goode
	Engineering Aspects of Fission Gas Removal	S. D. Clinton
	Engineering Aspects of Dissolution	W. S. Groenier
May 23	Transport of LMFBR Spent Fuel	A. R. Irvine
		R. S. Lowrie
		H. C. Young
		D. C. Watkin

CHEMICAL TECHNOLOGY DIVISION



ORNL-4422
 UC-10 - Chemical Separations Processes
 for Plutonium and Uranium

INTERNAL DISTRIBUTION

- | | |
|-------------------------------------|------------------------|
| 1. Biology Library | 217. H. W. Godbee |
| 2-4. Central Research Library | 218. H. E. Goeller |
| 5. Laboratory Shift Supervisor | 219. H. B. Graham |
| 6-7. ORNL - Y-12 Technical Library | 220. A. T. Gresky |
| Document Reference Section | 221. W. R. Grimes |
| 8. MIT Practice School | 222. P. A. Haas |
| 9-28. Laboratory Records Department | 223. J. P. Hammond |
| 29. Laboratory Records, ORNL R.C. | 224. C. S. Harrill |
| 30. H. I. Adler | 225. R. F. Hibbs |
| 31-32. R. D. Baybarz | 226. R. W. Horton |
| 33. S. E. Beall | 227. A. R. Irvine |
| 34. Arnold Berman | 228. R. L. Jolley |
| 35. D. S. Billington | 229. W. H. Jordan |
| 36. C. A. Blake | 230. M. A. Kastenbaum |
| 37. R. E. Blanco | 231. M. T. Kelley |
| 38. J. O. Blomeke | 232. A. D. Kelmers |
| 39. W. D. Bond | 233. F. Kertesz |
| 40. C. J. Borkowski | 234. N. A. Krohn |
| 41. G. E. Boyd | 235. E. Lamb |
| 42. R. E. Brooksbank | 236. J. A. Lane |
| 43. J. C. Bresee | 237. R. E. Leuze |
| 44. R. B. Briggs | 238. R. B. Lindauer |
| 45. F. N. Browder | 239. J. L. Liverman |
| 46. K. B. Brown | 240. R. S. Livingston |
| 47. F. R. Bruce | 241. M. H. Lloyd |
| 48. W. D. Burch | 242. H. G. MacPherson |
| 49. D. O. Campbell | 243. F. C. Maienschein |
| 50. W. H. Carr | 244. J. P. McBride |
| 51. G. I. Cathers | 245. W. J. McDowell |
| 52. J. M. Chandler | 246. L. E. McNeese |
| 53. W. E. Clark | 247. R. A. McNees |
| 54. C. F. Coleman | 248. A. B. Meservey |
| 55. W. C. Colwell | 249. R. P. Milford |
| 56. J. A. Cox | 250. E. C. Miller |
| 57. D. J. Crouse | 251. K. Z. Morgan |
| 58. F. L. Culler | 252. J. P. Nichols |
| 59. J. E. Cunningham | 253. E. L. Nicholson |
| 60. W. Davis, Jr. | 254. G. D. Novelli |
| 61-210. D. E. Ferguson | 255-256. R. B. Parker |
| 211. L. M. Ferris | 257. J. R. Parrott |
| 212. J. R. Flanary | 258. Helen Raen |
| 213. J. L. Fowler | 259. R. H. Rainey |
| 214. J. H. Frye, Jr. | 260. M. E. Ramsey |
| 215. R. C. Fuller | 261. J. T. Roberts |
| 216. J. H. Gillette | 262. A. F. Rupp |

- | | |
|-------------------------|----------------------------------|
| 263. A. D. Ryon | 277. C. D. Watson |
| 264. C. D. Scott | 278. B. S. Weaver |
| 265. H. E. Seagren | 279. A. M. Weinberg |
| 266. E. M. Shank | 280. M. E. Whatley |
| 267. L. B. Shappert | 281. J. C. White |
| 268. M. J. Skinner | 282. R. G. Wymer |
| 269. A. H. Snell | 283. B. J. Young |
| 270. M. G. Stewart | 284. Gale Young |
| 271. J. C. Suddath | 285. E. L. Youngblood |
| 272. D. A. Sundberg | 286. P. H. Emmett (consultant) |
| 273. E. H. Taylor | 287. J. J. Katz (consultant) |
| 274. W. E. Unger | 288. E. A. Mason (consultant) |
| 275. V. C. A. Vaughen | 289. J. L. Margrave (consultant) |
| 276. F. C. Von der Lage | 290. R. B. Richards (consultant) |

EXTERNAL DISTRIBUTION

291. D. F. Cope, RDT Site Office (ORNL)
292. Richard Hamburger, AEC, Washington
293. J. A. Swartout, 270 Park Avenue, New York 17, New York
294. Sylvania Electric Products, Inc.
295. Dr. Barendregt, c/o COMPRIMO, Europahuis, James Wattstraat 79, Amsterdam, Holland
296. Giacomo Calleri, Comitato Nazionale per l'Energia Nucleare, Programma EUREX, Saluggia (Vc), Italy
297. D. J. Carswell, Radiochemical Laboratory, The New South Wales University of Technology, P.O. Box 1, Kensington, Sydney, N.S.W., Australia
298. E. Cerrai, Laboratori CISE, Casella Postale N. 3986, Milano, Italy
299. David Dryssen, The Royal Institute of Technology, Department of Inorganic Chemistry, Kemisträgen 37, Stockholm 70, Sweden
300. Syed Fareeduddin, Indian Rare Earths Ltd., Army and Navy Building, 148 Mahatma Gandhi Road, Bombay 1, India
301. W. Wild, United Kingdom Atomic Energy Authority, Atomic Energy Research Establishment, Harwell, Berks, England
302. W. A. Graf, Manager, Plant Design, Atomic Products Division, General Electric Company, Box 450, Palo Alto, Calif.
303. T. Ishihara, Division of Fuel Research and Development, Tokai Research Establishment, JAERI, Tokai-mura, Ibaraki-ken, Japan
304. A. S. Kertes, Hebrew University, Jerusalem
305. Jorgen Klitgaard, Atomic Energy Commission Res. Estab. Risö, Roskilde, Denmark
306. Y. Marcus, Israel Atomic Energy Commission, Tel Aviv, Israel
307. E. Glueckauf, Atomic Energy Research Establishment, Harwell, Berks, England
308. P. Regnaut, C.E.N. Fontenay-aux-Roses, Boite Postale No. 6, Fontenay-aux-Roses, Seine, France
309. R. Rometsch, Eurochemic, Mol, Belgium
310. A. J. A. Roux, Director of Atomic Energy Research, South African Council for Scientific and Industrial Research, Box 395, Pretoria, South Africa
311. Jan Rydberg, Department of Nuclear Chemistry, Chalmers Tekniska Hogskola, Gibraltargatan 5 H. Goteborg, Sweden
312. M. Shaw, AEC, Washington
313. Erik Svenke, Director, Department of Chemistry, Atomic Energy Company, Stockholm 9, Sweden

314. D. G. Tuck, Associate Professor, Department of Chemistry, Simon Fraser University, Burnaby 2, British Columbia, Canada
315. B. F. Warner, United Kingdom Atomic Energy Authority, Production Group, Windscale and Calder Works, Sellafield, Seascale, Cumberland, England
316. M. Zifferero, Comitato Nazionale per l'Energia, Nucleare, Laboratorio Trattamento Elementi Combustibili, c/o Istituto di Chimica Farmaceutica e Tossicologica dell'Universita, Piazzale delle Scienze, 5, Rome, Italy
317. M. Claude Jean Jouannaud, Department Head, Plutonium Extraction Plant, Marcoule (Gard), France
318. Prof. Louis Gutierrez-Jadra, Director de Planta Pilotos e Industriales, Junta de Energia Nuclear, Ciudad Universitaria, Madrid (3), Spain
319. W. G. Belter, AEC, Washington
320. J. A. Lieberman, AEC, Washington
321. W. H. Regan, AEC, Washington
322. H. Bernard, AEC, Washington
323. P. Schmid, Federal Institute for Reactor Research, Wurenlingen, AG, Switzerland
324. Atou Shimozato, Nuclear Reactor Design Section, Nuclear Power Plant Department, Hitachi Ltd., Hitachi Works, Hitachi-Shi, Ibaraki-Ken, Japan
325. R. S. Brodsky, Division of Naval Reactors, Atomic Energy Commission, Washington, D.C.
326. R. W. Barber, AEC, Washington
327. Theodore Rockwell III, Chairman AIF Safety Task Force, MPR Associates, Inc., 815 Connecticut Avenue, N.W., Washington, D.C.
328. Guenther Wirths, NUKEM, Hanau, Germany
329. Riki Kobayashi, Professor, Rice University
330. W. Pollard, Oak Ridge Associated Universities
331. G. R. Hall, Nuclear Technology Laboratories, Department of Chemical Technology, Imperial College, Prince Consort Road, London, S.W. 7, England
332. Giuseppe Orsenigo, CNEN, Via Belisario 15, Rome, Italy
333. Laboratory and University Division, AEC, ORO
334. Werner Muller, European Transuranium Institute, Euratom, Postfach 2266, 75 Karlsruhe, West Germany
335. F. Baumgartner, Heidelberg University, Karlsruhe, Postfach 947, West Germany
336. Hugo Schumacher, Swiss Federal Institute for Reactor Research, Ch-5303 Wurenlingen, Switzerland
337. B. L. Vondra, NUMEC, Apollo, Pa.
338. W. H. McVey, AEC, Washington
339. E. E. Sinclair, AEC, Washington
340. A. R. Van Dyken, AEC, Washington
341. C. L. Sumrall, Gilbert Associates, Reading, Pa.
342. Dr. Narayanan Srinivasan, Head of Fuel Reprocessing Division, Bhabha Atomic Research Center, Bombay 74, India
343. D. M. Rafi, Pakistan Institute of Nuclear Science and Technology, P.O. Box Nilore, Rawal Pindi, Pakistan
344. D. E. Bloomfield, Battelle Northwest, Richland, Washington
345. P. A. DeJonghe, Centre d'Etude de l'Energie Nucleaire, Mol, Belgium
346. T. W. McIntosh, Division of Reactor Development and Technology, USAEC, Washington, D.C.
347. R. E. Pahler, AEC, Washington
348. D. R. Miller, AEC, Washington
349. J. J. Fardy, Australian Atomic Energy Commission; Lucas Heights, Sydney, Australia
350. R. E. Norman, Gulf General Atomic, P.O. Box 608, San Diego, California
351. H. O. G. Witte, Julich Nuclear Research Center, Julich, Germany
352. Alfred Richard Boettcher, Director, Julich Nuclear Research Center, Julich, Germany
353. Julich Nuclear Research Center Library, Julich, Germany

354. Hans W. Levi, Deputy Director, Hahn – Meitner – Institut für Kernforschung Berlin, Sektor Kernchemie, Glienicke Straße 100, 1 Berlin 39, Germany
355. William J. Lacy, Chief, Industrial Pollution Control Branch, Division of Applied Science and Technology, Federal Water Pollution Control Administration, Department of the Interior, Washington, D.C.
356. G. Rajan, Scientific Officer, Waste Treatment Division, Bhabha Atomic Research Centre, Bombay – 85 AS., India
357. C. Djordjevic, Chemistry Department, College of William and Mary, Williamsburg, Virginia
- 358–497. Given distribution as shown in TID-4500 under Chemical Separations Processes for Plutonium and Uranium (25 copies –CFSTI)